THE UNIVERSITY OF HULL

Department of Geography, Environment and Earth Sciences

The influence of Earth surface movements and human activities on the River Karun in lowland south-west Iran

being a Thesis submitted for the Degree of
Doctor of Philosophy
in the University of Hull

by

Kevin Paul Woodbridge
B.Sc. (Hons) (London)

October 2013

ABSTRACT

Earth surface movements are a primary external control on river system dynamics and evolution. It has often been observed that when responding to Earth surface motion driven by surface expression of folds, major rivers incise across young, active folds near their structural culminations and divert around others. This study shows that for the major rivers Karun and Dez in the Mesopotamian-Persian Gulf foreland basin, these different river responses are due to the need for narrow channel-belts to be maintained where a river incises across a fold, and the time it takes (at least several decades) for such narrow channel-belts to develop. In general, where a major river initially encounters a fold as an emerging fold "core", the river flows across the uplifting fold for sufficient time for the development of a narrow channel-belt, thus producing an incising river course across the fold (a single "water gap") in the vicinity of the fold "core" and the subsequent structural culmination. However, where a major river initially encounters a fold as a larger, emerged fold, the river does not flow across the uplifting fold for sufficient time, due to channel migration in response to lateral fold growth, thus producing a river course diverting around the fold "nose". Hence, river reaches across the fold axis for river incision are characterised by narrow channel-belts, low channel sinuosities, high specific stream powers, and river crossing locations relatively near to the fold "core" (generally nearer than 16 km). By contrast, river reaches across the fold axis projection for river diversion are characterised by average channel-belt widths and channel sinuosities with fairly wide ranging values, fairly low specific stream powers, and river crossing locations relatively far from the fold "core" (further than 22 km). A narrow average channel-belt width of less than c. 2.7 km is a threshold for the rivers Karun and Dez (mean annual discharges c. 575 m^3s^{-1} and 230 m^3s^{-1}) encountering folds in lowland south-west Iran (rates of uplift c. 0.1 - 2.3 mm yr^{-1}), and this probably has a precedence over other geomorphological changes for producing river incision across a fold in response to uplift. In general, slightly smaller rivers are more frequently diverted around the fold "nose", and small rivers and creeks, which are more easily "defeated" by fold growth, frequently develop a series of narrow "wind gaps" across a fold.

The influences of human impacts on major rivers can be distinguished from those of Earth surface movements by suites of river characteristics. There may be significant interactions where these two external factors coincide, most notably where fold uplift and major anthropogenic river channel straightening produce the persistence of long, near-straight river courses (channel sinuosity < 1.1 over a river course > 10 km long).

ACKNOWLEDGEMENTS

"From Hull, from Hell, from Halifax, 'tis this,
From all these three, Good Lord, deliver us."

(The Beggar's Litany, pre-1600 AD)

Firstly, I would like to give thanks to my main supervisor, Prof. Dan Parsons, for his excellent advice and encouragement. Our regular meetings and communications and the Bayfield Research Group Meetings with other researchers at the University of Hull have been invaluable. I give my sincere thanks to my initial main supervisors, Prof. Lynne Frostick and Dr. Martyn Pedley, especially for taking on a challenging research project about south-west Iran and for guiding me through the fieldwork, laboratory work and the initial writing up. I am also very grateful to my other supervisors, Dr. Jane Reed and Dr. Barbara Rumsby, for their input, comments and advice.

A research project of this extent in the Islamic Republic of Iran cannot take place without considerable assistance from people and organisations within Iran. In particular, my thanks go to Mr. Payman Forugipore and to his wife, Najleh Khandagh and their sons, Rezza and Maysam. Without their friendship and hospitality in Tehran and the tireless work of Payman contacting people with regards to applying for visas and permissions, searching for information and data, and enabling the involvement of a wide variety of organisations, this research project simply could not have taken place.

I am very grateful to the different organisations and people in Iran who have so kindly worked alongside me in the field and in their offices and in their homes. I have been amazed at the generosity, friendship and hospitality of the Iranian people. I thank the Geological Survey of Iran for assistance at their offices and library in Tehran, particularly the help of Dr. Manouchehr Ghoraishi and Dr. Mohammad Ghassemi in arranging for fieldwork logistics in south-west Iran, including the assistance of geologists, Amir Bolourchi and Babak Sedghi, and a surveyor, Hossein Akbarzadeh. I thank the Geological Survey of Iran in Ahvaz for assistance at their offices and in the field, particularly the help of Mr. Ali Mofid and Mr. Taher Shaverdi with the practicalities of field logistics in south-west Iran and for providing access to maps and remote sensing images. I am indebted to the Khuzestan Water and Power Authority in Ahvaz, particularly to Dr. Parvis Talebzadeh for providing access to information about the rivers and hydraulic engineering of south-west Iran. I am extremely grateful to Mr.

Ali Hadizadeh for his unfailing assistance, mainly with data relating to the rivers of south-west Iran. I am especially grateful to Prof. Saied Pirasteh, then of the Islamic Azad University in Dezful, for his dedicated and practical assistance. I thank him for his perseverance and skills with applying for visas and permissions, with arranging logistics for fieldwork in south-west Iran, including the assistance of a geologist, Omid Farshadi, and a surveyor, Mehdi Samsami, and with organising the excellent First GiT4NDM international conference in Isfahan.

There are many others who have helped me in Iran and I am very grateful to you all, even if you are not listed individually here. I thank the National Cartographic Center of Iran, the National Iranian Oil Company, the Iranian Remote Sensing Center, and Mr. Farrokh Barzegar of REPSOL for their help with maps, remote sensing images and data. I thank Prof. Abbas Alizadeh of the University of Chicago, U.S.A. for information regarding the archaeology of south-west Iran. I thank Mr. Pourghorban of the Ab Varzan Consulting Engineering Company for information about the ancient hydraulic structures in Shushtar. I thank Dr. Joe Langham, formerly of the University of Hull, for his excellent assistance in the field in south-west Iran. I thank Mr. Muhammad-e-Movaghar Assareh for his interpretation and translation, his assistance in the field, and his friendship.

I thank those who have generously given of their time and expertise in laboratory, office and remote sensing work. My thanks go to Prof. Hans van der Plicht of the University of Groningen, the Netherlands for radiocarbon dating of marine mollusc shell samples. I am greatly indebted to Prof. Mark Bateman of the University of Sheffield and Dr. Mortez Fattahi of the University of Oxford for their excellent work with the Optically Stimulated Luminescence (OSL) dating of river terrace sediment samples. I am grateful to Andy Smith and Jonathan Veal and of Sympatec GmbH for their advice on the use of the grain size analysis equipment. I am especially indebted to Dr. Michiel Dusar, Dr. Vanessa Heyvaert and Dr. Jan Walstra of the Geological Survey of Belgium and Prof. Michel Tanret of Ghent University, Belgium for their excellent collaboration and for access to their digital archive of remote sensing images, aerial photographs and maps of south-west Iran. I thank Jeremy Goff of BP Exploration for assistance with geological maps and the geology of south-west Iran. I also give thanks to University of Hull staff, including: Mark Anderson for general help with laboratory work, Tim Bettley and Mike Dennett for invaluable computer support, John Garner and Maxine Tyler for assistance with graphics and remote sensing images, Bob Knight for work on inductively coupled plasma spectrometry, Linda Love for administrative assistance and encouragement, and Brendan Murphy for assistance with GPS equipment.

I thank those who have kindly helped with information and advice, mainly with respect to the methodology and the findings of previous research in south-west Iran, particularly the following people: Dr. Abbas Moghaddam of the University of Sydney, Australia, Prof. Theodore Oberlander of the University of California, Berkeley, U.S.A., Prof. Helen Rendell of Loughborough University, Prof. Gerald Roberts of Birkbeck, University of London, Prof. Claudio Vita-Finzi of University College London, Prof. Tony Wilkinson of Durham University, and Prof. Henry Wright of the University of Michigan, U.S.A.

I am very grateful to those organisations which have provided financial assistance, mainly towards the costs of fieldwork in south-west Iran and laboratory work in the U.K. My sincere thanks go to the British Council, the British Institute of Persian Studies, the British Society for Geomorphology, the Quaternary Research Association, the Sir Philip Reckitt Educational Trust, and the University of Hull.

Most of all, I thank my wife, Marianne Heathcote Woodbridge, for graciously giving me all the time and space necessary to undertake this research and for putting up with the extreme disruption that it has caused to our family life. Thank you.

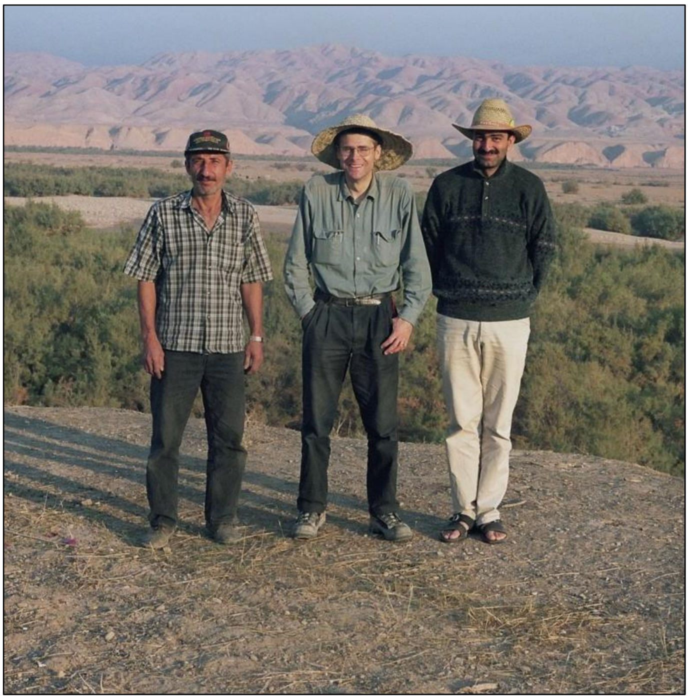

CONTENTS

Drink and dance and laugh and lie,
Love, the reeling midnight through,
For tomorrow we shall die!
(But, alas, we never do.) (Dorothy Parker, 1931 AD)

Trust, obey and rarely lie,
Praise the LORD, though weak and ill,
For tomorrow we may die!
(And, thank God, one day we will.) (Kevin Woodbridge, 2012 AD)

LIST OF FIGURES

Chapter 1

Chapter 2

Chapter 3

Chapter 4

Chapter 5

Chapter 6

Chapter 7

LIST OF TABLES

Chapter 1

Chapter 2

Chapter 4

Chapter 5

Chapter 6

NOTATION USED FOR DATES

Historical calendar dates are quoted as years Before Christ (BC) or Anno Domini (AD), using the Julian or Gregorian calendar.

For ease of comparison, radiometric dates obtained in this study are also quoted in years BC. Radiometric dates are quoted as conventional radiocarbon years Before Present (BP) (years before 1950 AD, using the standard Libby life value for ^{14}C of 5,568 ± 30 years) (Bowman, 1990) and as calibrated years Before Christ (cal.BC), by standard procedures using the OxCal Version 4.2 calibration program (Bronk Ramsey, 2013). Optically Stimulated Luminescence (OSL) dates are quoted as thousands of years before the present (ka) (Bateman and Fattahi, 2008, 2010) and as years Before Christ (BC). This is useful where radiometric dates overlap with historical dates, though it does mean that there are some unusual prehistoric date quotations, such as 23,860 ± 1,750 BC.

Dates given by other workers have been converted to years BC or AD, except where the nature of the quoted dates or the application of radiocarbon calibration was uncertain.

Geological ages are quoted in millions of years before the present (Ma) or thousands of years before the present (ka) (Aubry et al., 2009). Earth surface movement rates (rates of tectonic uplift, shortening and slip) are quoted in millimetres per year (mm yr^{-1}).

CHAPTER 1 INTRODUCTION

"If the Lord Almighty had consulted me before embarking on creation, I should have recommended something simpler."

Alfonso X, King of Castile and León (1221 - 1284 AD) (regarding the explanation of some astronomical phenomena)

1.1 Major rivers

1.1.1 The variability of major rivers

Rivers are naturally variable and complex. They have a wide range of forms, which extends over a wide range of scales, from that of river reaches (with a variety of channel patterns, such as meandering, braided and straight) to that of river catchments (with a variety of drainage networks, such as dendritic, rectangular and radial) (Leopold and Wolman, 1957; Howard, 1967; Knighton, 1998; Schumm et al., 2000; Schumm, 2005). Understanding this variability is useful in a variety of disciplines, including history and archaeology, due to the long dependence of humans on rivers (Schumm et al., 2000). Indeed, there may be relationships between the development of ancient civilizations and the nature of river variability. For instance, Schumm (2005) considered that the long-term stability and continuity of the Egyptian civilization might have been related to the River Nile (a relatively stable, single-thread river system) (Butzer, 1976; Said, 1993), the instability and flux of the Mesopotamian civilizations might have been related to the River Tigris/Euphrates (an unstable, anastomosing river system) (Adams, 1981), and the stability followed by catastrophe of the Harappan civilization might have been related to the River Indus (a single-thread river system subject to frequent major avulsions) (Flam, 1993).

A variability of forms and flows is prevalent in major rivers. Some variability may be inherent within the river system (such as channel pattern changes by migrations, cut-offs and avulsions), with autogenic changes of the river influenced by internal factors, such as aspects of river hydrology and sedimentology, and topography (Blum and Törnqvist, 2000; Lang et al., 2003; Vandenberghe, 2003; Downs and Gregory, 2004; Coulthard and Van de Wiel, 2007; Van de Wiel and Coulthard, 2010).

Some variability may be related to the environment of the river system, with allogenic changes of the river influenced by external factors. These external factors or external drivers of change include structural geology and active tectonics, human activities, relative sea-level (or base level) changes, and climate (Dollar, 2004). *Structural geology and active tectonics* influence rivers at the scales of both river reaches (mainly by folding, faulting and tilting) and river basins and catchments (mainly by broad-scale tectonic uplift, subsidence and tilting) by Earth surface movements causing changes in slopes (Schumm et al., 2000; Jones, 2002, 2004; Tandon and Sinha, 2007; Vergés, 2007; Whittaker et al., 2010). They also influence rivers by changing the surface sediments and bedrock which rivers encounter (Burbank et al., 1999; Burbank and Anderson, 2012). *Human activities* influence rivers at the scales of both river reaches (mainly by direct channel modifications and river regulation) and river basins and catchments (mainly by indirect impacts with changes in land use) (Brookes, 1994; Downs and Gregory, 2004; Brierley and Fryirs, 2005). *Relative sea-level changes* influence rivers at the scales of river reaches and coastal plains, by changes in overall river channel length, channel and floodplain slopes, and "accommodation space" (the amount of space available for sediment deposition), predominantly in coastal areas (Blum and Törnqvist, 2000; Coe, 2003; Woodroffe, 2003; Schumm, 2005). *Climate* influences rivers at the scales of river basins and catchments, mainly by changes in precipitation and temperature causing changes in river hydrology, sedimentology and vegetation (Jones et al., 1999b; Frostick and Jones, 2002; Vandenberghe, 2003).

Explaining how these factors may result in the variability that is observed in major rivers encounters difficulties for a number of reasons. These were summarised by Schumm (1991) who identified ten challenges within three broad classes:

1. Problems of scale and place - time, space, and location
2. Problems of cause and effect - convergence, divergence, efficiency, and multiplicity
3. Problems of system response - singularity, sensitivity, and complexity

Each of these challenges applies when explaining the variability of major rivers. In particular, different factors will be important at different temporal and spatial scales, different factors may result in similar effects, the same factor may produce different effects, the peak efficiency of a factor may occur at intermediate rather than maximal values, a river may respond non-linearly to change if it is close to a threshold for a factor, and major rivers are complex, interactive systems (Schumm, 1991; Downs and Gregory, 2004; Schumm, 2005). Furthermore, the variability of a river system may be dominated by autogenic, internally induced fluctuations, in which case any river response to external factors may be minimal or highly variable and very difficult to evaluate (Vandenberghe, 2003; Coulthard and Van de Wiel, 2007; Van de Wiel et al., 2011). A river system may frequently exhibit non-linearity (Phillips, 2003; Schumm, 2005) or self-organised criticality, being organised around a dynamic equilibrium in such a way that the same external disturbances to the system can initiate internal responses of highly variable magnitude (Bak et al., 1988; Fonstad and Marcus, 2003; Coulthard et al., 2005). One way of trying to tackle these various difficulties, as employed in this study, is to focus on certain spatial and temporal scales so that there can be an emphasis on just a few of the factors.

1.1.2 Earth surface movements and their impacts on major rivers

There are several forms of Earth surface movements by active tectonics, which can be sub-divided into forms of faulting, folding and tilting (Figure 1.1). Active tectonics have primary effects on rivers at reach scales that are either a local steepening or reduction of valley slope (Holbrook and Schumm, 1999), or lateral (cross-valley) tilting (Peakall, 1995; Peakall et al., 2000). There are secondary effects of river aggradation or incision as the river responds to the changed slopes. Also, there are tertiary effects, as the changed sediment loads influence the reaches downstream of the deformation and as changes in aggradation or incision in the deformed reach progress upstream (Ouchi, 1985; Schumm et al., 2000; Cohen et al., 2002; Bridge, 2003; Burbank and Anderson, 2012). These effects of active tectonics on rivers are quite well understood.

For instance, with regards to faulting, aseismic, gradual movements of faults have been associated with river incision across areas of movement (Burbank and Anderson, 2001); whereas seismic, abrupt movements of faults (and associated folds) have been associated with river diversion away from areas of movement, river channel avulsions and river damming (Meghraoui et al., 1988). With regards to folding, various detachment folds are generally associated with “wind gaps” (gaps of defeated, previous river courses which are now dry valleys) near the centre of a growing fold and “water gaps” (gaps of maintained river courses which are now river valleys) near the fold tips for small rivers. By contrast, fault bend folds are generally associated with multiple wind gaps cross-cutting a growing fold (Medwedeff, 1992; Burberry et al., 2010). Also, with regards to tilting, gradual, slow rates of tilting (less than c. 7.5 × 10^{-4} radians kyr^{-1}) appear to promote downtilt river channel lateral migrations (with river channels offset to one side of the basin and meander scars generally facing towards the channel); whereas abrupt, rapid rates of tilting (greater than c. 7.5 × 10^{-3} radians kyr^{-1}) appear to promote downtilt river channel avulsions (with river channels offset to one side of a basin and meander scars facing in both directions) (Alexander et al., 1994; Peakall et al., 2000).

Figure 1.1 Schematic diagrams of types of surface deformation (Plan view on left; cross-section on right; small arrows indicate direction of river flow; large arrows indicate direction of movement) (From Schumm et al., 2000)

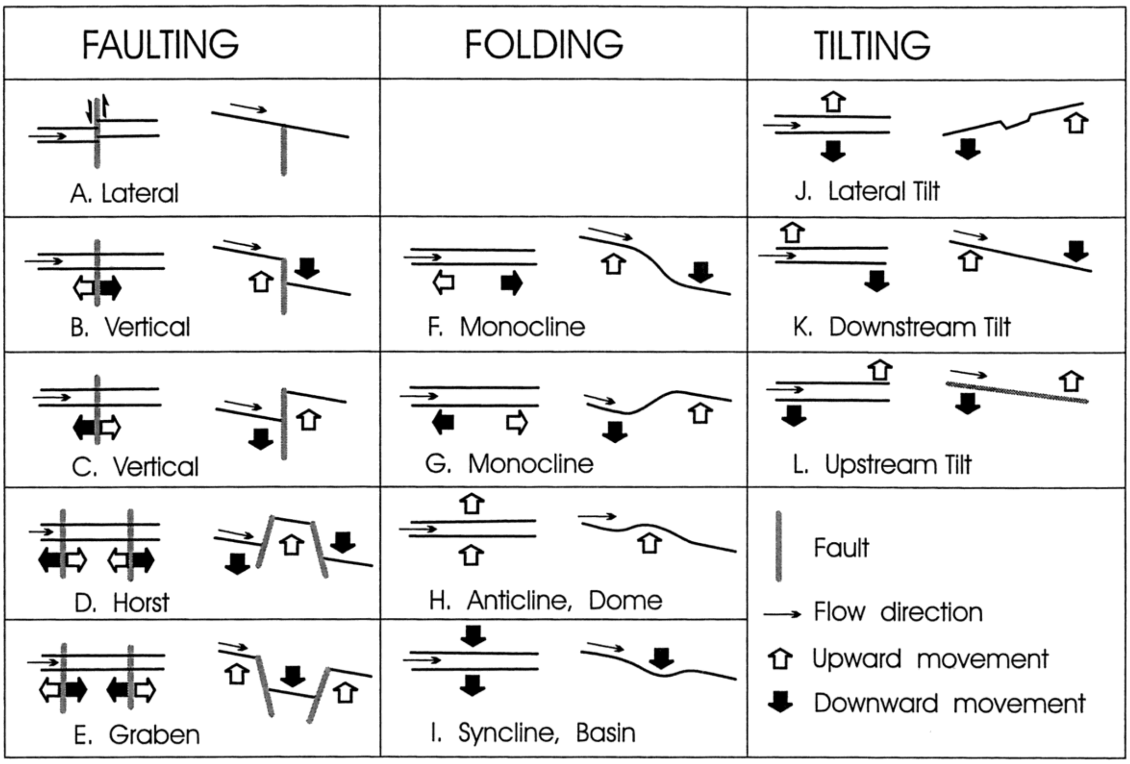

What is less well understood is the relative importance of these tectonic influences compared with other external factors, with a few workers considering the effects of tectonics on rivers to be rather localised with a relatively minor influence overall (Vandenberghe et al., 2011). Such views may be partly due to gaps in our knowledge, particularly for areas with moderate or high rates of Earth surface movements. A fairly large amount of work has been undertaken on smaller rivers in foothills and mountains (e.g. Mueller and Talling, 1997; Van der Beek et al., 2002; Ghassemi, 2005; Gabet et al., 2008) especially since some of the clearest examples of the effect of tectonics on rivers may be found associated with smaller rivers where the topography is most dramatic (Brocklehurst, 2010).

By contrast, major rivers have been much less well studied (Schumm et al., 2000). This is a notable gap in our knowledge, particularly considering that major rivers are very important in determining broad-scale geomorphology, they are important links of the sediment transfer system from continents to ocean basins, and their river systems (especially distributive fluvial systems) are a large component of the fluvial sedimentary rock record (Tandon and Sinha, 2007; Hartley et al., 2010; Ashworth and Lewin, 2012). Also, due to their low gradients and high discharges, major rivers may actually be the most significantly affected by the minor changes in slope that are related to deformation. To address this gap in our knowledge, more work on active tectonics and major rivers is needed (Schumm et al., 2000; Tandon and Sinha, 2007). In particular, a major river may incise across a fold, paradoxically, near to the structural culmination of the fold, or a major river may have a diversion of its course around the tip or "nose" of a fold (Oberlander, 1965; Alvarez, 1999; Burbank and Anderson, 2012). Only very rarely will a major river be "ponded" behind a fold due to the high discharges of a major river (Burbank et al., 1996).

1.2 The aim and objectives of this study

This study addresses this gap in our knowledge of tectonics and major rivers by investigating the major rivers Karun and Dez and their interactions with young, active folds in lowland south-west Iran. The aim of this study is to address this question:

Aim - Why do major rivers incise across some young, active folds near their structural culminations and divert around others?

For achieving this aim, the study has this objective:

First objective - Determine the distinguishing characteristics of major river responses to young, active folds and whether there are key characteristics which act as thresholds for river incision across a fold

Direct human impacts may have influences on major rivers over spatial and temporal scales that are similar to those for Earth surface movements associated with active folds. Thus, suites of distinguishing characteristics are important for disentangling the influences of the external factors of Earth surface movements and human activities, and for determining any interactions between them. Hence, the study also has this objective:

Second objective - Determine the distinguishing characteristics of direct human impacts on major rivers and whether there are interactions between Earth surface movements and these human impacts

1.3 The approach and scales of this study

The approach of this study is to investigate a major river system (the River Karun and its largest tributary, the River Dez) within the distal part of the wedge top and the proximal part of the foredeep of a foreland basin (the Khuzestan Plains in the Mesopotamian-Persian Gulf Foreland Basin), where there are series of folds at different levels of emergence (Sections 1.5, 2.4 and 4.1). By focussing on this part of the foreland basin, the rivers are studied both in locations where they are relatively free to move by migrations and avulsions across plains and in locations where they have become essentially “fixed” in quite deep river valleys. Furthermore, since a succession of folds often develops parallel to the orogenic axis in this part of the foreland basin, with progressively younger, less developed folds with distance from the orogen (Figure 1.2), an approximate relationship between location (distance of fold from the axis of the foreland basin) and time (degree of fold development since emergence on ground surface) can be utilised in the research.

For a study of major transverse rivers and active folds the issue of scale is important. There is a link between spatial and temporal scales, in that as the size of a landform increases, fewer of its characteristics can be explained by current conditions and more of its characteristics must be inferred from the past (Schumm, 1991). This effect and other factors, such as better “control” of other factors influencing major rivers (see Section 1.6.3), have been used to select these *main scales* for this study:

River scales - Major rivers which, generally, can incise to keep pace with active uplift. River scales are drainage basin areas greater than about 10,000 km^2 and mean annual water discharges greater than about 70 m^3s^{-1}/100 m^3s^{-1} (Meybeck et al., 1996). River scales focus on major river systems, rather than very large river systems (with drainage basin areas of about 100,000 km^2/800,000 km^2 or more (Tandon and Sinha, 2007)) which have a tendency to be less modified by small Earth surface movements (Pickering, 2010; Vandenberghe et al., 2011).

Spatial scales - Folds, river valleys, river reaches, river terraces, river channels, canals and dams. Horizontal scales are mainly from metres (river channel dimensions) to tens/hundreds of kilometres (fold dimensions and valley dimensions). Vertical scales are mainly from millimetres (river channel slopes and fold uplift) to tens/hundreds of metres (fold dimensions). In addition to these relatively fine spatial scales, there is some consideration of the broader scales of river basins and catchments.

Temporal scales - Earth surface movements associated with folds, river incisions, river migrations, changes to fluvial geomorphology, and the use and disuse of canals and dams. Temporal scales are mainly from decades (river migrations and small changes to fluvial geomorphology) to millennia (river incision and fold uplift). Temporal scales are subdivided into short timescales (less than 100 years) which include modern major dams and hydraulic engineering, intermediate timescales (100 - 2,000 years) which include ancient major dams and hydraulic engineering and Earth surface movements, and long timescales (more than 2,000 years) which include Earth surface movements and fold growth. There is a focus on the intermediates timescales of 100 - 2,000 years.

1.4 Applications of this research

An improved understanding of the influences of Earth surface movements and human activities on major rivers and any interactions between them is important in river management and its various associated disciplines, including hydrology, flood control, water management, irrigation, river engineering, agriculture, construction, industry, hydro-electric power, transport, town and country planning, fishing, ecology, and conservation (Chang, 2001; Downs and Gregory, 2004; Brierley and Fryirs, 2005).

For instance, major river floodplains upstream and downstream of an active fold are especially prone to channel migrations, avulsions and flooding (Section 1.5.5); hence, major construction, river engineering, power plants and roads should ideally be avoided in these locations, or built with considerable flood protection (Dumont, 1994; Schumm et al., 2000). By contrast, a major river course across an active fold will generally have very limited channel migration and a relatively deeply incised river valley (Burbank et al., 1996). Such locations are potentially good sites for major dams, bridges, reservoirs, irrigation, river engineering and hydro-electric power projects. An improved understanding of seismic and aseismic Earth surface movements and any interactions with human impacts at locations where rivers cross folds is important for the siting and long-term maintenance of such projects (Schumm et al., 2000). For instance, the incision immediately downstream of a dam may be increased as a result of structural uplift of the fold, especially if the dam is sited in the zone of maximal uplift, and this may lead to undesirable undermining of the dam structure (Komura and Simons, 1967; Brierley and Fryirs, 2005). Conversely, the desirable persistence of river channel straightening or realignment and near-straight canals across a fold may be enhanced as a result of fold uplift, though extra channel maintenance may be needed in the long-term on the fold limbs due to a progressive steepening of channel slopes with fold growth.

In addition to river management, this research has applications in other disciplines. For instance, in structural geology, locations where low sinuosity river reaches are maintained over decadal and centennial scales may indicate the location of a zone of uplift or of an emerging fold (Burbank and Tahirkheli, 1985; Schumm, 2005; Burbank and Anderson, 2012) Since anticlines are frequent traps for hydrocarbons in locations such as south-west Iran, this may aid oil and gas exploration, and rates of river incision across an anticline determined from features such as river terraces can indicate rates of anticlinal growth which can be used in models of the development and extent of oilfields (Schumm et al., 2000; Schumm, 2005).

This research is also useful in history and archaeology due to the considerable importance of major rivers to civilizations (Schumm, 2005). Tectonic uplift and accompanying river incision can lead to the disuse of ancient canals and the abandonment of irrigated lands, such as for the River Diyala in Iraq (Adams, 1965) and the River Moche and other coastal rivers in northern Peru (Moseley, 1983). Also, it is well known that previous courses of rivers and canals can account for linear distributions of settlements in semi-arid regions like Mesopotamia (Adams, 1981). An improved understanding of the interactions between rivers, Earth surface movements and human impacts can help elucidate how and why changes have taken place. For instance, within lowland south-west Iran there are two ancient canals cut across an active fold (the Shahur Anticline), one which is now dry and one which has developed into a small artificial river, with these changes mainly being related to uplift of the fold (Section 4.2.2 and 5.2.1; Lees and Falcon, 1952; Lees, 1955; Woodbridge, 2006).

1.5 Foreland basins

Major or large rivers are found in three main plate tectonic settings: rift settings, cratonic settings, and continental collision belts. Within a continental collision belt, major rivers frequently form in foreland basins which develop along the length of collisional plate margins or along compressional destructive margins (Tandon and Sinha, 2007).

A foreland basin is a depression that develops adjacent to and parallel to a mountain belt (or orogen), mainly as a result of the large mass of the crustal thickening associated with the formation of the orogen causing flexural bending of the relatively thin, elastic lithosphere of the tectonic plate floating above the relatively fluid substrate of the mantle (Turcotte and Schubert, 2002). The term “foreland” refers to the relatively undeformed continental crust over which major thrust faults move wedges of crust from the orogen and “hinterland”. These thrust wedges load the foreland plate which responds by the flexural bending to form the basin and form the uplifted areas that provide the main sediment sources to fill the basin (Leeder, 2011).

1.5.1 Types of foreland basin

There are two main types of basin: *peripheral foreland basins* (also termed pro-foreland basins) which occur on the tectonic plate that is subducted during plate convergence (e.g. the Mesopotamian-Persian Gulf Foreland Basin) (Baltzer and Purser, 1990), and *retroarc foreland basins* (also termed retro-foreland basins) which occur on the over-riding tectonic plate during plate convergence (e.g. the Central Andes basins) (DeCelles and Giles, 1996; Horton and DeCelles, 1997). The two types of foreland basin are distinctive in respect to tectonic position, but share the characteristics of flexure-induced subsidence by thrust loading and a variety of thrust faults and associated folds (Leeder, 2011). A succession of folds frequently develops in a foreland basin parallel to the orogenic axis associated with thrust faults and a basal décollement, with progressively younger folds with distance away from the highlands (Figure 1.2) (Keller and Pinter, 1996).

1.5.2 Foreland basin sediments and depozones

Sediments within the foreland basin are mostly derived from the orogeny and its associated fold-thrust belts. A foreland basin system can be considered to be comprised of four discrete sedimentary depozones: the wedge-top, the foredeep, the forebulge and the back-bulge (though the latter two depozones may be poorly developed or absent) (Figure 1.3) (DeCelles and Giles, 1996).

Figure 1.2 Idealised diagram of a subduction zone fold-and-thrust belt, and analogy to a moving snowplough (From Keller and Pinter, 1996)

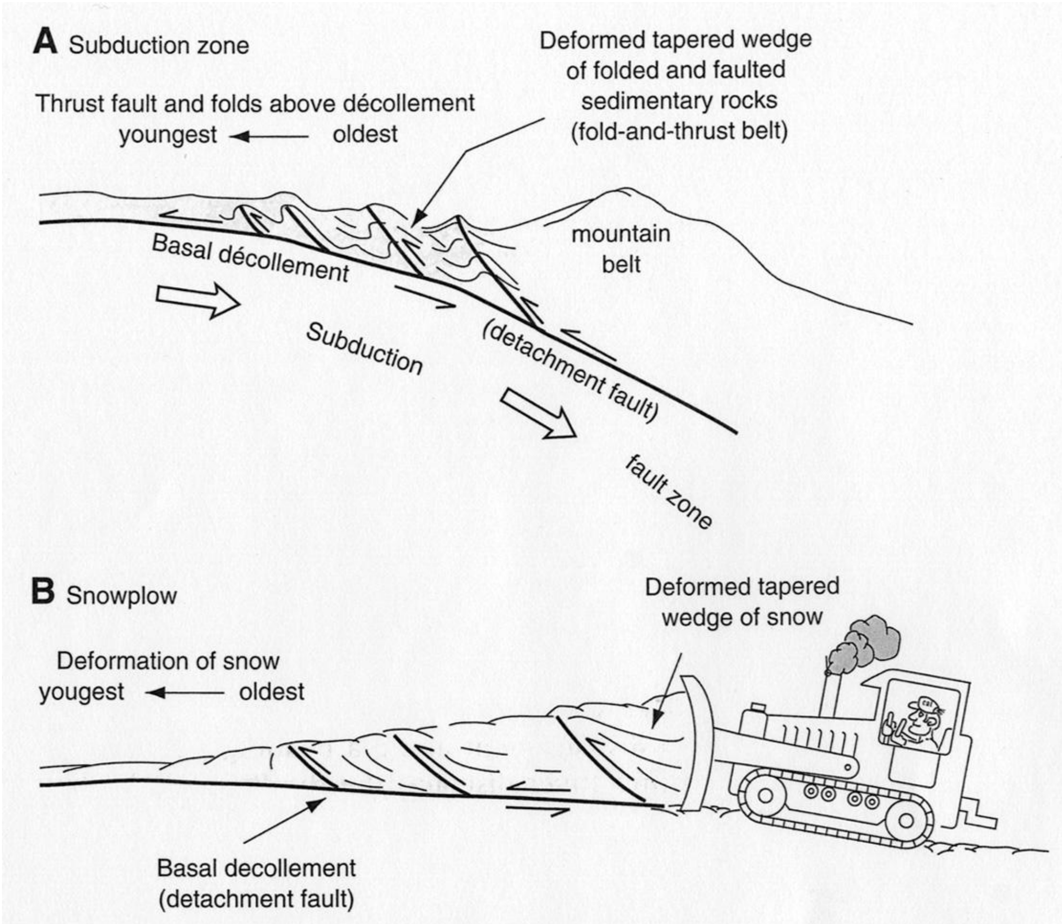

Figure 1.3 Schematic cross-section of a foreland basin system, showing the depozones (D is a duplex in the hinterland part of the orogenic wedge; TF is the topographic front of the thrust belt; TZ is the frontal triangle zone; short fanning lines associated with thrust tips represent the progressive deformation in the wedge-top) (From DeCelles and Giles, 1996)

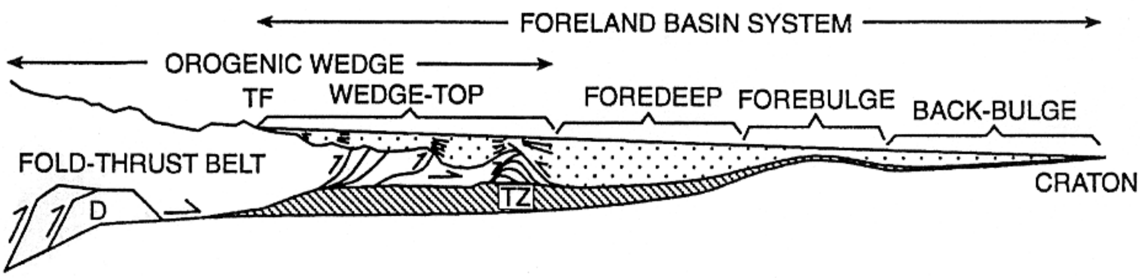

The *wedge-top* is the mass of sediment that accumulates on top of the orogenic wedge at its frontal end, frequently in small thrust-top (or "piggyback") basins lying on the back of low-angle thrust ramps, with various tectonic unconformities, growth structures and progressive deformation. It is generally characterised by coarse sediments, especially coarse-grained alluvial and fluvial sediments accumulating close to high topographic relief in sub-aerial settings, and mass flow and fine-grained shelf sediments in sub-aqueous settings (Ori et al., 1986; Baltzer and Purser, 1990; DeCelles and Giles, 1996). The *foredeep* is the sediment deposited between the frontal tip of the orogenic wedge (sometimes referred to as the "deformation front" (Hessami et al., 2001a; McQuarrie, 2004)) and the forebulge, and is the thickest part of the foreland basin with its overall thickness usually increasing markedly towards the orogeny. It is characterised by a wide variety of sediments, including longitudinal and transverse alluvial and fluvial systems in sub-aerial settings, and lacustrine, deltaic, shallow shelf and turbidite fans in sub-aqueous settings. Frequently in the foredeep of a peripheral foreland basin there is a transition from early deep-marine sedimentation ("flysch") to later coarse-grained, non-marine and shallow marine sedimentation ("molasse"), reflecting a typical structural evolution from ocean trench and ocean floor settings (deep marine sediments) to subduction zone and continental collision settings (shallow marine and non-marine sediments) (Sinclair and Allen, 1992; Sinha and Friend, 1994; DeCelles and Giles, 1996). The *forebulge* is the fairly broad region of potential flexural uplift along the distal side of the foredeep. It is frequently a site of erosion or relatively thin fluvial or aeolian sediments in sub-aerial settings and carbonate platform sediments in sub-aqueous settings (Crampton and Allen, 1995; DeCelles and Giles, 1996). The *back-bulge* (or "outer secondary basin") is the sediment that accumulates in the shallow but broad zone of potential flexural subsidence between the forebulge and the craton. It is characterised by relatively thin deposits of fine-grained shallow marine and non-marine sediments (Ben Avraham and Emery, 1973; Flemings and Jordan, 1989; Holt and Stern, 1994).

1.5.3 Rivers in peripheral foreland basins

Rivers develop with time in a peripheral foreland basin, flowing mainly from the orogen and the wedge-top into the subsiding foredeep, and are the principal agents of transfer of sediment from the orogen and the wedge-top into the foredeep. The major rivers may be longitudinal (also termed axial) rivers (like the Tigris and Euphrates in Iraq) flowing mostly parallel to axis of the foreland basin and the majority of the folds and thrusts, or transverse rivers (like the Karun and Dez in Iran) flowing mostly orthogonal to the axis of the foreland basin and the majority of the folds and thrusts (Baltzer and Purser, 1990).

Figure 1.4 Schematic diagrams showing the main contrasts between (a) underfilled and (b) overfilled foreland basins (From Crampton and Allen, 1995)

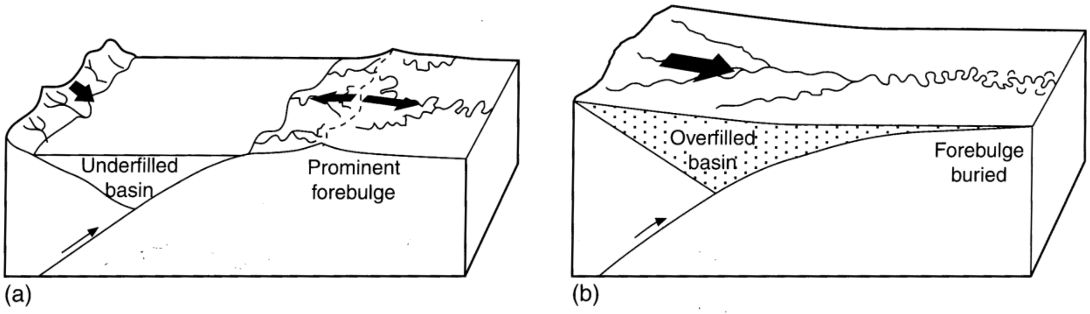

The overall form of a peripheral foreland basin and these longitudinal and transverse rivers depends on the balance between the rates of river sediment transfer (and the associated changes in crustal loading) and the rates of tectonic movement due to crustal thickening (and the associated changes in plate flexure) (Burbank and Anderson, 2001; Leeder, 2011). Where tectonic movements are dominant (as may occur early in the structural history of a foreland basin) there will be an "underfilled" basin, with slopes mainly determined by tectonic uplift creating short transverse rivers, a prominent foredeep, and a prominent forebulge. Where sediment transfer is dominant with sediment export down-system (as may occur later in the structural history of a foreland basin) there will be an "overfilled" basin (Leeder, 2011; Allen et al., 2013), with slopes mainly determined by deposits creating long transverse rivers, a slight foredeep, and a slight (or buried) forebulge (Figure 1.4) (Crampton and Allen, 1995; Jordan, 1995; Allen et al., 2013). Where foreland basins mainly have a regime of crustal thickening associated with tectonic loading, there will be maximal basin subsidence and prominent longitudinal rivers near to the mountain front that are fed by relatively short, curving transverse rivers. Alternatively, where foreland basins have a regime of mainly erosional unloading and associated basement isostatic uplift within both the active thrust front and proximal foreland, long transverse rivers may flow across almost the entire foreland basin before merging with longitudinal trunk rivers in the distal part of the foredeep (Burbank, 1992; Burbank and Anderson, 2012).

The division of major rivers into longitudinal and transverse rivers applies to their general setting within a foreland basin and not to the entire lengths of their courses. As shown in Figure 1.5, generally, a longitudinal major river (L) flowing parallel to the axis of a foreland basin in its lower reaches will have transverse river courses (Th) in its upper reaches in the hinterland of the orogenic wedge. Also, a transverse major river (T) mainly flowing orthogonal to the axis of a foreland basin will have some longitudinal river courses (Ld) in both the hinterland and foreland where diverted by thrust faults and associated folds (Burbank et al., 1996).

Figure 1.5 Conceptual depiction of different river orientations within a peripheral foreland basin (From Burbank et al., 1996)

Thrust faults delineate the uplifting hinterland and disrupt the proximal part of the foreland. Transverse rivers with hinterland catchments (**Th**) and with catchments entirely within the foreland (**Tf**) are tributary to the longitudinal river (**L**) which flows in a medial position in the foreland. Transverse rivers (**Th**) may be diverted by a thrust fault and its associated folds to flow longitudinally within the "piggyback" basin associated with the hanging wall of the thrust (**Ld**), or they may maintain their antecedent courses (**Ta**), undeflected across a thrust. Some thrusts or folds uplift parts of the foreland which subsequently act as local catchments (**Lc**) for rivers which flow into the piggyback basin or into the foreland.

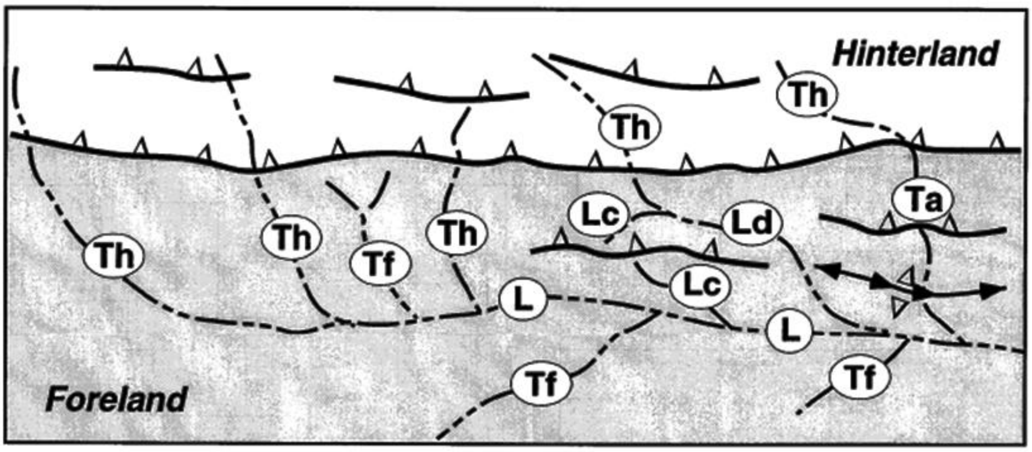

The influences of tectonics on longitudinal rivers are quite well understood. Generally, their courses develop in accordance with structural geology, with major rivers mainly flowing parallel to the mountain front, along, or parallel to, the axis of the geosyncline of the foreland basin and the axes of thrust faults and folds (Burbank et al., 1996; Schumm et al., 2000). Variations in river courses can be attributed to mechanisms such as lateral ground tilting causing channel belts to move away from the basin midline by gradual migrations or avulsions (Cox, 1994; Peakall, 1995) and uneven sediment accumulations by features such as tributary alluvial fans and megafans causing river course diversions (Baltzer and Purser, 1990; Leeder, 2011). Variations in river geomorphology can be attributed to mechanisms such as slope changes associated with localised zones of active uplift and subsidence. For instance, for the River Indus, anastomosing or fairly straight channel planforms were found in depositional basins upstream of active uplift zones, and meandering channel planforms were found on the downstream slopes of active uplift zones (Jorgensen et al., 1993; Burbank and Anderson, 2001).

1.5.4 Major transverse rivers in peripheral foreland basins

By contrast, the influences of tectonics on transverse rivers are less well understood. Generally, transverse river courses develop in discordance with structural geology, with major rivers mainly flowing in valleys and gorges across the axis of the geosyncline of the foreland basin and across the axes of thrust faults and folds (Burbank et al., 1996). The formation of transverse rivers across areas of structural uplift can be explained by four general mechanisms: antecedence, superimposition, piracy, and overflow, as shown in Figure 1.6 (Douglass et al., 2009). Each of these mechanisms may occur with a major river, with antecedence and superimposition more frequent with larger, higher discharge rivers, due to these rivers being more likely to produce the higher stream powers needed to maintain their courses by incision through uplifting bedrock. Smaller, lower discharge rivers are less likely to form and maintain transverse river courses and tend to be limited to the mechanism of piracy or the other three mechanisms where bedrock has low erosion resistance (Baltzer and Purser, 1990; Douglass and Schmeeckle, 2007; Douglass et al., 2009).

Antecedence is where a river followed a course that was developed prior to the tectonic uplift of the surrounding bedrock and subsequently maintained its course by river valley incision. *Superimposition* is similar to antecedence, except that there is also a less erosion resistant covermass (such as river sediments or softer rock formations) overlying the bedrock, with the river maintaining its course through both the covermass and the bedrock by river valley incision. Antecedence and superimposition are similar in that the through-going river predates the uplift and more recent exposures of the bedrock highland, with superimposition generally taking longer to develop due to the time needed for the deposition of the covermass and for the transport of both the eroded

Figure 1.6 Simplified diagrams and table of descriptions of the four general mechanisms of transverse drainage development (From Douglass et al., 2009)

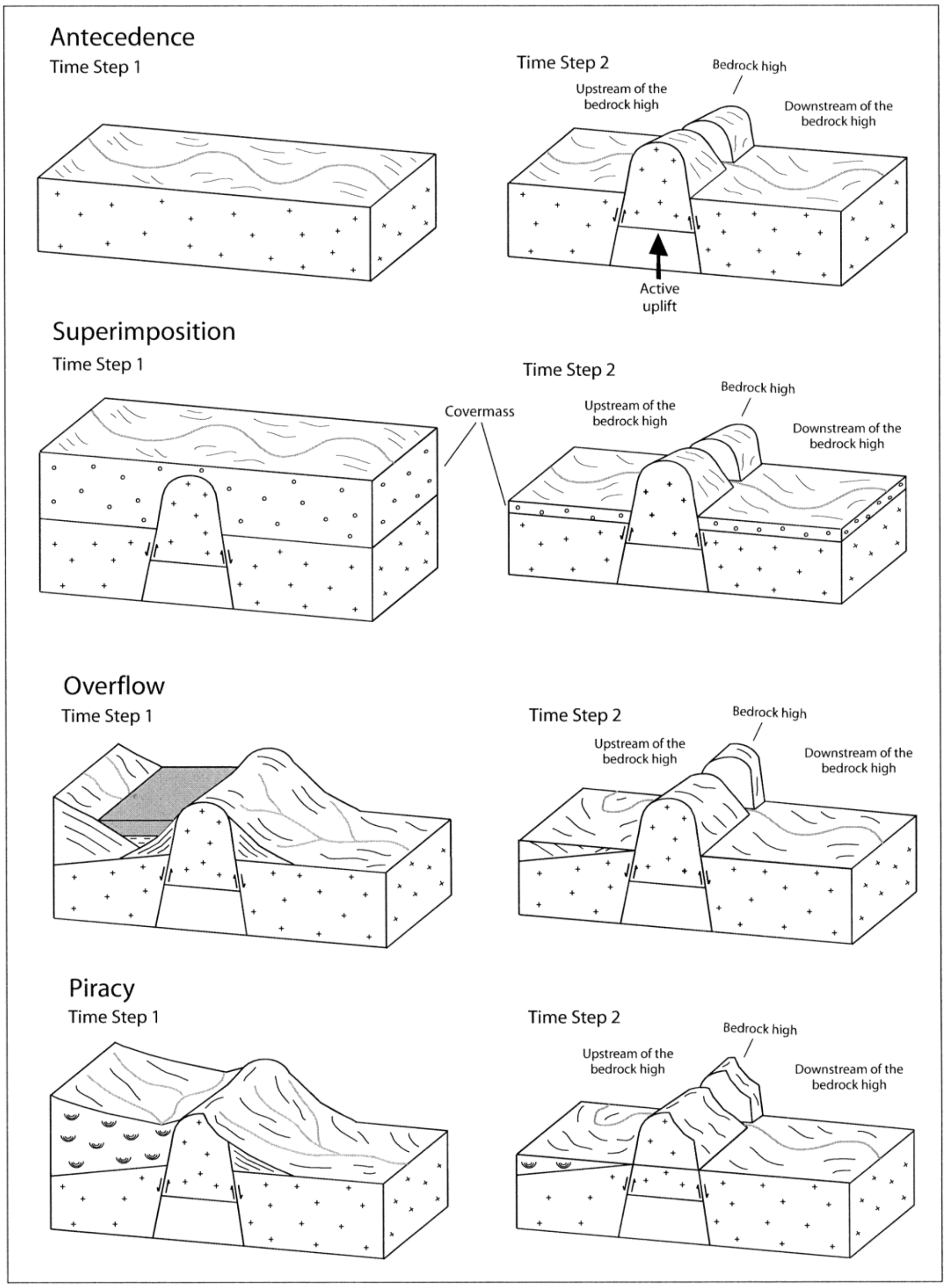

Mechanism	Generally located where:	Suggests mode of active tectonics that:	Relationship to stream order:
Antecedence	Streams flow across active or formerly active highlands with a capacity for erosion greater than the rock uplift rate.	Uplifts bedrock across the path of a through-flowing river.	Tend to be higher stream order channels because they require the capacity to erode through rising bedrock.
Superimposition	Streams develop transverse to resistant bedrock outcrops buried by nonresistant strata, alluvium, or lacustrine deposits and later become exposed following prolonged erosion.	Exposes strata, develop active mountain fronts flanked by alluvial fans, or disrupt fluvial systems and form interior-drained basins, which then experience extensive sedimentation.	Any stream order channel can be superimposed if the stream develops transverse to resistant bedrock buried by an erodible covermass.
Piracy	Streams flow in an indirect pattern with respect to regional topography and become captured across interfluves by channels with steeper gradients.	Disrupts drainage patterns such that streams have lower gradients than other potential stream paths.	Any stream order channels can be pirated as a drainage network becomes reorganized.
Overflow	Streams become ponded in interior-drained basins and eventually overspill at the lowest point of the basin rim.	Aggressively disrupts the regional drainage patterns so that formerly through-flowing channels become ponded in interior-drained basins.	Tend to be higher stream order channels because they form newly developed trunk channels that drain formerly interior-drained basins.

covermass and eroded bedrock. *Piracy* or "river capture" is where part of the course of one river channel changes to that of another. Where the point of capture is across a topographic high dividing two drainage systems, a pirated transverse drainage system will be formed. River capture may happen where the soon-to-be-captured river erodes, infiltrates, or flows over an intervening interfluve into a drainage basin with a steeper gradient; or, more rarely, where a river in a steeper basin erodes headward across a drainage divide and captures the discharge of a river on the other side. *Overflow* is where drainage becomes ponded in a lake in a closed basin before spilling across the lowest point of the basin rim as a result of tectonic activity or some other disruption. Overflow and piracy are similar in that the through-going river postdates the exposure of the bedrock structure, with overflow generally invoking a more marked disruption of the drainage pattern (Oberlander, 1965, 1985; Douglass and Schmeeckle, 2007; Douglass et al., 2009).

1.5.5 Major rivers interacting with growing folds in peripheral foreland basins

Within a foreland basin the main geological structures involving uplifted bedrock are growing folds, particularly growing folds associated with active thrust faults (Keller and Pinter, 1996; Leeder, 2011). Conceptual models of the interactions between rivers and growing folds have been constructed (e.g. Burbank et al., 1996; Amos and Burbank, 2007; Douglass et al., 2009; Burbank and Anderson, 2012). Such models indicate that where rates of river aggradation exceed rates of structural uplift associated with the fold, then a transverse river will flow without impedance across the fold, with little or no topographic relief developing. Where a fold does develop a surface topographic expression, then the river will either flow in a course across the fold by maintaining channel slopes which dip towards the foreland, or the river will be "defeated" by the growing fold. If the river is defeated, then it will be diverted around the fold by channel migrations or avulsions to flow through structural low points, or it will be ponded in a "piggyback" basin on top of moving thrust sheets upstream of the fold (Burbank et al., 1996; Burbank and Anderson, 2001; Amos and Burbank, 2007).

To maintain a transverse course across a fold, essentially, the river needs sufficient stream powers to erode and incise into the crest and across the axis of the fold at a rate greater than the difference between the rates of structural uplift and the rates of river aggradation (Burbank et al., 1996). To produce sufficient foreland-dipping channel slopes for maintaining erosive stream powers across the zone of greatest fold uplift, generally, a river will aggrade upstream and downstream of the fold (Holbrook and Schumm, 1999). If upstream aggradation or downstream aggradation is insufficient (especially as the fold widens with time) then the river may be "defeated", and if upstream aggradation is excessive then the river may also be "defeated" by producing slopes that promote channel migrations or avulsions to other upstream locations (Burbank et al., 1996). If downstream aggradation is excessive, then the river may be defeated by reducing channel slopes to such an extent that stream powers are insufficient to maintain erosion into the fold and maintain transport away of the eroded material (Douglass and Schmeeckle, 2007). Across the fold, generally, there will be greater erosion with higher discharge rivers, and, though the precise controls on river erosion are not agreed upon due to factors like bed armouring (Sklar and Dietrich, 2004; Brocklehurst, 2010), it is very likely that river erosion into bedrock and sediments will be increased with greater stream powers. Hence, to maintain erosion into the crest and across the axis of a fold, there may be changes in the river geomorphology across the fold which increase specific stream powers and river bed shear stresses; such as increases in channel water surface slopes, channel narrowing, reductions in channel sinuosity, and reductions in multiple channels and channel belt widths (Burbank and Anderson, 2001).

According to such conceptual models, the responses of rivers and major rivers should be fairly predictable, with a river either incising across an active fold as a "water gap" (a river valley of a maintained river course) or being defeated by the fold and diverted to leave a "wind gap" (a dry valley of a previous river course), with the configuration of these water and wind gaps varying with a number of factors, such as the type of fold (Burbank et al., 1996; Burberry et al., 2010; Burbank and Anderson, 2012). For instance, symmetric and asymmetric detachment folds would be expected to have a wind gap near the centre of the fold and a water gap near the propagating fold tip, and fault bend folds would be expected to a have a number of wind gaps across the length of the fold, with the defeated rivers diverted parallel to the fold axis (Figure 1.7) (Burberry et al., 2008, 2010).

However, in practice, the interactions of major rivers and active tectonics appear to be more complex and variable. For instance, some work (e.g. Yeromenko and Ivanov (1977) researching the meandering of the River Dniester in the former U.S.S.R.) has indicated that variations in erosion resistances of rocks and sediments are significant in influencing river responses, whereas other work (e.g. Burbank et al. (1996) reviewing research on rivers and growing folds in northern Alaska) has indicated that such variations in erosion resistances are not significant.

Figure 1.7 Diagrams of predicted configurations of "wind gaps" and "water gaps" for certain fold types (see Table APP 7.1 for details of fold measurements and indices)
a) Detachment fold with low aspect ratio and short hinge length, showing wind gap in centre of fold and water gap near fold tip
b) Fault-bend fold with high aspect ratio and long hinge length, showing multiple wind gaps and defeated streams diverted parallel to fold hinge line
c) Asymmetric detachment fold with steepened forelimb and incipient thrust fault in core, showing wind gap in centre of fold and water gap near fold tip
(From Burberry et al., 2008)

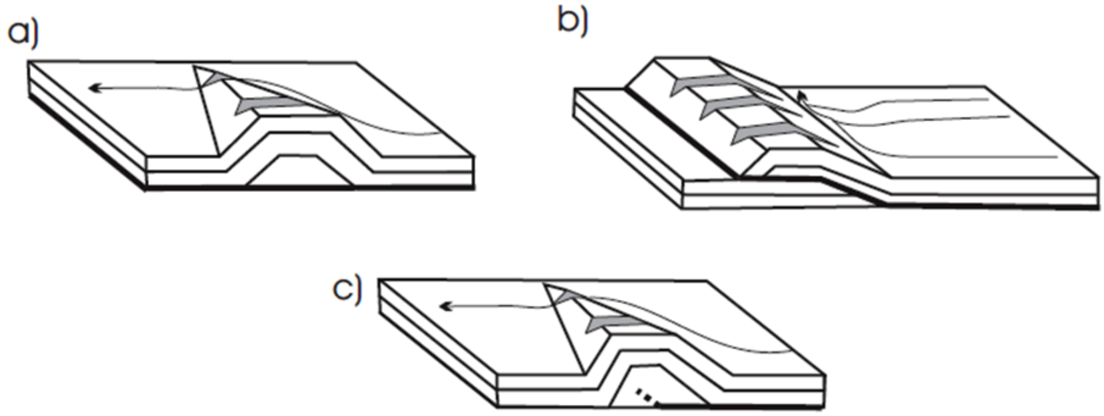

Also, paradoxically, there is a tendency for major rivers in fold-and-thrust belts to transect many growing anticlines at locations of their greatest structural and topographic relief (Oberlander, 1965, 1985; Alvarez, 1999). This may be due to the drainage network being superimposed from above via a structurally conformable more easily eroded horizon (Oberlander, 1985) or other mechanisms (Simpson, 2004; Montgomery and Stolar, 2006; Babault et al., 2012), all of which apply after the initial stages of fold development (see Section 6.1.2). However, this is only a tendency. Rivers may frequently cross a growing fold near to the laterally propagating tip or "nose" of the fold. This may be the result of capture of the discharge of rivers and streams from further within the "piggyback" basin upstream of the fold, due to greater widening within the fold "core" (the central part of the fold which emerges first) compared with the fold tips, causing rivers nearer the fold core to be defeated and diverted more readily (Jackson et al., 1996; Burbank and Anderson, 2001). Alternatively, rivers may be diverted around the fold tips of laterally propagating anticlinal fold segments until they coalesce; after which the river may divert from the coalesced fold to feed a longitudinal river, or incise across the coalesced fold at the topographic low of the merger location (Ramsey et al., 2008).

1.6 Determining the major river responses to active tectonics

1.6.1 Characteristics and thresholds of major river responses to active folds

Whilst conceptually it is clear that a major river should incise across an active fold in some cases and divert around an active fold in other cases, in practice frequently it is unclear as to how and why this occurs. This uncertainty is due to the naturally variable and complex nature of rivers (Section 1.1.1; Schumm, 2005). Multiple processes may act simultaneously and in combination to produce a particular phenomenon. Different factors may result in similar effects (Schumm, 1991). If a river as a complex system is modified in some way then it may not adjust in a progressive and systematic fashion (Schumm, 1991; Van de Wiel et al., 2011). Also, river systems may be dominated by autogenic, internally driven processes, with variability independent of external factors due to systems of non-linearity or self-organised criticality (dynamic equilibrium near a threshold condition) (Coulthard and Van de Wiel, 2007; Van de Wiel et al., 2011). Nevertheless, with such systems there may be a characteristic or characteristics of the river or the fold which act as a threshold which the river needs to cross for the dynamic equilibrium of river incision across an active fold to develop and be maintained (Knighton, 1998).

The characteristics which may act as thresholds will be those which are associated with the main controlling variables for the persistence of an antecedent river across a growing fold, as listed in Table 1.1 (Burbank et al., 1996). For instance, channel migration rate, channel-belt width, general river course direction, channel width, and channel width:depth ratio are associated with the rate of sediment aggradation, and degree of fold development and rate of fold uplift are associated with the rate of structural uplift. The sediment or rock type exposed in a fold and the degree of cementation are associated with the erosion resistance of the rocks and sediments in a fold. Mean annual water discharge, specific stream power, stream power per unit length, channel water surface slope, channel sinuosity, channel width, channel width:depth ratio, and channel-belt width are associated with the water discharge and stream power of the river. The width of geological structure at the river crossing is associated with the width of structure. Grain sizes of channel bed and channel bank sediments are loosely associated with sediment load, though, generally, good sediment load data for rivers is difficult to obtain in practice (IAEA, 2005; Allen et al., 2013). Gaps between fold segments are associated with transverse structures, though, generally, the locations of transverse structures are difficult to discern after initial fold emergence. In addition to these main controlling variables, the timing of interactions between rivers and growing folds is important, with, for instance, river incision across the central area or "core" of a fold mostly only occurring where the river encounters the fold at a very early stage in its development (Burbank et al., 1996; Allen and Talebian, 2011).

Table 1.1 The main controlling variables for the persistence of antecedent rivers and streams crossing growing folds (From Burbank et al., 1996)

Variable	Effect
Rate of sediment aggradation and rate of structural uplift	Lower rates of sediment aggradation and lower rates of structural uplift promote persistence of the antecedent river, due to less erosion of the fold hanging wall being required
Erosion resistance of rocks and sediments within fold	Lower erosion resistances (thick alluvial strata, poor cementation and readily erodible bedrock) mean that lower stream powers are required for persistence of the antecedent river
Water discharge and stream power of river	Higher water discharges and higher stream powers promote persistence of the antecedent river
Width of structure	Widening structures cause reduced channel water surface slopes and stream powers , promoting defeat of the antecedent river
Sediment load	Increased sediment load decreases proportion of stream power available for bed erosion, mantling of the bed with sediment precludes erosion of bed
Transverse structures	Provide zones of less erosion resistant rocks that cut across structures, exploited by antecedent rivers

Unravelling the influences of one or several characteristics within this complex system is difficult. External factors may be ramp type disturbances (associated with sustained and extensive shifts of variables to new levels) or pulsed type disturbances (associated with episodic low frequency, high magnitude events) (Brunsden and Thornes, 1979). There may be different reaction times, relaxation times and recurrence times for events, resulting in some river characteristics that are mainly transient and others that are more prolonged (Knighton, 1998). In short, with the complex systems of major rivers, simple cause and effect relationships are often not present.

1.6.2 Control of the various factors influencing major river responses in previous research

There has been limited previous research into the variable responses of rivers to the external factor of active tectonics. This previous research has often been focussed on only a few river characteristics, such as channel sinuosity (Zámolyi et al., 2010), or on very long time scales, such as 10^5 - 10^7 years (Humphrey and Konrad, 2000).

By contrast, a wide-ranging study was undertaken by Jorgensen (1990), who worked on four different small major rivers in western U.S.A. - the Neches River, Texas; the Humboldt River, Nevada; the Sevier River, Utah; and the Jefferson River, Montana. River water bankfull discharges were about 25 - 500 m^3s^{-1} and river types included suspended load, mixed load, and gravel-bed rivers. Active tectonic settings included uplift and extensional faulting, subsidence within a Basin and Range Province, uplift associated with an axial graben, and uplift within an extensional valley. River reach responses were sub-divided into eroding (with uplift or forward tilt) and depositing (with subsidence or stasis or decreasing uplift). Table 1.2 presents a summary of the results (Jorgensen, 1990; Schumm et al., 2000). Despite the different types of river and different types of tectonic setting, there are some characteristics that exhibited consistent directional changes with uplift and subsidence or stasis. Width:depth ratio showed a consistent decrease for reaches undergoing uplift and increase for reaches undergoing subsidence or stasis. Stream power and water surface slope showed a consistent increase for reaches undergoing uplift and decrease for reaches undergoing subsidence or stasis. Bed material size increased for reaches undergoing uplift and reduced for reaches undergoing subsidence or stasis. Sediment storage and bar size showed a decrease for reaches undergoing uplift and an increase for reaches undergoing subsidence or stasis (Jorgensen, 1990; Schumm et al., 2000).

Research such as this indicates that characteristics such as channel width:depth ratio and stream power are useful characteristics for investigating river responses to tectonics. However, what research such as this does not indicate is which characteristic or characteristics, if any, act as thresholds, and which external factor or factors, if any, are the main causative influences on these river characteristics. It has been assumed that the variations observed in channel width:depth ratios and stream powers are the product of Earth surface movements by active tectonics, mainly because a process for the changes

Table 1.2 Summary of the responses of the Neches, Humboldt, Sevier and Jefferson rivers in the U.S.A. to tectonic deformation (From Jorgensen, 1990; Schumm et al., 2000)

	Neches		Humboldt		Sevier		Jefferson	
Reach response	*Eroding*[1]	Depositing	*Eroding*	Depositing	*Eroding*	Depositing	*Eroding*	Depositing
Tectonic setting	*Uplift*	Subsidence	*Forward tilt*	Subsidence	*Uplift*	Decreasing uplift	*Uplift*	Subsidence or Stasis
Grain size	Suspended load (sand–clay)		Mixed load (gravel–sand)		Bed load (cobble–sand)		Bed load (cobble–sand)	
Response of valley and planform characteristics								
Planform	*Tight and irregular bends*	Two orders of meandering	*Tightly sinuous*	Broad, gentle meanders	*Slightly sinuous*	Irregular bends and narrows	*Straight to slightly sinuous*	Irregular, tight meanders
Sinuosity	*Increase*	Decrease	*Increase*	Decrease	*Decrease*	Increase	*Decrease*	Increase
Valley width	*Decrease*	Increase	*Increase*	Decrease	*Decrease*	Increase	*Decrease*	Increase
Valley slope	*Increase*	Decrease	*Increase*	Decrease	*Increase*	Decrease	*Decrease*	Increase
Migration rate	*Increase*	Decrease	*Decrease*	Increase	*Decrease*	Increase	*Decrease*	Increase
Response of channel shape								
Bankfull area	*Increase*	Decrease	*Decrease*	Increase	*Decrease*	Decrease	*Increase*	Decrease
Bankfull width	*Increase*	Decrease	*Decrease*	Increase	*Decrease*	Increase	*Decrease*	nc[3]
Bankfull depth	*Increase*	Decrease	*Decrease*	Increase	*Sl increase*	Decrease	*Sl increase*	nc
Width–depth ratio	*Decrease*	Increase	*Decrease*	Increase	*Decrease*	Increase	*Decrease*	Increase
Channel shape	*Asymmetric channel with deep scours and prominent sandy, point bars*	Symmetrical but debris choked, muddy channel with abrupt bends	*Narrow, smooth shape and regular profile*	Wide, irregular channel and irregular profile	*Narrow, smooth with high-relief coarse-grained bars*	Wide, shallow channel adjacent to large bars, stepped profile	*Smooth, U-shaped channel with low pool-riffle relief profile*	Asymmetric, sediment-filled channel with high, bar, pooled-riffle relief
Response of hydraulic variables								
Flow velocity	*nc*	Decrease	*Increase*	nc	*Increase*	Decrease	*Increase*	Decrease
Water surface slope	*Increase*	Decrease	*Increase*	Decrease	*Increase*	Decrease	*nc*	nc
Bankfull discharge	*Increase*	Decrease	*nc*	Increase	*Increase*	Increase	*Increase*	Decrease
Stream power	*Increase*	Decrease	*Increase*	Decrease	*Increase*	Decrease	*Increase*	Decrease
Response of sediment characteristics								
Bed material	*Coarsens*	Fines	[2]	Fines	*Coarsens*	Fines	*Coarsens*	Fines
Bar material	*Coarsens*	Fines	[2]	Fines	*Coarsens*	Fines	*nc*	Coarsens
Sediment storage	–[4]	–	*Decrease*	Increase	*Decrease*	Increase	*Decrease*	Increase
Bar size	–	–	*Decrease*	Increase	*Decrease*	Increase	*Decrease*	Increase
Armoring	–		*Less well developed armor on bar surfaces*	Well-developed armor surface on large bars	Uplift reaches are not armored in comparison to depositional reaches		Uplift reaches armored in comparison to depositional reaches	

Key

[1] The response of the study reaches have been generalised to those that are *eroding* over the long term (shown in *italics*) and those that are depositing over the long term (shown in conventional type)

[2] Result not clear [3] nc no change determined [4] – no data available

can be envisaged and because they correlate well with survey, seismic and geomorphic data which indicate the localities of the areas of active tectonics (Schumm et al., 2000). These are fairly reasonable assumptions, and confidence in these assumptions increases as more correlations of a similar nature are made, but there are notable uncertainties. The extent to which other factors have influenced the variations observed in the channel width:depth ratios and stream powers is uncertain, especially when the rivers and their environments are so different. For instance, width:depth ratios vary with factors such as human activities (such as dredging and channel straightening), climate (due to its influences on water and sediment discharges) and geology (especially sediment and bedrock erosion resistance), factors which were significantly different for each of the four rivers (Jorgensen, 1990).

What is needed is better "control" of the other external factors, so that the major river response to the external factor of structural geology and active tectonics can be distinguished. Burbank et al. (1996, p. 219) summarised the situation by stating: "Even when there is a clear conceptual understanding of the ways in which depositional and erosional processes may interact with growing structures, the multiplicity of independent, competing and often hard-to-calibrate variables often makes it difficult to resolve unambiguously the factors that control observed geomorphological or geological conditions."

One way of producing increased control of other factors was an investigation of two side-by-side upland rivers crossing rapidly uplifting folds (rates of uplift exceeding 10 mm yr^{-1}) in the Himalayan foreland of central Nepal (Hurtrez et al., 1999; Lavé and Avouac, 2000). This research found that both of the two rivers exhibited a significant reduction in channel width across the zone of rock uplift, though the smaller Bakeya River became steeper across the zone of rapid uplift whereas the larger Bagmati River showed no significant profile steepening across the same zone (Lavé and Avouac, 2000, 2001). This research indicated that channel width acts as a key characteristic of river responses, and that if structural uplift should become sufficiently great, the channel width will reduce to less than a certain threshold width value to maintain an incising river course across a zone of uplift. Channel narrowing to enhance incision rates appeared to take precedence over other changes, such as channel steepening (Lavé and Avouac, 2001; Burbank and Anderson, 2012); a scenario which has also been found with small upland channels in southern New Zealand (Amos and Burbank, 2007) and upland rivers in central Taiwan (Yanites et al., 2010).

1.6.3 Control of the various factors influencing major river responses in this study

In this study, the control of the various other factors is increased by having a focus on *specific spatial and temporal scales*, as described in Section 1.3. Though the many elements of a major river system are linked to each other, each element does not have similar response times or sensitivities to the changes imposed on it (Whipple and Tucker, 1999). In a drainage basin, there is a hierarchy of sensitivity to the majority of tectonically imposed changes which ranges from the catchment area (the least sensitive, with the greatest geomorphic inertia), to interfluves, hillslopes, and river channels (the most sensitive, with the smallest geomorphic inertia). Burbank and Anderson (2001) considered a conceptual example of rapid folding causing a region to be tilted by a total of 1º and the differences that this change would make to the various elements in a river drainage basin system. The catchment area and interfluves would be insensitive to such changes at short timescales, and hillslopes would be largely unaffected unless they were poised at maximum stable slope angles. However, rivers, and particularly river channels, typically have equilibrium slopes of less than 1º, frequently in the range of 0.006° to 0.6° (10^{-4} m m^{-1} to 10^{-2} m m^{-1}) (Howard, 1980; Peakall et al., 2000). Hence, a change in slope of the order of 1º would induce relatively rapid and pronounced responses in river channels (especially due to the large changes in stream powers induced), with responses such as river channel incision or river channel migration and avulsion. Therefore, this study with a focus on horizontal spatial scales of metres to tens/hundreds of kilometres and temporal scales of 100 - 2,000 years will have a focus on Earth surface movements of folds and faults influencing characteristics of river channels and river reaches (Brunsden and Thornes, 1979; Burbank and Anderson, 2001).

Also in this study, the control of other factors is increased by use of a *single major river* (the River Karun and its main tributary, the River Dez) in a single foreland basin (the Mesopotamian-Persian Gulf Foreland Basin) with similar areas of tectonic uplift (similar types and orientation of folds). With the same major river, the external factor of climate will be fairly similar over the drainage basin and will be essentially the same over horizontal spatial scales of metres to tens of kilometres, since climate zones (areas of effectively the same climate) are usually measured in thousands of km^2 (Potts, 1999; Badripour et al., 2006). Indeed, for some research (such as that of Cowie et al., 2008), rivers as far apart as central Italy and eastern Greece have been considered to be sufficiently similar since they were both within a central Mediterranean climate regime. Variations in climate are only likely to be significant at the local scales of river reaches in unusual instances such as channel widening, straightening and steepening in response to very large floods (Page and Nanson, 1996), or where climate changes cause a climate zone boundary to migrate across a river reach. With the same river and foreland basin, rates of sediment supply from the basin hinterland are likely to be similar at the scale of river reaches (Peng et al., 2010), except for slight changes where a river or its tributary streams flow across local outcrops of different lithologies. These changes may occur where river incision across an uplifting structure exposes rocks or sediments of different (usually greater) erosion resistances, so with a similar stratigraphic sequence throughout the same foreland basin the factor of sediment supply rate may be largely controlled (Burbank et al., 1996; Knighton, 1998). Similarly, with the same river and foreland basin, the erosion resistance of rocks and sediments in structures will be similar due to a similar stratigraphic sequence throughout the same foreland basin. Hence, the factor of bedrock and sediment erosion resistance will be largely controlled, with less control where there are local differences in the types and thicknesses of stratigraphic units (Burbank et al., 1996). Furthermore, the external factor of relative sea-level changes will be largely controlled, since many of the river reaches of this study are upstream of the limits of their influences; that is, upstream of a distance of about 150 km from the shoreline (Shanley and McCabe, 1993) and upstream of the extent of the river backwater length (Li et al., 2006; Blum et al., 2013).

1.7 Human activities

Human activities constitute the main external factor not controlled by this study approach, so this study investigates the influences of both Earth surface movements and human activities on major rivers. With Earth surface movements and human activities there are issues with convergence, with the two factors resulting in similar effects, especially with both active folds and direct human impacts having significant influences at river reach and channel scales. Also, there are issues with singularity and complexity, with possible interactions between the two factors, especially at locations where active folds and direct human impacts coincide (Schumm, 1991). However, it appears that previous research on any interactions between these two external factors has been limited to only tentative links. For instance, changes to the River Indus in Pakistan from an aggrading, anastomosing river into an incising, meandering river associated with the Jacobabad-Khairpur zone of uplift, have been considered to have been enhanced by the Sukkur Barrage which was constructed in 1932 AD (Harbor et al., 1994).

Over approximately the last 4,000 years (since the first major civilizations in south-west

Iran) and especially over the last 100 years, human activities have been the dominant form of disturbance to the fluvial environment, exerting a greater influence than adjustments related to climate changes, although extreme natural events have continued to be a significant cause of change (Petts, 1989; Brookes, 1994; Knighton, 1998). There are two broad categories of human impacts on rivers: direct human modifications to the river channel by river regulation and channel modifications, and indirect human impacts on the river catchment and river basin by land use changes (Table 1.3; Brookes, 1994; Brierley and Fryirs, 2005).

Table 1.3 Types of human impacts on rivers (Based on Brookes, 1994)

Direct human modifications (mainly reach scales)		***Indirect human impacts*** (mainly catchment and basin scales)
River regulation	Channel modifications	Land use changes
Water storage by dams, weirs and reservoirs, and water diversion schemes	River engineering. Channelization such as flood control works, bed/bank stabilisation structures and channel realignment	Changes to ground cover, including changes in agricultural practice and forest clearance
	Sand and gravel extraction and dredging	Urbanization and building/infrastructure construction
	Clearance of riparian vegetation and removal of woody debris	Mining activity

Direct human modifications by river regulation and channel modifications include: irrigation projects, dams, reservoirs, bunds, dikes, weirs, bridges, canals, straightened/realigned channels, widened channels, cuts, diversion channels, levées and embankments, bank protection, bed and bank stabilization structures, flood walls and lined channels, floodplain modifications, fish tanks, water pumps, dredging, sand and gravel extraction, and clearance of riparian vegetation, obstructions and woody debris. Generally, these direct modifications are intended (though unintended changes frequently also occur) and are undertaken with aims such as improving resource development, irrigation, navigation, flood protection or flood alleviation (Brookes, 1994; Downs and Gregory, 2004; Brierley and Fryirs, 2005).

Indirect human impacts are adjustments brought about as responses to changes to land use in the catchment that modify the water discharge and sediment load of the river by mechanisms such as changes in runoff and soil erosion (Kosmas et al., 1997) and, in general, are unintended. These indirect human impacts include: agriculture, vegetation clearance, forest clearance, irrigation, cultivation, pastoralism, grazing, urbanization, building and infrastructure constructions, drainage, sewage, and mining activity. Although indirect human impacts may appear less dramatic than direct disturbance responses, their effects are often more widespread and far-reaching (Brookes, 1994; Downs and Gregory, 2004; Brierley and Fryirs, 2005). There is considerable overlap between direct and indirect impacts (Brierley and Fryirs, 2005). In this study, with a focus on fine, river reach and channel scales, there is a greater emphasis on direct human modifications to the river channel.

Evidently, such a wide range of human activities may lead to a wide range of river responses, and the influences of human activities on rivers and landscape evolution have, generally, been poorly modelled (Wainwright, 2008). Hence, analyses of human impacts are best undertaken on an individual case basis, though some general principles do apply.

1.7.1 Direct human modifications to channels

It is the direct human modifications that have the greatest changes in impact between successive river reaches, and, especially with human modifications of greater magnitude, there may be impacts for appreciable distances both upstream and downstream of the main location of human impact. In this respect, *dams and reservoirs* are a pertinent example. As shown in Figure 1.8, dam construction traps a large quantity of river sediment (commonly more than 90 %) within a delta in the reservoir formed by the dam. In general, this may result in some aggradation upstream of the reservoir, though this may be limited or delayed depending on sediment supply conditions (Leopold and Bull, 1979). Also, in general, this results in prominent incision immediately downstream of the dam as a result of the clearer, “hungry” water that is able to expend its energy on the erosion of the channel bed and banks (Williams and Wolman, 1984; Kondolf, 1997). This downstream incision may result in changes in the channel capacity, width:depth ratio and channel sinuosity of the river (Gregory, 1987).

In extreme cases, basal scour may undermine the dam structure itself (Komura and Simons, 1967). The eroded sediment is transported by the river as a sediment “slug” which may accumulate at one location further downstream, as shown in Figure 1.8, or may be transported further distances and be deposited over a wide range of locations, so

Figure 1.8 Generalised geomorphological impacts of dam construction on river characteristics (From Brierley and Fryirs, 2005)

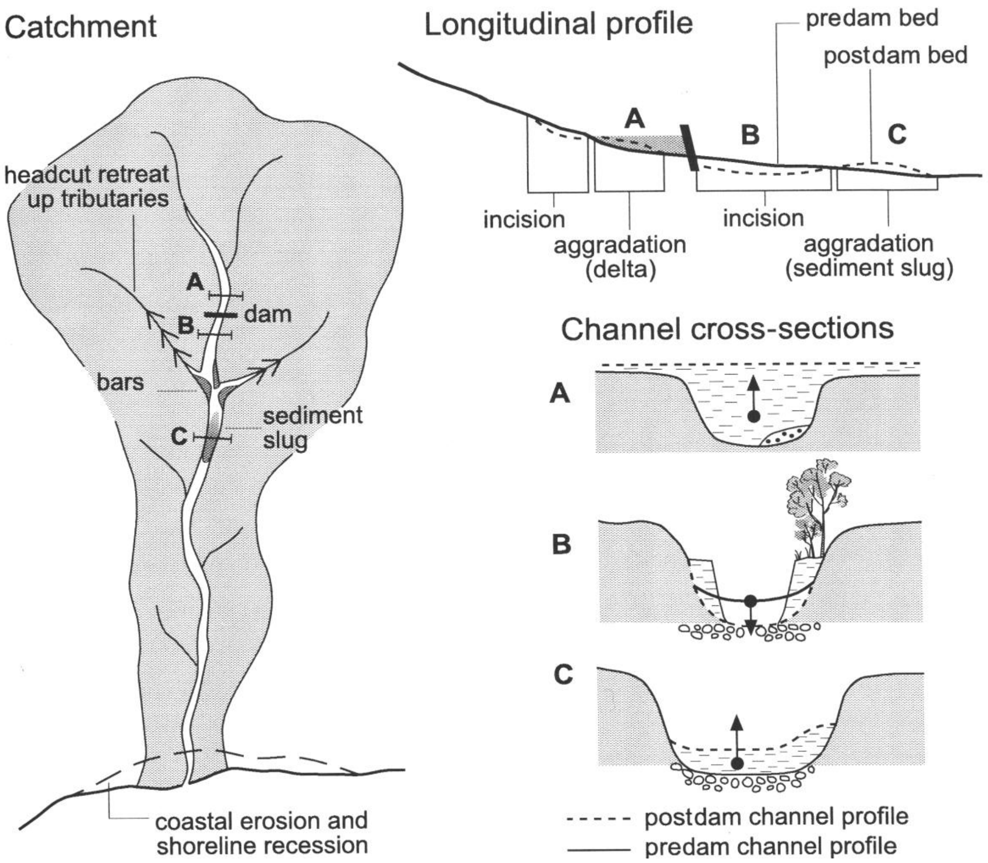

General changes which may occur with dam and reservoir construction include:
At location A, at the entrance to the reservoir, an accumulation zone develops, due to sediment being trapped within a delta in the reservoir.
At location B, immediately downstream of the dam, a slot channel with bed armouring develops with greater decoupling of the river channel form the floodplain, due to reduced bedload and increased erosion of the “hungry” river.
At location C, further downstream where the channel has contracted through the formation of lateral bars, there is sediment accumulation, due to deposition of the sediment “slug” eroded from location B propagating further downstream with time.
Offsite impacts may include tributary stream incision, and coastal erosion with altered morphodynamics of the coastline.

---

that net incision extends a long way downstream of the dam. Hence, whilst these general principles apply with dam construction, the details of the response will vary on an individual case basis. For instance, analysis of changes at 21 reservoir sites in central and south-west U.S.A. showed that in most cases there was channel bed degradation immediately downstream of the dam, though in some cases downstream channel width showed no appreciable change, in others it increased by as much as 100 %, in others it decreased by as much as 90 %, and at many cross-sections changes in bed elevation and channel width proceeded irregularly with time (Williams and Wolman, 1984). Also, the very large Aswan High Dam on the River Nile in Egypt, ultimately, only resulted in a maximum downstream degradation about 0.7 m (Wohl, 2000), whereas the small Black Butte Dam on Stony Creek in California, U.S.A. resulted in erosion of an equivalent of about 20 % of its average annual bedload from the downstream floodplain and a change in downstream channel pattern from braided to single-thread meandering (Kondolf and Swanson, 1993).

The river changes associated with a dam diminish with distance downstream, as non-regulated tributaries and boundary erosion provide sediment inputs, but large distances (tens of kilometres or more) may be required for the river to regain its sediment load and in some cases it may never do so (Williams and Wolman, 1984; Pitlick and Wilcock, 2001). In addition to this, dam and reservoir construction has a number of other effects on rivers, particularly on river flows, with, generally, reduced flood magnitudes and reduced seasonal variability of flows downstream of the dam (Downs and Gregory, 2004).

Human activities which straighten channels, such as canals, cuts, and channel straightening and realignment are especially important in this study, since they may be difficult to differentiate from reductions in channel sinuosity associated with a river eroding across an active fold (Burbank and Anderson, 2012). As partially shown in Table 1.4, human channel straightening may result in markedly reduced channel sinuosities and steepened channel slopes which become gentler with time as bed sediments are redistributed and channel pool depths are reduced, so that the river may change and become dominated by riffles (Brierley and Fryirs, 2005). As with all other human impacts, the details of the response of the river vary on an individual case basis, with, for instance, a study of 57 sites of channelization in England and Wales demonstrating a diversity of channel enlargement downstream with decreasing effects with distance downstream (Brookes, 1988). In general, and especially where channel straightening is accompanied by local bed steepening, there is net degradation upstream of a straightened reach by retreat of headcuts, and net aggradation downstream of a straightened reach leading to channel enlargement downstream which may increase channel capacity by as much as several hundred per cent (Daniels, 1960; Brookes, 1994). Degradation and widening may provide effective means of energy dissipation as systems adjust to channelization (Simon, 1992).

Table 1.4 Geomorphological impacts of some channelization procedures (Modified from Knighton (1998) and Brierley and Fryirs (2005) using various sources)

Short description of procedure	**Common reasons for procedure**	**Impacts of procedure**
Straightening/ realignment. River course is straightened by artificial cut-offs, cutting of a new channel, or diversion into a former canal.	Flood protection, infrastructure development, improved navigation, improved irrigation.	Gradient is steepened as flows follow shorter paths. Flow velocities and transport capacity are increased. Degradation ensues, progressing upstream as a headcut. Bed and bank erosion increase sediment load to the reach downstream, ultimately flattening its slope and promoting aggradation.
Levée and floodwall construction. River channel banks are raised, increasing channel capacity.	Maintenance of irrigation channels, flood protection, confining floodwaters.	Reduces floodplain inundation and sedimentation rates, causing major changes to wetland ecosystems. May "trap" floodwaters in extreme events, or concentration of flow may promote bed incision.
Channel stabilization and bank protection. Structures such as paving, dikes and subaqueous matting are used for strengthening.	Control of bank erosion.	Alters channel width and roughness components, with secondary effects on bed incision and subsequent sediment release, thereby adjusting channel slope. May promote sedimentation adjacent to the bank.
Resectioning/ overwidening. River channel is widened and/or deepened.	Increased conveyance capacity to reduce overbank flooding.	Widening reduces flow velocities and stream powers, thereby lowering sediment transport capacity and bench deposition.
Clearing and snagging. Obstructions are removed from the river.	Aiding flood passage and navigation capacity.	Decreases resistance and increases flow velocities, thereby promoting bed degradation, subsequent widening and marked increases in channel capacity.
Dredging. Bed sediment is removed to deepen the channel, especially along the thalweg in lower reaches.	Maintenance of navigable channels.	Dredging may promote degradation through lowering of base level enabling knickpoints to migrate upstream, thus contributing sediments to the dredged reach. Deepening may also promote bank collapse and upstream progressing degradation in tributaries.

Overall, *river engineering* generally produces a reduction in the sediment flux of a river, though the generation of sediment "slugs" may result in accumulations of sediments downstream, especially in lowland basins. *Dredging* may be undertaken to remove these and other sediments from the river bed, generally in order to maintain navigable channels. Depending on its extent, dredging will generally increase the local conveyance capacity and erosive power of the river. This may result in upstream degradation by knickpoint migration, which, if accompanied by erosion of the channel banks, may result in continued aggradation at the site of the dredging and further downstream. Sand and gravel extraction may have similar effects, which may be more marked if the gravel bed armour of a river is extracted (Downs and Gregory, 2004; Brierley and Fryirs, 2005).

Clearance of riparian vegetation and removal of woody debris will have greatest influence with extensive floodplain vegetation and sand bed alluvial rivers. In general, the effects of loss of riparian vegetation may be increased bank erosion, channel widening and shifting, bed degradation, and fall in the water table leading to secondary salinization (Burch et al., 1987; Brierley and Fryirs, 2005).

1.7.2 Indirect human impacts on catchments

The indirect impacts of humans on rivers have their principal influences at the larger spatial scales of catchments and basins, with relatively little variation between successive river reaches. In general, the *clearance of forest and vegetation cover and the establishment of agriculture* with cultivated and grazed land produce increases in runoff and large increases in sediment yield due to increased soil erosion. The details of the river response varies on an individual case basis, with more pronounced responses to extensive clearance and steeper slopes, but, generally, any changes that reduce the vegetation cover are likely to increase sediment discharge proportionally more than water discharge (Knighton, 1998). One scenario is that with the initial clearance of trees and changes to agriculture, there are fairly rapid increases in sediment yields and sediment discharges until a plateau is reached, after which they gradually reduce again once the more readily erodible soils have been removed (Bull, 1991). In some regions of the World these changes have taken place over relatively short time-scales, such as in the U.S.A. where the development of extensive agriculture dates to about the last 300 years (Downs and Gregory, 2004; Brierley and Fryirs, 2005). In other regions of the World these changes have taken place over longer time-scales, such as in south-west Iran where the development of extensive agriculture dates to about the last 4,000 years (Stevens et al., 2006). These river changes mainly apply at catchment spatial scales, though where there have been more recent clearances of trees and other vegetation for cultivation at local scales, river responses at reach scales may occur (Downs and Gregory, 2004).

Relative to the changes associated with vegetation cover, the human impacts associated with *urbanization* are usually more localised. Apart from during extensive construction phases when large amounts of soil are exposed and sediment yield may increase by up to two orders of magnitude (Wolman and Schick, 1967), the main general effects of urbanization are increased runoff and reduced sediment yields from impervious surfaces and from sewage and storm water systems (Brierley and Fryirs, 2005). These effects increase river water discharges, especially for smaller, more frequent floods, and reduce sediment discharges, producing accentuated erosion and channel enlargement, especially immediately downstream of urban areas (Wolman, 1967; Roberts, 1989).

Mining activities may have various pronounced impacts on river systems due to vegetation clearance, drainage modification and disposal of waste materials. Typically, they disrupt the hydrological regime, accelerate slope erosion and increase sediment delivery to rivers (Brierley and Fryirs, 2005).

1.8 Format of the study

This study aims to determine the influences of Earth surface movements and human activities on the major rivers Karun and Dez in lowland south-west Iran.

Chapter 2 describes the study area of south-west Iran and how the major rivers Karun and Dez, the folds, and other features are well suited to investigating the influences of major river responses to Earth surface movements and human activities.

Chapter 3 outlines the methods used in the study, with details of the methods given in Appendix 7.

Chapter 4 presents the results, sub-divided into those relating to Earth surface movement rates, river characteristics, and laboratory analyses, with further details given in the appendices.

Chapter 5 evaluates rates of Earth surface movements in lowland south-west Iran.

Chapter 6 evaluates the responses of the River Karun and River Dez to the influences of active folds and human impacts, including discriminating between the river responses of river incision across a fold, river diversion around a fold, and direct human impacts.

Chapter 7 evaluates the interactions of the influences of human impacts and Earth surface movements on the rivers Karun and Dez.

Chapter 8 presents the conclusions, including suggestions for future research.

Appendices 1 to 6 give details of the results in tables. Appendix 7 gives details of the methods.

CHAPTER 2 THE STUDY AREA

"We entered the Karun at Mohammerah on the 9th February, 1842. The river at that time, from violent and continued rains, had risen to an unusual height: the surrounding country was flooded for many miles, and had the appearance of a vast lake."

Austen Henry Layard, British traveller and archaeologist (1817 - 1894 AD)

2.1 Introduction

The study area is the Upper and Lower Khuzestan Plains of lowland south-west Iran (Figures 2.1, 2.2 and 2.3). This area was chosen since, as discussed in Section 1.6 and 1.7, it facilitates a study of the influences of Earth surface movements and human activities on major rivers, with good "control" of other external factors via a focus on reaches of the River Karun and its main tributary the River Dez in the Mesopotamian-Persian Gulf Foreland Basin.

The Khuzestan Plains within this single foreland basin have a fairly uniform semi-arid climate (Section 2.8), similar NW-SE trending folds which are progressively younger towards the south-west (Sections 2.4.6 and 2.4.7), and predominantly aseismic movements on folds and faults (Section 2.5). There is a long history of human activities on these plains, with the construction of major canals spanning over about four thousand years from the Elamite Period (c. 2,600 BC - 646 BC) to the Present (Section 2.11). Furthermore, the major rivers Karun and Dez move fairly freely across the Khuzestan Plains, with notable migrations or avulsions over the last four thousand years, in contrast with the Zagros Mountains region where, generally, river courses have been "fixed" over these timescales.

2.2 The major rivers of south-west Iran

There are five major rivers in south-west Iran: the rivers Karun, Dez, Karkheh, Jarrahi and Zohreh. They flow from the Zagros Mountains across the Upper and Lower Khuzestan Plains into the Huwayzah and Shadegan marshes and the Persian Gulf (Figures 2.2 and 2.3). The approximate length, drainage basin area, and average water discharge of each of these rivers in the Khuzestan Plains are given in Table 2.1.

Table 2.1 Length, drainage basin area, and average water discharge of the five major rivers of south-west Iran (Data from various sources, including Vali-Khodjeini, 1994; KWPA, 2003; Coad, 2009; PMIRIUN, 2009; UNH/GRDC, 2009; Masih, 2011)

River	Length	Drainage basin area	Average river water discharge in the Khuzestan Plains
River Karun	890 km (from source to the Persian Gulf)	45,230 km^2	575 m^3s^{-1} (at Ahvaz)
River Dez	515 km (from source to its confluence with the River Karun)	23,250 km^2	230 m^3s^{-1}
River Karkheh	755 km (from source to the Huwayzah marshes)	50,770 km^2	165 m^3s^{-1}
River Jarrahi	438 km (from source to the Shadegan marshes)	24,310 km^2	78 m^3s^{-1}
River Zohreh (or River Hendijan)	488 km (from source to the Persian Gulf)	13,590 km^2	80 m^3s^{-1}

Figure 2.1 The location of the study area and the broad-scale plate tectonics of the Middle East

Key to Figure 2.1

General direction of plate motion

Generalised tectonic plate boundary types

Divergent plate boundary

Convergent plate boundary

Strike-slip plate boundary

Dashed line area indicates the location of the study area shown in Figure 2.2

2.2.1 Regional importance of the rivers

The five major rivers shown in Figures 2.2 and 2.3 are of fundamental importance to Khuzestan province. Most of the Khuzestan Plains are too arid for dry farming, and irrigation using the major rivers and their tributaries has permitted extensive agriculture and civilization on the plains for thousands of years (Kirkby, 1977; Potts, 1999). The major rivers are important for urban development, especially water supply and sewage, with all cities on the Khuzestan Plains being sited on major rivers, and they are moderately important for navigation and transport, most notably for the River Karun downstream of Ahvaz (Golchin, 1977). From the mid-20th Century AD onwards, the major rivers in south-west Iran have been very important for major dams and reservoirs for hydro-electric power, and for extensive use of water in industry and processing plants (Afkhami et al., 2007; KWPA, 2010). However, recent over-developments have made Ahvaz the World's most air-polluted city and have radically reduced the flows of the River Karun, and improvements in river management are greatly needed (Afkhami et al., 2007; Heidari, 2009; Brett, 2013).

Key to Figure 2.2

Major faults:

Major thrust fault

Major right-lateral strike-slip fault

Major left-lateral strike-slip fault

Zagros Deformation Front (ZDF)

River basin margin (shown in upland areas only)

Figure 2.2 The major rivers and broad-scale geology of south-west Iran (Landsat (2000) false-colour image with three ETM+ bands: *Band 7* (mid-infrared, wavelength 2,090-2,350 nm) displayed as red; Band 4 (near-infrared, 750-900 nm) displayed as green; Band 2 (visible green, 525-605 nm) displayed as blue; Resolution 30 m) (NASA, 2012)

Key to abbreviations used in Figure 2.2

MFF Mountain Front Fault

Structural zones:
S-SZ Sanandaj-Sirjan (or metamorphic) Zone
IZ Imbricated Zone (or High Zagros)
SFZ Simple Folded Zone
FB Foredeep of the Mesopotamian-Persian Gulf Foreland Basin

Figure 2.3 The River Karun and other main rivers of the province of Khuzestan and its environs (Modified from Heyvaert et al., 2013)

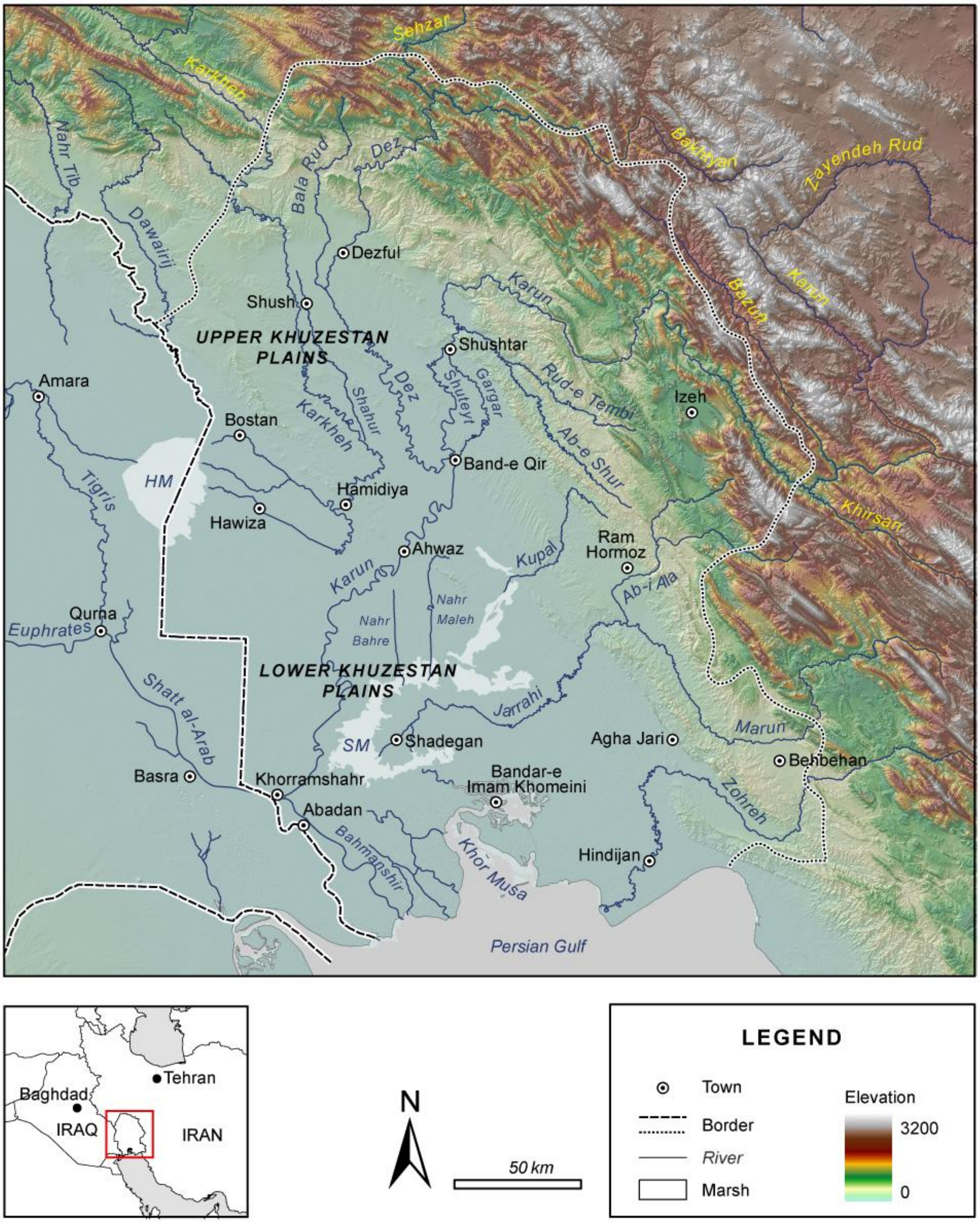

HM Huwayzah marshes *SM* Shadegan marshes

– – – – – – – – – International border

.... Border of Khuzestan province

2.2.2 River water discharges

The figures for river water discharges in Table 2.1 are approximate mean annual values. River water discharges vary throughout the year (with notably higher flows in the late winter and spring) and vary from year to year. The average water discharge curves for the River Karun at Ahvaz are shown in Figure 2.4 (a) for the years 1895 to 1930 AD (Ionides, 1937) and in Figure 2.4 (b) for the years 1965 to 1984 AD (CSGE, 2010).

The curves in Figure 2.4 are representative of the major rivers in the region, with peak flows with rainfall and Zagros snow-melt in the winter and spring, when floods are more frequent. On occasions, storms may cause large floods and examples of two flood hydrographs for the River Dez in its upper catchment at Taleh Zang are given in Figure 2.5 (Sadrolashrafi et al., 2008). Low flows occur in the late summer and autumn, when there may be very high salinities and navigational difficulties for larger vessels in the lower reaches of the River Karun. Due partly to high rates of evaporation, there are some trends to lower water discharges with distance downstream in the lower reaches of the rivers, particularly with the River Karkheh and River Jarrahi which flow into marshes. The curves also show that river water discharges have been reduced with the human impacts of extensive water extraction for agriculture and major dam construction from c. 1960 AD onwards (KWPA, 2010). The mean annual water discharge for the River Karun at Ahvaz was about 766 m^3s^{-1} for the period 1894 - 1932 AD (Ionides, 1937) and about 481 m^3s^{-1} to 575 m^3s^{-1} for the period 1965 - 1984 AD (UNH/GRDC, 2009; CSGE, 2010).

2.2.3 River sediment load

The sediment load carried by these major rivers is relatively high, mainly as a result of the relatively steep basin slopes in the Zagros and the high soil erodibility associated with the limited vegetation cover in the river catchments (Ludwig and Probst, 1998). River sediment supply can be difficult to measure (IAEA, 2005; Allen et al., 2013) and sediment load data for the rivers in Iran is scarce, though it is clear that there are large daily fluctuations and that sediment loads are usually very high during flood events. In the long-term, for the River Dez at Taleh Zang in its upper catchment it has been found that the mean suspended sediment load is about 7.5 to 12.4 × 10^6 tonnes yr^{-1} and the mean total sediment load is about 8.4 to 15.7 × 10^6 tonnes yr^{-1}, employing calculations using suspended sediment discharge/flow rating relationships (Jahani, 1992). The mean total sediment load at the mouth of the Tigris-Euphrates-Karun delta has been found to

Figure 2.4 Average water discharge curves for the River Karun at Ahvaz
(a) For the period 1895 - 1930 AD (From Ionides, 1937)
(b) For the period 1965 - 1984 AD (From CSGE, 2010)

a)

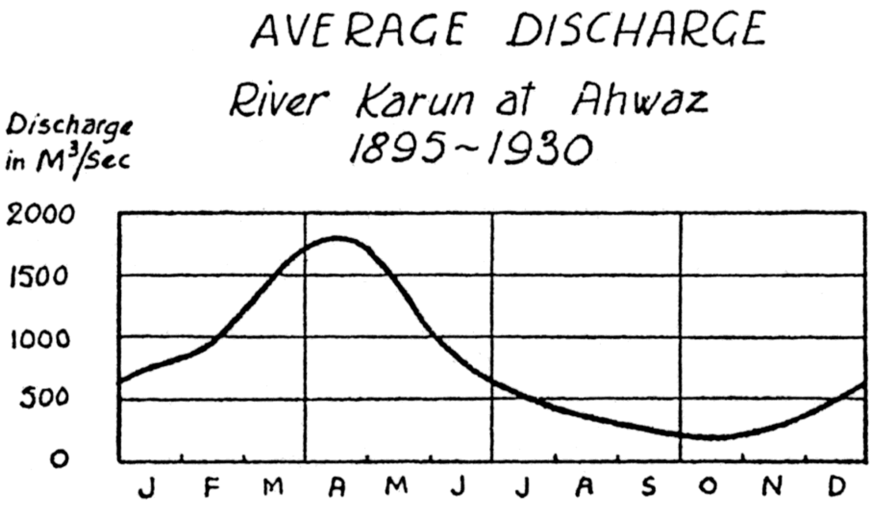

b)

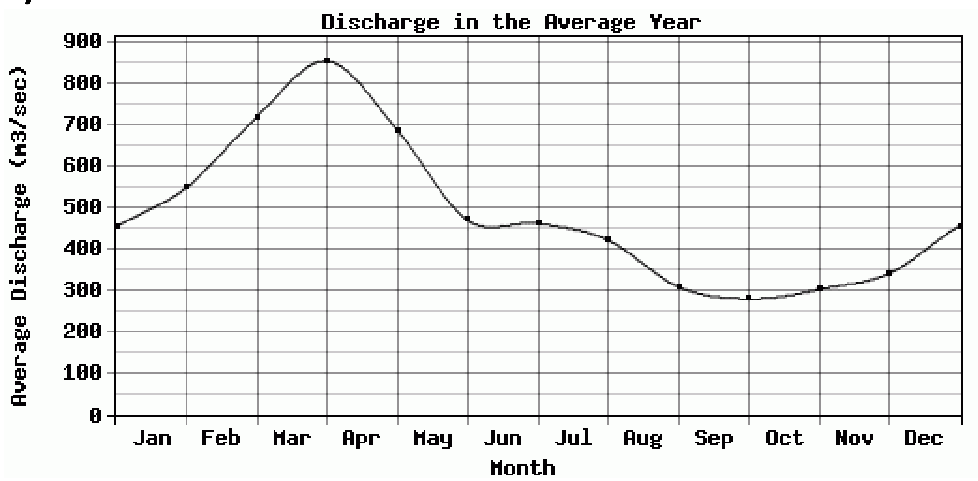

Figure 2.5 Flood hydrographs for the River Dez in its upper catchment at Taleh Zang (48°46'N 32°49'E) for storms in December 2001 and January 1993 (Rainfall is for the catchment of the Bakhtyari branch of the River Dez) (Modified from Sadrolashrafi et al., 2008)

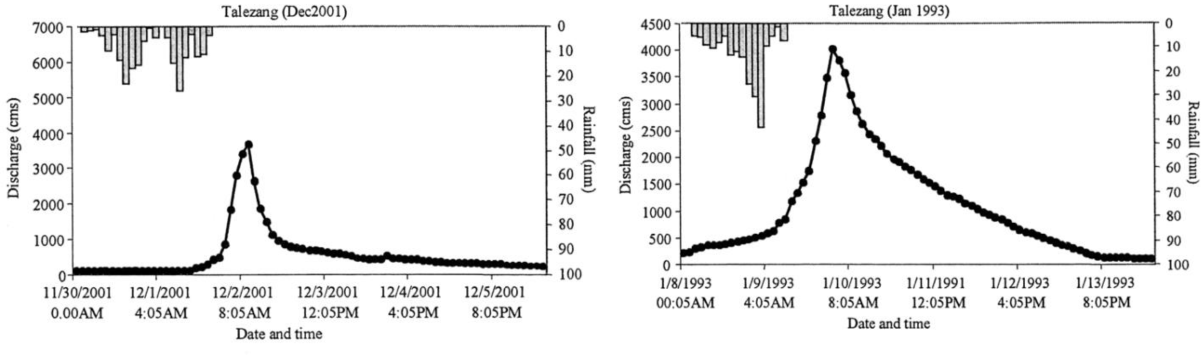

be greater than 53×10^6 tonnes yr^{-1} (Milliman and Syvitski, 1992), of which about 81 % - 90 % (or greater than 43×10^6 tonnes yr^{-1}) is derived from the River Karun (Cressey, 1958; Larsen and Evans, 1978).

2.2.4 River water salinity

The salinity of the River Karun is relatively high due to high rates of evaporation in the warm semi-arid climate, evaporite-rich rocks in the tributary catchments (most notably the Ab-e Shur or "salty river" just upstream of Shushtar), and, in recent times, the excessive extraction of water for agriculture. Average river water electrical conductivities were about 920 µS cm^{-1} at Gotvand and 1,630 µS cm^{-1} at Khorramshahr for the River Karun for the period 1967 - 2005 AD in its lower catchment, and about 530 µS cm^{-1} for the River Dez at the Dez Dam in its upper catchment (Afkhami, 2003; Naddafi et al., 2007).

2.3 The River Karun and the River Dez

2.3.1 The River Karun basin

The modern name of the largest river in Iran is the "Karun", a corruption of "Kuh Rang", namely the "yellow hills" or "coloured hills" of the region of Zardeh Kuh (peak elevation 4,548 m) in the Zagros Mountains, from which it descends. This region, which is the traditional source of both the Karun and the Zayendeh Rud (or "living stream" which flows internally through Isfahan), is an area of abundant springs (one part is called the "Chehel Cheshmeh" or "forty springs"), and from its source the Ab-e Kurang is a relatively large river (Layard, 1846). The River Karun and its various tributaries (including the rivers Wanak, Bazuft, Khirsan and Shur) wind their way through the Zagros Mountains, often in accordance with the general NW-SE structural grain and folding (Figure 2.6). The Karun passes the Mountain Front through a cleft in the "Kuh-e Tukak Anticline" north-west of the town of Izeh (or Malamir), and then crosses the Zagros foothills and the alluvial apron of mainly conglomerates of the Middle Pliocene - Pleistocene Bakhtyari Formation (Figure 2.6; Oberlander, 1965).

Near to Gotvand, the Karun flows out from a narrow gorge in the Turkalaki Anticline across the alluvial fan of the Aghili Plain of the Upper Khuzestan Plains (Oberlander, 1965; Kirkby, 1977). After receiving the salty Ab-e Shur tributary, the R. Karun crosses

Figure 2.6 The upper River Karun basin, prior to major dam construction (Modified from Oberlander, 1965, with main river course highlighted in yellow)

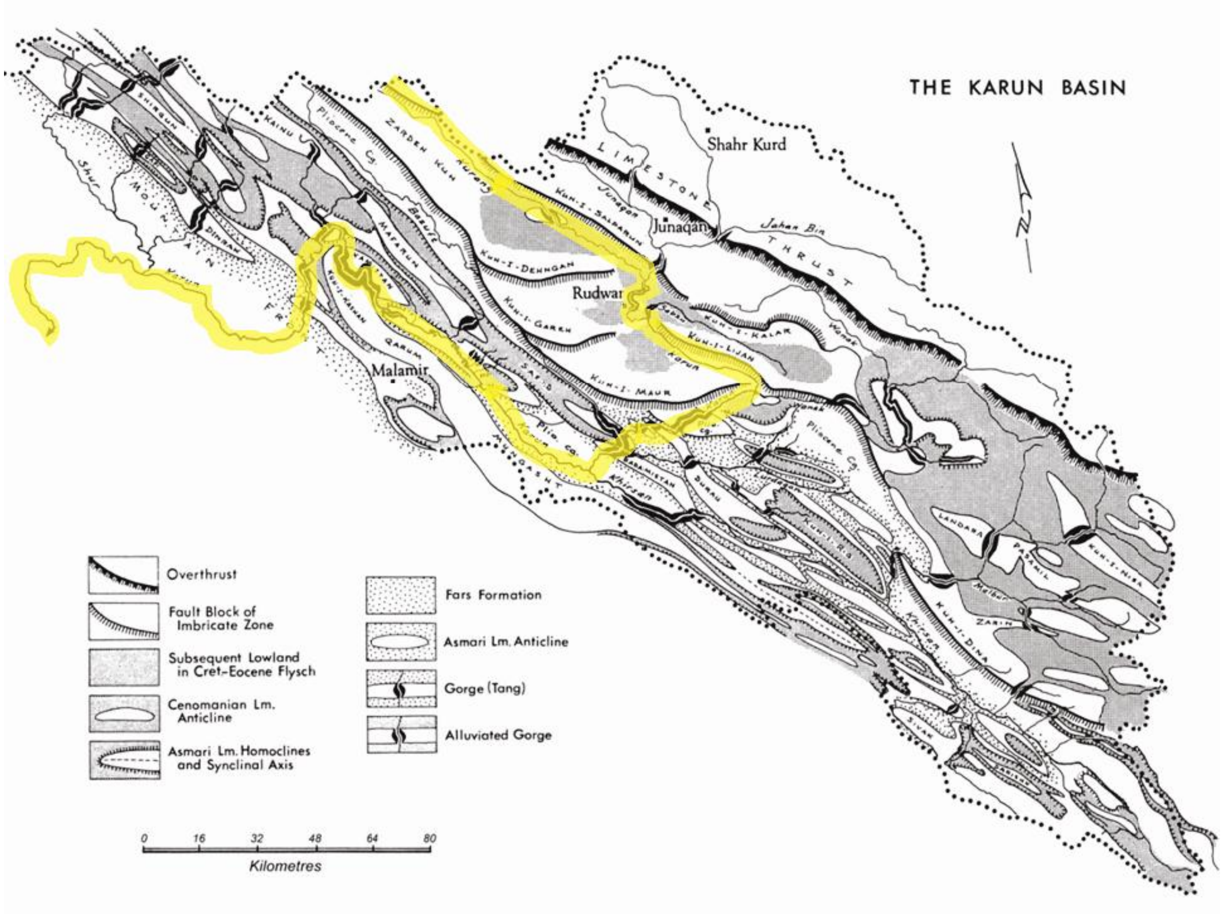

Shushtar Anticline and then flows across the alluvial fan of the upper Mianab Plain. As a result of major human impacts from the Sassanian Period (c. 224AD - 651 AD) onwards, the River Karun divides into two branches at Shushtar: the River Shuteyt (or "little river", known in the 14th - 15th Century AD as the "Chahar Danikah", or "four sixths") to the west, and the River Gargar (named after a part of Shushtar and known in the 14th - 15th Century AD as the "Du Danikah", or "two sixths") to the east (Figures 2.3 and 4.1 (b)). After flowing roughly southwards across the Mianab Plain, these two branches re-unite at Band-e Qir (meaning "bitumen dam/dike") at the confluence with the River Dez (Layard, 1846; Modi, 1905). The main geomorphological features of Upper Khuzestan are shown in Figure 2.7.

2.3.2 The River Dez basin

The River Dez in its upper catchment is generally known as the Sehzar (or "three yards", the reputed width of some of its narrowest defiles) which is formed at the town of Dorud by the confluence of the Burujird and Kamand rivers. The River Sehzar and its

Figure 2.7 The main physiographic zones and features of Upper Khuzestan (From Kirkby, 1977)

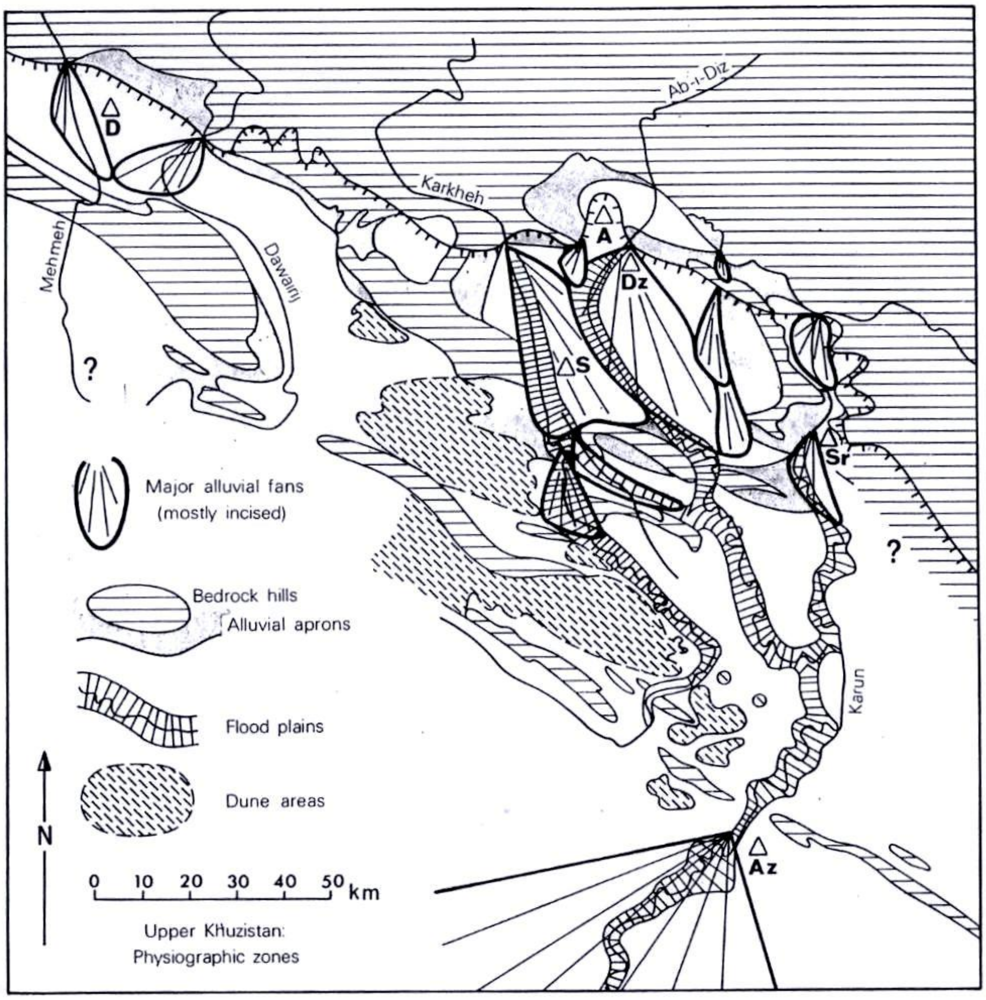

Key

A	Andimeshk	**Az**	Ahvaz	**D**	Deh Luran
Dz	Dezful	**S**	Shush (ancient Susa)	**Sr**	Shushtar

The town of Gotvand is about 25 km north of Shushtar near the mountain front

┬┬┬┬┬┬┬┬ Mountain front

---

main tributary, the River Bakhtyari, flow roughly south-westwards through the Zagros Mountains, mostly in discordance with the general NW-SE structural grain and folding, incising a succession of valleys and steep-sided gorges or *tangs*, such as the Tang-e Bahrein) (Figure 2.8). The discharge of the Sehzar is almost trebled by the addition of the Bakhtyari tributary and, after breaching anticlines in chasms approaching 1,500 m in depth, the river passes the Mountain Front near to Taleh Zang at the upstream end of the reservoir of the Dez Dam. It crosses the Zagros foothills and the alluvial apron in a deep canyon through the Pliocene-Pleistocene Bakhtyari Formation conglomerate cuesta, now filled by the reservoir of the Dez Dam (Figure 2.8; Oberlander, 1965).

Figure 2.8 The upper River Dez basin, prior to major dam construction (Modified from Oberlander, 1965, with main river course highlighted in yellow)

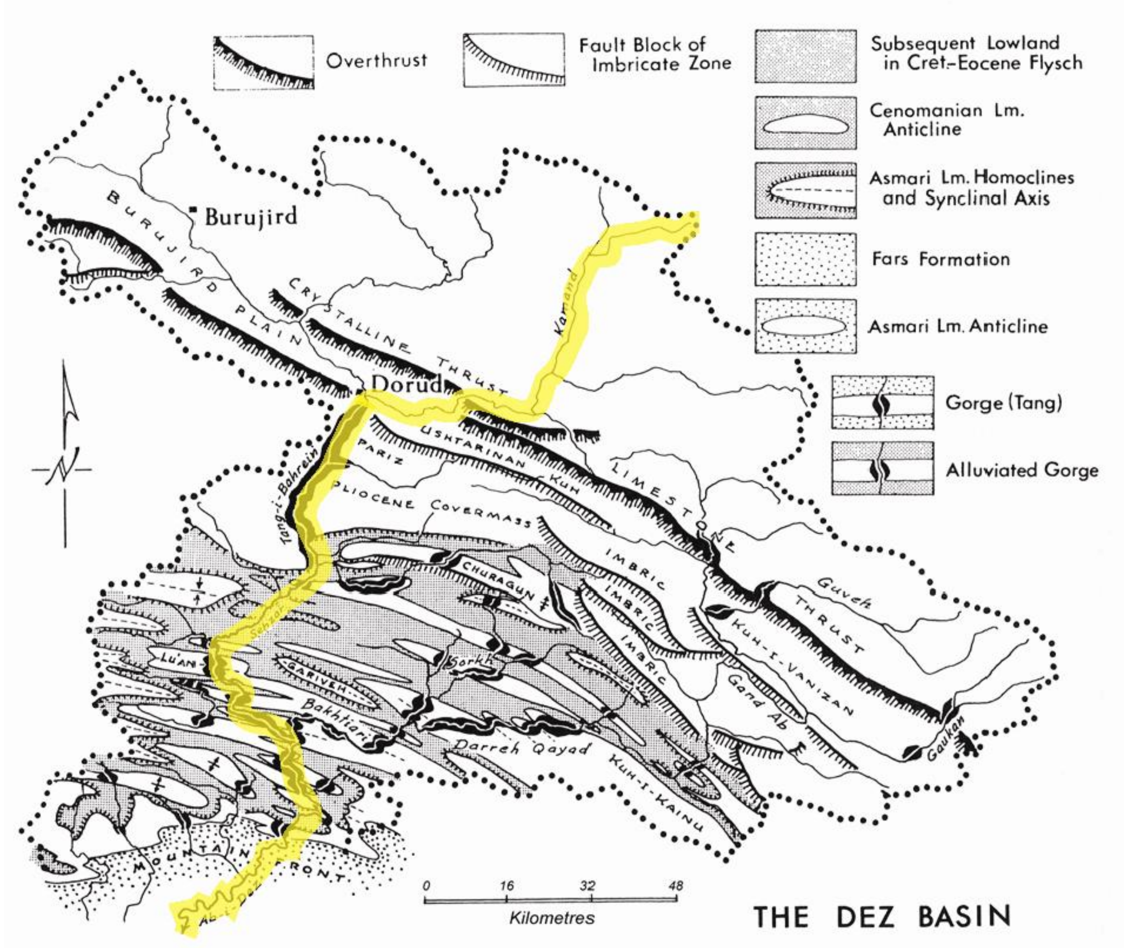

Downstream of the Mountain Front the river is known as the River Dez, this name being derived from Dezful (meaning “fortress bridge”), the city where the river flows across the Dezful Uplift and then out across a large alluvial fan on the Susiana Plain of the Upper Khuzestan Plains. After receiving the Bala Rud and Lureh tributaries, the R. Dez crosses the Sardarabad Anticline and, ultimately, flows into the River Karun at Band-e Qir (Figures 2.3, 4.1 (b) and (c); Layard, 1846; Oberlander, 1965; Kirkby, 1977).

2.3.3 The lower reaches of the River Karun

From Band-e Qir to Veys, the River Karun flows southwards along a c. 19 km long near-straight reach, most probably associated with the construction and subsequent disuse of the Sassanian Masrukan canal (Alizadeh et al., 2004). The Karun then turns roughly south-westwards to flow across the Ahvaz Anticline at Ahvaz. There are major rapids associated with anticlinal linear outcrops of Agha Jari Formation sandstone at Ahvaz, on which are the remains of the “Band of Ahvaz” (a barrage or dam dating to the Sassanian - Abbasid periods) (GBNID, 1945; Walstra et al., 2010a). Downstream of

Figure 2.9 The main geomorphological units of Lower Khuzestan (From Gasche et al., 2004)

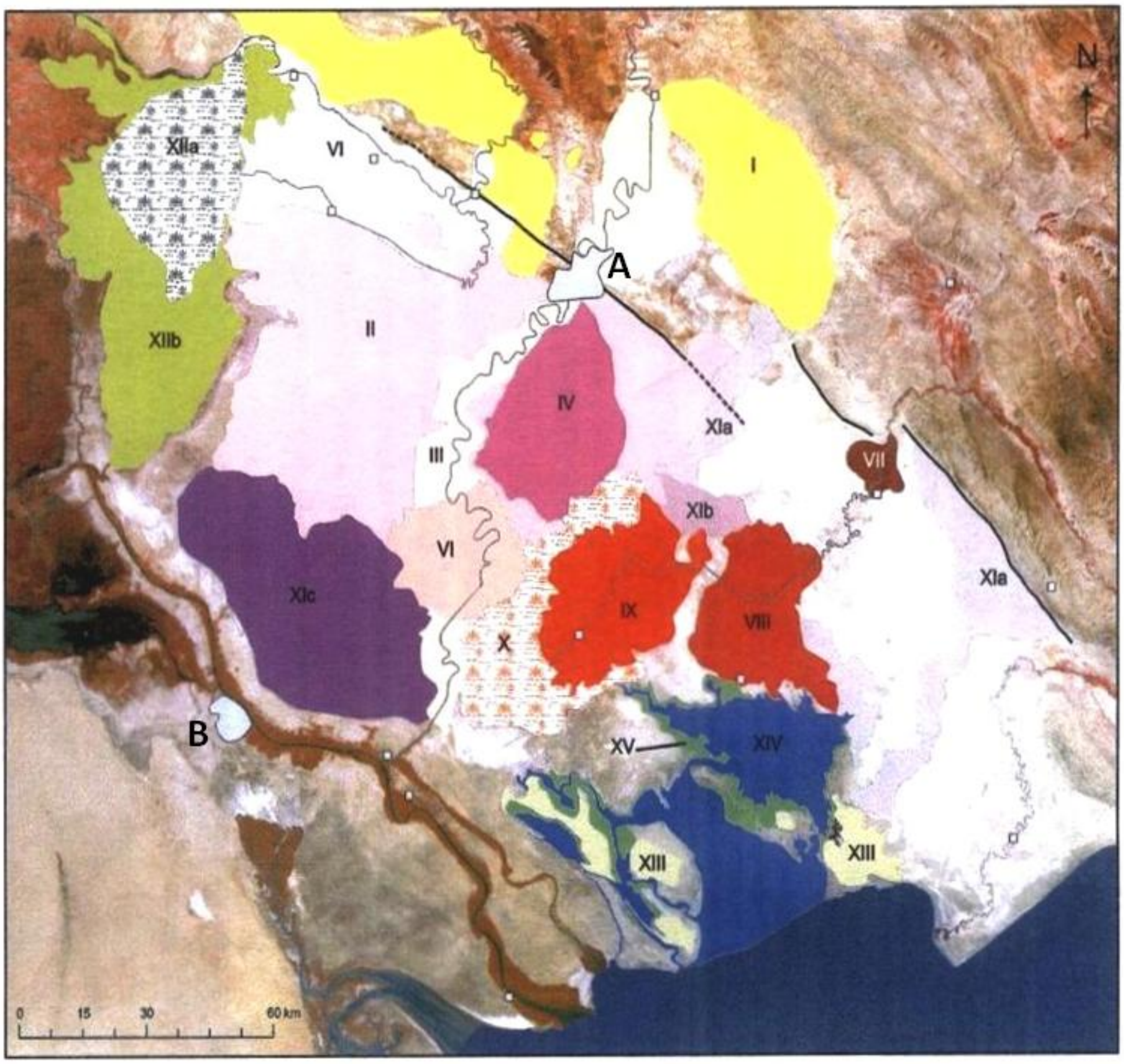

Key

Geomorphological units: **I** (on yellow) Dune fields
II, **III** and **VI** (on pink) Karun megafan, floodplain and crevasse splays
IV Karun canal lobe **VI** (on white) Karkheh floodplain
VII Small Jarrahi alluvial fan **VIII**, **IX** Jarrahi depositional lobes
X Shadegan freshwater marshes
XIa, **XIb** Ephemeral streams/continental sabkhas
XIc Ephemeral freshwater marsh/continental sabkha
XIIa, **XIIb** Huwayzah freshwater marshes **XIV** Tidal flats
XIII, **XV** Supra-tidal flats and salt marshes

Approximate locations of reverse faults are indicated by black lines

Large cities (**A** Ahvaz and **B** Basra) are shown as irregular grey areas, towns/villages as grey squares the Ahvaz Anticline, the River Karun flows over the Lower Khuzestan Plains across the broad Karun megafan and along two long near-straight reaches to its delta (Gasche et al., 2004, 2007). The Karun megafan and the other main geomorphological units of Lower Khuzestan are shown in Figure 2.9. The present-day Karun flows into the Persian Gulf via the Tigris-Euphrates-Karun delta along two main channels: a main course along the Shatt al-Arab (also known as the Arvand Rud) and a lesser course along the Bahmanshir River several km to the east (Figures 2.3, 2.11 and 3.4) (Larsen and Evans, 1978; Verkinderen, 2009; Walstra et al., 2010a).

2.3.4 River channel planforms

Across much of the Khuzestan Plains, the River Karun and River Dez have single-thread meandering channel planforms, the most frequent channel pattern for low-gradient rivers (Leopold, 1994), with some multi-thread braided and anastomosing channels and a few straight channels. Where there are some steeper slopes, such as across the alluvial fans centred on Gotvand, Shushtar and Dezful, the rivers mainly have multi-thread planforms, indicating that in the Upper Khuzestan Plains the major rivers have flow regimes that range across the meandering-braided transition (Schumm, 1985; Knighton, 1998).

2.3.5 Previous courses of the River Karun and River Dez

Over about the last four thousand years (the time of major civilizations in south-west Iran) (Section 2.11), it is most probable that there have been no major changes to the courses of the River Karun and Dez in their upper catchments in the Zagros Mountains. In the upper catchments, the river courses are generally “fixed” in deeply incised valleys, gorges and “tangs”, with significant changes only occurring over longer time-scales (by mechanisms such as river capture) and with changes associated with major dam construction since c. 1960 AD (Oberlander, 1965; KWPA, 2010).

By contrast, in the lower catchments, the major rivers are relatively mobile and have actively migrated or avulsed across the Khuzestan Plains over the last four thousand years; as they have since they first emerged on the plains, probably prior to 3 Ma (Vergés, 2007). River course changes have occurred by natural processes (such as migrations and avulsions into new channels, into pre-existing channels and by inundation of large areas of the floodplain to form avulsion belts) and with human influences (such as migrations and avulsions into canals, planned flow diversions by dams, canals and cuts, and unplanned flow diversions by disuse of canals and failure of dams and dikes) (Morozova, 2005). However, the details of these river course changes are poorly known.

Figure 2.10 Probable previous courses of the River Karun, Dez and Karkheh in Khuzestan, from c. 1,500 BC - Present (From Kirkby, 1977 and Potts, 2010)

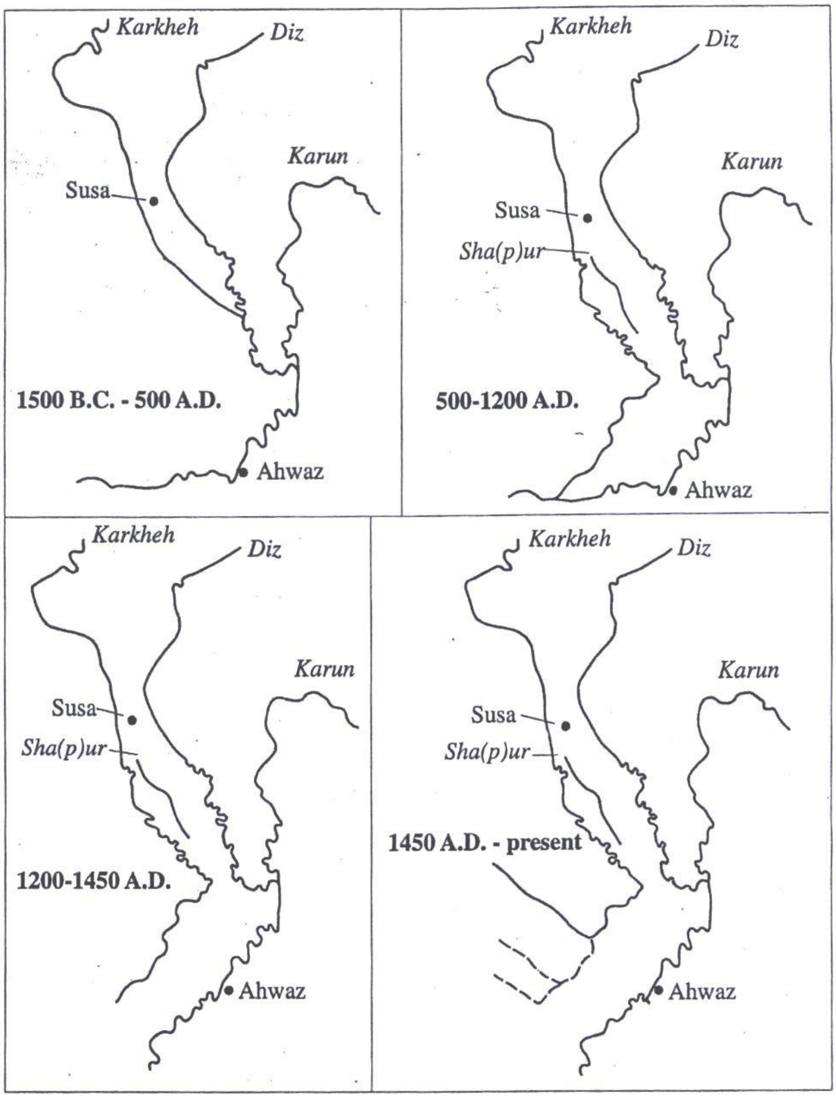

In Upper Khuzestan, four broad stages in the development of the rivers Karun, Dez and Karkheh over about the last four thousand years have been identified using evidence from archaeology, history, and the meander wavelengths of palaeochannels and river channels (Kirkby, 1977; Potts, 2010). Figure 2.10 summarising the work of Kirkby (1977) provides a good general picture of previous river courses, though there are a few errors (e.g. from 1,500 BC - 500 AD the River Karkheh most probably flowed across the Zeyn ul-Abbas and Hamidiyyeh Anticlines (Figure 4.1 (f)) and thence into the River

Figure 2.11 Geomorphological map of Lower Khuzestan showing palaeochannel belts of the River Karun (K1, K2, K3, K3a, K3b, and K3c from oldest to youngest) (From Heyvaert et al., 2013)

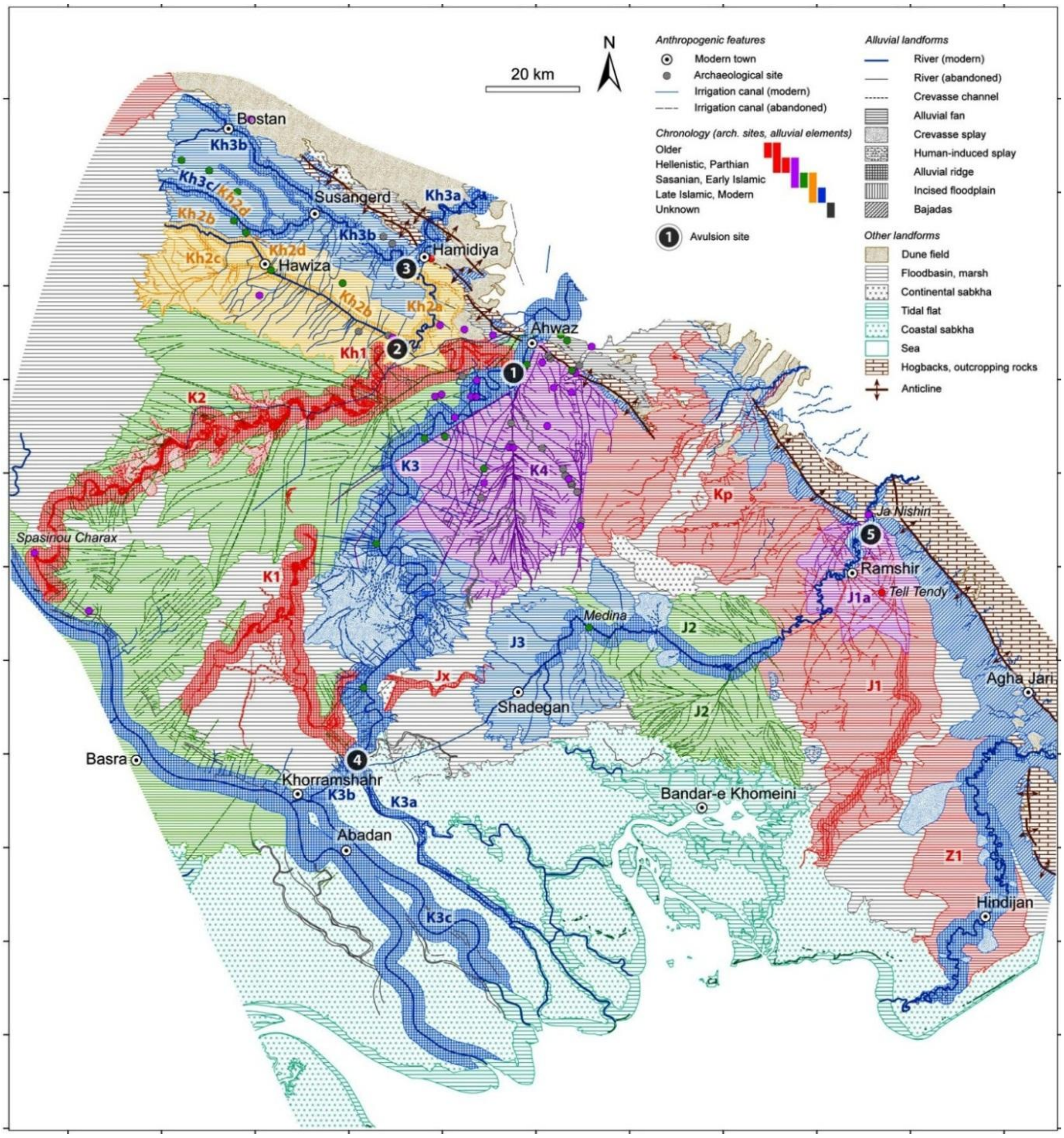

Key

Red, purple, green, orange and dark blue colours indicate chronology, as shown

Palaeochannel belts and channel belts (generally from oldest to youngest)

K1 K2 K3 K3a K3b K3c River Karun **K4** Karun canal lobe

Kh1 Kh2a Kh2b Kh2c Kh2d Kh3a Kh3b Kh3c River Karkheh

J1 J1a J2 J3 River Jarrahi

Kp River Kupal **Z1** River Zohreh

Karun), and details of river course changes are not provided. Other research based on soils, sediments, geomorphology and archaeology indicate that, over millennial timescales, the River Karun has migrated to the west and south-west across the Aghili and Mianab Plains (Figure 4.1 (b); Wright, 1969; Moghaddam and Miri, 2003), the River Dez has migrated to the west across the Susiana Plain (Figures 4.1 (b) and (c); Veenenbos, 1958; Kouchoukos and Hole, 2003), and the River Karkheh has migrated to the west across the Upper Khuzestan Plains (Veenenbos, 1958) (see Section 5.4).

In Lower Khuzestan, due to the balance between relative sea-level changes and river sediment supply, significant progradation of the coastline and major rivers only commenced after c. 550 BC (Coe, 2003; Heyvaert and Baeteman, 2007). Hence, recent river courses of the River Karun downstream of Ahvaz probably only developed subsequent to this date, burying previous river courses. In Lower Khuzestan three main palaeochannels and channels of the River Karun have been recognised (Figure 2.11):
K1, a bifurcated palaeochannel belt in the southern part of the plains aligned roughly North-South (dated as pre-Sassanian)
K2, a longer than 100 km palaeochannel belt aligned roughly WSW-ENE extending from Ahvaz to the Shatt al-Arab (dated to about pre-2nd Century BC - 7th Century AD)
K3/K3b/K3c and K3a, the courses of the present-day Karun and "Blind Karun" (all dating from pre-19th Century AD and possibly from pre-10th Century AD) - Present (Walstra et al., 2010a; Dupin, 2011; Heyvaert et al., 2013).
Other features include the Karun megafan roughly spreading out from Ahvaz (probably dating to after K1, at least in part) and the Karun canal lobe, K4, extending southwards from Ahvaz to the Shadegan marshes (Figures 2.9 and 2.11; Gasche et al., 2004, 2007; Walstra et al., 2010a; Heyvaert et al., 2013).

2.4 Geology of the study area

2.4.1 Regional structural geology

The foreland basin for the major rivers of south-west Iran is the Mesopotamian-Persian Gulf Foreland Basin; a sedimentary basin approximately 2,600 km long and 900 - 1,800 km wide in total, that extends from northern Syria and Turkey to the Gulf of Oman (Edgell, 1996). This foreland basin is adjacent to and parallel with the generally NW-SE trending Zagros Mountains, an approximately 200 - 300 km wide mountain range which is a part of the Alpine-Himalayan mountain chain that extends from Europe to south-east Asia (Hatzfeld and Molnar, 2010). The Zagros Mountains are one of the youngest fold mountain ranges on Earth, having formed from about the Oligocene - Early Miocene epoch onwards (about 35-23 Ma to the Present) as a result of the ongoing continent-continent collision between the Arabian Plate and the Iranian Block of the Eurasian Plate (Allen et al., 2004; Sherkati and Letouzey, 2004; Agard et al., 2005; Fakhari et al., 2008). Within south-west Iran, the Zagros Mountains are effectively narrower due to a structural unit known as the Dezful Embayment, a feature which effectively acts as a drainage node for the five major rivers flowing across the Khuzestan Plains (Figures 2.2, 2.12 and 2.14) (Oberlander, 1965).

2.4.2 Structural evolution of the Zagros region

These regional geological features have been determined by the relatively long and complex geological history of the convergence between the Arabian and the Eurasian lithospheric plates.

The structural evolution of the Zagros region, in general, is associated with the opening and closure of the Neo-Tethys Ocean. Prior to the formation of the southern margin of this ocean, the geology is only poorly known, due to very limited Proterozoic and early Palaeozoic rock outcrops in the Zagros, though the area appears to have been in an intra-cratonic setting. During the Neoproterozoic - Middle Cambrian (roughly 1,000 Ma - 500 Ma), strike-slip and extensional faulting affected the basin and established a structural framework of N-S trending structures that controlled the basin geometry and the subsequent deformation processes. The Hormuz Series salt basin formed at this time throughout much of the south-eastern Zagros, though deposition of halite and other evaporites in this basin most probably did not extend as far north-west as the Dezful Embayment and the study area (Sepehr and Cosgrove, 2004, Leturmy and Robin, 2010).

During the subsequent Palaeozoic there was mainly clastic sedimentation. This ceased in the Permian - Triassic (c. 300-200 Ma), with the separation of the Arabian Plate (which included the present Zagros region as its north-east margin) from the Eurasian Plate, including the rifting of an Iranian microcontinent away from the rest of south-west Iran. It is thought that the general NW-SE trending linear structural boundaries prevalent throughout much of the Zagros developed at this time, as the result of the development of normal faults (associated with crustal thinning) parallel to the previous

Figure 2.12 Overview of Zagros region structural geology

(a) Topography and structure of the Arabia-Eurasia plate collision (From Allen et al., 2004)

(b) Structural setting of the Zagros fold-thrust belt (From Sepehr and Cosgrove, 2004)

a)

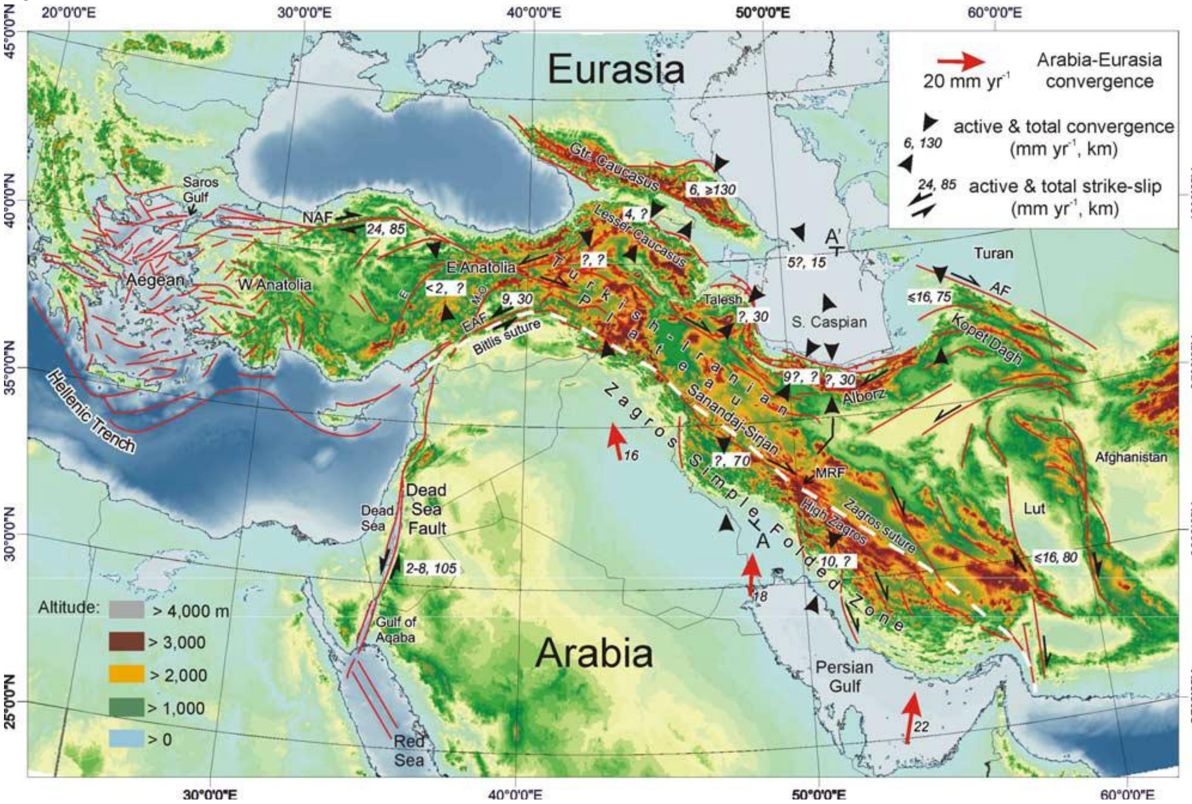

Key to Figure 2.12a

Numbers in italics indicate present shortening or slip rate in mm yr^{-1}, followed by finite shortening or strike-slip in km. Present Arabia-Eurasia convergence rates are from Sella et al. (2002). Red lines indicate main active faults, with thrusts marked by barbs.

Abbreviations: AF, Ashgabat fault; E, Ecemiş Fault; EAF, East Anatolian Fault; M-O, Malatya-Ovacik Fault; MRF, Main Recent Fault; NAF, North Anatolian Fault

b)

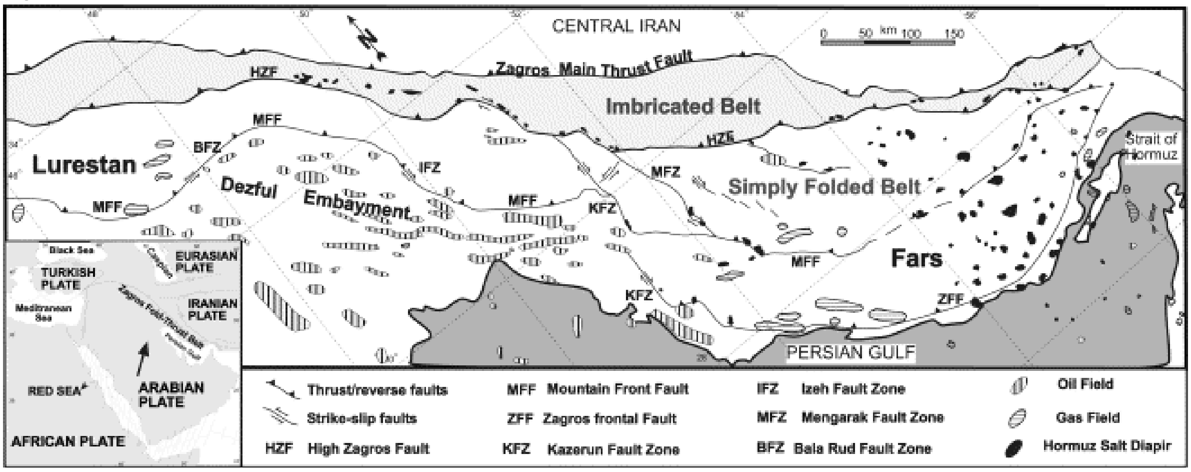

continental margin, the majority of which probably dipped towards the north-east (Berberian and King, 1981; Koop and Stoneley, 1982). This opening up of the Neo-Tethys Ocean brought about a general change from mainly clastic sediments in the Palaeozoic to mainly marine carbonate sediments during the Mesozoic and much of the Cenozoic. During the Jurassic - Early Cretaceous (c. 200-100 Ma) the basin was divided into two, with mainly shallow marine sediments in the southeast part of the Dezful Embayment and mainly deeper water sediments in the northwest. A single basin was restored in the Late Cretaceous (c. 100-66 Ma), at which time the NW-SE trend became the dominant trend of the basin (Beydoun et al., 1992; Sepehr and Cosgrove, 2004).

From the Middle Jurassic/Cretaceous to the Present there has been a convergence of the Arabian Plate and the Iranian Block of the Eurasian Plate. Until about the Oligocene - Early Miocene (c. 35-23 Ma), plate convergence was mainly by subduction of oceanic lithosphere of the Arabian Plate beneath the Iranian Block, forming metamorphic and igneous rocks along the north-east edge of the Zagros. There was a major obduction event in the Late Cretaceous (c. 100-66 Ma) on the margin of the Arabian Plate with a change of sedimentation associated with the formation of ophiolite-radiolarite nappes (or stacked thrust sheets). In the Palaeocene - Eocene (c. 66-34 Ma) the basin was divided into two basins by the Mountain Front Fault, with clastics and carbonates to the north-east, and deeper-water marls and shales to the south-west. Just prior to the closure of the Neo-Tethys ocean in the Oligocene - Early Miocene (about 35-23 Ma), shallow water conditions prevailed in the basin, with platform carbonates (mainly of the Asmari Formation) and evaporitic sediments (mainly of the Gachsaran Formation) being deposited (Sepehr and Cosgrove, 2004; Leturmy and Robin, 2010).

During the Oligocene - Early Miocene (about 35-23 Ma) there was a transition from oceanic subduction to continent-continent collision, as shown in Figure 2.13, which has continued to the present-day (Agard et al., 2005; Paul et al., 2010). From the Early Miocene (about 23-16 Ma) onwards, the Mountain Front Fault was a major structure controlling sedimentation in the basin, with mainly red beds and clastics (such as the Early Miocene Razak Formation) to the northeast and mainly marls, sands and evaporites (such as the Early Miocene Gachsaran Formation, c. 23-16 Ma) to the south-west in the foreland basin (Sepehr and Cosgrove, 2004). There was a first episode of folding in the Early Miocene during the deposition of the Gachsaran Formation evaporites (Sherkati et al., 2005). This was followed by a period of tectonic quiescence in the Middle - Late Miocene with the deposition of marls of the Middle Miocene Mishan Formation (about 16-10 Ma) and sandstones of the lower Agha Jari Formation. The main episode of folding appears to have been during the Middle Miocene to Middle Pliocene with the deposition of the sandstones of the upper Agha Jari Formation (about 10 Ma - 3 Ma for this formation as a whole). Variations in the folding appear to be mainly linked to lateral stratigraphic changes and the presence of deep-seated faults.

Figure 2.13 Schematic proposed model for the evolution of the lithospheric structure of the Zagros from (a) the onset of continental collision to (b) the present (no vertical exaggeration) (From Paul et al., 2010)
Blue and green colours relate to the Arabian Plate, orange to the Iranian Block of the Eurasian Plate. Abbreviations: ZFTB, Zagros Fold-Thrust Belt, SSZ, Sanandaj-Sirjan metamorphic Zone, MZRF, Main Zagros Reverse Fault

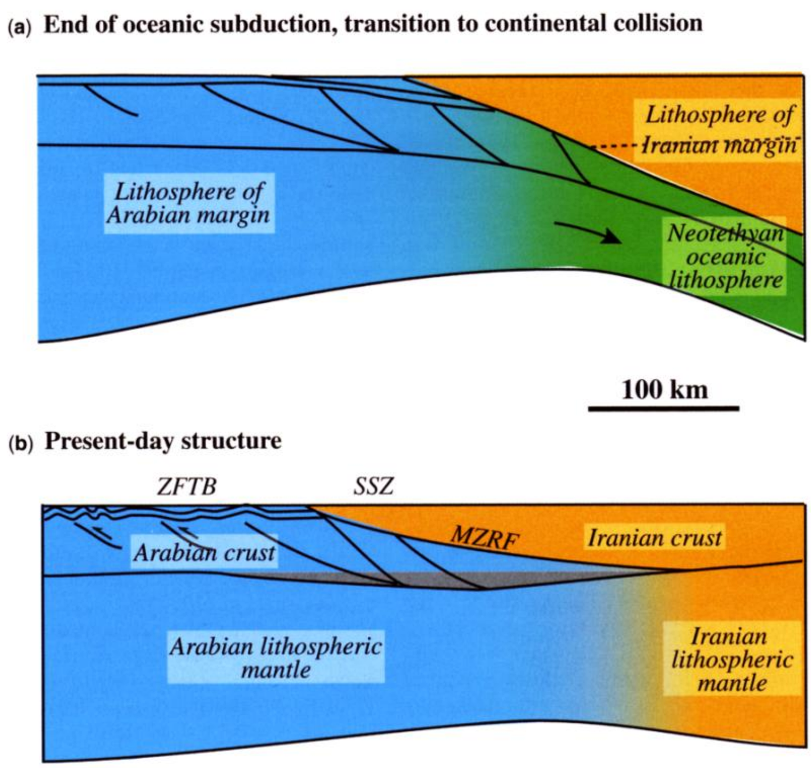

The last main tectonic event was the general involvement of deep-seated reverse basement faults during the Pliocene and Quaternary and the building of the topography of the Zagros Mountains, with deposition of the conglomerates of the Middle Pliocene - Pleistocene Bakhtyari Formation (mainly c. 3 Ma - 1 Ma in lowland south-west Iran) (Fakhari et al., 2008; Leturmy and Robin, 2010). Mainly from the Pliocene (c. 5 Ma) onwards (when there may have been a regional re-organisation of the plate collision due to the buoyancy of topographically high crust resisting further crustal thickening), there has been a migration of deformation away from the orogen towards areas of thinner crust to produce successions of thrust faults and folds on décollements in the Simple Folded Zone and in the Foreland Basin (Hessami et al., 2001a; Allen et al., 2004; McQuarrie, 2004; Sepehr and Cosgrove, 2004; Allen et al., 2011). As in other convergent fold-and-thrust belt settings, these thrust faults and folds are generally younger and less developed towards the south-west away from the orogen (Alavi, 1994; Keller and Pinter, 1996).

2.4.3 Structural zones in the Zagros region

In summary, this regional structural evolution has resulted in the broad-scale structural geology shown in Figures 2.2, 2.12 and 2.14 and the general stratigraphy of south-west Iran shown in Figures 2.15 and 2.16. The Zagros orogen in south-west Iran maintains the general NW-SE trend that was probably inherited from normal faults in the Permian - Triassic. Various sub-divisions have applied to the structure of the Zagros, and the region can be broadly sub-divided into these four NW-SE trending structural zones from the orogen in the north-east to the basin in the south-west (Figures 2.2 and 2.14):

The Sanandaj-Sirjan (or metamorphic) Zone (S-SZ)
The Imbricated Zone (or High Zagros) (IZ)
The Simple Folded Zone (SFZ) (including the Dezful Embayment)
The Mesopotamian-Persian Gulf Foreland Basin (FB) (mainly the foredeep)
(Stöcklin, 1968; Falcon, 1974; Alavi, 1994; Berberian, 1995; Hessami et al., 2001a; Blanc et al., 2003; Sepehr and Cosgrove, 2004; Abdollahie Fard et al., 2006).

2.4.4. The Sanandaj-Sirjan (or metamorphic) Zone

The *Sanandaj-Sirjan Zone* (S-SZ) is a zone approximately 50 km up to 250 km wide that is generally located to the north-east of the Main Recent Fault/Main Zagros Reverse Fault, the major strike-slip and thrust basement fault complex present along the entire length of the Zagros delineating the Arabian Plate from the Iranian Block (Khalaji et al., 2007). Some workers (such as Alavi, 1994) also include within the S-SZ some areas to the south-west of these faults. The S-SZ is comprised of mainly NW-SE trending metamorphic and igneous rocks, mostly of Mesozoic age, with some Palaeozoic rocks in the southeast (Azizi and Jahangiri, 2008). It is characterised by complexly deformed and metamorphosed rocks (especially of the greenschist facies) associated with plutons, as well as widespread Mesozoic volcanic rocks (Alavi, 1994; Haroni et al., 2000). Just

Figure 2.14 Simplified structural geological map of the central Zagros region and the study area, showing the structural zones, major faults, and major anticlines (Modified from Berberian (1995) using various sources)

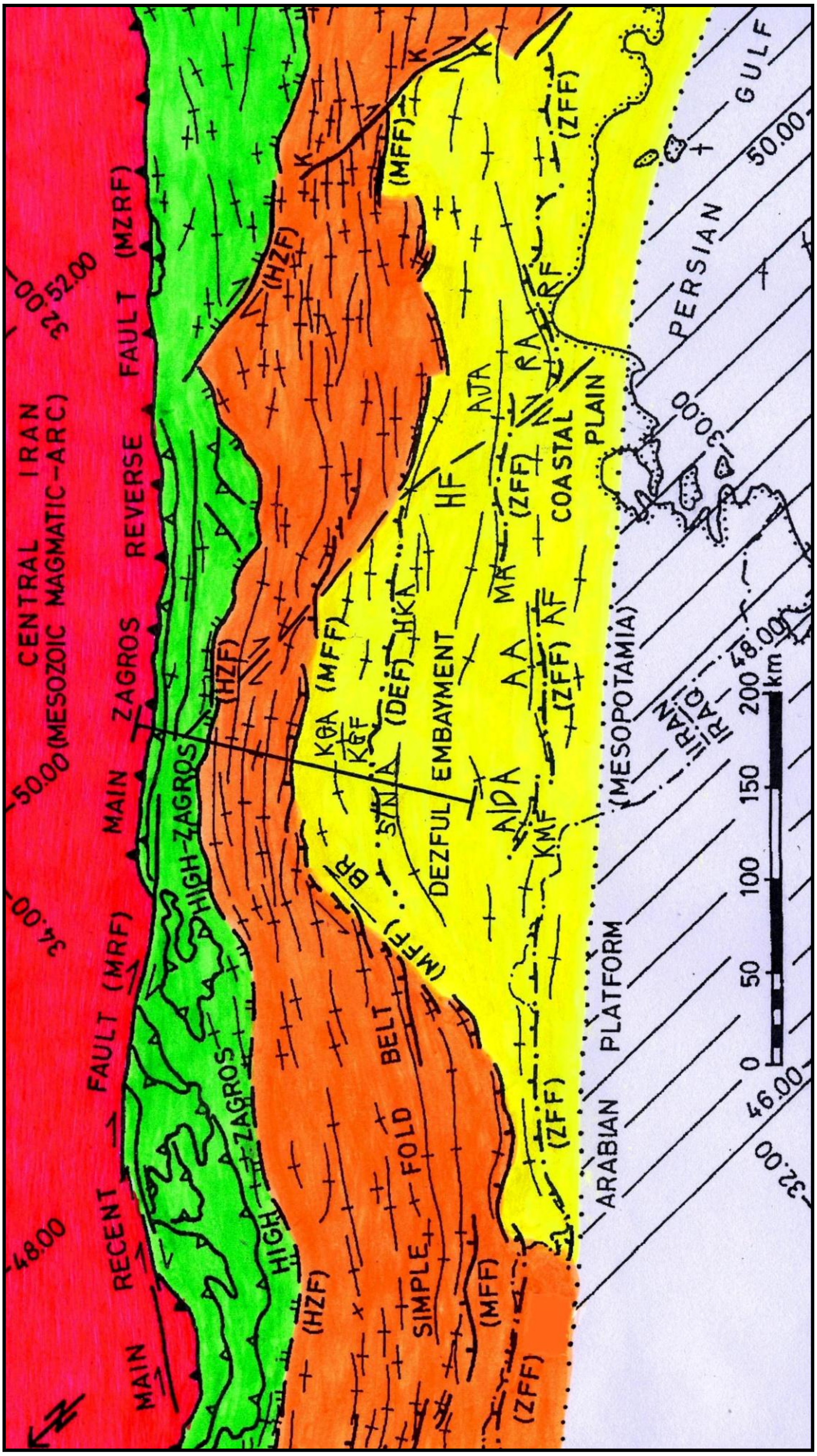

Key to Figure 2.14

Structural zones (colours)
Dark pink Central Iran (folds and faults not shown) - comprised of the Sanandaj-Sirjan (or metamorphic) Zone (S-SZ) with the Urumieh-Dokhtar Magmatic Assemblage (UDMA) to the NE
Green Imbricated Zone (or High Zagros) (IZ)
Orange Simple Folded Zone (SFZ)
Yellow Dezful Embayment
Light grey with diagonal lines Arabian Platform (only very few folds shown) - foredeep of the Mesopotamian-Persian Gulf Foreland Basin (FB)

Major faults delineating the structural zones

Main Recent Fault (MRF)
Main Zagros Reverse Fault (MRZF)
High Zagros Fault (HZF)
Mountain Front Fault (MFF)
Dezful Embayment Fault (DEF)
HF
Hendijan Fault (HF) (also known as the Izeh Fault)
K
Kazerun Fault Zone (K)
Zagros Foredeep Fault (ZFF) (delineating, within the Simple Folded Zone and Dezful Embayment, the "Zagros Foredeep" to the NE and the "Coastal Plain" to the SW)
Zagros Deformation Front (ZDF)

Other faults and folds

Thrust fault or reverse fault
Anticline

Selected faults and folds within the Dezful Embayment in the study area:
Associated with the Mountain Front Fault: BR Balarud Fault Zone (left-lateral strike slip fault zone)

Associated with the Dezful Embayment Fault:

KGF	Kuh-e Gach Thrust Fault	KGA	Kuh-e Gach Anticline
HKA	Haft Kel Anticline	S/N A	Shushtar/Naft-e Safid Anticline

Associated with the Zagros Foredeep Fault:

KMF	Kuh-e Mish Dagh Thrust Fault	A/D A	Abu ul-Gharib and Darreh-ye Viza Anticlines
AF	Ahvaz Thrust Fault	AA	Ahvaz Anticline
AJA	Agha Jari Anticline	MA	Marun Anticline
RF	Rag-e Safid Thrust Fault	RA	Rag-e Safid Anticline

Line indicates location of cross-section of Figure 2.16

Figure 2.15 Simplified stratigraphy of south-west Iran (Stratigraphic column from McQuarrie, 2004. Table based on various sources, including Veenenbos, 1958; James and Wynd, 1965; Colman-Sadd, 1978; Vita-Finzi, 1969, 1979; Kirkby, 1977; Brookes, 1982, 1989; Stöcklin and Setudehnia, 1991; Hamzepour et al., 1999; Blanc et al., 2003; Alizadeh et al, 2004; Abdollahie Fard et al., 2006; Fakhari et al., 2008)

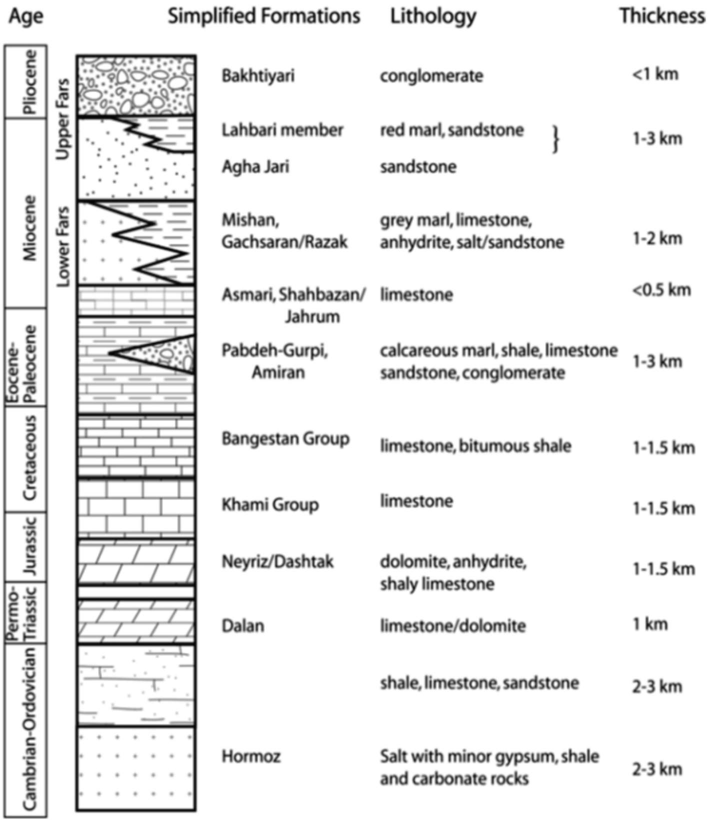

Stratigraphic group	Details of stratigraphic group
Late Quaternary fluvial deposits (see Section 2.6 for details)	"Younger fill" of Vita-Finzi (1969, 1979) and equivalents, such as "Unit IVb - Unit II" of Brookes (1982, 1989) (c. 700 AD - 1850 AD) Early - Middle Holocene fluvial aggradations, including sands and muds of "old alluvium" of Veenenbos (1958), floodplain aggradations of Kirkby (1977), "Unit V" of Brookes (1989), and post-4,500 BC Dar Khazineh area aggradations of Alizadeh et al. (2004) (c. 8,000 BC /6,500 BC - 1,500 BC /500 BC) "Older fill" of Vita-Finzi (1969, 1979) and equivalents, such as "Unit VI" of Brookes (1982, 1989) (c. 50 /38 ka - 7.3 /6.0 ka)
Passive Group	Quaternary deposits (generally unconsolidated alluvial gravels, sands and marls) Middle Pliocene - Pleistocene Bakhtyari Formation (c. 3 Ma - 1 Ma) (conglomerates, sandstones and mudstones) Middle Miocene - Middle Pliocene Agha Jari Formation (c. 10 Ma - 3 Ma) (sandstones, marls and mudstones) Middle Miocene Mishan Formation (c. 16 - 10 Ma) (marls, limestones and sandstones)
Upper Mobile Group	Early Miocene Gachsaran Formation (c. 23 - 16 Ma) (anhydrite and salt, limestones, marls and shales) (***potential major décollement***)
Competent Group	All Palaeozoic, Mesozoic and Cenozoic rocks to the top of the Oligocene - Early Miocene Asmari Formation (c. 35 - 23 Ma) (limestones and dolomites, marls, shales and sandstones). Within this "Competent Group" there are ***potential local décollements***, such as in the Triassic Dashtak Formation (c. 250 - 200 Ma)
Lower Mobile Group	Thick salt and evaporite deposits of the Neoproterozoic and Cambrian Hormuz Series (roughly 1,000 - 500 Ma) (***potential major décollement***)
Basement Group	Pre-Cambrian crystalline rocks (pre-1,000 Ma)

to the northeast of the S-SZ is the approximately 50 km wide *Urumieh-Dokhtar Magmatic Assemblage* (UDMA) (Schröder, 1944; Alavi, 1994). This can be considered to be an Andean type magmatic arc associated with subduction of oceanic lithosphere of the Arabian Plate, and is comprised of mainly Mesozoic deformed and undeformed plutons and Cenozoic (mainly Eocene) volcanics, especially lavas. (Mohajjel et al., 2003; Sepahi and Malvandi, 2008).

The headwaters of the River Dez flows across parts of the Urumieh-Dokhtar Magmatic Assemblage (Figure 2.8, R. Kamand), and the headwaters of the River Karun and the River Dez flow across the Sanandaj-Sirjan Zone (Figures 2.6 and 2.8, NE headwaters).

2.4.5 The Imbricated Zone (or High Zagros)

To the south-west of the Main Recent Fault/Main Zagros Reverse Fault complex various structural sub-divisions have been applied. One sub-division from north-east to south-west has the Imbricated Zone (or High Zagros) between the Main Recent Fault/Main Zagros Reverse Fault and the High Zagros Fault; the Simple Folded Zone between the High Zagros Fault and the Zagros Deformation Front (ZDF); and the Mesopotamian-Persian Gulf Foreland Basin as the basin undergoing subsidence to the south-west of the ZDF (Figure 2.14). In general, the intensity of the deformation progressively decreases towards the south-west from the S-SZ to the Mesopotamian-Persian Gulf Foreland Basin, and, thus, these structural zones grade into each other. There are changes at the High Zagros Fault and the ZDF (hence their use as structural boundaries), but, since the nature and location of the deep-seated major faults is debated (e.g. Alavi (2004) recognises a series of faults rather than a single Main Recent Fault or High Zagros Fault), the extent of the structural zones is quite poorly defined.

The *Imbricated Zone* (or High Zagros) is a NW-SE trending narrow thrust belt up to about 80 km wide containing highly imbricated slices of the Arabian margin and fragments of Cretaceous ophiolites. Structures include NW-SE trending thrust faults and folds (many of which are overturned), reverse faults, imbricate structures and slabs, fault blocks, “flower structures” and nappes (or stacked thrust sheets). The belt is strongly dissected by numerous reverse faults and is upthrusted to the south-west along segments of the High Zagros Fault. The Imbricated Zone is characterised by extensively deformed overthrust anticlines comprised mainly of Jurassic - Cretaceous outcrops with Palaeozoic cores along the reverse faults, Jurassic - Cretaceous limestones, obducted

Late Cretaceous radiolarite-ophiolite nappes, and Late Cretaceous - Oligocene flysch (Berberian, 1995, Blanc et al., 2003; Navabpour et al., 2010).

The Imbricated Zone essentially overthrusts the Simple Folded Zone and is topographically the highest part of the Zagros, with peaks over 4,000 m elevation. The traditional source of the River Karun is within this zone on the flanks of the Zardeh Kuh (elevation 4,548 m) and the Karun and its main tributaries flow mostly parallel to the NW-SE structures of the zone (Figure 2.6). By contrast, the source of the River Dez is upstream of this zone and the River Dez (known as the River Sehzar in this region) and its main tributaries flow mostly orthogonal to the NW-SE structures of the zone through deep, narrow gorges, such as the Tang-e Bahrein (Figure 2.8) (Oberlander, 1965).

2.4.6 The Simple Folded Zone

The *Simple Folded Zone* is a NW-SE trending belt about 200 - 300 km wide comprised of a thick sequence of simply folded sedimentary rocks (typically 6 km - 13 km thick) covering highly metamorphosed Pre-Cambrian basement rocks. The crystalline basement in the region is most probably an extension of the Proterozoic Arabian Shield which extends north-eastward to beneath the Sanandaj-Sirjan Zone (Giesse et al., 1983). The Simple Folded Zone is characterised by a series of fairly similar, NW-SE trending, simple parallel folds and associated NW-SE trending reverse and thrust faults, which are increasingly deformed and overturned towards the north-east part of the zone (Figures 2.14 and 2.16; Alavi, 1994).

2.4.6.1 Folds and faults within the Simple Folded Zone

The NW-SE trending folds form a succession of “obstacles” to the courses of the River Karun and River Dez as they flow as transverse rivers across the Simple Folded Zone from the NE and E towards the SW and W, in some cases incising across the folds in deep gorges and in other cases deflecting around them. The River Karun and its main tributaries (such as the River Khirsan) flow mostly parallel to NW-SE trending, Cretaceous (Bangestan Group) and Oligocene (Asmari Formation) Limestone anticlines (especially the vast Mungasht Anticline) and incise through them in some places in gorges (Figure 2.6). The River Dez (Sehzar) and its main tributaries (such as the River Bakhtyari) flow mostly orthogonal to the NW-SE trending, mainly Cretaceous (Bangestan Group) Limestone anticlines through deep, narrow gorges, such as that through the Kuh e- Lu’an (Figure 2.8) (Oberlander, 1965).

Figure 2.16 Possible balanced cross-section through the Dezful Embayment, Simple Folded Zone and Imbricated Zone (High Zagros) (From Blanc et al., 2003)

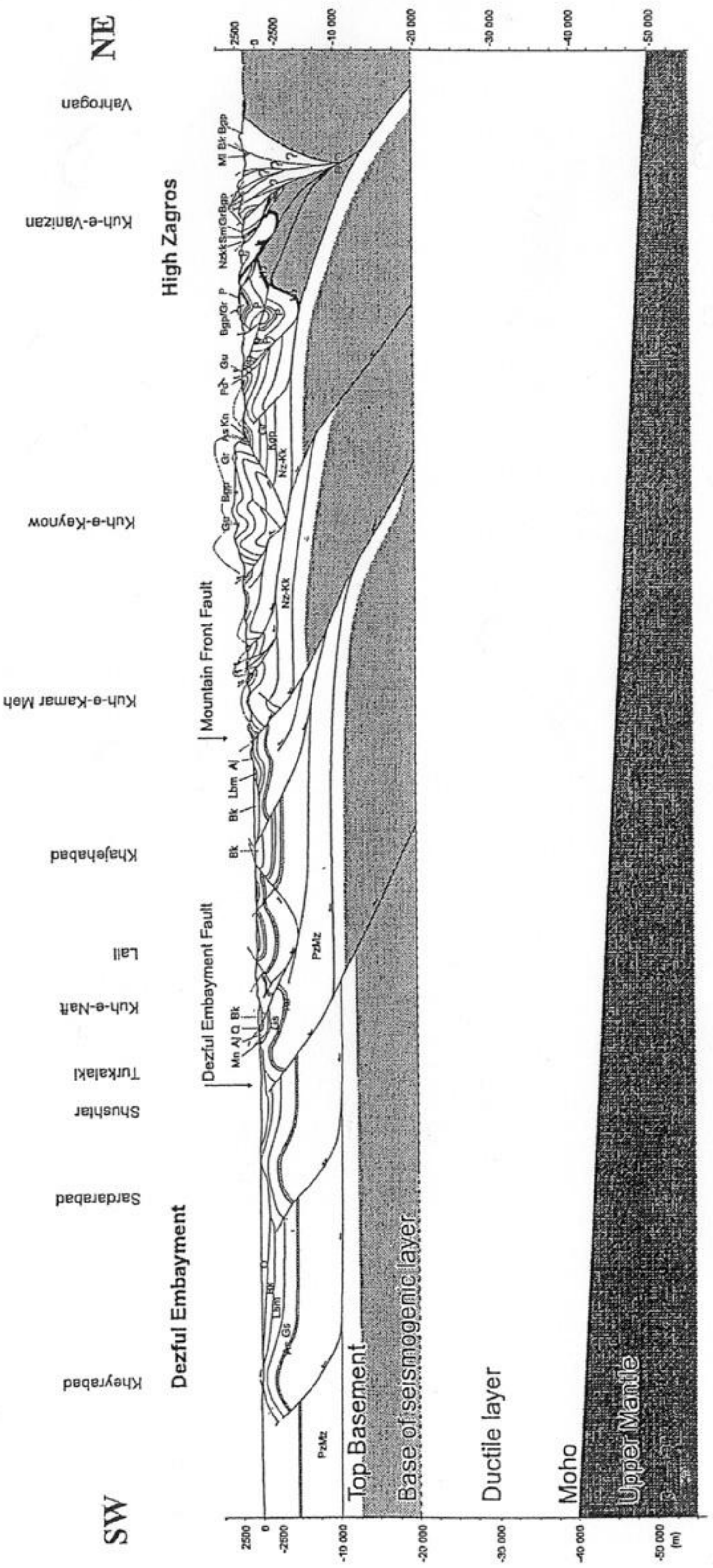

Key

Q: Quaternary
Bk: Bakhtyari
Lbm: Lahbari Member
Aj: Agha Jari
Mn: Mishan
Gs: Gachsaran
As / Light grey: Asmari Limestone
Kn: Kashkan
Pd: Pabdeh
Gu: Gurpi
Bgp: Bangestan Group
Gr: Garau
Kgp: Khami Group
Sm: Hith-Surmeh
Nz-Kk: Neyriz-Khaneh Kat
PzMz: Undivided Palaeozoic-Mesozoic
Hz / Black: Hormuz Series

Medium grey: Seismogenic basement
White: Ductile basement layer
Dark grey: Upper mantle

Bold black lines: Faults

The details of the folds and faults are debated, since with a general lack of exposed thrusts, published deep well logs and seismic profiles for the Zagros region (especially a lack of those reaching the basement), a variety of balanced cross-sections and models are plausible. Views vary from predominantly thick-skinned deformation with mainly deep-seated, basement décollements, thrust faults and associated folding (e.g. Alavi, 1994, 2004), to predominantly thin-skinned deformation with mainly shallow décollements, thrust faults and associated folding mostly within the sedimentary cover rocks (e.g. McQuarrie, 2004). For décollements, several active detachment horizons have been identified, including the Neoproterozoic - Middle Cambrian salt and other evaporites (the Hormuz Formation) (the main lower detachment), Triassic evaporites (the Dashtak Formation), Jurassic evaporates (the Gotnia Formation), Early - Late Cretaceous shales (the Gadvan, Kazhdumi and Gurpi Formations), and Miocene evaporites (the Gachsaran Formation) (the main upper detachment) (Sherkati and Letouzey, 2004; Abdollahie Fard et al., 2006; Sepehr et al., 2006). Based partly on Zagros seismicity (which indicates that larger earthquakes may be located on reverse faults with NW-SE strikes in the basement at depths of c. 5km - 15 km (Hatzfeld et al., 2010), many workers consider that the Simply Folded Zone is a combination of both thick- and thin-skinned deformation (e.g. Blanc et al., 2003; Figure 2.16). Indeed, cross-cutting structures, variations in structural style and the current seismicity of the basement indicate that there might have been an initial phase of mainly thin-skinned deformation during the Miocene - Pliocene, followed by a phase of mainly thick-skinned deformation from the Pliocene onwards (Molinaro et al., 2005; Leturmy et al., 2010).

2.4.7. The Dezful Embayment

The majority of the study area is within the major structural unit known as the *Dezful Embayment*, a unit which can be considered as a part of the Simple Folded Zone, though with its own structural framework (Sepehr and Cosgrove, 2004). In simple terms, the Dezful Embayment is an area of subdued relief and exhumation delineated by the Balarud Fault Zone and the Mountain Front Fault to the north and north-east, and by the Hendijan Fault (or Izeh Fault) and Kazerun Fault Zone to the south-east (Figure 2.14; Blanc et al., 2003; Abdollahie Fard et al., 2006). The Balarud, Hendijan and Kazerun strike-slip fault zones effectively act as oblique lateral ramps linking the various segments of the Mountain Front Fault (or Mountain Front Flexure), a major topographic front and thrust fault zone approximately coincident with both the 1,500 m - 2,000 m topographic contour and the zone of current seismicity (Sepehr and Cosgrove, 2004; Sepehr and Cosgrove, 2007). The Dezful Embayment is characterised by a lack of exposure of limestones of the Oligocene-Early Miocene Asmari Formation (except at the Kuh-e Asmari), which outcrops quite extensively around it (Blanc et al., 2003).

The origin and nature of the Dezful Embayment has been much debated. It may be related to the absence (or thinning) of the Hormuz Series salt to the north-west of the Kazerun Fault Zone, resulting in a less rapid migration of deformation away from the collision zone (and, thus, reduced relief and exhumation) within the Dezful Embayment. The Dezful Embayment has some characteristics of a foreland basin, with subsidence at the foot of the uplifting Mountain Front Fault and a thick post-Oligocene sedimentary rock sequence (McQuarrie, 2004; Sepehr et al., 2006).

2.4.7.1 Folds and faults within the Dezful Embayment

The Dezful Embayment is characterised by fairly similar, NW-SE trending, simple parallel folds and associated NW-SE trending, reverse and thrust faults, which within the Dezful Embayment generally all dip towards the north-east. As elsewhere in the Zagros, the details of these NW-SE trending folds and faults are debated, but at the ground surface they do have certain characteristics. A “typical” Dezful Embayment anticline is asymmetric at or near the ground surface, with a more steeply dipping fore-limb to the south-west (often associated with a northeast dipping reverse or thrust fault which generally does not penetrate the ground surface) and a more gently dipping back-limb to the north-east (Blanc et al., 2003; Figure 2.16). Also, these Dezful Embayment anticlines are an order of magnitude larger than structures to the north-east of the Mountain Front Fault (Sepehr et al., 2006). The folds of the area can be sub-divided into larger, asymmetric folds which are probably fault bend folds and fault-propagation folds, and smaller, more symmetrical folds which are probably detachment folds (Burberry et al., 2007, 2010). Also, it is generally agreed that within the Simple Folded Zone and Dezful Embayment, the deformation of the sedimentary cover (and, probably, also of the basement) has propagated towards the south-west with time (especially during the last 5 Ma), resulting in a succession of progressively younger and less developed folds towards the south-west, all the way to the Zagros Deformation Front (ZDF) where the folds die out (Haynes and McQuillan, 1974; Hatzfeld et al., 2010).

The main exceptions to the loose relationship of younger, less developed folds towards the south-west within the study area are the large, older folds (such as the Ahvaz Anticline) associated with "out of sequence" thrusts and reverse faults. Opinions vary (e.g. Alavi, 2004; McQuarrie, 2004), but there are probably a number of basement master "blind" thrust fault complexes, which for the region of the study may include: the Main Recent Fault/Main Zagros Reverse Fault, the High Zagros Fault, the Mountain Front Fault, the Dezful Embayment Fault and the Zagros Foredeep Fault (Berberian, 1995). These basement master "blind" thrust faults have limited surface expression. Within the study area, the Dezful Embayment Fault is probably associated with the Kuh-e Gach Thrust Fault, and with the Kuh-e Gach, Haft Kel, Shushtar and Naft-e Safid and Anticlines. Also, within the study area, the Zagros Foredeep Fault is probably associated with the Kuh-e Mish Dagh Thrust Fault and Abu ul-Gharib and Darreh-ye Viza Anticlines, the Ahvaz Thrust Fault and Anticline, the Agha Jari Thrust Fault and Anticline and Marun Anticline, and the Rag-e Safid Thrust Fault and Anticline (Figures 2.14 and 4.1 (a)).

Other tectonic features present within the study area include: deep-seated structural lineaments oriented approximately N-S and E-W, such as the "concealed fault/ deep-seated lineament" oriented E-W at about 31°47'N (Figure 4.1 (a); NIOC, 1977), and strike-slip faults and possibly oblique lateral ramps, many of which follow the general N-S structural trend of the Late Proterozoic - Middle Cambrian framework and the major lineaments in the adjacent Arabian Platform (Berberian, 1995; Edgell, 1996). One major N-S trending strike-slip fault in the eastern part of the study area is the Hendijan Fault (Figures 2.2 and 2.14), though it may not be currently seismically active (Hessami et al., 2001b; Bahroudi and Talbot, 2003). Also, there may be a slight general tectonic tilt of the Simple Folded Zone and Dezful Embayment towards the south-west, due to a regional, NW-SE trending "geo-flexure" with a hinge-line along the mountain front (Falcon, 1961) and a probable regional propagation of both shallow and basement deformation towards the south-west since about 5 Ma (Hatzfeld et al., 2010). In general, it is the folding (and to a lesser extent, the tilting) rather than the faulting that is most likely to influence the major rivers, since the majority of the faulting in the region does not break the ground surface. Indeed, no co-seismic surface ruptures have been observed in all studies in the Zagros region over the last fifty years or more, except for one Magnitude 6.4 earthquake in 1990 AD, located at the eastern termination of the High Zagros Fault (Walker et al., 2005).

2.4.8 The Mesopotamian-Persian Gulf Foreland Basin

The NW-SE trending folds die out at the Zagros Deformation Front, so that immediately to the south-west there is the *Mesopotamian Foredeep* of the subsiding *Mesopotamian-Persian Gulf Foreland Basin* (Figure 2.14). In the study area, this basin region is part of the East Arabian Block of the Arabian Platform, which is characterised by mainly N-S trending lineaments, uplifts and anticlines, of which the Dorquain Oilfield Anticline is an example (Figure 4.1 (a); Bahroudi and Talbot, 2003; Abdollahie Fard et al., 2006; Maleki et al., 2006). The Arabian Platform is considerably less seismically active than the Zagros and, correspondingly, these structures are generally propagating more slowly with, for instance, growth rates of about 0.01 mm yr^{-1} for deep-seated salt structures in the Persian Gulf (Edgell, 1996; Soleimany et al., 2011).

Figure 2.17 Geological cross-section of the Persian Gulf Basin (From Edgell, 1996)

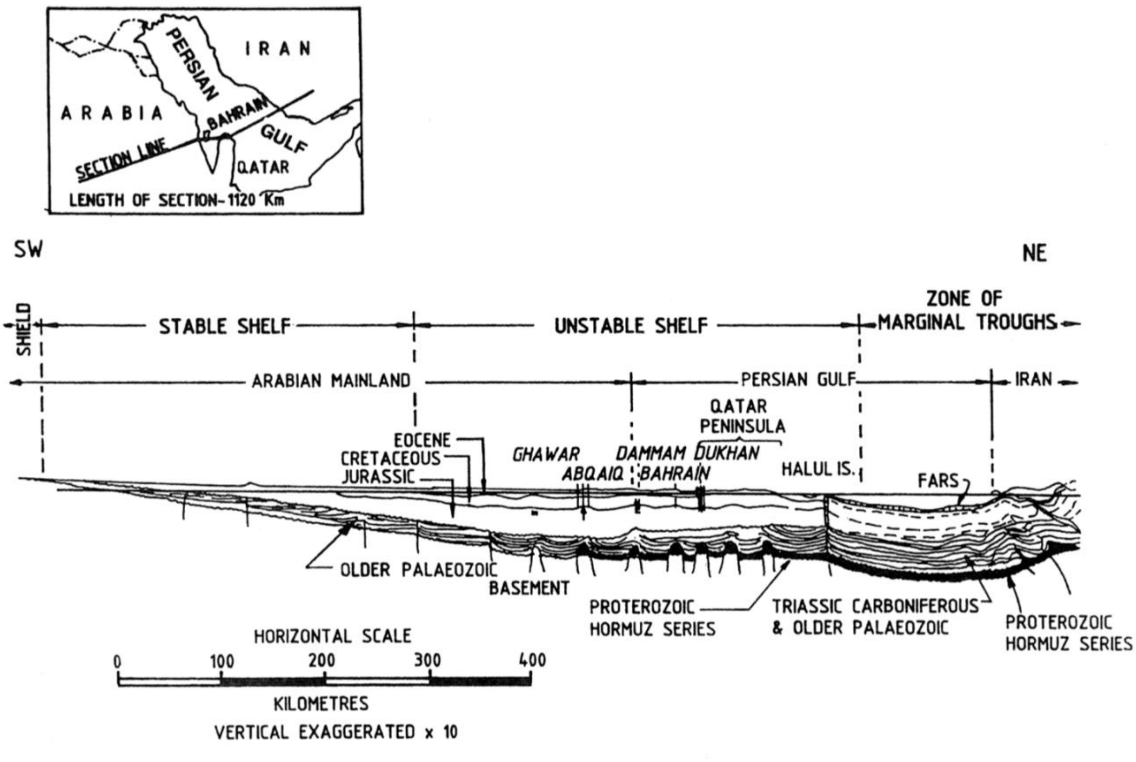

As described in Section 1.5, a foreland basin is a large system that can be considered to consist of a wedge-top, foredeep, forebulge and back-bulge depozones. For the Mesopotamian-Persian Gulf Foreland Basin, which is a peripheral foreland basin, the Dezful Embayment and much of the Simple Folded Zone can be considered to be the wedge-top, the main trough of the Mesopotamian Plain and the Persian Gulf to the south-west of the Zagros Deformation Front is the prominent foredeep, the Great Pearl Bank Barrier in the southern Persian Gulf is part of the slight forebulge, and the back-bulge is largely absent (DeCelles and Giles, 1996). The foreland basin can be considered to extend a long way into Arabia, as shown on Figure 2.17 (Edgell, 1996). There are some long transverse rivers, notably the River Karun and River Dez which interact with the folds of the wedge-top, and there is sediment export down-system by the River Tigris and River Euphrates longitudinal trunk rivers (Vergés, 2007). Hence, the Mesopotamian-Persian Gulf Foreland Basin can be considered to be an *"overfilled" basin*, especially within Mesopotamia and the areas to the north-west of Mesopotamia (Crampton and Allen, 1995; Jordan, 1995; DeCelles and Giles, 1996; Allen et al., 2013). It probably has a regime of mainly erosional unloading and associated basement isostatic uplift within both the active thrust front and the proximal foreland (Burbank, 1992; Burbank and Anderson, 2012).

2.5. Earth surface movements in the study area

2.5.1 Rates of convergence and shortening

The convergence of the Arabian Plate towards the Eurasian Plate is currently continuing in an approximately N-S direction (NNW-SSE in the northern Zagros to NNE-SSW in the southern Zagros) at rates of about 16 to 22 mm yr^{-1} (about 18 mm yr^{-1} in the study area of the Dezful Embayment), according to the GPS-based global plate motion model of Sella et al. (2002) (Allen et al., 2004; Figure 2.12a). The convergence rate increases towards the east because the pole of rotation for Arabia-Iran lies within the eastern Mediterranean region (Jackson and McKenzie, 1988; Allen et al., 2011).

This plate convergence is accommodated by a number of mechanisms, including: motion of neighbouring regions (such as NW Iran and the Alborz Mountains), various strike-slip faults (such as the Main Recent Fault in the northern Zagros and the Kazerun Fault in the southern Zagros), rotation of basement blocks in the southern Zagros, and motion of the many NW-SE trending folds and thrust faults throughout the Zagros (Hessami et al., 2001b; Tatar et al., 2002; Vernant et al., 2004). The present-day rate of N-S shortening that is accommodated by the Zagros mountain belt has been determined by different methods to be approximately 10 mm yr^{-1}. Geodetic measurements using

GPS across central Iran indicate shortening of about 4 to 10 mm yr^{-1} across the central Zagros mountain belt (Tatar et al., 2002; Vernant et al., 2004; Masson et al., 2005, Hatzfeld et al., 2010). Geomorphological and geological observations in the central Zagros suggest a shortening rate of about 10 to 14 mm yr^{-1} (an estimate of 50 km to 70 km of shortening since about 5 Ma) (Falcon, 1974; McQuarrie, 2004). Reconstructions of velocity vectors between Eurasia-Arabia-Iran based on earthquake focal mechanism slip vectors indicate approximate shortening rates of about 10 to 15 mm yr^{-1} (Jackson and McKenzie, 1988).

2.5.2 Seismic and aseismic movements

The *seismic* energy release calculated from earthquakes in the Zagros in the 20th Century AD can only account for a small part (about 10 % - 20 % at most) of the total deformation required by the convergence of the Arabian and Eurasian plates, though it could account for the deformation if the velocity field had larger absolute magnitudes. Hence, it is likely that much of the movement (probably c. 95 %) on folds and faults in the Zagros is by *aseismic* folding, faulting and stable creep (probably due to lubricated décollements on evaporite layers), or by other mechanisms such as "silent" or "slow" earthquakes (Beroza and Jordan, 1990), pressure solution and granular dislocations. The aseismic folding and faulting may be similar in style, orientation and distribution to that released seismically in earthquakes (Jackson et al., 1995; Masson et al., 2005; Hatzfeld et al., 2010). This is a feature of the study area which aids in elucidating the responses of major rivers to active tectonic uplift. With mainly gradual, aseismic movements of folds in the study area, it is likely that the time lags between Earth surface movements and river responses will be relatively short, probably resulting in closer relationships between tectonics and river characteristics.

2.5.3 Rates of active uplift and subsidence

Rates of active uplift and subsidence in the study area in south-west Iran are only very poorly known. To the north-east of the Zagros Deformation Front, there is regional uplift. Approximate indicators of general, long-term rates of uplift vary from about 0.2 mm yr^{-1} for the eastern Persian Gulf coast derived from Quaternary marine terraces (Reyss et al., 1998) to about 1 mm yr^{-1} for the central Zagros derived from geomorphological and geological observations (Falcon, 1974). In the neighbouring Fars region to the east of the Kazerun Fault Zone, rates of uplift of folds derived from incised terraces of the Dalaki and Mand rivers are about 0.2 to 3.2 mm yr^{-1} (Oveisi et al., 2008), and similar rates might be expected within the Dezful Embayment.

To the south-west of the Zagros Deformation Front, there is regional subsidence. In general, this is manifest by the deposition of river sediments in the Mesopotamian Plains and the Persian Gulf, particularly in marshes such as the Shadegan marshes (for the River Jarrahi), the Huwayzah marshes (for the River Karkheh) and the Hammar marshes (for the River Euphrates) (Baltzer and Purser, 1990). Also, more localised flooding of irrigation canals of the Sassanian Period (c. 224 - 651 AD) and Abbasid Period (c. 750 - 1258 AD) near to the present-day Khor Zubair (Iraq) and Khor-e Musa (Iran) tidal embayments, was interpreted as being due to tectonic subsidence by Lees and Falcon (1952). However, any evidence or data for rates of tectonic subsidence are very uncertain, due to complexity with other factors such as extensive sediment compaction, relative sea-level changes, and delta and coastline retreat and advance, which appear to have had greater influences on vertical movements. Indeed, using a variety of evidence, including Late Pleistocene and Holocene sediments from submarine platforms and borings from the Mesopotamian delta and the Persian Gulf (Figure 2.18), various workers (e.g. Purser, 1973; Larsen and Evans, 1978) considered an absence of major tectonic movements in that area during the Late Pleistocene and Holocene.

To the south-west of the Zagros Deformation Front, there a number of oil and gas fields (such as the Dorquain Oilfield). These are mainly NNW-SSE, N-S, NNE-SSW and NE-SW trending anticlines with reservoir rocks of Early Cretaceous limestones, such as those of the Early Cretaceous Fahliyan Formation, which may just be emerging on the land surface or sea-floor (Edgell, 1996; Maleki et al., 2006). There is some evidence that these anticlines may have undergone renewed faster growth during the Late Miocene - Present. Nevertheless, from evidence such as that from the Dorood Anticline in the north-west Persian Gulf, it is likely that fold uplift rates are still probably low in absolute terms, at around 0.024 mm yr^{-1} (Soleimany et al., 2011).

2.6 The Late Quaternary of south-west Iran

The stratigraphy, geomorphology and structural development of south-west Iran during the Quaternary are only very poorly known. With many Pleistocene sediments unexposed and unstudied, south-west Iran is still largely part of the “Blank on the Pleistocene map” described by Farrand (1979). Quaternary sediments in lowland south-west Iran are mainly fluvial deposits, with some aeolian deposits and significant deltaic, coastal and shallow marine deposits in Lower Khuzestan (Heyvaert et al., 2013).

For the Late Quaternary, a broad, loosely defined, two-fold fluvial aggradation sequence separated by erosion and river incision, was recognised in pioneering research in western and southern Iran (Figure 2.15; Vita-Finzi, 1969, 1979). The “Older fill” (c. 50 /38 ka - 7.3 /6.0 ka) of mainly alluvial fan/bajada gravels was probably deposited in a cold, fairly dry climate. The “Younger fill” (c. 700 AD -1850 AD) of mainly fluvial sands and muds (Vita-Finzi, 1969, 1979), was probably deposited during a southward shift of Mediterranean winter cyclone tracks associated with the “Neoglacial” (Rieben, 1955; Vita-Finzi, 1976). This sub-division only applies as a general pattern, and, for instance, Vita-Finzi (1969) found gullying and erosion followed by subsequent infilling of the “Older fill” at several locations. Brookes (1982, 1989) working in the Qara Su basin just to the north of the study area, found an alluvial sequence with a similar two-fold aggradation. An equivalent of the “Older fill” appeared to be “Unit VI” (assigned to the terminal Pleistocene by stratigraphic position and degree of calichification), comprised of cobbly alluvial fan gravels. An equivalent of the “Younger fill” appeared to be “Unit IVb - Unit II” (c. 850 AD/1600 AD - 1850 AD), comprised of silty sands and silty clays (Brookes, 1982, 1989) (Figure 2.15).

In addition to this, Early - Middle Holocene fluvial aggradations of sands and muds have been found in the upper plains of south-west Iran (Figure 2.15). In the Qara Su basin, Brookes (1989) found “Unit V” (c. 5,500 - 3,000 BC) comprised of reddish-brown muddy sands and silts. Kirkby (1977) found that aggradations of the rivers Karun and Karkheh (in the Khuzestan Plains) and the rivers Dawairij and Mehmeh (in the Deh Luran Plain) (Figures 2.7 and 2.15) were surprisingly synchronous, and concluded that aggradations of up to 5 m thickness had taken place in south-west Iran from c. 8,000 BC/ 6,500 BC to c. 1,500 BC/ 500 BC. In addition, the soil survey of Veenenbos (1958) in the Dezful area subdivided alluvial soils into those formed on “old alluvium”, “younger alluvium”, and “young alluvium”. Archaeological surveys of the Susiana Plain showed that Village Period sites (c. 7,000 - 4,000 BC) were biased towards being located on the “old alluvium”, rather than being buried beneath it. Hence, the “old alluvium” was probably an Early - Middle Holocene fluvial aggradation, for which deposition had ceased prior to c. 6,000 BC (Kouchoukos and Hole, 2003). In the Khuzestan Plains, Alizadeh et al. (2004) recorded some fluvial aggradations, including

Figure 2.18 The Late Quaternary stratigraphy of the Tigris-Euphrates-Karun delta region, from borings (From Larsen and Evans, 1978)

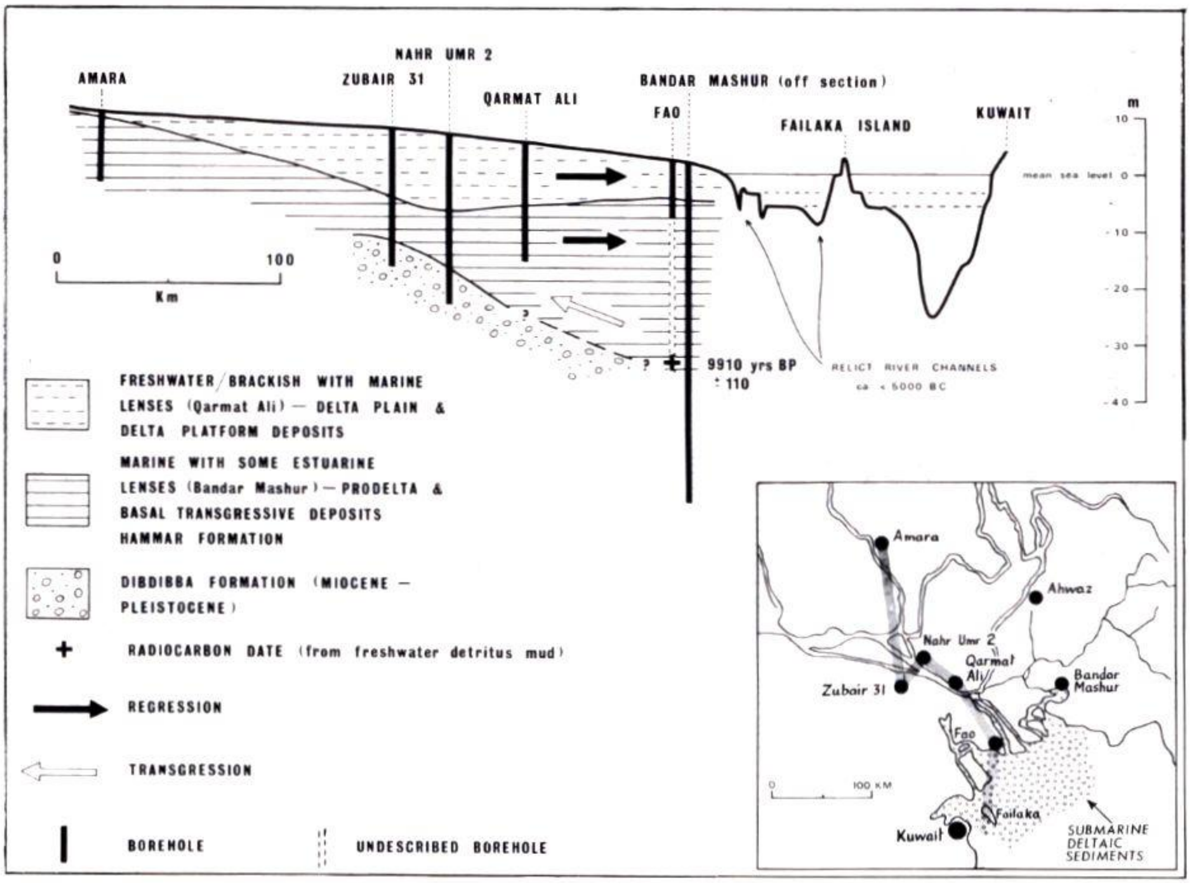

some in the Dar Khazineh area on the Mianab Plain approximately dated to post- 4,500 BC, which are probably also a part of this group of aggradations (Figure 2.15).

For the south-western Khuzestan Plains and Tigris-Euphrates-Karun delta region, the general Late Quaternary stratigraphy is shown in Figure 2.18. Typically, gravels and sands of the Late Miocene to Pliocene/Pleistocene Dibdibba Formation are unconformably overlain by marine, estuarine and deltaic silts and sands of the Holocene Hammar Formation associated with the sea-level transgression from the Last Glacial Maximum (c. 20,000 BC) to the probable Middle Holocene highstand (c. 6,000 BC - 3,500 BC) and the probable slight regression of c. 3,500 BC - 500 BC (Section 2.7; Lambeck, 1996). These are overlain by Middle - Late Holocene delta and floodplain silts, clays, and aeolian sands from the subsequent progradation of the coastline and the Tigris-Euphrates-Karun delta (Larsen and Evans, 1978; Aqrawi et al., 2006). The stratigraphic sequence in this area, with mostly very young Late Holocene surface sediments, is mainly the product of changes in relative sea-levels, the coastline and the delta (Purser, 1973; Heyvaert and Baeteman, 2007; Heyvaert et al., 2013).

2.7 Persian Gulf relative sea-level changes

2.7.1 Relative sea-level changes since the Last Glacial Maximum

Since the time of the Last Glacial (Marine oxygen Isotope Stage 2) (Lowe and Walker, 1997), changes in Persian Gulf relative sea-levels have been mainly associated with changes in eustatic (or global) sea-levels; especially the very large rise in eustatic sea-levels associated with the meltwater of the last deglaciation, as shown in Figure 2.19 (Stanford et al., 2011). During the Last Glacial Maximum (LGM) (c. 20,000 BC - 15,000 BC) sea-levels in the Persian Gulf, like global sea-levels, were very low at about $^{-}130$ m/$^{-}120$ m (Lambeck, 1996; Fleming et al., 1998; Stanford et al., 2011). At this time the Persian Gulf was mostly dry out to the Biaban Shelf in the Gulf of Oman and longitudinal rivers, such as the “Ur-Schatt River”, flowed along the axis of the present-day Persian Gulf. From the LGM onwards, and especially from c. 12,000 BC onwards when the Strait of Hormuz opened as a narrow waterway, there was a rapid rise in relative sea-levels, with an accompanying north-west migration of the head of the Persian Gulf (Lambeck, 1996; Kennett and Kennett, 2006; Smith et al., 2011). The details are debated, but this rise in relative sea-levels probably continued (with ^{14}C-dated submarine benches possibly indicating very short standstills within an interval of c. 11,000 BC - 8,000 BC (Sarnthein, 1972; Lambeck, 1996)) until sea-levels in the Persian Gulf sea-levels peaked at around 6,000 BC - 3,500 BC, as is typical for many “far-field sites” that are large distances from the polar ice sheets (Lambeck, 1996; Fleming et al., 1998; Woodroffe, 2003; Milne and Mitrovica, 2008; Stanford et al., 2011).

From roughly 6,000 BC onwards, changes in Persian Gulf relative sea-levels have been mainly associated with local isostatic effects related to the load of water in the Persian Gulf creating downwarping of the outer parts of the shelf and uplift of the shoreline (Lambeck, 1996; Woodroffe, 2003; Sanlaville and Dalongeville, 2005) (see Section 5.1.2.1). Holocene relative sea-level curves for the northern Persian Gulf have been constructed (Dalongeville and Sanlaville, 1987; Sanlaville, 1989; Lambeck, 1996), with some small-scale low-stands and high-stands of uncertain validity when the different areas of the Persian Gulf and the different settings of the relative sea-level indicators used are considered (Heyvaert and Baeteman, 2007). Nevertheless, there is fairly extensive evidence that highest relative sea-levels of about $^{+}1$ m to $^{+}3$ m in the northern Persian Gulf were reached about 6,000 BC - 3,500 BC, followed by a slight relative sea-

Figure 2.19 Eustatic sea-level curves for the last deglaciation (c. 20,000 BC - Present) (From Stanford et al., 2011)
a) The North Greenland Ice Core Project $\delta^{18}O$ record (on the GICC05 timescale)
b) Reconstructed sea-level curve, with the modelled sea-level probabilities shown alongside the data used to construct the Monte Carlo simulations
c) Rate of sea-level change (first derivative of the reconstructed sea-level change)
(In panels b) and c), 100 of the simulations are shown in light grey)
Since individual sea-level proxy records are all affected by local isostatic adjustments and depth and age uncertainties, these curves were constructed using a Monte Carlo style statistical analysis (using a 6 m coral depth uncertainty) to determine the highest-probability sea-level history from six key "far field" deglacial sea-level records.

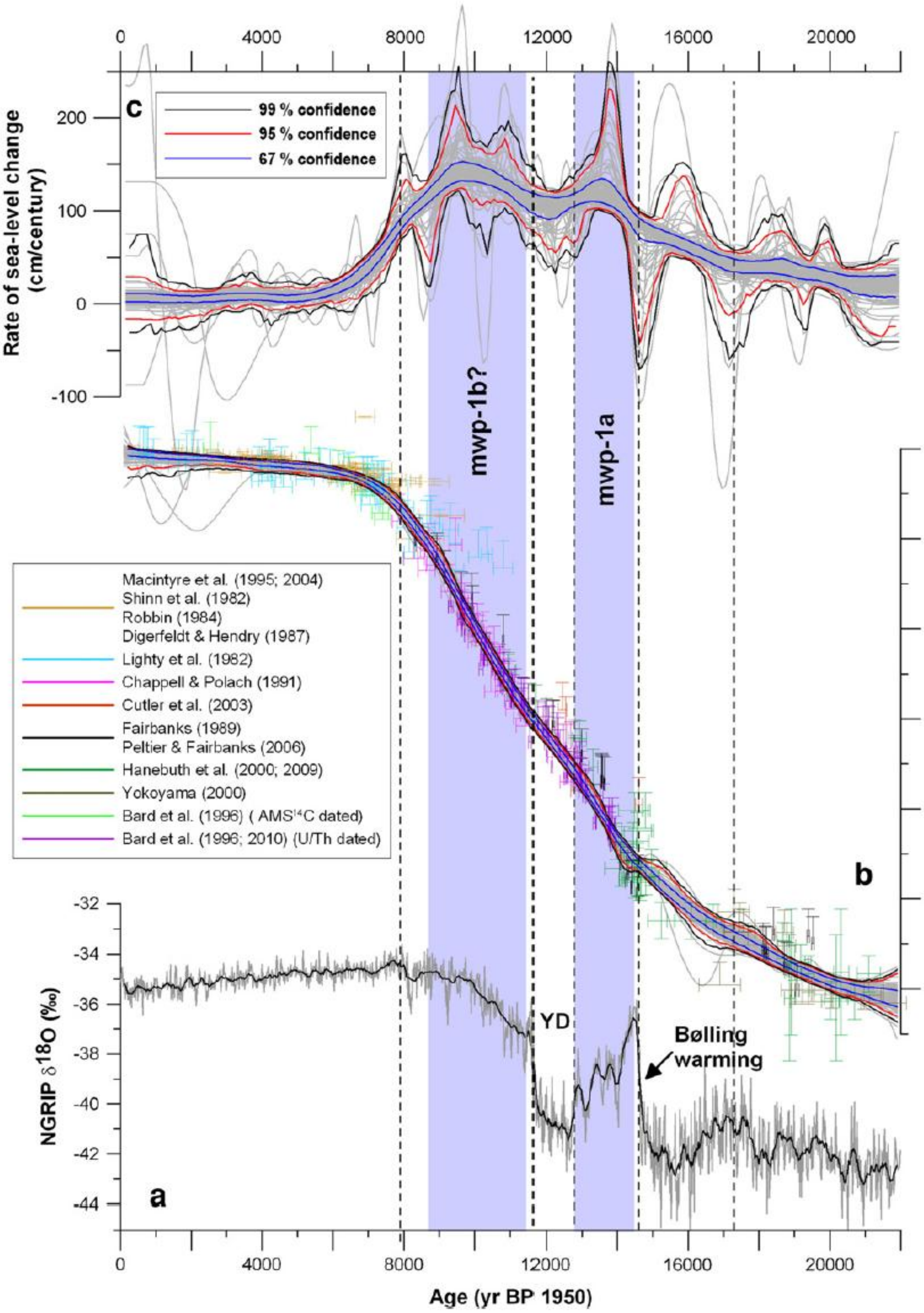

Key to Figure 2.19

mwp-1a meltwater pulse 1a (fairly short interval of high rates of sea-level rise)
mwp-1b? meltwater pulse 1b (longer interval of high rates of sea-level rise, existence has been debated)
YD Younger Dryas (short interval of cold climatic conditions)

---

level fall from about 3,500 BC - 550 BC, after which relative sea-levels have been very similar to that of today (Larsen and Evans, 1978; Cooke, 1987; Dalongeville and Sanlaville, 1987; Sanlaville, 1989; Lambeck, 1996; Reyss et al., 1998; Pournelle, 2003; Gasche et al., 2004, 2005). Such a pattern is often found in the Holocene for "far-field sites" (Fleming et al., 1998; Woodroffe, 2003; Kemp et al., 2011; Section 5.1.2.1). All of these changes in Persian Gulf relative sea-levels were principally due to glacio-hydro-isostatic effects and the effects of coastal tectonic movements were probably slight (Lambeck, 1996; Reyss et al., 1998).

From investigations of Holocene sediments in the Lower Khuzestan Plains using hand-operated cores and very limited outcrops, Heyvaert and Baeteman (2007) considered that both the Middle Holocene highstand of around 6,000 BC - 3,500 BC and the subsequent relative sea-level fall probably did not occur. Heyvaert and Baeteman (2007) based this assertion mainly on findings of very recent tidal and brackish-freshwater deposits near Bostan in Lower Khuzestan directly overlying the pre-transgressive surface at levels of $^{+}2$ m to $^{+}3$ m, and an absence of tidal deposits with an age of around 4,000 BC in southern parts of the Lower Khuzestan Plains. Whether this assertion is correct or not, the results of excellent multi-disciplinary investigations permitted fairly detailed reconstructions of the coastal environmental settings, as shown in Figure 2.20 (a-g). In general, these reconstructions indicate tidal flats and coastal sabkha over the south-west of the Lower Khuzestan Plains from c. 6,000 BC to c. 550 BC, and delta and coastline progradation from c. 550 BC onwards (Heyvaert and Baeteman, 2007; Heyvaert et al., 2013).

Key to Figure 2.20 (a-g)

Modern towns

B (on R. Karkheh)	Bostan	**B** (on Shatt el-Arab)	Basra
B (on Khawr-Musa)	Bandar-e Imam Khomeini		
H Hawiza		**K** Khorramshahr	
S (on R. Karkheh)	Susangerd	**S** (on R. Jarrahi)	Shadegan

Figure 2.20 (a-c) Reconstructions of the environmental setting of the Lower Khuzestan Plains from about 6,000 BC to about 3,000 BC (From Heyvaert and Baeteman, 2007)

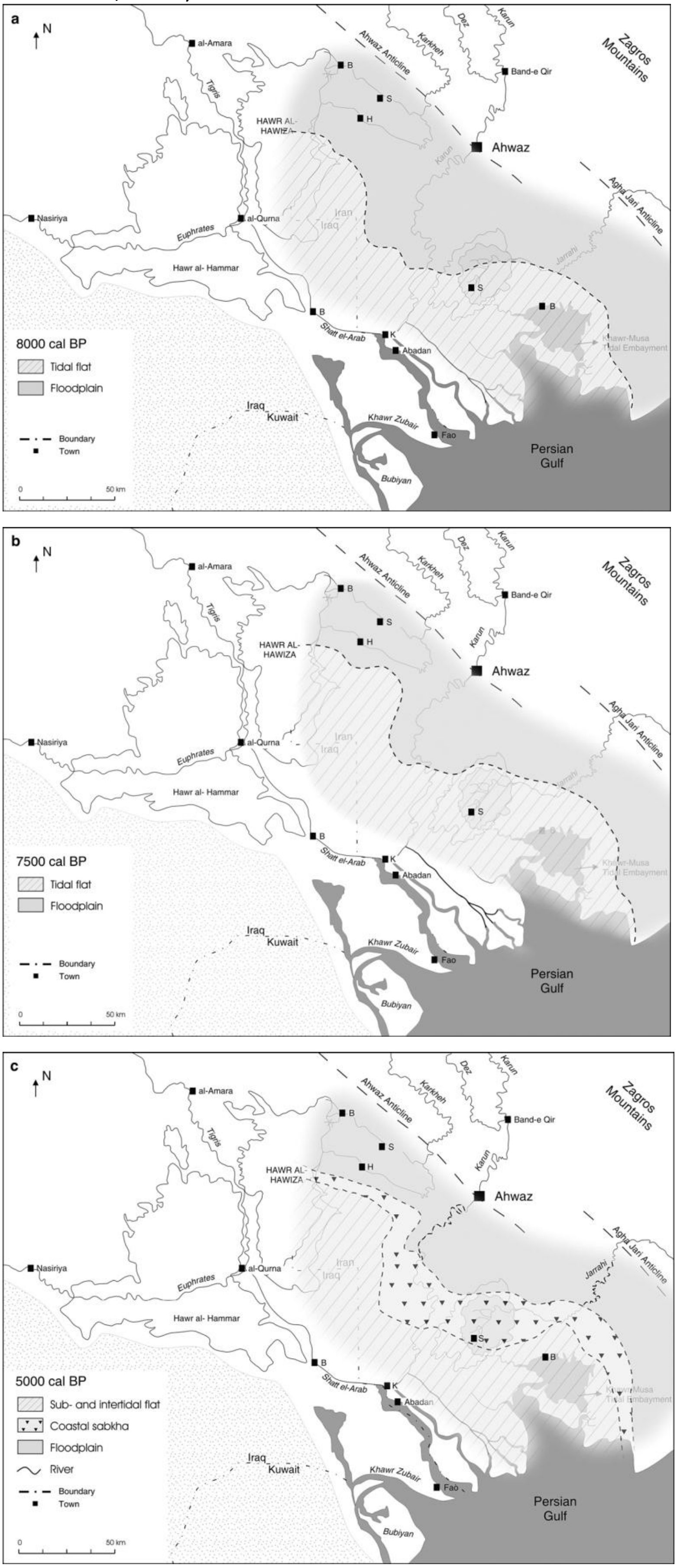

Figure 2.20 (d-f) Reconstructions of the environmental setting of the Lower Khuzestan Plains from about 550 BC to about 710 AD (From Heyvaert and Baeteman, 2007)

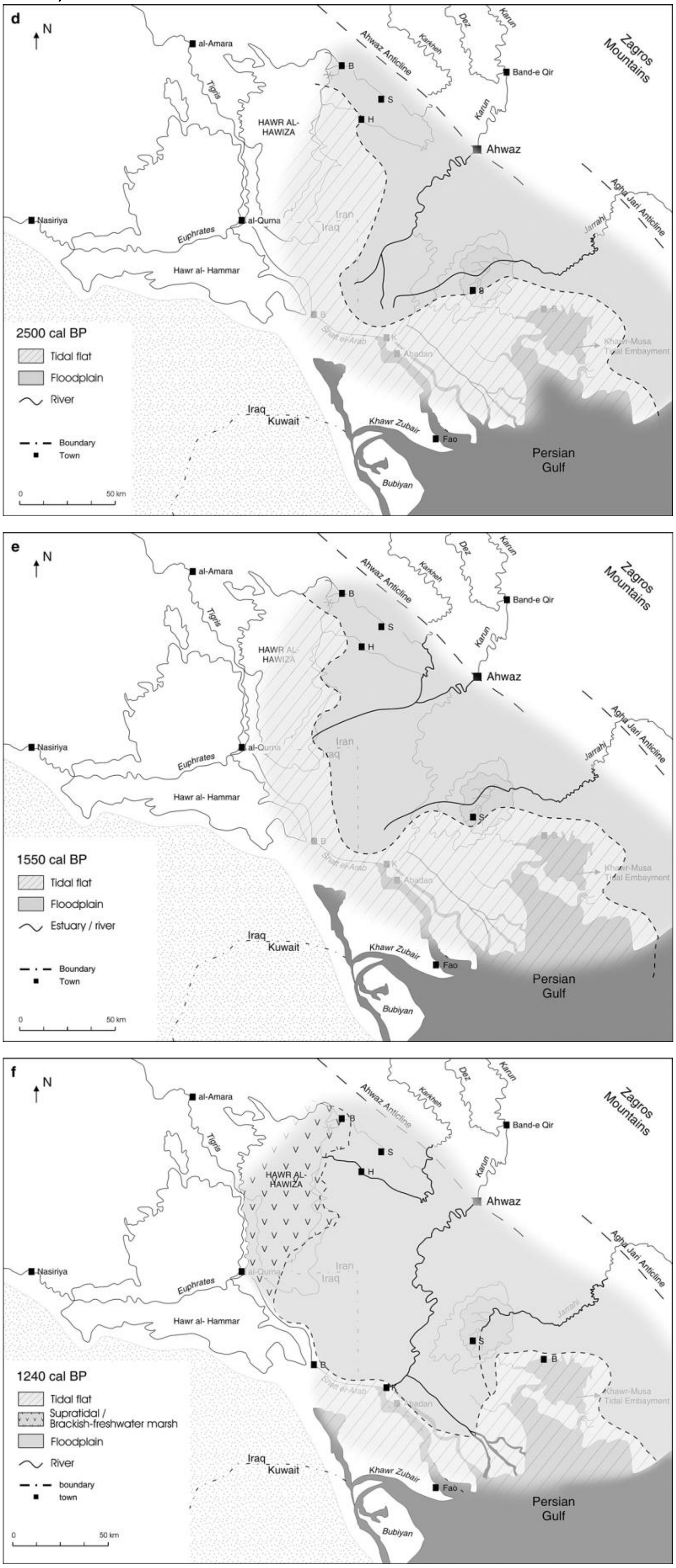

Figure 2.20 (g) Reconstruction of the environmental setting of the Lower Khuzestan Plains at about 1500 AD (From Heyvaert and Baeteman, 2007)

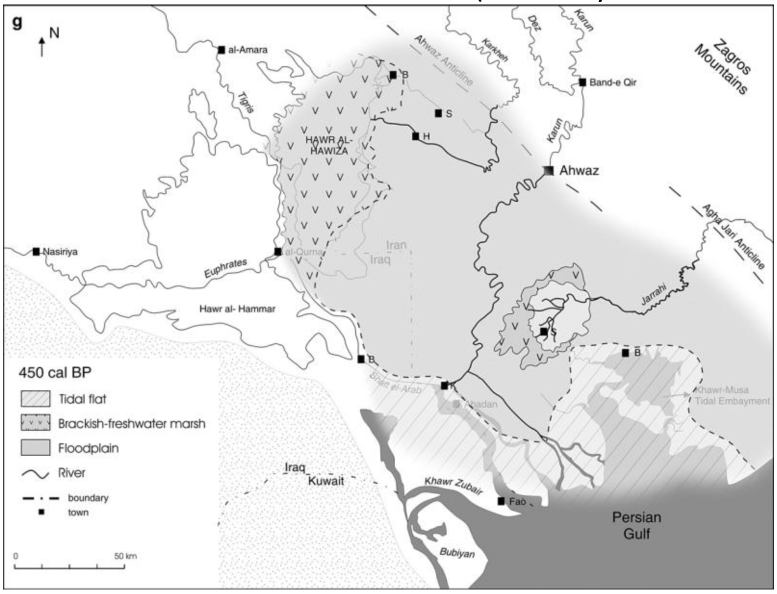

2.7.2 Influences of relative sea-level changes on the major rivers of south-west Iran

In the Upper Khuzestan Plains, the changes in Persian Gulf relative sea-levels and coastline will not have had significant influences on the major rivers, due to the long distances from the sea (more than 150 km from the shoreline (Shanley and McCabe, 1993)). For the River Karun in the Upper Khuzestan Plains, base-level is effectively the rapids in the vicinity of the “Band of Ahvaz” where the River Karun flows across the Ahvaz Anticline (Figure 6.3), and not relative sea-level. This is because this series of rapids, with a total fall of the river water surface of about 2.5 m due to the greater erosion resistance of exposures of Agha Jari Formation bedrock and uplift of the Ahvaz Anticline, effectively “decouples” the River Karun upstream of Ahvaz from the effects of coastal changes (Appendix 6.1; Kirkby, 1977). Also, there are no River Karun bed elevations upstream of the Ahvaz rapids (deepest channel bed scour at the Ahvaz rapids is $^{-}$0.07 m NCC, with many other Ahvaz rapids locations being several metres higher than this) which are below sea-level, so Ahvaz marks the upstream limit of the backwater length for the River Karun (Appendix 6.1; Blum et al., 2013). The backwater length is the distance over which the scoured channel base is at or below sea-level and so defines the distance over which there is a clear morphodynamic link with sea-level (Paola and Mohrig, 1996; Li et al., 2006). Upstream of Ahvaz, the rivers Karun and Dez in the Upper Khuzestan Plains can be classed as *mixed bedrock-alluvial valleys* where, in the long-term (10^6 years), river valleys are in a state of incision and deepening and longitudinal profiles reflect a balance between incision rates and rates of uplift (Whipple and Tucker, 1999; Blum et al., 2013), as manifested with the concave-up longitudinal profile for the Karun between Gotvand and Ahvaz (Figure 4.29).

In the Lower Khuzestan Plains, the changes in Persian Gulf relative sea-levels and coastline will have had prominent influences on the major rivers, due to the proximity of the sea and the very gentle slopes of the coastal plains. Downstream of Ahvaz is the backwater length of the River Karun, so there are clear morphodynamic links with sea-level in this region (Paola and Mohrig, 1996; Li et al., 2006) and onlap of Holocene floodplain strata onto earlier steeper-gradient channel-belt deposits (Blum et al., 2013). In the Lower Khuzestan Plains, the River Karun can be classed as a *coastal plain-valley* in which channels aggrade, channels are typically deep and migrate slightly, channel-belts are avulsive and distributive, and net deposition maintains slightly concave-up longitudinal profiles (Nittrouer et al., 2012; Blum et al., 2013), as manfiested with the longitudinal profile of the Karun between Ahvaz and the Persian Gulf (Figure 4.29) and the frequent Holocene avulsions of the Karun, Karkheh and Jarrahi (Figure 2.11; Walstra et al., 2010a; Heyvaert et al., 2012; Heyvaert et al., 2013). The lengths of major marine-attached avulsions frequently scale to backwater lengths (Jerolmack and Swenson, 2007), as manifested with the long palaeochannels associated with major river avulsions in the Lower Khuzestan Plains (Figure 2.11; Heyvaert et al., 2013).

The details of the major river responses in the Lower Khuzestan Plains depend on the balance between the rate of sea-level change and the rate of river sediment supply. From c. 20,000 BC to c. 6,000 BC Persian Gulf relative sea-level rise and progressive coastline retreat during the deglaciation would have promoted mainly river channel profile shortening and river aggradation in the coastal plains (Blum and Törnqvist, 2000; Schumm et al., 2000), with incision further upstream (especially at Ahvaz) to produce the sediments to partly fill the “accommodation space” in coastal areas (Miall, 1996; Coe, 2003; Woodroffe, 2003). During the subsequent period of c. 6,000 BC - 500 BC the influences of relative sea-levels are less clear, especially since the existence of a Middle Holocene highstand is debated (Heyvaert and Baeteman, 2007). If there were higher relative sea-levels of about $^{+}$1 m to $^{+}$3 m during c. 6,000 BC - 3,500 BC, then the probable retreat of the head of the Persian Gulf to the north-west indicates that relative sea-level rise continued to outpace river sediment supply. If there was then a slight relative sea-level fall from about $^{+}$1 m to $^{+}$3 m to present-day sea-level during c. 3,500

BC - 500 BC, then this was probably the period in which river sediment supply balanced and then outpaced relative sea-level changes to produce delta and coastline progradation from mainly c. 550 BC onwards (Heyvaert and Baeteman, 2007). This coastal progradation would have promoted river channel extension and some river incision across the Ahvaz Anticline and the upstream parts of the Lower Khuzestan Plains (Blum and Törnqvist, 2000; Schumm et al., 2000). The coastal and delta progradation was initially rapid in the centuries following 550 BC until around 400 AD (Hansman, 1978; Gasche et al., 2007; Heyvaert and Baeteman, 2007). Subsequently, any river changes were largely independent of sea-levels, since Persian Gulf sea-levels were relatively stable and similar to that of today (Cooke, 1987; Kemp et al., 2011).

2.8 Climate of the study area

2.8.1 Present-day climate of south-west Iran

South-west Iran can be considered to have a "warm steppic" climate. Using Strahler's climatic classification, the present-day climate of south-west Iran is part of the hot, arid desert climate (BWh) grading into cool, arid steppe (BSk) and temperate dry, hot summer "Mediterranean" climates (Csa) in the Zagros Mountains (Barry and Chorley, 1992). The region is characterised by: large annual air temperature ranges (c. 24°C in the plains), very high summer air temperatures (higher than 50°C on some summer days), low mean annual precipitation falling predominantly in the winter and spring (mainly between November and May), a long summer drought, and mainly moderate winds. There are some dust storms with stronger winds, particularly in the south of the region in the summer when a strong W/NW wind or *Shamal* may blow.

Climate data for the main cities of south-west Iran are summarised in Table 2.2 and the spatial distribution of annual precipitation is shown in Figure 2.21. These show the predominance of precipitation in the winter and spring between about November and May, the long summer drought, and the progressive increase in average precipitation from less than 200 mm in the south-west in the Lower Khuzestan Plains to more than 800 mm in the north-east in higher parts of the Zagros. The region is characterised by great swings in precipitation. Precipitation is frequently concentrated in storms, with some parts of central and southern Khuzestan receiving as little as 85 mm precipitation some years and as much as 580 mm in others (Adams, 1962; Potts, 1999; Alijani, 2008;

Table 2.2 Mean monthly temperature and precipitation data for cities in south-west Iran (From Potts, 1999)

City	m.a.s.l.	Temp/Rainfall	Jan	Feb	Mar	Apr	May	Jun	Jul	Aug	Sep	Oct	Nov	Dec	Total
Abadan	3	Max. temp.	18.8	21.4	25.5	32.4	37.9	43.3	44.5	45.1	42.4	36.4	26.5	19.1	
		Min. temp.	7.2	8.7	11.9	17.5	22.2	26.2	27.7	26.8	23.0	17.8	12.5	8.3	
		Rainfall	19.9	14.5	18.5	14.6	3.7	0.0	0.0	0.0	0.0	0.6	25.9	40.6	146.3
Ahwaz	20	Max. temp.	17.7	20.7	25.3	32.3	38.9	44.5	46.1	45.9	42.1	36.0	26.0	19.2	
		Min. temp.	7.8	8.2	12.2	17.1	22.0	24.9	26.9	25.6	21.3	17.3	12.8	8.6	
		Rainfall	33.5	25.2	16.9	17.3	3.5	0.0	0.0	0.0	0.1	1.8	26.7	33.5	158.5
Bushire	4	Max. temp.	18.9	20.4	24.4	30.8	34.7	37.1	38.9	39.7	37.4	33.3	26.8	20.5	
		Min. temp.	9.7	10.4	13.7	18.1	22.3	24.9	27.6	27.3	24.1	19.2	14.9	11.5	
		Rainfall	61.4	22.4	19.4	8.6	5.0	0.0	0.0	0.0	0.0	0.8	48.4	93.3	259.3
Dizful	143	Max. temp.	19.0	20.5	24.1	31.2	37.7	43.9	46.2	45.6	42.7	36.6	26.8	19.6	
		Min. temp.	8.7	9.3	12.0	17.6	23.4	26.9	30.3	30.2	26.5	20.7	14.7	10.0	
		Rainfall	65.0	45.9	48.6	30.3	4.0	0.0	1.0	0.0	0.0	5.0	80.0	75.6	355.4
Hamadan	1775	Max. temp.	4.8	6.4	10.5	16.8	22.2	28.4	32.2	33.1	28.5	20.9	11.1	5.6	
		Min. temp.	−4.9	−3.7	0.1	5.4	8.2	12.0	15.1	14.5	10.9	6.1	−0.8	−3.5	
		Rainfall	36.0	52.8	72.9	78.9	32.7	5.6	1.3	0.5	0.7	11.8	51.8	40.2	385.2
Khorramabad	1171	Max. temp.	11.7	13.3	16.7	22.4	29.3	36.3	39.9	39.8	36.0	29.1	18.7	13.0	
		Min. temp.	0.1	0.9	4.3	8.7	11.9	15.5	19.7	19.0	14.1	9.5	5.5	1.7	
		Rainfall	66.5	73.2	88.1	82.8	28.4	0.9	0.5	0.4	0.4	10.4	76.7	75.6	504.0
Kermanshah	1322	Max. temp.	8.4	10.3	13.8	19.8	25.9	33.0	37.2	36.5	32.5	25.6	15.6	9.7	
		Min. temp.	−3.5	−3.1	0.4	0.5	7.6	10.9	16.0	15.0	10.0	5.4	1.3	−1.9	
		Rainfall	37.8	46.3	67.8	68.0	30.0	2.9	0.0	0.1	1.3	13.3	55.3	50.9	372.7
Shiraz	1490	Max. temp.	12.4	14.6	18.5	24.1	29.8	34.9	36.9	36.0	33.5	27.6	19.8	13.5	
		Min. temp.	0.6	1.8	5.1	8.3	13.2	16.9	20.1	18.7	15.3	9.4	4.4	1.6	
		Rainfall	76.9	47.3	63.4	24.4	12.7	0.0	1.2	0.0	0.0	—	65.3	93.4	384.6

Figure 2.21 Spatial distribution of annual precipitation in south-west Iran (Isohyets in mm drawn parallel to the trend of the Zagros orogen) (Modified from Alijani, 2008)

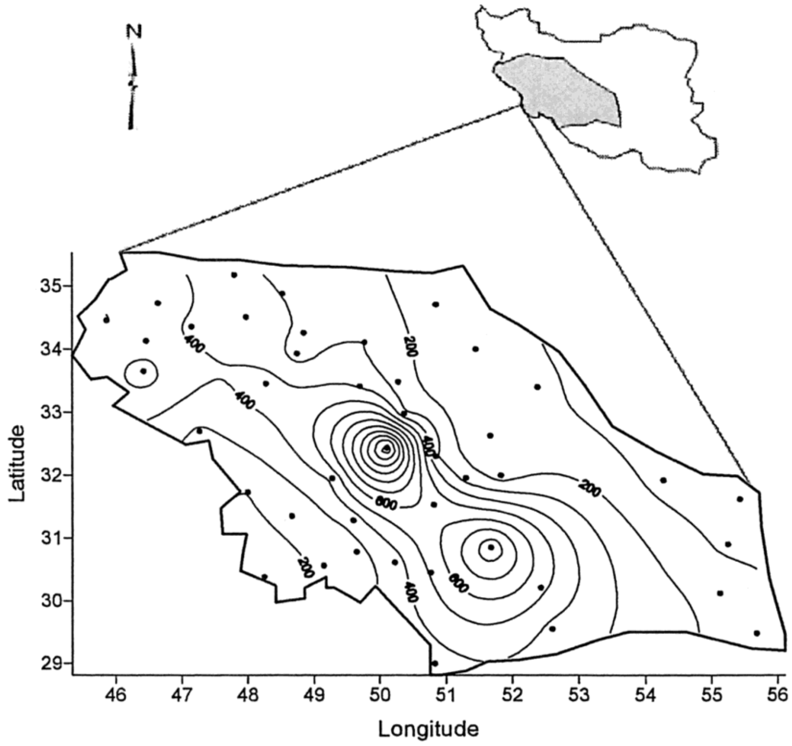

Djamali et al., 2010). The summer high air temperatures produce high evaporation rates of about 2,000 - 3,000 mm yr^{-1} in Khuzestan, of which 66 % occurs during May - September (FAO, 1992). Hence, evaporation greatly exceeds precipitation throughout most of the region, and only in areas above about 2,000 m elevation is a water surplus found (Oberlander, 1965).

South-west Iran can be broadly sub-divided into four climatic zones, mainly on the basis of mean annual precipitation (Carter and Stolper, 1984; Alizadeh, 1992; Potts, 1999):

The Arid Zone (c. 20,000 km^2) has a mean annual precipitation of less than 200 mm. It is confined to the south-west of Ahvaz on the Lower Khuzestan Plains. It is separated from central and northern parts of Khuzestan by a discontinuous low range of roughly NW-SE oriented hills running from Bostan to Ahvaz to Behbehan.

The Semi-Arid Zone (c. 15,000 km^2) has a mean annual precipitation of about 200 mm - 300 mm. It extends across the Upper Khuzestan Plains from Ahvaz to the series of roughly NW-SE oriented hills running from the Sardarabad Anticline towards Ram Hormuz. Mean monthly temperatures in the Arid Zone and Semi-Arid Zone range from c. 13°C in January to c. 37°C in July.

The Dry Zone (c. 25,000 km^2) has a mean annual precipitation of about 300 mm - 500 mm. It extends across the Upper Khuzestan Plains from the upper limit of the Semi-Arid Zone to as far north as Deh Luran and to the foothills of the Zagros Mountains (Potts, 1999; Alijani, 2008).

The Central Zagros Zone (c. 100,000 km^2), like most mountainous areas, has a notably variable climate, comprised of a myriad of smaller segments determined by local topography. In general, it is characterised by a mean annual precipitation of about 400 mm - 1,000 mm, with slightly more on a few high peaks. Temperatures are significantly lower than in the plains and winter minima fall below $^{-}$25°C in a few areas. Mean monthly temperatures in the valleys in the Central Zagros range from less than c. 2°C in January to c. 26 °C in July (Frey and Probst, 1986; Potts, 1999; Badripour et al., 2006; Alijani, 2008). On the higher peaks of the Zagros there is a high winter snowfall which accumulates as snow and ice fields, and above the theoretical snow line of c. 4,000 m there a few small glacier-like structures (Ehlers, 2001).

2.8.2 Climate changes in south-west Iran between the Last Glacial Maximum and the Holocene

Since the Last Glacial Maximum (LGM) (c. 20,000 BC - 15,000 BC), the climate of SW south-west Iran has undergone considerable changes. The details are quite poorly known, partly because the palaeoenvironmental data (such as pollen, ostracods and inferred lake levels from Lake Urmia, Lake Zeribar, Lake Mirabad and Lake Maharlou, and sediments from the sea-floor of the Persian Gulf and the Arabian Sea) come from slightly outside of south-west Iran. However, the general picture is fairly clear.

During the Last Glacial (the Weichselian (or Devensian) Glacial, Marine oxygen Isotope Stage 2) (Lowe and Walker, 1997) and especially during the LGM (c. 20,000 BC - 15,000 BC) the climate of south-west Iran was probably cool and treeless, with pollen analysis of lake cores indicating "*Artemisia* steppe" vegetation covering virtually the entire region (Van Zeist and Bottema, 1977; 1991). Parts of the Khuzestan Plains would have had very limited vegetation, and the formation of dune fields, such as those to the north of Hamidiyyeh, probably mainly occurred during the Last Glacial (Gasche et al., 2004). The broad picture of low ratios of Chenopodiaceae to *Artemisia* pollen, low percentages of Poaceae (grass) pollen, near absence of arboreal pollen, relatively high lake levels, lowering of the regional snowline by c. 1,500 m, and some valley glaciers and local ice fields in the Zagros, indicates a climate of cool, dry summers and moist, snowy winters (Farrand, 1979; El-Moslimany, 1987; Ferrigno, 1991; Kehl, 2009). The prominence of pollen of *Hippophaë rhamnoides* (a pioneer tree species which can grow on unstable soils, river beds and bars) in Lake Urmia cores indicate that there were cool winters, July temperatures above 11-12 °C (Kolstrup, 1980), and probably extensive fluvial activity in the absence of a well-developed vegetation cover (Djamali et al., 2008).

During the Deglacial of about 15,000 BC - 9,000 BC (Shakun and Carlson, 2010) there were changes in these indicators which showed that, with various oscillations, the climate generally became slightly warmer and, probably, drier, with very few trees and a pistachio-oak steppe over some of the Zagros (El-Moslimany, 1987; Kehl, 2009). A major oscillation with colder and drier conditions probably occurred during the Younger Dryas, with a significant increase in $\delta^{18}O$, maximum inferred lake salinity, and markedly low lake levels during about 10,600 BC - 10,000 BC (Kelts and Shahrabi, 1986; Snyder et al., 2001; Wasylikowa et al., 2006). Around 9,000 BC there was a change in the general nature of the sea-floor sediments of the Persian Gulf, with probable terrigenous sediments (greyish-brown detrital silts and detrital calcite) being overlain by probable autochthonous shallow marine sediments (greenish-grey carbonate muds with clay-sized aragonite needles and a sand fraction of oolites and pellets)

(Stoffers and Ross, 1979; Uchupi et al., 1999). This change might have been related to a reduction in precipitation in the Zagros region, resulting in less sediment from rivers being deposited on the sea-floor of the Persian Gulf.

2.8.3 Climate changes in south-west Iran during the Holocene

From about 9,000 BC onwards (the approximate commencement of the Holocene (or Flandrian) Interglacial, Marine oxygen Isotope Stage 1) (Lowe and Walker, 1997), there was a gradual, progressive increase in first grass cover (grass steppe) and then tree cover (forest steppe with mainly *Pistacia*, then *Quercus*). This change to tree cover occurred later in south-west Iran than in eastern Turkey and more gradually than in the relatively moist coastal Levant (Kehl, 2009). Maximum tree cover, similar to the present-day xerophilous “oak woodland” or “mountain forest steppe” natural vegetation, was probably reached around 5,200 BC/4,300 BC (Bottema, 1986; El-Moslimany, 1986, 1987; Van Zeist and Bottema, 1991; Stevens et al., 2006). This relatively gradual expansion of tree cover in south-west Iran was probably related to an intensification of the Indian Summer Monsoon (ISM) and NW shift of the Inter-Tropical Convergence Zone (ITCZ) in the Early Holocene which produced winter-dominated precipitation in the Zagros, with the establishment of both winter and spring precipitation being delayed until the Middle Holocene (Griffiths et al., 2001; Stevens et al., 2001, 2006; Fleitmann et al., 2007; Djamali et al., 2010).

Probably only from about 4,300 BC/2,600 BC onwards were fairly warm, moist winters and springs (from mid- to high- latitude westerly depressions) and hot summers, with no significant summer precipitation, established in south-west Iran (Van Zeist and Bottema, 1977, 1991; Rodwell and Hoskins, 2001). This climate has subsequently persisted to the present-day, with various fluctuations and a significant period of probably greater precipitation around 700 AD - 1850 AD (roughly corresponding to the Neoglacial) associated with greater southward penetration of mid- to high- latitude westerly depressions (Vita-Finzi, 1976, 1979; Brookes, 1989). From about 4,300 BC/2,600 BC onwards there was a change in the general nature of sea-floor sediments on the Mesopotamian Shelf of the northern Persian Gulf, with the aforementioned probable autochthonous greenish-grey carbonate muds being overlain (after a probable hiatus of deposition) by partly terrigenous sediments (olive-grey silty marls with a sand fraction of marine biogenic constituents) (Stoffers and Ross, 1979; Uchupi et al., 1999). This change to a greater terrigenous sediment input to the sea-floor of the

Mesopotamian Shelf may have been due to a time of higher regional precipitation and glacier melting roughly around 3,800 BC. However, it may also have been related to other factors, such as increased soil erosion with limited anthropogenic woodland depletion, and increased river and delta deposition following sea-level stabilisation.

These changes in vegetation essentially applied to the Zagros Mountains and foothills, with the present-day “oak woodland” being maintained in these areas by winter and spring precipitation (Griffiths et al., 2001; Stevens et al., 2001; Alijani, 2008; Djamali et al., 2010). Throughout the majority of lowland south-west Iran, the natural vegetation during the last 22,000 years has probably been mainly “arid steppe” and “semi-arid steppe” (Van Zeist and Bottema, 1991), apart from some woodland adjacent to the major rivers, as found as recently as the 19th Century AD within the Khuzestan Plains (Selby, 1844; Layard, 1846). Superimposed on all of these general changes in climate were various shorter duration changes. Examples include: variations in the intensity of the monsoon (Gasse and Van Campo, 1994), a regionally cooler and drier event around 6,400 BC - 6,000 BC (Weiss, 2000), a regionally drier interval around 3,600 BC - 3,000 BC (Magny and Haas, 2004; Stevens et al., 2006), a short period of greater aridity throughout the Middle East around 2,200 BC (Weiss et al., 1993), and a drier period around 500 AD - 650 AD (Wenke, 1976).

2.9 Soils of south-west Iran

The soils of south-west Iran reflect its climate. The soils of the Khuzestan Plains include steppe soils, alluvial soils, saline alluvial soils, halomorphic (salt marsh) soils, hydromorphic (river bank and swamp) soils, and some dune and loess-like soils (mainly Entisols, Inceptisols and Aridisols of the USDA soil classification). Most soils in the Khuzestan Plains are rich in carbonates, gypsum, and other evaporites, as a result of high rates of dissolution and evaporation. Soil salinities are high, with surface salt accumulations over large areas of the Lower Khuzestan Plains where the groundwater table is less than 1.5 m deep. The soils of the Zagros Mountains include steppe-forest soils (brown soils and chestnut soils), steppe soils, and alluvial soils (mainly Entisols and Xeric mountain soils of the USDA soil classification). In general, the soils of the region are quite poorly developed (Veenenbos, 1958; Dewan and Famouri, 1964; Birkeland, 1999; Badripour et al., 2006; Afkhami et al., 2007).

2.10 Natural vegetation of south-west Iran

The natural vegetation of south-west Iran similarly reflects its climate. The natural vegetation of the Arid Zone is a combination of arid desert steppe vegetation of mainly herbs (such *Artemisia* and the *Chenopodiaceae*) and grasses, and saline marshes. The Semi-Arid Zone and the Dry Zone have a semi-arid steppe vegetation of shrubs and herbs (such as *Artemisia* and the *Labiatae*, *Chenopodiaceae*, and *Compositae*) and grasses, with some saline soil vegetation (such as camelthorn, *Alhagi camelorum*). Throughout the Khuzestan Plains, woody herbs and shrubs and trees (such as *Ziziphus* and *Prosopis*) line the lower floodplains of the major rivers, and herbs and shrubs (like *Haloxylon*) partly cover some areas of sand dunes.

The Central Zagros, like most mountainous areas, has very varied vegetation. Its natural vegetation is mostly "Kurdo-Zagrosian steppe-forest", with a loose zoning according to elevation and precipitation. At lower elevations (up to c. 1,200 m), the semi-arid steppe vegetation grades into *Pistacia-Amygdalus* scrubs ("pistachio-almond scrubs"). At mid-elevations (c. 800 m - 1,800 m/2,300 m), there is a xerophilous "oak woodland" or "mountain forest steppe", comprised of mainly deciduous, broad-leaved shrubs and trees (mainly the xerophilous *Quercus brantii*, other *Quercus*, *Pistacia*, *Prunus* and *Pyrus*), with a ground cover of steppe vegetation (grasses and herbs, such as the *Labiatae* and *Compositae*). At higher elevations, especially over c. 1,800 m, grasses tend to predominate, and above c. 2,600m there is a high mountain sub-alpine and alpine vegetation of spiny cushion-like herbs (like *Astragalus*) and hardy grasses (Veenenbos, 1958; Zohary, 1963; Frey and Probst, 1986; Potts, 1999; Badripour et al., 2006; Djamali et al., 2010).

2.11 Human activities in south-west Iran

There is a long history of human activities in south-west Iran, and the main archaeological and historical periods of south-west Iran are summarised in Table 2.3.

2.11.1 Indirect human impacts on the vegetation and environment of south-west Iran

The natural vegetation of south-west Iran has been greatly modified over the course of history by human influences. For instance, in the Khuzestan Plains, herbs like *Artemisia* have been considerably reduced by cultivation and associated weed plants, and trees and

Table 2.3 Summary of the main archaeological and historical periods in south-west Iran

Archaeological or historical period	**Approximate dates**
Palaeolithic and Mesolithic Periods (the "Old Stone Age" and "Middle Stone Age", with hunter-gatherer technologies)	Mainly pre-9,000 BC
Neolithic Period (the "New Stone Age", with the development of agriculture and the "Village Period" from c. 7,000 - 4,000 BC)	9,000 - 4,500 BC
Chalcolithic Period (the "Copper Age", including the Uruk Period, from c. 4,000 - 3,100 BC, with larger settlements)	4,500 - 3,100 BC
Proto-Elamite Period	3,100 - 2,600 BC
Elamite Period (with the first major civilization in Khuzestan)	2,600 BC - 646 BC
Persian Empire Periods (Neo-Assyrian and Achaemenid empires)	646 BC - 330 BC
Seleucid Period	330 BC - 139 BC
Parthian Period (or Arsacid Period)	139 BC - 224 AD
Sassanian Period	224 AD - 633/651 AD
Early Islamic Period (Islamic conquest and Umayyad Caliphate)	633 AD - 750 AD
Abbasid Period (including the Zanj Rebellion of c. 869 - 883 AD and less influence of the Abbasid caliphs after c. 946 AD)	750 AD - 1219/1258 AD
Mongol Period (Mongol invasion and rule (c. 1258 AD onwards) - Mongol empire (Ilkhanate) and Jalayirid sultanate)	1219 - 1393/1432 AD
Timurid dynasty (and Shi'a sects)	1393 - 1506/1510 AD
Safavid and Zand dynasties	1510 -1794 AD
Qajar dynasty (with British and Russian colonialism during c. 1856 - 1945 AD)	1794 - 1925 AD
Pahlavi dynasty	1925 - 1979 AD
Islamic Republic	1979 AD - Present

shrubs now only line river floodplains at a few localities, mainly along braidplains where grazing and cultivation is very limited. Also, in the Zagros Mountains, tree and scrub clearance for agriculture, cultivation, grazing, firewood and timber has greatly reduced both the "pistachio-almond scrubs" and the "oak woodland" (Potts, 1999; Badripour et al., 2006; Djamali et al., 2009).

Woodland depletion associated with agriculture and civilization commenced very early in the Middle East. It has been noted as early as c. 7,000 BC in north-west Syria, and descriptions of forest depletion in the Epic of Gilgamesh from Mesopotamia and the domestication of goats in the Zagros as early as c. 8,000 BC, suggest that anthropogenic woodland depletion in south-west Iran probably commenced early in the Holocene (Yasuda et al., 2000; Zeder and Hesse, 2000). The details and timing of anthropogenic woodland depletion in south-west Iran are only poorly known, due to limited evidence and due to difficulties with distinguishing human influences from climate induced changes. Human activities, such as wood cutting and burning of the landscape, probably had some influence on the relatively gradual expansion of tree cover in the Zagros during the Early-Middle Holocene (Hillman, 1996; Roberts, 2002). It has been hypothesised that significant human-influenced degradations of the natural vegetation and partial deforestation in south-west Iran occurred as early as approximately 2,500 BC (Bobek, 1959). This is supported by limited environmental and archaeological evidence, which indicates that anthropogenic woodland depletion occurred mostly after about 4,900 BC/2,600 BC (Van Zeist and Bottema, 1991; Potts, 1999). It is also supported by strong increases in percentages of *Gramineae* and *Plantago lanceolata* pollen (often taken as indicators of human disturbance) at c. 2,000 BC in Lake Mirabad cores (Stevens et al., 2006) and the appearance of cultivated tree species (such as *Juglans*, *Olea* and *Vitis*) at c. 2,300 BC in Lake Maharlou cores (Djamali et al., 2009). The first major civilization in south-west Iran which practiced extensive agriculture and irrigation, the Elamite civilization, dates from c. 2,600 - 646 BC (De Miroschedji, 2003), so it is to be expected that the rate of vegetation degradation and woodland depletion would have increased subsequent to 2,600 BC. This vegetation degradation probably continued at varying rates through historical times, with, for instance, profound degradation of *Pistacia-Amygdalus* scrubs in the Zagros being found at around 700 BC in Lake Maharlou cores, presumably with increased human activities around the time of the commencement of the Persian empires (Djamali et al., 2009). Descriptions by 19th Century AD travellers (Selby, 1844; Layard, 1846) of woods lining the major rivers of lowland Khuzestan (especially the Dez with thick woods of poplar and tamarisk), indicate that some final woodland clearance occurred in the late 19th Century AD and 20th Century AD.

Other major human impacts on the environment of south-west Iran have included *irrigation and hydrological engineering*. One effect of irrigation systems is the accumulation of fine-grained “irrigation silts”, which may be present as early as about 5,000 BC with flood recession agriculture (Kouchoukos, 1999). In later periods (mainly from the time of the Elamite civilization onwards), appreciable thicknesses (several metres) and appreciable rates of aggradation (greater than 1 mm yr^{-1} for parts of the Mianab Plain of the River Karun) have been reported, which resulted in reductions in the overall gradients of the plains (Alizadeh et al., 2004).

2.11.2 Direct human impacts on the river channels and floodplains of south-west Iran

The construction of *major canals* in lowland south-west Iran dates from the Elamite civilization, such as the canal system of c. 1,250 BC that supplied water from the River Karkheh to the Elamite settlements of Haft Tepe and Choga Zanbil. Canal construction in Khuzestan continued throughout subsequent historical times. Important times of canal construction were probably the Persian Empire periods (c. 646 BC - 330 BC) when qanats (subterranean canals) were first widely used in Khuzestan, the Sassanian and Early Islamic Periods (c. 224 AD - 750 AD), the Early Abbasid Period (c. 750 - 946 AD), and the Qajar dynasty - the Present (c. 1794 AD - Present) (Kirkby, 1977).

The height of irrigation development in south-west Iran in antiquity was the Sassanian Period (c. 224 - 651 AD), when a regional network of irrigation canals and qanats extended over much of the Upper Khuzestan Plains and the Lower Khuzestan Plains. Flow was regulated by intricate hydraulic engineering including bunds (or dikes), dam-bridges, levées, cuts, reservoirs, sluices, weirs, tunnels and water mills (Alizadeh et al., 2004; Walstra et al., 2010a). An especially important Sassanian hydraulic system was that related to the monumental Band-e Qaisar dam-bridge across the River Karun at Shushtar (Section 4.2.3). This was used to raise water levels to feed both the Darian canal irrigation system serving the northern Mianab Plain and the Masrukan canal irrigation system serving the Shushtar water mills, the southern Mianab Plain, the "*sawad*" plains (now deserted marshlands) between the Kupal and Ahvaz Anticlines, and also parts of the Lower Khuzestan Plains to the south of Ahvaz. Use of these canal systems probably continued into the subsequent Early Islamic Period (c. 633 - 750 AD), but they were later abandoned and the Band-e Mahibazan dam, about 4 km south of Shushtar, subsequently collapsed (Alizadeh et al., 2004; Verkinderen, 2009; Moghaddam, in press). The timing of this abandonment is uncertain, as historical records are hard to interpret. According to Ibn Serapion in the 10th Century AD, the River Karun (then called the Dujayl) flowed parallel to the Masrukan down to its tidal estuary; whereas Mustawfi in the 14th Century AD mentions that the Masrukan poured back into the River Karun near the city of Askar Mukram (just to the north-east of Band-e Qir) (Le Strange, 1905). Hence, disuse of the system and avulsion/diversion from the river in a palaeochannel between Chamlabad and Ummashiyyeh-ye Yek (the original Dujayl) into a near-straight reach of the present-day River Karun between

Band-e Qir and Veys (the original Masrukan canal), probably took place in the time of political instability (which included the Mongol invasion) that was the 10th - 14th Centuries AD (Figure 4.1 (d); Bakker, 1956). The Masrukan canal system was so large that, apparently, with disuse it incised and developed into the meandering River Gargar. Hence, the construction and disuse of the Masrukan canal system resulted in the present-day River Karun having two branches, the larger River Shuteyt and the smaller River Gargar, and an approximately 19 km long near-straight river reach between Band-e Qir and Veys (Figure 4.1 (b); Alizadeh et al., 2004).

Near-straight reaches (with very low sinuosities of less than about 1.1) are very rare in nature (Frenette and Harvey, 1973; Rosgen, 1994; Wang and Ni, 2002) and in lowland south-west Iran, with mainly meandering rivers and straight canals, long near-straight reaches can be considered to be primarily related to human activities (Alizadeh et al., 2004). Some river reaches have been straightened mainly for navigation (such as the Haffar cut, that was originally dug in the 10th Century AD to allow access to the deeper Shatt al-Arab and which probably became the main course of the Karun after construction of a bund in the 18th Century AD (Layard, 1846; Potts, 2004)), and some mainly for irrigation (such as the Karkheh Kur towards Huveyzeh, that was probably dug between the 7th and 19th Centuries AD (Alai, 2010; Heyvaert et al., 2012)).

From the *20th Century AD onwards*, irrigation and hydrological engineering has been greatly expanded with a very extensive network of dams, reservoirs, pumping stations, canals and concrete channels, that has involved some major constructions and levelling of the land, to enable large areas of the Khuzestan Plains to come under cultivation (Alizadeh et al., 2004). Since around 1960 AD, when the Khuzestan Water and Power Authority (KWPA) was founded, the scale of this work was greatly increased, with the construction of large reservoir dams on the major rivers in the Zagros foothills and mountains. The first large reservoir dam on the River Dez (the Dez Dam) was constructed in 1959 - 1962 AD, the first large reservoir dam on the River Karun (the Karun 1 or Shahid Abbasspour Dam) was constructed in 1969 - 1976 AD, and the first large reservoir dam on the River Karkheh (the Karkheh Dam) was constructed in 1992 - 2001 AD (KWPA, 2010). These reservoir dams and the extensive extraction and diversion of water for agriculture have significantly changed the flow regimes of the major rivers. River water and sediment discharges downstream of the dams and irrigation canals are now generally lower, especially in the lower reaches of the Karkheh and Karun in the summer, and there are higher levels of salinity, especially in the Shatt al-Arab region (Afkhami, 2003; Salarijazi et al., 2012). River regulation means that flows are less “flashy”, though major floods do still occur, including rare occasions when dams are overtopped and events like the failure of the Karun 1 dam in spring 1993 AD (Kopytin, 1996; Emami et al., 2003; Heidari, 2009).

Similarly, other human impacts on major rivers in south-west Iran date mainly from the 20th Century AD onwards. These include river channelization programs such as flood control works, urbanization (mainly in Ahvaz and Dezful), dredging (mainly on the River Karun downstream of Ahvaz), fish tanks, limited river gravel and sand extraction for building projects, and very limited impacts through mining (Afkhami et al., 2007).

CHAPTER 3 METHODS

"Far and away the best prize that life has to offer is the chance to work hard at work worth doing."

Theodore Roosevelt, U.S. President (1858 - 1919 AD)

3.1 Introduction

The methods and techniques employed in this study were according to standard procedures as outlined in this chapter, with details of the methods being given in Appendix 7. The methods used fall into three main groups:

3.2 Methods for investigating Earth surface movement rates

3.3 Methods for investigating river characteristics influenced by Earth surface movements and human activities

3.4 Laboratory analyses for investigating Earth surface movement rates and for investigating river characteristics

3.2 Methods for investigating Earth surface movement rates

The Khuzestan Plains of lowland south-west Iran were investigated in this study since the major rivers have been significantly influenced by Earth surface movements of emerging folds in the region for many millennia. However, the rates of Earth surface movements in south-west Iran are only very poorly known. For the area of the Khuzestan Plains there are no sequential high-precision levelling or GPS surveys, and no notable published rates of uplift for the folds that form a succession of "obstacles" to the major rivers. Interpretations of interactions between rivers and tectonics may be significantly limited where details of Earth surface movements are only poorly known (Ouchi, 1985; Schumm et al., 2000). Hence, to remedy this deficiency, a variety of fieldwork and dating techniques to derive dated indicators of vertical Earth surface movements were undertaken in the environs of the study area. The fieldwork undertaken included surveying, geomorphological and sedimentological description, and sampling for laboratory analyses, including the radiometric dating techniques of radiocarbon dating and Optically Stimulated Luminescence (OSL) dating.

3.2.1 Fieldwork and dating for marine terraces along the north-east coast of the Persian Gulf

Marine terraces along the north-east coast of the Persian Gulf were investigated to determine general rates of Earth surface movements within the Dezful Embayment near to the Zagros Deformation Front, both regionally and on the limbs of an active fold. Marine terraces with sediments exhibiting minimal compaction were selected for this investigation, so that relative sea-level changes were principally due to tectonic movements and glacio-hydro-isostatic effects (Lambeck, 1996). This was in contrast to the alluvial and coastal sediments of the Lower Khuzestan Plains, where sediment aggradation, incision and compaction were complicating factors (Larsen and Evans, 1978; Lambeck, 1996; Coe, 2003; Heyvaert and Baeteman, 2007).

Surveying was undertaken using a dumpy level and surveyor's staff, using standard procedures outlined by Bettess (1992) and Bannister et al. (1998). Locations of temporary bench marks were determined as latitude and longitude in the WGS 84 (World Geodetic System 1984) reference system, using a Garmin GPS 12 (Global Positioning System) hand-held unit, which had a horizontal positional accuracy of within 100 m (and probably within 15 m) when placed at a bench mark for several hours (Garmin, 2011). Surveys were relative to Mean High Water strand lines. Closure of each survey indicated vertical measurement errors of approximately 5 cm or less. Details of the surveying methods are given in Appendix 7.1.1.

Geomorphological and sedimentological description of marine terrace deposits and bedrock, including photography and logging, was undertaken, using established procedures including those outlined by by Gardiner and Dackombe (1983), Goudie et al. (1990), Tucker (1993), Miall (1996), Todd (1996), Jones et al. (1999a), Garrison (2003), and Stow (2005).

Radiocarbon dating was undertaken on marine mollusc shell samples from marine terrace sediments, using standard procedures for sampling (Gillespie, 1984; Aitken, 1990; Pilcher, 1991).

The laboratory used for radiocarbon dating was the Centre for Isotope Research radiocarbon laboratory in the University of Groningen, the Netherlands. The radiocarbon dating undertaken was conventional (beta-radioactivity) radiocarbon dating for larger shell samples (greater than 15g mass) and Accelerator Mass Spectrometry (AMS) radiocarbon dating for smaller shell samples. This was undertaken following the standard procedures used by the laboratory (Mook and Streurman, 1983; Van der Plicht and Lanting, 1994; Van der Plicht et al., 2000). Details of the radiocarbon dating methods are given in Appendix 7.1.2.

The results obtained were quoted as conventional radiocarbon years Before Present (BP) (years before 1950 AD, using the standard Libby half-life value for ^{14}C of 5,568 ± 30 years) ± one standard deviation (one σ, confidence interval 68.3 %) for each sample (Bowman, 1990; Griffin, 2004). The results were also quoted as calibrated radiocarbon years Before Christ (cal.BC) ± one standard deviation, using the Julian/Gregorian calendar. Calibration was undertaken with the OxCal Version 4.2 calibration program (Bronk Ramsey, 2013), using the Marine09 modelled ocean average calibration curve of Reimer et al. (2009) and a ΔR offset of $^{+}$180 years for the nearest location (Doha in Qatar) within the CHRONO Marine Reservoir Database (Southon et al., 2002).

3.2.2 Fieldwork and dating for ancient canals and other ancient hydrological engineering cut across anticlines

Two abandoned ancient canals cut across an anticline and the intake tunnels of an ancient canal system cut through an anticline were investigated to determine rates of Earth surface movements associated with two folds. The methods of ***surveying*** and ***geomorphological and sedimentological description*** followed established procedures, as employed with the marine terraces. Historical and archaeological evidence was used to determine dating.

3.2.3 Fieldwork and dating for river terraces of the Karun river system in the Upper Khuzestan Plains

River terraces of the Karun river system in the Khuzestan Plains were investigated to determine rates of Earth surface movements associated with active folds within the study area. The Upper Khuzestan Plains were used for these investigations, since in the predominantly very flat Lower Khuzestan Plains no preserved river terraces were found. The limbs of anticlines were selected for the fieldwork, since reasonably well preserved river terraces were found on the limbs of anticlines as a result of some lateral river migration. Also, at some locations on anticlinal limbs, river cliffs had cut into the river terraces to produce relatively accessible exposures of river terrace deposits and bedrock.

By contrast, for river courses across anticlinal axes, it was mostly found that the river terraces had been entirely eroded away by constrained river vertical incision, as is well known for other rivers, such as the River Arun in the U.K. (Bates and Briant, 2009). This approach to the fieldwork facilitated an initial investigation into the Late Pleistocene and Holocene river terraces of the Karun river system, which was useful as there had been no significant previous research on river terraces within Khuzestan.

Surveying was undertaken using Total Station equipment, using standard procedures outlined by Bettess (1992), Bannister et al. (1998) and Kavanagh (2009). Locations of temporary bench marks were determined using a Garmin GPS 12 hand-held unit, as with the marine terraces. Surveys were relative to the nearest river water surface and, where available, relative to a National Cartographic Center of Iran (NCC) bench mark (such as that shown in Figure 3.1). The NCC datum is a "modified" Indian Spring Low Water - a tidal datum approximating the lowest water level observed at a place (similar to the Lowest Astronomical Tide), originally devised by G. H. Darwin for the tides of India at a level below Mean Sea Level (Hareide, 2004). Closure of each survey indicated vertical measurement errors of approximately 2 cm or less. Details of the surveying methods are given in Appendix 7.1.3.

Figure 3.1 A National Cartographic Center of Iran (NCC) bench mark

Geomorphological and sedimentological description of river terrace deposits and bedrock followed established procedures, as with the marine terraces.

Assignment of river terrace names was undertaken since there was no significant previous published research on the river terraces of the Khuzestan Plains. Each terrace was assigned a new name (either from a nearby village or from the fold on which it was located), in accordance with recommended stratigraphic practice (Salvador, 1994). A system of numbers for the river terraces was not used, since numbered terraces can be confusing when additional lower, intermediate or higher river terraces are discovered and when subsequent research alters the interpretations of correlations between river terraces (Bridgland, 1994; Demir et al., 2007).

Figure 3.2 Carving out two adjacent block sediment samples from a Khuzestan river terrace exposure for OSL dating

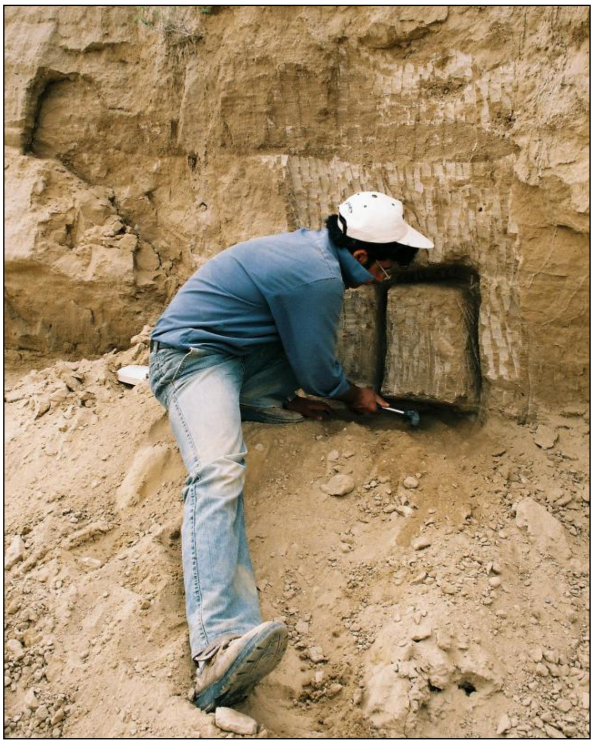

Optically Stimulated Luminescence (OSL) dating was undertaken on sediment samples from river terrace deposits, using standard procedures for sampling (Aitken, 1998). Care was taken to sample from relatively homogeneous deposits containing fine sand and very fine sand (since quartz grains in the size range 90 - 250 µm were to be used for dating), with the homogeneity and near absence of gravels extending to a sphere of radius of about 0.3 m around each sampling point (Rendell, H. M., Loughborough University, personal communication, 2005). Gamma rays emitted up to a distance of 0.3

m from a sample can contribute to the annual dose-rate and by applying these precautions when sampling, the need for on-site measurement of the gamma dose-rate was circumvented. Sampling targeted sands at least several decimetres above probable bedload coarse sands and gravels, to increase the likelihood that the fluvial sediments had originally been transported mainly as suspended load and had received sufficient exposure to sunlight for complete "bleaching" of the OSL signal (Aitken, 1998; Colls et al., 2001). The majority of the sediments in the Khuzestan river terrace exposures were very well indurated and cemented, so samples were carefully extracted by carving out two adjacent approximately 10 cm square blocks with a geological hammer and chisel and a very strong, sharp knife (Figure 3.2). By sampling such a relatively large block, sediments deeper within the block were not exposed to light.

The laboratory used for Optically Stimulated Luminescence (OSL) dating was the Sheffield Centre for International Drylands Research (SCIDR) luminescence laboratory in the University of Sheffield, U.K. The OSL dating was undertaken according to standard procedures (Aitken, 1998), as outlined in two Quartz Optical Dating Reports (Bateman and Fattahi, 2008, 2010).

Incomplete bleaching during the last period of transport and deposition is frequently a major source of inaccuracies in the calculated palaeodose value, resulting in OSL ages that are older than the true age of sediment burial (Richards et al., 2001). To varying degrees, all of the samples from Khuzestan exhibited some signs of incomplete bleaching, with a high amount of replicate scatter and replicates having a wide range of palaeodose (De) values. Thus, steps were taken statistically to isolate burial OSL ages for each of the samples. In two cases, this was achieved by removal of aliquots whose palaeodoses were outside of two standard deviations of the dataset mean and by application of the Central Age Model (Galbraith et al., 1999). This statistical model was sufficient where the De replicate datasets produced essentially unimodal De distributions. In the majority of cases, the palaeodose replicate datasets were statistically analysed by Finite Mixture Modelling (Galbraith and Green, 1990) to extract the different multiple components contained within the De distributions (Figure 3.3). Where the principal cause of De scatter is partial bleaching the youngest component is generally a better indicator of the true burial age, hence, the lowest component which represented more than 10 % of the data was selected for the calculation of OSL ages (Bateman et al., 2007, 2010).

Figure 3.3 Example application of the Central Age Model and Finite Mixture Modelling to the palaeodose (De) results for one sediment sample ('Dar Khazineh terrace', HGWS05 Bed 7hgw, laboratory code Shfd08207)

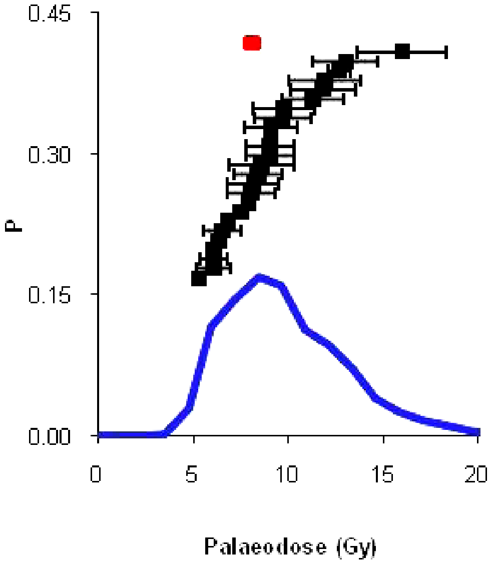

Graph shows plots of Probability, P against Palaeodose, De (Gy):
Probability density curve (blue curve) Probability mean (red point)
Ranked palaeodose (De) data (black points with error bars)

Palaeodose of aliquot, De (Gy)	Error (one SD)
5.36	0.19
6.10	0.22
6.10	0.72
6.10	0.87
6.36	0.22
6.55	0.98
6.87	0.23
7.54	0.20
7.92	0.31
8.08	1.22
8.18	1.37
8.45	1.28
8.62	1.69
9.06	1.28
9.07	1.24
9.09	0.30
9.13	1.41
9.73	1.48
9.77	1.63
11.85	1.74
11.93	1.89
11.32	1.59
12.68	0.59
13.05	1.69
16.00	2.33

Statistical models		
Unweighted Mean		
Mean De (Gy)	Standard Deviation, SD	Standard Error, SE
9.00	2.61	0.52
Central Age Model		
Mean De (Gy)	Standard Deviation, SD	Overdispersion, OD (%)
8.54	0.48	25.48
Finite Mixture Modelling		
Component	Mean De (Gy) ± Error (one SD)	Proportion
1	6.84 ± 0.33	0.51
2	10.72 ± 0.66	0.49

Table shows:
De data derived from individual aliquots
Unweighted Mean De is 9.00 ± 2.61 Gy
Mean De by Central Age Model is 8.54 ± 0.48 Gy
Mean De by Finite Mixture Modelling is 6.84 ± 0.33 Gy;
with annual dose-rate this gives OSL age of 5.68 ± 0.36 ka

The results obtained using the equation OSL age = Palaeodose, De / Annual dose-rate (Aitken, 1998) were quoted as thousands of years before the present (ka) ± one standard deviation (one σ, confidence interval 68.3 %). This incorporated systematic uncertainties with the dosimetry data, uncertainties with the palaeomoisture content, and errors associated with the De determination (Bateman and Fattahi, 2008, 2010). The results were also quoted as years Before Christ (BC) ± one standard deviation, using the Julian/Gregorian calendar. Details of the Optically Stimulated Luminescence (OSL) dating methods are given in Appendix 7.1.4.

3.3 Methods for investigating river characteristics influenced by Earth surface movements and human activities

The River Karun and its largest tributary, the River Dez, were chosen for this study for a number of reasons, including their large size and their courses which interact with various anticlines and emerging anticlines in the Khuzestan plains before debouching into the Persian Gulf. The river courses studied were the River Karun downstream of the Gotvand Regulating Dam, the River Dez downstream of the Dez Regulating Dam in northern Dezful to its confluence with the Karun at Band-e Qir (7 km north of Molla Sani), and the River Karun downstream to the Persian Gulf at the mouth of the Bahmanshir River. Both the River Shuteyt and River Gargar branches of the River Karun were studied, plus some aspects of the Ab-e Shur, Rud-e Tembi and Ab-e Gulestan tributaries of the River Karun (Figure 3.4). The river courses had been subjected to a detailed survey by the Dez Ab Engineering Company during the period of about 1997 - 2000 AD, with survey locations at fairly regular intervals, typically several kilometres apart. These survey locations were used to sub-divide the major rivers into a succession of straight-line river “reaches”, as illustrated in Figure 3.5. A river reach in this study was defined as a length of channel with homogeneous morphology and discharge (Hogan and Luzi, 2010).

The reaches were of an average length of about 8.0 km and had a range of lengths from about 0.8 km (in the city of Shushtar) to an extreme of about 50.5 km (for the Bahmanshir River). Any significant or pronounced changes in general course direction, channel planform, channel pattern, channel sinuosity, or meander wavelength were used to demarcate the end of one reach and the start of the next. This sub-division was undertaken so that various river characteristics (such as the valley slope and the channel

Figure 3.4 Map showing the rivers and major dams of south-west Iran, with the river courses of the study highlighted (Modified from KWPA, 2004)

The river courses studied were the River Karun downstream from the Gotvand Regulating Dam (including the Ab-e Shur, Rud-e Tembi and Ab-e Gulestan tributaries and the River Shuteyt and River Gargar branches), the River Dez downstream from the Dez Regulating Dam in northern Dezful to its confluence with the Karun near Molla Sani, and the River Karun downstream to the Persian Gulf at the mouth of the Bahmanshir River.

Scale approx. 1:1,480,000 River courses studied highlighted in yellow

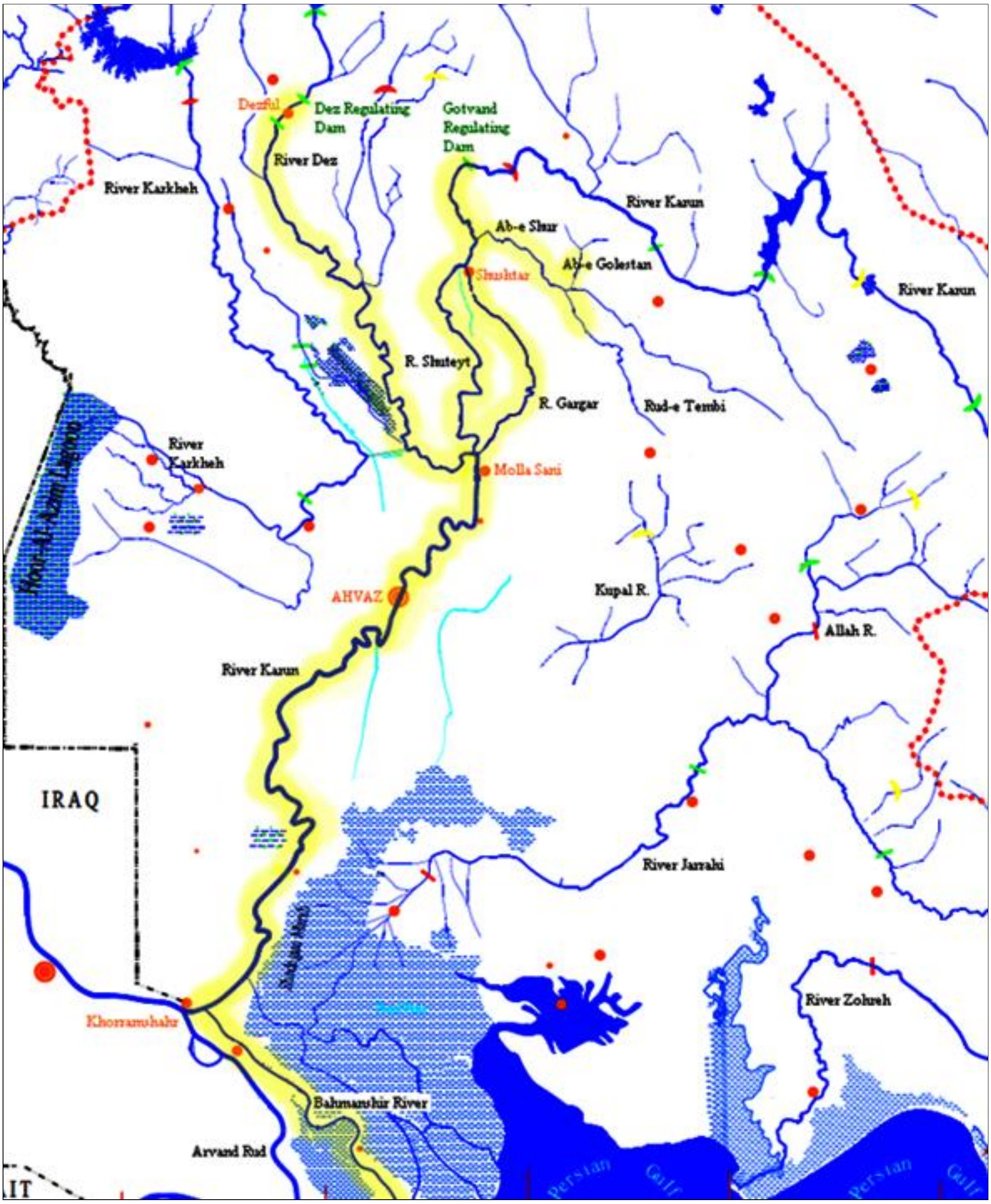

Key to Figure 3.4

River

River investigated in this study

Canal

Lake, marsh or lagoon

Reservoir dam

Diversion dam

Regulating dam

(Green indicates operational, red indicates under construction, yellow indicates projected)

International boundary

Khuzestan Province boundary

Town or city

---

sinuosity) could be better quantified and so that river reaches upstream of a fold, across the axis of a fold, and downstream of a fold could be compared.

The survey data, fieldwork data, and map and remote sensing data were compiled and analysed. The map and remote sensing data had a wide variety of sources and dates, including:

1:25,000 and 1:50,000 scale topographical maps (various uncertain dates for original IOOC and NCC surveys, probably 1961 - 2001 AD)

1:100,000 scale geological maps (IOOC, various dates, mainly 1960's and 1970's AD)

1:1,000,000 scale geological map of south-west Iran (NIOC, 1973)

1:2,500,000 scale tectonic map of south-west Iran (NIOC, 1977)

1:63,000 scale aerial photographs of some parts of the study area (1955 AD)

CORONA satellite images (missions 1035-1 and 1045-2, revolutions 040D and 182D, frames 12-20 and 65-74), with a maximum resolution of c. 3m (23 September 1966 AD and 5 February 1968 AD) (Walstra et al., 2010a)

Landsat Enhanced Thematic Mapper Plus satellite images (paths 165-166, rows 38-39) of various dates and spectral bands, each pan-sharpened with panchromatic Band 8, with a resolution of c. 30 m (2000 AD with three Landsat ETM+ bands: *Band 7* (mid-infrared, wavelength 2,090-2,350 nm) displayed as red, Band 4 (near-infrared, 750-900 nm) displayed as green, and Band 2 (visible green, 525-605 nm) displayed as blue) to highlight variations in lithology and vegetation) (28 July and 4 August 2001 AD with three Landsat ETM+ bands: Band 4 displayed as red, *Band 3* (visible red, 630-690 nm)

Figure 3.5 The sub-division of the River Karun (Shuteyt and Gargar branches) and River Dez into straight-line river "reaches"

(Landsat (2001) false-colour image with three ETM+ bands: Band 4 (near-infrared, wavelength 750-900 nm) displayed as red; *Band 3* (red, 630-690 nm) displayed green; Band 2 (visible green, 525-605 nm) displayed as blue; Resolution 30 m) (NASA, 2012)
Scale approx. 1:1,350,000 River "reaches" shown as green lines

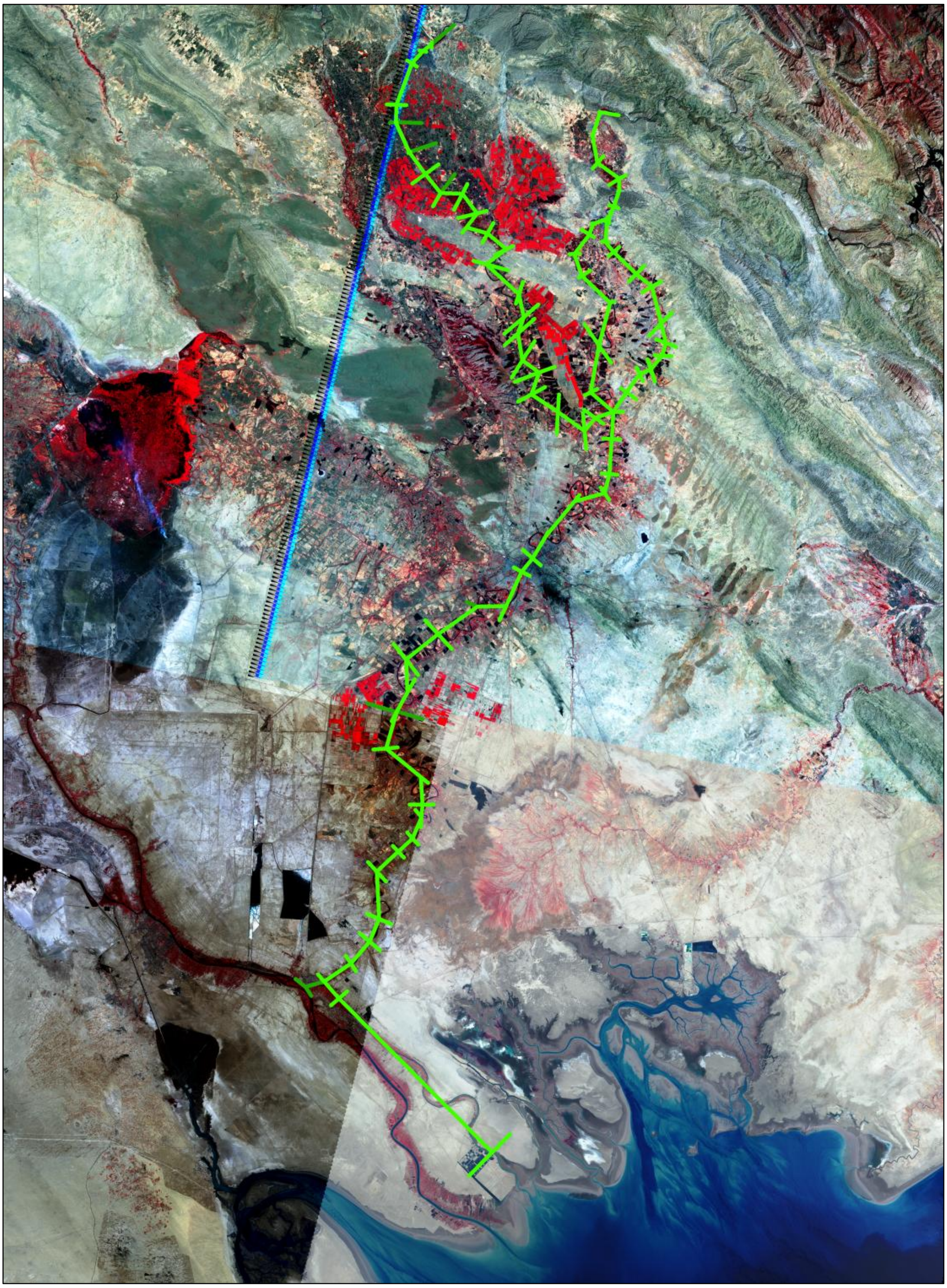

displayed as green, and Band 2 displayed as blue) (Drury, 2001; Gutman et al., 2008; Walstra et al., 2010a; NASA, 2012)

Since these maps and remote sensing images had different dates there were differences between them, particularly due to changes in human activities and river geomorphology with time. To avoid errors involved with these changes, a standard date of 2000 AD was employed for characteristics, the approximate date of completion of the Dez Ab Engineering Company survey and the approximate date of the analysed Landsat ETM+ satellite images. The compiled data set was used to determine the following:

River longitudinal profiles, with plots of valley/average river floodplain elevation, average channel banks elevation, river water surface elevation, and deepest channel bed elevation against valley distance (the distance measured along the valley in a succession of straight-line "reaches", in a manner similar to that used by Burnett, 1982)
Structural geology, including locations and characteristics of anticlines and emerging oilfield anticlines
Human activities
River geomorphology, river hydrology, and river sedimentology
River migration, with data from each river reach for the CORONA (1966 and 1968) satellite images and the Landsat (2001) satellite images which had been superimposed in an ArcGIS® database by the Geological Survey of Belgium (Walstra et al., 2010a) being used to determine river channel migration over a mean period of 34.2 years (Shields et al., 2000; Giardino and Lee, 2011). Channel-belt dimensions were also determined as indicators of river aggradation and channel migration over longer periods, mainly timescales of millennia (Alexander et al., 1994; Burbank and Anderson, 2001)

These characteristics of the rivers, the structural geology and the human activities were compiled to investigate the influences of Earth surface movements and human activities on the major rivers Karun and Dez. Details of the methods used are given in Appendix 7.2. The various characteristics were analysed to determine relationships between them. The methods used included standard statistical techniques (Upton and Cook, 1996; Rogerson, 2006; Salkind, 2010). For instance, analysis of variance (ANOVA) was applied to different groups of river reaches (such as river incision across a fold) for different variables (such as average channel-belt width) and regression analysis was applied to determine the strength of correlation between selected variables and river valley distance from the nearest fold axis (Rogerson, 2006; Salkind, 2010).

3.4 Laboratory analyses for investigating Earth surface movement rates and for investigating river characteristics

To improve the descriptions and interpretations of Earth surface movement rates and river characteristics, and to determine elemental concentrations necessary for OSL dating, a variety of laboratory analyses were undertaken. Details of these laboratory analyses are given in Appendix 7.3.

3.4.1 Gravel lithological analysis

Analysis of the gravel lithologies of river bed samples and river terrace deposits were undertaken using a hand lens, Leica S6 zoom stereo-microscope, a sharp-pointed steel probe and dropper bottles of hydrochloric acid, following established procedures (Bridgland, 1986; Gale and Hoare, 1991; Dietrich, 2011).

3.4.2 Thin section analysis

Thin sections of fine-grained sediment and rock samples from river banks and beds, river terraces, ancient constructions and bedrock were prepared using established methods (Heinrich, 1965; Adams et al., 1984; Miller, 1988). General descriptions and point counting of these thin sections were undertaken using an Olympus BH-2 petrographic microscope, following established procedures (Harwood, 1988; Miller, 1988; Garrison, 2003).

3.4.3 Inductively coupled plasma spectrometry

For derivation of the annual dose-rate in each sediment sample for OSL dating, the concentrations of naturally occurring uranium (U), thorium (Th), potassium (K) and rubidium (Rb) were determined by inductively coupled plasma spectrometry. These measurements were made by Inductively Coupled Plasma Mass Spectrometry (ICP-MS) using a PerkinElmer SCIEX ELAN DRC II ICP-MS (PerkinElmer SCIEX, 2001), and by Inductively Coupled Plasma Optical Emission Spectrometry (ICP-OES) using a PerkinElmer Optima 5300 DV ICP-OES (PerkinElmer, 2004), according to established procedures (Fairchild et al., 1988; Boss and Fredeen, 2004).

3.4.4 Grain size analysis

In the field, grain size assessments of sediments and rocks were based on observations, direct measurements (including a-axis, b-axis and c-axis measurements of gravel clasts (Gale and Hoare, 1991)), use of grain scales, and touch (UTA, 2011). In the laboratory, fine-grained sediment and rock samples (fine gravels and smaller) from river banks, beds and floodplains, river terraces, and ancient constructions had their grain size distributions analysed in more detail. After pre-treatments, each sub-sample was wet sieved through a 63 μm sieve. The less than 63 μm fraction was kept in solution and analysed using a laser diffraction particle size analyser. The equipment used was the Sympatec GmbH HELOS helium-neon laser diffraction sensor and the QUIXEL wet dispersing system, following recommended methods (Sympatec GmbH, 1994; Witt and Heuer, 1998). The greater than 63 μm fraction was dried in a drying oven and analysed using a laser imaging particle size analyser. The equipment used was the Sympatec GmbH QICPIC image analysis sensor and the GRADIS dry gravity dispersing system, following recommended methods (Sympatec GmbH, 1995, 1998; Witt et al., 2005).

CHAPTER 4 RESULTS

"Hofstadter's Law: It always takes longer than you expect, even when you take into account Hofstadter's Law."

Douglas Hofstadter, American academic (1945 AD -)

4.1 Introduction

The results of the study are given in this chapter, mainly as tables, graphs, and annotated maps, remote sensing images and photographs, and also in Appendices 1 to 6 as tables. The results are considered in more depth in Chapters 5, 6 and 7 where the results are discussed, statistically analysed, and interpreted. The results fall into three main groups:

4.2 Results relating to Earth surface movement rates

4.3 Results for river characteristics influenced by Earth surface movements and human activities

4.4 Results of laboratory analyses

The results of using map and remote sensing data, fieldwork data, and data from published articles (including Sherkati and Letouzey, 2004; Abdollahie Fard et al., 2006; Maleki et al., 2006; Soleimani et al., 2008) to determine the locations of anticlines, oilfields, and oilfield anticlines in lowland south-west Iran are given in Figure 4.1. This summary figure includes an annotated overview map of south-west Iran (Figure 4.1 (a), modified NIOC (1973) geological map) and annotated remote sensing images of selected areas (Figures 4.1 (b) to (g), Landsat (2000) false-colour images).

4.2 Results relating to Earth surface movement rates

4.2.1 Results for marine terraces along the north-east coast of the Persian Gulf

Fieldwork and remote sensing images show that there are two marine terraces along the north-east coast of the Persian Gulf. There is a lower terrace, Marine terrace A, of terrace surface elevation about $^{+}0.7$ m to $^{+}3$ m above Mean High Water, and a higher terrace, Marine terrace B, of terrace surface elevation about $^{+}10$ m to $^{+}30$ m above Mean High Water (Woodbridge, 2006).

Figure 4.1 (a) Geological map of south-west Iran showing selected anticlines, oilfields, and oilfield anticlines in the lowlands and the locations of other figures (Modified from NIOC (1973) using various sources)

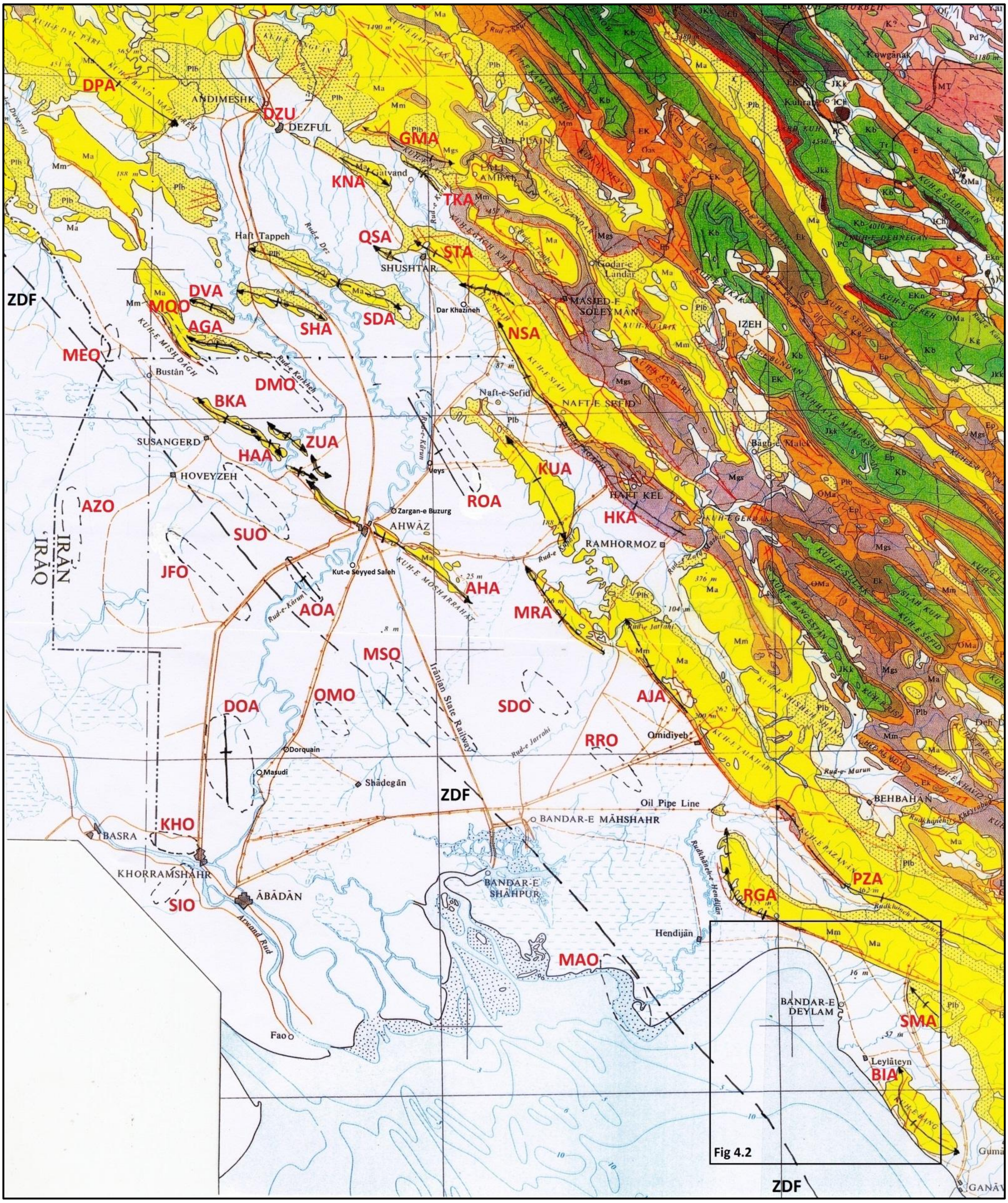

Figure 4.1 (a) (continued) Geological map of central Khuzestan showing the locations of six other figures, with **Key** to geological map symbols (Modified from NIOC (1973) using various sources)

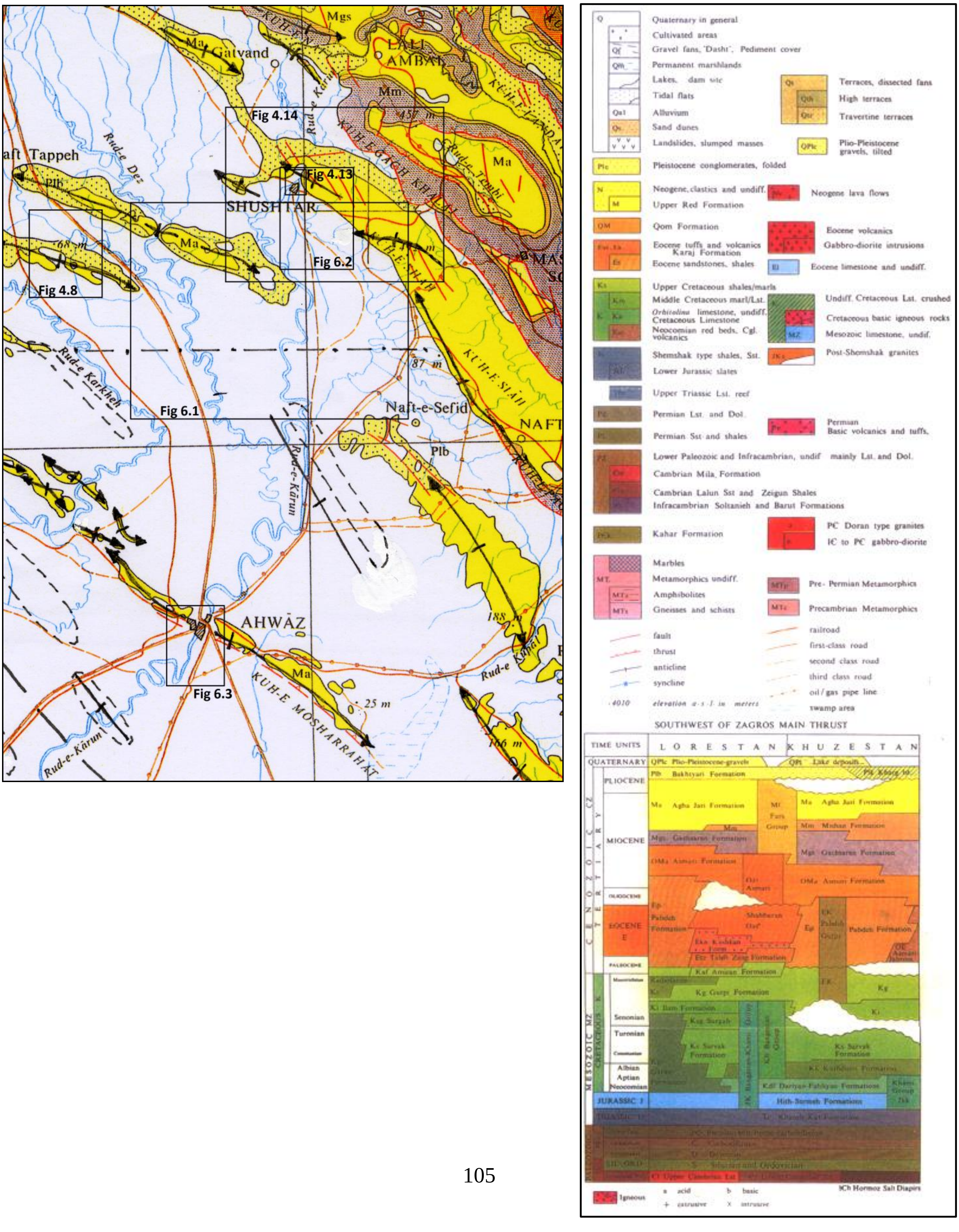

Key to annotations on Figure 4.1 (a)

— — — — — — **ZDF** Zagros Deformation Front

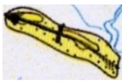 Axis of anticline (arrow indicates direction of plunge)

 Oilfield

Oilfield anticline

 "Concealed fault/deep-seated lineament" oriented E-W at 31°47'N

Abbreviations for selected anticlines and oilfields

AGA	Abu ul-Gharib Anticline	**AHA**	Ahvaz Anticline
AJA	Agha Jari Anticline	**AOA**	Ab-e Teymur Oilfield Anticline
AZO	Azadegan Oilfield	**BIA**	Binak Anticline
BKA	Band-e Karkheh Anticline	**DMO**	Dasht-e Mishan Oilfield
DOA	Dorquain Oilfield Anticline	**DPA**	Dal Parri Anticline
DVA	Darreh-ye Viza Anticline	**DZU**	Dezful Uplift
GMA	Gach-e Moh Anticline	**HAA**	Hamidiyyeh Anticline
HKA	Haft Kel Anticline	**JFO**	Jufeyr Oilfield
KHO	Khorramshahr Oilfield	**KNA**	Kuhanak Anticline
KUA	Kupal Anticline	**MAO**	Mahshahr Oilfield
MEO	Mehr Oilfield	**MQO**	Mushtaq Oilfield
MRA	Marun Anticline	**MSO**	Mansuri Oilfield
NSA	Naft-e Safid Anticline	**OMO**	Omid Oilfield
PZA	Pazanan Anticline	**QSA**	Qal'eh Surkheh Anticline
RGA	Rag-e Safid Anticline	**ROA**	Ramin Oilfield Anticline
RRO	Ramshir Oilfield	**SDA**	Sardarabad Anticline
SDO	Shadegan Oilfield	**SHA**	Shahur Anticline
SIO	Siba Oilfield	**SMA**	Siah Makan Anticline
STA	Shushtar Anticline	**SUO**	Susangerd Oilfield
TKA	Turkalaki Anticline	**ZUA**	Zeyn ul-Abbas Anticline

The oilfields in this region are anticlines

The annotated remote sensing images of Figures 4.1 (b) to (g) are of smaller areas within lowland south-west Iran:

Figure 4.1 (b) covers Central Khuzestan (same area as the smaller geological map), including the Shushtar Anticline (STA) and Ahvaz Anticline (AHA)
Figure 4.1 (c) covers the vicinity of Dezful, including the Dezful Uplift (DZU)
Figure 4.1 (d) covers the vicinity of Veys, including the Ramin Oilfield Anticline (ROA)
Figure 4.1 (e) covers the lower reaches of the River Karun, including the Ab-e Teymur Oilfield Anticline (AOA) and Dorquain Oilfield Anticline (DOA)
Figure 4.1 (f) covers the lower reaches of the River Karkheh, including the Darreh-ye Viza Anticline (DVA) and Susangerd Oilfield (SUO)
Figure 4.1 (g) covers the lower reaches of the River Jarrahi, including the Marun Anticline (MRA) and the Mansuri Oilfield (MSO)

Figure 4.1 (b) Central Khuzestan (Landsat (2000) false-colour image showing main rivers and anticlines)

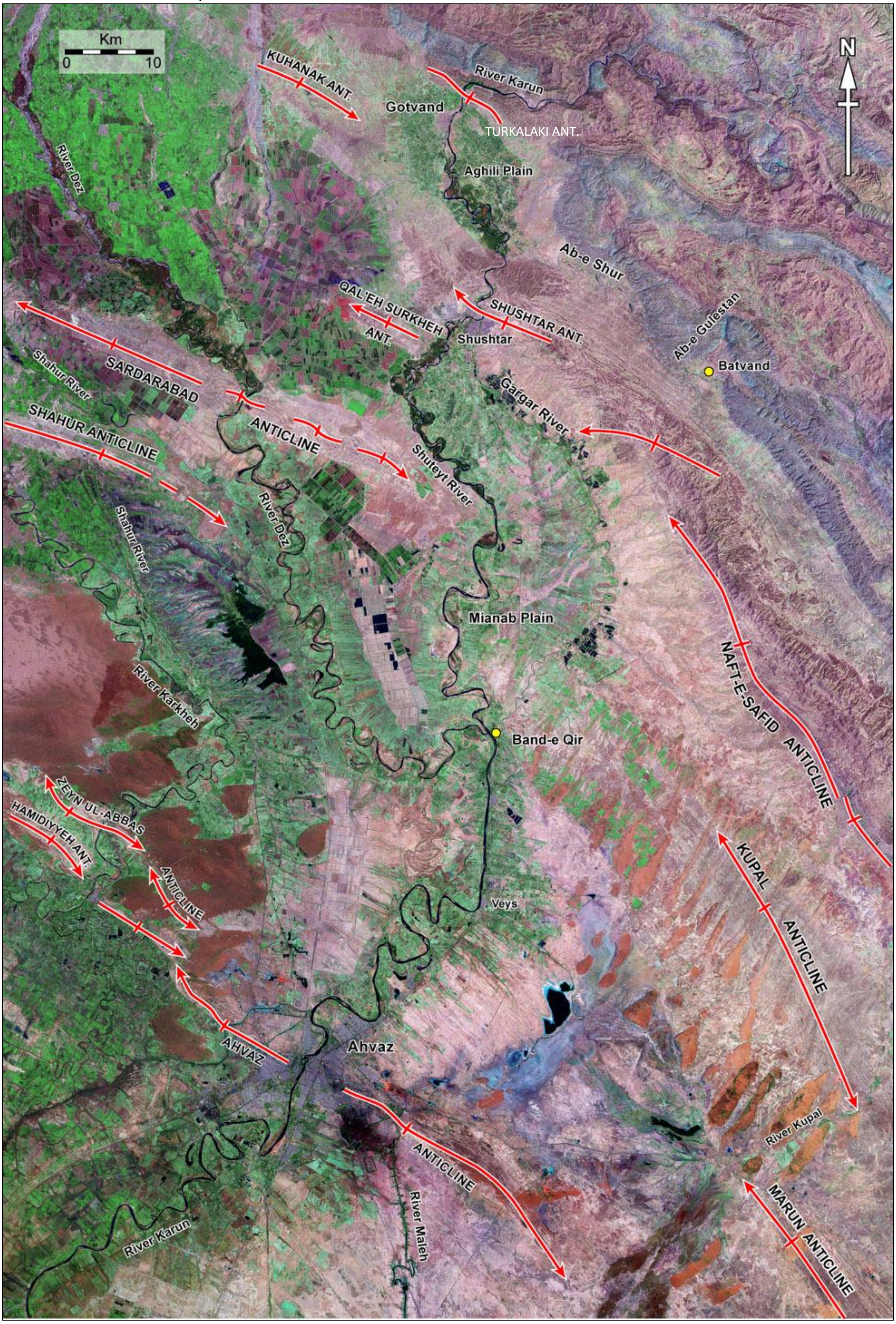

Figure 4.1 (c) The vicinity of Dezful (Landsat (2000) false-colour image showing the Dezful Uplift, which extends to the NW off image and to the SE to near the Shirin Ab)

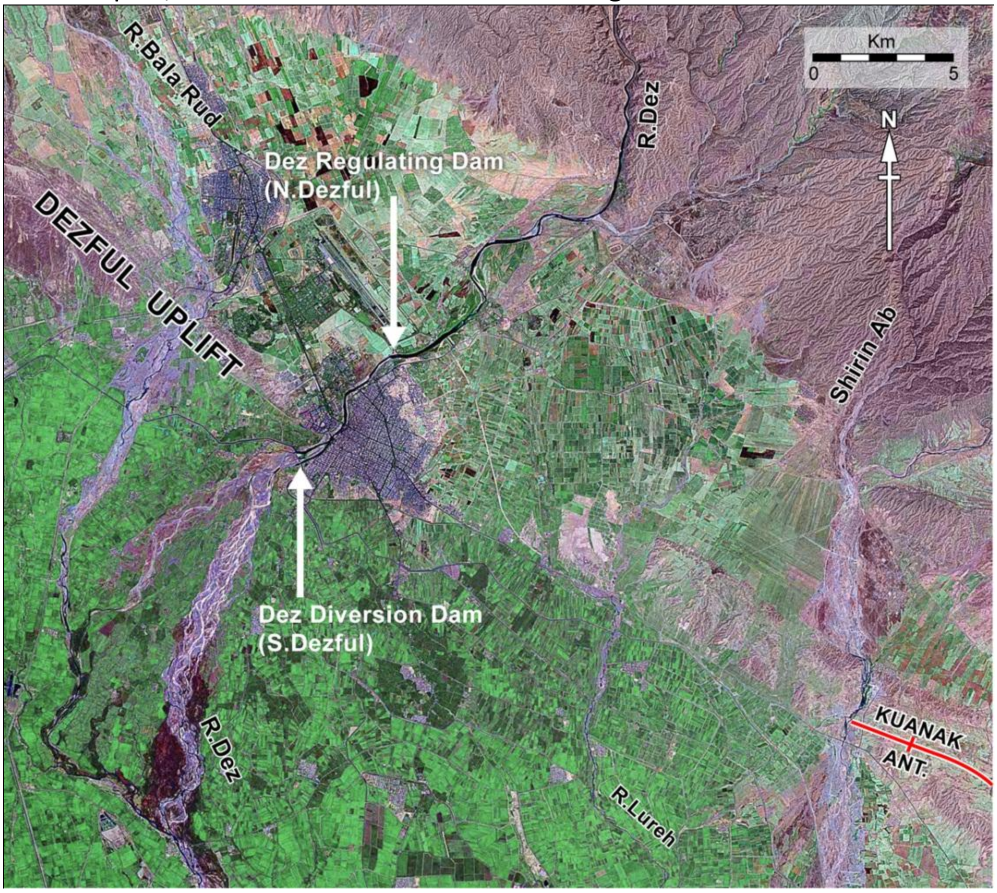

Figure 4.1 (d) The vicinity of Veys and Band-e Qir (Landsat (2000) false-colour image showing main rivers and the Ramin Oilfield Anticline)

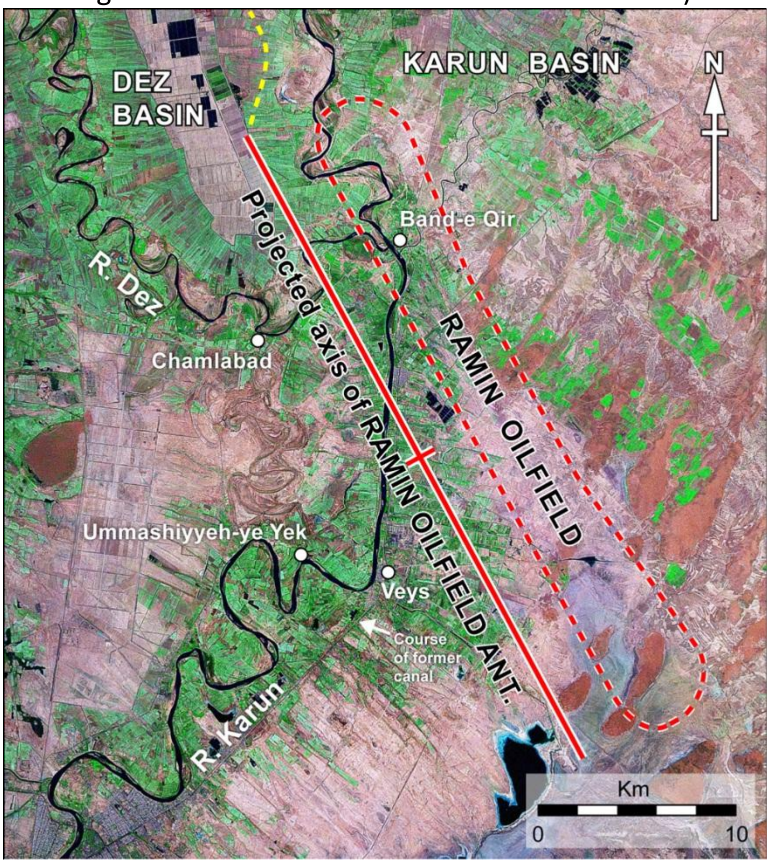

Figure 4.1 (e) The lower reaches of the River Karun (Landsat (2000) false-colour image showing main rivers, anticlines and oilfields)
Scale approx. 1:490,000

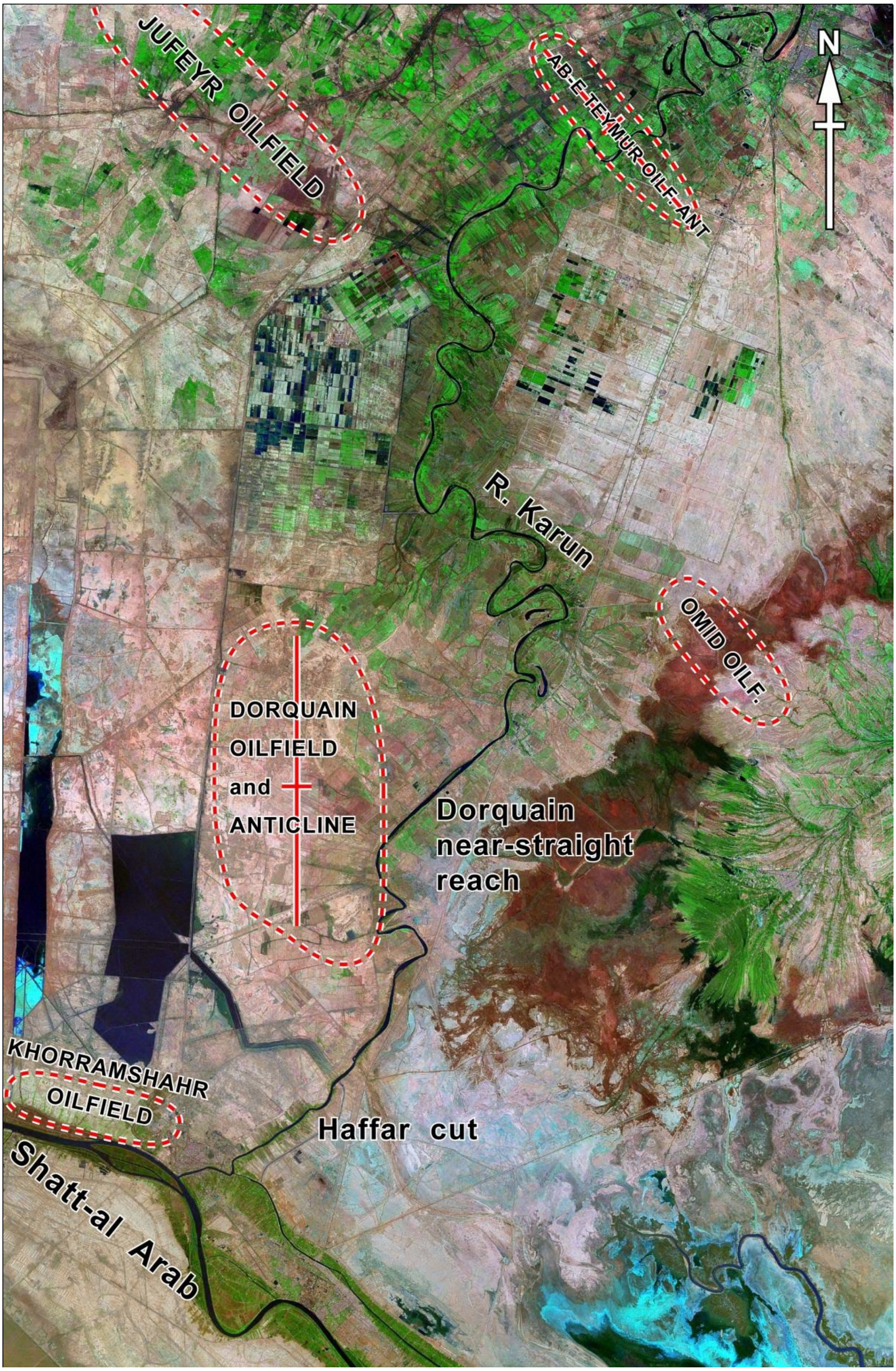

Figure 4.1 (f) The lower reaches of the River Karkheh (Landsat (2000) false-colour image showing main rivers, anticlines and oilfields)

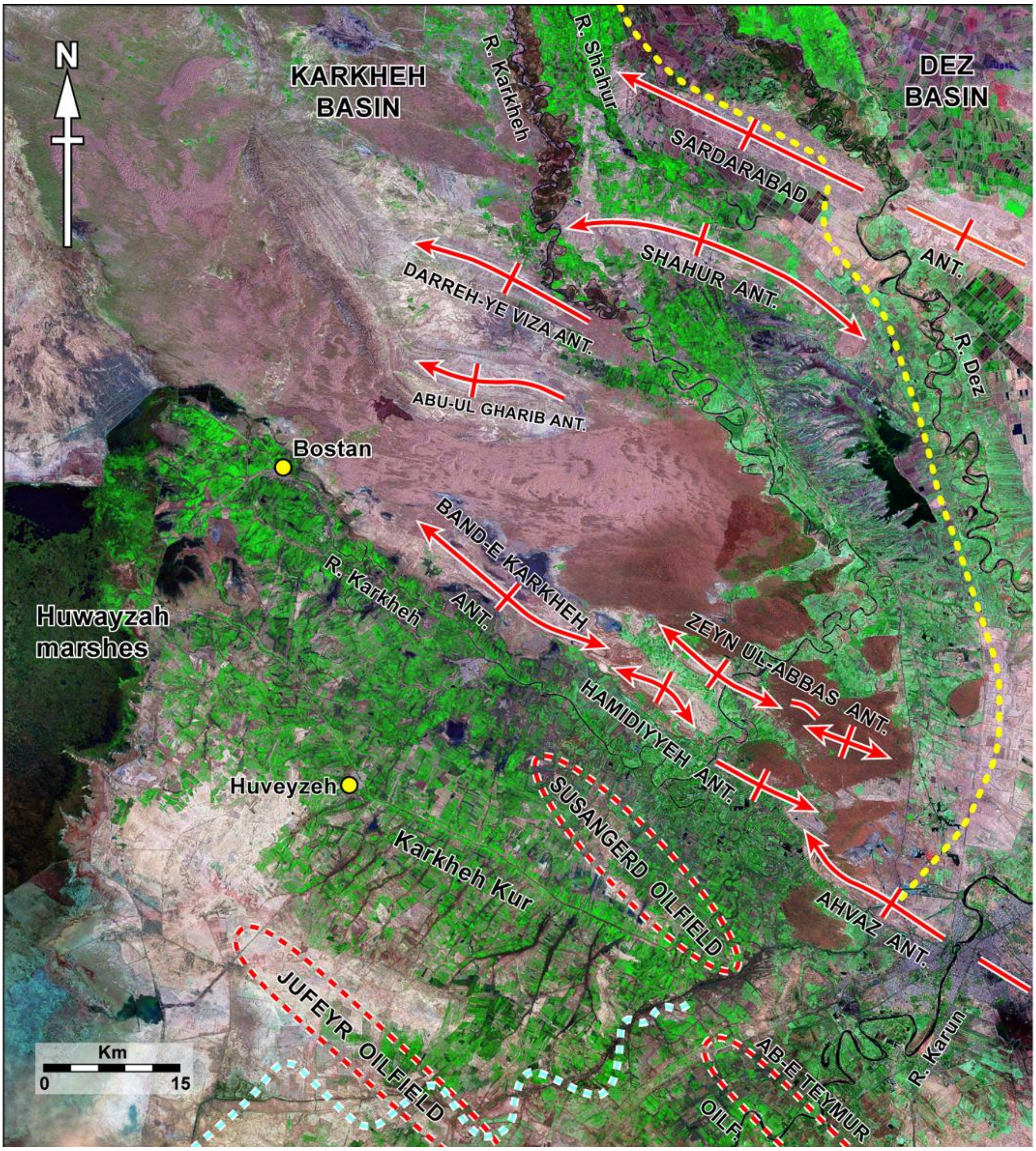

Figure 4.1 (g) The lower reaches of the River Jarrahi (Landsat (2000) false-colour image showing main rivers, anticlines and oilfields)

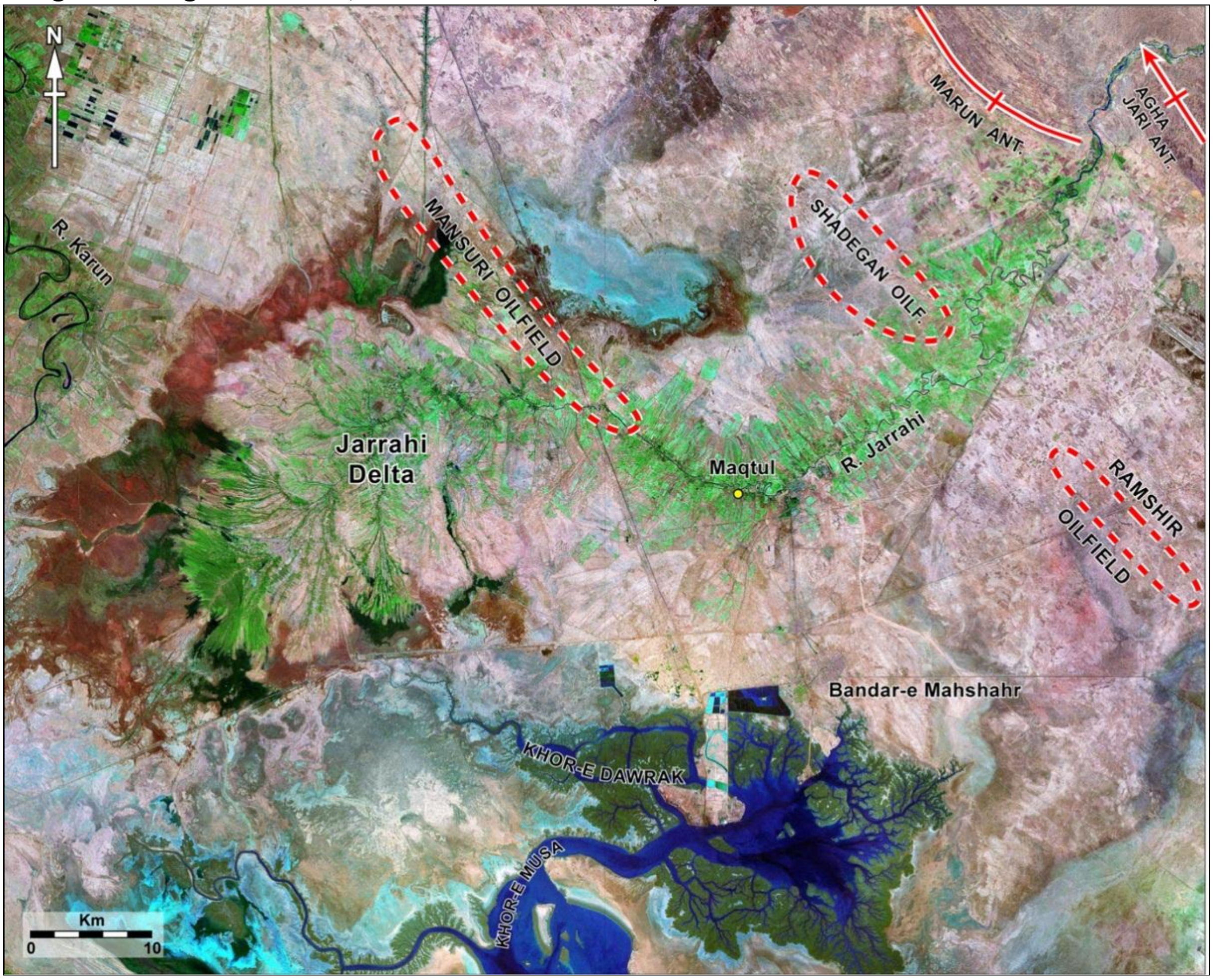

Key to Figure 4.1 (b) to Figure 4.1 (g)

Thick red line with cross bar - Axis of anticline (arrow indicates direction of plunge)
Yellow dashed line - River basin margin (approx. location on Fig. 4.1 (d) and Fig. 4.1 (f))

Red dashed line - Oilfield margin (approx. interpreted extent from maps and articles)

Pale blue dashed line - Course of palaeochannel of River Karun ("K2" of Fig. 2.10, Heyvaert et al., 2013)

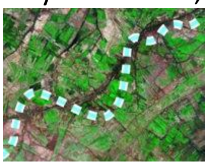

○ or ○ Modern settlement

The locations of the two marine terraces are shown in Figure 4.2.

Figure 4.2 Marine terraces A and B along the north-east coast of the Persian Gulf (Landsat (2000) false-colour image)

Marine terrace A is a moderately continuous ridge or berm, generally parallel to the coastline, extending from the north-east head of the Persian Gulf, through location BANDN1 and Bandar-e Deylam, to location BINAK3 (very near to BINAK4) and beyond.

Marine terrace B is a discontinuous, gently sloping, planar surface preserved as a capping on high rock outcrops mainly on the W limb of the Binak Anticline, particularly at location BINAK4. There are progressively fewer terrace fragments preserved to the N and NNW of the Binak Anticline, extending about as far north as Bandar-e Deylam.

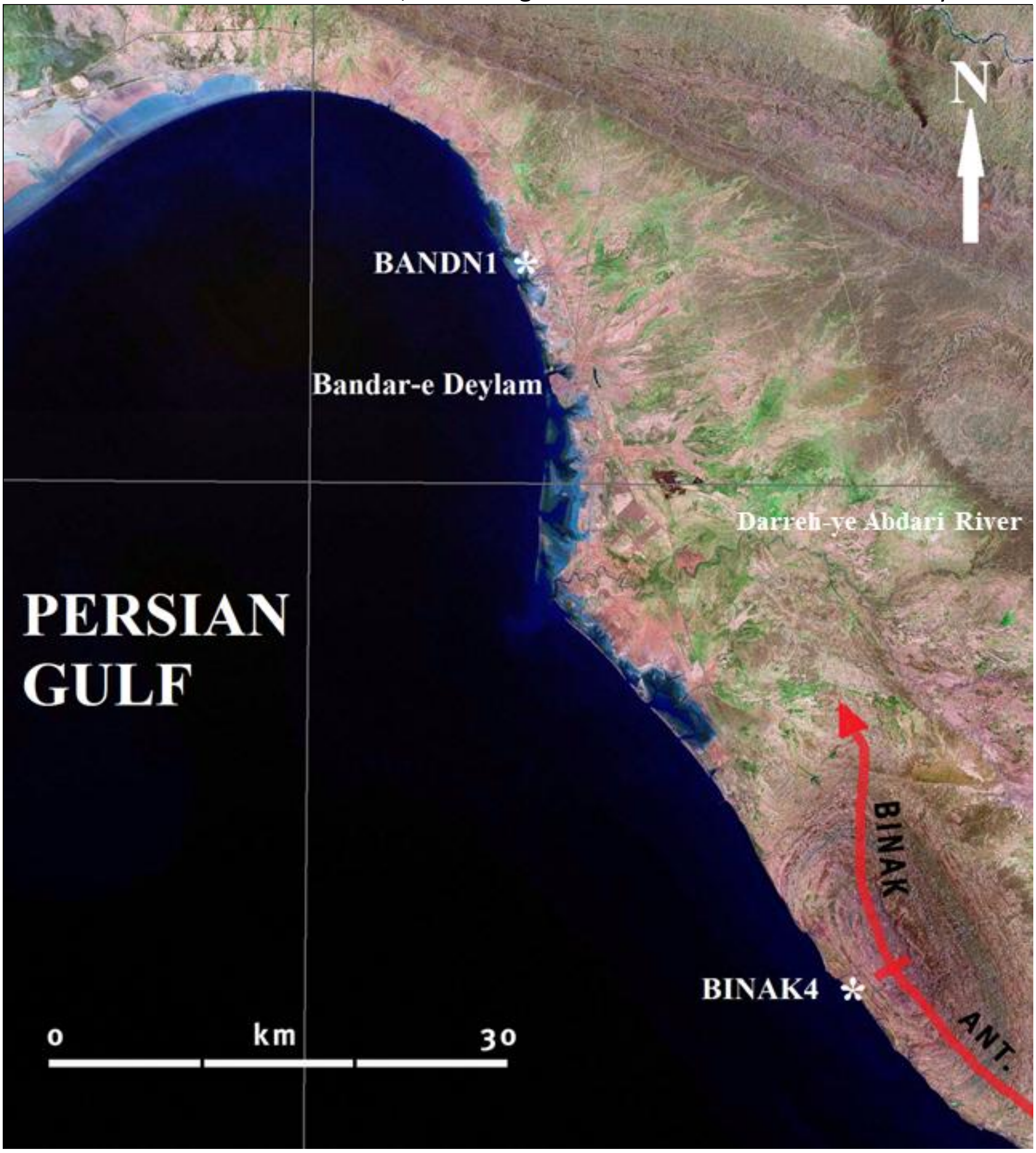

Key

Red line with cross bar Axis of Binak Anticline (arrow indicates direction of plunge)

∗BANDN1 Location north of Bandar-e Deylam, 30°06’47”N 50°07’44”E

∗BINAK4 Location near Binak, 29°43’39”N 50°20’28”E

The general geomorphology of the two marine terraces is shown in Figure 4.3 and 4.4.

Figure 4.3 Marine terrace A north of Bandar-e Deylam - general view (near 30°06’47’’N 50°07’44’’E looking NW)

Figure 4.4 Marine terraces A and B near Binak - general view (near 29°43’30’’N 50°20’23’’E looking SE)

Exposures of the terrace deposits of Marine terraces A and B are shown in Figure 4.5 and Figure 4.6, with the locations of marine mollusc shell samples taken for radiocarbon dating indicated. The findings for Marine terraces A and B are summarised in Table 4.1 and Table 4.2.

Figure 4.5 Exposure of terrace deposits of Marine terrace A near location BINAK3 (near 29°43'30''N 50°20'23''E looking NE, hammer 30 cm long)

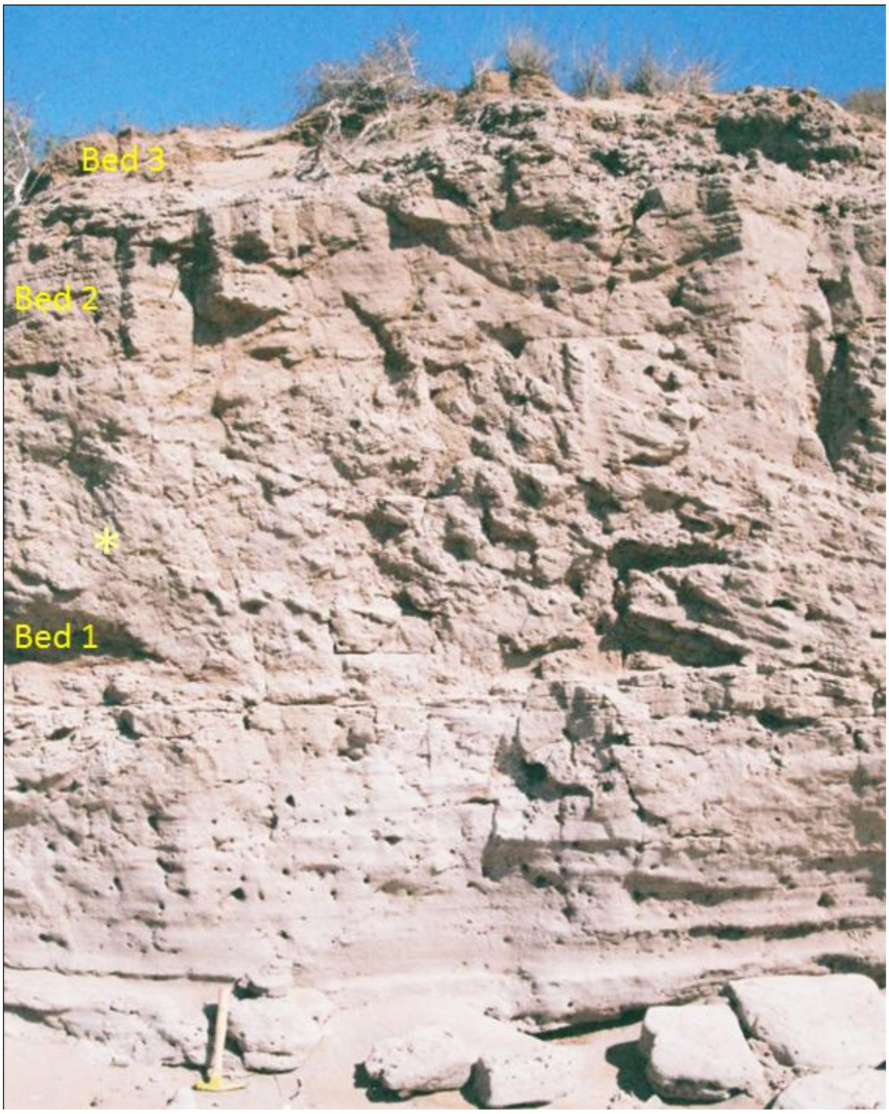

Yellow asterisk indicates location of marine mollusc shell from Bed 1, dated by conventional radiocarbon dating to 3,310 ± 60 BP (GrN-25106), calibrated to **1,390 ± 91 cal.BC**

Figure 4.6 Exposure of upper terrace deposits of Marine terrace B at location BINAK4 (near 29°43’39’’N 50°20’28’’E)

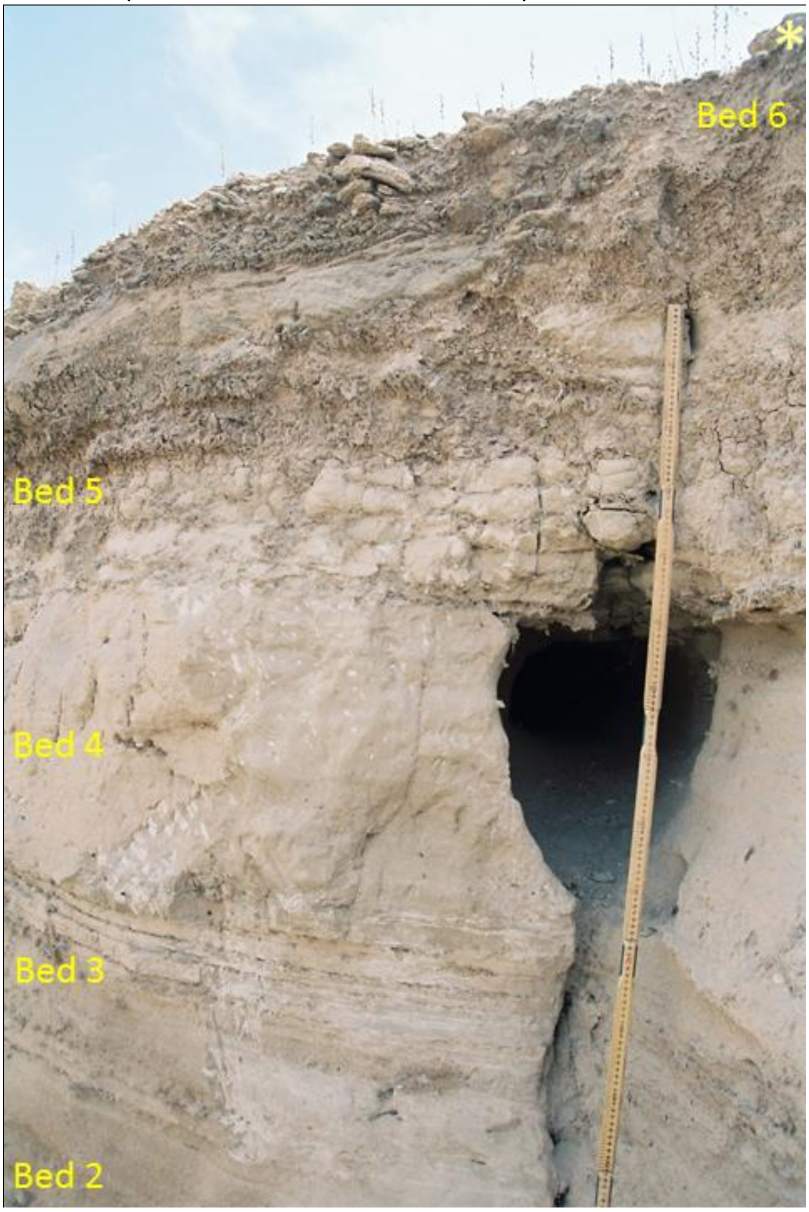

Yellow asterisk indicates location of marine mollusc shell from Bed 6, dated by AMS radiocarbon dating to **> 43,000 BC** (GrA-21606) (**infinite radiocarbon age**)

Marine mollusc shell sample from Bed 6 was *Ostrea sp.* from shell encrustation around *in situ* small boulder within sandy and shelly beachrock

Table 4.1 Summary of findings for Marine terrace A

Marine terrace	**Elevation**	**Short description**	**Probable age**
Marine terrace A Located along the NE coast of the Persian Gulf, including: BANDN1 (north of Bandar-e Deylam, 30°06’47’’N 50°07’44’’E) BINAK3 (near Binak on SW limb of Binak Anticline at 29°43’18’’N 50°20’44’’E)	About $^{+}$0.7 m to $^{+}$3.0 m above Mean High Water (MHW) strand lines	A moderately continuous linear ridge or berm, generally parallel to the present-day coastline. At some locations it forms a barrier ridge behind which small lagoons, tidal flats and coastal sabkhas have developed. The terrace deposits are mainly sands plus some shells, in places well-cemented as sandy beachrock. General stratigraphic sequence north of Bandar-e Deylam (BANDN1, 30°06’47’’N 50°07’44’’E) (top of sequence at c. $^{+}$2.80 m above MHW): Bed 3 (c. 33 cm thick) - Modern light grey sands, with shell fragments and plant rootlets. Bed 2 (c. 17 cm thick) - Quite well cemented light grey finely bedded sands with shell fragments, well cemented beachrock in upper few cm. Bed 1 (more than 61 cm thick) - Quite well cemented orange-brown sands with shell fragments, well cemented beachrock in upper few cm.	Marine mollusc shell (*Diplodonta sp.*, mass 6 g) from ridge of sandy beachrock north of Bandar-e Deylam (location BANDN1, Bed 2) at $^{+}$2.51 m above MHW, dated by AMS radiocarbon dating to 2,820 ± 50 BP (GrA-15580) (Woodbridge, 2006). OxCal Version 4.2 (Bronk Ramsey, 2013), marine data from the curve of Reimer et al. (2009), and ΔR offset of $^{+}$180 years (Southon et al., 2002) produce a calibrated radiocarbon date of **815 ± 87 cal.BC** 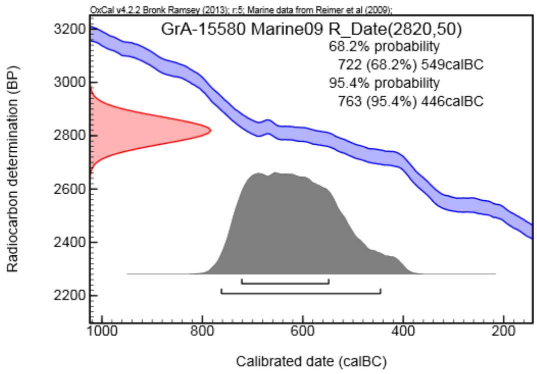 Marine mollusc shell (*Acrosterigma sp.* mass 22 g) from beachrock near Binak (location BINAK 3, Bed 1) on ***SW limb of the Binak Anticline*** at $^{+}$1.62 m above MHW, dated by conventional radiocarbon dating to 3,310 ± 60 BP (GrN-25106) (Woodbridge, 2006). OxCal Version 4.2 (Bronk Ramsey, 2013), marine data from Reimer et al. (2009), and ΔR offset of $^{+}$180 years (Southon et al., 2002) produce a calibrated radiocarbon date of **1,390 ± 91 cal.BC** 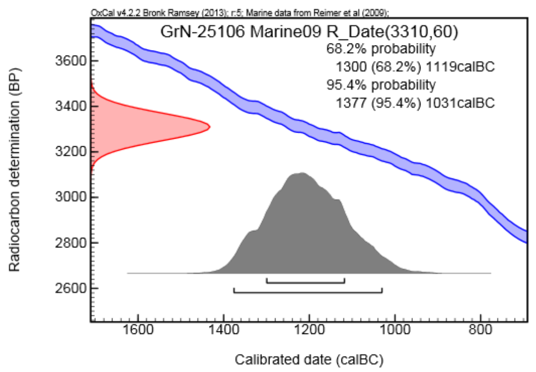

Table 4.2 Summary of findings for Marine terrace B

Marine terrace	**Elevation**	**Short description**	**Probable age**
Marine terrace B Located along the NE coast of the Persian Gulf, mainly near Binak, including: BINAK4 (near Binak, on SW limb of Binak Anticline at 29°43’39’’N 50°20’28’’E)	About $^{+}$10 m to $^{+}$30 m above Mean High Water (MHW) strand lines	A discontinuous, gently sloping, planar terrace surface preserved as a capping on high rock outcrops. Progressively fewer preserved terrace fragments are present north of the environs of the Binak Anticline. The terrace deposits are mainly well cemented sands and shells (beachrock), with other deposits occasionally preserved at greater depths. General stratigraphic sequence near Binak (BINAK4, 29°43’39’’N 50°20’28’’E) (top of sequence at c. $^{+}$15 m above MHW): Bed 6 (more than 70 cm thick) - Very well cemented light grey sands and abundant shells (beachrock), with some gravels and few small boulders; multi-directional “herring-bone” cross-bedded sands in lower part. Bed 5 (c. 60 cm thick) - Light grey silt/clay, well-cemented by abundant gypsum/anhydrite; nodular structure in lower part, massive structure in upper part. Bed 4 (c. 50 cm thick) - Mainly high-angle cross-bedded sands with very small shell fragments; vertical burrows (probably *Skolithos*) in upper few cm. Bed 3 (c. 34 cm thick) - Laminated sands and silt/clays with some gypsum and occ. shell fragments; planar and wavy cross-laminations. Bed 2 (c. 400 cm thick) - Alternating bands of angular gravels and light grey laminated and cross-laminated sands and silts; generally fining upwards. Bed 1 (c. 105 cm thick) - Poorly sorted conglomerates, with thin bands of light grey fine sand. Agha Jari Formation bedrock (calcareous sandstones and mudstones).	Marine mollusc shell (*Ostrea sp.*, mass 1 g) from shell encrustation around *in situ* boulder within sandy/shelly beachrock (Bed 6) near Binak (location BINAK4) on ***SW limb of Binak Anticline*** at c. $^{+}$15 m above MHW, dated by AMS radiocarbon dating to **> 43,000 BC** (GrA-21606) (**infinite radiocarbon age**) (Woodbridge, 2006)

4.2.2 Results for ancient canals cut across the Shahur Anticline

Fieldwork and remote sensing images show the traces of two ancient canals (SC1 and SC2) with a roughly NNE-SSW orientation that cut across the Shahur Anticline (Figure 4.8). The traces of ancient canal SC1 are a series of dry, linear canal remnants (Figures 4.7 and 4.8).

Figure 4.7 Remnant of ancient canal SC1 cut across the Shahur Anticline (near 31°57′10′′N 48°22′02′′E (location A on Fig. 4.7) looking S)

Key to Figure 4.8

Axis of anticline

River channel - flow of R. Shahur is from the NW towards the S and SE

Palaeochannel - prior to and probably during the Early Sassanian Period (c. 224 - 379 AD) the River Karkheh may have bifurcated a few km upstream of the Shahur Anticline. Probably, there was a branch flowing to the north and east of the Shahur Anticline (the present-day River Shahur and the palaeochannel indicated flowing to the River Dez to the SE) and a branch to the west and south of the Shahur Anticline (similar to the present-day River Karkheh) (Gasche et al., 2007)

Trace of ancient canal

SC1 Sassanian Canal 1 SC2 Sassanian Canal 2

∗A Location of photograph of canal SC1 for Figure 4.7
∗B Location of photograph of canal SC2 for Figure 4.9
∗C Location of photograph of canal SC2 for Figure 4.10
KDD Kheyrabad Diversion Dam (or Sadd-e Karkheh) on the R. Shahur

Figure 4.8 Traces of two ancient canals (SC1 and SC2) cut across the Shahur Anticline (Landsat (2000) false-colour image and interpretation)

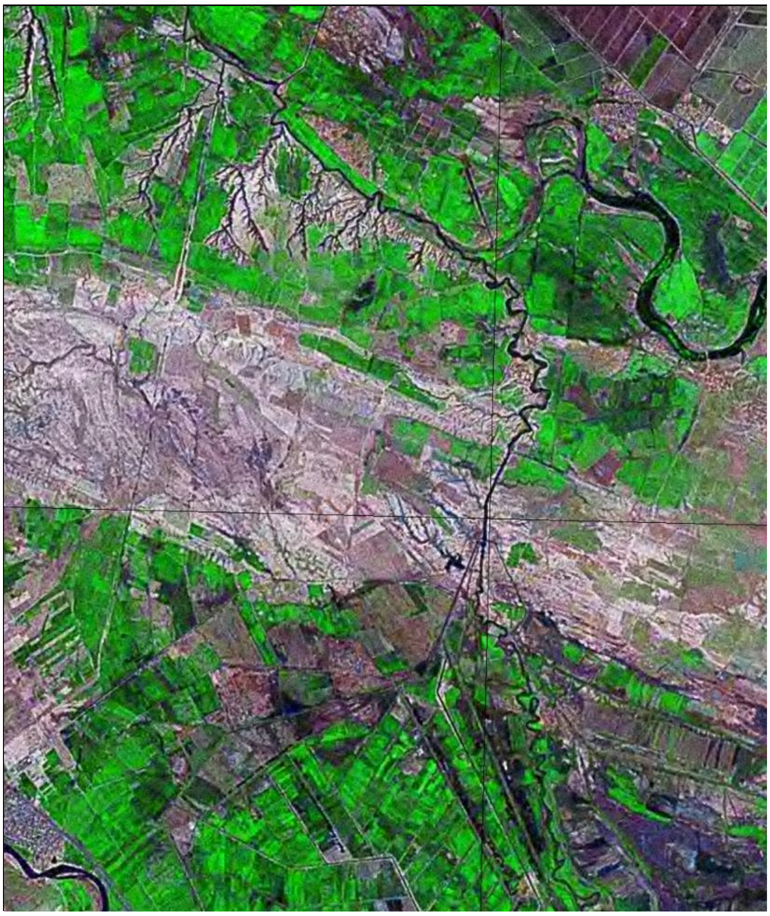

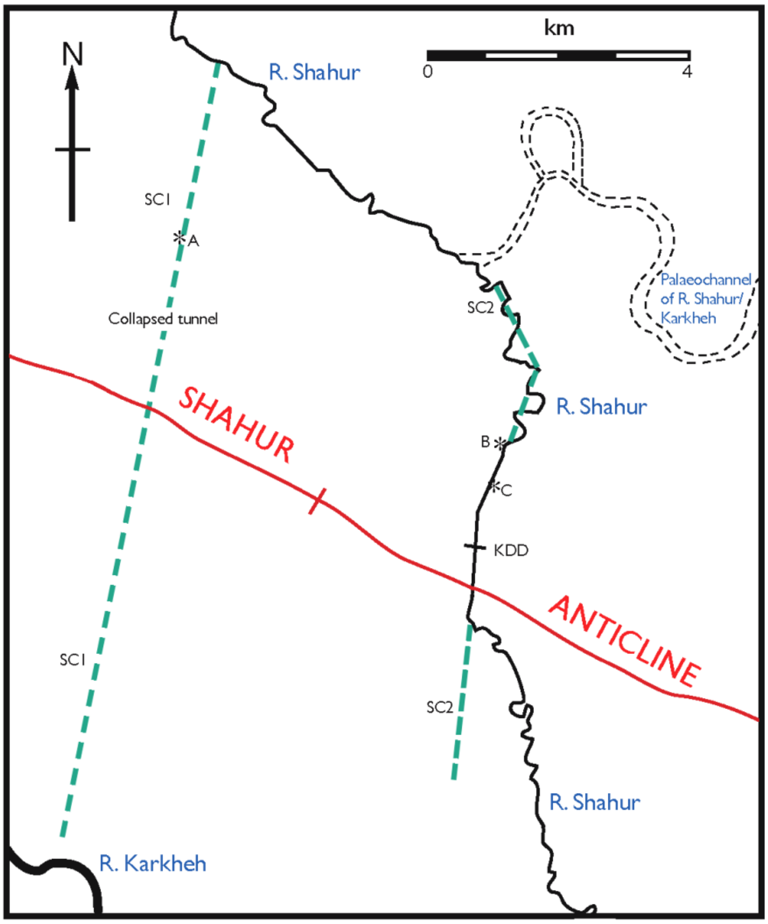

The traces of ancient canal SC2 are partly a series of linear canal remnants and partly the course of the present-day Shahur River (Figures 4.8, 4.9 and 4.10). An exposure of the sequence associated with ancient canal SC2 is shown in Figure 4.10.

Figure 4.9 Remnant of ancient canal SC2, now partly occupied by the Shahur River (near 31°55'30''N 48°25'10''E (location B on Fig. 4.8) looking NNE - i.e. N of the Shahur Anticline axis, looking upstream towards 020° along the course of the ancient canal)

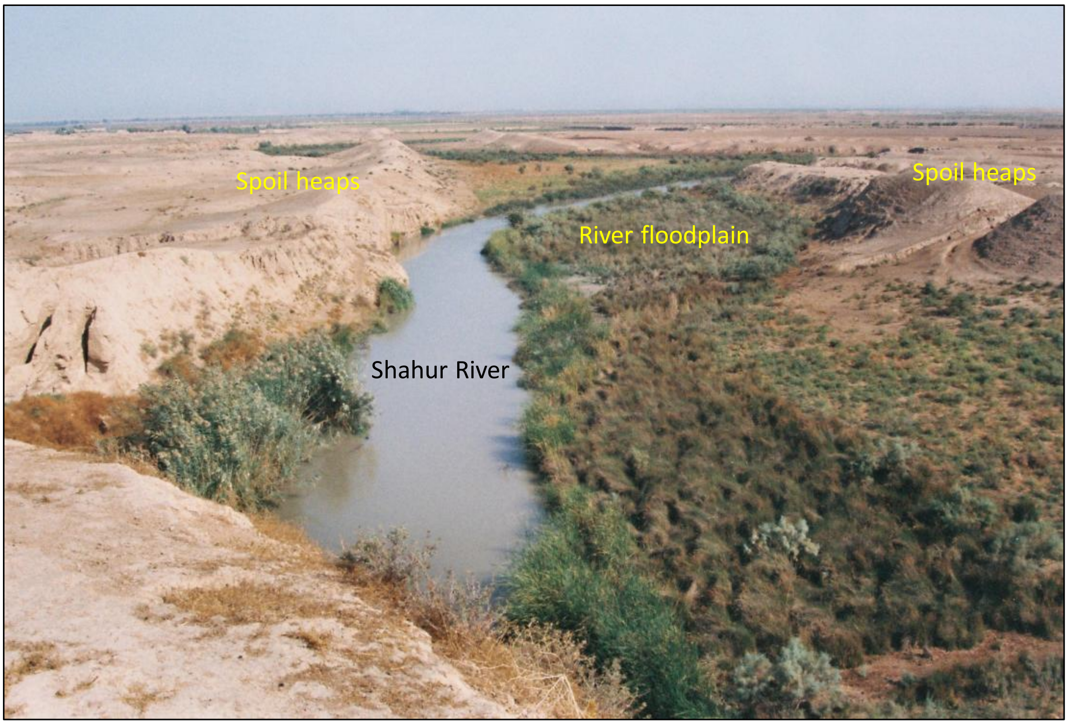

Figure 4.10 Sequence at a locality near the Shahur Anticline axis, where the Shahur River flows along a near-straight reach coincident with ancient canal SC2 (near 31°55'22''N 48°25'07''E (location C on Fig. 4.8) looking WNW, width of view c. 25 m)

The findings for ancient canals SC1 and SC2 are summarised in Table 4.3.

Table 4.3 Summary of findings for the two ancient canals cut across the Shahur Anticline

Ancient canal	**Short description**	**Probable age**
Ancient canal SC1 Approx. location 31°57'N 48°22'E	The course of an ancient canal, now dry. A straight canal remnant, with an approx. NNE-SWS course (original flow towards 190°) across the Shahur Anticline from the present-day Shahur River to the River Karkheh, which is well preserved. About 0.9 km - 1.5 km north of the axis of the Shahur Anticline (the crest of the anticlinal ridge),the ancient canal was cut through a tunnel, now collapsed. At a number of locations, remnants of the ancient canal (mostly infilled with sediment), ancient canal banks, and spoil heaps could be distinguished (Figure 4.7). A short survey to the north of the collapsed tunnel on the ***back-limb of the Shahur Anticline*** shows that the canal bank remnants slope fairly gently from S to N (i.e. opposite to the original flow direction of the canal), with an average slope (over a horizontal distance of 948.1 m) of 0.003159 m m^{-1} ≈ 0.18° (Woodbridge, 2006)	Probably constructed during the Early Sassanian Period (**c. 224 - 379 AD**) (Lees and Falcon, 1952; Lees, 1955; Woodbridge, 2006)
Ancient canal SC2 Approx. location 31°55'N 48°25'E	The course of an ancient canal, now partly occupied by the present-day Shahur River. A generally straight canal remnant, with an approx. NNE-SSW course (original flow generally towards 200°) across the Shahur Anticline from a palaeochannel east of the Shahur River to the River Karkheh, which is partially preserved. About 1.1 km - 2.0 km north of the axis of the Shahur Anticline, the present-day Shahur River flows along a near-straight reach coincident with the course of the ancient canal. This stretch is in the vicinity of the ***crest of the Shahur Anticline*** and just upstream of the modern Kheyrabad Diversion Dam (or Sadd-e Karkheh), operational since about 1940 AD (KWPA, 2010). Upstream and downstream of this near-straight reach, the Shahur River is slightly sinuous and wandering, with an overall approx. N-S course (flow towards about 170°) (Figures 4.8 and 4.9). A short survey in the vicinity of the near-straight reach of the Shahur River found this sequence at some localities: Extensive spoil heaps (sands and silts) Remnant of surface of ancient canal banks Cut through Agha Jari Formation bedrock (fairly coarse calcareous sandstone) Present-day river water surface In the vicinity of location C on Figure 4.8, relative to the present-day river water surface, the ancient canal bank surface is at elevation $^{+}$3.45 m and the top of the spoil heap is at $^{+}$7.91 m (see Figure 4.10) (Woodbridge, 2006)	Probably constructed during the Early Sassanian Period (**c. 224 - 379 AD**) (Lees and Falcon, 1952; Lees, 1955; Woodbridge, 2006)

4.2.3 Results for ancient hydrological engineering cut across the Shushtar Anticline

The elements of a monumental ancient hydrological engineering cut across the Shushtar Anticline at Shushtar are shown in Figures 4.11, 4.12 and 4.13. The main findings for this ancient hydrological engineering system are summarised in Table 4.4.

Figure 4.11 The Band-e Qaisar at Shushtar in 1884 AD, showing how it raised water levels upstream of it to feed the Masrukan and Darian canals (From Dieulafoy, 1885)

Figure 4.12 Citadel reservoir beneath the Salasel Castle in Shushtar (location of Salasel Castle shown on Fig. 4.13, looking W, staff divided into 10 cm graduations)
This photograph of March 2002 AD shows the ancient citadel reservoir was not being filled by water from the River Shuteyt, even with spring seasonal high river water levels

Figure 4.13 Ancient hydraulic structures in Shushtar (CORONA (1968) satellite image and interpretation)

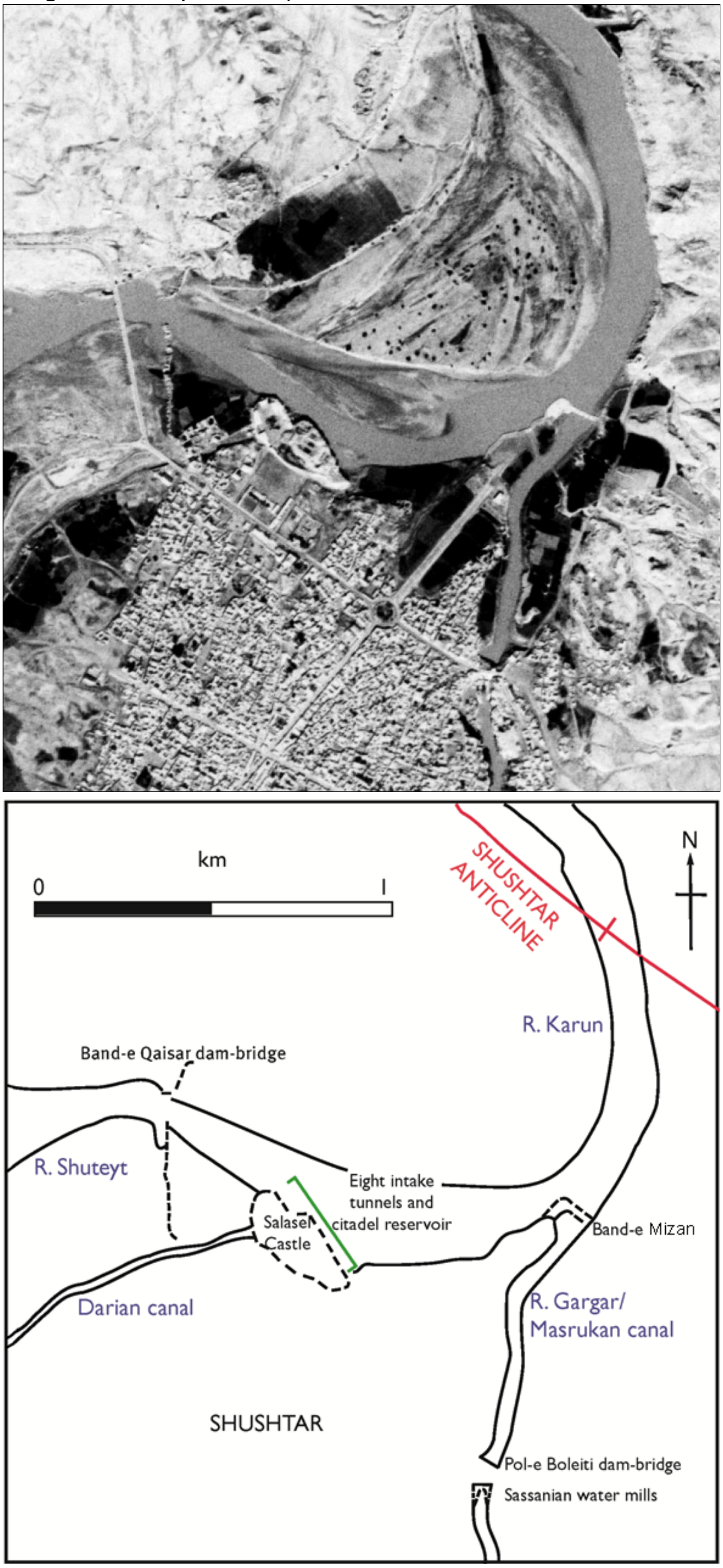

Key Red line indicates axis of anticline R. Karun flows from the N to the S & W

Table 4.4 Summary of findings for the ancient hydrological engineering system cut across the Shushtar Anticline

Ancient engineering	Short description	Probable age
Shushtar ancient hydraulic structures in the vicinity of the Salasel Castle - Eight intake channels of small aperture all serving a larger aperture main channel of the Darian canal system and Citadel reservoir beneath the Salasel Castle Approx. location 32°03'N 48°51'E	The remnants of monumental hydrological engineering cut through Agha Jari Formation sandstones and marls of the ***fore-limb of the Shushtar Anticline*** in Shushtar on the south bank of the R. Karun (Shuteyt branch) (Figure 4.13). In antiquity, ***eight intake tunnels of small aperture*** all serving a larger aperture main channel of the Darian canal system were cut, with intakes at different elevations ranging from about $^{+}37$ m to $^{+}42.5$ m above NCC Datum. This was used to optimise flow in the main channel in antiquity for the typical range of R. Karun discharges from low river water levels (in the autumn) to high river water levels (in the spring). Water flow in a tunnel is slower when full of water, so the higher tunnels helped maintain fast flows in the main channel at times of high river levels by increasing the effective aperture. Also in antiquity, a simple ***citadel reservoir*** was cut in the Agha Jari Formation sandstones beneath the Salasel Castle to provide a water supply, especially in the summer. In 2001 AD, average river water levels for the south bank of the R. Karun (Shuteyt branch) in the vicinity of the Salasel Castle at Shushtar ranged from about $^{+}37$ m to about $^{+}42$ m NCC Datum through the year. When investigated during March 2002 AD (a time of fairly high river water levels of c. $^{+}39$ m NCC Datum), the R. Karun (Shuteyt) water level was about 2.5 m below the base of the citadel reservoir (Figure 4.12) and about 1 m to 3.5 m below the intakes for the three highest tunnels of the Darian canal system (Pourghorban, Ab Varzan Consulting Engineering Company, personal communication, 2002; Woodbridge, 2006). This indicates that, for the R. Karun at this location, river water levels in the 21st Century AD were considerably lower than during the main period of construction and use of the Shushtar large-scale hydrological engineering (the Early Sassanian Period, c. 224 - 379 AD). The total relative fall in river water levels was probably at least about 3 m (Woodbridge, 2006); and, if during use in antiquity, the tunnel intakes and the citadel reservoir were at least partly filled during the autumn months, the total relative fall was most probably about 5 m. Much of the relative fall in river water levels can be attributed to the disuse (and eventual collapse in 1885 AD) of the ***Band-e Qaisar*** or *shadhurvan* (Verkinderen, 2009). This dam-bridge, with its associated flagstone pavement on the river bed, was constructed in early Sassanian times just downstream of the tunnels, partly to raise the river water levels (probably by about 3m to 4 m (Hartung and Kuros, 1987)) for the tunnel intakes to the Darian canal system. In early December 2005 AD (a time of low river water levels), the upper surface of the remnants of the Sassanian base of the Band-e Qaisar at its northern end were found to be c. 1.34 m above the R. Karun (Shuteyt) water level.	The large-scale hydrological engineering system in Shushtar was most probably constructed during the Early Sassanian Period (**c. 224 - 379 AD**). Only the Sassanians had the imperial policy and planning needed for such a monumental system and the assistance of Roman engineers (part of the entire Roman army under Valerian captured by Shapur I (c. 240 - 272 AD)) needed for the characteristic Roman concrete and masonry bound with mortar used in the Band-e Qaisar. This dam-bridge, which was built over solid sandstone rock outcrops after draining of the R. Shuteyt branch of the R. Karun, originally functioned as a weir, with water always flowing over the top of its base (Figure 4.11; Smith, 1971; Hartung and Kuros, 1987; Hodge, 1992; Moghaddam and Miri, 2007).

4.2.4 Results for river terraces of the Karun river system in the Upper Khuzestan Plains

Fieldwork and remote sensing images show that there are a number of river terraces of the Karun at various elevations of up to $^{+}$35 m and more above present-day river water levels in the Upper Khuzestan Plains. These river terraces had not been described before and were assigned new names, in accordance with recommended stratigraphic practice (Salvador, 1994; Section 3.2.3).

There are four river terraces associated with the Naft-e Safid Anticline: the ‘Dar Khazineh terrace’, the ‘Batvand terrace’, the ‘Naft-e Safid terrace’ and the ‘Abgah terrace’. There is one river terrace associated with the Sardarabad Anticline: the ‘Kabutarkhan-e Sufla terrace’ on its back-limb. There is one river terrace associated with the Shushtar Anticline: the ‘Kushkak terrace’ on its back-limb. All of these river terraces have underlying terrace deposits dating to the Late Quaternary, as shown by Optically Stimulated Luminescence (OSL) dating. The locations of these river terraces are shown in Figure 4.14.

There are higher, presumably Pleistocene, river terraces in the region. There are higher terraces in the vicinity of the Shushtar to Naft-e Safid Road on the fore-limb of the Naft-e Safid Anticline and near the village of Abgah on the back-limb of the Naft-e Safid Anticline. These terrace fragments are relatively small and poorly preserved, and no terrace names were assigned to them. There are higher terraces on the back-limb of the Shushtar Anticline, though no exposures of their underlying terrace deposits were found.

The general geomorphology of the six named river terraces and exposures of their river terrace deposits are shown in Figures 4.15 to 4.27, with the locations of sediment samples taken for Optically Stimulated Luminescence (OSL) dating indicated. The findings for these river terraces are summarised in Tables 4.5 to 4.9. The results for the river terraces are presented in this order: ‘Dar Khazineh terrace’, ‘Kabutarkhan-e Sufla terrace’, ‘Batvand terrace’, ‘Kushkak terrace’, ‘Naft-e Safid terrace’, and ‘Abgah terrace’.

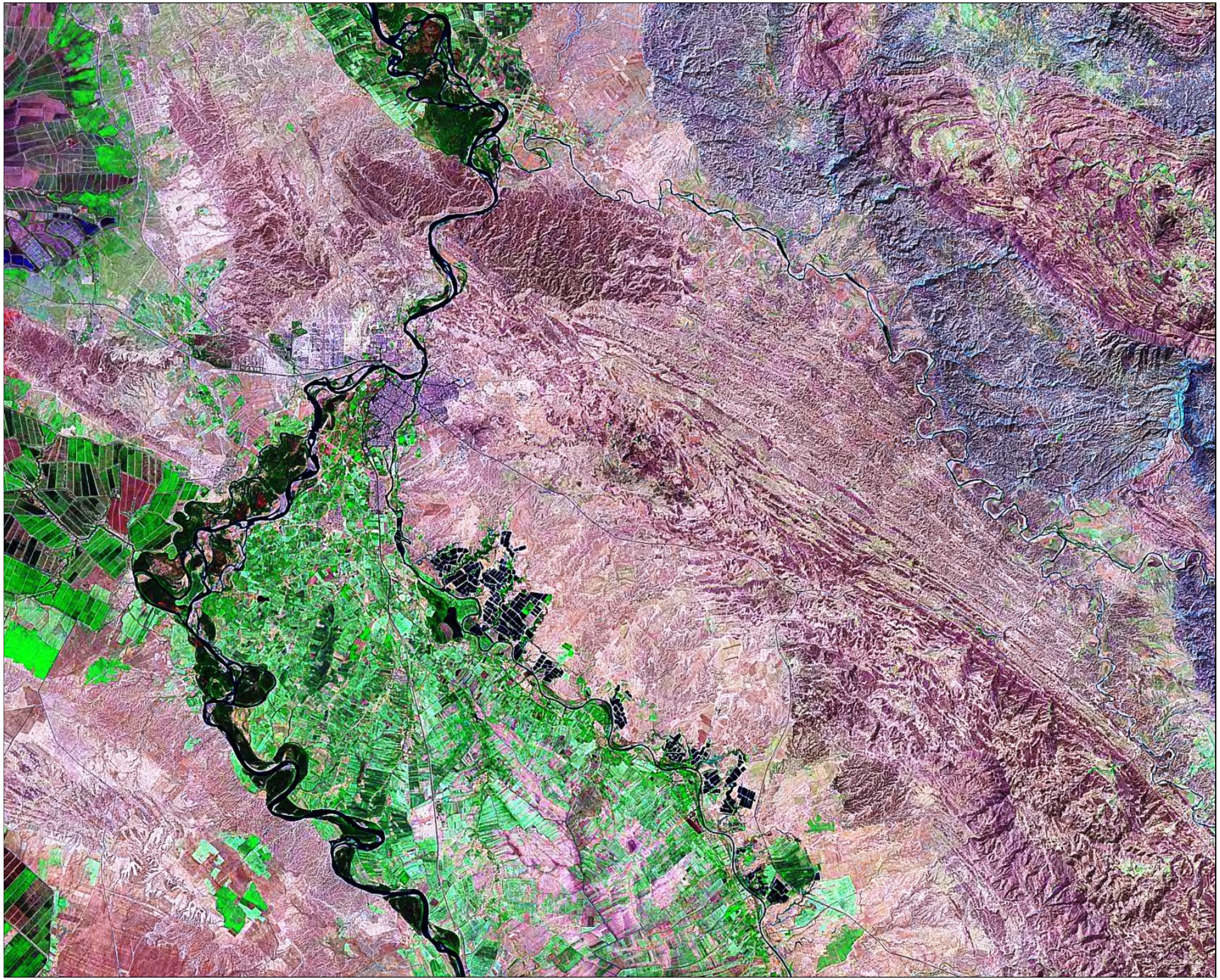

Figure 4.14
River terraces of the Karun river system in the Upper Khuzestan Plains

(Landsat (2000) false-colour image with interpretation on next page)

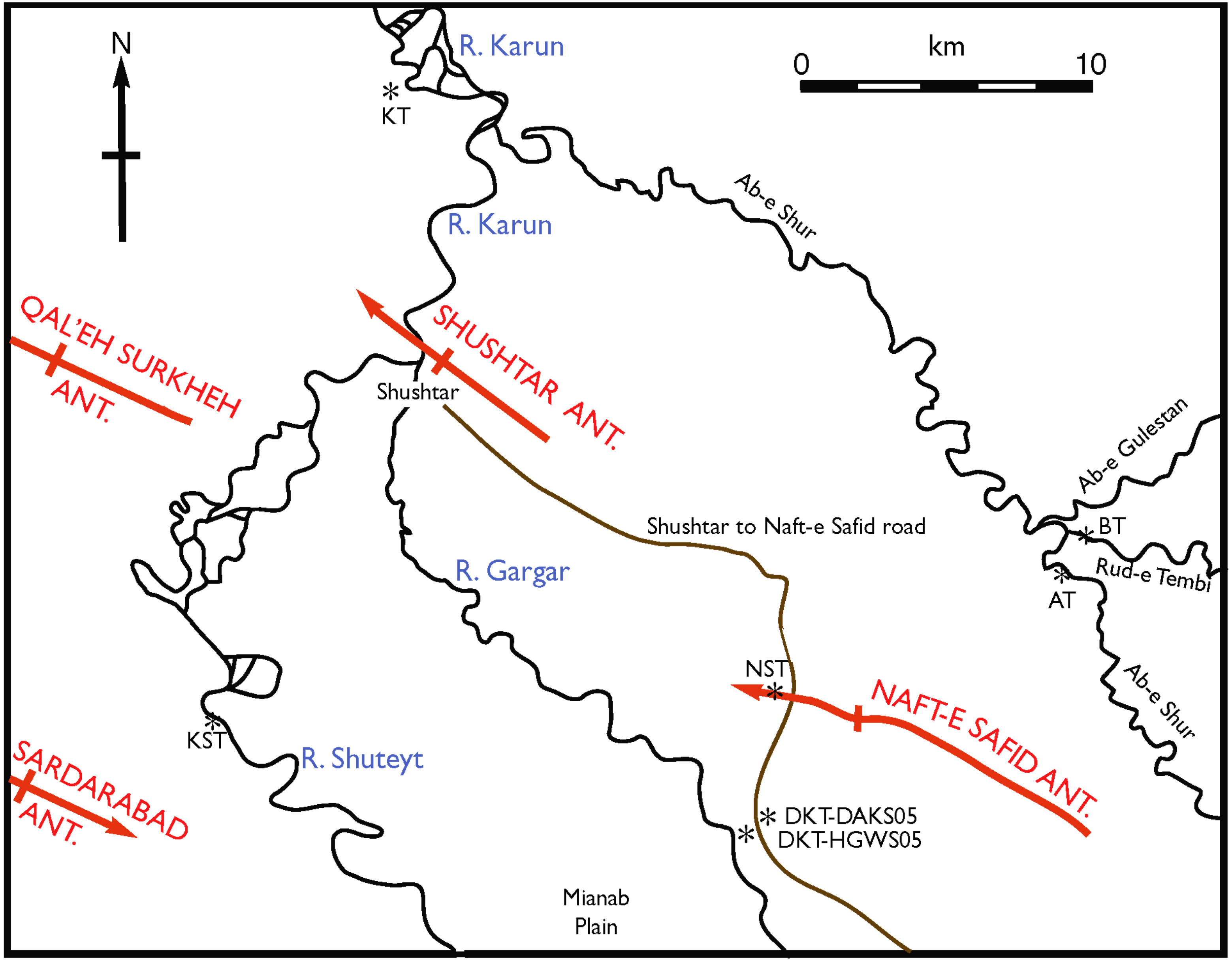

Figure 4.14 (continued) River terraces of the Karun river system in the Upper Khuzestan Plains (interpretation)

Red line indicates axis of anticline, with arrow for direction of plunge. The Qal'eh Surkheh Anticline plunges towards the NW. For each anticline, the fore-limb is to the SW of the anticlinal axis and the back-limb is to the NE of the anticlinal axis. Brown line is Shushtar to Naft-e Safid road.

∗AT Abgah terrace
∗BT Batvand terrace
∗DKT-DAKS05 Dar Khazineh terrace location DAKS05
∗DKT-HGWS05 Dar Khazineh terrace location HGWS05
∗KST Kabutarkhan-e Sufla terrace
∗KT Kushkak terrace
∗NST Naft-e Safid terrace

Figure 4.15 'Dar Khazineh terrace' - general view (near location HGWS05 at 31°54'N 48°59'E looking NE across the extensive terrace surface)

Figure 4.16 'Dar Khazineh terrace' - exposure of "hanging wadi channel" at location HGWS05 (near 31°54'35''N 48°59'09''E looking NNE, wooden rule 2 m long, blue circles show lower edge of channel)

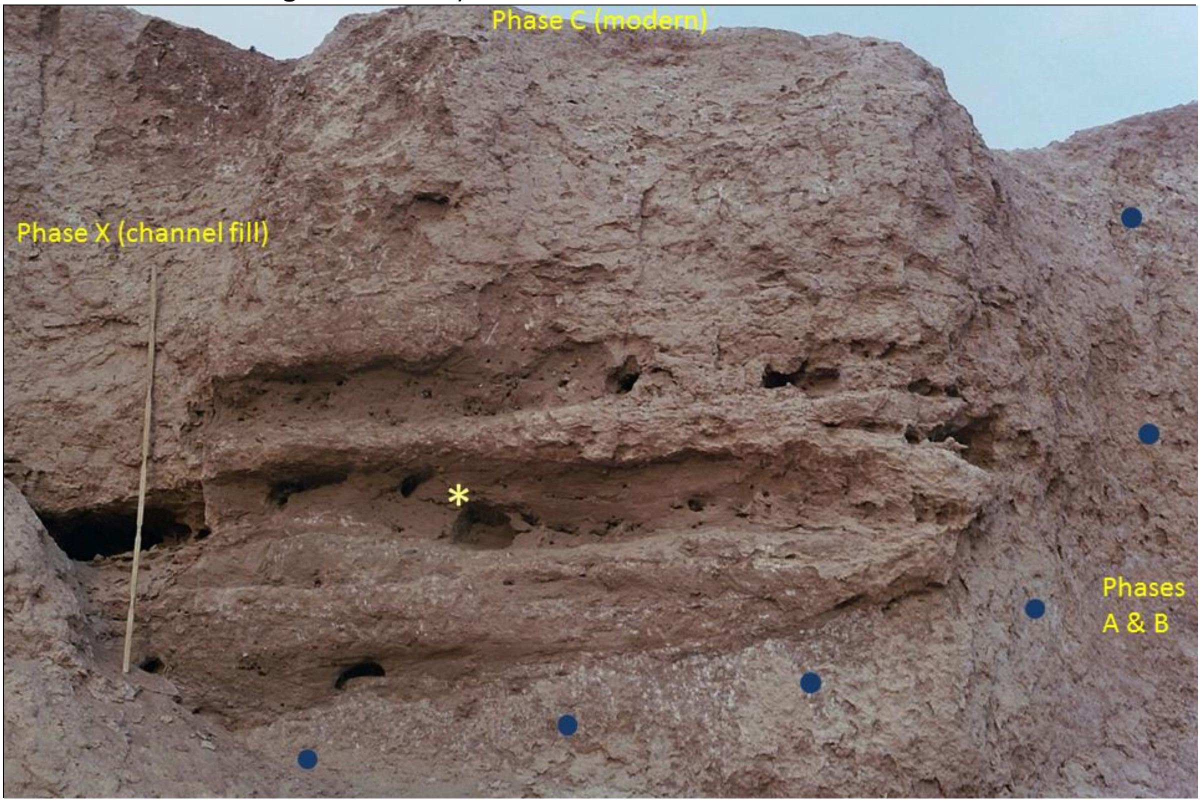

Yellow asterisk indicates location of OSL Sample 4 from Bed 7hgw in Phase X, dated to 5.68 ± 0.36 ka (Shfd08207), equivalent to **3,670 ± 360 BC**

Figure 4.17 'Dar Khazineh terrace' - exposure of terrace deposits of Phases A and B at location DAKS05 (near 31°54'47''N 48°59'29''E looking E, wooden rule 2 m long)

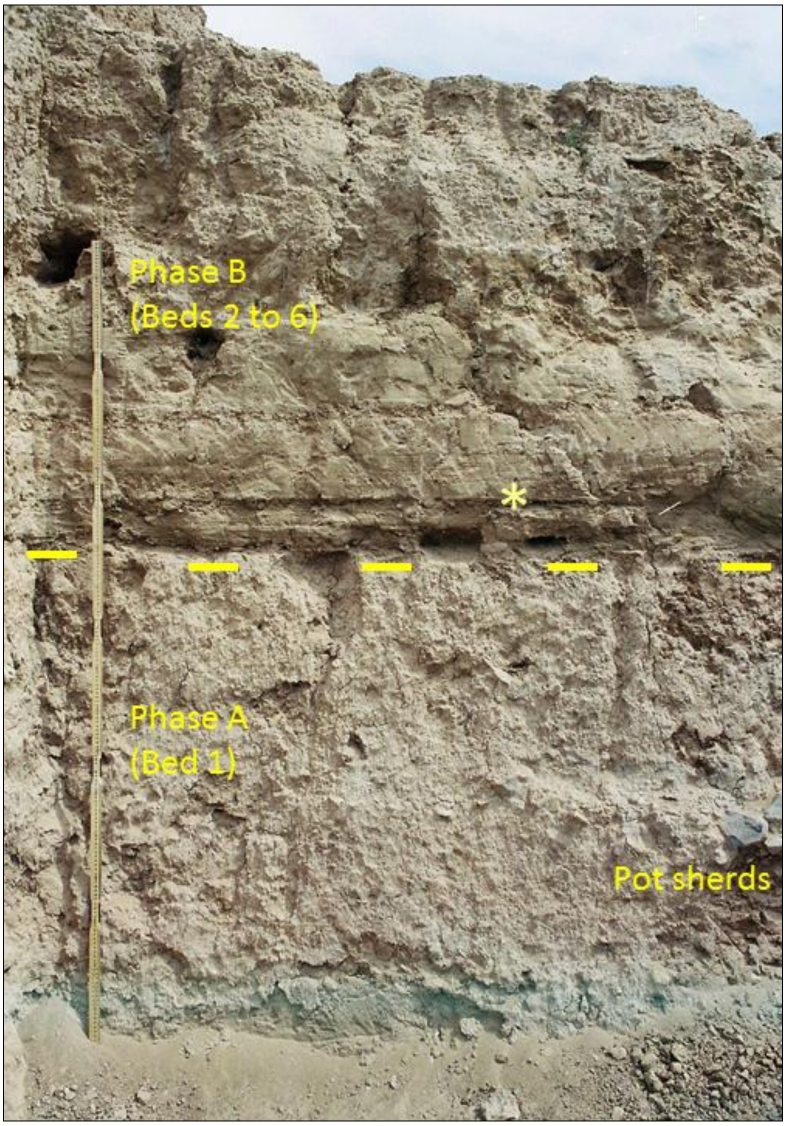

Yellow asterisk indicates location of OSL Sample 3 from Bed 2 in Phase B, dated to 2.49 ± 0.19 ka (Shfd08206), equivalent to **480 ± 190 BC**

Pot sherds in Bed 1 were dated to the Late Susiana 1 and Late Susiana 2 Periods, **c. 4,800 BC - 4,000 BC**

Figure 4.18 ‘Dar Khazineh terrace’ - exposure of terrace deposits of Phases A, B and C at location DKLTFH (near 31°54’46’’N 48°59’23’’E looking SSW, wooden rule 2 m long)

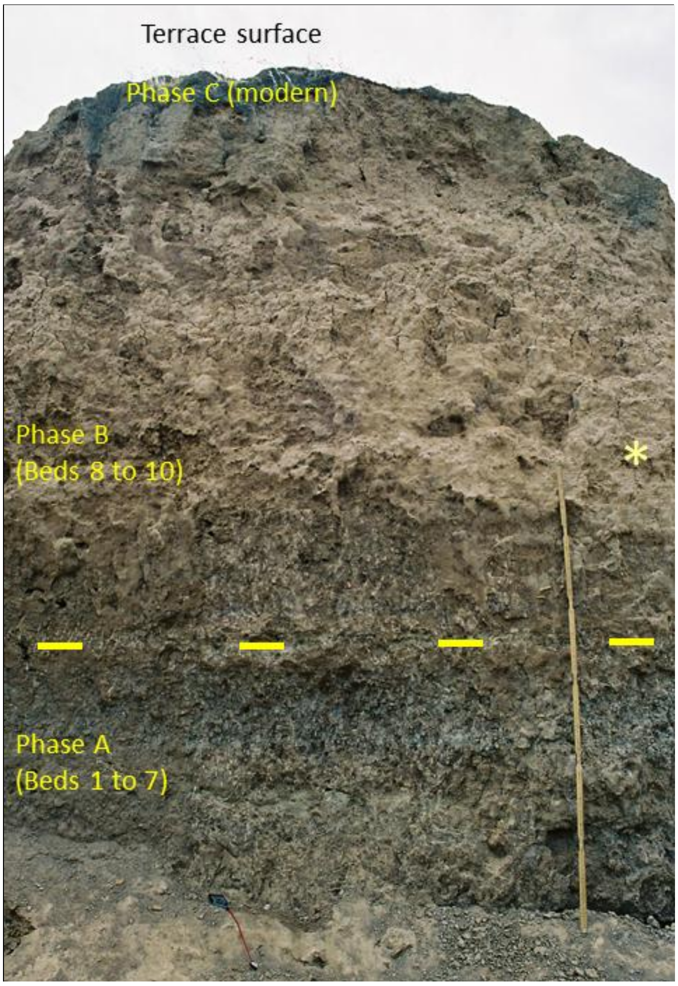

Yellow asterisk indicates location of OSL Sample 11 from Bed 10 in Phase B, dated to 2.83 ± 0.22 ka (Shfd08202), equivalent to **820 ± 220 BC**

In the vicinity of location DKLTFH, deposits equivalent to Phase B included pottery from the Elamite Period, **c. 2,600 BC - 646 BC**

Figure 4.19 'Kabutarkhan-e Sufla terrace' - general view looking SE (looking downstream along River Shuteyt), and exposure of terrace deposits of Beds 2 and 4 at location KBS4OS (near 31°56'28''N 48°47'21''E looking SSW, steel rule 0.5 m long)

Yellow asterisk indicates location of OSL Sample 9 from Bed 2, dated to 18.3 ± 1.4 ka / 16.4 ± 0.9 ka (Shfd08021), equivalent to **15,590 ± 2,100 BC**
Bed 3 is laterally variable and is absent in the exposure for OSL Sample 9 from Bed 2

Figure 4.20 'Batvand terrace' - general view (near 32°00'08''N 49°06'08''E looking NNE across the floodplains of the Rud-e Tembi and Ab-e Gulestan rivers)

Figure 4.21 'Batvand terrace' - part of extensive exposure of terrace deposits of Phases A, B and C in the vicinity of location BFLS05 (near 32°00'08''N 49°06'08''E looking SSW, width of view c. 13 m)

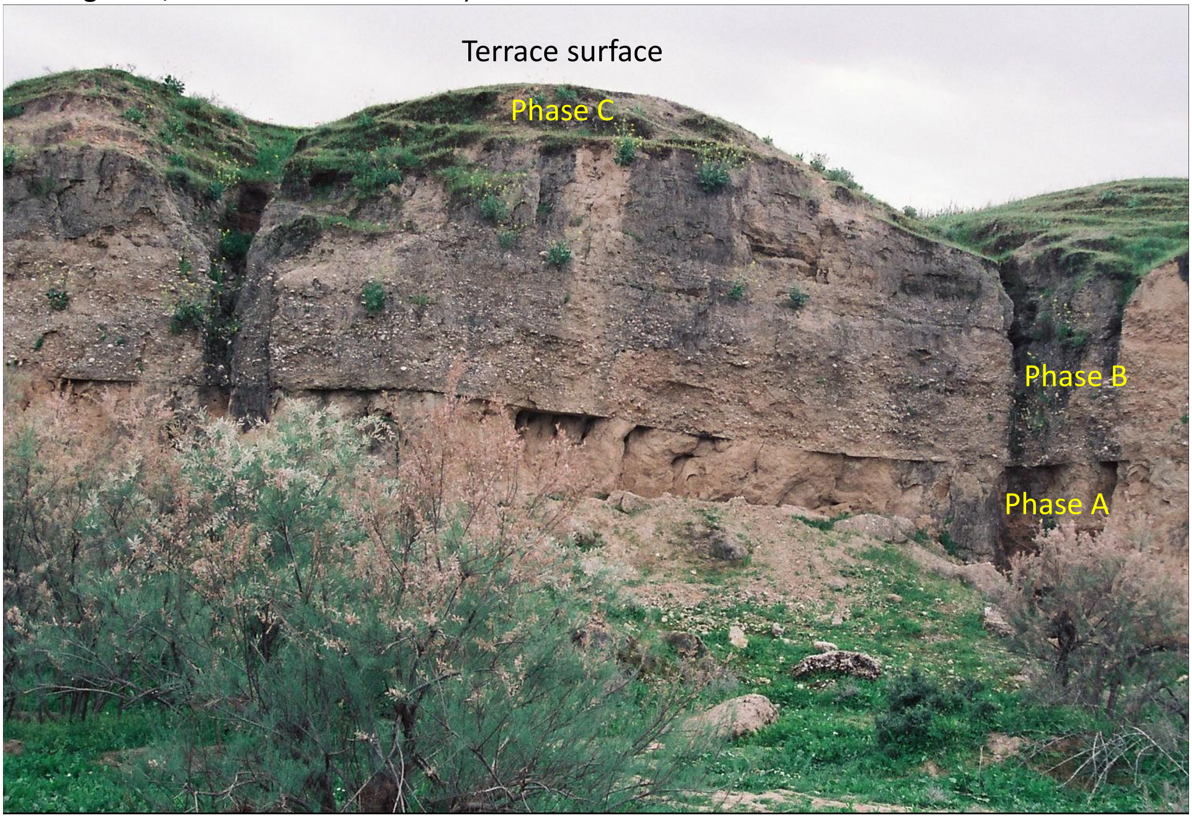

Figure 4.22 'Batvand terrace' - part of extensive exposure of terrace deposits of Phases A and B at location BFLS05 (near 32°00'08''N 49°06'06''E looking SSW, width of view c. 4 m)

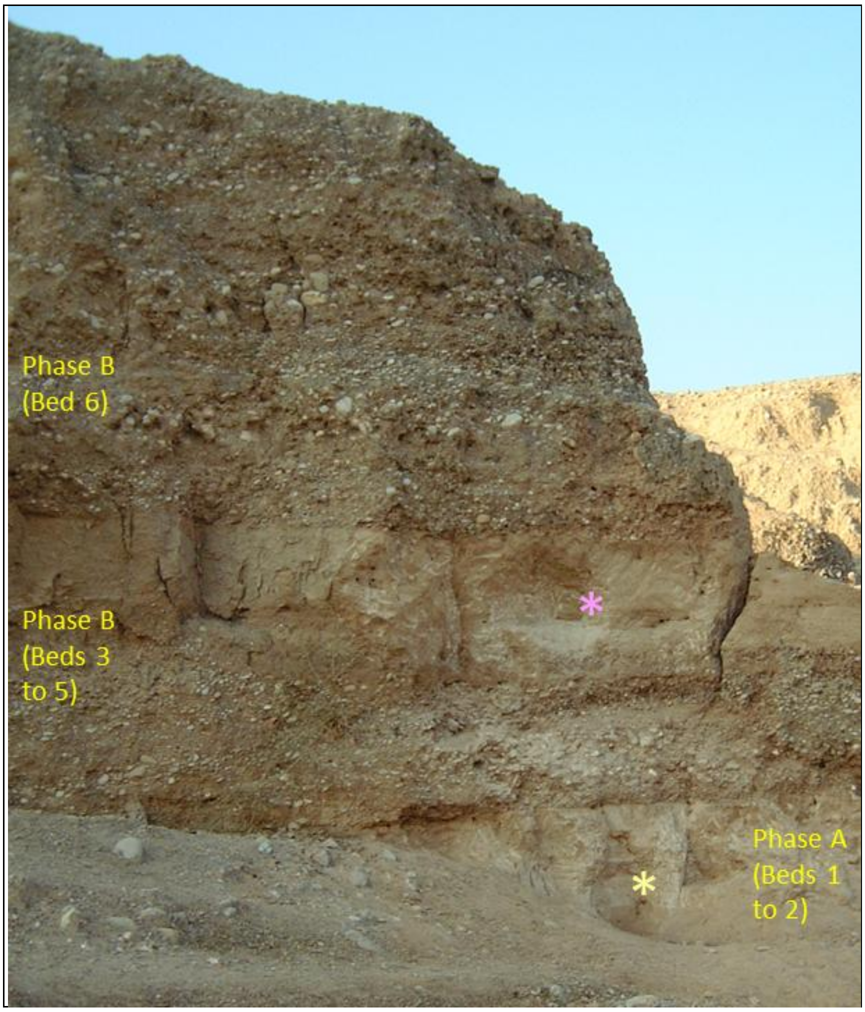

Pink asterisk (higher) indicates location of OSL Sample 1 from Bed 5 in Phase B, dated to 10.49 ± 0.83 ka (Shfd08204), equivalent to **8,480 ± 830 BC**

Yellow asterisk (lower) indicates location of OSL Sample 2 from Bed 2 in Phase A, dated to 25.87 ± 1.75 ka (Shfd08205), equivalent to **23,860 ± 1,750 BC**

Figure 4.23 'Kushkak terrace' - general view, and exposure of terrace deposits of Beds 1, 2 and 3 near location KUHKL3 (near 32°08'07''N 48°50'34''E looking SW, wooden rule 2 m long)

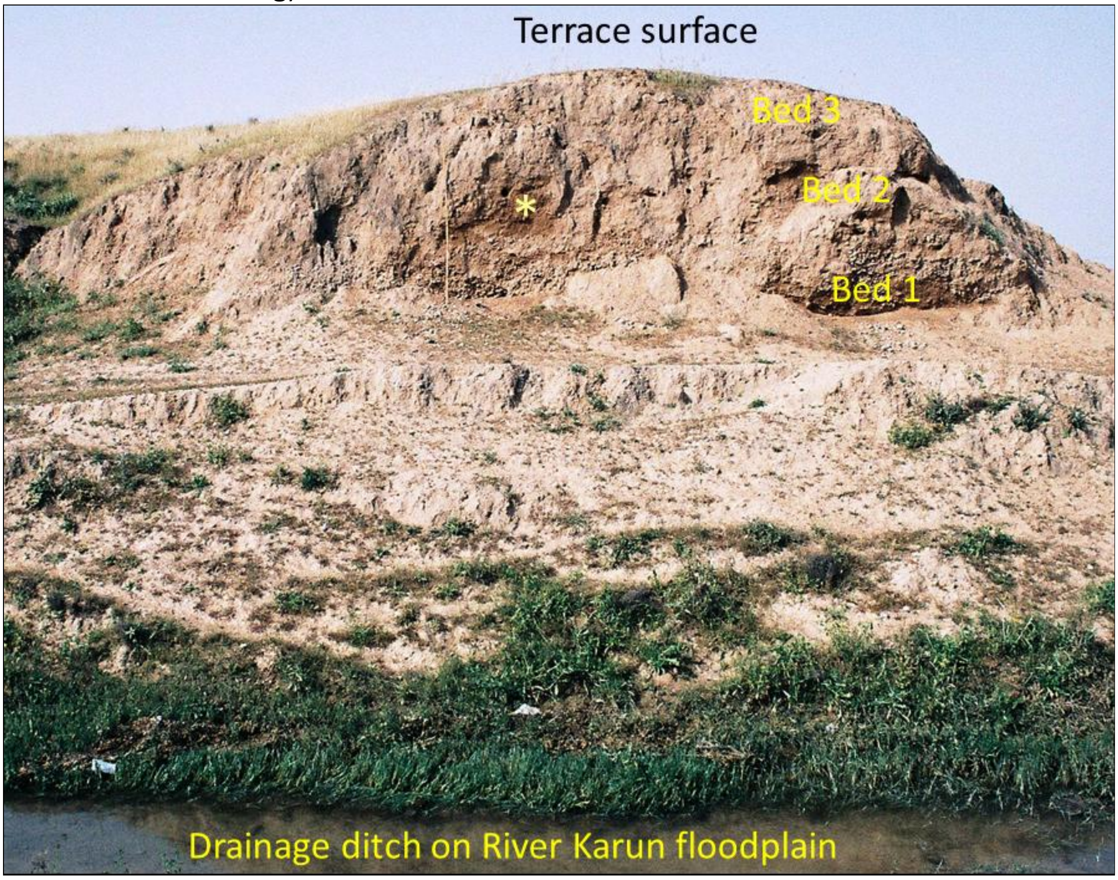

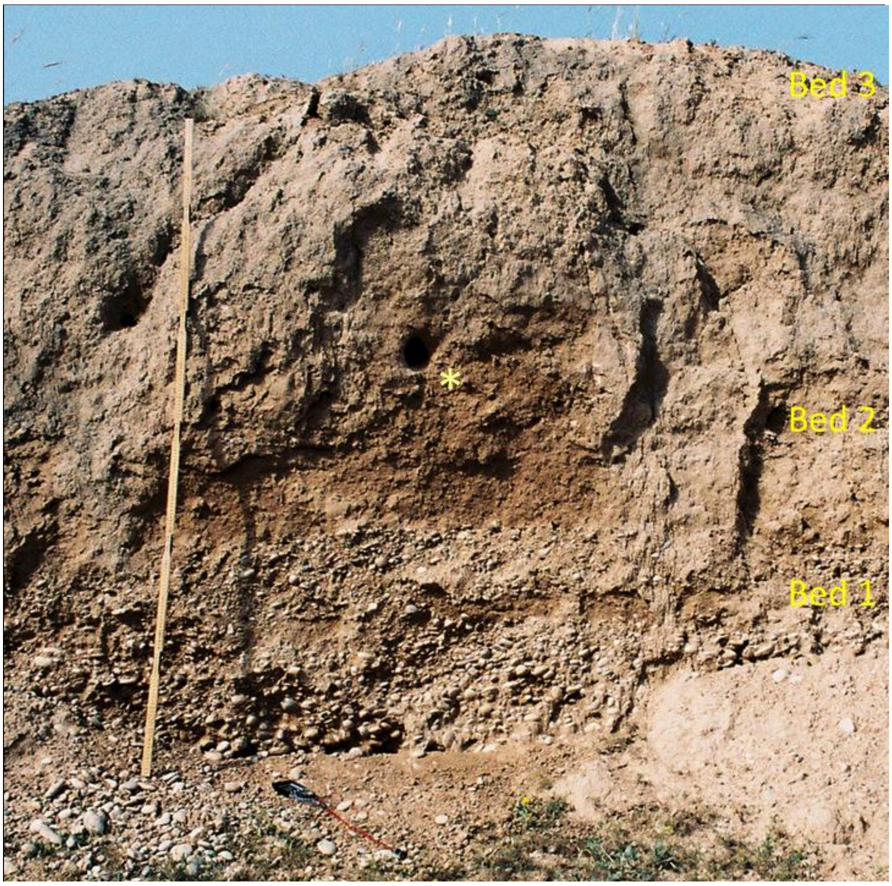

Yellow asterisk indicates location of OSL Sample 10 from Bed 2, dated to 19.98 ± 2.00 ka (Shfd08210), equivalent to **17,970 ± 2,000 BC**

Figure 4.24 'Naft-e Safid terrace' - general view (near 31°57'14''N 48°59'42''E looking W towards the Mianab Plain)

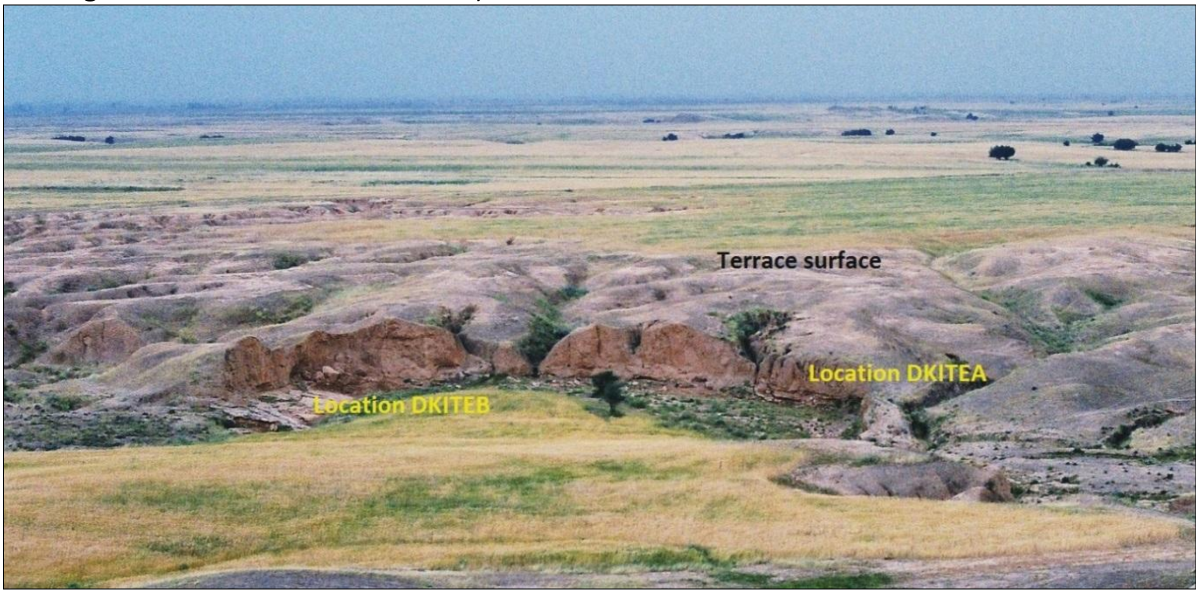

Figure 4.25 'Naft-e Safid terrace' - exposure of terrace deposits of Beds 1, 2, 3 and 4 at location DKITEB (near 31°57'15''N 48°59'32''E looking SSW, wooden rule 2 m long)

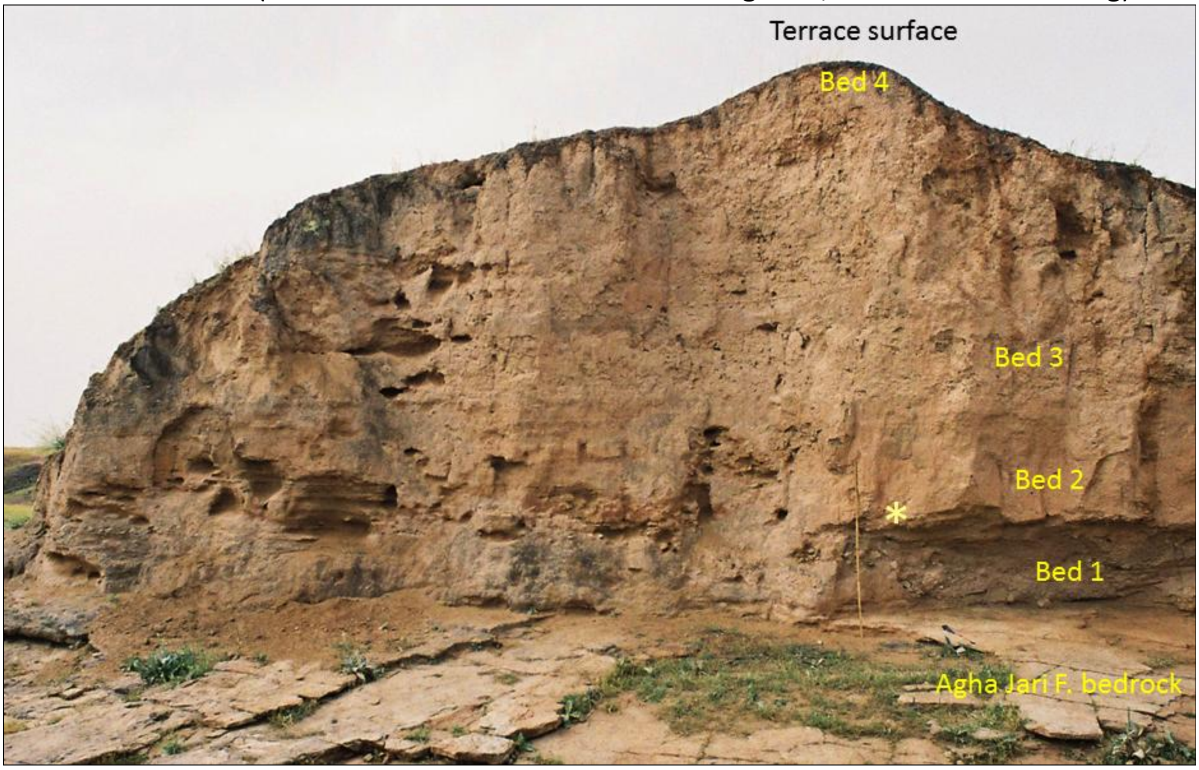

Yellow asterisk indicates location of OSL Sample 8 from Bed 2, dated to 22.5 ± 1.1 ka (Shfd08019), equivalent to **20,490 ± 1,100 BC**

Figure 4.26 'Naft-e Safid terrace' - exposure of terrace deposits of Beds 1 and 2 at location DKITEB (near 31°57'15''N 48°59'32''E looking SSW, wooden rule 2 m long)

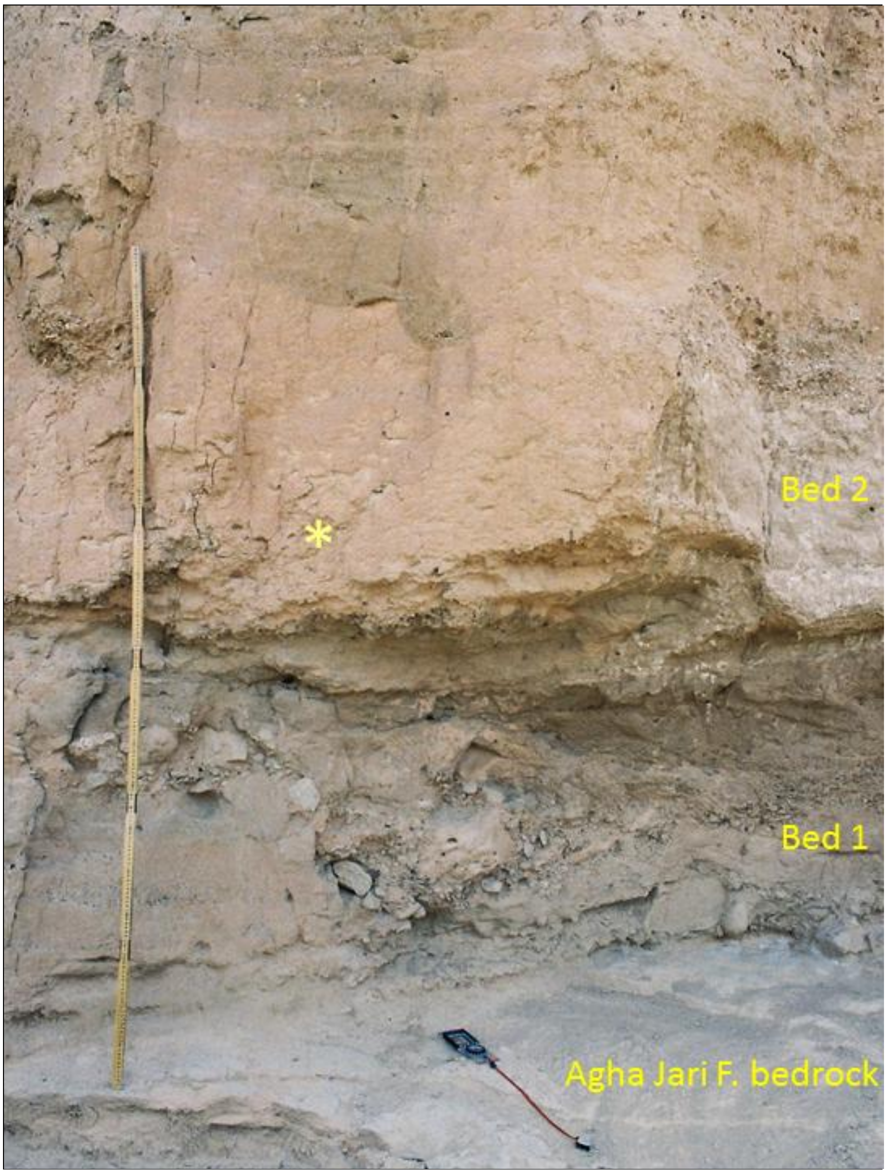

Yellow asterisk indicates location of OSL Sample 8 from Bed 2, dated to 22.5 ± 1.1 ka (Shfd08019), equivalent to **20,490 ± 1,100 BC**

Figure 4.27 'Abgah terrace' - general view (width of view c. 37 m), and exposure of terrace deposits of Phase B (Beds 4 and 5) near location BAF2BR (near 31°59'32''N 49°05'43''E looking SW, wooden rule 2 m long)

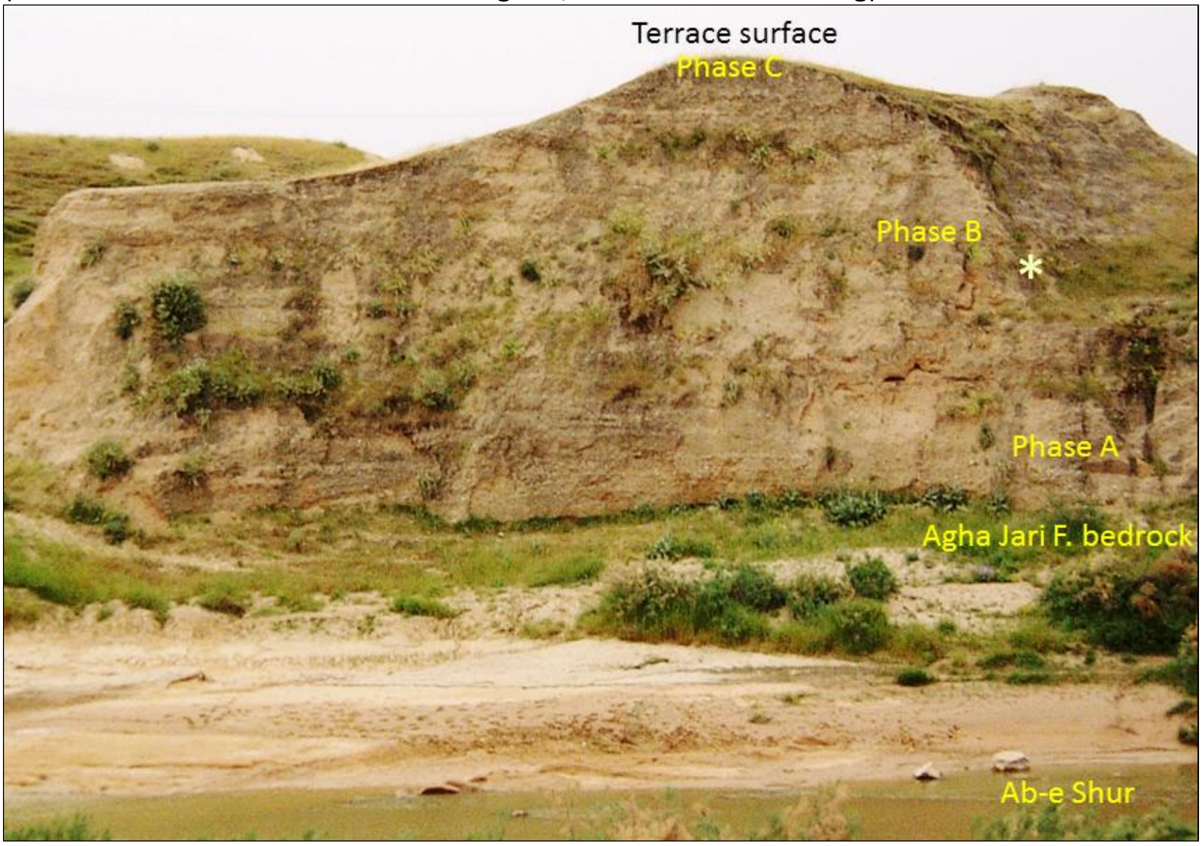

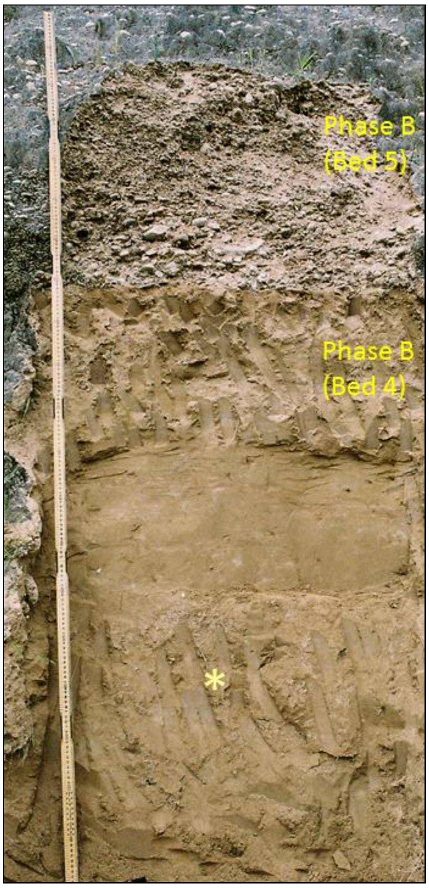

Yellow asterisk indicates location of OSL Sample 7 from Bed 4 in Phase B, dated to 20.60 ± 3.13 ka (Shfd08209), equivalent to **18,590 ± 3,130 BC**

Table 4.5 (a) Summary of findings for river terraces in the Upper Khuzestan Plains - 'Dar Khazineh terrace'

River terrace	Elevation	Short description	Probable age
'**Dar Khazineh terrace**' Type locality: Vicinity of the village of Dar Khazineh, on edge of south-west limb of Naft-e Safid Anticline Includes: DAKS05 31°54'47''N 48°59'29''E DKLTFH 31°54'46''N 48°59'23''E HGWS05 31°54'35''N 48°59'09''E	Terrace surface from less than c. $^{+}$31.21 m to more than c. $^{+}$37.28 m NCC Datum (from about <$^{+}$9.41 m to >$^{+}$15.48 m above River Gargar water level, which was $^{+}$21.80 m NCC Datum at L44)	A slightly concave terrace surface, which slopes from the NE to the SW on the ***fore-limb of the Naft-e Safid Anticline*** down towards the River Gargar at the type locality (Figure 4.15). The terrace surface is heavily dissected by fluvial erosion from wadis and numerous small channels, and by wind erosion. Where preserved, the terrace surface is smooth. The terrace surface is very extensive, esp. over the eastern part of the Upper Khuzestan Plains. Its downstream slope is similar to that of the main river valley. The terrace deposits are mostly sands and silts, with some fine gravels. There is a stratigraphic sequence with at least four main phases of sediment deposition in the vicinity of Dar Khazineh (Figure 4.16 to 4.18): Phase C (c. $^{+}$30.92 m to >$^{+}$32.96 m NCC Datum): Bed 7 (c. 90 cm thick) at DAKS05; Bed 11 (less than 160 cm thick) at DKLTFH; Bed 12 (c. 130 cm thick) at HGWS05 - Modern light grey/brown silts and sands, with soil structures and plant rootlets. Phase B (c. $^{+}$29.67 m to $^{+}$31.92 m NCC Datum): Beds 2 to 6 (total c. 110 cm thick) at DAKS05 - Mainly light grey/brown laminated and cross-bedded sands and silts, with occ. gravels, clay lenses and worm burrows; and Beds 8 to 10 (more than 170 cm thick) at DKLTFH - Light grey/brown laminated and cross-bedded sands and silts, with occ. pottery fragments in lower parts. Prominent, very sharp, bounding surface at c. $^{+}$29.82 m NCC Datum at DAKS05 and at c. $^{+}$29.67 m NCC Datum at DKLTFH with some features of a former land surface, such as worm burrows, surface cracks and ash fragments.	Phase C: Modern, with major soil formation processes over about the last 500 years. Phase B: OSL Sample 3 ($^{+}$29.89 m NCC Datum) from Bed 2 at DAKS05 dated to 2.49 ± 0.19 ka (Shfd08206), equivalent to **480 ± 190 BC** OSL Sample 11 ($^{+}$30.52 m NCC Datum) from Bed 10 at DKLTFH dated to 2.83 ± 0.22 ka (Shfd08202), equivalent to **820 ± 220 BC** In the vicinity of Dar Khazineh, deposits equiv. to Phase B included pottery from the Elamite Period (**c. 2,600 BC - 646 BC**) and more recent periods, and there was an Elamite Period well which had been sunk through Phase B equivalent deposits. (continued on Table 4.5 (b))

Table 4.5 (b) Summary of findings for river terraces in the Upper Khuzestan Plains - 'Dar Khazineh terrace' (continued)

River terrace	Elevation	Short description	Probable age
'**Dar Khazineh terrace**' (continued)		Phase X (c. $^{+}$27.36 m to $^{+}$30.93 m NCC Datum): Cutting and filling of small-scale river channels c. 10 m - 50 m wide (the "hanging wadi channels" of Alizadeh et al. (2004)) - Beds 2hgw to 9hgw (total c. 160 cm thick) - Channel fill of mainly light grey/brown laminated and cross-bedded sands and silts, with some thin clay layers, gravels and clay clasts and Beds 10hgw to 11hgw (total c. 197 cm thick) at HGWS05 - Channel fill of light grey/brown low-angle and high-angle cross-bedded sands and silts, with occ. thin clay layers in lower parts. Phase A (c. <$^{+}$28.51 m to $^{+}$29.82 m NCC Datum): Bed 1 (more than 100 cm thick) at DAKS05 - Mainly brown silts and sands, with some columnar structures and very poorly sorted gravels, including fragments of pottery, worked stone and mud-bricks; and Beds 1 to 7 (more than 116 cm thick) at DKLTFH - Mainly brown and grey silts and sands, with a few pottery sherds and fragments, some columnar and blocky structures, and occasional nodules.	Phase X: OSL Sample 4 ($^{+}$28.37 m NCC Datum) from Bed 7hgw at HGWS05 dated to 5.68 ± 0.36 ka (Shfd08207), equivalent to **3,670 ± 360 BC** Phase A: Pottery sherds from Bed 1 at DAKS05 (at elevation c. $^{+}$28.82 m to c. $^{+}$29.32 m NCC Datum) and from elsewhere nearby (Alizadeh et al., 2004) date to the Late Susiana 1 and Late Susiana 2 Periods, **c. 4,800 BC - 4,000 BC**

Table 4.6 Summary of findings for river terraces in the Upper Khuzestan Plains - 'Kabutarkhan-e Sufla terrace'

River terrace	Elevation	Short description	Probable age
'**Kabutarkhan-e Sufla terrace**' Type locality: Just SE of the hamlet of Kabutarkhan-e Sufla, on north-east limb of Sardarabad Anticline Includes: KBS4OS 31°56'28''N 48°47'21''E	Terrace surface from less than c. $^{+}$36.67 m to more than c. $^{+}$39.87 m NCC Datum (from about <$^{+}$11.34 m to >$^{+}$14.54 m above River Shuteyt water level)	A slightly concave terrace surface which slopes gently from the SW to NE on the ***back-limb of the Sardarabad Anticline*** down towards the River Shuteyt at the type locality (Figure 4.19). The terrace surface is slightly undulating due to erosion from water run-off and, to a lesser extent, due to wind erosion. The terrace surface is fairly extensive along the north-east limb of the Sardarabad Anticline. Its downstream slope is similar to that of the main river valley. The terrace deposits are a variety of fine gravels, sands, silts and clays. There is a stratigraphic sequence with five main beds near Kabutarkhan-e Sufla (Figure 4.19): Bed 5 (c. <$^{+}$34.48 m to >$^{+}$37.01 m NCC Datum, more than 253 cm thick) - Modern light grey/brown silts and sands, eroded by slope wash. Bed 4 (c. $^{+}$30.34 m to <$^{+}$34.48 m NCC Datum, less than 414 cm thick) - Succession of light grey finely bedded and cross-bedded sands, silts and fine gravels, and occ. silt/clay bands and lenses, separated by erosional "scour" bounding surfaces often associated with gravels. Sharp bounding surface at base of Bed 4 at c. +29.80 m to +30.34 m NCC Datum. Bed 3 (c. $^{+}$29.92 m to $^{+}$30.34 m NCC Datum, c. 42 cm thick) - Laterally variable bed of mainly laminated grey and brown sands, silts and clays, with occ. thin bands of red-brown clay-silts and very occ. blocky structures. Bed 2 (c. $^{+}$25.66 m to $^{+}$30.28 m NCC Datum, c. 462 cm thick) - Planar and trough cross-bedded sands and gravels alternating with thin bands of sands and muds; generally fining upwards. Bed 1 (c. <25 m to +25.66 m NCC Datum, more than 200 cm thick) - Brown laminated clays and silts, with occ. worm burrows.	OSL Sample 9 ($^{+}$29.90 m NCC Datum) from upper part of Bed 2 at KBS4OS dated to 16.4 ± 0.9 ka (Shfd08021) (Finite Mixture Modelling) 18.3 ± 1.4 ka (Shfd08021) (*Central Age Model*), equivalent to **15,590 ± 2,100 BC**

Table 4.7 (a) Summary of findings for river terraces in the Upper Khuzestan Plains - 'Batvand terrace' and 'Kushkak terrace'

River terrace	Elevation	Short description	Probable age
'**Batvand terrace**' Type locality: Just SW of the village of Batvand, on edge of north-east limb of Naft-e Safid Anticline Includes: BFLS05 32°00'08''N 49°06'06''E	Terrace surface from less than c. $^{+}$104.78 m to more than c. $^{+}$108.88 m NCC Datum (from about <$^{+}$11.62 m to >$^{+}$15.72 m above Rud-e Tembi river water level)	A very gently sloping and slightly undulating terrace surface which slopes very slightly from the SW to the NE on the ***back-limb of the Naft-e Safid Anticline*** down towards the Rud-e Tembi at the type locality (Figure 4.20). The terrace surface is extensive and, generally, well preserved downstream from Batvand to the confluence of the Ab-e Shur with the River Karun, as a smooth surface on both sides of the Ab-e Shur/Rud-e Tembi floodplain. Its downstream slope is similar to that of the Ab-e Shur/Rud-e Tembi river valley. The terrace deposits are mainly poorly sorted gravels with some light grey/brown sands, especially in the lowermost part of the sequence. There is a stratigraphic sequence with at least three main phases of sediment deposition near Batvand (Figure 4.21 and 4.22):	
		Phase C (c. >$^{+}$104.95 m to >$^{+}$108.88 m NCC Datum) - Modern light grey/brown silts and sands, with gravels from lower beds, eroded by slope wash and small channels.	Phase C: Modern, with major soil formation processes over about the last 500 years.
		Phase B (c. $^{+}$98.97 m to >$^{+}$104.95 m NCC Datum): Cutting and filling of large-scale river channels (channel gravels and sands extend over more than 200 m width in exposures at BFLS05) Beds 3 to 5 (total c. 125 cm thick) - Poorly sorted gravels and light grey-brown sands with medium-scale bedding and cross-bedding (with "channel" sedimentary structures up to c. 25 m or more in width); overlain by Beds 6 to 7 (more than 473 cm thick) - Poorly sorted, generally rounded, gravels with large-scale bedding and cross-bedding (with "channel" sedimentary structures up to c. 75 m or more in width), and matrix of light grey-brown sands, especially in Bed 7.	Phase B: OSL Sample 1 ($^{+}$99.85 m NCC Datum) from Bed 5 at BFLS05 dated to 10.49 ± 0.83 ka (Shfd08204), equivalent to **8,480 ± 830 BC** (continued on Table 4.7 (b))

Table 4.7 (b) Summary of findings for river terraces in the Upper Khuzestan Plains - 'Batvand terrace' and 'Kushkak terrace' (continued)

River terrace	Elevation	Short description	Probable age
'**Batvand terrace**' (continued)		Very prominent, very sharp, gently undulating major bounding surface at c. $^{+}$98.93 m to c. $^{+}$101.07 m NCC Datum Phase A (c. <$^{+}$98.32 m to $^{+}$98.97 m NCC Datum): Beds 1 to 2 (total more than 65 cm thick) - Light grey/brown laminated sands and silts.	Phase A: OSL Sample 2 ($^{+}$98.49 m NCC Datum) from Bed 2 at BFLS05 dated to 25.87 ± 1.75 ka (Shfd08205), equivalent to **23,860 ± 1,750 BC**
'**Kushkak terrace**' Type locality: Vicinity of the village of Kushkak, on edge of north-east limb of Shushtar Anticline Includes: KUHKL3 32°08'07''N 48°50'34''E	Terrace surface from less than approx. $^{+}$60.40 m to more than approx. $^{+}$69.90 m NCC Datum (from approx. <$^{+}$10.60 m to approx. >$^{+}$20.10 m above River Karun water level, which was $^{+}$49.80 m NCC Datum at LB15)	Terrace surface on ***the back-limb of the Shushtar Anticline***, with a high degree of undulation due to extensive erosion by water run-off and wind erosion. Terrace surface preserved as quite large fragments on the west bank of River Karun upstream as far as Jallekan and Gotvand. Terrace surface has a downstream slope, probably with a gentler downstream slope on the north-east limb of the Shushtar Anticline. The terrace deposits, where exposed, are mostly gravels, overlain by sands and silts. There is a stratigraphic sequence with three beds was near Kushkak (Figure 4.23): Bed 3 (c. $^{+}$59.51 m to >$^{+}$60.22 m NCC Datum, more than 71 cm thick) - Mainly modern light brown laminated sands and silts, with soil structures and plant rootlets in upper parts. Bed 2 (c. $^{+}$58.46 m to $^{+}$59.51 m NCC datum, c. 105 cm thick) - Light grey and grey-brown laminated and slightly cross-laminated sands and silts, with occ. clay laminae and band of gravels near base. Bed 1 (c. <$^{+}$57.69 m to $^{+}$58.46 m NCC Datum, more than 77 cm thick) - Moderately rounded gravels with poorly defined bedding and planar cross-bedding and matrix of brown sands.	Archaeological survey of sites on this terrace surface included Tepe-i Jallekan dated by pottery to the "Susa A" and "Susa B" periods, c. 4,100 BC - 3,100 BC (Wright, 1969) OSL Sample 10 (approx. $^{+}$58.98 m NCC Datum) from Bed 2 at KUHKL3 dated to 19.98 ± 2.00 ka (Shfd08210), equivalent to **17,970 ± 2,000 BC** There are fragments of higher (probably Pleistocene) terraces in the vicinity on the north-east limb of the Shushtar Anticline, though no exposures of their underlying terrace deposits were found

Table 4.8 Summary of findings for river terraces in the Upper Khuzestan Plains - 'Naft-e Safid terrace'

River terrace	Elevation	Short description	Probable age
'**Naft-e Safid terrace**' Type locality: Quite near to Qareh Sultan by the Shushtar - Dar Khazineh - Naft-e Safid road, very near to the axis of a segment of the Naft-e Safid Anticline Includes: DKITEB 31°57'15''N 48°59'32''E DKITEA 31°57'16''N 48°59'34''E	Terrace surface from less than c. $^{+}$54.08 m to more than c. $^{+}$56.95 m NCC Datum (from about <$^{+}$32.02 m to >$^{+}$34.89 m above River Gargar water level, which was $^{+}$22.06 m NCC Datum at L40)	A planar terrace surface which slopes from the NE to the SW, away from ***the axis of the Naft-e Safid Anticline***. Terrace surface is relatively smooth, but is only preserved as small terrace fragments, due to heavy dissection by fluvial erosion from small channels and water run-off (Figure 4.24). The terrace deposits are alternating bands of cross-bedded gravels and sands, with significant lateral variations. There is a stratigraphic sequence with four main beds at DKITEB (Figure 4.25 and 4.26): Bed 4 (c. $^{+}$52.88 to >$^{+}$53.08 m NCC Datum, more than 20 cm thick) - Modern light grey sands and silts with limited soil structures. Bed 3 (c. $^{+}$50.24 m to $^{+}$52.88 m NCC Datum, c. 264 cm thick) - Succession of alternating bands of bedded and cross-bedded light grey sands and gravels. Generally fining upwards, with more trough cross-bedding near base and more horizontal bedding near top. Bed 2 (c. $^{+}$49.54 m to $^{+}$50.24 m NCC Datum, c. 70 cm thick) - Alternating bands of light grey planar and trough cross-bedded coarse and fine sands. Bed 1 (c. $^{+}$48.56 m to $^{+}$49.54 m NCC datum, c. 98 cm thick) - Variable deposits of very poorly sorted bedded and cross-bedded gravels and coarse sands. Very sharp and prominent, planar or gently undulating major bounding surface at c. $^{+}$47.79 m to c. $^{+}$51.04 m NCC Datum. Agha Jari Formation bedrock (calcareous sandstones, with bands of calcareous mudstones).	OSL Sample 8 ($^{+}$49.67 m NCC Datum) from Bed 2 at DKITEB dated to 22.5 ± 1.1 ka (Shfd08019) (*Central Age Model*), equivalent to **20,490 ± 1,100 BC** There are fragments of higher (probably Pleistocene) terraces in the vicinity, though these are relatively small and poorly preserved

Table 4.9 Summary of findings for river terraces in the Upper Khuzestan Plains - 'Abgah terrace'

River terrace	Elevation	Short description	Probable age
'**Abgah terrace**' Type locality: Just NE of the village of Abgah, on north-east limb of Naft-e Safid Anticline Includes: BAF2BR 31°59'32''N 49°05'43''E	Terrace surface from less than approx. $^{+}$119.82 m to more than approx. $^{+}$121.92 m NCC Datum (from approx. <$^{+}$11.90 m to approx. >$^{+}$14.00 m above Ab-e Shur river water level for high flows)	Terrace surface on ***back-limb of Naft-e Safid Anticline*** with a high degree of undulation due to extensive erosion by water run-off and wind erosion. Terrace surface is only preserved as small fragments and, notably as fairly high cliffs next to the Ab-e Shur river. Slope of terrace surface is uncertain. The thick terrace deposits are cross-bedded gravels, overlain by alternating bands of cross-bedded sands and gravels, with sand units being dominant in the upper parts of the sequence. There is a stratigraphic sequence with three main phases of sediment deposition at BAF2BR (Figure 4.27): Phase C (approx. $^{+}$121.62 m to $^{+}$121.92 m NCC Datum): Bed 6 (c. 30 cm thick) - Modern sands and silts with limited soil structures.	
		Phase B (approx. $^{+}$111.02 m to $^{+}$121.62 m NCC Datum): Succession of alternating bands of bedded/laminated and cross-bedded orange-brown and light brown sands (including Bed 2 (c. 100 cm thick) and Bed 4 (c. 290 cm thick)), and faintly bedded and cross-bedded fine gravels (including Bed 3 (c. 70 cm thick) and Bed 5 (c. 90 cm thick)). Generally fining upwards, with thinner and more widely spaced gravel beds in upper parts.	OSL Sample 7 (approx. $^{+}$114.82 m NCC Datum) from quite near top of Bed 4 at BAF2BR dated to 20.60 ± 3.13 ka (Shfd08209), equivalent to **18,590 ± 3,130 BC**
		Phase A (approx. $^{+}$107.92 m to $^{+}$111.02 m NCC Datum): Bed 1 (c. 310 cm thick) - Mainly cross-bedded gravels with a sand matrix; coarser gravels in lower parts, and finer gravels and more sand and silt lenses in upper parts. Very sharp, gently undulating major bounding surface at approx. $^{+}$107.92 m NCC Datum. Agha Jari Formation bedrock (calcareous sandstones, with bands of calcareous mudstones).	There are fragments of higher (probably Pleistocene) fill and strath terraces in the area to the SW, though these are relatively small and poorly preserved

4.2.5 Results for Optically Stimulated Luminescence (OSL) dating of river terrace sediments

The main aspects of the OSL dating results for the Karun river system terrace sediment samples from the Upper Khuzestan Plains are given in Table 4.10 and 4.11.

Table 4.10 (a) Optically Stimulated Luminescence (OSL) dating results for Karun river system terrace sediment samples - 'Dar Khazineh terrace' and 'Kabutarkhan-e Sufla terrace'

Sample location, sample number, block sample dimensions, and laboratory code	Sample elevation		Depth below ground surface (m)	Radioactivity data			
	Above NCC Datum (m)	Above river water level (m)		Uranium U (ppm in orig. dry solid)	Thorium Th (ppm in orig. dry solid)	Rubidium Rb (ppm in orig. dry solid)	Potassium K (% in orig. dry solid
'Dar Khazineh terrace' DAKS05 Bed 2 31°54'47''N 48°59'29''E OSL Sample 3 16 x 14 x 10 cm Shfd08206	+29.89	+8.09	1.93	1.51	2.0	15.2	0.43
'Dar Khazineh terrace' DKLTFH Bed 10 31°54'46''N 48°59'23''E OSL Sample 11 7 x 6 x 6 cm Shfd08202	+30.52	+8.72	2.44	1.75	3.8	34.0	0.92
'Dar Khazineh terrace' HGWS05 Bed 7hgw 31°54'35''N 48°59'09''E OSL Sample 4 15 x 10 x 9 cm Shfd08207	+28.37	+6.57	2.99	1.60	2.2	19.3	0.53
'Kabutarkhan-e Sufla terrace' KBS4OS Bed 2 31°56'28''N 48°47'21''E OSL Sample 9 10 x 7 x 8 cm Shfd08021	+29.90	+4.57	4.58	1.49	4.56	—	0.95

Table 4.10 (b) Optically Stimulated Luminescence (OSL) dating results for Karun river system terrace sediment samples - 'Dar Khazineh terrace' and 'Kabutarkhan-e Sufla terrace' (continued)

Sample location, sample number, block sample dimensions, and laboratory code	Dosimetry data		Total no. of aliquots measured, statistical model used	De (Gy)	Dose rate (µGy a^{-1})	Age
	D_{cosmic} (µGy a^{-1})	Moisture content (%)				
'Dar Khazineh terrace' DAKS05 Bed 2 31°54'47''N 48°59'29''E OSL Sample 3 16 x 14 x 10 cm Shfd08206	156 ± 8	1.7 ± 3	24 Finite Mixture Modelling	2.72 ± 0.18	1,090 ± 43	2.49 ± 0.19 ka, equivalent to **480 ± 190 BC**
'Dar Khazineh terrace' DKLTFH Bed 10 31°54'46''N 48°59'23''E OSL Sample 11 7 x 6 x 6 cm Shfd08202	146 ± 7	2.4 ± 3	15 Finite Mixture Modelling	4.82 ± 0.32	1,706 ± 72	2.83 ± 0.22 ka, equivalent to **820 ± 220 BC**
'Dar Khazineh terrace' HGWS05 Bed 7hgw 31°54'35''N 48°59'09''E OSL Sample 4 15 x 10 x 9 cm Shfd08207	135 ± 7	1.5 ± 3	25 Finite Mixture Modelling	6.84 ± 0.33	1,205 ± 49	5.68 ± 0.36 ka, equivalent to **3,670 ± 360 BC**
'Kabutarkhan-e Sufla terrace' KBS4OS Bed 2 31°56'28''N 48°47'21''E OSL Sample 9 10 x 7 x 8 cm Shfd08021	99 ± 5	1.8 ± 3	26 Central Age Model & Finite Mixture Modelling	31.51 ± 2.06 (Central Age Model) 28.22 ± 1.01 (Finite Mixt. Modelling)	1,723 ± 73	18.3 ± 1.4 ka (Central Age Model) 16.4 ± 0.9 ka (Finite Mixture Modelling), equivalent to **15,590 ± 2,100 BC**

Table 4.11 (a) Optically Stimulated Luminescence (OSL) dating results for Karun river system terrace sediment samples - 'Batvand terrace', 'Kushkak terrace', 'Naft-e Safid terrace' and 'Abgah terrace'

Sample location, sample number, block sample dimensions, and laboratory code	Sample elevation		Depth below ground surface (m)	Radioactivity data			
	Above NCC Datum (m)	Above river water level (m)		Uranium U (ppm in orig. dry solid)	Thorium Th (ppm in orig. dry solid)	Rubidium Rb (ppm in orig. dry solid)	Potassium K (% in orig. dry solid)
'Batvand terrace' BFLS05 Bed 5 32°00'08''N 49°06'06''E OSL Sample 1 14 x 10 x 10 cm Shfd08204	$^{+}$99.85	$^{+}$6.69	6.04	0.71	0.9	6.2	0.18
'Batvand terrace' BFLS05 Bed 2 32°00'08''N 49°06'06''E OSL Sample 2 8 x 8 x 12 cm Shfd08205	$^{+}$98.49	$^{+}$5.33	7.40	1.21	2.8	24.0	0.60
'Kushkak terrace' KUHKL3 Bed 2 32°08'07''N 48°50'34''E OSL Sample 10 10 x 10 x 8 cm Shfd08210	Approx. $^{+}$58.98	Approx. $^{+}$9.18	1.24	2.52	3.5	28.7	0.77
'Naft-e Safid terrace' DKITEB Bed 2 31°57'15''N 48°59'32''E OSL Sample 8 8 x 8 x 7 cm Shfd08019	$^{+}$49.67	$^{+}$27.61	3.41	1.26	2.42	—	0.71
'Abgah terrace' BAF2BR Bed 4 31°59'32''N 49°05'43''E OSL Sample 7 8 x 6 x 7 cm Shfd08209	Approx. $^{+}$114.82	Approx. $^{+}$6.90	7.10	1.41	3.2	21.3	0.60

Table 4.11 (b) Optically Stimulated Luminescence (OSL) dating results for Karun river system terrace sediment samples - 'Batvand terrace', 'Kushkak terrace', 'Naft-e Safid terrace' and 'Abgah terrace' (continued)

Sample location, sample number, block sample dimensions, and laboratory code	Dosimetry data		Total no. of aliquots measured, statistical model used	De (Gy)	Dose rate (μGy a^{-1})	Age
	D_{cosmic} (μGy a^{-1})	Moisture content (%)				
'Batvand terrace' BFLS05 Bed 5 32°00'08''N 49°06'06''E OSL Sample 1 14 x 10 x 10 cm Shfd08204	112 ± 6	1.2 ± 3	22 Finite Mixture Modelling	5.61 ± 0.39	535 ± 20	10.49 ± 0.83 ka, equivalent to **8,480 ± 830 BC**
'Batvand terrace' BFLS05 Bed 2 32°00'08''N 49°06'06''E OSL Sample 2 8 x 8 x 12 cm Shfd08205	96 ± 5	1.9 ± 3	24 Finite Mixture Modelling	32.32 ± 1.72	1,249 ± 52	25.87 ± 1.75 ka, equivalent to **23,860 ± 1,750 BC**
'Kushkak terrace' KUHKL3 Bed 2 32°08'07''N 48°50'34''E OSL Sample 10 10 x 10 x 8 cm Shfd08210	173 ± 9	10.2 ± 3	19 Finite Mixture Modelling	32.44 ± 2.97	1,624 ± 66	19.98 ± 2.00 ka, equivalent to **17,970 ± 2,000 BC**
'Naft-e Safid terrace' DKITEB Bed 2 31°57'15''N 48°59'32''E OSL Sample 8 8 x 8 x 7 cm Shfd08019	110 ± 6	1.1 ± 3	29 Central Age Model	29.22 ± 0.71	1,301 ± 55	22.5 ± 1.1 ka, equivalent to **20,490 ± 1,100 BC**
'Abgah terrace' BAF2BR Bed 4 31°59'32''N 49°05'43''E OSL Sample 7 8 x 6 x 7 cm Shfd08209	84 ± 4	9.9 ± 3	24 Finite Mixture Modelling	20.60 ± 3.13	1,131 ± 47	20.60 ± 3.13 ka, equivalent to **18,590 ± 3,130 BC**

4.2.6 Summary of results relating to Earth surface movement rates

All of the radiometric dating results are summarised in Table 4.12.

Table 4.12 Summary of radiometric dating results

In this table, FMM indicates Finite Mixture Modelling and CAM indicates Central Age Model for the statistical analysis of the De distributions for OSL dating (Section 3.2.3)

Sample location (Terrace name, location code, and bed number)	Latitude and longitude	Elevation above MHW (Mean High Water), NCC datum or rwl (river water level)	Sample type	Method of radiometric dating and laboratory code	Age (years BC or years cal.BC with error ± one σ)
Marine terraces					
Marine terrace A BANDN1 Bed 2	30°06'47''N 50°07'44''E	+2.51 m above MHW	Marine mollusc shell	AMS ^{14}C dating GrA-15580	**815 ± 87 cal.BC**
Marine terrace A BINAK3 Bed 1	29°43'18''N 50°20'44''E	+1.62 m above MHW	Marine mollusc shell	Convent. ^{14}C dating GrN-25106	**1,390 ± 91 cal.BC**
Marine terrace B BINAK 4 Bed 6	29°43'39''N 50°20'28''E	Approx. +18 m above MHW	Marine mollusc shell	AMS ^{14}C dating GrA-21606	**> 43,000 BC (infinite ^{14}C age)**
River terraces					
'Dar Khazineh terrace' DAKS05 Bed 2	31°54'47''N 48°59'29''E	+29.89 m NCC +8.09 m rwl	Sediment (90 - 180/ 250 μm)	OSL dating FMM Shfd08206	**480 ± 190 BC**
'Dar Khazineh terrace' DKLTFH Bed 10	31°54'46''N 48°59'23''E	+30.52 m NCC +8.72 m rwl	Sediment (90 - 180/ 250 μm)	OSL dating FMM Shfd08202	**820 ± 220 BC**
'Dar Khazineh terrace' HGWS05 Bed 7hgw	31°54'35''N 48°59'09''E	+28.37 m NCC +6.57 m rwl	Sediment (90 - 180/ 250 μm)	OSL dating FMM Shfd08207	**3,670 ± 360 BC**
'Kabutarkhan-e Sufla terrace' KBS4OS Bed 2	31°56'28''N 48°47'21''E	+29.90 m NCC +4.57 m rwl	Sediment (90 - 180/ 250 μm)	OSL dating CAM/FMM Shfd08021	**15,590 ± 2,100 BC**
'Batvand terrace' BFLS05 Bed 5	32°00'08''N 49°06'06''E	+99.85 m NCC +6.69 m rwl	Sediment (90 - 180/ 250 μm)	OSL dating FMM Shfd08024	**8,480 ± 830 BC**
'Batvand terrace' BFLS05 Bed 2	32°00'08''N 49°06'06''E	+98.49 m NCC +5.33 m rwl	Sediment (90 - 180/ 250 μm)	OSL dating FMM Shfd08205	**23,860 ± 1,750 BC**
'Kushkak terrace' KUHKL3 Bed 2	32°08'07''N 48°50'34''E	Approx. +58.98 m NCC +9.18 m rwl	Sediment (90 - 180/ 250 μm)	OSL dating FMM Shfd08210	**17,970 ± 2,000 BC**
'Naft-e Safid terrace' DKITEB Bed 2	31°57'15''N 48°59'32''E	+49.67 m NCC +27.61 m rwl	Sediment (90 - 180/ 250 μm)	OSL dating CAM Shfd08019	**20,490 ± 1,100 BC**
'Abgah terrace' BAF2BR Bed 4	31°59'32''N 49°05'43''E	Approx. +114.82 m NCC +6.90 m rwl	Sediment (90 - 180/ 250 μm)	OSL dating FMM Shfd08209	**18,590 ± 3,130 BC**

Figure 4.28 Summary diagram showing the results for the river terraces in relation to the River Karun longitudinal profile and the axes of anticlines in Upper Khuzestan

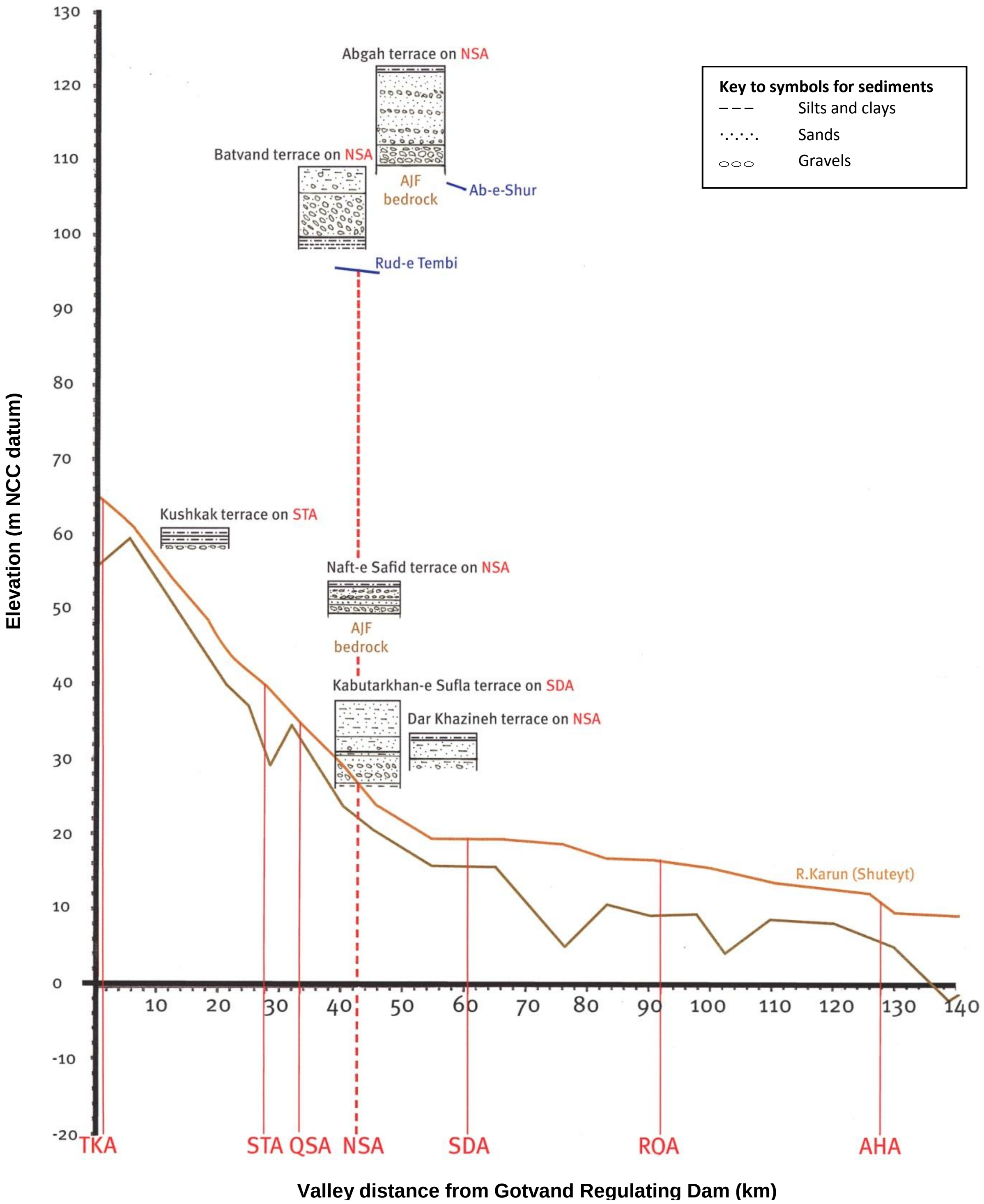

Key

AHA	Ahvaz Anticline	**AJF bedrock**	Agha Jari Formation bedrock	**NSA**	Naft-e Safid Anticline
QSA	Qal'eh Surkheh Anticline	**ROA**	Ramin Oilfield Anticline	**SDA**	Sardarabad Anticline
STA	Shushtar Anticline	**TKA**	Turkalaki Anticline	——— or ------	Axis of anticline

——— Water surface of tributary ——— Water surface of R. Karun ——— Deepest channel bed of R. Karun

The results for the river terraces are summarised in Figure 4.28, which shows how the river terraces and their deposits relate to the anticlines of Upper Khuzestan and the longitudinal profile of the River Karun and its tributaries.

4.3 Results for river characteristics influenced by Earth surface movements and human activities

4.3.1 Results for river reaches

The sub-division of the major river courses into a total of 78 straight-line river "reaches" are shown in Figures 3.4 and 3.5. These successive reaches are designated by their upstream end and downstream end channel locations on the detailed survey, e.g. reach LG2 to LG6 and are used to define the longitudinal valley distance. There are 40 reaches for the River Karun (River Shuteyt) from the Gotvand Regulating Dam to the Persian Gulf at the mouth of the Bahmanshir River. There are 12 reaches for the River Karun (River Gargar) from its bifurcation to its confluence with the River Shuteyt at Band-e Qir. There are 23 reaches for the River Dez from the Dez Regulating Dam in northern Dezful to its confluence with the River Karun at Band-e Qir. There are 3 other reaches: the River Karun upstream of the Gotvand Regulating Dam, the River Dez upstream of the Dez Regulating Dam, and the River Karun from its bifurcation with the Bahmanshir River to its confluence with the Shatt-al Arab at Khorramshahr. The results for these river reaches for structural geology, human activities, river geomorphology, river hydrology, river sedimentology and river migration are given in tables in Appendices 5 and 6.

The results for selected river reaches for selected characteristics relating to general river form, stream powers, river sedimentology and river migration are given in Tables 4.13, 4.14 and 4.15. The river reaches are categorised as upstream, across axis, and downstream of a fold based on the surface extent of the fold limbs ("across axis" includes the reaches between the extent of the fold limbs) on geological and topographical maps, remote sensing images and published articles (as detailed in Section 3.3). Selected river reaches more than about 5 km valley distance from active folds and direct human modifications (such as major dams and major anthropogenic river channel straightening) are categorised as having "minimal" influences from them.

Thirteen cases of fold-river interactions are considered, as follows:

River Karun (River Shuteyt) between the Gotvand Regulating Dam and the vicinity of Band-e Qir:

A) Turkalaki Anticline - Incision across the fold

B) Shushtar Anticline - Incision across the fold

C) Qal'eh Surkheh Anticline - Incision across the projection of the fold

D) Sardarabad Anticline - *Diversion* around the "nose" of the fold

River Gargar between Shushtar and Band-e Qir:

E) Qal'eh Surkheh Anticline - Incision across the projection of the fold

F) Kupal Anticline - Incision across the fold (incision near to the fold "nose")

River Dez between the Dez Regulating Dam in northern Dezful and Band-e Qir:

G) Dezful Uplift - Incision across the uplift

H) Sardarabad Anticline - Incision across the fold

I) Shahur Anticline - *Diversion* around the "nose" of the fold

River Karun and River Dez in the vicinity of Band-e Qir to Veys:

J) Ramin Oilfield Anticline - Incision across the emerging fold

River Karun between Veys and Kut-e Seyyed Saleh (c. 10 km downstream of Ahvaz):

K) Ahvaz Anticline - Incision across the fold

River Karun between Kut-e Seyyed Saleh and the Persian Gulf:

L) Ab-e Teymur Oilfield Anticline - Incision across the emerging fold

M) Dorquain Oilfield Anticline - *Diversion* around the "nose" of the emerging fold

For the selected river characteristics there are expected general trends for river incision across a fold. For instance, with channel sinuosity, an increase in sinuosity upstream of a fold, a decrease in sinuosity across a fold axis, and an increase in sinuosity downstream of a fold is a frequent trend (Jorgensen, 1990; Schumm et al., 2000; Burbank and Anderson, 2001). In Tables 4.13 to 4.15, a ✓ or a ✗ is used to indicate whether changes are in accordance with expected general trends or not.

Table 4.13 (a) Characteristics of general river form for river reaches associated with active folds in lowland south-west Iran

✓ **In accordance with general trends between reaches upstream, across axis, and downstream of fold**
× **Not in accordance with expected general trends between reaches**

Details of fold and reaches of the River KARUN	**Braiding index**	**Channel sinuosity**	**Average channel-belt width (km)**	**General river course direction (bearing degrees)**
A) **Turkalaki Anticline** - Incision across fold				
Upstream of fold	Single-thread 1	Low sinuosity 1.125	Narrow channel belt c. 0.4	c. 50° to fold axis c. 280
Across axis of fold LG2 to LG16	Single-thread 1 ✓	Low sinuosity 1.074 ✓	Narrow channel-belt 1.214 ×	c. 50° to fold axis 200 ×
Downstream of fold LG16 to LB8	Increase to 240 % 2.4 ✓	Increase to 127 % 1.368 ✓	Increase to 215 % 2.613 ✓	170
Reach with “minimal” influences from active folds and direct human modifications				
LG16 to LB8	2.4	1.368	2.613	170
B) **Shushtar Anticline** - Incision across fold				
Upstream of fold LB8 to LB19 LB19 to LB26	Decrease to 77 % 2.0 1.7 ×	Increase to 111 % 1.704 1.345 ✓	Increase to 118 % 3.679 2.469 ✓	130 180
Across axis of fold LB26 to LB31 LB31 to LB34	Single-thread 1 1 ✓	Decrease to 90.5 % 1.431 1.329 ✓	Decrease to 17.3 % 0.485 0.580 ✓	c. 80° to fold axis 200 200 ✓
Downstream of fold LB34 to LB46/1 along R. Shuteyt	Increase to 200 % 2.0 ✓	Increase to 101 % 1.392 ✓	Increase to 168 % 0.893 ✓	250
C) **Qal’eh Surkheh Anticline** - Incision across projection of the fold				
Upstream of fold LB34 to LB46/1 along R. Shuteyt	Increase to 200 % 2.0 ✓	Increase to 101 % 1.392 ✓	Increase to 168 % 0.893 ✓	250
Across axis of fold LB46/1 to LB49 along R. Shuteyt	Multi-thread 2.0 ×	Decrease to 83.9 % 1.168 ✓	Increase to 252 % 2.253 ×	c. 80° to fold axis 200 ✓
Downstream of fold LB49 to LB 56 along R. Shuteyt	Increase to 155 % 3.1 ✓	Increase to 110 % 1.283 ✓	Increase to 129 % 2.895 ✓	220
D) **Sardarabad Anticline** - *Diversion* around nose of the fold				
Upstream of fold LB56 to LB68/1 LB68/1 to LB84	Decrease to 52 % 2.1 1.1	Increase to 124 % 1.389 1.798	Decrease to 71.8 % 2.355 1.805	0°-20° to fold axis 160 140 ✓
Across axis of fold LB84 to LB101	Single-thread 1	Increase to 104 % 1.647	Increase to 162 % 3.359	Change of c. 50° around fold nose 190 ✓
Downstream of fold LB101 to LB116	No change 1	Increase to 102 % 1.682	Decrease to 74.2 % 2.494	190

Table 4.13 (b) Characteristics of general river form for river reaches associated with active folds in lowland south-west Iran (continued)

✓ **In accordance with general trends between reaches upstream, across axis, and downstream of fold**
× **Not in accordance with expected general trends between reaches**

Details of fold and reaches of the River GARGAR	**Braiding index**	**Channel sinuosity**	**Average channel-belt width (km)**	**General river course direction (bearing degrees)**
E) **Qal'eh Surkheh Anticline** - Incision across projection of the fold				
Upstream of fold LB34 to L3 along R. Gargar	No change 1 ✓	Decrease to 80.2 % 1.066 ×	Decrease to 11.7 % 0.068 ×	200
Across axis of fold L3 to L15	Single thread 1 ✓	Increase to 109 % 1.164 ×	Increase to 284 % 0.193 ×	c. 90° to fold axis 190 ✓
Downstream of fold L15 to L20	No change 1 ✓	Increase to 107 % 1.243 ✓	Increase to 284 % 0.548 ✓	140
Reach with "minimal" influences from active folds and direct human modifications				
L37 to L44	1	1.281	0.360	140
F) **Kupal Anticline** - Incision across fold (incision near to fold nose)				
Upstream of fold L71 to L78 L78 to L88	No change 1 1 ✓	Decrease to 62.3 % 1.354 2.629 ×	Decrease to 29.8 % 0.302 0.564 ×	210 250
Across axis of fold L88 to L95 L95 to LM1	Single thread 1 1 ✓	Decrease to 64.3 % 1.259 1.301 ✓	Decrease to 47.2 % 0.234 0.175 ✓	c. 70° to fold axis 210 210 ✓
Downstream of fold LM1 to LM8 along R. Karun	No change 1 ✓	Decrease to 81.6 % 1.061 ×	Increase to 355 % 0.725 ✓	180
Details of fold and reaches of the River DEZ	**Braiding index**	**Channel sinuosity ($m\ m^{-1}$)**	**Average channel-belt width (km)**	**General river course direction (bearing degrees)**
G) **Dezful Uplift** - Incision across uplift				
Upstream of fold L1-A / L2 to L6	Single-thread 1 ✓	Low sinuosity 1.036 ×	Narrow channel-belt 0.231 ×	230
Across axis of fold L6 to L40	Increase mainly over last 1 km 1.9 ×	Increase to 107 % 1.104 ×	Large increase mainly over last 2 km 2.579 ×	c. 90° to fold axis 220 ✓
Downstream of fold L40 to L54-A	Increase to 342 % 6.5 ✓	Increase to 103 % 1.140 ✓	Increase to 298 % 7.674 ✓	200
Reaches with "minimal" influences from active folds and direct human modifications				
L93 to L100	2.1	1.194	3.434	140
L100 to L109	2.1	1.197	2.995	140

Table 4.13 (c) Characteristics of general river form for river reaches associated with active folds in lowland south-west Iran (continued)

✓ In accordance with general trends between reaches upstream, across axis, and downstream of fold
× Not in accordance with expected general trends between reaches

Details of fold and reaches of the River DEZ	Braiding index	Channel sinuosity	Average channel-belt width (km)	General river course direction (bearing degrees)
H) **Sardarabad Anticline** – Incision across the fold				
Upstream of fold	No signif. change	Increase to 116 %	Decrease to 66.9 %	
L135 to L145	1	1.199	3.621	220
L145 to L158	1	2.156	3.164	120
L158 to L168	1	1.417	2.832	130
	✓	✓	×	
Across axis of fold	Single thread	Decrease to 70.4 %	Decrease to 43.7 %	c. 80° to fold axis
L168 to L175	1	1.120	1.402	230
	✓	✓	✓	✓
Downstream of fold	No signif. change	Increase to 144 %	Increase to 391 %	
L175 to L190	1.1	1.585	4.875	130
L190 to L199	1	1.629	6.091	170
	✓	✓	✓	
I) **Shahur Anticline** - *Diversion* around nose of the fold				
Upstream of fold	No signif. change	Increase to 144 %	Increase to 391 %	c. 10° to fold axis, then 40° change around fold nose
L175 to L190	1.1	1.585	4.875	130
L190 to L199	1	1.629	6.091	170
				✓
Across axis of fold	Single thread	Decrease to 95.2 %	Decrease to 75.1 %	Change of 40°-70° around fold nose
L199 to L206	1	1.792	4.163	200
L206 to L214	1	1.270	4.067	170
				✓
Downstream of fold	No change	Increase to 123 %	Decrease to 83.7 %	
L214 to L225	1	2.231	3.959	130
L225 to L233	1	1.537	2.929	190
Reach with "minimal" influences from active folds and direct human modifications				
L233 to L246	1	1.858	4.139	120
Details of fold and reaches of the River KARUN	**Braiding index**	**Channel sinuosity**	**Average channel-belt width (km)**	**General river course direction (bearing degrees)**
J) **Ramin Oilfield Anticline** - Incision across emerging fold (with some *diversion of a palaeochannel*)				
Upstream of fold	No change	Increase to 101 %	Unchanged	
LB116 to LM1	1	1.702	2.494	130
	✓	✓	✓	
Across axis of fold	Single thread	Decrease to 61 %	Decrease to 28.8 %	c. 40° to fold axis
LM1 to LM8	1	1.061	0.725	180
LM8 to LM16	1	1.010	0.344	180
LM16 to LM20	1	1.043	1.085	190
	✓	✓	✓	×
Downstream of fold	No change	Increase to 238 %	Increase to 685 %	
LM20 to LM36	1	2.468	4.920	250
	✓	✓	✓	
Reach with "minimal" influences from active folds and direct human modifications				
LM36 to LM61	1.1	2.200	4.431	220

Table 4.13 (d) Characteristics of general river form for river reaches associated with active folds in lowland south-west Iran (continued)

✓ In accordance with general trends between reaches upstream, across axis, and downstream of fold
× Not in accordance with expected general trends between reaches

Details of fold and reaches of the River KARUN	**Braiding index**	**Channel sinuosity**	**Average channel-belt width (km)**	**General river course direction (bearing degrees)**
K) **Ahvaz Anticline** - Incision across fold				
Upstream of fold LM36 to LM61 LM61 to A11/A12	No signif. change 1.1 1.2 ✓	Decrease to 88.5 % 2.200 2.167 ×	Decrease to 66 % 4.431 2.060 ×	 220 210
Across axis of fold A11/A12 to B11/B12	Single thread 1.2 ✓	Decrease to 48 % 1.047 ✓	Decrease to 20.2 % 0.656 ✓	c. 70° to fold axis 220 ✓
Downstream of fold B11/B12 to A49/A50 A49/A50 to A85/A86	No signif. change 1 1 ✓	Increase to 208 % 1.078 3.283 ✓	Increase to 451 % 0.918 5.002 ✓	 200 270
L) **Ab-e Teymur Oilfield Anticline** - Incision across emerging fold				
Upstream of fold A49/A50 to A85/A86	No change 1 ✓	Increase to 304 % 3.283 ×	Increase to 545 % 5.002 ×	 270
Across axis of fold A85/A86 to B33/B34	Single thread 1 ✓	Decrease to 56.6 % 1.858 ✓	Decrease to 52.1 % 2.604 ✓	c. 90° to fold axis 230 ✓
Downstream of fold B33/B34 to B49/B50 B49/B50 to B63/B64	No change 1 1 ✓	Decrease to 63.7 % 1.176 1.192 ×	Decrease to 36.2 % 0.831 1.056 ×	 230 180
Reaches with "minimal" influences from active folds and direct human modifications				
B97/B98 to C37/C38	1	2.094	3.428	130
C37/C38 to C63/C64	1	2.751	5.232	180
M) **Dorquain Oilfield Anticline** - *Diversion* around nose of the emerging fold				
Upstream of fold C79/C80 to C85/C86 C85/C86 to E3/F3 E3/F3 to E12/F12	No signif. change 1.2 1.1 1	Decrease to 64.5 % 1.002 1.002 1.675	Decrease to 26.5 % 0.546 0.473 1.208	c. 50° then c. 0° to fold axis 230 230 180 ✓
Across axis of fold (& sl. downstr. of fold) E12/F12 to E15/F15 E15/F15 to E19/F19 E19/F19 to E27/F27	Single thread 1 1 1	Decrease to 85.6 % 1.049 1.088 1.014	Decrease to 50.4 % 0.509 0.385 0.228	Change of 20°-50° around fold nose 200 220 230 ✓

Table 4.14 (a) Characteristics relating to stream powers for river reaches associated with active folds in lowland south-west Iran

✓ **In accordance with general trends between reaches upstream, across axis, and downstream of fold**
× **Not in accordance with expected general trends between reaches**

Details of fold and reaches of the River KARUN	**Channel water surface slope ($m\ m^{-1}$)**	**Channel width:depth ratio**	**Specific stream power ($W\ m^{-2}$)**	**Stream power per unit length ($W\ m^{-1}$)**
A) **Turkalaki Anticline** - Incision across fold				
Upstream of fold	—	—	—	—
Across axis of fold LG2 to LG16	Qu. steep channel water surface slope 0.0006427	Very low width:depth ratio 17.6	High specific stream power 16.339	Mod. stream power per unit length 1,986.8
Downstream of fold LG16 to LB8	Increase to 131 % 0.0008394 ×	Increase to 727 % 127.9	Decrease to 54.2 % 8.861 ✓	Increase to 131 % 2,594.9 ×
Reach with "minimal" influences from active folds and direct human modifications				
LG16 to LB8	0.0008394	127.9	8.861	2,594.9
B) **Shushtar Anticline** - Incision across fold				
Upstream of fold LB8 to LB19 LB19 to LB26	Decrease to 93.8 % 0.0005306 0.0010434	Increase to 118 % 127.2 175.6	Decrease to 92.8 % 5.116 11.336	Decrease to 93.8 % 1,640.4 3225.6
Across axis of fold LB26 to LB31 LB31 to LB34	Decrease to 63.6 % 0.0005988 0.0004018 ×	Decrease to 21.4 % 37.1 27.6 ✓	Increase to 154 % 11.451 13.912 ✓	Decrease to 70.6 % 2,056.1 1,379.8 ×
Downstream of fold LB34 to LB46/1 along R. Shuteyt	Increase to 122 % 0.0006103 ×	Increase to 224 % 72.4 ✓	Decrease to 77.1 % 9.776 ✓	Increase to 122 % 2,095.7 ×
C) **Qal'eh Surkheh Anticline** - Incision across projection of the fold				
Upstream of fold LB34 to LB46/1 along R. Shuteyt	Increase to 122 % 0.0006103	Increase to 224 % 72.4	Decrease to 77.1 % 9.776	Increase to 122 % 2,095.7
Across axis of fold LB46/1 to LB49 along R. Shuteyt	Increase to 153 % 0.0009313 ✓	Decrease to 92.8 % 67.2	Increase to 133 % 13.006 ✓	Increase to 152.6 % 3,197.8 ✓
Downstream of fold LB49 to LB 56 along R. Shuteyt	Decrease to 64.3 % 0.0005987 ✓	Increase to 129 % 86.7	Decrease to 34.2 % 4.450 ✓	Decrease to 64.3 % 2,055.8 ✓
D) **Sardarabad Anticline** - *Diversion* around nose of the fold				
Upstream of fold LB56 to LB68/1 LB68/1 to LB84	Decrease to 82.3 % 0.0007075 0.0002778	Decrease to 74.0 % 51.9 76.5	Increase to 235 % 14.706 6.234	Decrease to 93.8 % 2,768.5 1,086.9
Across axis of fold LB84 to LB101	Decrease to 0.7 % 0.0000035	Decrease to 60.4 % 38.8	Decrease to 0.8 % 0.082	Decrease to 0.7 % 13.9
Downstream of fold LB101 to LB116	Increase to 1,220 % 0.0000433	Increase to 163 % 63.4	Increase to 707 % 0.580	Increase to 1,220 % 169.5

Table 4.14 (b) Characteristics relating to stream powers for river reaches associated with active folds in lowland south-west Iran (continued)

✓ In accordance with general trends between reaches upstream, across axis, and downstream of fold
× Not in accordance with expected general trends between reaches

Details of fold and reaches of the River GARGAR	**Channel water surface slope ($m\ m^{-1}$)**	**Channel width:depth ratio**	**Specific stream power ($W\ m^{-2}$)**	**Stream power per unit length ($W\ m^{-1}$)**
E) **Qal'eh Surkheh Anticline** - Incision across projection of the fold				
Upstream of fold LB34 to L3 along R. Gargar	Very large decrease -0.0001993	Decrease to 27.9 % 7.7	Very large decrease -2.983	Very large decrease -89.7
Across axis of fold L3 to L15	Very large increase 0.0028614 ✓	Increase to 809 % 62.3	Very large increase 17.825 ✓	Very large increase 1,287.6 ✓
Downstream of fold L15 to L20	Decrease to 19.5 % 0.0005577 ✓	Decrease to 26.6 % 16.6	Decrease to 40.5 % 7.216 ✓	Decrease to 19.5 % 251.0 ✓
Reach with "minimal" influences from active folds and direct human modifications				
L37 to L44	0.0000308	11.1	0.357	13.8
F) **Kupal Anticline** - Incision across fold (incision near to fold nose)				
Upstream of fold L71 to L78 L78 to L88	Increase to 345 % 0.0002809 0.0001087	Increase to 107 % 8.7 8.4	Increase to 370 % 3.304 1.411	Increase to 345 % 126.4 48.8
Across axis of fold L88 to L95 L95 to LM1	Decrease to 85.3 % 0.0001278 0.0002047 ×	Increase to 112 % 10.8 8.3	Increase to 109 % 1.446 3.705 ✓	Decrease to 85.3 % 57.5 92.1 ×
Downstream of fold LM1 to LM8 along R. Karun	Decrease to 0.4 % 0.0000007 ✓	Increase to 261 % 24.9	Decrease to 0.8 % 0.021 ✓	Decrease to 5.6 % 4.2 ✓
Details of fold and reaches of the River DEZ	**Channel water surface slope ($m\ m^{-1}$)**	**Channel width:depth ratio**	**Specific stream power ($W\ m^{-2}$)**	**Stream power per unit length ($W\ m^{-1}$)**
G) **Dezful Uplift** - Incision across uplift				
Upstream of fold L1-A / L2 to L6	Moderate channel water surface slope 0.0006645	Low width:depth ratio 20.8	Moderate specific stream power 16.960	Mod. stream power per unit length 1,586.1
Across axis of fold L6 to L40	Increase to 290 % 0.0019238 ✓	Decrease to 90.9 % 18.9	Increase to 397 % 67.342 ✓	Increase to 290 % 4,592.1 ✓
Downstream of fold L40 to L54-A	Increase to 123 % 0.0023614 ×	Increase to 519 % 98.0	Decrease to 61.0 % 41.103 ✓	Increase to 123 % 5,636.5 ×
Reaches with "minimal" influences from active folds and direct human modifications				
L93 to L100	0.0012345	168.6	30.129	2,946.7
L100 to L109	0.0010156	139.6	10.857	2,424.3

Table 4.14 (c) Characteristics relating to stream powers for river reaches associated with active folds in lowland south-west Iran (continued)

✓ **In accordance with general trends between reaches upstream, across axis, and downstream of fold**
✗ **Not in accordance with expected general trends between reaches**

Details of fold and reaches of the River DEZ	**Channel water surface slope ($m\ m^{-1}$)**	**Channel width:depth ratio**	**Specific stream power ($W\ m^{-2}$)**	**Stream power per unit length ($W\ m^{-1}$)**
H) **Sardarabad Anticline** – Incision across the fold				
Upstream of fold L135 to L145 L145 to L158 L158 to L168	Decrease to 68.2% 0.0003018 0.0003328 0.0003438	Increase to 101 % 89.6 105.3 44.3	Decrease to 43.2 % 4.731 4.437 6.621	Decrease to 68.2 % 720.4 794.3 820.8
Across axis of fold L168 to L175	Decrease to 92.0 % 0.0002999 ✗	Decrease to 71.4 % 56.9	Decrease to 88.5 % 4.659 ✗	Decrease to 92.0 % 715.9 ✗
Downstream of fold L175 to L190 L190 to L199	Decrease to 48.4 % 0.0001240 0.0001664 ✓	Increase to 107 % 59.4 62.7	Decrease to 33.1 % 1.039 2.042 ✓	Decrease to 48.4 % 296.0 397.3 ✓
I) **Shahur Anticline** - *Diversion* around nose of the fold				
Upstream of fold L175 to L190 L190 to L199	Decrease to 48.4 % 0.0001240 0.0001664	Increase to 107 % 59.4 62.7	Decrease to 33.1 % 1.039 2.042	Decrease to 48.4 % 296.0 397.3
Across axis of fold L199 to L206 L206 to L214	Decrease to 82.6 % 0.0001682 0.0000718	Increase to 102 % 64.3 59.7	Increase to 116 % 2.496 1.063	Decrease to 82.6 % 401.5 171.4
Downstream of fold L214 to L225 L225 to L233	Increase to 114 % 0.0001211 0.0001528	Decrease to 83.5% 42.7 60.8	Increase to 117 % 2.416 1.763	Increase to 114 % 289.1 364.7
Reach with "minimal" influences from active folds and direct human modifications				
L233 to L246	0.0001268	96.0	1.313	302.6
Details of fold and reaches of the River KARUN	**Channel water surface slope ($m\ m^{-1}$)**	**Channel width:depth ratio**	**Specific stream power ($W\ m^{-2}$)**	**Stream power per unit length ($W\ m^{-1}$)**
J) **Ramin Oilfield Anticline** - Incision across emerging fold (with some *diversion of a palaeochannel*)				
Upstream of fold LB116 to LM1	Increase to 358 % 0.001551	Decrease to 60.1 % 38.1	Increase to 429 % 2.488	Increase to 358 % 606.8
Across axis of fold LM1 to LM8 LM8 to LM16 LM16 to LM20	Decrease to 53.0 % 0.0000007 0.0001104 0.0001354 ✗	Increase to 152 % 24.9 95.8 52.8	Decrease to 66.8 % 0.021 2.027 2.941 ✗	Decrease to 76.2 % 4.2 621.1 761.4 ✗
Downstream of fold LM20 to LM36	Increase to 102 % 0.0000839 ✗	Decrease to 97.0 % 56.1	Decrease to 93.6 % 1.557 ✓	Increase to 102 % 471.9 ✗
Reach with "minimal" influences from active folds and direct human modifications				
LM36 to LM61	0.0000516	78.8	0.921	290.3

Table 4.14 (d) Characteristics relating to stream powers for river reaches associated with active folds in lowland south-west Iran (continued)

✓ In accordance with general trends between reaches upstream, across axis, and downstream of fold
× Not in accordance with expected general trends between reaches

Details of fold and reaches of the River KARUN	Channel water surface slope ($m\ m^{-1}$)	Channel width:depth ratio	Specific stream power ($W\ m^{-2}$)	Stream power per unit length ($W\ m^{-1}$)
K) **Ahvaz Anticline** - Incision across fold				
Upstream of fold	Decrease to 51.4 %	Increase to 130 %	Decrease to 50.9 %	Decrease to 51.4 %
LM36 to LM61	0.0000516	78.8	0.921	290.3
LM61 to A11/A12	0.0000347	67.2	0.663	195.1
Across axis of fold	Increase to 1,422 %	Decrease to 44.8 %	Increase to 1,361 %	Increase to 1,422 %
A11/A12 to B11/B12	0.0006136 ✓	32.7	10.777 ✓	3,451.4 ✓
Downstream of fold	Decrease to 7.3 %	Increase to 130 %	Decrease to 7.5 %	Decrease to 7.3 %
B11/B12 to A49/A50	0.0000296	30.7	0.631	166.4
A49/A50 to A85/A86	0.0000597 ✓	54.5	0.978 ✓	336.0 ✓
L) **Ab-e Teymur Oilfield Anticline** - Incision across emerging fold				
Upstream of fold	Increase to 202 %	Increase to 178 %	Increase to 155 %	Increase to 202 %
A49/A50 to A85/A86	0.0000597	54.5	0.978	336.0
Across axis of fold	Decrease to 35.5 %	Decrease to 57.4 %	Decrease to 41.8 %	Decrease to 35.5 %
A85/A86 to B33/B34	0.0000212 ×	31.3	0.409 ×	119.3 ×
Downstream of fold	Increase to 323 %	Increase to 119 %	Increase to 395 %	Increase to 323 %
B33/B34 to B49/B50	0.0000614	46.1	1.228	345.3
B49/B50 to B63/B64	0.0000758 ×	28.4	2.003 ×	426.2 ×
Reaches with "minimal" influences from active folds and direct human modifications				
B97/B98 to C37/C38	0.0000318	24.7	0.700	200.3
C37/C38 to C63/C64	0.0000422	27.1	1.143	266.0
M) **Dorquain Oilfield Anticline** - *Diversion* around nose of the emerging fold				
Upstream of fold	Increase to 104 %	Decrease to 92.6 %	Decrease to 97.6 %	Increase to 104 %
C79/C80 to C85/C86	0.0000770	23.4	1.646	485.4
C85/C86 to E3/F3	0.0000132	23.2	0.427	83.4
E3/F3 to E12/F12	0.0000140	44.7	0.330	88.5
Across axis of fold (& sl. downstr. of fold)	Increase to 143 %	Decrease to 76.1 %	Increase to 190 %	Increase to 143 %
E12/F12 to E15/F15	0.0000637	34.4	1.740	401.4
E15/F15 to E19/F19	0.0000356	11.9	1.306	224.1
	Large decrease	Decrease to 82.5 %	Large decrease	Large decrease
E19/F19 to E27/F27	0	19.1	0	0

Table 4.15 (a) Characteristics of river migration and river sedimentology for river reaches associated with active folds in lowland south-west Iran

✓ In accordance with general trends between reaches upstream, across axis, and downstream of fold (brackets indicate no change) × Not in accordance with expected general trends between reaches

Details of fold and reaches of the River KARUN	**Greatest channel bank migration distance 1966/68 - 2001 (m)**	**Average channel migration rate 1966/68 - 2001 (m yr^{-1})**	**Description of channel bed surface sediments (grain size)**	**Description of channel bank sediments (grain size)**
A) **Turkalaki Anticline** - Incision across fold				
Upstream of fold	—	—	—	—
Across axis of fold LG2 to LG16	223	1.096	P gr (esp pb), P sa & si	P gr & sa, P sa & si
Downstream of fold LG16 to LB8	Increase to 222 % 494 ✓	Increase to 285 % 3.123 ✓	No change P gr (esp pb), P sa & si (✓)	No change P gr & sa, P sa & si (✓)
Reach with "minimal" influences from active folds and direct human modifications				
LG16 to LB8	494	3.123	P gr (esp pb), P sa & si	P gr & sa, P sa & si
B) **Shushtar Anticline** - Incision across fold				
Upstream of fold LB8 to LB19 LB19 to LB26	Increase to 261 % 1626 956	Increase to 288 % 9.239 8.728	Slight increase M gr (esp pb wi s cb, Dmax=47.9-114.1 mm), s sa & si ×	No change P gr & sa, P sa & si (B=87.5 %)
Across axis of fold LB26 to LB31 LB31 to LB34	Decrease to 25.9 % 411 259 ✓	Decrease to 18.0 % 1.774 1.468 ✓	No signif. change M gr (esp pb wi s cb, Dmax= 77.7 mm), s sa & si (✓)	Very slight increase M sa & si (B=79.5%) & gr ✓
Downstream of fold LB34 to LB46/1 along R. Shuteyt	Increase to 129 % 432 ✓	Increase to 218 % 3.540 ✓	No signif. change M gr (esp pb wi s cb), s sa & si (✓)	Very slight decrease P gr & sa, P fine sa & mu ✓
C) **Qal'eh Surkheh Anticline** - Incision across projection of the fold				
Upstream of fold LB34 to LB46/1 along R. Shuteyt	Increase to 129 % 432	Increase to 218 % 3.540	No signif. change M gr (esp pb wi s cb), wi s sa & si (✓)	Very slight decrease P gr & sa, P fine sa & mu
Across axis of fold LB46/1 to LB49 along R. Shuteyt	Increase to 186 % 802 ×	Increase to 125 % 4.430 ×	No signif. change M gr (esp pb wi s cb, Dmax=88.2 mm), wi s sa & si (✓)	No change P gr & sa, P fine sa & mu (B=77.9 %) (✓)
Downstream of fold LB49 to LB 56 along R. Shuteyt	Increase to 205 % 1644 ✓	Increase to 408 % 18.072 ✓	No signif. change M gr, wi s sa & si (✓)	No change P gr & sa, P fine sa & mu (✓)
D) **Sardarabad Anticline** - *Diversion* around nose of the fold				
Upstream of fold LB56 to LB68/1 LB68/1 to LB84	Decrease to 67.6 % 1119 1104	Decrease to 42.8 % 8.792 6.663	Decrease P sa & si (Dfine=723.8 μm), P gr (Dmax=82.5 mm)	Decrease M sa & si (B=61.6 %)' few gravels
Across axis of fold LB84 to LB101	Decrease to 53.0 % 589	Decrease to 57.0 % 4.403	Decrease M sa & si	Decrease Sa & mu (B=97.3-99.0%)
Downstream of fold LB101 to LB116	Increase to 271 % 1598	Increase to 124 % 5.468	No change M sa & si	Very slight increase Sa & mu (B=89.8 %)

Table 4.15 (b) Characteristics of river migration and river sedimentology for river reaches associated with active folds in lowland south-west Iran (continued)

✓ In accordance with general trends between reaches upstream, across axis, and downstream of fold (brackets indicate no change) × Not in accordance with expected general trends between reaches

Details of fold and reaches of the River GARGAR	Greatest channel bank migration distance 1966/68 - 2001 (m)	Average channel migration rate 1966/68 - 2001 (m yr^{-1})	Description of channel bed surface sediments (grain size)	Description of channel bank sediments (grain size)
E) **Qal'eh Surkheh Anticline** - Incision across projection of the fold				
Upstream of fold LB34 to L3 along R. Gargar	Decrease to 8.9 % 23	Decrease to 7.8 % 0.114	Large decrease M sa & si, few gr ✓	Large decrease M sa & mu
Across axis of fold L3 to L15	Increase to 191 % 44 ×	Decrease to 71.1 % 0.081 ✓	No signif. change M sa & si, few gr (Dmax=89.1 mm) (✓)	No change M sa & mu (B=65.4 %), P sa & gr (✓)
Downstream of fold L15 to L20	Large decrease 0 ×	Large decrease 0 ×	Decrease M sa & si ✓	Decrease Sa & mu (B=97.0 %) ✓
Reach with "minimal" influences from active folds and direct human modifications				
L37 to L44	24	0.012	M sa & si	M mu, wi s sa
F) **Kupal Anticline** - Incision across fold (incision near to fold nose)				
Upstream of fold L71 to L78 L78 to L88	Increase to 594 % 109 271	Increase to 534 % 0.161 0.430	No change M sa & si (✓)	No change M mu, wi s sa
Across axis of fold L88 to L95 L95 to LM1	Decrease to 14.2 % 27 27 ✓	Decrease to 5.6 % 0.010 0.023 ✓	No change M sa & si (✓)	No change M mu, wi s sa (✓)
Downstream of fold LM1 to LM8 along R. Karun	Increase to 433 % 117 ✓	Very large increase 0.730 ✓	No signif. change M sa & si (Dfine=21.1 µm) (✓)	Increase Sa & mu (B=81.2 %) ×
Details of fold and reaches of the River DEZ	**Greatest channel bank migration distance 1966/68 - 2001 (m)**	**Average channel migration rate 1966/68 - 2001 (m yr^{-1})**	**Description of channel bed surface sediments (grain size)**	**Description of channel bank sediments (grain size)**
G) **Dezful Uplift** - Incision across uplift				
Upstream of fold L1-A / L2 to L6	86	0.566	M gr (esp pb w s cb), few sa & si	P gr & sa, P fine sa & mu
Across axis of fold L6 to L40	Increase to 314 % 270 ×	Decrease to 94.3 % 0.534 ✓	No signif. change M gr (esp pb & cb, Dmax=91.6 mm), few sa & si (✓)	No change P gr & sa, P fine sa & mu (✓)
Downstream of fold L40 to L54-A	Increase to 279 % 754 ✓	Increase to 1,096 % 5.852 ✓	No change M gr (esp pb w s cb), few sa & si (✓)	Very slight decrease M sa wi s gr, P fine sa & mu ✓
Reaches with "minimal" influences from active folds and direct human modifications				
L93 to L100	696	5.763	P gr, P sa & si	M sa & si, few gr
L100 to L109	1572	15.863	P gr., P sa & si	M sa & si, few gr

Table 4.15 (c) Characteristics of river migration and river sedimentology for river reaches associated with active folds in lowland south-west Iran (continued)

✓ **In accordance with general trends between reaches upstream, across axis, and downstream of fold (brackets indicate no change)** ✗ **Not in accordance with expected general trends between reaches**

Details of fold and reaches of the River DEZ	**Greatest channel bank migration distance 1966/68 - 2001 (m)**	**Average channel migration rate 1966/68 - 2001 ($m\ yr^{-1}$)**	**Description of channel bed surface sediments (grain size)**	**Description of channel bank sediments (grain size)**
H) **Sardarabad Anticline** – Incision across the fold				
Upstream of fold L135 to L145 L145 to L158 L158 to L168	Decrease to 87.3 % 1096 521 1775	Decrease to 90.6 % 4.936 3.511 11.129	V. slight decrease P sa & si (Dfine=99.5 μm), P gr (Dmax=69.2 mm) ✓	No signif change M sa & si (B=51.8 %), few gr
Across axis of fold L168 to L175	Decrease to 22.7 % 257 ✓	Decrease to 24.2 % 1.578 ✓	No signif. change P sa & si, P gr (✓)	Very slight decrease M sa & si (B=67.0 %), few gr ✗
Downstream of fold L175 to L190 L190 to L199	Increase to 361 % 946 911 ✓	Increase to 318 % 4.502 5.538 ✓	Decrease M sa & si (Dfine=129.1 μm) ✓	Slight decrease Sa & mu (B=68.4 %) ✓
I) **Shahur Anticline** - *Diversion* around nose of the fold				
Upstream of fold L175 to L190 L190 to L199	Increase to 361 % 946 911	Increase to 318 % 4.502 5.538	Decrease M sa & si (Dfine=129.1 μm)	Slight decrease Sa & mu (B=68.4 %)
Across axis of fold L199 to L206 L206 to L214	Decrease to 35.1 % 308 344	Decrease to 54.0 % 2.841 2.578	No signif. change M sa & si	No signif. change Sa & mu
Downstream of fold L214 to L225 L225 to L233	Decrease to 95.9 % 405 220	Decrease to 52.6 % 1.890 0.960	No change M sa & si	No change Sa & mu
Reach with “minimal” influences from active folds and direct human modifications				
L233 to L246	179	1.909	M sa & si	Sa & mu
Details of fold and reaches of the River KARUN	**Greatest channel bank migration distance 1966/68 - 2001 (m)**	**Average channel migration rate 1966/68 - 2001 ($m\ yr^{-1}$)**	**Description of channel bed surface sediments (grain size)**	**Description of channel bank sediments (grain size)**
J) **Ramin Oilfield Anticline** - Incision across emerging fold (with some *diversion of a palaeochannel*)				
Upstream of fold LB116 to LM1	Decrease to 46.2 % 739	Decrease to 89.7 % 4.907	No signif. change M sa & si (Dfine=28.8 μm) (✓)	Very slight increase Sa & mu (B=66.0 %)
Across axis of fold LM1 to LM8 LM8 to LM16 LM16 to LM20	Decrease to 17.8 % 117 162 116 ✓	Decrease to 15.5 % 0.730 0.712 0.847 ✓	No signif. change M sa & si (Dfine=21.1 μm) (✓)	Very slight decrease Sa & mu (B=81.2 %) ✗
Downstream of fold LM20 to LM36	Increase to 245 % 323 ✓	Increase to 355 % 2.711 ✓	Very slight increase M sa & si (Dfine=69.1 μm) ✗	Very slight increase Sa & mu (B=63.6 %) ✗
Reach with “minimal” influences from active folds and direct human modifications				
LM36 to LM61	651	4.061	M sa & mu	Mu & sa

Table 4.15 (d) Characteristics of river migration and river sedimentology for river reaches associated with active folds in lowland south-west Iran (continued)

✓ **In accordance with general trends between reaches upstream, across axis, and downstream of fold (brackets indicate no change)** ✗ **Not in accordance with expected general trends between reaches**

Details of fold and reaches of the River KARUN	**Greatest channel bank migration distance 1966/68 - 2001 (m)**	**Average channel migration rate 1966/68 - 2001 (m yr^{-1})**	**Description of channel bed surface sediments (grain size)**	**Description of channel bank sediments (grain size)**
K) **Ahvaz Anticline** - Incision across fold				
Upstream of fold LM36 to LM61 LM61 to A11/A12	Increase to 150 % 651 315	Decrease to 89.3 % 4.061 0.781	No signif. change M sa & mu (Dfine=10.7-65.7 µm) (✓)	No signif. change Mu & sa (B=79.8-97.4 %)
Across axis of fold A11/A12 to B11/B12	Decrease to 40.8 % 197 ✓	Decrease to 41.6 % 1.008 ✓	Slight increase M sa & mu (Dfine=10.6-152.7 µm), wi s gr (Dmax=69.5 mm) ✓	Slight increase Sa & mu (B=49.8-65.7 %) ✓
Downstream of fold B11/B12 to A49/A50 A49/A50 to A85/A86	Increase to 163 % 320 323 ✓	Increase to 269 % 3.224 2.198 ✓	Slight decrease M sa & mu (Dfine=150.7 µm) ✓	Very slight decrease Mu & sa (B=63.8-74.7 %) ✓
L) **Ab-e Teymur Oilfield Anticline** - Incision across emerging fold				
Upstream of fold A49/A50 to A85/A86	Increase to 101 % 323	Decrease to 68.2 % 2.198	Slight decrease M sa & mu (Dfine=150.7 µm) ✓	Very slight decrease Mu & sa (B=63.8-74.7 %)
Across axis of fold A85/A86 to B33/B34	Increase to 116 % 374 ✗	Increase to 128.9 % 2.833 ✗	Very slight decrease Sa & mu ✗	No signif. change Mu & sa (✓)
Downstream of fold B33/B34 to B49/B50 B49/B50 to B63/B64	Decrease to 57.9 % 177 256 ✗	Decrease to 63.2 % 0.982 2.601 ✗	No change Sa & mu (✓)	No change Mu & sa (✓)
Reaches with "minimal" influences from active folds and direct human modifications				
B97/B98 to C37/C38	799	3.231	Sa & mu	M mu
C37/C38 to C63/C64	634	3.316	Sa & mu	M mu
M) **Dorquain Oilfield Anticline** - *Diversion* around nose of the emerging fold				
Upstream of fold C79/C80 to C85/C86 C85/C86 to E3/F3 E3/F3 to E12/F12	Increase to 131 % 110 247 296	Increase to 144 % 0.841 3.471 1.819	No change Sa & mu (✓)	No signif. change M mu (esp si/clay & clay) (✓)
Across axis of fold (and sl. downstream of fold) E12/F12 to E15/F15 E15/F15 to E19/F19	Decrease to 85.9 % 195 179	Decrease to 42.3 % 0.855 0.873	No change Sa & mu (✓)	No change M mu (✓)
E19/F19 to E27/F27	Decrease to 34.8 % 65	Decrease to 49.8 % 0.430	No change Sa & mu (✓)	No change M mu (✓)

Key to abbreviations for Table 4.15 (a-d)

B	% of channel bank sediments less than 63 µm			cb	cobbles
Dfine	mean grain size for fine gravels, sands and muds				
Dmax	mean grain size for 10 largest gravel clasts				
gr	gravels	M	mainly	mu	muds
P	partly	pb	pebbles	s	some
sa	sands	si	silts	wi	with

4.3.2 Plots of river characteristics against valley distance

River longitudinal profiles of elevation plotted against valley distance (as a succession of "reaches") for the River Karun (Shuteyt), River Karun (Gargar) and River Dez are given in Figures 4.29 to 4.31. The river geomorphological characteristics of channel and valley slopes, channel sinuosity, braiding index, average channel-belt width and general river course direction are plotted against valley distance in Figures 4.32 to 4.37. The river hydrological characteristics of channel water surface slope, channel width:depth ratio and specific stream power are plotted against valley distance in Figures 4.38 to 4.40. The river sedimentological characteristics of greatest channel bank migration distance and average channel migration rate 1966/1968 - 2001 are plotted against valley distance in Figures 4.41 to 4.43. On these graphs, the locations of the main geological structures are indicated by the use of symbols and abbreviations, or by the use of red lines and the letter codes given in Section 4.3.1 for the fold axes or uplift limbs.

4.4 Results of laboratory analyses

The results of the laboratory analyses are presented in the Appendices as tables. Appendix 1 gives the results of the gravel lithological analysis for 50 typical gravel clasts for samples from river bed gravels and river terrace gravels. Appendix 2 gives the results of the thin section analysis of fine-grained sediment and rock samples from river banks and beds, river terraces, ancient constructions and bedrock. Appendix 3 gives the results of the grain size analysis for the 10 largest gravel clasts and 50 typical gravel clasts for samples of river bed gravels and river terrace gravels. Appendix 4 gives the results of grain size analysis of fine-grained sediment and rock samples from river banks and beds, river terraces and floodplains, and ancient constructions. Results from the laboratory analyses are also incorporated in Appendices 5 and 6 about river characteristics.

Figure 4.29 Longitudinal profile of the River **Karun** (River **Shuteyt** branch) from Gotvand to the Persian Gulf

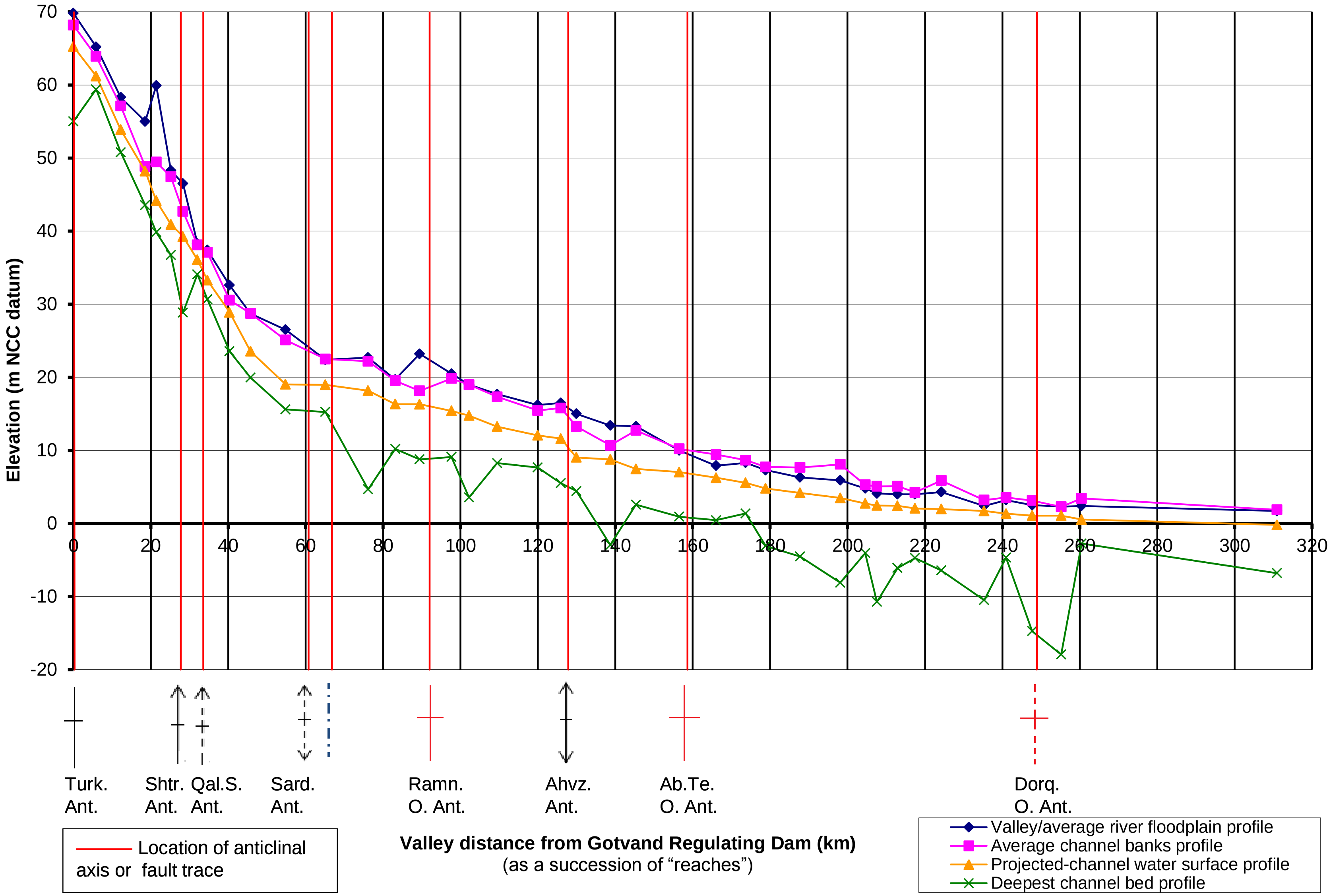

Figure 4.30 Longitudinal profile of the River Karun (River **Gargar** branch) from Gotvand - near Zargan-e Buzurg

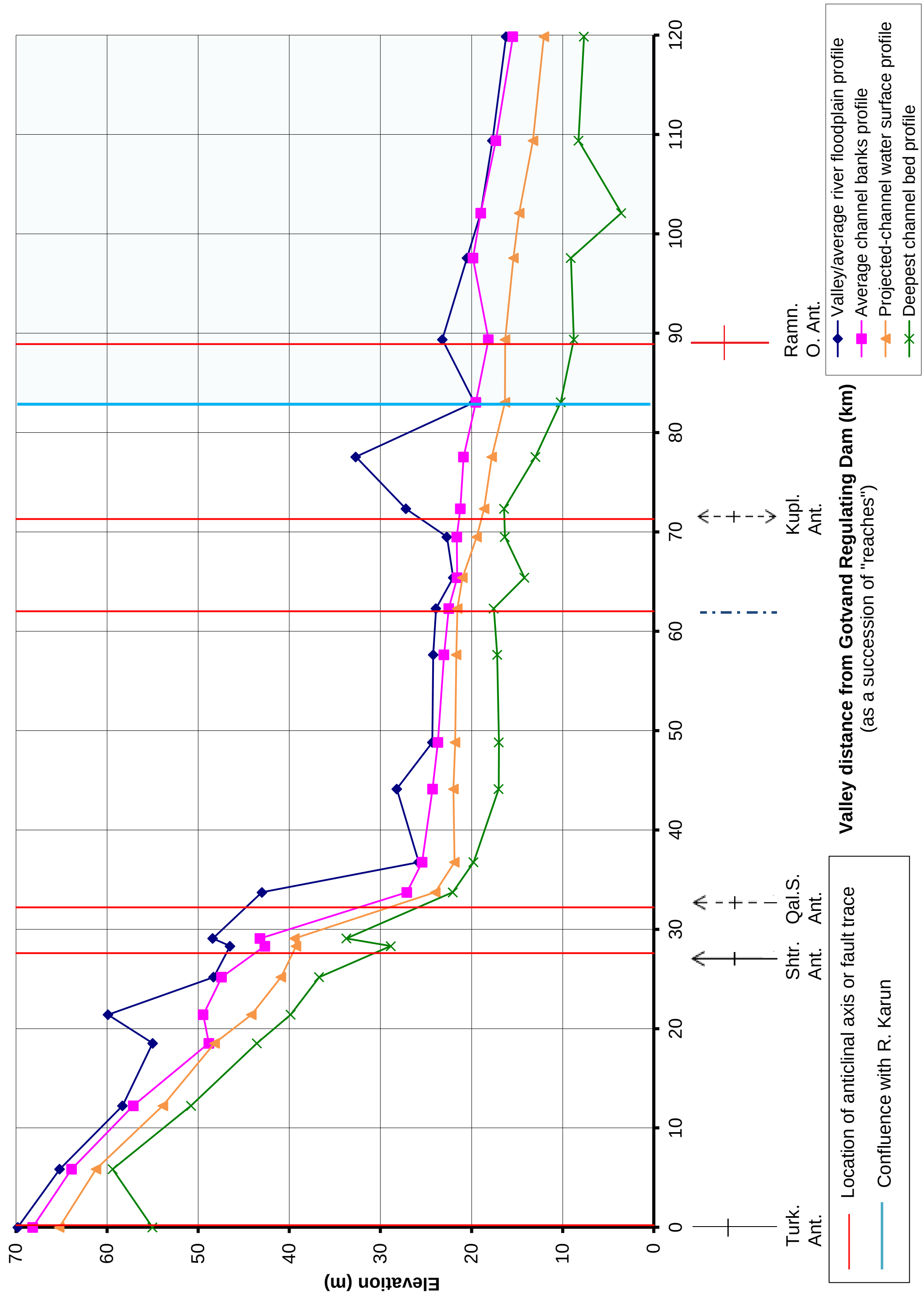

Key to abbreviations used in Figures 4.29, 4.30 and 4.31

Ab.Te. O. Ant.	Ab-e Teymur Oilfield Anticline		
Ahvz. Ant.	Ahvaz Anticline	Dorq. O. Ant.	Dorquain Oilfield Anticline
Kupl. Ant.	Kupal Anticline	Qal.S. Ant.	Qal'eh Surkheh Anticline
Ramn. O. Ant.	Ramin Oilfield Anticline		
Sard. Ant.	Sardarabad Anticline	Shah. Ant.	Shahur Anticline
Shtr. Ant.	Shushtar Anticline	Turk. Ant.	Turkalaki Anticline

Figure 4.31 Longitudinal profile of the River **Dez** from northern Dezful - near Zargan-e Buzurg

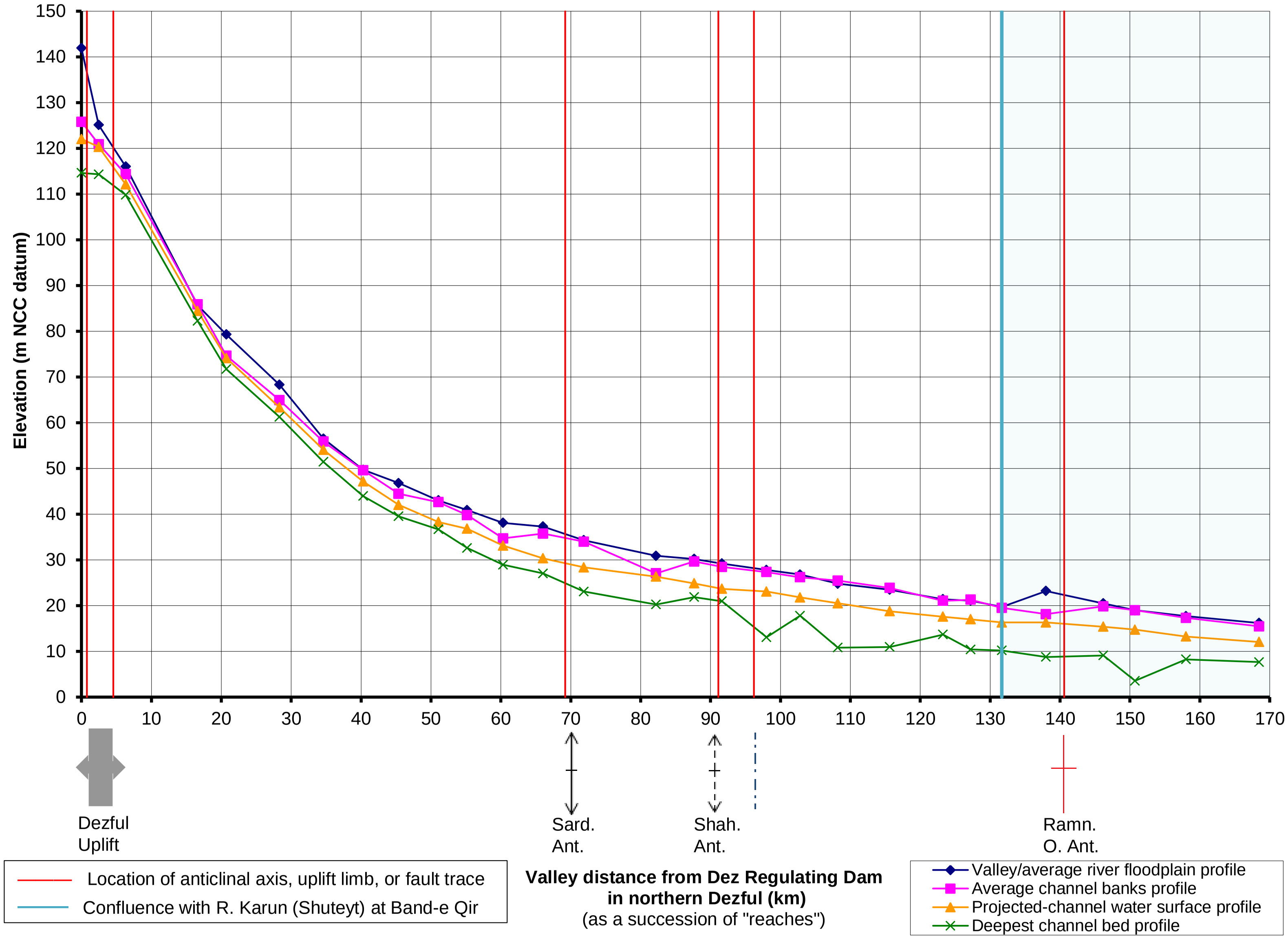

Figure 4.32 Channel/valley slopes and channel sinuosity of the River **Karun** (**Shuteyt**) from Gotvand to the Persian Gulf

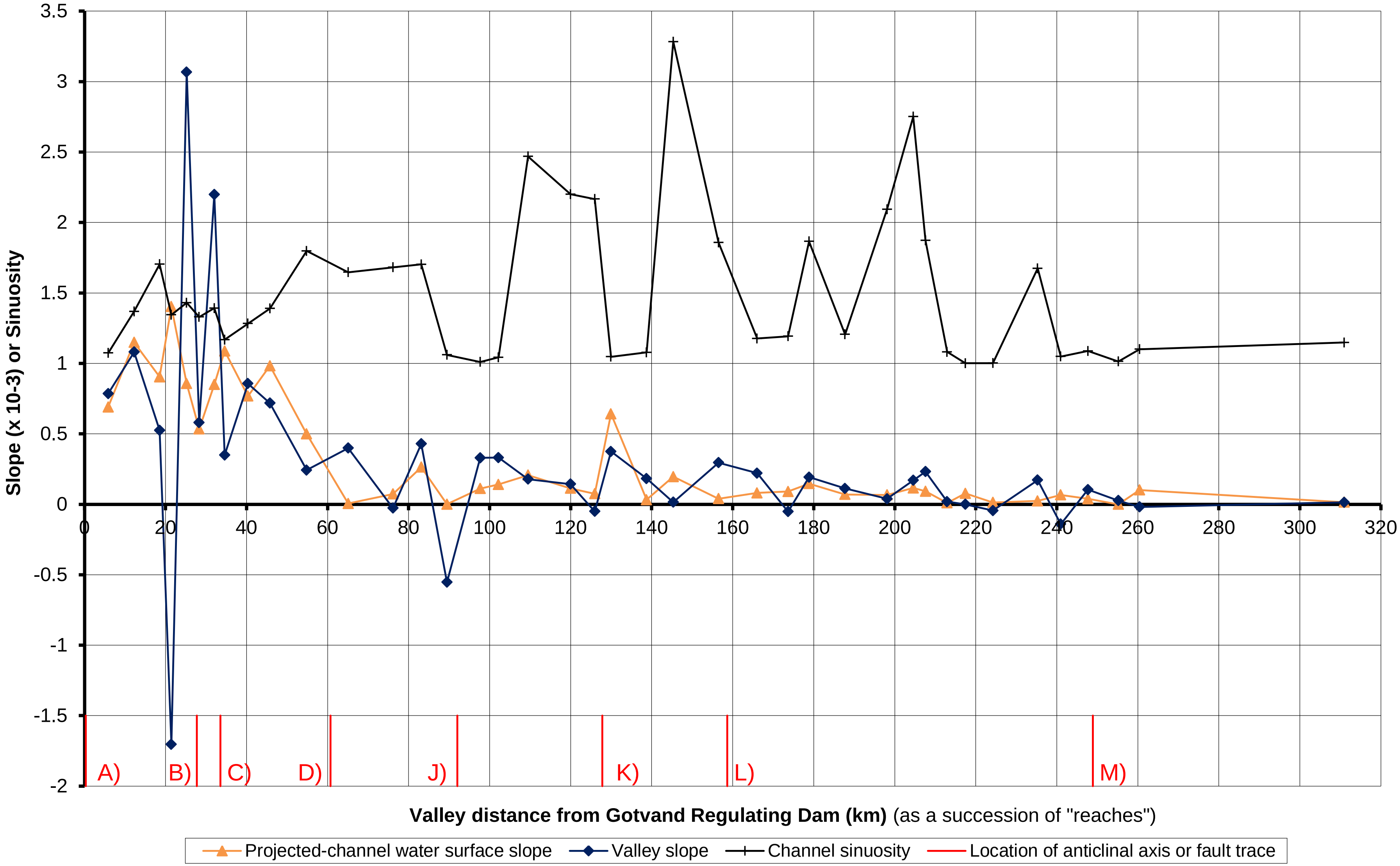

Figure 4.33 Channel/valley slopes and channel sinuosity of River Karun (**Gargar**) from Gotvand - nr. Zargan-e Buzurg

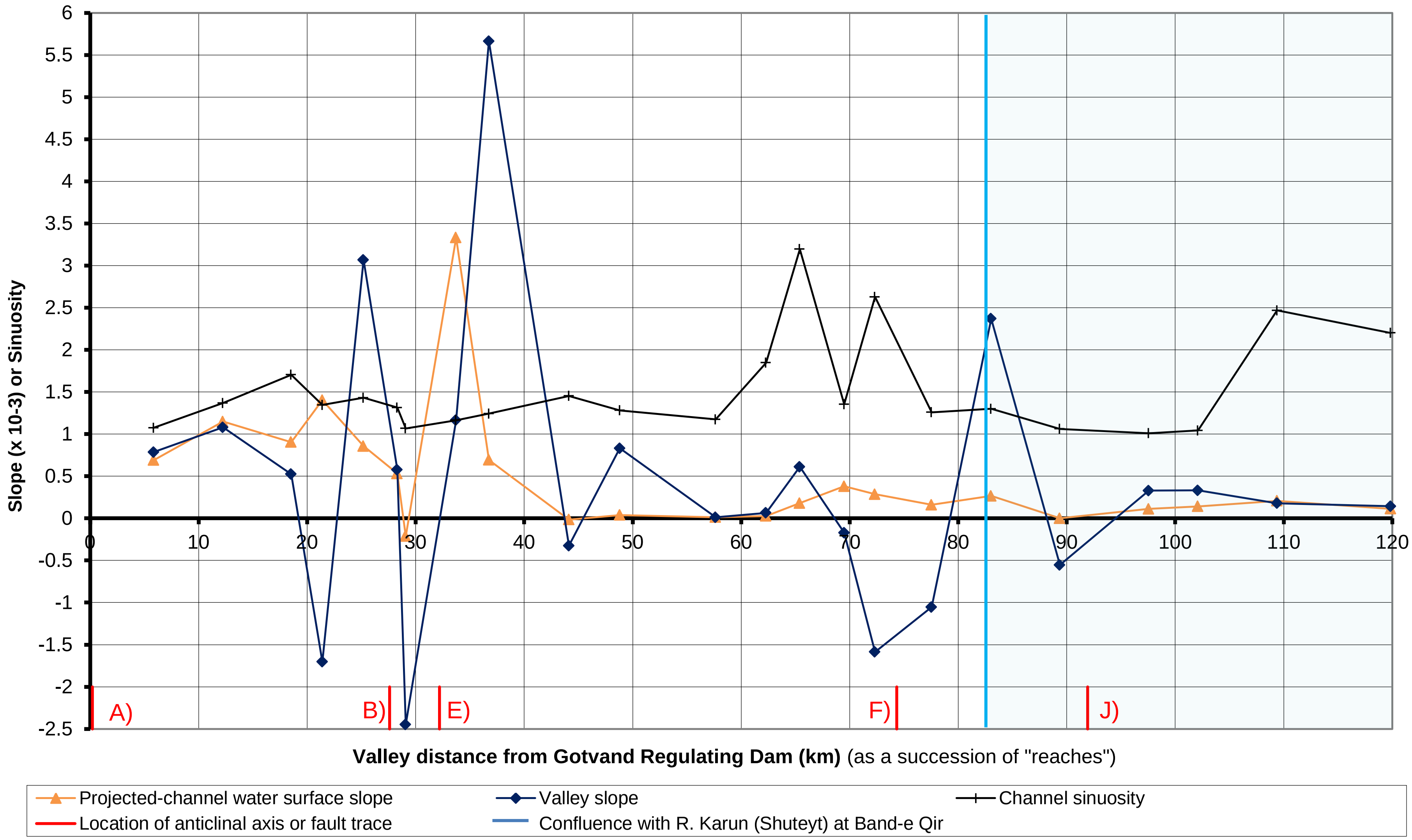

Figure 4.34 Channel/valley slopes and channel sinuosity of the River **Dez** from northern Dezful - nr. Zargan-e Buzurg

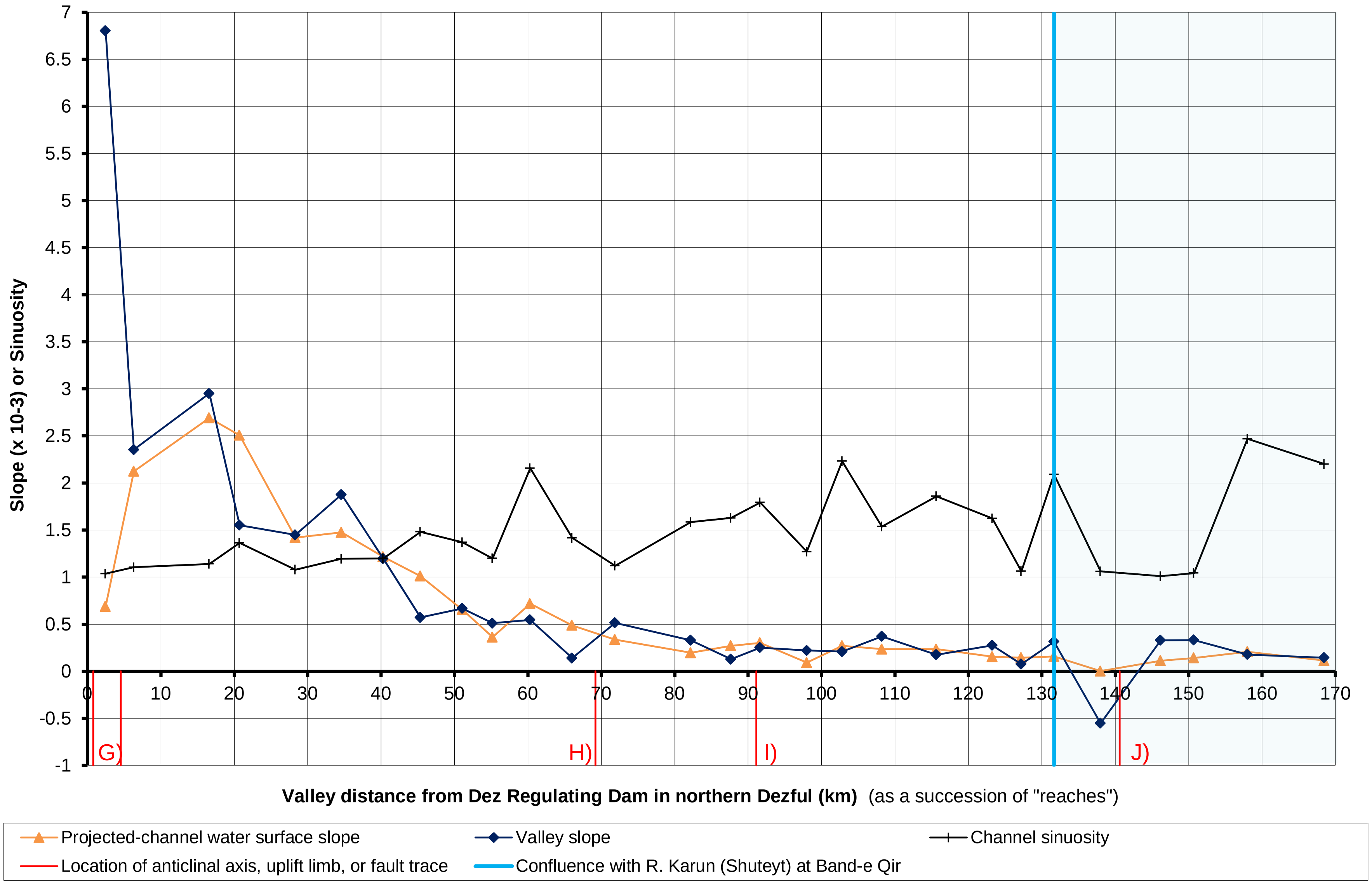

Figure 4.35 Characteristics of general river form for the River **Karun** (**Shuteyt**) from Gotvand to the Persian Gulf

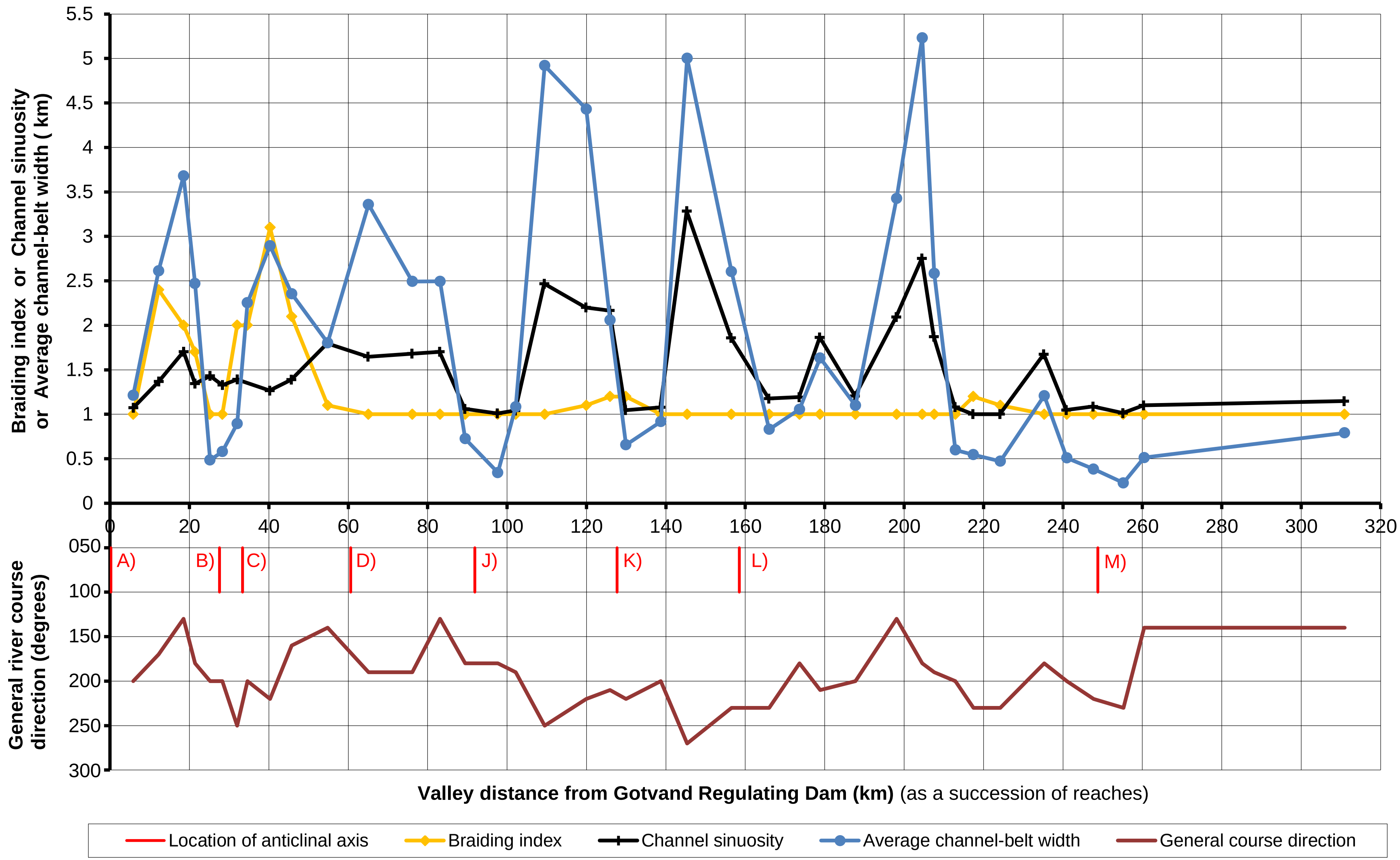

Figure 4.36 Characteristics of general river form for the River Karun (**Gargar**) from Gotvand - nr. Zargan-e Buzurg

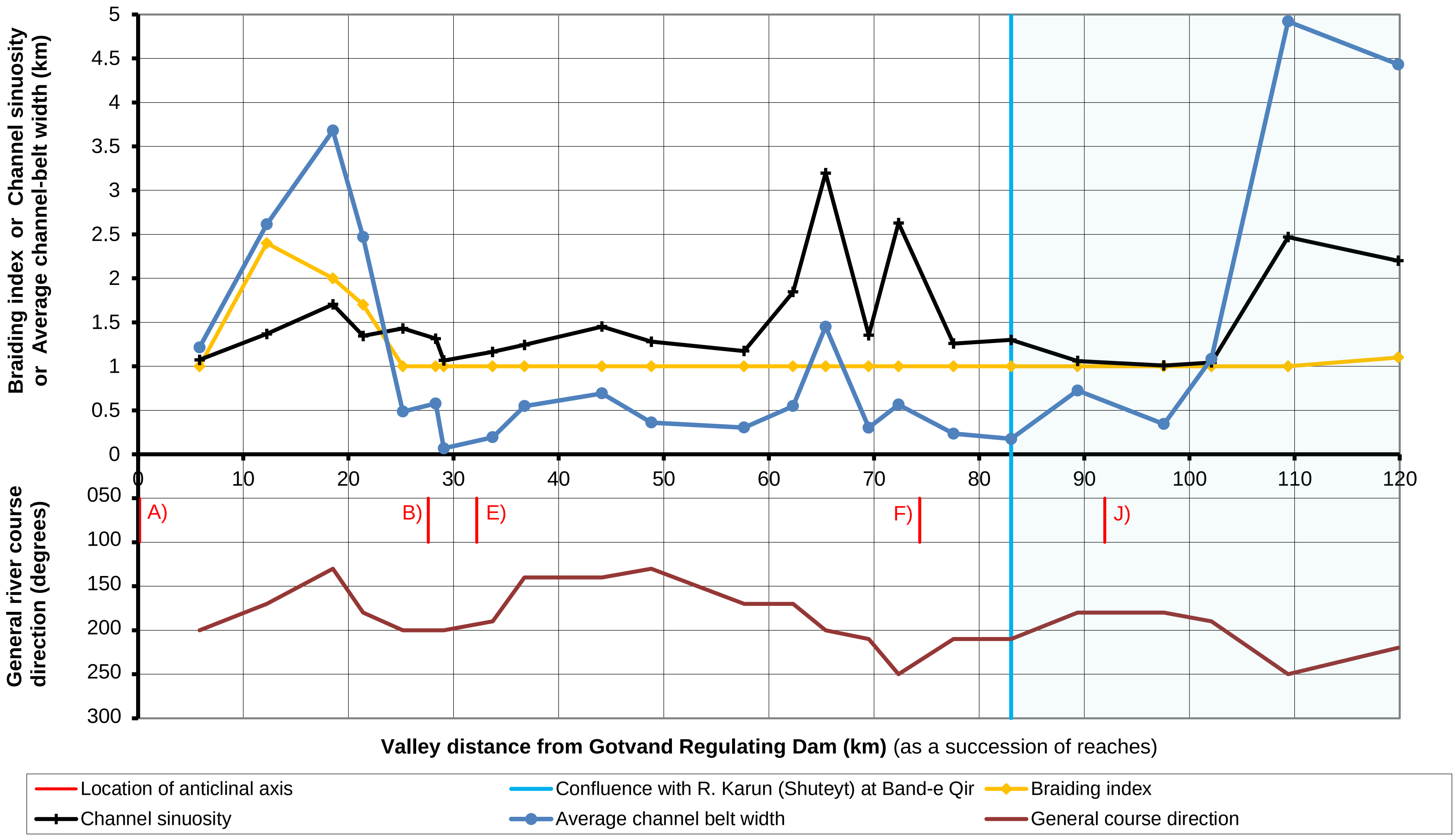

Figure 4.37 Characteristics of general river form for the River **Dez** from northern Dezful - nr. Zargan-e Buzurg

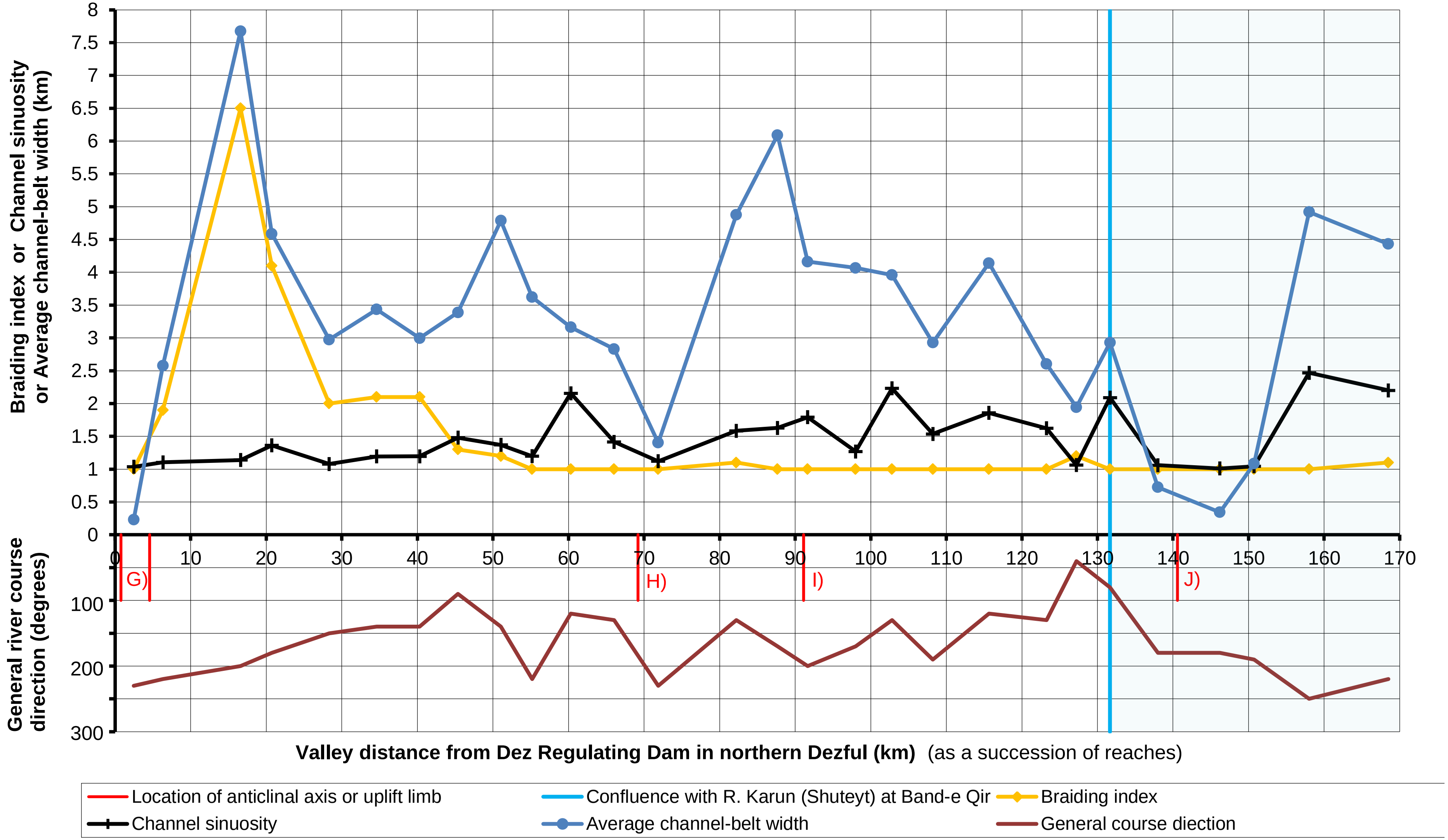

Figure 4.38 Characteristics relating to stream powers for the River **Karun** (**Shuteyt**) from Gotvand to the Persian Gulf

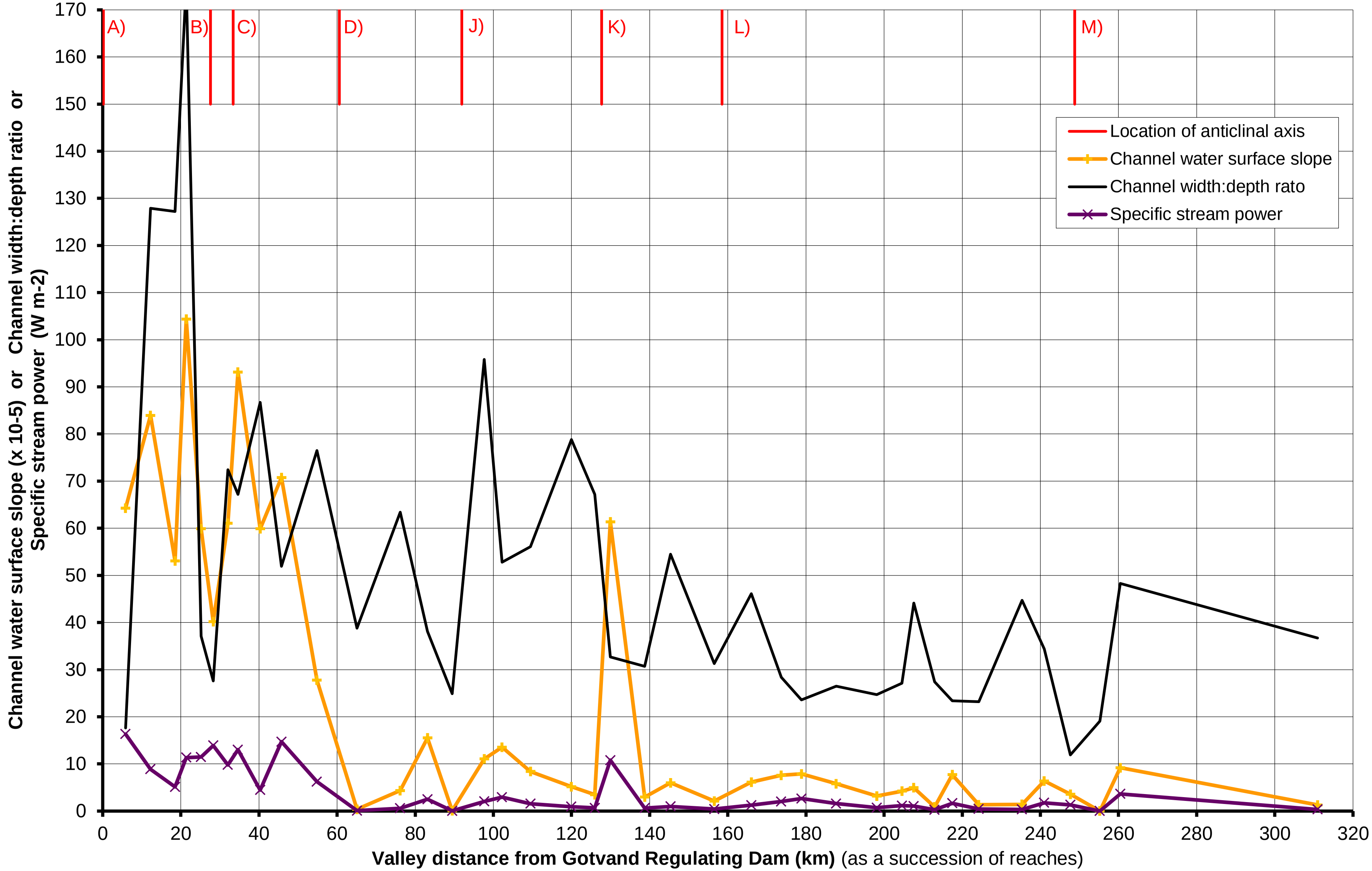

Figure 4.39 Characteristics relating to stream powers for the River Karun (**Gargar**) from Gotvand - nr. Zargan-e Buzurg

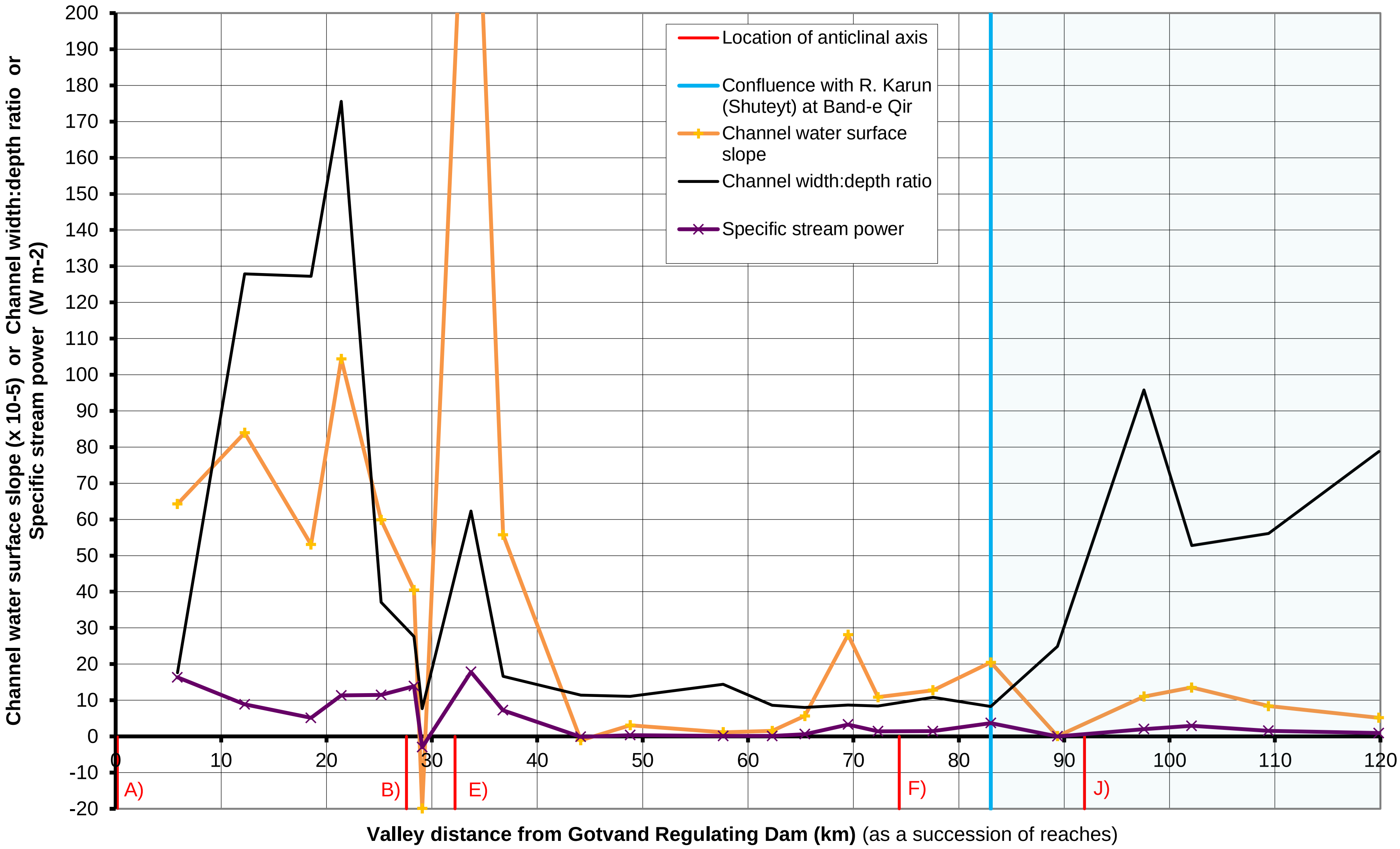

Figure 4.40 Characteristics relating to stream powers for the River **Dez** from northern Dezful - nr. Zargan-e Buzurg

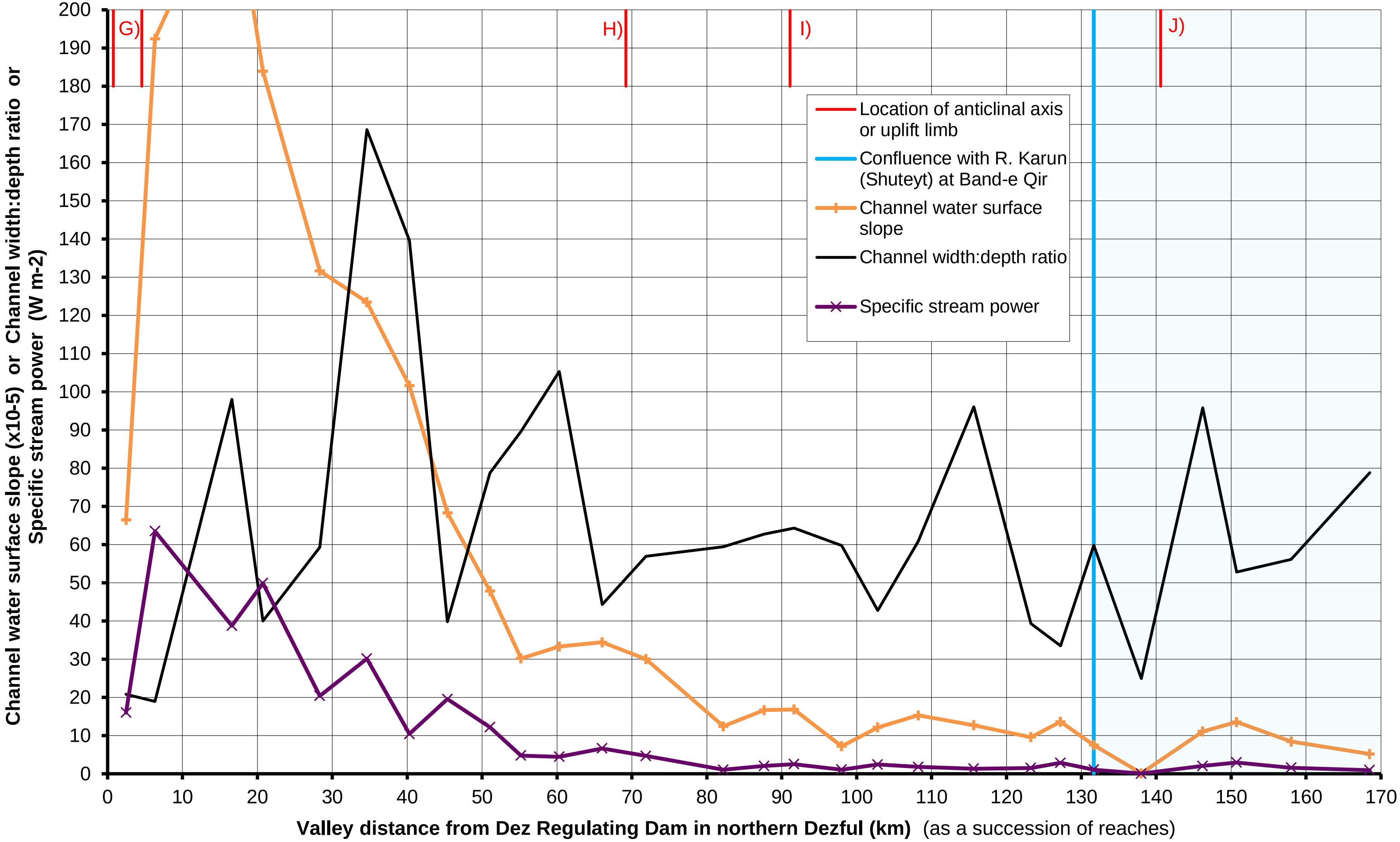

Figure 4.41 Characteristics of river sedimentology for the River **Karun** (**Shuteyt**) from Gotvand to the Persian Gulf

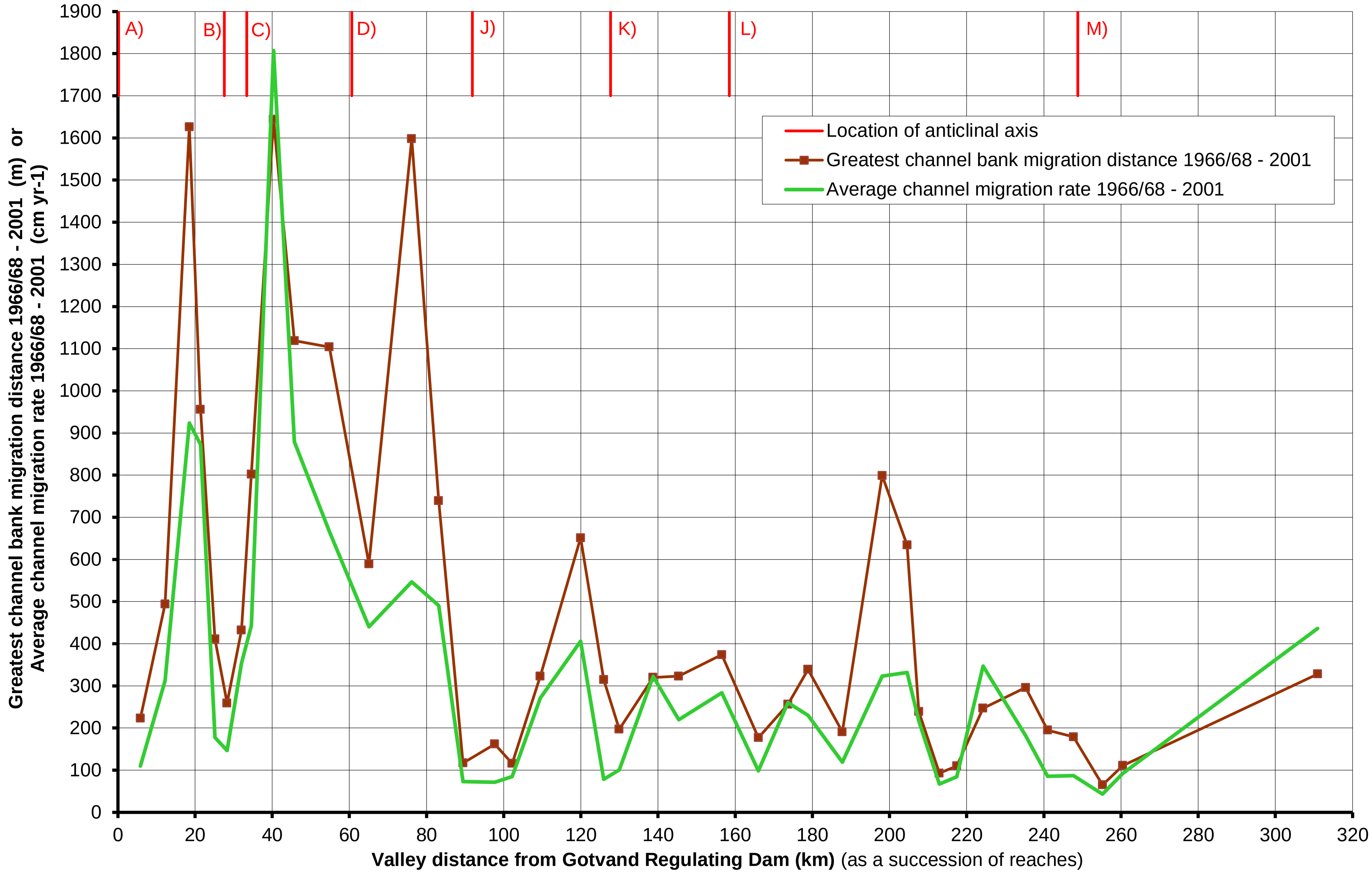

Figure 4.42 Characteristics of river sedimentology for the River Karun (**Gargar**) from Gotvand - nr. Zargan-e Buzurg

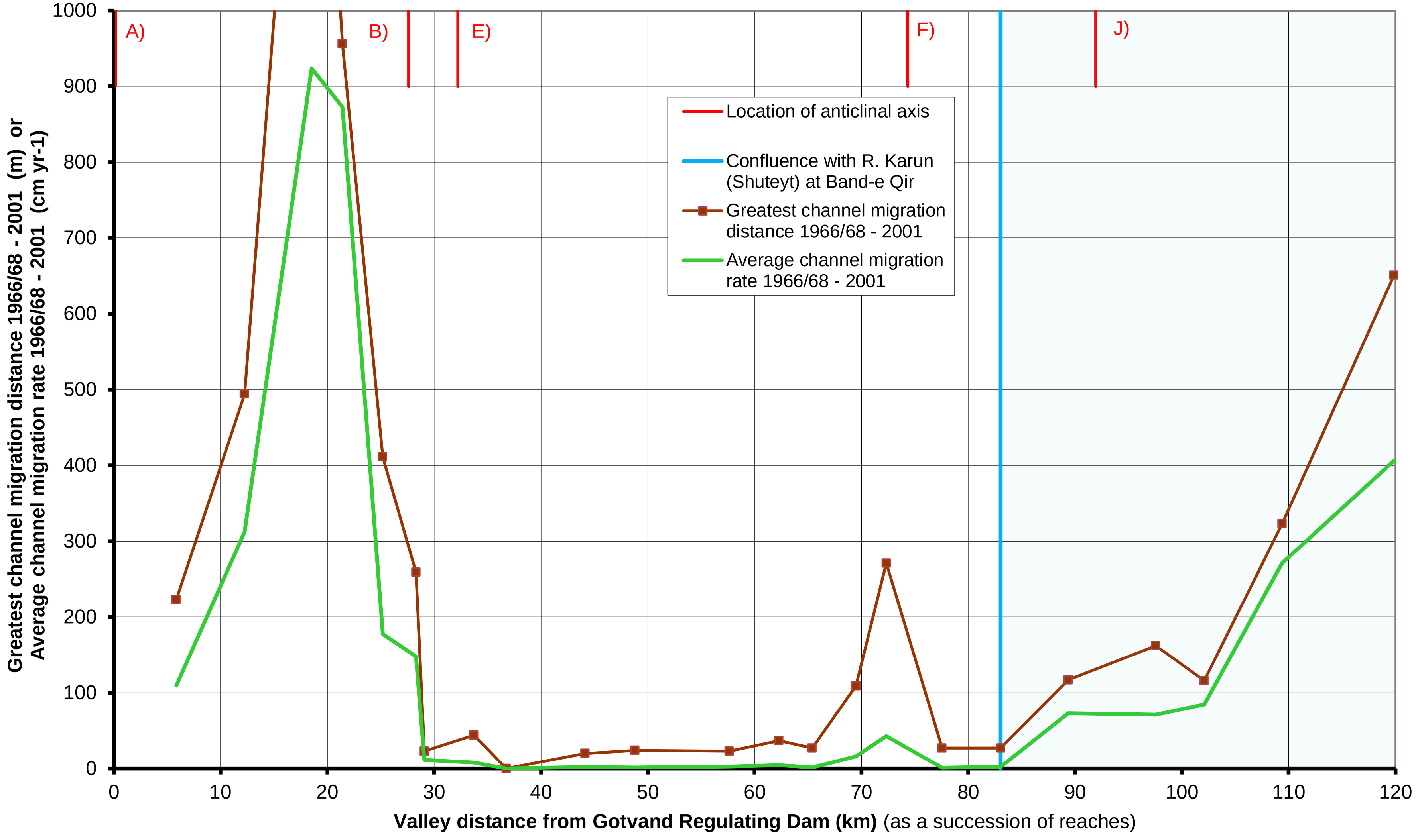

Figure 4.43 Characteristics of river sedimentology for the River **Dez** from northern Dezful - nr. Zargan-e Buzurg

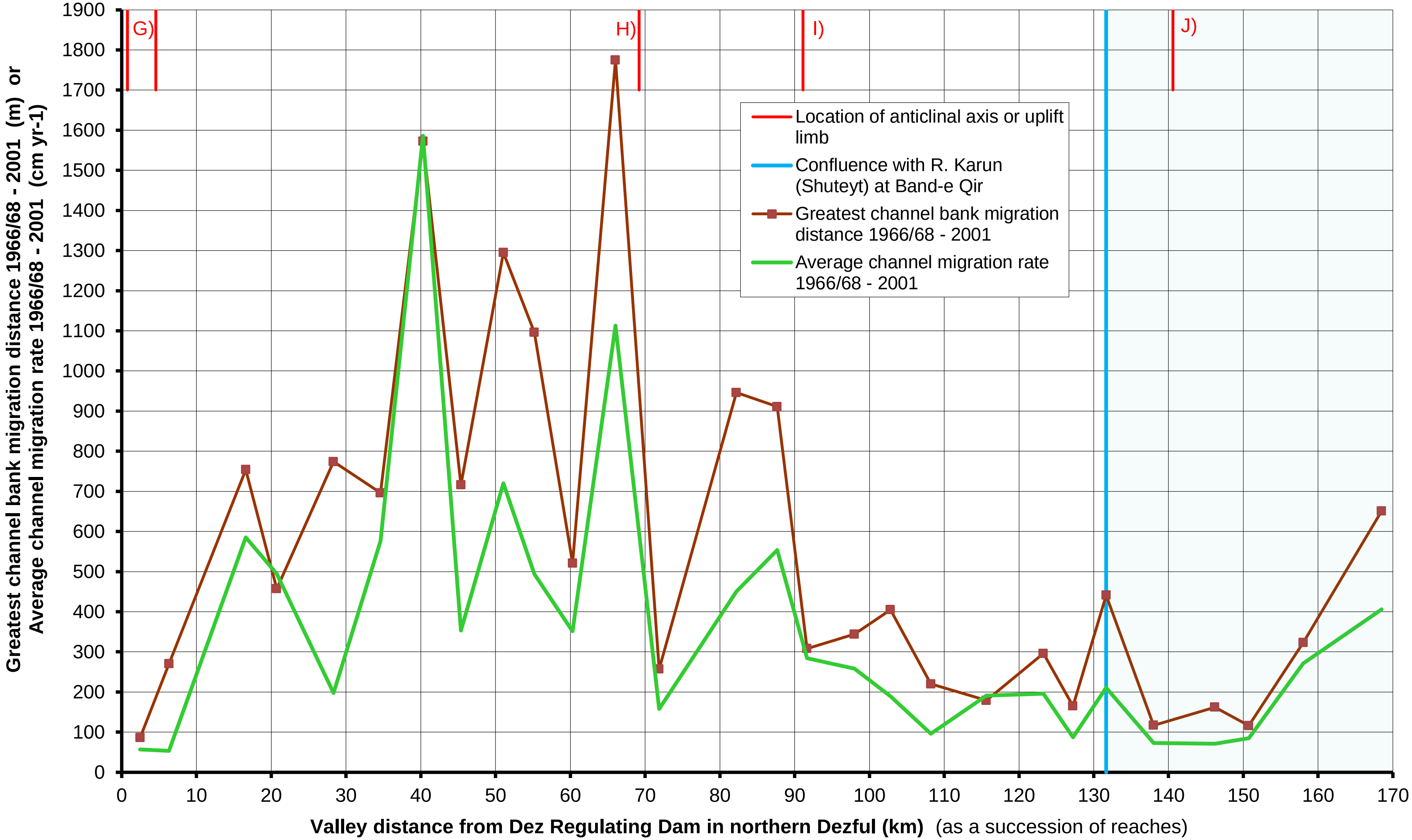

CHAPTER 5 RATES OF EARTH SURFACE MOVEMENTS

"Geology gives us a key to the patience of God."

Josiah Gilbert Holland, American author and poet (1819 - 1881 AD) (attributed)

5.1 Earth surface movement rates in the Dezful Embayment along the north-east Persian Gulf coast

5.1.1 Marine terraces of the north-east Persian Gulf coast

Two marine terraces (Marine terrace A and Marine terrace B) are present along the north-east coast of the Persian Gulf. These marine terraces are moderately continuous along mainly linear shorelines near Bandar-e Deylam and Binak, with Marine terrace A forming a barrier ridge at some locations behind which small lagoons, tidal flats and coastal sabkhas have developed (Figure 4.3 and 4.4). The morphologies and sediments of the terraces are mainly the product of coastal processes (Tables 4.1 and 4.2). At locations BANDN1, BINAK3 and BINAK4, there are only very small rivers and ephemeral streams and thus limited fluvial influences. This is the case along the north-east coast of the Persian Gulf shown in Figure 4.2, except for the Darreh-ye Abdari River which forms a small delta about 10 km south of Bandar-e Deylam. Hence, these terraces are relatively good indicators for interpreting relative sea-level changes, unlike locations on the Lower Khuzestan Plains where the complicating factors of fluvial aggradation and incision and sediment compaction are considerably more pronounced (Larsen and Evans, 1978; Lambeck, 1996; Coe, 2003; Heyvaert and Baeteman, 2007).

5.1.2 Marine terrace A

Marine terrace A is a moderately continuous linear ridge or berm, with deposits of mainly sands and shell fragments and some well cemented beachrock in its upper parts. Evidently, this marine "terrace" was mainly formed through wave energy, with the sandy sediments deposited above Mean High Water (MHW) probably being the products of both high wave energies during storms and relative sea-level changes. Beachrock is the cementation together of beach deposits ranging from fine sands to boulders by the precipitation of carbonates. This precipitation of mainly calcite or aragonite in warm waters by inorganic precipitation from sea water and ground water and by microbial activity forms layers of hard sandstones, conglomerates or breccias, usually with a slight seaward slope (Pirazzoli, 1996; Bird, 2000). Though some researchers ascribe such beachrock formation to supratidal locations (e.g. Kelletat, 2006), it is generally considered to form mainly within the intertidal zone (Pirazzoli, 1996; Bird, 2000). Hence, the thin deposits of beachrock in Marine terrace A are most probably indicative of higher relative sea-levels in the past, though with a range of uncertainty relating to factors such as storm deposition. Radiocarbon dating was applied to marine mollusc shell samples from these beachrock deposits at elevations of $^{+}$2.51 m above MHW at BANDN1 north of Bandar-e Deylam and $^{+}$1.62 m above MHW at BINAK3 on the SW limb of the Binak Anticline (Table 4.1). If the measured relative elevation changes were solely due to tectonics, then rates of tectonic uplift of about 0.47 - 0.92 mm yr^{-1} are indicated (Table 5.1).

5.1.2.1 Errors involved with the rates of tectonic uplift for Marine terrace A

The figures of about 0.47 - 0.92 mm yr^{-1} probably overestimate the rates of tectonic uplift for two main reasons. Firstly, slightly higher relative sea-levels in the Persian Gulf are to be expected during the approximate period 1,500 BC - 500 BC due to *isostasy*. Though there are uncertainties, as considered by Heyvaert and Baeteman (2007), it is likely that highest relative sea-levels of about $^{+}$1 m to $^{+}$3 m in the northern Persian Gulf were reached about 6,000 BC - 3,500 BC, followed by a slight relative sea-level fall from about 3,500 BC - 500 BC, after which relative sea-levels may have been very similar to that of today (see Section 2.7). Such a pattern is frequently found in “far-field sites” like the Persian Gulf which are large distances from the polar ice sheets, with a Deglacial and Holocene sea-level curve similar to the pattern of ice melt that rises to near or slightly above present around 4,000 BC, followed by a slight fall, as a result of hydro-isostatic adjustment and some equatorial ocean siphoning (Fleming et al., 1998; Woodroffe, 2003). Hence, Earth surface movements of the shoreline during the period of formation of Marine terrace A have been significantly influenced by hydro-isostatic effects, with the slight relative sea-level fall from about 3,500 BC - 500 BC being mainly due to hydro-isostatic effects of the load of water in the Persian Gulf causing downwarping of the outer parts of the shelf and uplift of the shoreline (Lambeck, 1996; Woodroffe, 2003; Sanlaville and Dalongeville, 2005). Thus, the approximate period of 1,500 BC - 500 BC (the period of dated samples from deposits of Marine terrace A) was part of a period of shoreline uplift due to hydro-isostatic effects, with the vertical movements due to hydro-isostasy probably being of the order of about $^{+}$0.7 m. If that were the case, then subtracting 0.7 m from the elevation values of the two dated shell samples in Table 5.1, provides rates of tectonic uplift for Marine terrace A of about 0.26 - 0.66 mm yr^{-1}.

Table 5.1 Summary of findings relating to rates of tectonic uplift for marine terraces along the north-east coast of the Persian Gulf

Location	**Type of sample and elevation**	**Age**	**Approximate rate of tectonic uplift,** assuming relative elevation changes solely due to tectonics (or assuming vertical movements due to hydro-isostasy of c. $^{+}0.7$ m)
Marine terrace A Location: BANDN1 North of Bandar-e Deylam, 30°06’47’’N 50°07’44’’E	Marine mollusc shell from sandy beachrock at $^{+}2.51$ m above Mean High Water (MHW)	815 ± 87 cal.BC (Calibrated AMS radiocarbon dating, GrA-15580)	0.89 ± 0.03 mm yr^{-1} or **0.86 - 0.92 mm yr^{-1}** (or assuming hydro-isostasy of c. $^{+}0.7$ m, **0.62 - 0.66 mm yr^{-1}**)
Marine terrace A Location: BINAK3 Near Binak, 29°43’18’’N 50°20’44’’E	Marine mollusc shell from sandy beachrock at $^{+}1.62$ m above MHW	1,390 ± 91 cal.BC (Calibrated conventional radiocarbon dating, GrN-25106)	0.48 ± 0.01 mm yr^{-1} or **0.47 - 0.49 mm yr^{-1}** (or assuming hydro-isostasy of c. $^{+}0.7$ m, **0.26 - 0.28 mm yr^{-1}**)
Marine terrace B Location: BINAK4 Near Binak, 29°43’39’’N 50°20’28’’E	Marine mollusc shell from shell encrustation around *in situ* boulder at c. $^{+}18$ m above MHW	> 43,000 BC (infinite radiocarbon age) (AMS radiocarbon dating, GrA-21606) Marine terrace B sediments probably deposited during the Last Interglacial MIS 5e (c. 120,000 BC), when eustatic sea-levels peaked at c. $^{+}5.5$ m to $^{+}9.0$ m (Kopp et al., 2009; Dutton and Lambeck, 2012) and sea-levels in the Red Sea peaked at c. $^{+}6.0$ m to $^{+}9.0$ m (Rohling et al., 2008)	< 0.40 mm yr^{-1} **less than 0.40 mm yr^{-1}** If sample deposited c. 120,000 BC, then accounting for eustatic sea-levels of c. $^{+}6.0$ m to $^{+}9.0$ m (Rohling et al., 2008), rate is 0.09 ± 0.02 mm yr^{-1} or **0.07 - 0.11 mm yr^{-1}**

Secondly, storm waves are an important factor in beach ridge and beach berm formation. Storm waves are significantly lower in the Persian Gulf than in the Indian Ocean, but maximum significant wave height is still of the order of 5.5 m for a 12 year period (Rakha et al., 2007). Large, high energy waves associated with storms may deposit sediments, marine mollusc shells and other materials at locations a few metres above the intertidal zone, producing anomalously high elevations for samples and, thus, anomalously high rates of tectonic uplift (Pirazzoli, 1996; Bird, 2000). The errors associated with such effects may have been relatively small in this study since the beds of Marine terrace A selected for sampling were finely bedded sands and the marine mollusc shells selected for sampling were complete shells with intact valves and, therefore, were most probably *in situ* or subjected to limited transport.

Countering these two factors are effects which may cause radiocarbon dating of samples to underestimate rates of tectonic uplift. In particular, beach formation necessarily precedes the cementation of beachrock (Pirazzoli, 1996). Due to this, and possible reworking of shell samples, radiocarbon dates for marine mollusc shells within beachrock provide oldest dates for the sea-level at which cementation occurred and thus may produce underestimations of rates of tectonic uplift.

Overall, this indicates that the rates of tectonic uplift along the north-east coast of the Persian Gulf over the last few thousand years were probably in the range of about 0.26 - 0.92 mm yr^{-1}.

5.1.3 Marine terrace B

Marine terrace B is a discontinuous, gently sloping, planar terrace surface preserved as a capping on high rock outcrops, with deposits of mainly sandy and shelly beachrock. At a few locations (such as BINAK4 near Binak, with six beds totalling more than 7 m thick), thicker stratigraphic sequences with different sedimentary environments are preserved, attesting to relatively long times for deposition (Table 4.2; Figure 4.6). At BINAK4 the sequence was one of probable fluvial deposits (poorly sorted conglomerates generally fining upwards to medium and fine sands), overlain by supra-tidal and coastal sabkha deposits (sands and silts with shell fragments and gypsum-rich layers), overlain by coastal beach deposits (very well cemented sands and shells). Similar deposits from the lower part of the sequence were found to be preserved at only a few locations, whereas the coastal beach deposits at the top of the sequence were extensively preserved. Being mainly comprised of beachrock of very well cemented sands, gravels and shells, these deposits were erosion resistant and formed the gently sloping, planar surface of Marine terrace B (Table 4.2; Figure 4.4).

5.1.3.1 Errors involved with the rates of tectonic uplift for Marine terrace B

The age of Marine terrace B is not known, other than it being older than approximately 43,000 BC (infinite age by Accelerator Mass Spectrometry (AMS) radiocarbon dating of a marine mollusc shell from an encrustation around an *in situ* boulder). For the sample elevation of about $^{+}$18 m above MHW, assuming that the relative elevation changes were solely due to tectonics, this dating provides a long-term rate of tectonic uplift of less than 0.40 mm yr^{-1}, as shown in Table 5.1. Unfortunately, logistical and security limitations precluded returning to the area to take samples for Optically Stimulated Luminescence dating. Nevertheless, the presence of coastal beach deposits at significantly higher elevations than those of today is indicative of deposition during an interglacial period, rather than during a glacial period with low eustatic sea-levels. If, as seems likely, this were the Last Interglacial (the Eemian (or Ipswichian) Interglacial, c. 120,000 BC, Marine oxygen Isotope Stage 5e) (Lowe and Walker, 1997) when eustatic sea-levels peaked at about $^{+}$5.5 m to $^{+}$9.0 m (Kopp et al., 2009; Dutton and Lambeck, 2012) and sea-levels in the Red Sea peaked at about $^{+}$6.0 m to $^{+}$9.0 m (Rohling et al., 2008), then, as shown in Table 5.1, the long-term rate of tectonic uplift in the vicinity of the Binak Anticline is about 0.07 - 0.11 mm yr^{-1}. If the coastal beach deposits were associated with an earlier interglacial period (such as the Dömnitz (or Hoxnian) Interglacial, c. 340,000 BC, Marine oxygen Isotope Stage 9) (Lowe and Walker, 1997), then the long-term rate of tectonic uplift would be even less.

These figures probably overestimate the rates of tectonic uplift, due to hydro-isostatic effects causing flexure of the continental crust with downwarp of the outer shelf and uplift of the shoreline, and storm waves producing deposits a few metres above the intertidal zone. However, due the relatively large elevations ($^{+}$18 m) and long timescales (probably c. 122,000 years, an interglacial-glacial-postglacial cycle) involved, these errors are likely to be proportionally less for Marine terrace B than for the lower terrace.

5.1.4 Summary of Earth surface movement rates in the Dezful Embayment along the north-east Persian Gulf coast

In summary, in the Dezful Embayment along the north-east coast of the Persian Gulf, at locations roughly 20 - 60 km to the north-east of the Zagros Deformation Front, there is evidence for Earth surface movements due to tectonics. The rates of tectonic uplift are low, in the range of about 0.07 - 0.92 mm yr^{-1}, with the true long-term rates of tectonic uplift probably being in the lowest parts of this range.

5.2 Earth surface movement rates in the Dezful Embayment in the Upper Khuzestan Plains

The fieldwork relating to the ancient canals, ancient hydraulic structures and river terraces of the Karun river system in the Upper Khuzestan Plains is related to four main anticlines: the Shahur Anticline, the Shushtar Anticline, the Naft-e Safid Anticline and the Sardarabad Anticline.

5.2.1 Ancient canals on the Shahur Anticline

Two ancient canals (SC1 and SC2) had been cut across the Shahur Anticline in antiquity (during the Early Sassanian Period of c. 224 - 379 AD, most probably during the reigns of the Sassanian rulers Ardashir I and Shapur I of c. 224 - 272 AD) and which had subsequently fallen into disuse (Figure 4.8, Table 4.3). These ancient canals were originally constructed as approximately straight channels, with gentle slopes from N/NNE to S/SSW from the present-day Shahur River to the River Karkheh for irrigation of lands to the south of the Shahur Anticline (Lees and Falcon, 1952; Lees, 1955; Woodbridge, 2006). Hence, some changes in their morphology since disuse are mainly attributable to tectonic movements of the Shahur Anticline.

Ancient canal SC1

After disuse, ancient canal SC1 subsequently ceased flowing and developed a slope from S to N (i.e. opposite to its original flow direction) and there was collapse of a canal tunnel which had been cut through the crest of the anticlinal ridge of the Shahur Anticline. The nature and timing of the canal disuse is not known, though it was probably around the time of the end of the Sassanian Period, c. 633 AD/651 AD (Kirkby, 1977; Gasche et al., 2007). If no major modifications were made to ancient canal SC1 after its construction, then any changes to the slope of its canal bank remnants can be attributed mainly to tectonic movements of the Shahur Anticline since the time of canal construction. If these reasonable assumptions are valid, then these changes to canal bank slopes indicate a steepening of the back-limb of the Shahur Anticline at a rate of about $1.02 - 1.12 \times 10^{-4}$ ° yr^{-1}, equivalent to $1.78 - 1.95 \times 10^{-3}$ radians kyr^{-1}, as shown in Table 5.2.

Ancient canal SC2

After disuse, ancient canal SC2 continued flowing and developed into the Shahur River, flowing roughly from N to S (generally towards 170°) across the Shahur Anticline.

Fieldwork and remote sensing images show that the Shahur River is a wandering, suspended load, meandering channel of fairly low sinuosity along most of its length. A notable exception is about 1.1 km - 2.0 km north of the axis of the Shahur Anticline where it flows along a near-straight course coincident with that of the ancient canal, flowing straight from NNE to SSW (generally towards 200°) along the ancient canal remnant (Figures 4.8 and 4.9). This near-straight reach might have been partly human influenced, since it was just upstream of a modern dam, the Kheyrabad Diversion Dam that was implemented in 1940 AD (KWPA, 2010).

Table 5.2 Summary of findings for ancient canals relating to rates of tectonic uplift for the Shahur Anticline in the Upper Khuzestan Plains

Location	**Summary of main geomorphological changes**	**Age**	**Approximate rate of tectonic movements,** assuming that geomorphological changes were solely due to tectonics
Ancient canal SC1 Approximate location 31°57'N 48°22'E	Ancient canal originally constructed with a slight slope from N to S. Survey of ancient canal bank remnants about 1.5 km - 2.5 km north of axis of Shahur Anticline indicates average slope from S to N of 0.003159 $m\ m^{-1} \approx 0.18°$ (Woodbridge, 2006)	Constructed during Early Sassanian Period (c. 224 - 379 AD	Steepening of back-limb of the Shahur Anticline at a rate of $1.07 \pm 0.05 \times 10^{-4}$ ° yr^{-1} ($1.02 - 1.12 \times 10^{-4}$ ° yr^{-1}) equivalent to $1.86 \pm 0.09 \times 10^{-3}$ radians kyr^{-1} or **$1.78 - 1.95 \times 10^{-3}$ radians kyr^{-1}**
Ancient canal SC2 Approximate location 31°55'N 48°25'E	Ancient canal originally constructed with near-straight course with flow from NNE to SSW (generally towards 200°). Survey of ancient canal remnants indicates canal had developed into the sinuous Shahur River with flow from N to S (generally towards about 170°). About 1.1 km - 2.0 km north of the axis of the Shahur Anticline river had a near-straight course coincident with canal remnants (generally towards 200°) and had incised so that river water surface was at elevation of 3.45 m below canal bank remnants (Woodbridge, 2006)	Constructed during Early Sassanian Period (c. 224 - 379 AD)	Uplift of crest of the Shahur Anticline at a rate of 2.03 ± 0.10 mm yr^{-1} or **$1.94 - 2.13$ mm yr^{-1}**

However, the features of the changes in course direction and sinuosity both upstream and downstream of this near-straight reach, its coincidence with the ancient canal remnant, and its close proximity to the axis of the anticline (generally the area of greatest anticlinal uplift), strongly indicate that the Shahur River has maintained this near-straight course since the Sassanian Period. This is because very low sinuosity channels maximise channel slopes and stream powers to produce high rates of river incision which may keep pace with anticlinal uplift (Burbank et al., 1996; Burbank and Anderson, 2001). This is further evidenced by the way in which the spoil heaps associated with the canal construction were generally not cut into by minimal river migration along the near-straight reach (see foreground of Figure 4.9), whereas they were cut into by river migration elsewhere (see background of Figure 4.9).

Along this near-straight reach, the River Shahur has incised through Agha Jari Formation bedrock (mainly fairly coarse calcareous sandstone), and, near the locality illustrated in Figure 4.10, this near-straight channel incision through bedrock has produced a present-day river water surface 3.45 m below the ancient channel bank surface (Woodbridge, 2006). The nature and timing of the disuse of this canal is not precisely known. It is not known whether human activities in antiquity aided the maintaining of the course of the River Shahur across the Shahur Anticline for irrigation; as was the case for the Kheyrabad Diversion Dam, the Shavour Diversion Dam further south, and various irrigation canals from the early 20th Century AD onwards for irrigation of lands to the south of the Shahur Anticline (Gasse et al., 2007; KWPA, 2010). However, fieldwork indicated no signs of such human activities, neither along the near-straight reach in the vicinity of axis of the Shahur Anticline, nor along the gently meandering reaches upstream and downstream of the near-straight reach. Hence, there have probably been only limited human influences on the development of the Shahur River since the disuse of ancient canal SC2 (possibly around the end of the Sassanian Period, c. 633 AD/651 AD) until modern times (possibly the early 20th Century AD onwards). If this were the case, then, as considered by previous workers (Lees and Falcon, 1952; Lees, 1955), the vertical distance of 3.45 m between ancient channel banks and present-day water surface measured for the near-straight reach can be mostly attributed to vertical incision since the time of construction of ancient canal SC2 (about 224 - 379 AD) in response to tectonic uplift. If these reasonable assumptions are valid, then these changes indicate tectonic uplift of the crest of the Shahur Anticline since Sassanian times at an average rate of about 1.94 - 2.13 mm yr^{-1}, as shown in Table 5.2.

5.2.2 Ancient hydraulic structures at Shushtar on the Shushtar Anticline

The remnants of the ancient hydraulic system in Shushtar in the vicinity of the Salasel Castle clearly indicate a relative fall in river water levels for the River Karun (Shuteyt branch) since their main period of construction and use (Figures 4.11 to 4.13). Parts of the Shushtar ancient hydraulic system have been assigned to as early as the 5th Century BC associated with the Achaemenids of the Persian Empire Periods (Torfi et al., 2007). However, as described in Table 4.4, the monumental scale of the system and the use of cut sandstone blocks bonded by mortar and iron clamps and filled with Roman concrete (Smith, 1971; Hartung and Kuros, 1987), indicate that the main period of construction and use was the Early Sassanian Period (c. 224 - 379 AD). In Shushtar during the Early Sassanian Period, and, presumably, for the Sassanian Period as a whole (c. 224 - 651 AD), the high degree of imperial organisation of the Sassanians would have ensured that the Band-e Qaisar dam-bridge was maintained and that the Darian canal intake tunnels and the Salasel Castle citadel reservoir were at least partly filled throughout the year. The findings of River Karun water levels several metres too low for these to be operational during the late 20th/early 21st Century AD indicate a fall in relative river water levels over the last one to two thousand years. How much of this is attributable to the disuse (and eventual collapse in 1885 AD) of the Band-e Qaisar (or *shadhurvan*) (Verkinderen, 2009), and how much was attributable to river incision and tectonic uplift of the fore-limb of the Shushtar Anticline, is not known precisely, but can be estimated.

As described in Table 4.4, in early December 2005 AD (a time of low river water levels), the upper surface of the remnants of the Sassanian base of the Band-e Qaisar at its northern end were found to be about 1.34 m above the River Karun (Shuteyt) water level. If this base top were at a similar elevation to when in use during the Sassanian Period, then this indicates that the Band-e Qaisar, which originally functioned as a weir with water flowing over the top of its base throughout the year (Hodge, 1992), raised the river water level upstream of it during use by a maximum of about 1.34 m. Allowing for slumping and subsidence of the structure since disuse (though slumping was least at its northern end) and lower river water levels than in December 2005 AD, then a maximum raising of the river water level by as much as 3 m to 4 m (as considered by Hartung and Kuros, 1987) could be envisaged (but not more than this and not as much

Table 5.3 Summary of findings for ancient hydraulic structures relating to rates of tectonic uplift for the Shushtar Anticline in the Upper Khuzestan Plains

Location	**Summary of main river water level changes**	**Age**	**Approximate rate of tectonic uplift,** assuming that river incision changes were solely due to tectonics
Shushtar ancient hydraulic structures - Eight intake channels of small aperture all serving a larger aperture main channel of the Darian canal system Approximate location 32°03’N 48°51’E	Intake tunnels for the Darian canal system originally constructed at a range of elevations from about $^{+}37$ m to $^{+}42.5$ m NCC Datum. In March 2002 AD, River Shuteyt water levels (c. $^{+}39$ m NCC Datum) were c. 3.5 m below the level of the highest intake tunnel. Assuming that high flow river water levels in antiquity immersed the highest intake tunnel by at least $^{+}0.5$ m and that the Band-e Qaisar raised river water levels in antiquity by c. $^{+}1.34$ m to $^{+}4.0$ m, this indicates river incision of c. 4.0 m - (1.34 m to 4.0 m) = about 0 m to 2.66 m since antiquity.	Mainly constructed and used during the Early Sassanian Period (c. 224 - 379 AD)	Uplift of fore-limb of the Shushtar Anticline at a rate of 0.78 ± 0.86 mm yr^{-1} or **0 - 1.64 mm yr^{-1}**
Shushtar ancient hydraulic structures - Citadel reservoir beneath the Salasel Castle Approximate location 32°03’N 48°51’E	Citadel reservoir originally constructed for water storage throughout the year, including autumn low river flows. In March 2002 AD, River Shuteyt water levels (c. $^{+}39$ m NCC Datum, c. $^{+}2.0$ m above low flows) were c. 2.5 m below the base of the citadel reservoir. Assuming that low flow river water levels in antiquity immersed the reservoir base by at least $^{+}0.5$ m and that Band-e Qaisar raised river water levels in antiquity by c. $^{+}1.34$ m to $^{+}4.0$ m, this indicates river incision of c. 5.0 m - (1.34 m to 4.0 m) = about 1.0 m to 3.66 m since antiquity.	Mainly constructed and used during the Early Sassanian Period (c. 224 - 379 AD)	Uplift of fore-limb of the Shushtar Anticline at a rate of 1.37 ± 0.89 mm yr^{-1} or **0.56 - 2.26 mm yr^{-1}**

as 7 m, as considered by O’Connor, 1993). In Table 5.3, derivations of rates of river incision and tectonic uplift of the Shushtar Anticline are based on the Band-e Qaisar causing a rise of the river water levels by about 1.34 m to 4.0 m during its main period of construction and use in the Early Sassanian Period (c. 224 - 379 AD).

In antiquity, eight small aperture tunnels with intakes at a range of elevations from $^+37$ m to $^+42.5$ m above NCC Datum all served a larger aperture main channel of the Darian canal system, with a design to optimise flow in the main channel in antiquity for the usual range of River Karun (Shuteyt) flows from low river water levels (in the autumn) to high river water levels (in the spring) (Table 4.4). Water flow in a tunnel is slower when full of water, so the higher tunnels helped maintain fast flows in the main channel at times of high river water levels (in the spring) by increasing the effective aperture. In March 2002 AD (before modern constructions caused loss of access to the ancient hydraulic structures in the vicinity of the Salasel Castle) at a time of fairly high river water levels, the River Karun (Shuteyt) water levels in the vicinity of the Darian canal intake tunnels were about $^+39$ m NCC Datum. Assuming that in antiquity such high flow river water levels immersed the highest intake tunnel by at least $^+0.5$ m, then this probably indicates tectonic uplift of the fore-limb of the Shushtar Anticline since Sassanian times of about 0 - 1.64 mm yr^{-1}, as shown in Table 5.3.

Similarly, in March 2002 AD, the River Shuteyt water levels were a considerable c. 2.5 m below the base of the citadel reservoir beneath the Salasel Castle at Shushtar (Figure 4.12). Assuming that low river flows in antiquity immersed the base of the simple reservoir by at least $^+0.5$ m, then, also as shown in Table 5.3, tectonic uplift of the fore-limb of the Shushtar Anticline at average rates of about 0.56 - 2.26 mm yr^{-1} since Sassanian times are probably indicated.

These rates of uplift for the Shushtar Anticline are necessarily approximate due to uncertainties associated with both the heights by which the Band-e Qaisar (or *shadhurvan*) raised river water levels in antiquity and the depths to which the intake tunnels and water storage structures were designed to be immersed in antiquity. The Band-e Qaisar was a monumental structure during its main periods of use in the Sassanian and Early Islamic periods, with an original length of about 520 m and a superstructure of at least 40 arches which originally carried a bridge (Figure 4.11; Torfi et al., 2007; Verkinderen, 2009). Some Medieval geographers claimed that the construction of the *shadhurvan* caused the water of the river to rise to the gate of the city of Shushtar, and its efficiency in diverting river water (prior to its demise and ultimate collapse in 1885 AD) was such that as late as the 19th Century AD the Gargar branch of the River Karun was still preferred to the Shuteyt branch for river navigation

(Verkinderen, 2009). Hence, it is conceivable that the changes in river water levels can be accounted for by human activities alone.

5.2.3 River terraces on anticlines in the Upper Khuzestan Plains

The results of the fieldwork and dating of the river terraces of the Karun river system on the Naft-e Safid Anticline, the Sardarabad Anticline and the Shushtar Anticline can be used to determine average rates of incision since deposition of the terrace deposits. As is well known, river incision depends on various factors, such as changes in sediment supply with time due to changes in climate, vegetation and land use, and due to river channel modifications such as canal and dam construction. Nevertheless, average rates of river incision can be a guide to average rates of tectonic uplift, particularly over periods of thousands or tens of thousands of years, since over longer timescales the influences of changes in aggradation and incision due to changes in sediment supply tend to be evened out (Bull, 1991, Burbank and Anderson, 2001).

River terraces associated with the Naft-e Safid Anticline

Four river terraces are associated with the Naft-e Safid Anticline: the ‘Dar Khazineh terrace’ on the fore-limb of the anticline, the ‘Naft-e Safid terrace’ on the axis of the anticline, and the ‘Batvand terrace’ and the ‘Abgah terrace’ on the back-limb of the anticline. This good coverage and dating of a variety of different terrace deposits by Optically Stimulated Luminescence (OSL) dating and by archaeological dating, provides robust estimates of the rates of river incision. Assuming that these rates of river incision are solely due to tectonics then for the Naft-e Safid Anticline there have been rates of tectonic uplift of between about 0.19 - 3.82 mm yr^{-1} during the Late Quaternary, as shown in Table 5.4.

The wide range of rates of tectonic uplift of 0.19 - 3.82 mm yr^{-1} for the Naft-e Safid Anticline can be sub-divided into an upper range of 1.71 - 3.82 mm yr^{-1} for river terrace deposits of Phase B of the ‘Dar Khazineh terrace’, and a lower range of 0.19 - 1.29 mm yr^{-1} for all of the other river terrace deposits (Table 5.4). The deposits of Phase B of the ‘Dar Khazineh terrace’ relate to an approximate timespan of 2,600 BC - 290 BC and are most probably unrepresentative of rates of tectonic uplift for the Naft-e Safid Anticline for two reasons.

Firstly, the construction of the monumental Masrukan canal system in the Early Sassanian Period (c. 224 - 379 AD) and its subsequent development into the meandering

Table 5.4 Summary of river terrace findings relating to rates of tectonic uplift for the Naft-e Safid Anticline in the Upper Khuzestan Plains

Location	**Type of sample and elevation**	**Age** (OSL dates use De derived from Finite Mixture Model, except OSL Sample 8)	**Approximate rate of tectonic uplift**, assuming that river incision changes were solely due to tectonics
'Dar Khazineh terrace' Locations: DAKS05 (for Phase A and Phase B) 31°54'47''N 48°59'29''E DKLTFH (for Phase A and Phase B) 31°54'46''N 48°59'23''E HGWS05 (for Phase X) 31°54'35''N 48°59'09''E	Phase B: Block of river terrace sediment of mean grain size 112.8 µm Elevation: $^{+}$29.89 m NCC Datum, $^{+}$8.09 m above river water level for River Gargar Block of river terrace sediment of mean grain size 24.3 µm Elevation: $^{+}$30.52 m NCC Datum, $^{+}$8.72 m above river water level for River Gargar Deposits equivalent to Phase B (elevation c. $^{+}$29.67 m to $^{+}$31.92 m NCC, c. $^{+}$7.87 m to $^{+}$10.12 m above River Gargar water level) in the vicinity of Dar Khazineh included Elamite Period pottery and an Elamite Period well Phase X: Block of river terrace sediment of mean grain size 255.0 µm Elevation: $^{+}$28.37 m NCC Datum, $^{+}$6.57 m above river water level for River Gargar Phase A: Pottery sherds from Late Susiana 1 & 2 Periods from Bed 1 at DAKS05 Elevation c. $^{+}$28.82 m to c. $^{+}$29.32 m NCC Datum, c. $^{+}$7.02 m to c. $^{+}$7.52 m above river water level for River Gargar	Phase B: 480 ± 190 BC (OSL dating, OSL Sample 3, Shfd08206) 820 ± 220 BC (OSL dating, OSL Sample 11, Shfd08202) 2,600 BC - 646 BC (Archaeological dating, Pottery and well from Elamite Period) Phase X: 3,670 ± 360 BC (OSL dating, OSL Sample 4, Shfd08207) Phase A: 4,800 BC - 4,000 BC (Archaeological dating, Pottery sherds from Late Susiana 1 & 2 Periods)	Phase B: Uplift of fore-limb of the Naft-e Safid Anticline at rates of: 3.25 ± 0.27 mm yr^{-1} (or 3.02 - 3.52 mm yr^{-1}) 3.08 ± 0.26 mm yr^{-1} (or 2.86 - 3.34 mm yr^{-1}) 2.76 ± 1.06 mm yr^{-1} (or 1.71 - 3.82 mm yr^{-1}) (Uplift rates for Phase B range from **1.71 - 3.82 mm yr^{-1}**) Phase X: Uplift of fore-limb of the Naft-e Safid Anticline at a rate of 1.16 ± 0.07 mm yr^{-1} (or **1.09 - 1.23 mm yr^{-1}**) Phase A: Uplift of fore-limb of the Naft-e Safid Anticline at a rate of 1.14 ± 0.11 mm yr^{-1} (or **1.03 - 1.25 mm yr^{-1}**)

'Naft-e Safid terrace' Location: DKITEB Bed 2 31°57'15''N 48°59'32''E	Block of river terrace sediment of mean grain size 119.0 µm Elevation: $^{+}$49.67 m NCC Datum, $^{+}$27.61 m above river water level for River Gargar	20,490 ± 1,100 BC (OSL dating, OSL Sample 8, Shfd08019, *Central Age Model*)	Uplift of the axis of the Naft-e Safid Anticline at a rate of 1.23 ± 0.06 mm yr^{-1} (or **1.17 - 1.29 mm yr^{-1}**)
'Batvand terrace' Location: BFLS05 Bed 5 (Phase B) and Bed 2 (Phase A) 32°00'08''N 49°06'06''E	Phase B: Block of river terrace sediment of mean grain size 498.2 µm Elevation: $^{+}$99.85 m NCC Datum, $^{+}$6.69 m above river water level for Rud-e Tembi Phase A: Block of river terrace sediment of mean grain size 55.5 µm Elevation: $^{+}$98.49 m NCC Datum, $^{+}$5.33 m above river water level for Rud-e Tembi	Phase B: 8,480 ± 830 BC (OSL dating, OSL Sample 1, Shfd08204) Phase A: 23,860 ± 1,750 BC (OSL dating, OSL Sample 2, Shfd08205)	Phase B: Uplift of back-limb of the Naft-e Safid Anticline at a rate of 0.64 ± 0.05 mm yr^{-1} (or **0.59 - 0.69 mm yr^{-1}**) Phase A: Uplift of back-limb of the Naft-e Safid Anticline at a rate of 0.21 ± 0.02 mm yr^{-1} (or **0.19 - 0.22 mm yr^{-1}**)
'Abgah terrace' Location: BAF2BR Bed 4 31°59'32''N 49°05'43''E	Block of river terrace sediment of mean grain size 74.6 µm Elevation: Approx.$^{+}$114.82 m NCC Datum, Approx. $^{+}$6.90 m above river water level for Ab-e Shur	18,590 ± 3,130 BC (OSL dating, OSL Sample 7, Shfd08209)	Uplift of back-limb of the Naft-e Safid Anticline at a rate of 0.33 ± 0.06 mm yr^{-1} (or **0.29 - 0.39 mm yr^{-1}**)

River Gargar after its disuse, probably in the 10th - 14th Centuries AD, resulted in rapid vertical river incision over a relatively short period of time (Le Strange, 1905; Alizadeh et al., 1994). Surveying with a Total Station in the vicinity of Qulramzi (about 6 km upstream of Dar Khazineh) in this study indicated about 8.5 m of vertical incision between ancient canal bank remnants considered to be those of the Masrukan or "Gargar Channel" and the river water level of the present-day River Gargar (Moghaddam, in press). If vertical incision associated with disuse of the Masrukan canal were similar in the vicinity of Dar Khazineh, then this would account for the c. $^{+}$7.87 m to $^{+}$10.12 m elevation differences between deposits equivalent to Phase B and the River Gargar water level at Dar Khazineh, and would indicate little (< 0.61 mm yr^{-1}) or no tectonic uplift associated with the Naft-e Safid Anticline.

Secondly, in the vicinity of Dar Khazineh between Phase A and Phase B at elevations of c. $^{+}$29.67 m to $^{+}$29.82 m NCC Datum (see Table 4.5, Figure 4.17 and Figure 4.18), there is a prominent, very sharp bounding surface with some features of a former land surface, such as worm burrows, surface cracks and ash fragments. This appears to be a very extensive bounding surface, and an equivalent may be the sharp bounding surface at the base of Bed 4 at elevations of c. $^{+}$29.80 m to $^{+}$30.34 m NCC Datum for the 'Kabutarkhan-e Sufla terrace' at location KBS4OS about 18 km away on the west side of the Mianab Plain. This extensive bounding surface, which may have been a former land surface, indicates that there was probably a period of erosion and non-deposition prior to the deposition of the Phase B at Dar Khazineh, which would make the sediments of Phase B poor indicators of rates of tectonic uplift. It is likely that sediments of Phase A (dating to around 4,800 BC - 4,000 BC) originally extended to elevations of around $^{+}$31 m NCC Datum or more at Dar Khazineh and then were truncated by erosion prior to the deposition of Phase B. If that were the case, then lower rates of tectonic uplift of the order of 1.35 - 1.53 mm yr^{-1} for the fore-limb of the Naft-e Safid Anticline are indicated.

In summary, the terrace deposits of the four river terraces on the limbs of the Naft-e Safid Anticline most probably indicate average rates of tectonic uplift for the fold of about 0.19 - 1.53 mm yr^{-1}.

River terrace associated with the Sardarabad Anticline

One river terrace is associated with the Sardarabad Anticline: the 'Kabutarkhan-e Sufla terrace' on the back-limb of the Sardarabad Anticline. As shown in Table 5.5, one OSL date (using both the Finite Mixture Model and the Central Age Model) from river terrace deposits indicates rates of tectonic uplift for the fold of about 0.23 - 0.29 mm yr^{-1}.

Table 5.5 Summary of river terrace findings relating to rates of tectonic uplift for the Sardarabad Anticline in the Upper Khuzestan Plains

Location	**Type of sample and elevation**	**Age** (OSL dates use De derived from Finite Mixture Model & Central Age Model)	**Approximate rate of tectonic uplift**, assuming that river incision changes were solely due to tectonics
'Kabutarkhan-e Sufla terrace' Location: KBS4OS 31°56'28''N 48°47'21''E	Block of river terrace sediment of mean grain size 93.0 µm Elevation: $^{+}$29.90 m NCC Datum, $^{+}$4.57 m above river water level for River Shuteyt	15,590 ± 2,100 BC (OSL dating, OSL Sample 9, Shfd08021, combination of Finite Mixture Model and *Central Age Model*)	Uplift of back-limb of the Sardarabad Anticline at a rate of 0.26 ± 0.03 mm yr^{-1} (or **0.23 - 0.29 mm yr^{-1}**)

River terrace associated with the Shushtar Anticline

One river terrace is associated with the Shushtar Anticline: the 'Kushkak terrace' on the back-limb of the Shushtar Anticline. As shown in Table 5.6, assuming that rates of river incision were solely due to tectonics, archaeological dating indicates rates of tectonic uplift for the Shushtar Anticline of less than about 2.5 mm yr^{-1} and OSL dating of river terrace deposits indicate rates of tectonic uplift for the Shushtar Anticline of about 0.42 - 0.51 mm yr^{-1}. Though the OSL dating is based on only one sample from one terrace, it is for a relatively long time span of about 20,000 years and, hence, is probably representative of the average long-term rates of tectonic uplift for the fold.

Table 5.6 Summary of river terrace findings relating to rates of tectonic uplift for the Shushtar Anticline in the Upper Khuzestan Plains

Location	**Type of sample and elevation**	**Age** (OSL dates use De derived from Finite Mixture Model)	**Approximate rate of tectonic uplift,** assuming that river incision changes were solely due to tectonics
'Kushkak terrace' Location: KUHKL3 32°08'07''N 48°50'34''E	Block of river terrace sediment of mean grain size 87.4 µm Elevation: Approx. $^{+}$58.98 m NCC Datum, Approx. $^{+}$9.18 m above river water level for River Karun	17,970 ± 2,000 BC (OSL dating, OSL Sample 10, Shfd08210)	Uplift of back-limb of the Shushtar Anticline at a rate of 0.46 ± 0.05 mm yr^{-1} (or **0.42 - 0.51 mm yr^{-1}**)
	Archaeological survey sites on this terrace surface (elevation approx. <$^{+}$10.60 m to approx. >$^{+}$20.10 m above river water level for River Karun) included Tepe-i Jallekan with pottery of the "Susa A" and "Susa B" periods (Wright, 1969)	Terrace surface is older than c. 4,100 BC (Archaeological dating, Pottery from "Susa A" and "Susa B" periods)	Uplift of back-limb of the Shushtar Anticline at a rate of *less than c. 2.5 ± 0.8 mm yr^{-1}*

5.2.3.1 Errors involved with the rates of tectonic uplift for river terraces on anticlines

With river terrace data there is uncertainty as to the amount of vertical incision due to tectonic uplift, since the amount of river incision and aggradation due to other factors (especially changes in sediment supply due to changes in climate and human impacts) is not known. There is a general tendency for data from river terrace sediments to slightly overestimate rates of fold uplift, since a period of river sediment aggradation or river flooding followed by river incision is necessary for river terrace sediments to be preserved and then exposed (Bull, 1991; Bridgland, 2000; Burbank and Anderson, 2001).

Nevertheless, this is only a tendency and in major periods of river sediment aggradation (as may have occurred in the study area around the time of the Last Glacial Maximum, c. 20,000 BC - 15,000 BC and the time of the Early - Middle Holocene, c. 8,000 BC - 500 BC) (Section 2.6 and 2.7), there may be sediment aggradation even though tectonic uplift is present, resulting in an underestimation of rates of fold uplift. Indeed, it is interesting that no notable equivalents of the "Younger fill" of c. 700 AD - 1850 AD of Vita-Finzi (1969, 1979) associated with the "Neoglacial" (Rieben, 1955; Vita-Finzi, 1976), were found in the deposits of the river terraces of the Upper Khuzestan Plains investigated in this study. This is probably because greater winter precipitation during the Neoglacial did produce a tendency towards sediment aggradation, but, due to other factors, such as the removal in earlier periods of most of the readily erodible sediment and soil cover as a consequence of extensive agriculture and woodland depletion (Bobek, 1959; Djamali et al., 2009), this tendency only produced a reduced rate of sediment incision rather than sediment aggradation within the Upper Khuzestan Plains (Bull, 1991). Hence, these factors probably only cause slight overestimations, so that dated river terrace sediments may be good indicators of actual rates of tectonic uplift. This is particularly the case with terrace deposits older than about 15,000 BC, considering the large changes in climate and relative sea-levels that have taken place from the time of the Last Glacial Maximum to the present. Over these longer timespans the effects of periods of river sediment aggradation and incision due to factors other than tectonics will tend to be evened out (Bull, 1991). Additionally, over these longer timespans, the total vertical distance associated with tectonic uplift (both by stable creep and seismicity) will, typically, be of the order of several metres and thus more likely to exhibit a significant geomorphological expression (Burbank and Anderson, 2001).

Furthermore, there are two main types of error associated with the river terrace data which tend to underestimate rates of uplift. Firstly, as already touched upon, there are errors involved with the locations of the river terraces and dated samples relative to the axis of the anticline. Apart from the 'Naft-e Safid terrace' with dated river terrace exposures less than 0.5 km from one part of the axis of the Naft-e Safid Anticline, all of the dated terrace exposures are on fold limb locations several kilometres from the anticlinal axis. The vicinity of the axis or crest of an anticline is the area where the rate of vertical uplift is greatest (Suppe, 1985), though the greater total vertical uplift for the fold crest compared with the fold limbs is generally small in field studies for river terraces less than c. 30 ka in age (Molnar et al., 1994; Burbank and Anderson, 2012). Hence, except for the 'Naft-e Safid terrace', the data for the river terrace sediments associated with all of the river terraces slightly underestimate the rates of crestal uplift for the Shushtar, Naft-e Safid and Sardarabad Anticlines.

Secondly, there are errors associated with the Optically Stimulated Luminescence (OSL) dating of the river terrace sediments. Despite the precautions with sampling, all of the samples in this study exhibited some signs of incomplete bleaching to varying degrees (Bateman and Fattahi, 2008, 2010). This is most probably due to inherent problems such as the attenuation of light through the water column and the input of non-bleached sediment from the erosion of older deposits and river banks (Rittenour, 2008). This is countered to a large extent by statistical modelling to isolate burial OSL ages for each of the samples (Galbraith and Green, 1990; Galbraith et al., 1999), but if the bleaching during the last period of sediment transport and deposition was less complete than expected or modelled for, then the OSL dates obtained will be overestimates of the age of sediment burial (Richards et al., 2001; Zhang et al., 2003). If that were the case, then the river terrace data will underestimate the rates of river incision and tectonic uplift.

Whilst these underestimation errors are probably of a lesser magnitude than the overestimation errors associated with the amounts of river aggradation and incision, together they will tend to balance these overestimations. Hence, the quoted uplift rates for the anticlines in this study are thought to be good guides to the actual rates of tectonic uplift.

5.2.4 Summary of Earth surface movement rates in the Dezful Embayment in the Upper Khuzestan Plains

In summary, in the Dezful Embayment along the north-east coast of the Persian Gulf, at locations roughly 60 - 130 km to the north-east of the Zagros Deformation Front, there is evidence for Earth surface movements due to tectonics. The rates of tectonic uplift are moderate, probably in the range of about 0.19 - 2.26 mm yr^{-1}.

5.3 Earth surface movements within lowland south-west Iran relative to the Zagros Deformation Front

The data of this study relating to Earth surface movements falls into two broad groups at different distances from the Zagros Deformation Front (ZDF), the approximate NW-SE oriented line where folds associated with the Simple Folded Zone and Dezful Embayment ultimately die out (Haynes and McQuillan, 1974; Berberian, 1995; Hessami et al., 2001a). The first broad group, which is approximately 20 km - 60 km to the north-east of the ZDF, includes the interpreted data from the marine terraces, with approximate rates of tectonic uplift of 0.07 - 0.66 mm yr^{-1} (assuming hydro-isostasy of c. $^{+}$0.7 m). The second broad group, which is approximately 60 km - 130 km to the north-east of the ZDF, includes the interpreted data from the river terraces, ancient canals and ancient hydraulic structures, with approximate rates of tectonic uplift of 0.19 - 2.26 mm yr^{-1}. The data is shown in Table 5.7. As discussed, there are errors and uncertainties involved with both broad groups of data, particularly with *hydro-isostasy for the marine terraces*, so the data relating to the marine terraces are less reliable indicators of rates of tectonic uplift than the other types of data. Nevertheless, the two broad groups do exhibit some significant differences, with, generally, lower rates of tectonic uplift in a “zone” about 20 - 60 km to the NE of the ZDF and, generally, higher rates of tectonic uplift in a “zone” about 60 - 130 km to the NE of the ZDF (Table 5.7 and Figure 5.2).

5.3.1 Zones of Earth surface movements relative to the ZDF

The general differences in Earth surface movements in these two “zones” is supported by data for the GPS-detected horizontal surface motion of the Zagros (the Eurasian Plate) relative to Arabia (the Arabian Plate) (Figure 5.1; Tatar et al., 2002; Walpersdorf et al., 20006; Tavakoli et al., 2008; Hatzfeld et al., 2010). In the Dezful Embayment, this relative horizontal surface motion is from N / NE to S / SW at rates varying from roughly zero in the vicinity of the Zagros Deformation Front (ZDF), to roughly 0.5 mm yr^{-1} - 3 mm yr^{-1} in the vicinity of Ahvaz and the NE Persian Gulf about 20 - 60 km to the north-east of the ZDF, up to roughly 2 mm yr^{-1} - 6 mm yr^{-1} in the vicinity of Dezful, Masjed-e Soleyman and Haft Kel about 60 - 130 km to the north-east of the ZDF (Figure 5.1; Hatzfeld et al., 2010). Rates of surface horizontal movements and rates of surface uplift are related (Suppe, 1985; Hardy and Poblet, 2005) and using interpolation, approximate equivalent rates of surface uplift for each of these zones are given in Table 5.7.

Figure 5.1 GPS-detected surface motion of the Zagros relative to Arabia (Arrows show direction and rate of horizontal motion, with 95 % confidence ellipses) (From Tatar et al., 2002; Walpersdorf et al., 2006; Tavakoli et al., 2008; Hatzfeld et al., 2010)

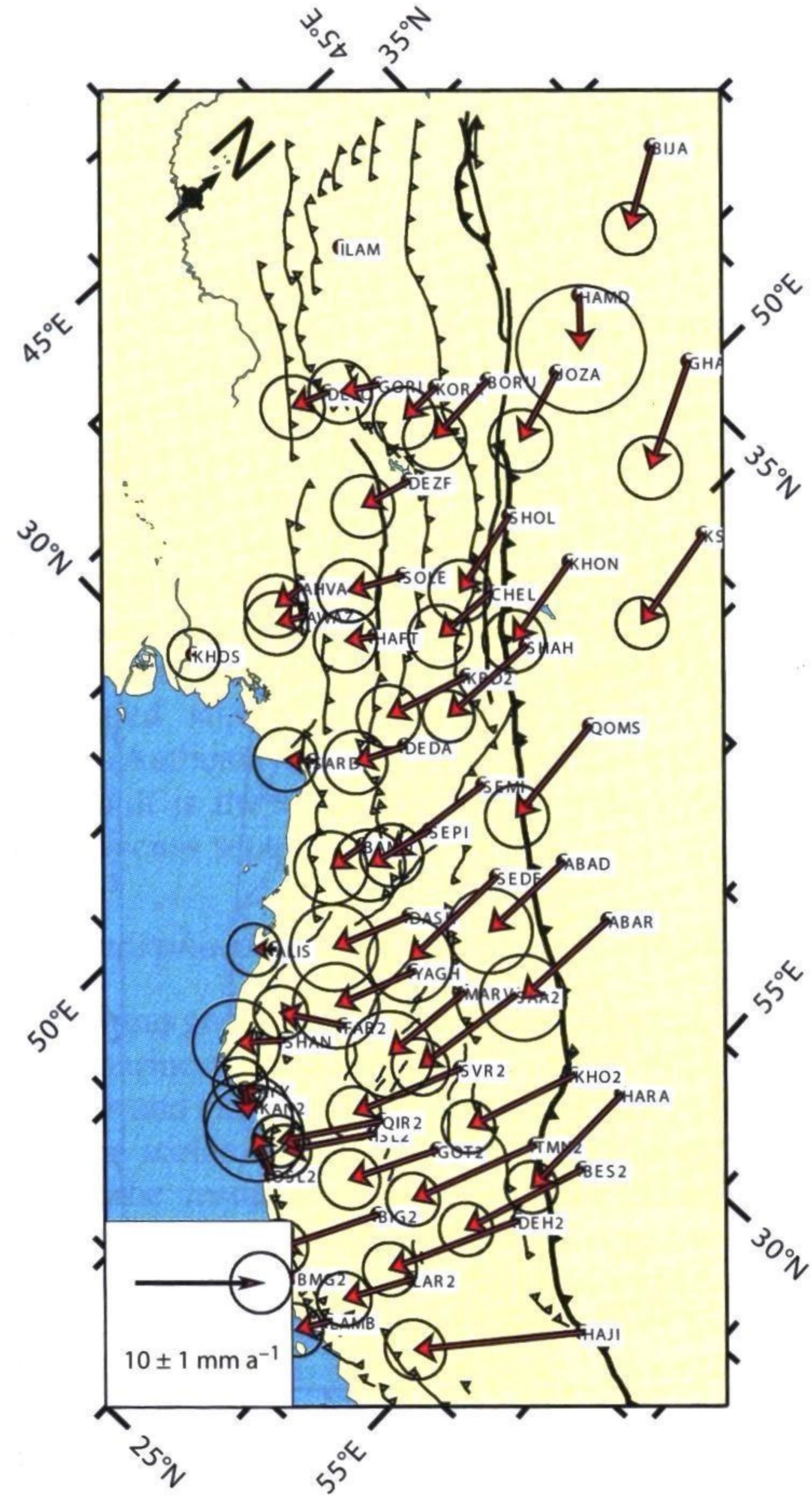

Table 5.7 Summary of Earth surface movements within lowland south-west Iran in NW-SE trending structural zones relative to the Zagros Deformation Front

Location of NW-SE trending zone relative to the Zagros Deformation Front (ZDF)	**Approximate rates of tectonic uplift,** based on interpreted data for marine terraces, river terraces, ancient canals and ancient hydraulic structures	**Approximate rates of GPS-detected horizontal surface motion** for Zagros relative to Arabia and **Approximate equivalent rates of surface uplift using interpolation**	**Approximate rates of uplift** (range in mm yr^{-1} to one decimal place)
Vicinity of Zagros Deformation Front (ZDF) (approx. 0 - 20 km to the NE and SW of the ZDF)	—	Horizontal motion of Zagros relative to Arabia approximately zero, so rates of surface uplift approximately zero	**Rates of uplift approximately zero**
Approximately 20 - 60 km to the NE of the ZDF	Most probable range of rates of tectonic uplift based on interpreted data for marine terraces: North of Bandar-e Deylam (Marine terrace A at BANDN1, assuming hydro-isostasy of c. $^{+}$0.7 m): 0.62 - 0.66 mm yr^{-1} SW limb of Binak Anticline (Marine terrace A at BINAK3, assuming hydro-isostasy of c. $^{+}$0.7 m): 0.26 - 0.28 mm yr^{-1} SW limb of Binak Anticline (Marine terrace B at BINAK4): 0.07 - 0.11 mm yr^{-1}	Approximate rates of horizontal surface motion (in the vicinity of Ahvaz and the NE Persian Gulf coast): 0.5 mm yr^{-1} - 3 mm yr^{-1} Approximate equivalent rates of surface uplift using interpolation: 0.1 - 0.8 mm yr^{-1}	**Uplift at rates of approximately 0.1 - 0.8 mm yr^{-1}**
Approximately 60 - 130 km to the NE of the ZDF	Most probable range of rates of tectonic uplift of folds based on interpreted data for river terraces, ancient canals and ancient hydraulic structures: Naft-e Safid Anticline: 0.19 - 1.53 mm yr^{-1} Sardarabad Anticline: 0.23 - 0.29 mm yr^{-1} Shahur Anticline: 1.94 - 2.13 mm yr^{-1} Shushtar Anticline: 0 - 2.26 mm yr^{-1}	Approximate rates of horizontal surface motion (in the vicinity of Dezful, Masjed-e Soleyman and Haft Kel): 2 mm yr^{-1} - 6 mm yr^{-1} Approximate equivalent rates of surface uplift using interpolation: 0.5 - 1.5 mm yr^{-1}	**Uplift at rates of approximately 0.2 - 2.3 mm yr^{-1}**

Figure 5.2 Zones of Earth surface movements in lowland south-west Iran relative to the Zagros Deformation Front (ZDF) (Landsat (2000) false-colour image with yellow ring and blue ring symbols to indicate magnitudes of interpreted ranges of uplift rates)

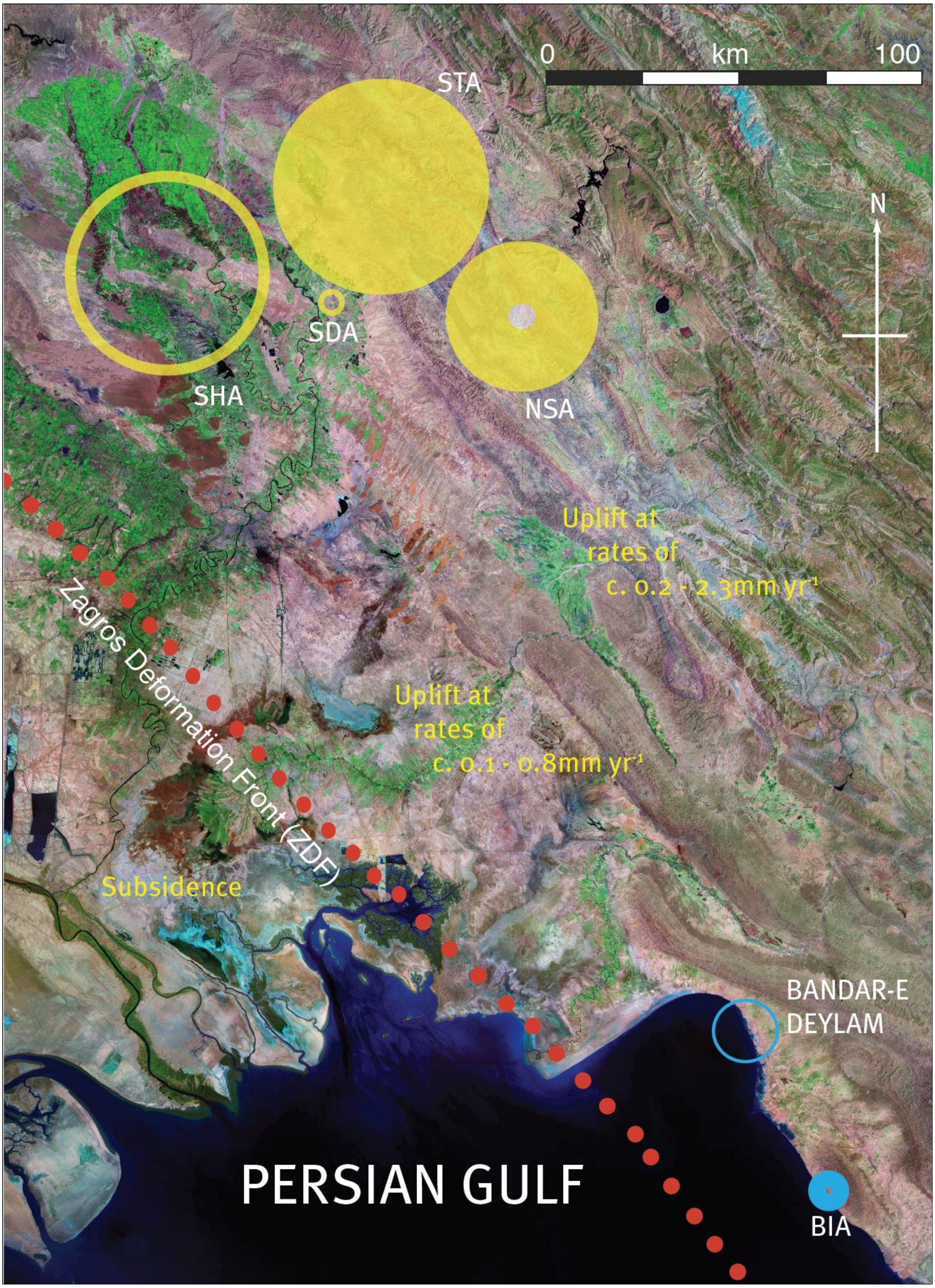

Key

● ● ● ● ● Zagros Deformation Front (ZDF)

Key to ring symbols in Figure 5.2

Yellow rings indicate magnitudes of interpreted ranges of rates of uplift at locations within the Upper Khuzestan Plains: NSA Naft-e Safid Anticline; 0.19 - 1.53 mm yr^{-1}
SDA Sardarabad Anticline; 0.23 - 0.29 mm yr^{-1}
SHA Shahur Anticline; 1.94 - 2.13 mm yr^{-1} STA Shushtar Anticline; 0 - 2.26 mm yr^{-1}

Blue rings indicate magnitudes of interpreted rates of uplift at locations along the north-east Persian Gulf Coast:
BANDAR-E DEYLAM North of Bandar-e Deylam; 0.62 - 0.66 mm yr^{-1}
BIA Binak Anticline; 0.07 - 0.28 mm yr^{-1}
These rates of uplift for marine terraces include a correction for $^{+}$0.7 m of hydro-isostasy, but this correction is only an estimate so the blue ring symbols are less reliable indicators of rates of tectonic uplift than the yellow ring symbols

---

Figure 5.3 Earthquake focal mechanisms, major active faults, and topography in south-west Iran, with an inset showing the Balarud Line (From Nissen et al., 2011)

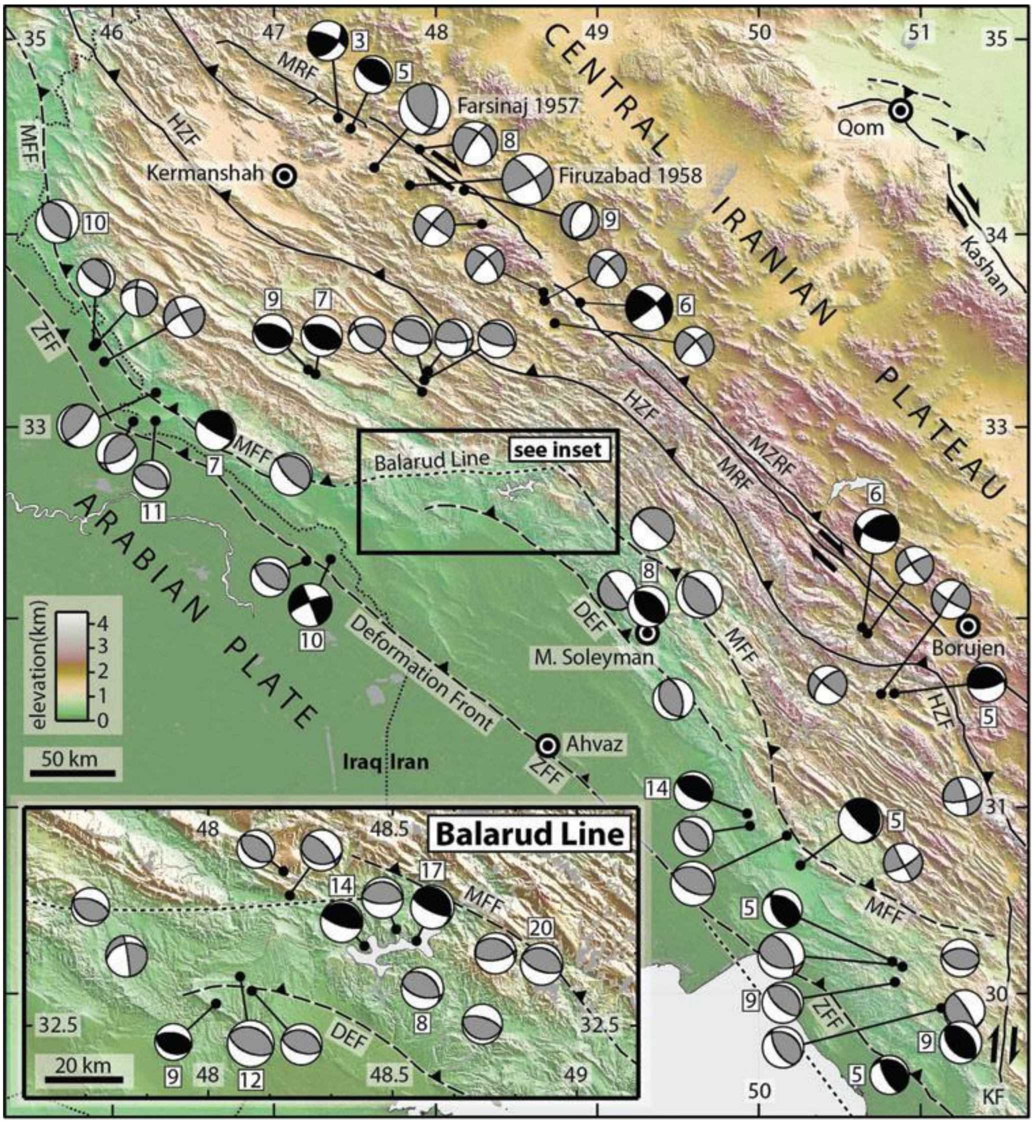

Focal mechanism diagrams show compressions in black or grey and tensions in white. Black mechanisms were determined from full *P* and *SH* body-wave modelling, all with centroid depths in km. Grey mechanisms were from the Global CMT catalogue, some with centroid depths in km (Nissen et al., 2011).

As shown in Table 5.7 and Figure 5.2, Earth surface movements in lowland south-west Iran can be considered in four broad groupings or NW-SE trending zones relative to the Zagros Deformation Front (ZDF) in the region of the Dezful Embayment:

South-west of the ZDF: Subsidence

Vicinity of the Zagros Deformation Front (approximately 0 - 20 km to the SW and NE of the ZDF): Minimal vertical Earth surface movements

Approximately 20 - 60 km to the NE of the ZDF: Uplift at rates of approximately 0.1 - 0.8 mm yr^{-1}

Approximately 60 - 130 km to the NE of the ZDF: Uplift at rates of approximately 0.2 - 2.3 mm yr^{-1}

These zones are approximate and overlap to some degree due to errors involved with the data and due to the natural variation of tectonic movements, especially variations between individual folds. Nevertheless, the general trends of subsidence to the SW of the ZDF, minimal vertical movements in the vicinity of the ZDF, and increasing uplift with distance to the NE of the ZDF are broadly in accordance with what is known of the structural geology of the region, as described in Section 2.4. Subsidence is present to the SW of the ZDF, due to lithospheric flexure of the Arabian Plate within the Mesopotamian-Persian Gulf Foreland Basin (DeCelles and Giles, 1996; Edgell, 1996). Within the vicinity of the Zagros Deformation Front there are interactions between the N-S trending Arabian-type anticlines and the NW-SE trending Zagros-type anticlines, though with limited vertical movements (Abdollahie Fard et al., 1996). Increasing uplift is present with distance to the NE of the ZDF in the Simple Folded Zone and Dezful Embayment, due to a propagation of the deformation of the sedimentary cover towards the south-west with time (especially since about 5 Ma) (Allen et al., 2004), with NW-SE trending Zagros-type folds of decreasing age and magnitude towards the south-west (Berberian, 1995; Alavi, 2004; Hatzfeld et al, 2010).

The rates of uplift found in this study (approximately 0.1 - 0.8 mm yr^{-1} and 0.2 - 2.3 mm yr^{-1}) are of the same order as that found in previous work using geomorphological and geological observations in the central Zagros (about 1 mm yr^{-1}, Falcon, 1974), Persian Gulf marine terraces south-east of the Kazerun Fault Zone (about 0.2 mm yr^{-1} (Reyss et al., 1998) in a region where deformation may be more concentrated in the shore area (Walpersdorf et al., 2006)), and incised Dalaki and Mand river terraces on folds (0.2 - 3.2 mm yr^{-1}, Oveisi et al., 2008). Also, the general trends are in accordance with the recorded earthquake history of the region, with very few earthquakes to the SW of the ZDF, and earthquakes to the NE of the ZDF with focal mechanisms mainly indicative of reverse faults oriented roughly NW-SE (Figure 5.3; Allen and Talebian, 2011; Nissen et al., 2011).

5.3.2 Earth surface movements to the south-west of the ZDF

To the south-west of the Zagros Deformation Front, there is no data in this study relating to tectonic movements. As discussed in Section 2.5, rates of tectonic subsidence within this foredeep area are not known from previous work due to the complexity of other factors such as sediment compaction, relative sea-level changes, and delta and coastline changes, which have had greater influences on relative vertical movements during the Late Pleistocene and Holocene (Larsen and Evans, 1978; Heyvaert and Baeteman, 2007). There are some mainly NNW-SSE, N-S and NNE-SSW trending anticlines within the region, but rates of uplift are very low, with deep-seated salt structures and anticlines in the northern Persian Gulf undergoing uplift at rates of about 0.01 to 0.024 mm yr^{-1} (Edgell, 1996; Soleimany and Sàbat, 2010; Soleimany et al., 2011).

In summary, for this region of general subsidence and low rates of anticlinal uplift to the SW of the ZDF, it is likely that the influences of tectonics on major rivers are only slight, especially since the influences of the external factors of relative sea-level changes and human impacts have been great (Lambeck, 1996; Walstra et al, 2010a, 2010b; Heyvaert et al., 2012).

5.3.3 Earth surface movements to the north-east of the ZDF

To the north-east of the Zagros Deformation Front, the data from this study and previous work indicate moderate rates of tectonic uplift with a total range of about 0.1 - 2.3 mm yr^{-1} and a general trend for higher rates of uplift with increasing distance from the ZDF.

This trend is only a slight, general trend. There are variations between individual folds, with, for instance, the Shahur Anticline having measured rates of uplift (about 1.94 -

2.13 mm yr^{-1}) which are much greater than those of the neighbouring Sardarabad Anticline (about 0.23 - 0.29 mm yr^{-1}). The reason for this difference is uncertain. It may be partly because there was some incision into the Shahur Anticline when ancient canal SC2 developed into the Shahur River to produce the typically slightly steeper gradients characteristic of rivers, thus overestimating the rate of uplift. It may be partly because compressive stresses built up on fault bend folds to the south-west associated with the Zagros Foredeep Fault (ZFF), producing detachment folding and associated uplift first at the Sardarabad Anticline, then at the Shahur Anticline, and then at the Zeyn ul-Abbas Anticline (Figure 4.1 (f); Burberry et al., 2010).

Also, as described in Section 2.4, there are some folds (such as the Ahvaz Anticline) associated with "out of sequence" thrusts and reverse faults (such as the ZFF) (Figure 2.14) that are significantly older and larger than their distance from the ZDF would indicate. It is likely that rates of uplift associated with these folds are anomalously greater than that indicated by the simple general "zones" (with, *possibly*, the Ahvaz Anticline having rates of uplift of the order of about 1.5 mm yr^{-1}).

In summary, for this region of general uplift and moderate rates of anticlinal uplift to the NE of the ZDF, it is likely that the influences of tectonics on major rivers are great; especially since the rivers are upstream of sea-level influences (Figure 4.29; Kirkby, 1977; Blum et al., 2013) and the rivers frequently interact with the anticlines of growing folds (Allen and Talebian, 2011).

5.4 Rates of tilting in the study area

The difference in tectonic uplift rates between the Zagros Deformation Front (ZDF) (approximately zero) and within the Dezful Embayment about 60 - 130 km to the north-east of the ZDF (approximately 0.2 - 2.3 mm yr^{-1}) would be sufficient to produce regional tilting. If the tectonic uplift were generally organised into NW-SE oriented tectonic uplift "zones", then this regional tilting would be from the NE and ENE towards the SW and WSW at average rates of tilt of approximately 1.5×10^{-6} to 3.8×10^{-5} radians kyr^{-1}. These average rates of tilt are considerably less than the rates of tilting of approximately of 7.5×10^{-4} to 7.5×10^{-3} radians kyr^{-1} proposed by Peakall et al. (2000) as being the lower threshold necessary for avulsions.

These tilt directions are consistent with the general crustal thickening towards the NE and ENE associated with the Arabian-Eurasian plate collision (Blanc et al., 2003; Sepehr and Cosgrove, 2004; Abdollahie Fard et al., 2006), as described in Chapter 2. Similarly, they are consistent with a regional, NW-SE “geo-flexure” with a hinge-line along the mountain front (Falcon, 1961) and a probable regional propagation of both shallow and basement deformation towards the south-west since about 5 Ma (Allen et al., 2004; Hatzfeld et al., 2010).

These tilt directions are also consistent with the tendency for major rivers in the Upper Khuzestan Plains to migrate towards the west and south-west over millennial timescales. The River Karun (Shuteyt) currently occupies a course near the west and south-west margin of both the Aghili Plain and the Mianab Plain (Figure 4.1 (b)). Meander scars to the east of the river channel which generally face towards the river and the distributions of prehistoric, Elamite and Parthian Period archaeological sites (c. 9,000 BC - 224 AD) further east within these plains (Wright, 1969; Moghaddam and Miri, 2003), suggest that the River Karun was located several km further east thousands of years ago and then migrated west and south-west to its present-day course (Alexander et al., 1994; Burbank and Anderson, 2012). Similarly, the River Dez occupies the west and south-west part of the Susiana Plain, with its furthest eastward extent being the “fixed” location of the incision across the Sardarabad Anticline (Figure 4.1 (b)). Soils, sediments, relict levées and archaeological survey suggest that the River Dez has migrated westwards with time (especially with different courses across the Dezful Uplift, such as the one now occupied by the Shirin Ab), probably from prior to the “Village Period” (c. 7,000 BC/4,000 BC) to the present (Figures 4.1 (b) and (c); Veenenbos, 1958; Kouchoukos and Hole, 2003). The River Karkheh may also have migrated westwards with time occupying first a course similar to the present-day River Dez on the Susiana plain, then one similar to the Shahur River, then its present-day course (Veenenbos, 1958). These changes are consistent with a regional tilt towards the SW and WSW. However, the avulsions indicate that higher rates of tilt or other factors may also be involved.

CHAPTER 6 RESPONSES OF THE RIVER KARUN AND RIVER DEZ TO ACTIVE FOLDS AND HUMAN IMPACTS

"It is hardly less difficult to visualize the mighty Rustam standing astride the mountains and laying about with strokes of his gigantic sword than it is to attribute the *tangs* and stream pattern of this region to one of the classical hypotheses of transverse drainage formation."

Theodore Oberlander, American geologist, in the book "The Zagros Streams" (1965 AD)

6.1 The major rivers Karun and Dez, active folds and direct human impacts in lowland south-west Iran

The structural development of a foreland basin greatly influences and broadly determines the development of major rivers within a foreland basin (Burbank et al., 1996; Leeder, 2011). In the Mesopotamian/Persian Gulf peripheral foreland basin in south-west Iran, the largest river system is the River Karun with its main tributary, the River Dez. This river system is the main agent of sediment transfer from the Zagros orogen and wedge-top into the foredeep of Lower Khuzestan, southern Mesopotamian and the northern Persian Gulf. As discussed in Chapter 2, the River Karun and River Dez mainly flow as transverse rivers across the Upper and Lower Khuzestan Plains roughly from the north to the south and south-west. They encounter the similar, mainly NW-SE trending active anticlines and uplifts of the Dezful Embayment as a succession of significant "obstacles" with progressively younger, less developed folds to the south-west with distance downstream towards the Zagros Deformation Front (ZDF) (Haynes and McQuillan, 1974). They also encounter the mainly N-S trending emerging anticlines and uplifts of the Mesopotamian foredeep as a number of lesser "obstacles" to the south-west of the ZDF (Abdollahie Fard et al., 2006; Hatzfeld et al., 2010).

Like many rivers, the River Karun and River Dez respond to each of these "obstacles" either by maintaining a course across a growing fold or by being defeated by a growing fold and thus following a diverted course around the fold. Being "ponded" behind a fold in an internal drainage basin is not a condition which has persisted for the rivers Karun and Dez in the Khuzestan Plains, most probably due to their large catchment areas and high water discharges (Burbank et al., 1996). Indeed, though the smaller River Karkheh was "ponded" in lakes (the Saidmarreh, Jaidar and other small lakes probably totalling c. 290 km^2) by the vast Saidmarreh Landslip (covering c. 170 - 270 km^2) of pre-9,000

BC, with time the River Karkheh had incised a course through the slide debris by a gorge that is currently about 20 km long and up to 180 m deep (Watson and Wright, 1969; Shoaei and Ghayoumian, 2000).

As the folds grow laterally and, in some cases, coalesce to form larger folds, and regional uplift continues to extend over the entire Khuzestan Plains, the River Karun and River Dez will, ultimately, incise across many areas of uplift in the Khuzestan Plains. River incision is necessary if they are to maintain their courses as major rivers, as they have done further upstream in the Zagros Mountains (Oberlander, 1965, 1985). Within the Zagros orogen the courses of the major rivers are varied, with the River Karun mostly flowing in accordance with the general NW-SE structural grain and folding, and with the River Dez mostly flowing in discordance with this structural grain and folding (see Section 2.3.1 and 2.3.2). In the Zagros Mountains, rivers cross anticlines at a variety of locations with, paradoxically, a strong tendency for the transection of anticlines at locations of their greatest structural and topographic relief (Oberlander, 1965, 1985). These crossing locations in the Zagros Mountains will have been mainly determined at a much earlier stage in the development of the Zagros orogen when structural and topographic relief in the Zagros was less. In parts of the Zagros two resistant limestone formations are separated by a unit of easily erodible flysch which is thicker than the amplitude of folding. It is likely that a key period of determining river crossing locations was when a relatively flat erosion surface developed in the folded flysch, and from this surface the rivers and streams were superimposed onto the folded limestone unit below (Oberlander, 1965). Another key period for determining river crossing locations may have been earlier still, when the folds were just emerging on the ground surface in a scenario quite similar to the Khuzestan Plains of the present-day. Hence, it is probable that the interactions between the young, active folds of the Khuzestan Plains and the River Karun and River Dez are important in determining the courses of these major rivers both now and during many millennia to come, once tectonic uplift has progressed sufficiently for the river courses to become “fixed” within relatively deep valleys.

6.1.1 River size, form, hydrology, sedimentology and migration

Within the Khuzestan Plains the most frequent response of the River Karun and River Dez to an interaction with an active fold is river incision across the fold, even though the folds are at relatively young stages in their development and there are areas of the plains between neighbouring folds into which rivers can divert. As listed in Section 4.3, there are 13 cases of fold-river interactions, of which the majority of 10 cases (or 77 %) involve river incision across a fold and 3 cases (or 23 %) involve river diversion around a fold. These are shown in Tables 4.13 to 4.15 and in the plots of river characteristics against valley distance shown in Figures 4.29 to 4.43.

The predominance of river incision across a fold is probably mainly related to the relatively high average and peak discharges of the major rivers Karun and Dez, which provide sufficient erosive powers to maintain a course across a fold over long periods of time. Though not investigated in detail in this study, *two slightly smaller rivers* in lowland south-west Iran, the River Karkheh and the River Jarrahi (mean annual water discharges c. 165 m^3s^{-1} and 78 m^3s^{-1}, respectively), divert around the “nose” of a fold much more frequently. The River Karkheh diverts around the “nose” of the Dal Parri Anticline, Shahur Anticline, Darreh-ye Viza Anticline and the Dasht-e Mishan Oilfield. The River Karkheh only appears to incise across the Zeyn ul-Abbas Anticline and the Hamidiyyeh Anticline (Figure 4.1 (a) and (f)). These two folds are of slight to moderate development and 1:100,000 scale geological maps (IOOC, 1969a, 1969b, 1969c) indicate that they are most probably forming as a coalescence of two or three separate fold segments. The River Jarrahi diverts around the “nose” of the Marun Anticline, Shadegan Oilfield and Mansuri Oilfield. The River Jarrahi only appears to incise across the Agha Jari Anticline, with the incision near to the laterally propagating tip of the fold after a long roughly SE-NW course of the River Marun parallel to the axis of the Agha Jari Anticline (Figure 4.1 (a) and (g)). Hence, with these slightly smaller rivers, out of 10 cases of fold-river interactions, there are only 3 cases (30 %) of river incision across a fold and 7 cases (70 %) of river diversion around a fold.

There is a contrast of responses between very small rivers, such as the easily defeated creeks associated with the Wheeler Ridge anticline in California, U.S.A. (Keller et al., 1998) and the easily diverted small rivers in the south-east Zagros (Ramsey et al., 2008), and very large rivers, such as the minimally altered River Ganges incising across the Mohand Anticline in northwest India (Pickering, 2010). This is fairly well understood from previous work (Burbank et al., 1996; Schumm et al., 2000).

A good example of the differences in general river forms for the two groups is shown in Figure 6.1 for the Sardarabad Anticline. The River Dez incises across the central part of

Figure 6.1 Incision of the River Dez across the Sardarabad Anticline and diversion of the River Karun (Shuteyt) around the Sardarabad Anticline
(a) Landsat (2000) false-colour image
(b) Landsat TM image at 50 % transparency draped over SRTM digital topography (scale saturated at 100 m elevation) (From Allen and Talebian, 2011)

a)

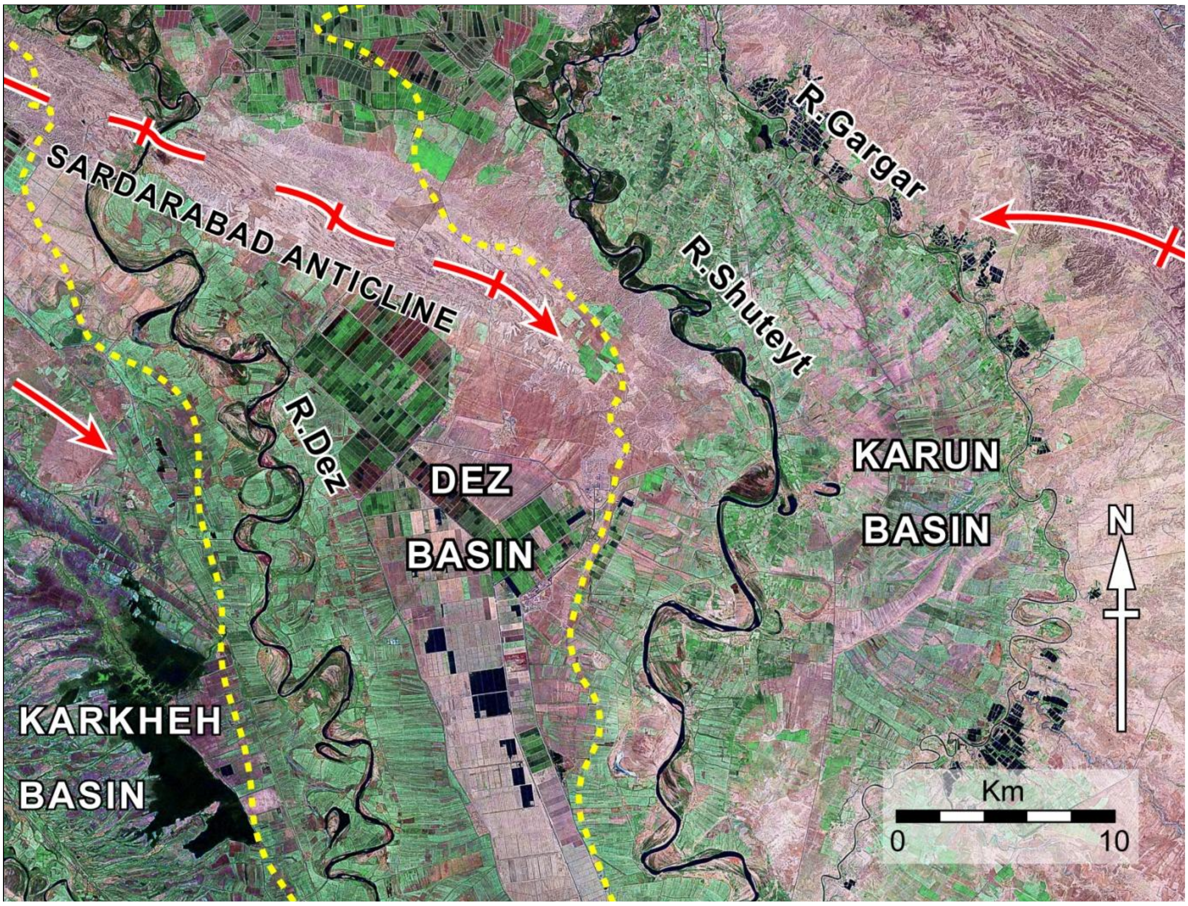

Key to Figure 6.1 (a)
Thick red line with cross bar - Axis of anticline (arrow indicates direction of plunge)
Yellow dashed line - River basin margin (approximate location)

b)

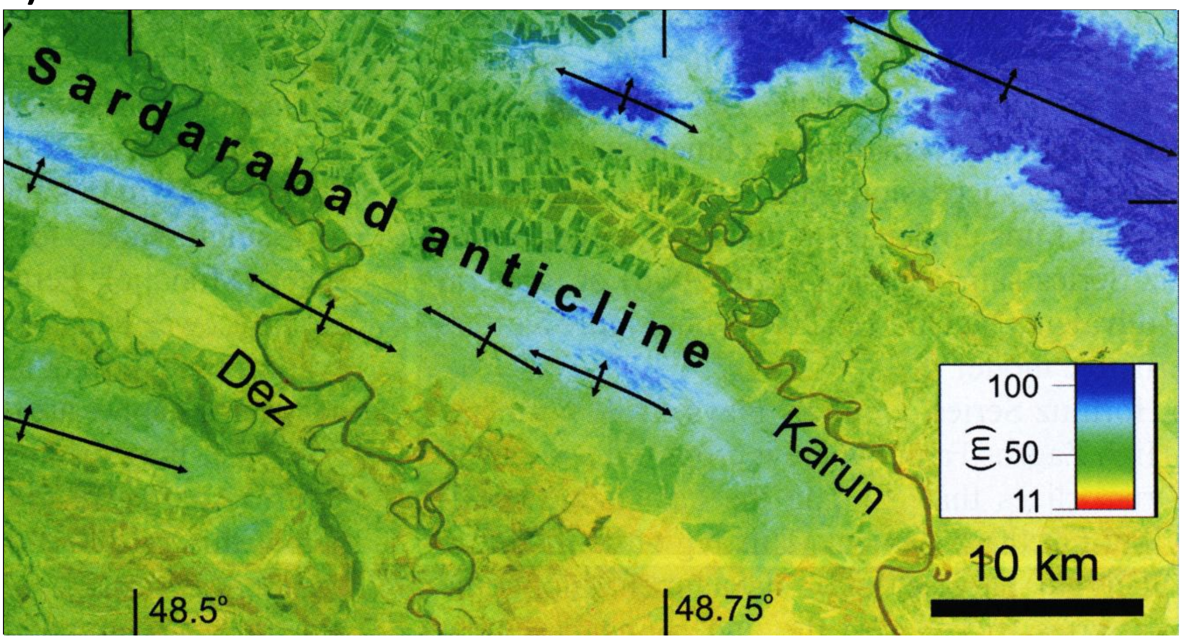

the Sardarabad Anticline, with the reaches across the fold axis having a narrow channel-belt width, low channel sinuosity, and a general river course across the fold which is approximately orthogonal to the fold axis. The River Karun diverts around the "nose" of the Sardarabad Anticline, with the reaches across the projection of the fold axis having a moderate channel-belt width, moderate channel sinuosity, and a general river course which changes by approximately 20° to 70° to flow around the nose of the fold (Allen and Talebian, 2011).

Key characteristics of general river form, river hydrology, river sedimentology and river migration which help to differentiate between river incision across a fold and river diversion around a fold are summarised in Table 6.2. Specific stream powers for each reach were determined using the mean annual water discharge from the nearest river gauging station and using the channel water surface slopes and channel widths on the day of the survey, as described in Appendices 7.2.2.3 and 7.2.2.4. These specific stream powers allow for comparison between reaches, but are underestimates of the stream powers which will have influenced the river geomorphology. This is because sediment bedloads were not measured, water discharges would have been higher in previous millennia before major dams were constructed (Ionides, 1937; Knighton, 1998), and sediment discharges would have been higher prior to loss of upland soil cover with forest clearance (Bull, 1991). Also, it is generally considered that greater water discharges associated with seasonal floods (rather than mean annual water discharges) are most influential in determining river geomorphology (Leopold et al., 1964; Andrews, 1980; Bridge, 2003).

6.1.2 Fold structural geology

The predominance of river incision across a fold over river diversion around a fold for the Karun and Dez (Section 4.3), may be related in some way to fold structural geology.

A high incidence of river incision across a fold when alternative diverted courses are available, such as the River Dez incising across the centre of the Sardarabad Anticline when a diverted course to the west to join the River Karkheh is an alternative (Figure 4.1 (b) and (f)), is poorly understood. Previous research, such as that of Oberlander (1965, 1985) further upstream in the Zagros Mountains, found a tendency for rivers to incise across anticlines near locations of greatest structural relief. A number of mechanisms may account for this tendency (Simpson, 2004; Montgomery and Stolar, 2006; Babault et al., 2012), including the superimposition of the drainage network via a structurally conformable more easily eroded horizon (Oberlander, 1985); though these mechanisms apply after the initial stages of fold development. In particular, the folds in the study area are too small to have net river erosion which is sufficient to be significantly different from surrounding areas to induce focussed rock uplift (the mechanism of Montgomery and Stolar, 2006) or to significantly unload the crust and produce a doubly plunging anticline with a river valley at its centre (the mechanism of Simpson, 2004). Indeed, doubly plunging anticlines are clearly produced in the study area by different mechanisms, since there are some well-developed, doubly plunging anticlines within lowland south-west Iran, such as the Kupal Anticline and the Binak Anticline, which have no notable stream incising across the centre. Also, the folds are much too young and the structural relief is much too gentle for the capture of longitudinal rivers by transverse rivers in response to an amplification of the regional slope (the mechanism of Babault et al., 2012). In short, the structural geology and the *early stages* of the structural development of folds may be important factors influencing the predominance of river incision across the young, active folds of lowland south-west Iran.

As described in Section 2.4, the folds in the study area of the Dezful Embayment and in the foredeep of the Mesopotamian-Persian Gulf Foreland Basin are relatively similar. Hence, as shown in Table 6.1, a number of characteristics of fold structural geology are similar for river incision and river diversion, though the sample size is small. The types of fold are similar, with no larger fault bend folds and fault propagation folds associated with cases of river diversion. The degree of fold development is similar, with mainly moderately developed folds in both scenarios. The estimated rates of structural uplift are of similar ranges, with a mean range of 0.16 - 1.71 mm yr^{-1} for river incision and a mean range of 0.72 - 0.84 mm yr^{-1} for river diversion. The width of the fold (or its projection) at the location of the river crossing is similar in both scenarios, and even the estimated erosion resistance of the folds are similar in both scenarios.

The main differences between cases of river incision and river diversion appear to be associated with the location where the river crosses the fold axis (or its projection) relative to the fold "core" and the fold "nose". Models of fold development indicate that many folds initially emerge on the ground surface as a relatively small, oval fold "core" from which the lateral propagation of the fold develops, usually from one or both of the

Table 6.1 Characteristics of fold structural geology for river incision across a fold and river diversion around a fold in lowland south-west Iran

Characteristic of fold structural geology	**River incision across a fold**	**River diversion around a fold**
Probable type of fold AsDF: Asymmetric detachment fold DF: Detachment fold FBendF: Fault bend fold FPropF: Fault propagation fold Monocl: Monocline OLR: Oblique lateral ramp	A) AsDF B) FBendF truncated by OLR C) AsDF E) AsDF F) Short FBendF G) Monocl/AsDF H) AsDF J) DF K) FPropF L) DF Mode: **Asymmetric detachment fold**	D) AsDF I) AsDF M) DF Mode: **Asymmetric detachment fold**
Degree of development of fold Max. topographic expression: High: Well developed (>100 m) Mod: Moderately developed (30 m - 100 m above surrounding plains) Slight: Slightly developed (8 m - 30 m) Emerg: Emerging (<8 m)	A) High B) High C) Mod E) Mod F) High G) Mod H) Mod J) Emerg K) High L) Emerg Mode: **Moderate / High**	D) Mod I) Mod M) Emerg Mode: **Moderate**
Estimate of approximate rate of structural uplift (range in mm yr^{-1})	A) 0.2-2.3 B) 0-2.26 C) 0.2-2.3 E) 0.2-2.3 F) 0.2-2. G) 0.2-1.5 H) 0.23-0.29 J) 0.2-1.5 K) 0.2-1.5 L) 0-0.8 Mean: **0.16 - 1.71 mm yr^{-1}**	D) 0.23-0.29 I) 1.94-2.13 M) 0-0.1 Mean: **0.72 - 0.84 mm yr^{-1}**
Width of fold (or its projection) where crossed by river (distance in km between extent of fold limbs)	A) 2.3 B) 7.4 C) 7.5 E) 7.5 F) 6.8 G) 2.8 H) 4.3 J) 4.0 K) 2.3 L) 4.4 Mean: **4.9 ± 2.2 km**	D) 4.1 I) 4.9 M) 9.2 Mean: **6.1 ± 2.7 km**
Approximate distance from fold "core" to river crossing (distance in km along fold axis or its projection)	A) 3.9 B) 4.5 C) 1.2 E) 4.8 F) 43.6 G) 15.1 H) 1.3 J) 1.7 K) 8.5 L) 0.6 Mean: **8.5 ± 13.1 km**	D) 32.2 I) 22.8 M) 26.5 Mean: **27.2 ± 4.7 km**
Approximate distance from fold "nose" to river crossing (distance in km along fold axis or its projection)	A) 2.7 B) 8.8 C) 11.8 E) 15.7 F) 8.4 G) 12.5 H) 25.8 J) 15.0 K) 18.1 L) 9.0 Mean: **12.8 ± 6.4 km**	D) 3.8 I) 6.3 M) 14.3 Mean: **8.1 ± 5.5 km**
"River crossing location ratio" of Fold "core" to river crossing distance Fold "core" to fold "nose" distance (approximate ratio measured along fold axis, expressed as %)	A) 59 B) 34 C) 11 E) 45 F) 124 G) 55 H) 5 J) 10 K) 32 L) 6 Median: **33 %** Mean: **38 ± 36 %**	D) 113 I) 138 M) 217 Median: **138 %** Mean: **156 ± 54 %**
Approximate distance from fold "core" to river basin margin (distance in km, measured roughly along fold axis, from fold "core" to nearest river basin margin for the river crossing the fold) **+** ve indicates fold "core" within the river basin, **-** ve indicates fold "core" outside the river basin	A) +3.9 B) +8.6 C) +3.6 E) -3.6 F) -16.0 G) +9.9 H) +3.8 J) +18.0 K) +22.0 L) +15.0 Median: **+6.3 km** Mean: **+6.5 ± 11.0 km**	D) -25.7 I) -20.7 M) +43.0 Median: **-20.7 km** Mean: **-1.1 ± 38.3 km**

Table 6.1 Characteristics of fold structural geology for river incision across a fold and river diversion around a fold in lowland south-west Iran (continued)

Characteristic of fold structural geology	River incision across a fold	River diversion around a fold
Estimate of degree of general erosion resistance of fold (overall estimate - across fold for cases of river incision, just upstream of fold for cases of river diversion) Low & Qu low: Unlithified floodplain sediments Mod: Agha Jari Formation bedrock (mainly sandstones and siltstones) High: Bakhtyari Formation bedrock (mainly conglomerates)	A) Mod/High B) High/Mod C) Low E) Mod/Qu. low F) Qu. low G) Mod/High H) Qu. low J) Low K) Mod L) Qu. low Median: **Quite low / Moderate**	D) Mod I) Low M) Qu. low Median: **Quite low**

Letter codes A) to M) for cases of fold-river interactions are as given in Section 4.3.1

---

ends of the core (Jackson et al., 1996; Burbank et al., 1999; Keller et al., 1999; Champel et al., 2002). A fold "nose" is the end of a laterally propagating fold tip of a plunging fold (Jackson et al., 1996; Burbank and Anderson, 2001). Folds appear to grow in this way in lowland south-west Iran, with a general sequence of folds of progressively longer hinge length and higher amplitude with increasing distance to the north-east of the ZDF (Haynes and McQuillan, 1974; Hatzfeld et al., 2010). As described in Appendix 7.2.2.1, the fold "core" (the location on the fold axis on geological maps interpreted as having emerged first based on structural geology, topography, and drainage; generally, the area on the fold axis with greatest structural relief) and the fold "nose" (the location on the fold axis on geological maps of the tip of the fold; generally, the point where the fold curves back on itself) had been determined for each fold.

As shown in Table 6.1, the "river crossing location ratio" has a low mean value of 38 ± 36 % for river incision across a fold. The approximate distance from the fold "core" to the river crossing has a low mean value of 8.5 ± 13.1 km for river incision across a fold, compared with a high mean value of 27.2 ± 4.7 km for river diversion around a fold. The fold-river interactions for cases E) and F) associated with the artificial River Gargar are likely to have been greatly influenced by the location of the former monumental Masrukan canal from which it developed (Section 2.11). If these two cases are excluded, then river incision across a fold is characterised by a river crossing that is less than 16.0 km from the fold "core", and river diversion around a fold is characterised by a river crossing that is more than 22.0 km from the fold "core". These findings of river incision near to the fold "core" suggest that major river incision across a fold is frequently initiated at a very early stage in fold development.

Also, as shown in Table 6.1 and Figure 6.1, there is a strong tendency for the fold "core" to be located within the margins of the river basin of a river incising across a fold, and beyond the margins of the river basin of a river diverting around a fold. For river incision, the approximate distance from the fold "core" to the river basin margin has a median value which is $^{+}$ve ($^{+}$6.3 km), and, if cases E) and F) are excluded, river incision is always characterised by a fold "core" that is located within the river basin margins. For river diversion, the approximate distance from the fold "core" to the river basin margin has a median value which is $^{-}$ve ($^{-}$20.7 km), and only case M) has a $^{+}$ve value. This exception of the Dorquain Oilfield Anticline being within the basin margins of the diverted River Karun is to be expected since the River Karun has such an extensive river basin (more than 70 km across) in its lower reaches. These findings indicate that fold growth and river migration are important factors influencing the major river response to young, active folds.

6.1.3 Direct human impacts

There are four main categories of direct human modifications to river channels of the River Karun and River Dez in lowland south-west Iran: major dams, ruins of major dams, major anthropogenic river channel straightening, and artificial river development.

6.1.3.1 Major dams

There are three major dam complexes in the study area: the Gotvand Regulating Dam about 4 km north of Gotvand on the River Karun (KWPA, 2010) across the Turkalaki Anticline; the Dez Regulating Dam in northern Dezful and the Dez Diversion Dam in southern Dezful on the River Dez across the Dezful Uplift (Figure 4.1 (c); KWPA, 2010); and the Band-e Mizan weir, Pol-e Boleiti dam-bridge and water mills in Shushtar on the River Gargar on the forelimb of the Shushtar Anticline (Section 4.2.3; Figure 6.2; Selby, 1844; Torfi et al., 2007; Verkinderen, 2009; Moghaddam, in press). These major dams are characterised by a large drop in river water levels across the dam (of the order of about 3 m - 15 m), a reservoir upstream of the dam (of variable size according to seasonal flows, typically about 1.9 km - 8.3 km long by about 0.3 km - 0.7 km wide), and some prominent vertical river incision immediately downstream of the dam (about 3 m - 20 m or more below the surrounding plains). At channel distances of about 0 - 6 km

Figure 6.2 Landsat (2000) false-colour image showing features relating to ancient dams and canals associated with the River Shuteyt and River Gargar in the vicinity of Shushtar and photograph of ruins and foundations of the Band-e Mahibazan built on a WNW-ESE oriented linear outcrop of Agha Jari Formation sandstone (near 31°00’01”N 48°51’25”E, looking S, wooden rule 2 m long)

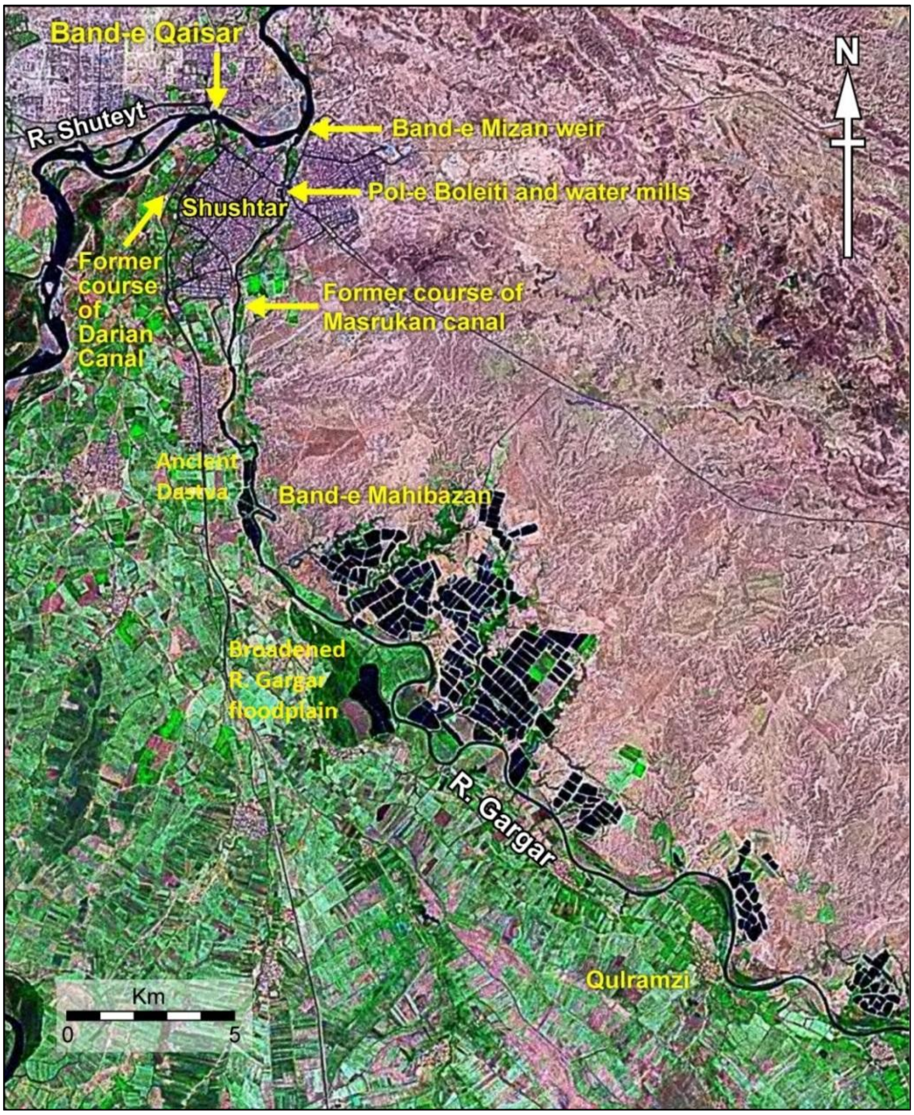

Figure 6.3 CORONA (1968) satellite image showing the Karun near-straight river course between the "Band of Ahvaz" (BA) and Kut-e Seyyed Saleh (KS) and the trace of the ancient East Bank Canal (EBC) which had an intake in northern Ahvaz (A) and photograph of the ruins of the "Band of Ahvaz" at low water (From Aleyasin, 2001)

downstream of the dam, the high rates of river incision associated with the clearer, "hungry" water emerging from the dam (Kondolf, 1997) produce high specific stream powers (about 16.3 - 67.3 W m^{-2}) and low average channel migration rates (less than 1.1 m yr^{-1} for the period 1966/1968 - 2001) (Table 6.2).

6.1.3.2 Ruins of major dams

There are the ruins of three major dams (or bunds) in the study area: the Band-e Qaisar or *shadhurvan* in Shushtar on the River Shuteyt on the fore-limb of the Shushtar Anticline (Section 4.2.3; Figure 6.2; Torfi et al., 2007; Verkinderen, 2009); the Band-e Mahibazan on the River Gargar (Figure 6.2; Moghaddam et al., 2005; Verkinderen, 2009; Moghaddam, in press); and the "Band of Ahvaz" or *shadhurvan* in Ahvaz on the River Karun across the Ahvaz Anticline (Figure 6.3; Ainsworth, 1838; Graadt van Roggen, 1905; GBNID, 1945; Aleyasin, 2001; Verkinderen, 2009; Walstra et al., 2010a). These ruins of major dams are characterised by a reservoir remnant upstream of the dam ruins, with an increase in channel width of about 45 % - 900 % (to channel widths of c. 101 m - 850 m) at channel distances of c. 1.5 km upstream of the ruins compared with c. 4.0 km upstream of the ruins (Table 6.2).

6.1.3.3 Major anthropogenic river channel straightening

There are four major near-straight river courses in the study area: the c. 19 km long near-straight N-S course between Band-e Qir and Veys (Figure 4.1 (d); Layard, 1846; Le Strange, 1905; Bakker, 1956; Alizadeh et al., 2004; Verkinderen, 2009); the c. 11 km long near-straight NNE-SSW course between the "Band of Ahvaz" and Kut-e Seyyed Saleh (Figure 6.3; Graadt van Roggen, 1905; Verkinderen, 2009; Walstra et al., 2010a); the c. 13 km long near-straight NE-SW course between Dorquain and Masudi (Figure 4.1 (e); Chesney, 1850; Gasche et al., 2005; Verkinderen, 2009); and the c. 18 km long near-straight NE-SW course of the Haffar cut upstream of Khorramshahr (Figure 4.1 (e); Curzon, 1890; Le Strange, 1905; Potts, 1994; Walstra et al, 2010a; Heyvaert et al, 2013). These near-straight river courses are considered to be mainly human-influenced due to historical records, near-straight alluvial channels being rare and usually temporary in nature (Frenette and Harvey, 1973; Rosgen, 1994; Wang and Ni, 2002), and the longest presumed natural near-straight river course in the study area (the River Dez across the Sardarabad Anticline) being only about 6 km long. These anthropogenic straightenings are characterised by very low channel sinuosity (generally less than c. 1.1) over more than 10 km river course length, a narrow channel-belt (average channel-belt width less than 1.1 km), and a relatively broad, shallow channel (mean channel width greater than c. 180 m, mean channel width:depth ratio greater than c. 20) with a tendency (along c. 70 % of the near-straight reach) for trapezoidal or rectangular channel cross-sections (Table 6.2).

6.1.3.4 Artificial river development

The only artificial river development in the study area is that of the c. 55 km long River Gargar between Shushtar and Band-e Qir. This developed from the ancient Masrukan canal system (probably mostly constructed during the Early Sassanian Period, c. 224 - 379 AD) when this monumental canal system probably fell into disuse in the 10th - 14th Centuries AD (Figure 4.1 (b) and Figure 6.2; Le Strange, 1905; Alizadeh et al., 2004; Bosworth, 1987; Moghaddam and Miri, 2007; Moghaddam, in press). This artificial river development is characterised by many human constructions and their traces associated with the river, including the Band-e Mizan weir, the Pol-e Boleiti dam-bridge, the Shushtar water mills, the ruins of the Band-e Mahibazan, canal traces on remote sensing images, canal remnants and spoil heaps, and archaeological settlement sites on its banks, such as the ruins of Askar Mukram and Dastva (Alizadeh et al., 2004; Moghaddam and Miri, 2007; Moghaddam, in press). It is also characterised by some prominent vertical river incision (about 2 m - 10 m or more below the surrounding plains), a narrow channel-belt (average channel-belt width less than 2.0 km), and low average channel migration rates (less than 0.5 m yr^{-1} for the period 1966/1968 - 2001) (Table 6.2). This very limited river channel lateral migration is manifest as meander development limited to migrations from a single, often straight, former course, and a lack of features of mature meandering channels, with an absence of meander cut-offs and oxbow lakes (Alizadeh et al., 204; Verkinderen, 2009).

6.2 River characteristics which help to differentiate between the influences of active folds and direct human impacts

Key river characteristics which help to differentiate between river incision across a fold, river diversion around a fold, and direct human modifications to rivers are summarised in Table 6.2. These characteristics are useful, though they need to be interpreted carefully.

Table 6.2 (a) Key characteristics (general river forms and human constructions) which help to differentiate between the influences of active folds and direct human impacts

Especially useful characteristics for discriminating are highlighted in ***bold and italics***
Useful characteristics for discriminating are highlighted in *italics*

Type of external factor influencing river reaches	**Characteristic of river** (general river forms and human constructions)			
	General river course direction (compass bearing in degrees)	**Channel sinuosity**	**Vertical river incision** (m)	**Human constructions (and their traces) associated with river reaches**
River incision across a fold	Reaches across fold axis: ***Generally approx. orthogonal (70° - 90°) to fold axis***	Reaches across fold axis: ***Generally less than 1.4*** (for reaches with no major direct human impacts, lowest value is 1.12) and ***reduced (by mean 0.368) compared to upstream and downstream***	Reaches across fold axis: *Generally prominent vertical river incision, c. 2 m - c. 7 m to 20 m or more* below surrounding plains	No consistent changes of note
River diversion around a fold	***Approx. parallel (0° - 20°) to fold axis upstream of fold nose, changing by approx. 20° - 70° to flow around fold nose***	Reaches across fold axis projection: Fairly wide range of values (for reaches with no major direct human impacts, range is c. 1.27 - 1.79) and *reduced (by mean 0.117) compared to upstream and downstream)*	No consistent changes of note	No consistent changes of note
Major dams	No consistent changes of note	Compared with prior to major dam: Slight decrease by c. 0.017 - 0.046 upstream of dam (associated with reservoir)	Within 2.5 km channel distance downstream of major dam: *Prominent vertical river incision, c. 3 m - c. 8 m to 20 m or more* below surrounding plains	***Major dam and reservoir***
Ruins of major dams	No consistent changes of note	No consistent changes of note	No consistent changes of note	***Ruins of major dam and reservoir remnant***
Major river channel straightening	No consistent changes of note	***Generally less than 1.1 over a greater than 10 km long river course***	No consistent changes of note	***Channel straightening***
Artificial river development	No consistent changes of note	Wide range of values (c. 1.07 - 3.20)	*Prominent vertical river incision, c. 2 m - c. 8.5 m to 10 m or more* below surrounding plains	***Many human constructions*** (including four major structures, many canal traces and remnants, and two large ancient towns)

Table 6.2 (b) Key characteristics (river hydrology and channel dimensions) which help to differentiate between the influences of active folds and direct human impacts

Type of external factor influencing river reaches	**Characteristic of river** (river hydrology, channel slopes and channel cross-sections)			
	Channel water surface slope ($m\ m^{-1}$)	**Channel width** (m)	**Channel width:depth ratio** (and **channel cross-sectional shape**)	**Specific stream power** ($W\ m^{-2}$)
River incision across a fold	Reaches across fold axis: ***Generally greater than 1.5 × 10^{-4} $m\ m^{-1}$***	No consistent changes of note	Reaches across fold axis: Less than 70 (variety of cross-sectional forms)	Reaches across fold axis: ***Gen. greater than 1.6 $W\ m^{-2}$*** and ***gen. increased (by mean 8.285) compared with upstr. & downstr.***
River diversion around a fold	Reaches across fold axis projection: ***Less than 1.3 × 10^{-4} $m\ m^{-1}$*** & ***generally reduced (by mean 1.11 × 10^{-4} $m\ m^{-1}$) compared to upstream and downstream***	No consistent changes of note	Reaches across fold axis projection: Less than 70 (variety of cross-sectional forms)	Reaches across fold axis projection: Wide range of values, ***all less than 2.5 $W\ m^{-2}$***
Major dams	***Large drop in river water levels across major dam of the order of c. 3 m - 15 m***	Within reservoir (up to c. 8.3 km long) *upstream* of major dam: *Widening by c. 0 - 196 m* Within 2.5 km channel distance downstream of dam: *Less than about 160 m* (range c. 62 m - 154 m; c. 20 m - 57 m for R. Gargar)	Within 2.5 km channel distance downstream of major dam: *Less than 50*, with range of values c. 3 - 50 (*mainly triangular* cross-sections)	Within 6.0 km channel distance downstream of major dam: ***Greater than about 16.0 $W\ m^{-2}$*** (range of values c. 16.3 - 67.3 $W\ m^{-2}$)
Ruins of major dams	No consistent changes / very slight drop in river water levels across the dam ruins of c. 0 - 1 m	Within about 1.5 km channel distance *upstream*: *Widening to c. 101 m - 850 m* associated with the reservoir remnant	No consistent changes of note	No consistent changes of note
Major river channel straightening	No consistent changes of note	***Mean channel width of greater than about 180 m*** (range c. 140 m - 500 m)	***Mean channel width:depth ratio greater than about 20***, with range of values c. 7 - 150 (***trapezoidal or rectangular cross-sections along more than 70 % of its length***)	No consistent changes of note
Artificial river development	No consistent changes of note	Less than about 80 m	Generally less than 20 (though range c. 7 - 63) (mainly triangular & other cross-sections)	No consistent changes of note

Table 6.2 (c) Key characteristics (river migration and river sedimentology) which help to differentiate between the influences of active folds and direct human impacts

D_{fine} is mean grain size for fine gravels, sands and muds (µm)

Type of external factor influencing river reaches	**Characteristic of river** (river migration and river sedimentology)			
	Average channel-belt width (km)	**Average channel migration rate 1966/68 - 2001** (m yr^{-1})	**Average grain size of channel bed surface sediments**	**Average grain size of channel bank sediments**
River incision across a fold	Reaches across fold axis**: *Less than 2.7 km (generally less than 1.5 km)*** and ***reduced (by mean 1.2 km) compared to upstream and downstream***	Reaches across fold axis: *Generally less than 1.8 m yr^{-1}*	No consistent changes / slightly increased (e.g. D_{fine} increases from average of c. 38.2 µm to c. 81.7 µm for R. Karun across axis of Ahvaz Anticline) across fold axis compared to upstream and downstream (21 % of cases) / slightly decreased just upstream of fold compared with reaches further upstream (37 % of cases)	No consistent changes / slightly increased (e.g. D_{fine} increases from average of c. 21.3 µm to c. 73.4 µm for R. Karun across axis of Ahvaz Anticline) across fold axis compared to upstream and downstream (31 % of cases) / slightly decreased just upstream of fold compared with reaches further upstream (37 % of cases)
River diversion around a fold	Reaches across fold axis proj.: Wide range of values, *mostly greater than 2.7 km*	Reaches across fold axis projection: Wide range of values, *mostly greater than 1.8 m yr^{-1}*	No consistent changes of note	No consistent changes of note
Major dams	No consistent changes of note	Within 6.0 km channel distance of major dam: Low rates of *less than c. 1.1 m yr^{-1}* (range c. 0.53 m yr^{-1} - 1.10 m yr^{-1}; c. 0.08 m yr^{-1} for R. Gargar)	Not known (probably decrease in grain size just upstream of major dam and increase in grain size just downstream of dam)	Not known (probably decrease in grain size just upstream of major dam and increase in grain size just downstream of dam)
Ruins of major dams	No consistent changes of note	No consistent changes of note	No consistent changes of note	No consistent changes of note
Major river channel straightening	***Less than 1.1 km*** (range of values c. 0.22 km - 1.09 km)	*Less than c. 3.5 m yr^{-1}* (and generally less than c. 1.0 m yr^{-1})	No consistent changes of note / slightly decreased (e.g. D_{fine} decreases from average of c. 49.0 µm to c. 25.1 µm for R. Karun between Band-e Qir and Veys) along near-straight reach compared to upstream & downstream	No consistent changes of note / slightly decreased (e.g. D_{fine} decreases from average of c. 54.9 µm to c. 25.8 µm for R. Karun between Band-e Qir and Veys) along near-straight reach compared to upstream & downstream
Artificial river development	***Less than 2.0 km*** (mostly less than 0.6 km)	Very low rates of ***less than 0.5 m yr^{-1} throughout*** (and mostly less than 0.2 m yr^{-1})	No consistent changes of note	No consistent changes of note

Firstly, there are overlaps and interactions between some of the categories. Folds within a basin are often quite closely spaced, so the river reaches downstream of a river incision may be the same as the river reaches upstream of a river diversion. Major dams may frequently be located where a river incises across a fold axis, due to a number of characteristics, such as outcrops of firm bedrock and narrow valleys and channel-belts, which are favourable for dam construction. Major anthropogenic river channel straightening may frequently be located where a river incises across a fold axis, probably due to channel meandering being inhibited to maximise stream powers and river erosion in response to active uplift.

Secondly, care is needed to avoid circular reasoning. For instance, it may be reasoned that humans cause channel straightening by cuts, diversions into former canals, or canalisation, thus all channels of very low sinuosity of less than 1.1 are due to the human impact of major anthropogenic river channel straightening. However, such reasoning is flawed, since straight rivers of low sinuosity may occur in nature due to factors like very cohesive sediments, bedrock outcrops, or tectonic influences like faults and zones of uplift (Schumm, 1981; Burbank and Tahirkheli, 1985; Burbank and Anderson, 2001). Nevertheless, long straight alluvial river courses are rare in nature (Wang and Ni, 2002) and tend to be associated with braided channel belts rather than single course meandering river systems (e.g. the braided/straight Paraná River studied by Orfeo and Stevaux, 2002). Hence, as stated in Table 6.2, it is better to consider that, *generally*, channel sinuosity of less than 1.1 over a river course of greater than 10 km length is a characteristic of major anthropogenic river channel straightening.

Thirdly, some characteristics are more useful in differentiating between the categories than others. For instance, the characteristic of channel sinuosity generally less than 1.1 over greater than 10 km river course length for major anthropogenic straightening is highlighted in ***bold and italics*** in Table 6.2 as it is very useful for discrimination, since channel sinuosity that low is not found over such long distances for the other categories. Prominent vertical river incision (greater than about 2m or 3 m below the surrounding plains) is highlighted in *italics* in Table 6.2 as it is useful in discriminating between categories, since it may be present for the three categories of river incision across a fold, major dams, and major anthropogenic river channel straightening. By contrast, the characteristic of a wide range of values (c. 1.07 - 3.20) for channel sinuosity for artificial river development is in normal text in Table 6.2 as it is poor for discrimination, since it overlaps with most of the other categories.

6.3 Statistical analyses of characteristics of the rivers and structural geology

To investigate which characteristics are especially discriminative between the river responses of river incision across a fold and river diversion around a fold, statistical analyses have been applied (Upton and Cook, 1996; Rogerson, 2006; Salkind, 2010). There is a comparison between groups of river reaches for categories of: *river incision* for reaches across the fold axis, *river diversion* for reaches across the fold axis projection, *major anthropogenic river channel straightening* (since this may not always be clearly human-influenced and may be related to interactions with fold uplift), and *minimal influences from active folds and direct human modifications* (as a control). From the results in Table 6.2, Tables 4.13 to 4.15, and Appendices 5 and 6, it is evident that certain characteristics may be more useful in discriminating between the two categories of river incision and river diversion, and between all four of the categories.

6.3.1 Analysis of variance (ANOVA)

Analysis of variance (ANOVA) has been applied to determine whether there are statistically significant differences between the four categories of river reaches for each of these useful characteristics of the river and the structural geology, and the findings are summarised in Table 6.3.

The findings shown in Table 6.3 indicate that there are eight characteristics which exhibit differences between categories (either between river incision and river diversion or between all four categories) which are statistically significant (p-value ≤ 0.05 which is equivalent to a 5 % significance level) or nearly statistically significant (t statistic exceeds critical value or p-value ≤ 0.06) (Salkind, 2010). These eight characteristics are: *channel sinuosity*, *average channel-belt width*, *channel-belt width* at location of fold axis or midpoint of near-straight reach or minimally influenced reach, *valley depth over the extent of the channel-belt*, *general river course direction*, *average grain size of channel bank sediments*, *distance from fold "core" to river crossing location*, and *"river crossing location ratio"*. These eight characteristics with differences of greater statistical significance are likely to be useful in discriminating between the different categories of river reaches.

Table 6.3 Analysis of variance (ANOVA) between categories of river reaches for different characteristics of the river or structural geology

Characteristic of the river or characteristic of structural geology	**ANOVA between two categories of river incision** (across fold axis) **and river diversion** (across fold axis projection)	**ANOVA between four categories of river incision** (across fold axis)**, river diversion** (across fold axis projection)**, major anthropogenic river channel straightening,** and **minimal influences**
Channel sinuosity	F = 1.275 F *crit* = 4.844 p-value = 0.283	**F = 3.847 F *crit* = 3.127 p-value = 0.026**
Average channel-belt width (km)	*F = 3.234 F crit = 4.844 p-value = 0.100 t = -1.798 t crit = 1.796*	**F = 5.386 F *crit* = 3.127 p-value = 0.007**
Channel-belt width at location of fold axis or midpoint of near-straight reach (m)	**F = 4.924 F *crit* = 4.844 p-value = 0.048**	**F = 4.213 F *crit* = 3.127 p-value = 0.019**
Valley depth over extent of channel-belt (m)	F = 1.703 F *crit* = 4.844 p-value = 0.219	*F = 3.046 F crit = 3.127 p-value = 0.054*
General river course direction (bearing in degrees)	F = 1.633 F *crit* = 4.844 p-value = 0.228	**F = 5.897 F *crit* = 3.127 p-value = 0.005**
General river course direction change compared with reaches just upstream (bearing in degrees)	F = 0.560 F *crit* = 4.844 p-value = 0.470	F = 0.215 F *crit* = 3.127 p-value = 0.885
Channel water surface slope (m m^{-1})	F = 1.897 F *crit* = 4.844 p-value = 0.196	F = 1.535 F *crit* = 3.127 p-value = 0.238
Channel width (m)	F = 0.015 F *crit* = 4.844 p-value = 0.906	F = 0.596 F *crit* = 3.127 p-value = 0.625
Channel width:depth ratio	F = 0.039 F *crit* = 4.844 p-value = 0.847	F = 2.734 F *crit* = 3.127 p-value = 0.072
Specific stream power (W m^{-2})	F = 1.340 F *crit* = 4.844 p-value = 0.271	F = 1.052 F *crit* = 3.127 p-value = 0.392
Stream power per unit length (W m^{-1})	F = 2.848 F *crit* = 4.844 p-value = 0.120	F = 1.423 F *crit* = 3.127 p-value = 0.267
Greatest channel bank migration distance 1966/1968 - 2001 (m)	F = 0.502 F *crit* = 4.844 p-value = 0.493	F = 1.509 F *crit* = 3.127 p-value = 0.244
Average channel migration rate 1966/1968 - 2001 (m yr^{-1})	F = 1.789 F *crit* = 4.844 p-value = 0.208	F = 1.837 F *crit* = 3.127 p-value = 0.175
Average grain size of channel bed surface sediments (Code from 1 - smallest to 10 - largest)	F = 3.092 F *crit* = 4.844 p-value = 0.106	F = 2.147 F *crit* = 3.127 p-value = 0.128
Average grain size of channel bank sediments (Code from 1 - smallest to 10 - largest)	*F = 3.373 F crit = 4.844 p-value = 0.093 t = 1.836 t crit = 1.796*	F = 2.270 F *crit* = 3.127 p-value = 0.113
Width of geological structure (or its projection) at river crossing location (distance in km between extent of fold limbs)	F = 0.568 F *crit* = 4.844 p-value = 0.467	
Distance from fold "core" to river crossing location (km along fold axis or its projection)	**F = 5.568 F *crit* = 4.844 p-value = 0.038**	
Distance from fold "nose" to river crossing location (km along fold axis or its projection)	F = 1.294 F *crit* = 4.844 p-value = 0.279	
"River crossing location ratio" (fold "core" to river crossing distance/ fold "core" to fold "nose" distance expressed as %)	**F = 19.883 F *crit* = 4.844 p-value = 0.001**	
Distance from fold "core" to river basin margin (km)	F = 0.369 F *crit* = 4.844 p-value = 0.556	
Estimate of degree of general erosion resistance of fold (Code from 1 - least to 6 - greatest)	F = 0.445 F *crit* = 4.844 p-value = 0.519	

Key to abbreviations used in Table 6.3

F Obtained F value (mean sums of squares due to between-group differences/ mean sums of squares due to within-group differences)

F crit The critical *F* value needed to reject the null hypothesis

p-value The level of significance of the *F* value (p = 0.05 is equivalent to a 5 % significance level or a 95 % confidence level)

t Obtained value of *t* statistic (Student's *t*-test which compares the actual difference between two means in relation to the variation in the data, expressed as the standard deviation of the difference between the means)

t crit The critical *t* statistic value needed to reject the null hypothesis for a one-tailed test (characteristic has $^{+}$ve values only)

Bold text indicates statistically significant: *p*-value ≤ 0.05 (equivalent to a 5 % significance level or a 95 % confidence level or better)

Italic text indicates nearly statistically significant: *t* statistic exceeds critical value or *p*-value ≤ 0.06 (equivalent to 6 % significance level or 94 % confidence level or better) (Upton and Cook, 1996; Rogerson, 2006; Salkind, 2010)

Codes for average grain size (from 1 - smallest to 10 - largest) of channel bed surface sediments and channel bank sediments:

1.0 Mainly muds
2.0 Mainly muds, with some sands
3.0 Muds and sands
3.5 Sands and muds
4.0 Mainly sands and muds
4.5 Mainly sands and silts
5.0 Mainly sands and muds, slight gravels
5.5 Mainly sands and silts, few gravels
6.0 Mainly sands and muds, partly sands and gravels
7.0 Partly sands and silts, partly gravels
7.5 Partly gravels and sands, partly fine sands and muds
8.0 Partly gravels & sands, partly sands & silts
8.5 Partly gravels (esp. pebbles), partly sands and silts
9.5 Mainly gravels (esp. pebbles with some cobbles), some sands and silts
10.0 Mainly gravels (esp. pebbles and cobbles), few sands and silts

---

6.3.2 Comparison of categories using box-and-whisker plots

The results for these eight characteristics (plus, for completeness, the two characteristics of specific stream power and average grain size of channel bed surface sediments) are shown as box-and-whisker plots for the different categories of river reaches in Figures 6.4 to 6.13. In these plots, the "box" indicates the 25th percentile, 50th percentile (the median) and 75th percentile, and the "whiskers" indicate the minimum value, 10th percentile, 90th percentile and maximum value (McGill et al., 1978; Frigge et al., 1989). On Figures 6.4 to 6.13 a summary of the results for ANOVA is included next to the box-and-whisker plots.

N.B.: In the box-and-whisker plots of Figure 6.4 to Figure 6.13, the results for river reaches are displayed in up to four categories; with the "box" indicating the 25th percentile, 50th percentile (the median) and 75th percentile, and the "whiskers" indicating the minimum value, 10th percentile, 90th percentile and maximum value

Figure 6.4
Channel sinuosity

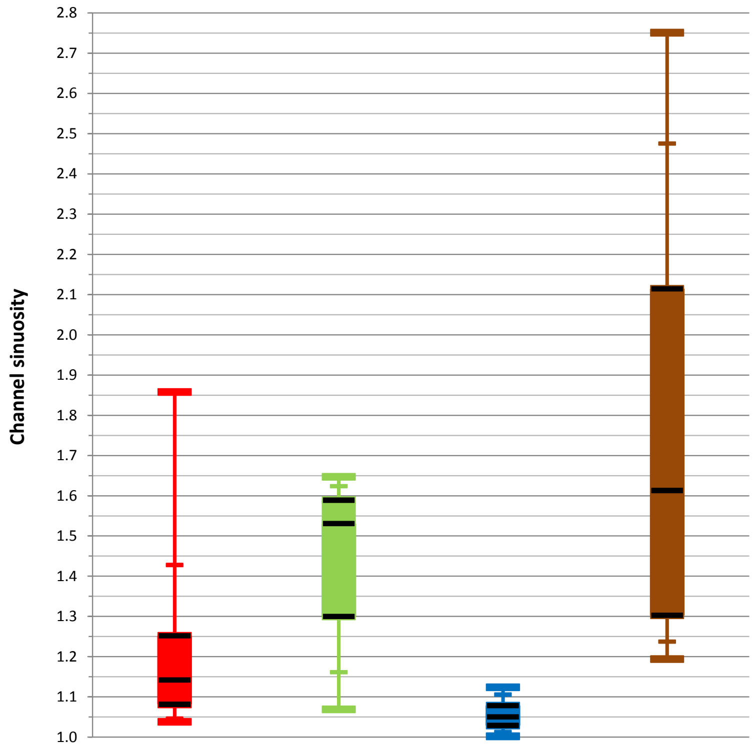

ANOVA (Analysis of variance)
Between the two categories of river incision across a fold and river diversion around a fold
F = 1.275 *F crit* = 4.844 *p*-value = 0.283
Between all four categories
F = 3.847 *F crit* = 3.127 *p*-value = 0.026

Correlation (best straight line) with river valley distance from nearest fold axis to mid-point of river reach (km)
For river incision only *r* squared = 0.258
For river diversion only *r* squared = 0.014
For all four categories *r* squared = 0.023

River incision (across fold axis)
River diversion (across fold axis projection)
Major anthropogenic river channel straightening
Minimal influences from active folds and direct human modifications

Figure 6.5
Average channel-belt width (km)

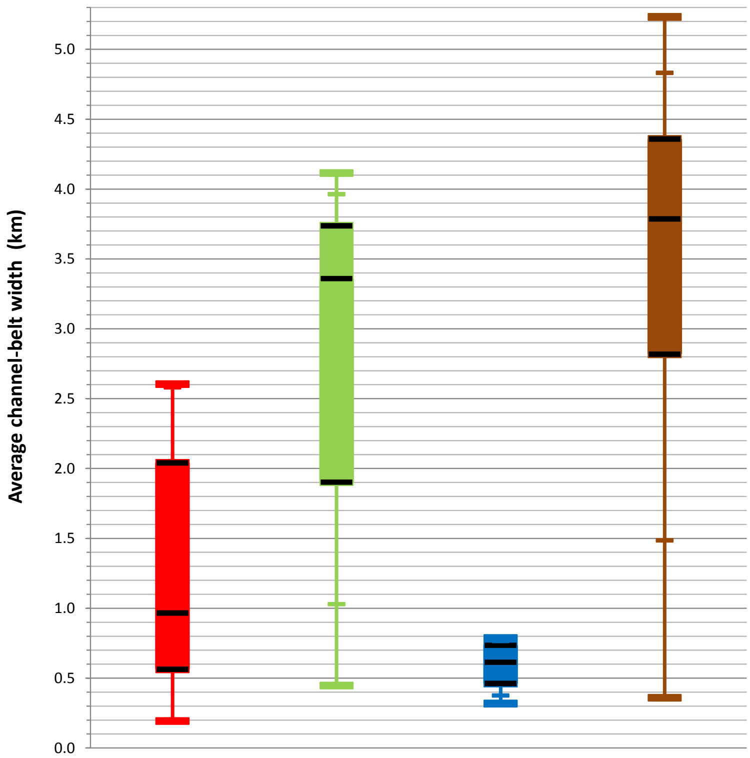

ANOVA (Analysis of variance)
Between the two categories of river incision across a fold and river diversion around a fold
F = 3.234 *F crit* = 4.844 *p*-value = 0.100
Between all four categories
F = 5.386 *F crit* = 3.127 *p*-value = 0.007

Correlation (best straight line) with river valley distance from nearest fold axis to mid-point of river reach (km)
For river incision only *r* squared = 0.179
For river diversion only *r* squared = 0.056
For all four categories *r* squared = 0.027

River incision (across fold axis)
River diversion (across fold axis projection)
Major anthropogenic river channel straightening
Minimal influences from active folds and direct human modifications

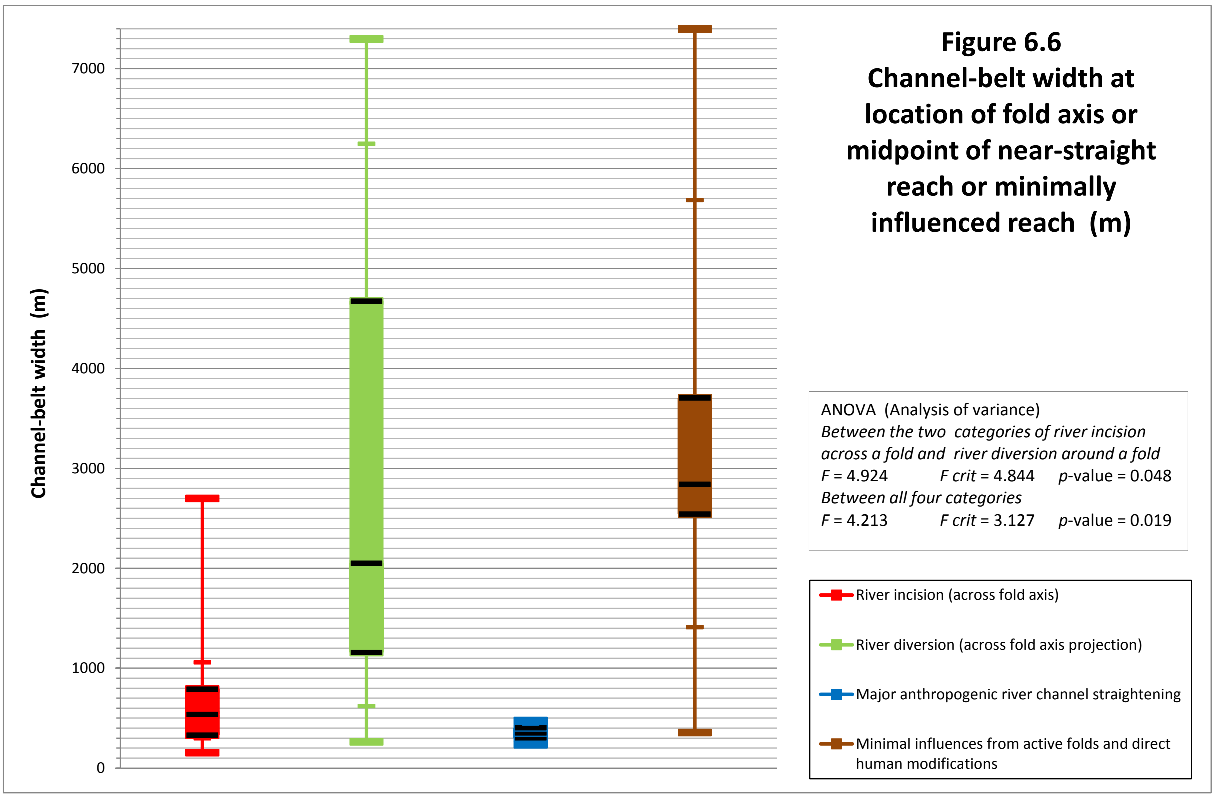

Figure 6.6
Channel-belt width at location of fold axis or midpoint of near-straight reach or minimally influenced reach (m)
Channel-belt width (m)
7000
6000
5000
4000
3000
2000
1000
0
ANOVA (Analysis of variance)
Between the two categories of river incision across a fold and river diversion around a fold
F = 4.924 F crit = 4.844 p-value = 0.048
Between all four categories
F = 4.213 F crit = 3.127 p-value = 0.019
River incision (across fold axis)
River diversion (across fold axis projection)
Major anthropogenic river channel straightening
Minimal influences from active folds and direct human modifications

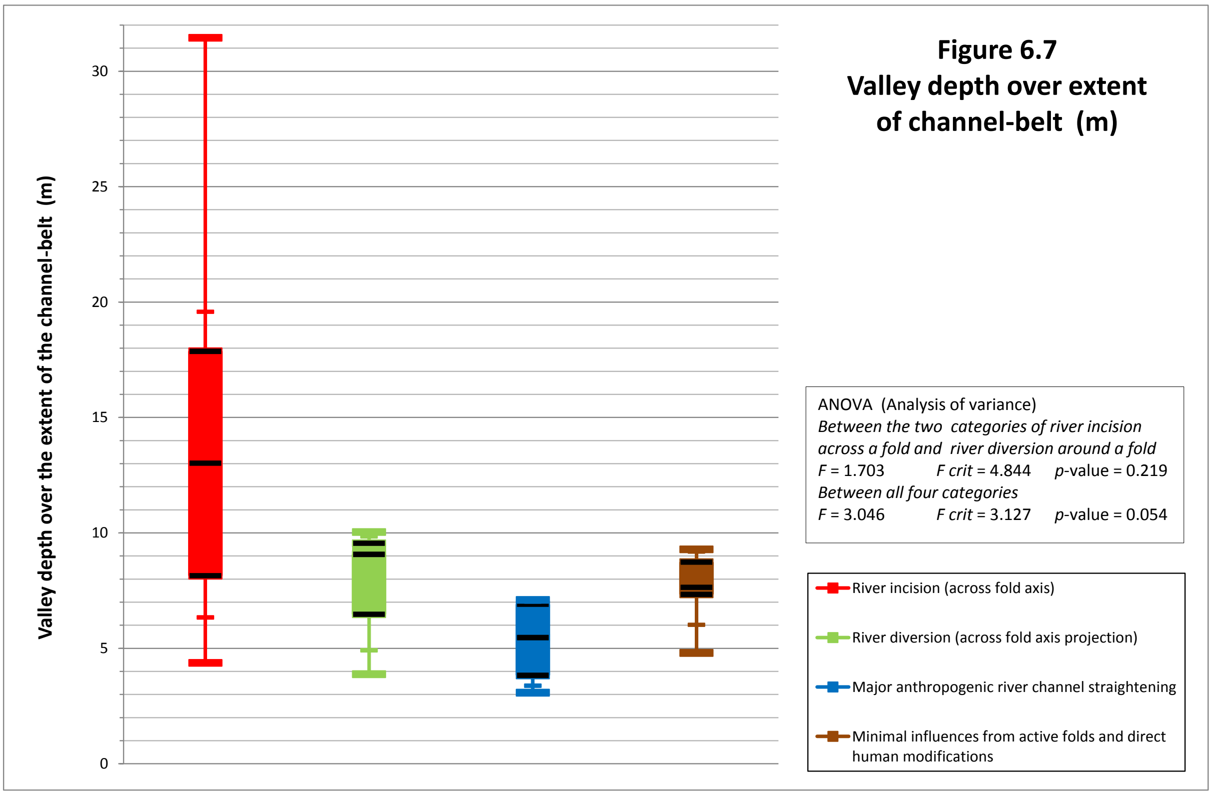

Figure 6.7
Valley depth over extent of channel-belt (m)
Valley depth over the extent of the channel-belt (m)
30
25
20
15
10
5
0
ANOVA (Analysis of variance)
Between the two categories of river incision across a fold and river diversion around a fold
F = 1.703 F crit = 4.844 p-value = 0.219
Between all four categories
F = 3.046 F crit = 3.127 p-value = 0.054
River incision (across fold axis)
River diversion (across fold axis projection)
Major anthropogenic river channel straightening
Minimal influences from active folds and direct human modifications

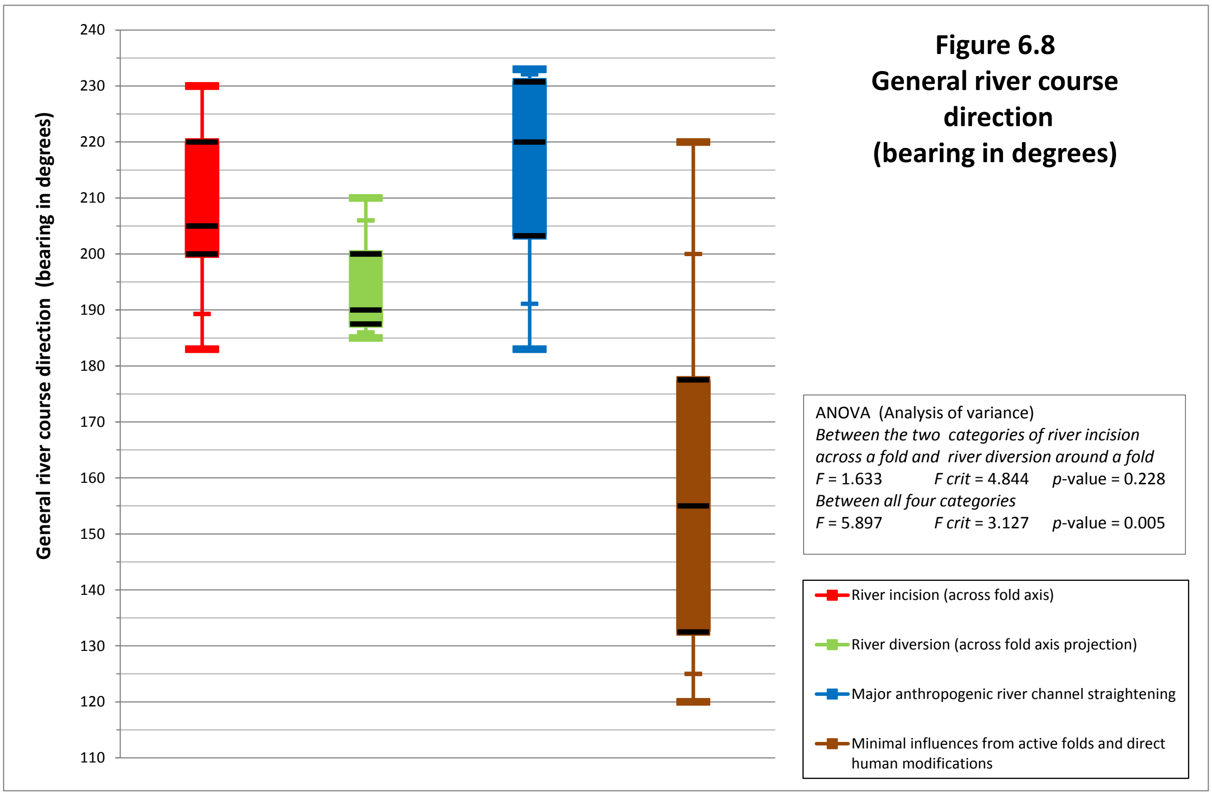

Figure 6.8
General river course direction
(bearing in degrees)

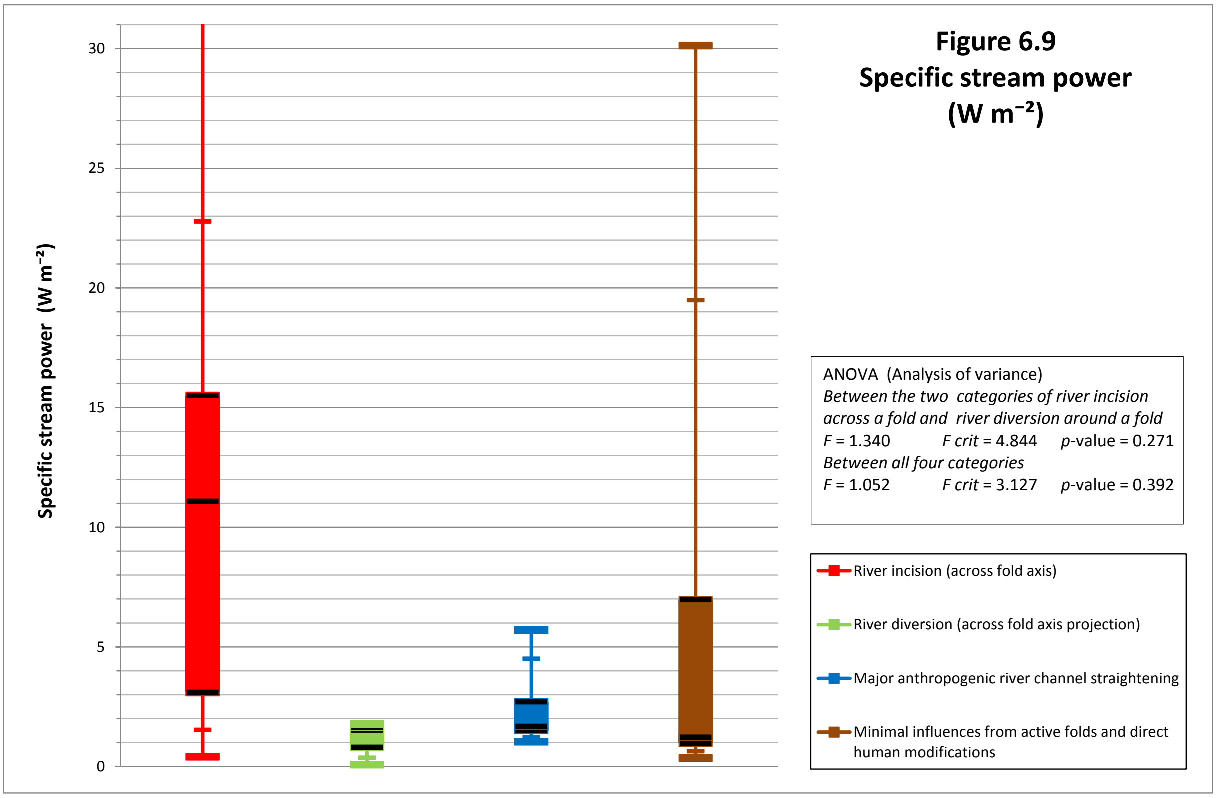

Figure 6.9
Specific stream power
($W\ m^{-2}$)

N.B.: In Figure 6.10 and Figure 6.11 the codes for average grain size range from 1.0 for mainly muds, to 3.5 for sands and muds, to 5.0 for mainly sands and muds with slight gravels, to 10.0 for mainly gravels with few sands and silts. Full details of the codes are given with Table 6.3.

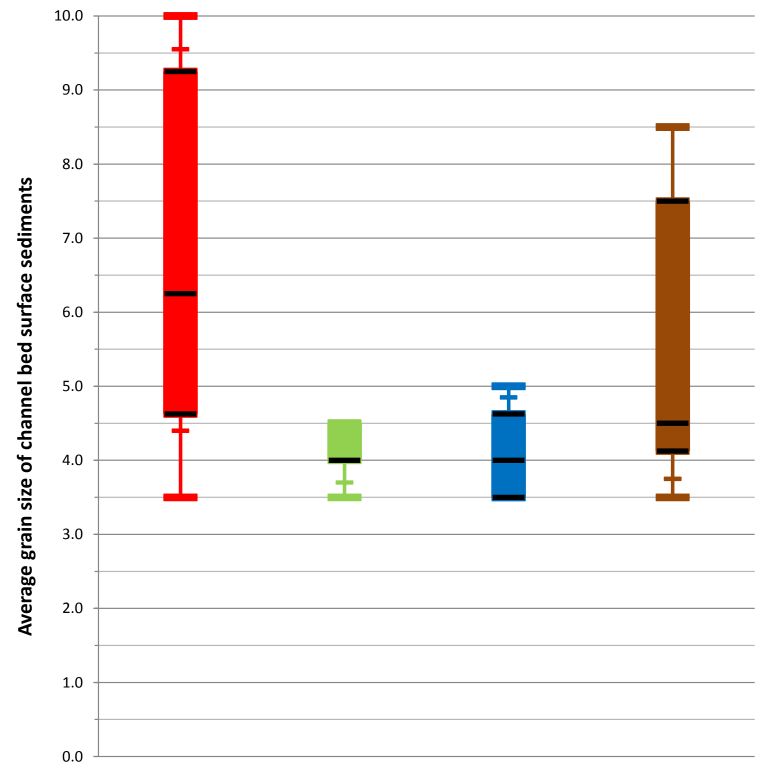

Figure 6.10
Average grain size of channel bed surface sediments (Code from 1 - smallest to 10 - largest)

ANOVA (Analysis of variance)
Between the two categories of river incision across a fold and river diversion around a fold
F = 3..092 *F crit* = 4.844 *p*-value = 0.106
Between all four categories
F = 2.147 *F crit* = 3.127 *p*-value = 0.128

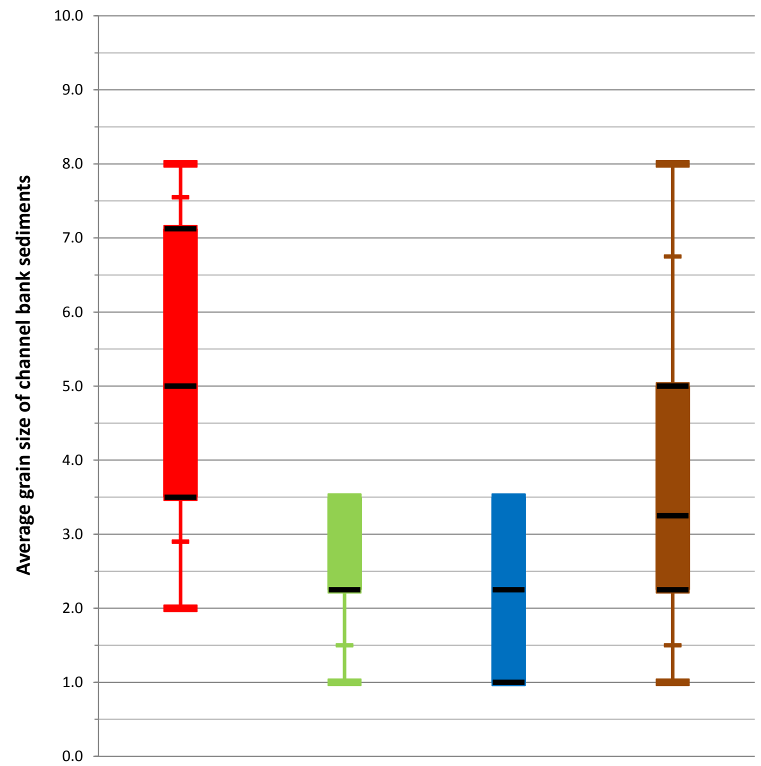

Figure 6.11
Average grain size of channel bank sediments (Code from 1 - smallest to 10 - largest)

ANOVA (Analysis of variance)
Between the two categories of river incision across a fold and river diversion around a fold
F = 3.373 *F crit* = 4.844 *p*-value = 0.093
Between all four categories
F = 2.270 *F crit* = 3.127 *p*-value = 0.113

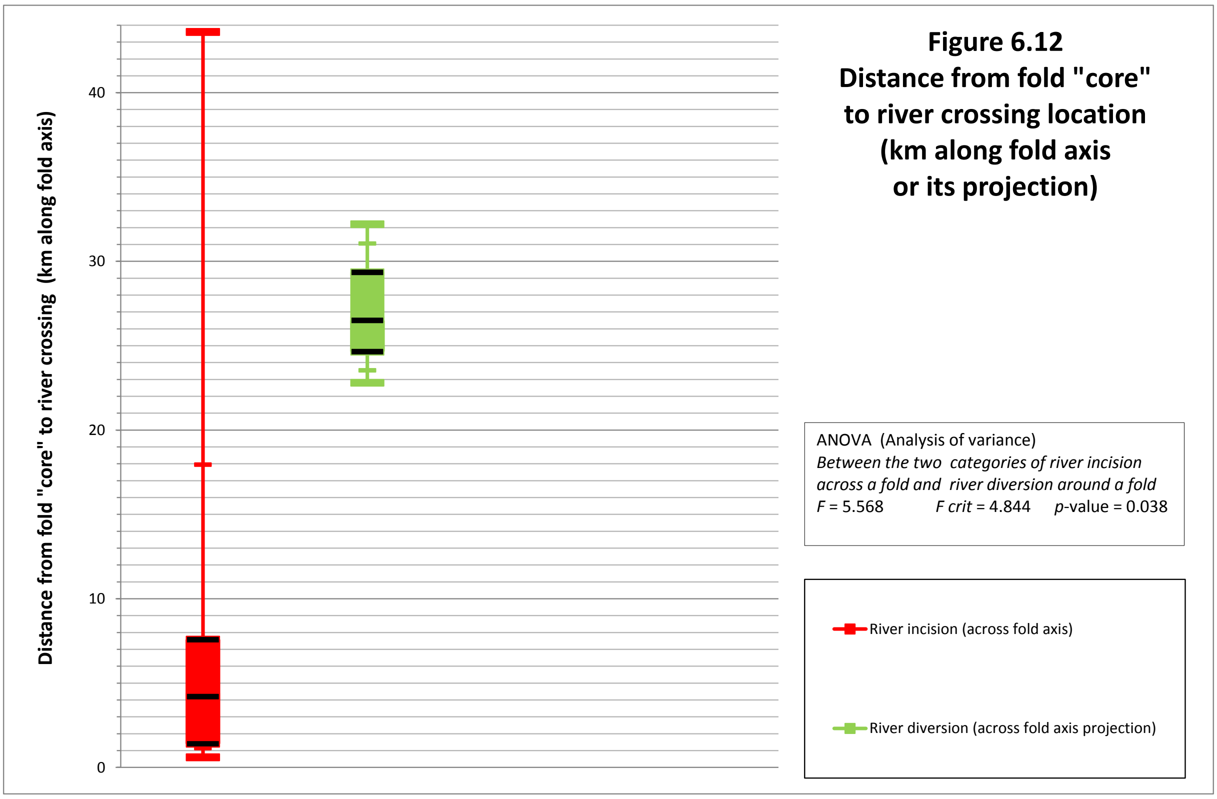
Figure 6.12
Distance from fold "core" to river crossing location (km along fold axis or its projection)
Distance from fold "core" to river crossing (km along fold axis)
0
10
20
30
40
ANOVA (Analysis of variance)
Between the two categories of river incision across a fold and river diversion around a fold
F = 5.568 F crit = 4.844 p-value = 0.038
River incision (across fold axis)
River diversion (across fold axis projection)

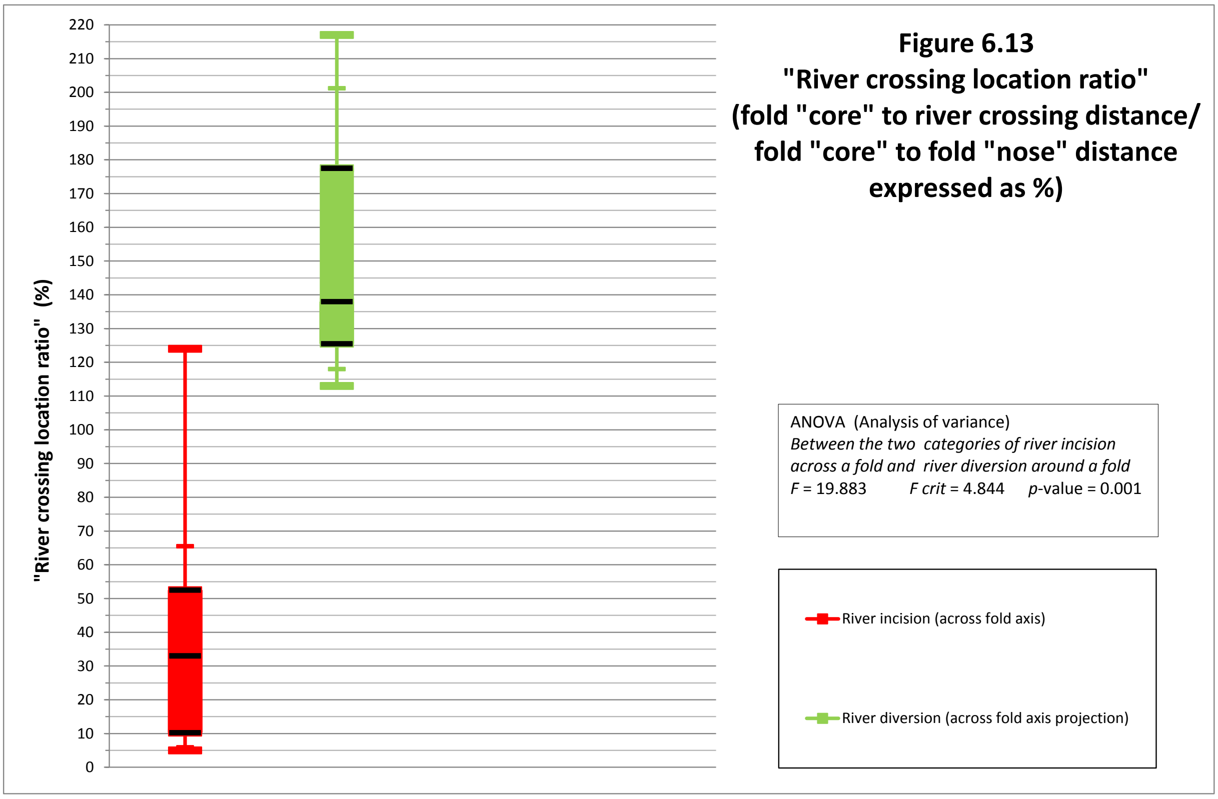
Figure 6.13
"River crossing location ratio" (fold "core" to river crossing distance/ fold "core" to fold "nose" distance expressed as %)
"River crossing location ratio" (%)
0
10
20
30
40
50
60
70
80
90
100
110
120
130
140
150
160
170
180
190
200
210
220
ANOVA (Analysis of variance)
Between the two categories of river incision across a fold and river diversion around a fold
F = 19.883 F crit = 4.844 p-value = 0.001
River incision (across fold axis)
River diversion (across fold axis projection)

N.B.: In the scatter plots of Figure 6.14 and Figure 6.15 for river reaches associated with river incision across a fold, the black line is a straight regression line through the points and r^2 is the value of Pearson's product-moment correlation coefficient squared

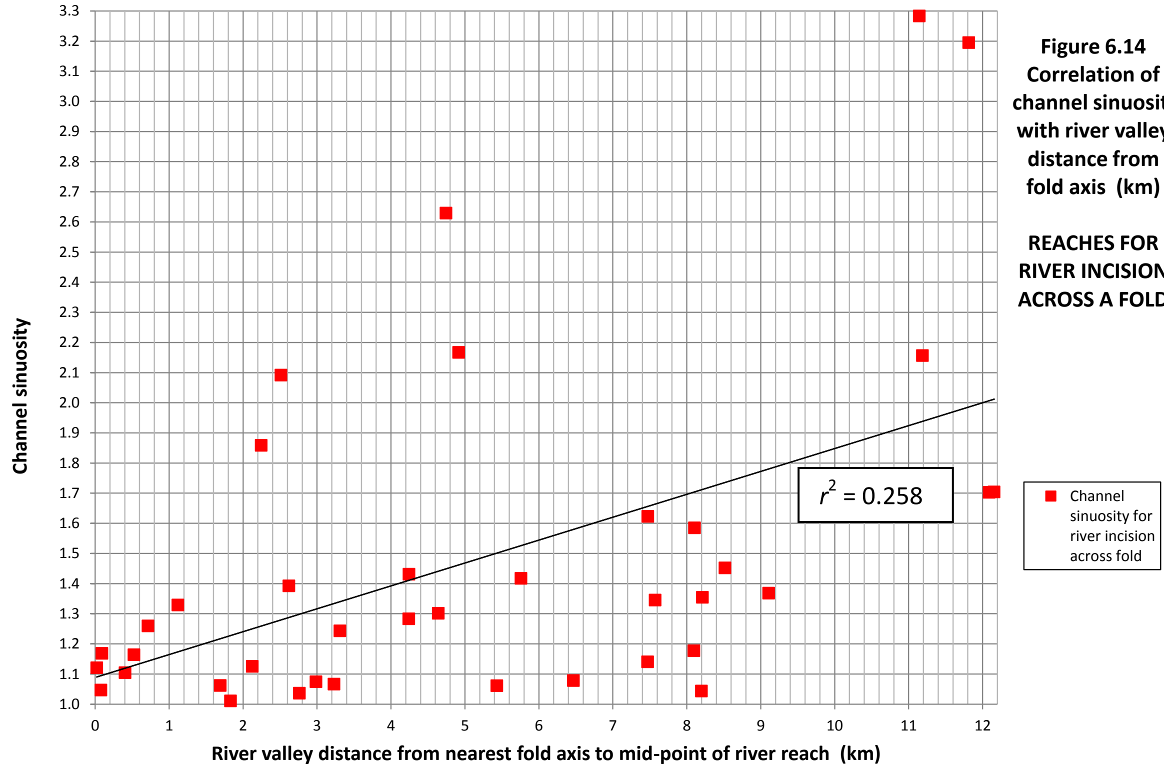

Figure 6.14
Correlation of channel sinuosity with river valley distance from fold axis (km)

REACHES FOR RIVER INCISION ACROSS A FOLD

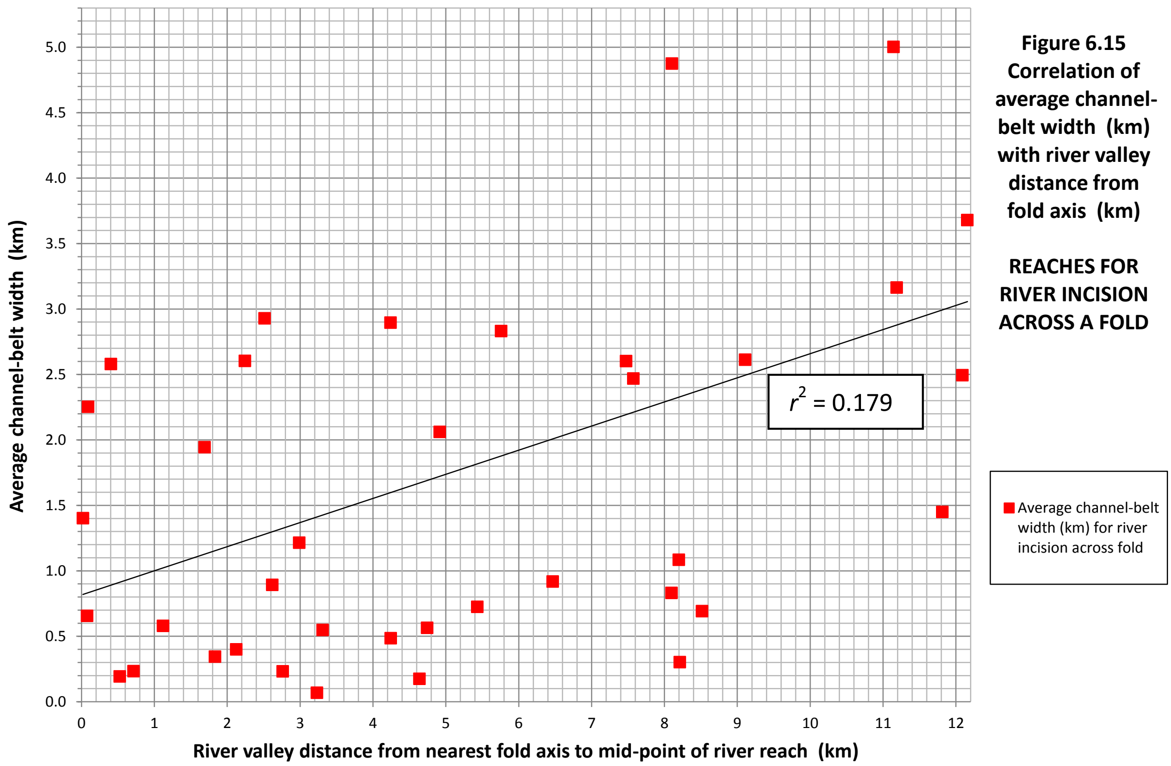

Figure 6.15
Correlation of average channel-belt width (km) with river valley distance from fold axis (km)

REACHES FOR RIVER INCISION ACROSS A FOLD

6.3.3 Correlation with river valley distance from the nearest fold axis

On Figure 6.4 (channel sinuosity) and Figure 6.5 (average channel-belt width), the values of r^2 (Pearson's product-moment correlation coefficient squared, or the coefficient of determination; Salkind, 2010) are included for a linear correlation between the river characteristic and river valley distance from the nearest fold axis (best straight line through a scatter plot) (Rogerson, 2006).

For all of the river characteristics, the only notable linear correlation with a value of r^2 of just greater than 0.25 (usually indicative of a moderate relationship; Salkind, 2010), is that between channel sinuosity and river valley distance from the nearest fold axis out to a distance of 12.2 km, for the category of river incision across a fold. The scatter plot with this correlation is shown in Figure 6.14. A similar linear correlation, though with a lesser value of r^2 of 0.179 (usually indicative of a weak to moderate relationship; Salkind, 2010), is present for average channel-belt width for the category of river incision across a fold, as shown in the scatter plot of Figure 6.15.

6.4 Discriminating between the river responses of river incision across a fold and river diversion around a fold

The ANOVA findings in Table 6.3 indicate that there are only three characteristics which have **statistically significant** differences at the 5 % significance level (or 95 % confidence level) between categories of river reaches for river incision across a fold and river diversion around a fold. These three characteristics are: *"river crossing location ratio"*, *distance from fold "core" to river crossing location*, and *channel-belt width*.

It is to be expected that *"river crossing location ratio"* discriminates between the two categories of river reaches, since river incision naturally occurs between the fold "core" and the fold "nose" (crossing ratio of less than 100 %) and river diversion naturally occurs beyond the fold "nose" (crossing ratio of more than 100 %). The apparent exception of the River Gargar incision across the Kupal Anticline (case F) is due to the fold extending further to the NW under Quaternary sediments than its indicated extent on geological maps. Nevertheless, it is interesting that the two populations are so clearly divided by "river crossing location ratio", as shown in Section 6.1.2, with a low mean value of 38 ± 36 % for river incision across a fold, indicating that river incision preferentially occurs nearer to the fold "core" than the fold "nose" for these young and emerging folds. This is also shown by *distance from the fold "core" to the river crossing location* discriminating between river incision across a fold and river diversion around a fold at the 5 % significance level. As shown in Section 6.1.2, river incision across a fold is characterised by a river crossing that is less than 16.0 km from the fold "core", and river diversion around a fold is characterised by a river crossing that is more than 22.0 km from the fold "core". These results and the ANOVA findings clearly indicate that there is tendency for a major river to incise across a fold at or near to the location of the fold "core". Since the folds in this study are all in early stages of their development, this indicates that major river incision across a fold, at, or near, the fold "core" is initiated at a very early stage in fold development, probably when the fold is emerging on the ground surface.

The third characteristic which is significantly different at the 5 % significance level for river incision and river diversion is ***channel-belt width*** at the location of the fold axis. As shown in Table 6.2 and Table 6.3, channel-belt width is an important characteristic for discriminating between river incision across a fold and river diversion around a fold. Channel-belt width at the location of the fold axis is significantly different between the two categories of river incision and river diversion, and also between these categories and major anthropogenic river channel straightening and minimal influences from active folds and direct human impacts for the mid-point of the reach. *Average channel-belt width* across a fold axis or its projection may have a wide range of values for river diversion. However, for river incision, average channel-belt width is always (100 % of cases) less than 2.7 km across the fold axis (and in 70 % of cases it is less than 1.5 km), and it is generally (75 % of cases) reduced (by a mean value of 1.2 km) compared with reaches just upstream and downstream of the fold. These findings for river incision are consistent with broader channel-belts immediately upstream and downstream of the fold due to increased aggradation to maintain foreland-dipping channel slopes across the fold, and narrow channel-belts across the fold due to increased erosion across the fold to keep pace with fold uplift (Burbank et al., 1996; Holbrook and Schumm, 1999; Douglass and Schmeeckle, 2007). Hence, channel-belt width may act as a statistically significant threshold which needs to be crossed for a river to incise across an active fold. For the folds of this study (with uplift rates of about 0.1 - 2.3 mm yr^{-1}) and the major rivers of this study (with mean annual water discharges of approximately 230 m^3s^{-1} and 575 m^3s^{-1}), an average channel-belt width of less than 2.7 km needs to be maintained across the surface expression of the fold if the river is to incise across the fold in the long-term, over timescales of centuries and millennia (Wright, 1969; PGL, 2004; Lahiri and Sinha, 2012).

A narrow channel-belt is required for the maintenance of a major river course across an active fold over long-term, mainly millennial, timescales because it entails limited lateral migration of the river, thus focussing river incision across the fold at one location (or “water gap”). If the channel-belt were wide (wider than about 2.7 km in this study), then, in the long-term, the proportion of the energy of the river expended in lateral migration and in erosion and removal of sediment over a large area would be too great to maintain river incision in response to fold uplift. It is a narrow channel-belt which is a key geomorphological characteristic, since channel-belts change over relatively long timescales (mainly decades and centuries; Wright, 1969; PGL, 2004) that are similar, though less than, the long timescales (mainly centuries and millennia; Burbank and Anderson, 2001) of the mainly gradual, aseismic movements of fold uplift. The importance of channel-belt width in fold-river interactions is demonstrated in the graphs of Figures 4.35 to 4.37, with a prominent general pattern of low values of average channel-belt width at locations where a river incises across a fold axis and mainly high values elsewhere.

In addition to the maintenance of a narrow channel-belt, there are other characteristics associated with a major river incising across a fold (Sections 4.3, 6.1 and 6.2; Tables 6.2 and 6.3), though these characteristics have less statistical significance.

In particular, for river incision across a fold, *channel sinuosity* is generally (90 % of cases) less than 1.4 across the fold axis and is generally (80 % of cases) reduced (by a mean value of 0.368) compared with reaches upstream and downstream of the fold. Channel sinuosity for river incision across a fold has a significant correlation (r^2 of 0.258 is typical for a moderate relationship; Salkind, 2010) with valley distance from the nearest fold axis, showing linearly increasing channel sinuosity with increasing valley distance from the fold axis up to a distance of 12.2 km (Figure 6.14). A similar correlation is present for specific stream power for river incision across a fold, with linearly decreasing specific stream power with increasing valley distance from the fold axis, though a lower value of r^2 of 0.136 is typical for a weak to moderate relationship (Salkind, 2010). Across the fold axis, the reductions in channel sinuosity contribute to increases in channel water surface slopes (generally greater than 1.5×10^{-4} m m^{-1}) and thus increases in specific stream powers (generally greater than 1.6 W m^{-2}), which increase the erosion and removal of sediment to keep pace with fold uplift (Burbank et al., 1996; Schumm et al., 2000; Burbank and Anderson, 2001).

This is demonstrated by the general pattern in the valley distance plots of Figures 4.32 to 4.40 of mainly low values of channel sinuosity and mainly high values of specific stream power at locations where a major river incises across a fold axis, and mainly high values of channel sinuosity elsewhere. This is only a general pattern for channel sinuosity and is not as prominent as for average channel-belt width. In general, channel sinuosity is less well correlated with fold locations than channel-belt width because it changes over shorter timescales, is more influenced by major changes to river flows with recent intensive agriculture and monumental dams since c. 1960 AD, and is notably influenced by other factors (such as anthropogenic river channel straightening and cohesiveness of channel bank sediments). Also, some previous research on other rivers (e.g. Ouchi (1985) and Bullard and Lettis (1993) on different rivers in California, U.S.A.) has found increased channel sinuosity at locations across flexures and folds due to accompanying stable or decreased channel slopes, demonstrating the variable nature of channel sinuosity response to active uplift. Channel water surface slopes and specific stream powers are even less well correlated and do not reach statistical significance at the 95 % confidence level in this study because they vary with other factors, especially a natural reduction with distance downstream.

General river course direction for river incision across a fold is generally (80 % of cases) approximately orthogonal (i.e. at a bearing of 70° - 90°) to the fold axis across the fold, and this contributes to increases in channel water surface slopes and increases in specific stream powers across the fold. By contrast, general river course direction for river diversion around a fold is always (100 % of cases) approximately parallel (i.e. at a bearing of 0° to 20°) to the fold axis immediately upstream of the fold nose and then changes by about 20° - 70° to flow around the fold nose at the projection of the fold axis. The actual general river course directions do not exhibit statistically significant differences between these two cases due to the similar orientations of the folds (approximately NW-SE). There are statistically significant differences between all four cases due to the “minimal influences” category being largely independent of the folds.

In conjunction with channel-belt narrowing there is valley deepening for river incision across a fold, as shown by Figure 6.7. In this study, *valley depth over the extent of the channel-belt* of greater than about 10 m is only found with river incision across a fold, due to continued erosion at the same crossing location forming a “water gap” (Burbank and Anderson, 2001). This contrasts with river diversion around a fold, with mainly channel lateral migration and only limited vertical incision which continues until the river can no longer divert, such as when neighbouring fold tips coalesce (Ramsey et al., 2008). This is as expected, though differences in valley depth are not statistically significant between the two categories of river incision and river erosion at the 95 % confidence level, due to the short periods of time and low rates of uplift associated with the very young folds in the study area. There is nearly statistical significance between all four categories, since major anthropogenic river channel straightening is associated with a very narrow channel-belt.

Average grain size for both channel bed surface sediments and channel bank sediments is greater for river incision across a fold than for river diversion around a fold (Figures 6.10 and 6.11). However, these differences are not quite statistically significant (ANOVA *p*-values of 0.106 and 0.093) and are mainly simply related to the cases of river incision having generally larger grain sizes due to being mainly located further upstream than the cases of river diversion. More informative are changes relating to each case of river incision across a fold, with some previous work on folds and areas of uplift indicating decreases in grain size for aggrading reaches upstream of the fold or area of uplift, increases in grain size for incising reaches across the structural axis, and decreases in grain size for aggrading reaches downstream of the fold or uplifted area (Jorgensen, 1990; Holbrook and Schumm, 1999; Schumm et al., 2000; Whittaker et al., 2007, 2010; Burbank and Anderson, 2012). Such trends are found in this study, though the trends are only slight, as shown in Table 4.15 and Table 6.2. For river *incision* across a fold, grain sizes of channel bed surface sediments are increased across the fold axis compared with reaches upstream and downstream in only 21 % of cases (with no change in 68 % of cases). For river incision across a fold, grain sizes of channel bank sediments are increased across the fold axis compared with reaches upstream and downstream in 31 % of cases (with no change in 42 % of cases). Also, for river incision, the reaches just upstream of the fold have decreased grain sizes for both channel bed and bank sediments compared with reaches further upstream in 37 % of cases (with no change in 50 % of cases). For river *diversion* around a fold, there are no clear patterns to grain size change. This generally poor correlation between grain sizes and folds may be due to factors such as reduced and modified discharges since recent monumental dam construction, deeper bed sediments being more related to sediment and bedrock erosion, and any changes in grain size associated with folds being relatively small. This probably indicates that grain size is not an important factor in fold-river interactions, especially in downstream locations where, in general, sediments are uniformly fine-grained. Some previous research (Holbrook and Schumm, 1999; Schumm et al., 2000) has found increased grain sizes associated with localities of uplift, though the findings which can be distinguished from the many other causes of grain size variations mainly relate to gravels greater than 10 mm grain size in upland catchments (Whittaker et al., 2007, 2010; Pickering, 2010).

6.4.1 The importance of a narrow channel-belt for river incision across a fold

Since the main river characteristic associated with the highest levels of statistical significance in this study is channel-belt width and there is a threshold of average channel-belt width of less than c. 2.7 km which needs to be maintained for the major rivers Karun and Dez to incise across a fold, it is proposed that channel-belt width is a key driver of change in fold-river interactions. When a major river encounters an active fold (such as where it flows across the "core" of an emerging fold), if it is to incise a transverse river course across the fold and maintain that river course in the long-term, then the characteristics of the river will change in response to the fold and its associated anticlinal uplift. The channel-belt width will be reduced to (or maintained at) less than c. 2.7 km across the fold and, usually, will be increased immediately upstream and downstream of the fold. These changes in channel-belt width will occur gradually (over decadal to centennial timescales) in response to fold uplift in the form of mainly gradual, aseismic movements, punctuated by occasional earthquakes.

For river incision across the fold, a narrow channel-belt width is associated with changes in other river characteristics. As shown in Table 6.2 and Table 6.3, generally these changes are reductions in channel sinuosity (to less than 1.4), river course directions approximately orthogonal to the fold axis, and increases in channel water surface slopes (to greater than 1.5×10^{-4} m m^{-1}, and frequently much greater), all of which increase specific stream power (to greater than 1.6 W m^{-2}, and frequently much greater) and thus increase river erosion and incision across the fold (Burbank et al., 1996; Brocklehurst, 2010; Burbank and Anderson, 2012). There may be changes in other characteristics, such as increased grain size of channel bed and bank sediments (Whittaker, 2010), though in this study these changes are small with only slight increases in average grain sizes across a fold in only c. 21 - 31 % of cases (Table 6.2).

Though channel width and channel width:depth ratio for river incision across a fold and river diversion around a fold are not statistically different in this study (Table 6.2 and Table 6.3), it is interesting that other research in upland catchments has found that channel narrowing is associated with river incision across a fold and that this can occur independently of other changes such as channel steepening (Lavé and Avouac, 2001; Amos and Burbank, 2007; Yanites et al., 2010). Similar to a finding in upland catchments of a probable precedence of channel narrowing over other geomorphological changes in producing river incision in response to high rates of fold uplift (more than 10 mm yr^{-1} in the Himalayan foreland of Nepal; Lavé and Avouac, 2001), in this study in lowland catchments there is a probable precedence of channel-belt narrowing over other geomorphological changes in producing river incision across a fold in response to fold uplift. The threshold average channel-belt width of less than 2.7 km with associated limited lateral channel migration can be sufficient to enable incision of the rivers Karun and Dez to keep pace with fold uplift in lowland south-west Iran. However, with increased rates of fold uplift and exposure of fold core rocks of increased erosion resistance, other changes such as further reductions in channel-belt widths (frequently to average widths of less than 1.5 km, Table 6.2) and increases in channel water surface slopes will develop to enable the river to maintain an incising course across a fold.

6.4.2 The importance of the timing of fold-river interactions in the development of a narrow channel-belt across a fold

Since it takes time, at least several decades (PGL, 2004; Lahiri and Sinha, 2012), for a narrow channel-belt to develop and be maintained across an active fold, this can account for the division of the findings into major rivers incising across young, active folds relatively near to the fold “core” (generally, less than 16.0 km from the fold “core”), and major rivers diverting around young, active folds relatively far from the fold “core” (generally, greater than 22.0 km from the fold “core”) (Section 6.1.2).

Where a major river flows across an area of an emerging, active fold *at or very near to the fold “core”* for a period of decades to centuries, then it will be gradually modified to have a river course with a narrow channel-belt in response to the fold uplift it experiences. As the fold grows vertically and laterally from the fold “core”, this incising river course with a narrow channel-belt will be maintained in preference to a new incised river course across another part of the fold, since the river will not have a period of decades to centuries at the new location to develop a new narrow channel-belt, provided that the original river course across the fold “core” continues to be maintained. In this way, there is a strong tendency for a major river to flow across the “water gap” location at or near to the fold “core” that it incised with its first long-term encounter with the fold. A smaller river, with lesser discharges and stream powers, has less capacity to develop and maintain a narrow channel-belt across an active fold “core” and thus diverts around a fold much more frequently (Section 6.1.1).

By contrast, where a major river flows across an area of a young, emerged, active fold *very near to the fold “nose”*, then, unless the river maintains the same course for a period of at least several decades to allow for the development of an incising narrow channel-belt, the river will divert around the “nose” of the fold. With river migration away from the fold “nose” being promoted by lateral growth of the fold, the maintenance of the same river course for a period of decades to centuries is unlikely. Thus the river will continue to divert around the fold, unless there are factors which counter this river migration, such as a lack of an “easier” alternative river course (as with the coalescence of neighbouring folds (Ramsey et al., 2008)) or high river discharges and stream powers (as with significant tributary confluences upstream of the fold “nose” (Jackson et al., 1996; Burbank and Anderson, 2012)).

6.4.3 Model of the development of river incision across a fold and river diversion around a fold

Hence, there will be a difference in fold-river interactions depending on whether the major river first encounters the fold as a fold “core” of an emerging or very young fold, or first encounters the fold as a fold “nose” of a more developed fold. A model illustrating how this may occur and lead to the different responses of river incision across a fold and river diversion around a fold in is shown in Figure 6.16. The cartoons in the model in Figure 6.16 are based on a growing fold oriented roughly ESE-WNW (like the Sardarabad Anticline in Figure 6.1) and two similar major rivers flowing roughly from north to south (a west river like the River Dez in Figure 6.1 and an east river like the River Karun (Shuteyt) in Figure 6.1).

Figure 6.16 Cartoons showing a model of the development of a major river incision across a growing fold and a major river diversion around a growing fold

A growing fold oriented ESE-WNW (like the Sardarabad Anticline on Fig. 6.1) develops near to two major rivers flowing roughly from N to S: one to the west (like the R. Dez) incises across the fold and one to the east (like the R. Karun) diverts around the fold.

Figure 6.16 (a)
Time 1 (very approx. 100 ka): Due to river migration, the west river flows across part of the emerging fold "core" at location A-B (with modifications due to fold uplift), with an alternative course around the fold at location AA-BB. The east river flows from S-T but does not encounter the fold since it is beyond the margins of its basin.

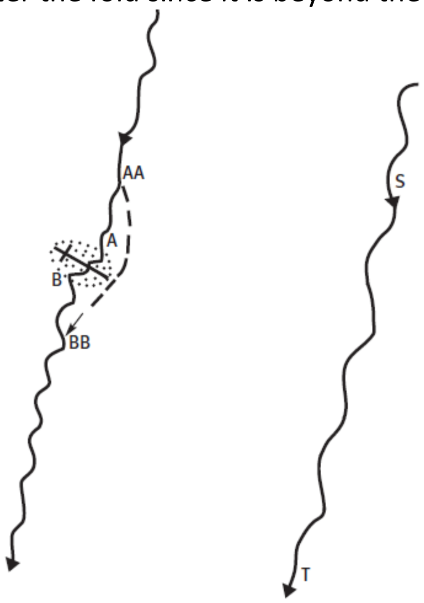

Figure 6.16 (b)
Time 2 (very approx. 70 ka): The west river flows across the slightly developed fold at "fixed" location A-B (with modifications due to fold uplift), with a rare, temporary course between two fold segments at location CC-DD. The east river flows from U-V but does not encounter the fold since it is beyond the margins of its basin.

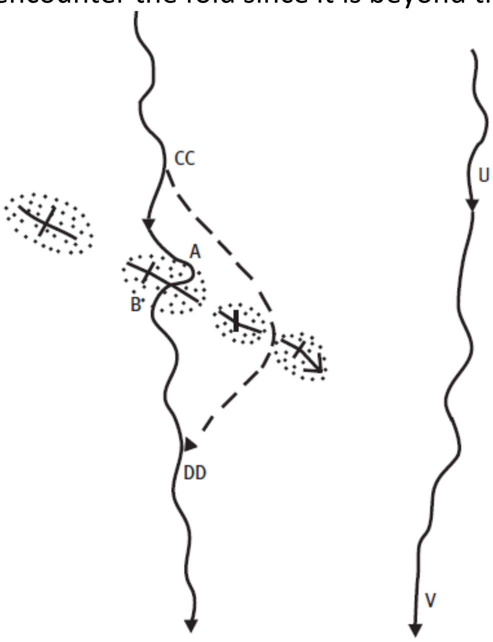

Figure 6.16 Cartoons showing the development of a major river incision across a growing fold and a major river diversion around a growing fold (continued)

Figure 6.16 (c)
Time 3 (the Present): The west river flows across the moderately developed fold at "fixed" location A-B (with modifications due to fold uplift), with an extremely rare course around the fold at location EE-FF. The east river flows from W-X with a diversion around the "nose" of the fold which it has encountered due to lateral fold growth.

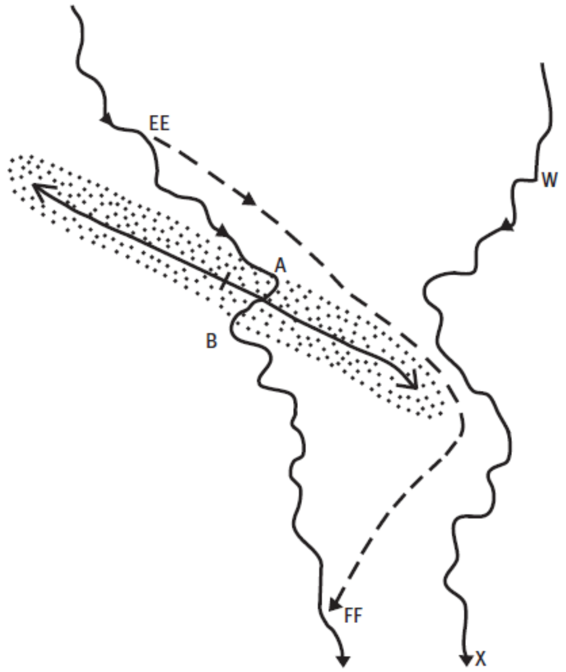

Key

River course

Alternative river course

Fold (solid line with bar is axis of anticline, arrow indicates direction of plunge)

The west river in Figure 6.16 (like the River Dez encountering the Sardarabad Anticline) migrates to and fro across the plains over the centuries as a result of internal and external factors (including slight tectonic tilting) and, with time, will flow across the "core" of the fold. At first, river aggradation will keep pace with the structural uplift of the fold, especially if rates of tectonic uplift for the emerging fold are initially relatively low. The river will flow without impedance across the fold with no significant topographic relief developing (Burbank et al., 1996). With time, as tectonic uplift of the fold continues (and possibly increases) and slight topographic relief (approximately 0 to 2 m) develops, when the river flows over the fold "core" it will be influenced by the greater uplift associated with the “core” (as opposed to adjacent parts of the plains with no fold yet emerged) and will undergo slight changes to its river characteristics (Figure 6.16 (a), “Time 1”). These changes across the fold “core” will, generally, include reduced channel sinuosities, increased channel water surface slopes, increased specific stream powers, and, possibly, slightly increased channel bed and bank grain sizes, which over the course of decades and centuries will lead to a narrow channel-belt, as discussed.

Similar initial fold-river interactions may be occurring at the present-day for the River Karun encountering the “core” of the emerging Ab-e Teymur Oilfield Anticline (Figure 4.1 (e) and (f)). For the river reaches immediately downstream of the mapped oilfield extent (river reach B33/B34 to B49/B50, which may correspond to the area of greatest uplift on the ground surface; Appendix 6.1) there are reductions in channel sinuosity (from 1.858 to 1.176), increases in specific stream power (from 0.409 W m^{-2} to 1.228 Wm^{-2}), and reductions in average channel-belt width (from 2.604 km to 0.831 km) (Tables 4.13 and 4.14; Appendix 6.1). The course of the River Karun has been coincident with the “core” of the emerging Ab-e Teymur Oilfield Anticline at its present-day location for an uncertain length of time, though probably for more than 150 years considering the dating of shrine-tombs and canals associated with the modern K3 channel (Figure 2.11; Gasche et al., 2005; Verkinderen, 2009; Walstra et al., 2010a; Heyvaert et al., 2013). During this time, the characteristics of the River Karun have been modified, including a reduction of parts of the channel-belt to average widths of less than 0.9 km, as described earlier.

Once these modified river characteristics and a narrow-channel belt have developed significantly at one location within the fold “core” (location A-B on Figure 6.16 (a)), then, as the fold subsequently grows laterally and vertically, this location may become the “preferred” river course. If the river should migrate a few km laterally so that the upstream course is still upstream of the “core” area, it will tend not to flow across the “core” at a different location. Since it takes time, at least several decades (PGL, 2004; Lahiri and Sinha, 2012), for a narrow-channel belt to develop, then, as shown in Figure 6.16 (a), the river will either be diverted into the already modified course with a narrow channel-belt at location A-B or it will be diverted around the end of the fold “core” at location AA-BB (or a similar course around the western end of the fold “core”). Thus, the river will tend to occupy or re-occupy the course with the narrow channel-belt at A-

B in the fold "core" so that, with time, A-B becomes more deeply incised than any other location within the fold "core" or anywhere else along the fold as it propagates. As the fold continues to grow laterally and vertically, location A-B will continue to have a narrow channel-belt and river reaches of low sinuosity across the fold axis, and a progressively longer diversion of the river course around the nose of the fold (location CC-DD) will require the expenditure of progressively more energy than continuing river incision at A-B (Figure 6.16 (b), "Time 2"). As a result, the river will only flow at locations (such as CC-DD) other than A-B at times of major flooding, so that the river becomes "fixed" at location A-B (Figure 6.16 (b)), effectively being "captured" by the fold.

Similar fold-river interactions may be occurring at the present-day for the River Karkheh interacting with the Zeyn ul-Abbas Anticline, a slightly developed fold comprised of three fold segments, the largest of which peaks at about 22 m above the surrounding plains (Figure 4.1 (f)). Though not investigated by survey and fieldwork in this study, the River Karkheh incises across the Zeyn ul-Abbas Anticline near to the structural culmination of its largest fold segment, the "core" of which most probably emerged first on the ground surface. The River Karkheh has a narrow channel belt (less than 0.6 km wide) and low channel sinuosity across the axis of the Zeyn ul-Abbas Anticline at this fold "core" location and so has maintained this incised, effectively "fixed" river course (like A-B in Figure 6.16 (b)) even though there is an apparently "easier" course between fold segments (like CC-DD in Figure 6.16 (b)) only about 7 km to the south-east (Figure 4.1 (f)).

As lateral and vertical fold growth continues further, then the modified course with a narrow channel-belt at A-B will become the only notable course of the river, with a very long course around the fold at EE-FF (or similar) being extremely rare during times of catastrophic flooding, or non-existent (Figure 6.16 (c), "Time 3"). In this way, provided that the river is not "defeated" by factors such as the increased fold width, landslides, or the exposure of more erosion resistant rocks within the fold (Section 1.6.1; Burbank et al., 1996), the river will become firmly "fixed" at location A-B and will continue to incise across the fold at or near to its location of greatest structural relief.

As described earlier, similar fold-river interactions are occurring at the present-day for the River Dez interacting with the Sardarabad Anticline, a moderately developed fold which peaks at more than 70 m above the surrounding plains and which probably developed from the coalescence of four fold segments (Figure 6.1; Allen and Talebian, 2011). For the river reaches across the fold axis there are reductions in channel sinuosity (from 1.591 to 1.120), unexpected slight decreases in specific stream power (from 5.263 W m^{-2} to 4.659 W m^{-2}) and reductions in average channel-belt width (from 3.246 km to 1.402 km) (Table 4.13 and 4.14; Appendix 6.3). These river characteristics indicate that the River Dez is incising across the Sardarabad Anticline, though with present-day flows the channel slopes, stream powers and erosion across the fold are being reduced.

The east river in Figure 6.16 (like the River Karun (Shuteyt) encountering the Sardarabad Anticline) migrates to and fro across the plains over the centuries, though it does not encounter the growing fold at “Time 1” and “Time 2” because the fold is beyond the margins of its river basin. During this time, river courses S-T and U-V flow roughly from north to south with no notable influences from the growing fold, as shown in Figure 6.16 (a) and (b). With continued vertical and lateral growth of the fold and continued migration of the river across the plains, the “nose” of the fold interacts with the river in the western parts of the river basin at “Time 3” (Figure 6.16 (c)). Since at this time the fold is a moderately developed fold with a large topographic expression, the river is diverted around the “nose” of the fold along river course W-X, as shown in Figure 6.16 (c). Since, as discussed in Section 6.4.2 above, it takes time for a narrow channel-belt to develop, unless the river maintains the same course for at least several decades the river will continue to divert around the “nose” of the fold in response to lateral growth of the fold (Keller et al., 1999). This lateral channel migration away from the fold “nose” will generally occur even though rates of uplift may be relatively low for locations on the fold near to the fold “nose” compared with nearer to the structural culmination (Hurtrez et al., 1999; Burbank and Anderson, 2012), because these rates of uplift are still notably greater than the merely regional rates of uplift on the adjacent plains beyond the fold “nose”. Only when there are factors which counter lateral river migration away from the propagating fold “nose” (such as increased stream powers (Burbank and Anderson, 2012) or the closure of “easier” alternative courses (Ramsey et al., 2008)), will the river develop a narrow channel-belt and incise across the fold.

As described earlier, similar fold-river interactions are occurring at the present-day for the River Karun encountering the “nose” of the Sardarabad Anticline (Figure 6.1; Allen and Talebian, 2011). The River Karun flows approximately parallel to the axis of the

Sardarabad Anticline (flow approximately towards 150°) upstream of the fold "nose" and then changes its general course direction (flow approximately towards 190° across the fold axis projection) to flow around the "nose" of the fold. For the river reaches across the projection of the fold axis there are slight increases in channel sinuosity (from 1.594 to 1.647), decreases in specific stream power (from 10.470 W m^{-2} to 0.082 W m^{-2}) and increases in average channel-belt width (from 2.080 km to 3.359 km) (Table. 4.13 and 4.14; Appendix 6.1). These river characteristics indicate that the River Karun is not currently incising across the fold "nose" and so is continuing to divert around the Sardarabad Anticline.

Hence, this relatively simple model can account for the way in which fold-river interactions divide quite clearly into categories of river incision across a fold (mostly with river crossings less than 16.0 km from the fold "core") and river diversion around a fold (with river crossings more than 22.0 km from the fold "core"). It demonstrates that a key factor determining the river response is the timing of the fold-river interactions. The west river in Figure 6.16 first encounters the fold at very early stages in the development of the fold when the fold is emerging and of limited topographic expression (much less than 8m above the plains, Table 6.1), due to the fold "core" being within the margins of its river basin. This scenario is like the fold "core" of the Sardarabad Anticline being within the margins of the river basin of the River Dez (see Figure 6.1). By contrast, the east river in Figure 6.16 first encounters the fold and the fold "nose" at later stages in the development of the fold when the fold is at least slightly developed (more than 8 m above the plains, Table 6.1), due to the fold "core" being outside of the margins of its river basin and the fold "nose" propagating towards the river. This scenario is like the fold "core" of the Sardarabad Anticline being beyond the margins of the river basin of the River Karun (see Figure 6.1).

Thus, this difference in the timings of fold-river interactions can help to account for the division of fold-river interactions into categories of river incision across a fold and river diversion around a fold. It explains why the majority of cases of river incision for the rivers Karun and Dez are characterised by distances from the fold "core" to the nearest basin margin which are $^{+}$ve (fold "core" within the river basin), whereas the majority of cases of river diversion are characterised by distances from the fold "core" to the nearest basin margin which are $^{-}$ve (fold "core" outside the river basin) (Section 6.1.2, Table 6.1).

6.4.4 The importance of a narrow channel-belt in the development of "wind gaps" and "water gaps" for rivers of different sizes

This model can also help to account for why rivers incise across active folds as discrete "wind gaps" (dry valleys of previous river courses) and "water gaps" (river valleys of maintained river courses), rather than incising across great swathes of a fold. On occasions, river incision may bevel off the top of an emerging fold tip so that the emerging fold has little or no topographic relief (Burbank and Anderson, 2001). In some cases, a major river may flow across an actively uplifting fold with little or no topographic relief developing, if river aggradation keeps pace with or exceeds the rate of structural uplift of the subsurface fold (Burbank et al., 1996). Examples are known from the rock record, with beds of syntectonic growth strata thinning across the crest of folds in the Spanish Pyrenees (Riba, 1976; Burbank and Vergés, 1994). An example in the study area is the River Karun flowing across the Ab-e Teymur Oilfield Anticline with less than 2 m of topographic relief developing (Figure 4.1 (e); Appendix 5.5). However, for a growing fold to produce little or no topographic relief in the long-term, generally, rates of structural uplift need to be low. In south-west Iran such interactions are mainly limited to the vicinity of the Zagros Deformation Front and the Mesopotamian-Persian Gulf foredeep where rates of uplift are about 0.1 mm yr^{-1} or less (Section 5.3; Edgell, 1996; Soleimany and Sàbat, 2010; Soleimany et al., 2011).

In most interactions between active folds and transverse rivers, the rate of river aggradation is less than the rate of structural uplift of the fold, and wind and water gaps are cut across the fold. For *small rivers*, such as the streams and creeks associated with the Wheeler Ridge Anticline in California, U.S.A. (Medwedeff, 1992; Keller et al., 1998) and the Bana Bawi and Safeen Anticlines in Iraq (Bretis et al., 2011), often there are series of wind gaps and water gaps across a fold, with wind gaps of decreasing elevation being geomorphic indicators of lateral fold propagation (Keller et al., 1999). When a small river encounters a part of an active fold as it initially emerges on the ground surface, it takes a period of time (probably decades) for a narrow channel-belt to develop, with increased channel slopes and specific stream powers to increase erosion across the fold to keep pace with the fold uplift. This produces a narrow channel-belt and a narrow valley across the fold (a water gap) rather than an incision across a wide expanse of the emerging part of the fold, in a manner similar to that given in the model in Section 6.4.3 above.

For such small rivers, each water gap is typically less than about 1 km wide (Keller et al., 1998; Bretis et al., 2011), since small rivers with low discharges need an especially narrow channel-belt to produce sufficient stream powers and erosion to keep pace with tectonic uplift. When the small river is subsequently "defeated" by the fold (due to factors such as increased fold width; Burbank et al., 1996), the river is unable to cut a new valley near to the previous valley due to vertical and lateral growth of the fold producing a large topographic "obstacle". Hence, the river diverts around the "nose" of the fold. This produces a wind gap. Near to the fold "nose" the small river may develop a new narrow channel-belt across the fold (due to factors such as narower fold width or capture of other streams; Jackson et al., 1996) over a period of time in response to fold uplift. This produces a new channel-belt and narrow valley less than about 1 km wide across the fold; a new water gap. With continued vertical and lateral fold growth this water gap may be subsequently defeated to produce a new wind gap, and, by the repetition of such processes, a series of wind gaps will form. Hence, a series of narrow "gaps", rather than very wide valleys, forms because narrow channel-belts are necessary for a river to incise across a fold and it takes time for these narrow channel-belts to form. Alternatively, small rivers may be ponded behind the fold as internal drainage, such as in the Qara Su basin in central west Iran (Brookes, 1989).

Multiple wind gaps may form with *major rivers*, but this is much less likely since their greater discharges and stream powers very frequently enable the river to maintain its initial course or water gap across the fold, as in the model in Section 6.4.3 above. For the River Karkheh (mean annual discharge c. 165 m^3s^{-1}), there are very occasional wind gaps, such as the wind gap across the Kuh-e Chenareh Anticline in the Zagros foothills to the north of the Khuzestan Plains (Allen and Talebian, 2011). For the slightly larger River Karun and River Dez in this study (mean annual discharges c. 575 m^3s^{-1} and 230 m^3s^{-1}, respectively), there are no notable wind gaps associated with their interactions with folds in the Khuzestan Plains, and there are prominent changes in river form where these rivers cross folds. There are three water gaps across the Dezful Uplift to the SW of Dezful (which may be associated with former anastomoses or courses of the River Dez; Figure 4.1 (c); Veenenbos, 1958) because this fold may be emerging as a long "core" at low rates of uplift which both large and small river channels can incise across (similar to that shown in Figure 1.7 (b)). For the larger River Ganges in north-west India (mean annual discharge c. 1,200 m^3s^{-1} at Rishikesh), there are no notable wind gaps associated with interactions with folds in the Dehradun basin, and there are only fairly slight changes in river form where the river crosses folds, though average channel-belt widths narrow to less than about 3 km across the Mohand Anticline (Pickering, 2010).

6.5 Discriminating between the river responses to active folds and direct human impacts

To interpret the interactions between active folds and major rivers, the factor of human activities needs to be considered, as discussed in Chapter 1. As with Earth surface movements associated with folds, direct human modifications to rivers may have pronounced influences at river reach scales, hence there may be issues of convergence, with the two different external factors resulting in similar effects (Schumm, 1991).

6.5.1 Discriminating the river responses to major dams

The size and location of major dams on the River Karun and River Dez in the study area are readily distinguishable, as are their associated river characteristics in the vicinity of the dam and many kilometres upstream and downstream of the dam (Section, 1.7.1; Section 6.2). The main significant difficulty is interpreting which characteristics were present before the dam was constructed (and thus are due to Earth surface movements) and which characteristics developed after the dam was constructed (and thus are mainly due to human activities). Major dams are frequently constructed where a river incises across a moderately or well-developed fold, due to the features such as low channel sinuosities, low braiding indices, narrow valleys and channel-belts, and outcrops of firm bedrock which make these locations good sites for dams (Weaver and Bruce, 2007).

In the study area, there are three major modern dams located near to the fold axis of the Turkalaki Anticline and the Dezful Uplift on the rivers Karun and Dez, and one ancient dam still in use located on the forelimb of the Shushtar Anticline on the River Gargar (Section 4.2.3 and Section 6.1.3.1). Though there are no detailed survey data available prior to their construction (c. 1963 - 1977 AD and c. 224 - 379 AD), it is clear that some of their characteristics, such as a large drop in river water levels across the dam and a reservoir upstream of the dam, are due to human activities. What is less clear is which proportion of the river incision downstream of these dams (with high specific stream powers of 16.3 - 67.3 W m^{-2} and low average channel migration rates of less than 1.1 m yr^{-1} for the period 1966/1968 - 2001) is attributable to clearer, “hungry” water emerging from the dam (Kondolf, 1997), and which proportion was present prior to dam construction and thus attributable to uplift of the fold. In this respect, the characteristic of average channel-belt width is a very useful discriminator. The narrow channel-belts with average widths of 1.214 km, 2.579 km and 0.533 km across the fold axis of the Turkalaki Anticline, Dezful Uplift and Shushtar Anticline, respectively, are likely to have taken centuries to develop and are of similar widths on remote sensing images before and after the time of construction of the three modern dams. Hence, an average channel-belt width of less than 2.7 km across a fold axis appears to be predominantly due to river incision in response to fold uplift, rather than river incision associated with major dam construction and use.

6.5.2 Discriminating the river responses to ruins of major dams

There are three major dam ruins in the study area: one located near to the fold axis of the Ahvaz Anticline, and two on the forelimb of the Shushtar Anticline (one of which is on a linear sandstone outcrop) (Section 4.2.3 and Section 6.1.3.2). Since they are clearly ruins and their only notable associated river modifications are increases in channel widths about 1.5 km upstream of the dam ruins (Section 6.2), there are no notable difficulties in distinguishing their influences on the major rivers from those of fold-river interactions.

6.5.3 Discriminating the river responses to major anthropogenic river channel straightening

In the study area, there are four locations of major anthropogenic river channel straightening of greater than 10 km river course length (Section 6.1.3.3). It is particularly important to distinguish these from the influences of Earth surface movements, since some co-workers informally considered that they might be primarily related to faulting or sedimentology, and for one case (the near-straight river course c. 13 km long between Dorquain and Masudi) there are no historical records linking it to human activities. Hence, to aid in discrimination, major anthropogenic river channel straightening was included as a category in the Analysis of Variance (ANOVA) in Section 6.3.

The ANOVA findings in Table 6.3 indicate that there are only four characteristics which have **statistically significant** differences at the 5 % significance level between the four categories of river reaches for river incision across a fold, river diversion around a fold, major anthropogenic river channel straightening, and minimal influences from active folds and direct human impacts. These four characteristics are more likely to be useful in discriminating between the influences of Earth surface movements associated with active folds and the direct human impacts of major anthropogenic river channel straightening. It is to be expected that *general river course direction* discriminates between categories of river reaches associated with active folds and major human influenced channel straightening. However, the differences are only slight, since, as will be discussed in Chapter 7, three out of the four major near-straight courses in the study area are associated with river incision across a fold. Thus, like river incision across a fold, human influenced near-straight reaches are preferentially oriented to flow approximately orthogonal to the WNW-ESE and NW-SE structural trend of most of the folds in the study area; that is, towards a bearing of about 180° - 235°.

Channel sinuosity is a key characteristic which distinguishes major anthropogenic river channel straightening from river reaches associated with active folds and from all other river reaches, as shown in Section 6.3, Table 6.2 (a) and Figure 6.4. Very low channel sinuosity of generally less than 1.1 over more than 10 km river course length is indicative of direct human modifications in the study area, almost by definition, since such long near-straight alluvial river courses are very rare in nature (Wang and Ni, 2002) and tend to be associated with braided channel belts rather than single-thread meandering river systems. In the Khuzestan Plains, humans have constructed numerous canals, cuts, levées and straightened channels over the centuries, which have frequently been many kilometres long and very nearly straight (Kirkby, 1977; Alizadeh et al., 2004; Verkinderen, 2009). The only notable uncertainty with the assignation of long, very low channel sinuosity reaches to direct human modifications is their association with courses across active folds. However, as will be discussed in Chapter 7, this is probably indicative of their preferential preservation in such scenarios rather than humans not being involved in their original construction.

The third and fourth characteristics which are significantly different between all four categories at the 5 % significance level are associated with ***channel-belt width***. Both average channel-belt width and channel-belt width at the location of the fold axis or midpoint of the near-straight reach are highly discriminative (with low *p*-values of 0.007 and 0.019, respectively; Table 6.3). *Average channel-belt width* with major anthropogenic river channel straightening is less than 1.1 km in nearly all cases, reflecting how the river is confined to the near-straight reach except in times of very high flows. This confinement is probably due to human factors such as the use of levées and embankments and dredging (Alizadeh et al., 2004; Downs and Gregory, 2004; Brierley and Fryirs, 2005), but may also be related to incision in response to fold uplift, as will be discussed in Chapter 7.

As a consequence of the channel-belt being narrow for major anthropogenic river channel straightening, the *valley depth over the extent of the channel-belt* is relatively shallow for these long, near-straight reaches. However, the valley can be as deep as about 7 m (for the Band-e Qir to Veys and “Band of Ahvaz” to Kut-e Seyyed Saleh near-straight reaches), notably overlapping with the ranges of valley depths for each of the three other categories. Thus, valley-depth over the extent of the channel-belt is only nearly statistically significant (*p*-value 0.054) between all four categories.

6.5.4 Discriminating the river responses to artificial river development

There is only one artificial river development in the study area, that of the c. 55 km long River Gargar which developed from the monumental ancient Masrukan canal system. It is readily distinguishable by the many human constructions associated with it and by its lack of features of mature meandering channels (Alizadeh et al., 2004; Moghaddam and Miri, 2007; Moghaddam, in press). It is characterised by prominent vertical river incision (about 2 m - 10 m or more below the surrounding plains), a narrow channel-belt (average channel-belt width less than 2.0 km), and low average channel migration rates (less than 0.5 m yr^{-1} for the period 1966/1968 - 2001) (Section 6.1.3.4 and Table 6.2). Many of the features of the River Gargar are partly natural, such as its gently meandering course, its capture of tributary wadis from the east, and its incision across folds (Verkinderen, 2009), but findings like straight canal traces, no meander cut-offs, and stream confluences at unnatural angles show that these features have developed after disuse of a human cut canal (Alizadeh et al., 2004).

6.6 Summary

Fold-river interactions between the transverse major rivers Karun and Dez and the young and emerging folds of lowland south-west Iran are clearly differentiated into categories of river incision across an active fold and river diversion around the “nose” of an active fold. River incision across a fold is the predominant response for the rivers

Karun and Dez (mean annual discharges c. 575 m^3s^{-1} and 230 m^3s^{-1}, respectively), occurring in 10 out of 13 cases (77 % of cases). By contrast, river diversion around a fold is the predominant response for the slightly smaller rivers Karkheh and Jarrahi (mean annual discharges c. 165 m^3s^{-1} and 78 m^3s^{-1}, respectively), occurring in 7 out of 10 cases (70 % of cases).

Incision of a major river across a fold occurs in cases where the river initially encounters the fold at an early stage in its development, when the "core" of the fold is emerging on the ground surface and when the fold has very limited topographic expression. River incision which keeps pace with fold uplift occurs for the rivers Karun and Dez where average channel-belt width is 2.7 km or less, and with time (over a period of at least several decades) the river reaches across the fold will undergo reduced lateral channel migration so that an incising river, with a narrow channel-belt of less than the threshold 2.7 km width, is formed. Provided this narrow channel-belt is maintained over the millennia as the fold grows, this river course will be maintained as a "water gap" across the fold near to its location of greatest structural relief. River diversion around a fold occurs in cases where the river initially encounters the fold at a later stage in its development, after the fold "core" has emerged and when the fold has a significant topographic expression. Since it takes time for a narrow channel-belt to develop and be maintained, the river will not incise across the fold until there are factors which counter lateral migration away from the fold "nose" in response to lateral and vertical fold growth. The time taken to develop an incising narrow channel-belt accounts for river incision occurring relatively near to the fold "core" (less than c. 16.0 km) and river diversion occurring relatively far from the fold "core" (more than c. 22.0 km) for the rivers Karun and Dez. It can also account for how rivers generally cut a series of discrete "wind gaps" and "water gaps" across a fold, rather than incising across large areas of an active fold.

Due to its association with long-term channel migration and human-influenced channel confinement, channel-belt width is a key river characteristic for discriminating river incision (always less than 2.7 km), river diversion (wide range of values), and major anthropogenic river channel straightening (always less than 1.1 km). In conjunction with other useful characteristics (such as channel sinuosity), the influences on river reaches of different categories of Earth surface movements and direct human impacts can be differentiated.

CHAPTER 7 INTERACTIONS OF THE INFLUENCES OF HUMAN IMPACTS AND EARTH SURFACE MOVEMENTS ON THE RIVERS KARUN AND DEZ

"The main stream flows behind the island about shouting distance to a *shadhurvan*, remarkably built from the rock, and the river forms a lake. Here are foaming jets of water and marvellous sights. The barrage holds back the water, and divides it into three streams which flow to the domains of the inhabitants of Ahvaz and irrigate their fields."

Al-Muqaddasi, Arabic geographer (c. 946 - 990 AD) describing the "Band of Ahvaz"

7.1 Coinciding interactions of Earth surface movements and human activities

Locations of direct human modifications to river channels and active folds may coincide, as described in Chapter 6. This may be due to human design at a location, such as with the Gotvand Regulating Dam constructed in the relatively deep, narrow valley across the axis of the Turkalaki Anticline (Section 6.5.1). Alternatively, this may be due to the preferential preservation or maintenance of the characteristics of human constructions, such as with the near-straight reach between Band-e Qir and Veys which is generally considered to be a reach of the former near-straight ancient Masrukan canal (Layard, 1846; Bakker, 1956; Alizadeh et al., 2004).

The external factors of Earth surface movements and human activities may have notable interactions at the locations where they coincide, but only where they are acting over similar timescales (Schumm, 1991). Earth surface movements associated with folds often act over an earthquake cycle with slow elastic deformation strain accumulation on associated faults over long interseismic periods of many years, followed by sudden elastic rebound in the opposite direction on associated faults over very short coseismic periods of seconds (and post-seismic periods of days to years) (Thatcher, 1993; Hyndman and Wang, 1995). Though there are a number of models (e.g. Reid, 1910; Shimaki and Nakata, 1980), it is clear that Earth surface movements associated with the growth of active folds are partly comprised of large, sudden coseismic (and post-seismic) movements associated with earthquakes, and partly comprised of gradual movements associated with mechanisms such as fault creep, aseismic folding and faulting, "silent" or "slow" earthquakes, pressure solution, and granular dislocations (Beroza and Jordan, 1990; Keller and Pinter, 1996; Burbank and Anderson, 2001).

As discussed in Section 2.5, in the study area and the Zagros region in general, earthquakes only account for a small part (about 10 % - 20 % at the most) of the total deformation required by the convergence of the Arabian and Eurasian plates. It is likely that much of the movement (probably c. 95 %) on faults and folds in the Zagros region is by aseismic folding, faulting and stable creep (probably due to lubricated décollements on evaporite layers) (Jackson et al., 1995; Masson et al., 1995; Hatzfeld et al., 2010). These mainly gradual vertical movements are of the order of about 0.1 - 2.3 mm yr^{-1} at distances of about 20 - 130 km to the north-east of the Zagros Deformation Front (Section 5.3).

These rates of tectonic movements are slow compared with the relatively rapid changes associated with direct human impacts and human constructions. Hence, influences on the reaches of major rivers can be sub-divided into three broad timescales:
Short timescales (less than 100 years) for which the influences of direct human impacts predominate (Downs and Gregory, 2004)
Intermediate timescales (about 100 - 2,000 years) for which there may be interactions between direct human impacts and Earth surface movements
Long timescales (more than about 2,000 years) for which the influences of Earth surface movements predominate, especially prior to the commencement of the monumental irrigation systems of the Sassanian Period (c. 224 AD) and prior to the first major civilization in the Elamite Period (c. 2,600 BC) (Burbank and Anderson. 2001; De Miroschedji, 2003; Alizadeh et al., 2004)

7.2 Interactions between direct human impacts and Earth surface movements at reach scales

7.2.1 Interactions between major dams and Earth surface movements

The three modern major dams in the study area have only been in use over about the last 50 years (Section 6.1.3.1). During this short time interval with uplift at rates of about 0.1 - 2.3 mm yr^{-1} (Section 5.3.1), total vertical Earth surface movements will have been small, of the order of about 0.01 m - 0.12 m. Hence, there have been no notable interactions between Earth surface movements and direct human impacts to date. With time, uplift of the Turkalaki Anticline should increase sediment aggradation upstream of the Gotvand Regulating Dam located very near the fold axis, and enhance river incision

Figure 7.1 Photograph showing water emerging from the Shushtar water mills as jets or "waterfalls" and then flowing as the River Gargar through a relatively deep, narrow, gently meandering gorge (view from Pol-e Boleiti dam-bridge in Shushtar (Figure 4.13) looking S)

The descriptions of Al-Muqaddasi (c. 946 - 990 AD), an ancient Arabic geographer, indicate that similar jets of water emerged from the dam-bridge or "Band of Ahvaz" across the River Karun at Ahvaz when it was in use (Collins, 2001)

immediately downstream of this dam. With time, uplift of the Dezful Uplift should enhance river incision between the two dams located near the edges of the limbs of the Dezful Uplift. These probable changes would be undesirable since they may promote undermining of the Gotvand Regulating Dam and the Dez Regulating Dam (Komura and Simons, 1967; Downs and Gregory, 2004), especially in the case of an earthquake.

The Pol-e Boleiti dam-bridge in Shushtar on the River Gargar (Figure 4.13) is a much older major dam. Its original construction probably dates to the Early Sassanian Period (c. 224 AD - 379 AD) and, with various repairs and constructions through history, it is likely that some dam or structure holding back the River Gargar has been present at the locality for more than 1,700 years from the time of the Sassanians to the present (Alizadeh et al., 2004; Verkinderen, 2009). Over this relatively long time interval there will have been some notable vertical Earth surface movements associated with uplift of the SW limb of the Shushtar Anticline. If these vertical movements were uplift at rates of about 0 - 2.26 mm yr^{-1} (Section 5.2.2 and 5.2.3), then total vertical movements over this time span would have been of the order of about 0 m - 3.8 m. It is difficult to determine the influences that this uplift has had on the characteristics of the River Gargar. This is due to the other large changes which have occurred through history, particularly the changes from the Masrukan canal to the River Gargar in the c. 10^{th} -14^{th} Centuries AD and the collapse of the Band-e Qaisar dam-bridge in c. 1885 AD which changed the River Gargar into a much smaller river (Le Strange, 1905; Modi, 1905; Verkinderen, 2009). It may be that the deep, narrow gorge downstream of the Pol-e Boleiti dam-bridge in Shushtar (Figure 7.1) is partly natural due to river incision in response to long-term uplift of the SW limb of the Shushtar Anticline (Woodbridge, 2006) and that incision through this gorge since the construction of the Masrukan canal has been enhanced by continued anticlinal uplift.

7.2.2 Interactions between ruins of major dams and Earth surface movements

As summarised in Section 6.1.3.2 and Table 6.2, the ruins of three major dams in the study are associated with river characteristics of channel broadening to about 101 m - 850 m within about 1.5 km channel distance upstream of the dam ruins and very slight drops in river water levels of about 0 m - 1 m across the dam ruins. The influences of the dams and ruins have been present over intermediate timescales of about 115 years to 1,000 years or more (Curzon, 1892; Hodge, 1992; Bosworth et al., 1984; Moghaddam and Miri, 2007; Verkinderen, 2009; Walstra et al., 2010; Moghaddam, in press). These timescales are sufficiently long for interactions with Earth surface movements to have taken place.

For the Shushtar Anticline with uplift rates of about 0 - 2.26 mm yr^{-1} (Section 5.2.2 and 5.2.3), total vertical movements have probably been about 0 m - 0.26 m for the Band-e Qaisar on the River Karun (Shuteyt) and about 0 m - 1.35 m for the Band-e Mahibazan on the River Gargar. For the Ahvaz Anticline with probable uplift rates of about 0.1 - 0.8 mm yr^{-1} (Section 5.3), total vertical movements have probably been about 0.07 m - 0.56 m for the “Band of Ahvaz” on the River Karun. These moderate vertical Earth surface movements, and the greater erosion resistance of the linear rock outcrops on which the ancient dams were constructed, will have promoted the persistence of the drop in river water levels at the dam location, contributing to the slight drop in river water levels of c. 0 m - 1 m across the dam ruins. Also, these vertical Earth surface movements may have promoted river incision and narrowing of the reservoir remnant upstream of the dam ruins. In short, there are probable interactions between Earth surface movements associated with active folds and major dam ruins, though their effects on major rivers are only slight and localised.

7.2.3 Interactions between major anthropogenic river channel straightening and Earth surface movements

In contrast to major dams and major dam ruins, major anthropogenic river channel straightening interact with Earth surface movements associated with active folds with more prominent effects on major rivers. River courses with major river channel straightening (i.e. river courses of very low sinuosity of generally less than 1.1 over a greater than 10 km long river course) (Section 6.1.3.3; Table 6.2) have probably been present in the study area over intermediate timescales of about 200 - 1,000 years. These timescales are due to the long history of use and disuse of major canals and cuts in lowland south-west Iran (Alizadeh et al., 2004; Verkinderen, 2009), and are sufficiently long for interactions with Earth surface movements to have taken place.

Whilst there are uncertainties with each case, it is possible to determine the likely minimum length of time that each long near-straight river course has been in existence with only limited human maintenance. The c. 19 km long River Karun near-straight course between Band-e Qir and Veys probably developed by avulsion or diversion into the ancient Masrukan canal, with very limited human impacts for about the last 600 years (Le Strange, 1905; Bosworth, 1987). The c. 11 km long River Karun near-straight course between the "Band of Ahvaz" and Kut-e Seyyed Saleh probably developed from channelization procedures employed by the Sassanians and subsequent peoples, with only limited human impacts, such as rebuilding a dam at the location of the *shadhurvan* and maintenance of the East Bank large Canal (Ainsworth, 1838; Verkinderen, 2009), over about the last 700 years or more. The c. 13 km long River Karun near-straight course between Dorquain and Masudi may have developed from a branch of the Mubaraki Canal, with very limited human impacts for maybe 200 - 700 years (Chesney, 1850; Bosworth et al., 1984). The c. 18 km long River Karun near-straight course of the Haffar cut was originally dug in the 10^{th} Century AD, with some fairly limited human impacts over the last 1,000 years (Le Strange, 1905; Potts, 2004). Over these intermediate timescales of about 200 - 1,000 years, rates of uplift of about 0.1 - 0.8 mm yr^{-1} (Section 5.3) will have produced total vertical movements of the order of about 0.02 m - 0.80 m.

It is unexpected that these long, near-straight river courses should have persisted over hundreds of years with only limited subsequent direct human modifications. It is particularly unexpected when it is considered that some features (such as the canal traces) indicate that ancient canals originally extended beyond the preserved near-straight courses, and also that when the ancient Masrukan canal fell into disuse across the Mianab Plain it did not retain its original near-straight course but developed into the meandering River Gargar (Figure 4.1 (b) and Figure 6.2). Three out of four cases of major anthropogenic river channel straightening have river courses across the axis of an anticline and the fourth (the near-straight river course between Dorquain and Masudi) has a river course immediately upstream of an emerging anticline. Hence, it is very likely that Earth surface movements associated with active folds are key factors in the persistence of these long, near-straight river courses.

There are details of the near-straight river courses which support this interpretation. The c. 19 km long River Karun *near-straight N-S course between Band-e Qir and Veys* and a c. 4 km long River Dez short near-straight SW-NE reach upstream of Band-e Qir both coincide with the approximate projected surface location of axis of the emerging Ramin Oilfield Anticline (Figure 4.1 (a) and Figure 4.1 (d)). Along these very low sinuosity reaches (1.038 and 1.062, respectively), average channel-belt widths are narrow (about 0.718 km and 1.944 km, respectively) and specific stream powers are moderate (about 1.663 W m^{-2} and 2.849 W m^{-2}, respectively). By contrast, immediately upstream and downstream of the near-straight reaches, the average channel-belt widths are broader (about 2.494 - 4.920 km) and the specific stream powers are slightly less (about 1.485 - 2.488 W m^{-2}) (Appendices 5.4, 6.1 and 6.3). This indicates that the human-influenced near-straight reaches are being preferentially maintained in response to the structural uplift of the Ramin Oilfield Anticline, even though the rates of uplift of this anticline are not known. The mechanism whereby this takes place is that across the axis and crest of the anticline where uplift rates are greatest, very low channel sinuosities, narrow channel-belts, and relatively high specific stream powers are promoted to maximise river erosion and incision in response to fold uplift (Burbank and Anderson, 2001; Brocklehurst, 2010). Upstream and downstream of this area of higher structural uplift rates, any promotion of river incision is much less and the river is “free” to migrate away from the confines of the human-influenced near-straight reaches and to have a natural, meandering course.

Figure 7.2 Large ancient irrigation systems of the western Lower Khuzestan Plains, as mapped from CORONA satellite images (Modified from Verkinderen, 2009)

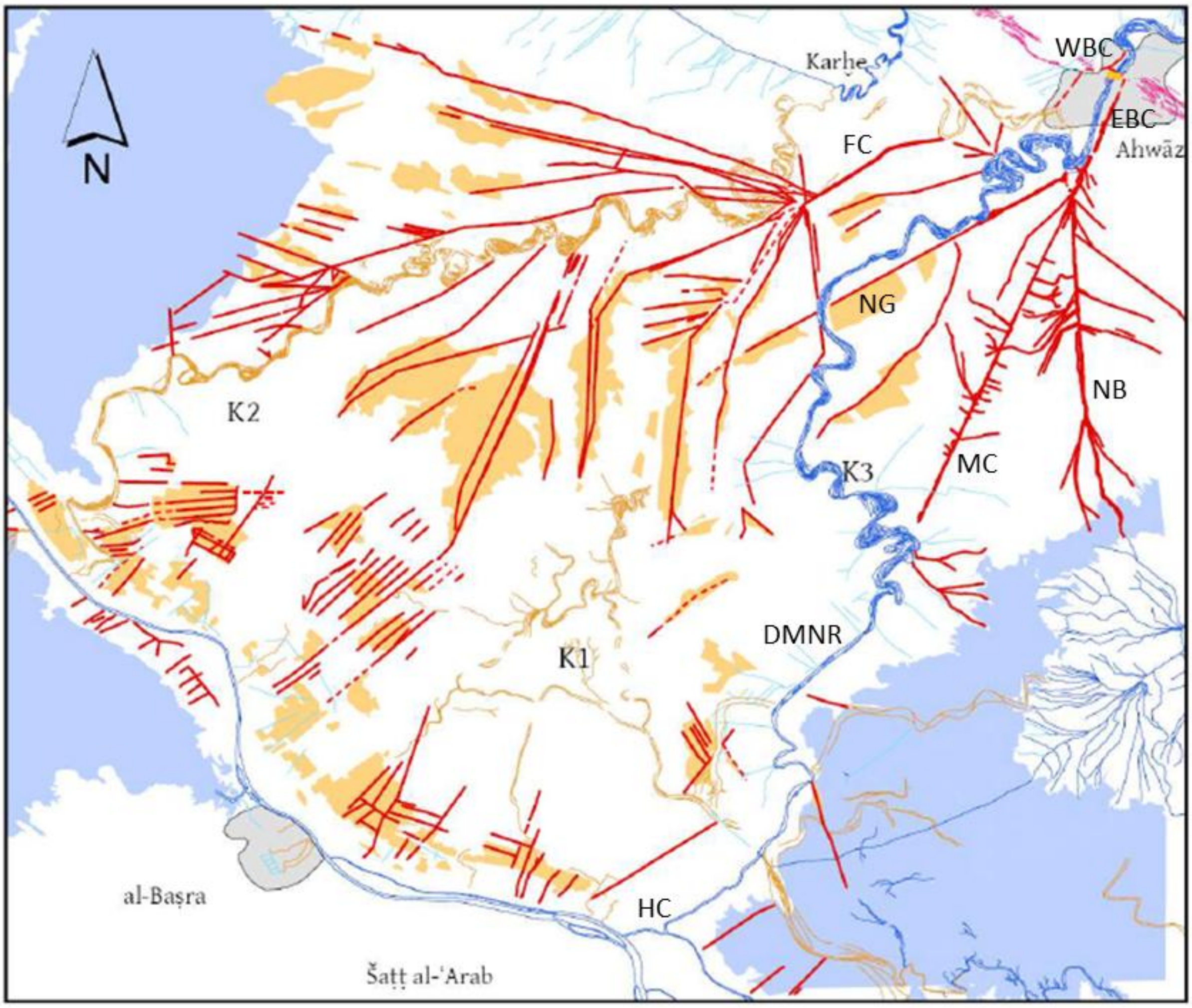

Key

Red Main fossil irrigation canals:

EBC East Bank large Canal serving: NG Nahr Gumalq MC Mubaraki Canal
NB Nahr Bahreh

WBC West Bank large Canal probably serving: FC Feeder Canal

Pale blue Other canals Blue Wetlands (wet season extent)

Dark blue Active rivers including: DMNR Dorquain to Masudi Near-straight Reach
HC Haffar Cut

Grey Modern cities (Ahvaz and Basra)

Orange "Feather canals" and fossil meanders (K1 K2 K3 are River Karun palaeochannel belts shown on Figure 2.11)

The c. 11 km long River Karun *near-straight NNE-SSW course between the "Band of Ahvaz" and Kut-e Seyyed Saleh* coincides with the axis of Ahvaz Anticline. Along this very low sinuosity reach (1.063), average channel-belt width is narrow (about 0.787 km) and specific stream power is high (about 10.777 W m^{-2}) along the initial c. 3 km of the near-straight reach. By contrast, immediately upstream and downstream of the near-straight reach, the average channel-belt widths are broader (about 2.060 - 5.002 km) and the specific stream powers are less (about 0.663 - 0.978 W m^{-2}) (Appendices 5.5 and 6.1). This pattern is similar to that for the River Karun and River Dez across the Ramin Oilfield Anticline and similarly suggests that the human-influenced c. 11 km long near-straight reach is being preferentially maintained in response to structural uplift of the Ahvaz Anticline.

However, there are differences between the initial c. 3 km of the near-straight reach coincident with the axis and outcrops of the Ahvaz Anticline (which includes the Ahvaz rapids and high specific stream powers of c. 10.777 W m^{-2}) and the final c. 8 km of the near-straight reach beyond the outcrops of the Ahvaz Anticline (which includes alternating point bars accumulating on a previously very straight course and low specific stream powers of c. 0.631 W m^{-2}) (Figure 6.3; Appendix 6.1). Hence, it appears that structural uplift and greater rock erosion resistance associated with the Ahvaz Anticline greatly influences the initial c. 3 km of the near-straight reach, whereas the influences of the Ahvaz Anticline on the final c. 8 km of the near-straight reach are only slight. Hence, it is likely that the diversion away from the near-straight course at Kut-e Seyyed Saleh towards the west, is influenced by other factors in addition to tectonics, such as the slightly elevated “Karun canal lobe” (IV on Figure 2.9 and K4 on Figure 2.11) to the south. This probably developed from sedimentation associated with disuse of channels and canals, such as the Mubaraki Canal, from about the Early Islamic Period (c. 633 - 750 AD) onwards (Figure 7.2; Gasche et al., 2004; Verkinderen, 2009; Heyvaert et al., 2013).

The c. 13 km long River Karun *near-straight NE-SW course between Dorquain and Masudi* does not coincide with any anticlines or oilfield anticlines known from geological maps or published articles (Figure 4.1 (a) and (e)). If this NE-SW near-straight channel was originally an extension of Mubaraki Canal to the north-east (Figure 7.2) which was retained as a course of the River Karun when the canal fell into disuse, then its NE end near Dorquain is expected due to the slightly elevated “Karun canal lobe” which the course of the River Karun diverts around (Figures 2.9, 2.11, 4.1 (a) and (e); Gasche et al., 2004; Verkinderen, 2009; Heyvaert et al., 2013). The reasons for it not having a downstream extent further SW than Masudi are unclear, though tectonic uplift associated with the Dorquain Oilfield Anticline might be an influence. The course of the River Karun diverts to the south on encountering the margin of the Dorquain Oilfield Anticline at Masudi (Figure 4.1 (a) and (e)) and has a reduction in channel water surface slopes (from 7.70×10^{-5} to 1.32×10^{-5} m m^{-1}) and specific stream powers (from 1.646 to 0.427 W m^{-2}) with distance along the near-straight course (Appendices 5.6 and 6.1). These could be features associated with tectonic uplift of the Dorquain Oilfield Anticline, though there does not appear to be a topographic high at the mapped location of the Dorquain Oilfield and it is probable that rates of uplift associated with its anticline are slight at around 0.1 mm yr^{-1} (Section 5.3; Abdollahie Fard et al., 2006; Soleimany and Sàbat, 2010). In summary, Earth surface movements probably have had an influence on the Dorquain to Masudi near-straight reach, though the influence is fairly slight and it is associated with the south-west extent of the near-straight reach. Other factors, such the constraining influence of the River Jarrahi delta to the east (Figure 4.1 (e) and (g)), may have been more influential in the persistence of this near-straight river course (Heyvaert et al., 2013).

For the c. 18 km long River Karun *near-straight NE-SW course of the Haffar cut upstream of Khorramshahr* there are associations with tectonics in that the Haffar cut flows across the southern projection of the Dorquain Oilfield Anticline (Figure 4.1 (e)). Since this anticline probably extends beyond the mapped extent of the oilfield and there is a N-S structural trend in its vicinity (Edgell, 1996; Abdollahie Fard et al., 2006; Maleki et al., 2006), it is probable that the reaches just upstream of the Haffar cut and along the initial c. 14 km of the Haffar cut, flow across an area of uplift. Along this stretch across the projection of the anticlinal axis, values of channel sinuosity (1.050) and average channel-belt width (about 0.374 km) are low, and slightly less than values for reaches immediately upstream and downstream (channel sinuosity about 1.125 - 1.675 and average channel-belt width about 0.321 - 1.208 km) (Appendices 5.6 and 6.1). This suggests that uplift associated with the Dorquain Oilfield Anticline is promoting the persistence of the straightness of the Haffar cut, by promoting river incision and inhibiting meandering. However, across the projection of the Dorquain Oilfield Anticline values for channel water surface slopes (about 3.31×10^{-5}) and specific stream powers (1.015 W m^{-2}) are rather low and certainly are not greater than for reaches just downstream (Appendices 5.6 and 6.1). Also, as stated above, rates of uplift associated with the Dorquain Oilfield Anticline are probably slight at around 0.1 mm yr^{-1} (Section 5.3; Abdollahie Fard et al., 2006; Soleimany and Sàbat, 2010), which over the c. 1,000 years since the Haffar cut was initially dug (Potts, 2004) would only entail total vertical movements of the order of about 0.10 m. Such vertical movements might be sufficient to influence a major river on the very gently sloping Abadan Plain, but would be a fairly small influence compared with other factors like the mid-18th Century AD channel widening and recent dredging programs (Potts, 2004; Verkinderen, 2009). In summary, Earth surface movements probably have exerted an influence on the persistence of the near-straight river course of the Haffar cut, but other human impacts may have exerted a greater influence.

7.2.4 Interactions between artificial river development and Earth surface movements

The only artificial river development in the study area, the River Gargar, is a major feature. It has a valley length of c. 55 km and a mean annual discharge of c. 46 m^3s^{-1}, with considerably greater discharges in the past (in the 14th - 15th Centuries AD it was known as the “Du Danikah” or “two sixths” (Layard, 1846; Modi, 1905) implying that its water discharges were roughly three times that of today).

Along its length, the artificial River Gargar encounters the projections of two anticlines, the Qal’eh Surkheh Anticline and the Kupal Anticline. As described in Section 6.1.3.4 and Table 6.2, the River Gargar is characterised by some prominent vertical river incision (about 2 m - 10 m or more below the surrounding plains), a narrow channel-belt (average channel-belt width less than 2.0 km), and low average channel migration rates (less than 0.5 m yr^{-1} for the period 1966/1968 - 2001). As a result, the River Gargar incises across the fold axis projections of the Qal’eh Surkheh Anticline and Kupal Anticline with little change in average channel-belt widths (an increase from c. 0.068 km to 0.193 km, and a decrease from c. 0.433 km to 0.205 km, respectively) and at an unusually long distance of 43.0 km from the fold “core” of the Kupal Anticline (Tables 4.13 and 6.1; Appendices 5.2 and 5.4). These fold-river interactions for the artificial River Gargar are significantly different to the fold-river interactions for the comparatively natural River Karun (Shuteyt) and River Dez. Hence, the exclusion of fold-river interactions associated with the artificial River Gargar (cases E) and F) listed in Section 4.3) when considering some characteristics (such as distance from fold “core” to river crossing location) of fold-river interactions associated with natural rivers in Chapter 6 is reasonable.

The different response of the artificial River Gargar to these folds compared with the natural River Karun and River Dez is related to the very limited lateral migration of the River Gargar. Throughout its history of about 600 - 1,000 years it has produced no meander cut-offs or oxbow lakes and so probably has had channel-belts of average width similar to the 2.0 km or less of the present-day (Le Strange, 1905; Alizadeh, 2004; Verkinderen, 2009). With such limited lateral migration, the River Gargar will only respond to encountering an active fold by incising across the fold or by being "defeated" by the fold, and in both cases the river was not "defeated". For the Qal'eh Surkheh Anticline, the incision across the fold is not unexpected since the extent of the ESE influence of the fold is unclear. For the Kupal Anticline, the incision across the fold near the fold "nose" is somewhat unexpected, especially since the course across the fold axis has developed into a meandering channel (albeit of fairly low channel sinuosities of c. 1.259 - 1.301), rather than retaining the original near-straight channel of the ancient Masrukan canal which would have maximised incision across the fold. It may be that with possibly rapid breaches or collapse of the Band-e Mahibazan, there was a short period of rapid incision, flooding (especially in the broadened R. Gargar floodplain shown in Figure 6.2) and gentle meander formation, which acted at a rate that was too rapid (perhaps a few decades) to be influenced by the Earth surface movements of the order of c. 1.0 mm yr^{-1}. Subsequently, when rates of incision and other changes had slowed as the artificial River Gargar trended towards an equilibrium, the River Gargar may have responded to tectonic uplift associated with the Kupal Anticline by slight decreases in channel sinuosity and average channel-belt width, in a manner similar to that found for natural rivers incising across active folds (Burbank and Anderson, 2001; Brocklehurst, 2010). More research on the development of the artificial River Gargar is needed to interpret its interactions with active folds.

The River Gargar also encounters the c. 110 km long "concealed fault/ deep-seated lineament" oriented E-W at about 31°47'N (NIOC, 1977) and is influenced by it. As shown in Figures 4.1 (a), 4.1 (b) and 4.30, the location of this E-W lineament corresponds closely with a highly sinuous reach of the River Gargar which has prominent E-W oriented meanders (reach L62 to L71 in Appendix 6.2). Whilst the details of the movements associated with this deep-seated lineament are not known, the majority of extensive lineaments with lengths of tens of kilometres are associated with fault zones or shear zones bounding structural blocks in the Pre-Cambrian basement which produce joints and small vertical displacements that may be of the order of one or two metres (Mason, 1992; Gay, 2012). Such a vertical displacement appears to be manifest as fairly steep valley slopes (6.121×10^{-4} m m^{-1}) for reach L62 to L71 of the River Gargar, with high channel sinuosity (3.195) developing to maintain fairly typical Gargar channel water surface slopes (5.65×10^{-5} m m^{-1}) across the slight vertical displacement of the lineament. The E-W meander orientation for this reach most probably is related to the approximate E-W orientation of the lineament and associated joints, especially since they may act as hydraulic conduits or barriers (Park, 1997; Gleeson and Novakowski, 2009; Gay, 2012). The River Karun (Shuteyt) and the River Dez flow across this extensive structural lineament with no significant modifications to their form (Figures 4.1 (a) and (b)), probably due to their greater water and sediment discharges and greater stream powers.

7.3 Interactions between direct human impacts and Earth surface movements at valley and basin scales

In summary, there are interactions between the influences of Earth surface movements and direct human modifications on the river reaches of the rivers Karun and Dez in lowland south-west Iran. Due to these interactions and the large size of some human constructions, direct human modifications may also have influences at valley and basin scales, due to their influences on the development of river courses.

The most significant influences on the drainage network and drainage basin are associated with the locations where rivers incise across emerged folds. As demonstrated in the model in Section 6.4.3, once a river has developed and maintained a narrow channel-belt across a fold for several millennia (as shown by the west river in Figure 6.16 (b), "Time 2" and by the incising course of the River Karkheh across the Zeyn ul-Abbas Anticline in Figure 4.1 (f)), the river course effectively becomes "fixed" at that location. The river course may change from this "fixed" or "captured" river course if the river is subsequently "defeated" by the active fold, but, as discussed earlier, this is unlikely with major rivers due to their relatively high discharges and stream powers.

Major dams may have influences on these "fixed" river course locations, though their influences are slight. Major dams may enhance river incision across the fold where they are constructed on a river near to where it is incising across a fold axis, as is the case with the Gotvand Regulating Dam on the River Karun across the Turkalaki Anticline and the two major dams on the River Dez across the Dezful Uplift (Figure 4.1 (c)). However, the River Karun across the Turkalaki Anticline near Gotvand and the River Dez across the Dezful Uplift at Dezful originally developed these “fixed” locations many millennia ago. The major dams will only significantly influence their future development if they are maintained for centuries to come. The ruins of major dams in this study demonstrate that a dam may have significant influences on river characteristics and development, but that these influences rapidly reduce if the dam should collapse and not be restored. The Band-e Qaisar which was probably constructed in the 3rd Century AD, created the monumental Masrukan canal/River Gargar and the Darian canal, but with its disuse and collapse in the 19th Century AD, the River Gargar and the Darian canal became considerably reduced in size and water flows (Modi, 1905; Verkinderen, 2009). Thus, the influences of a major dam on river courses are dependent on human activities in the future.

Major anthropogenic river channel straightening and artificial river development may have more prominent influences on these “fixed” river course locations. In the Upper Khuzestan Plains, the development of the disused ancient Masrukan canal into the River Gargar has greatly altered the course of the River Karun on the Mianab Plain. At Shushtar, the river divides into two main branches, with the artificial Gargar branch having a course through a gorge just south of Shushtar and across the Kupal Anticline near its fold “nose”. If conditions and human impacts are similar for centuries to come, the “new” River Gargar will become a “fixed” branch of the River Karun, and the N-S river course on the limb of the Shushtar Anticline near the water mills and the NE-SW across the Kupal Anticline upstream of Band-e Qir will both become “fixed” (Figure 4.1 (b) and Figure 6.2). Further south, the influence of the Masrukan canal has altered the courses of the River Karun and River Dez so that they now have a confluence at Band-e Qir rather than at Chamlabad, and a near-straight course further east between Band-e Qir and Veys (the former course of the Masrukan canal) rather than between Chamlabad and Ummashiyyeh-ye Yek (Figure 4.1 (d); Section 2.11.2). If the near-straight course between Band-e Qir and Veys is maintained for many centuries to come, then a “fixed” river course will develop N-S across the Ramin Oilfield Anticline. Thus, the influences of major anthropogenic river channel straightening and artificial river development on river courses are dependent on human activities in the future. It is interesting to consider that a length of the ancient Masrukan canal (the c. 19 km near-straight N-S course between Band-e Qir and Veys) may persist for millennia to come as a result of structural uplift of the Ramin Oilfield Anticline.

The major anthropogenic river channel straightening between the "Band of Ahvaz" and Kut-e Seyyed Saleh is likely to be maintained, even with limited future human impacts, since the narrow channel-belt course of the River Karun across the Ahvaz Anticline has been established for many millennia with an incised valley that is tens of metres deep. The human-straightened channel increases stream powers and erosion across the Ahvaz Anticline and thus promotes the maintenance of this "fixed" NNE-SSW river course across the fold. The straightened course has merely developed alternating point bars and very gentle meandering over about the last 700 years since its general disuse (Figure 6.3), indicating that this near-straight river course is likely to be maintained for centuries and millennia to come.

7.3.1 "Fixed" locations in the drainage networks of the River Karun and River Dez in the Khuzestan Plains

Thus, there is a succession of "fixed" locations that have developed and are developing in the drainage networks of the River Karun and River Dez in the Khuzestan Plains. All of these locations are related to river incision across a fold, with cases where direct human impacts may be enhancing this incision being indicated by *italics*.

For the River Karun, these "fixed" locations in the Upper Khuzestan Plains include: the *R. Karun across the Turkalaki Anticline a few km upstream of Gotvand*, the R. Karun across the Shushtar Anticline just upstream of Shushtar, the *R. Gargar across the Shushtar Anticline in the vicinity of the Shushtar water mills*, the *R. Gargar across the Kupal Anticline upstream of Band-e Qir*, the *R. Karun across the Ramin Oilfield Anticline between Band-e Qir and Veys*, and the *R. Karun across the Ahvaz Anticline in the vicinity of the "Band of Ahvaz"* (Figure 4.1 (a)). The three well-developed "fixed" locations of the R. Karun near Gotvand, Shushtar, and Ahvaz effectively confine the River Karun to a general river course from N to S in the Upper Khuzestan Plains. The four "fixed" locations which are still developing will strengthen this general N to S river course with time, particularly the c. 19 km long N-S near-straight former course of the Masrukan, if it continues to be maintained over the coming centuries. Most of these "fixed" locations are point sources for alluvial fans, particularly the Karun megafan extending over the Lower Khuzestan Plains from southern Ahvaz (Figures 2.9 and 2.11; Gasche et al., 2004; Walstra et al., 2010b).

For the River Dez, these “fixed” locations in the Upper Khuzestan Plains include: the *R. Dez across the Dezful Uplift in the vicinity of Dezful,* the R. Dez across the Sardarabad Anticline near Chogha Zanbil, and the *R. Dez short near-straight reach upstream of Band-e Qir* (Figure 4.1 (a)). The two well-developed “fixed” locations in the vicinity of Dezful and Chogha Zanbil confine the River Dez to a general NNW to SSE course in the Upper Khuzestan Plains. In the Susiana Plain upstream of the Sardarabad Anticline, the River Dez follows a course between these two “fixed” locations which is towards the western edge of the plain and the river drainage basin (Figure 4.1 (b) and (c)), probably as a result of a regional tilt to the SW and WSW (Section 5.4). Most of these “fixed” locations are point sources for alluvial fans, particularly the Dezful alluvial fan which extends over the western Susiana Plain from southern Dezful (Figure 2.7; Kirkby, 1977).

For the River Karun in the Lower Khuzestan Plains, there are no “fixed” locations because all of the folds on these very gently sloping plains are sub-surface folds or emerging folds with maximum topographic expressions of considerably less than 8.0 m (Table 6.1). The River Karun is interacting with the “core” of the emerging Ab-e Teymur Oilfield Anticline as described in Section 6.4.3, but these interactions are in very early stages, probably many centuries before the development of a “fixed” location. It is evident from maps, remote sensing images and palaeochannel traces that the River Karun has migrated and avulsed extensively across the Lower Khuzestan Plains over the last few millennia (Figure 2.11; Heyvaert et al., 2013), and it is likely that river migrations and avulsions will continue in these coastal plains for millennia to come (Hudson and Kesel, 2000; Blum et al., 2013).

7.4 Summary

There are interactions between the influences of direct human impacts and Earth surface movements on the major rivers Karun and Dez in the Upper Khuzestan Plains. These interactions mainly have effects over intermediate timescales (about 100 - 2,000 years) at the spatial scales of river reaches. Major anthropogenic river channel straightening may be preferentially maintained as incising river reaches across an active fold in response to fold structural uplift. Artificial river development may promote river incision across a fold at locations which are unusually long distances from the fold “core”, due to artificially low rates of channel migration, narrow channel-belts, and high rates of vertical incision.

Where maintained over centuries and millennia, river reaches incising across folds (both with and without significant influences from direct human modifications) develop into “fixed” locations of the rivers Karun and Dez which shape the subsequent development of their drainage networks and river basins. “Fixed” locations on the River Karun are yet to develop in the Lower Khuzestan Plains because all of the folds on these very gently sloping plains are either sub-surface folds or emerging folds.

CHAPTER 8 CONCLUSIONS

"Study the past if you would define the future."

Confucius, Chinese philosopher (c. 551 - 479 BC)

8.1 Conclusions relating to the aim and objectives of the study

8.1.1 Aim - Why do major rivers incise across some young, active folds near their structural culminations and divert around others?

In lowland south-west Iran, fold-river interactions between major rivers and young and emerging active folds are clearly differentiated into two categories: river incision across an active fold and river diversion around the "nose" of an active fold. The different major river responses are due to the need for incising river reaches with narrow channel-belts and limited lateral channel migration to be developed and maintained at a location where a river follows a course across an active fold in the long-term, and due to the time it takes for narrow channel-belts to develop at a location and be maintained in response to fold uplift.

Where a major river initially encounters a fold at an early stage of fold development (e.g. as an emerging fold "core" of very limited topographic expression) the river generally flows across the fold (at a location in the vicinity of the fold "core") for a sufficient length of time (at least several decades) for incising river reaches with narrow channel-belts to form (PGL, 2004; Lahiri and Sinha, 2012). Such cases result in river incision across the fold, with a river crossing location near to the structural culmination that generally develops over the location of the original fold "core" with subsequent vertical fold growth. Where a major river initially encounters a fold at a later stage of fold development (e.g. as an emerged, laterally propagating fold of more than about 8 m topographic expression) the river generally does not flow across the fold (at a location in the vicinity of the fold "nose") for a sufficient length of time for incising river reaches with narrow channel-belts to form. Such cases result in river diversion around the "nose" of the fold, as a result of repeated channel migration away from the fold "nose" in response to lateral fold growth (Burbank and Anderson, 2012). In such cases a river will continue to divert around the fold, unless there are factors which counter this river migration, such as a lack of an "easier" alternative river course (as with the coalescence of neighbouring folds (Ramsey et al., 2008)) or high river discharges and stream powers (as with significant tributary confluences upstream of the fold "nose" (Jackson et al., 1996; Burbank and Anderson, 2012)).

8.1.2 First objective - Determine the distinguishing characteristics of major river responses to young, active folds and whether there are key characteristics which act as thresholds for river incision across a fold

There are suites of characteristics which can distinguish between river incision across a fold and river diversion around a fold for the major rivers Karun and Dez in lowland south-west Iran. *River incision across a fold* is characterised by a general river course orthogonal to the fold axis where the river crosses the fold. The river reaches across the fold axis for river incision are characterised by: narrow channel-belts (average channel-belt width < 2.7 km and generally < 1.5 km), low channel sinuosities (generally < 1.4), steep channel water surface slopes (generally > 1.5×10^{-4} m m^{-1}), high specific stream powers (generally > 1.6 W m^{-2}), and a river crossing location relatively near to the fold "core" (generally nearer than 16 km). *River diversion around a fold* is characterised by a general river course parallel to the fold axis upstream of the fold and a change in river course bearing of about 20° - 70° to flow around the fold. The river reaches across the fold axis projection for river diversion are characterised by: average channel-belt widths and channel sinuosities with fairly wide ranging values (c. 0.4 km - 4.2 km and c. 1.1 - 1.8, respectively), gentle channel water surface slopes (< 1.3×10^{-4} m m^{-1}), fairly low specific stream powers (< 2.5 W m^{-2}), and a river crossing relatively far from the fold "core" (further than 22 km). Interestingly, channel width, grain size of channel bed and bank sediments, rate of structural uplift, general erosion resistance of fold rocks and sediments, and width of geological structure were not discriminative characteristics in this study at the 5 % significance level.

For the River Karun and River Dez (mean annual discharges c. 575 m^3s^{-1} and 230 m^3s^{-1}, respectively) to incise across the young, active folds in lowland south-west Iran (rates of uplift c. 0.1 - 2.3 mm yr^{-1} and fold rock erosion resistances varying from fluvial sediments to well-cemented conglomerates), average channel-belt width needs to be *less than a threshold average channel-belt width of about 2.7 km* for river reaches across the fold. Average channel-belt widths are also reduced (by a mean value of 1.2 km) compared with river reaches immediately upstream and downstream of the fold. These changes provide the necessary long-term incision across the fold and long-term aggradation immediately upstream and downstream of the fold for producing sufficient foreland-dipping slopes to maintain erosion into the uplifting fold and to transport away the eroded material (Holbrook and Schumm, 1999; Douglass and Schmeeckle, 2007). The flows of the major rivers Karun and Dez are sufficient to maintain these narrow channel-belts and vertical incision in response to fold uplift over many millennia. Hence, for the rivers Karun and Dez in lowland south-west Iran, river incision across the fold at or near the location of the original fold "core" is the predominant river response, occurring in about 77 % of cases. For the rivers Karun and Dez, river diversion around the fold "nose" mainly only occurs where the river encounters the fold later in its development (such as when a fold propagates laterally towards a river from beyond the river basin margins) and is the less frequent river response, occurring in about 23 % of cases. This leads either to a "water gap" across the fold near its structural culmination (less than about 16 km from the fold "core") where the river incises across the "core" of the fold at an early stage in the development of the fold and maintains this incision as the fold grows, or a "water gap" across the fold far from its structural culmination (more than about 22 km from the fold "core") where the river incises across the fold near to the propagating "nose" of the fold at a later stage in the development of the fold.

Channel-belt width with its association with long-term lateral channel migration is very important in determining fold-river interactions, though other factors are involved, particularly the *size of the river*. Smaller rivers, with lesser water and sediment discharges, will generally have threshold average channel-belt widths which are narrower, possibly about 1 km for small streams across the Bana Bawi and Safeen Anticlines in Iraq (Bretis et al., 2011). Small rivers and creeks tend to develop a series of "wind gaps" across a fold, since smaller rivers are more likely to be "defeated" by factors like increases in fold width and increases in fold rock erosion resistance (Brozovic et al., 1995; Burbank et al., 1996; Keller et al., 1998). Rivers which are slightly smaller than the rivers Karun and Dez are more frequently diverted around the "nose" of a fold, like the rivers Karkheh and Jarrahi in lowland south-west Iran with mean annual discharges of c. 165 m^3s^{-1} and 78 m^3s^{-1}, respectively, for which river incision across a fold occurs in only 30 % of cases. Larger rivers, with greater water and sediment discharges, will generally have threshold average channel-belt widths which are broader, possibly about 3 km for the River Ganges (mean annual discharge c. 1,200 m^3s^{-1} at Rishikesh) across the Mohand Anticline in north-west India (Pickering, 2010), and just one “water gap” tends to develop across a fold (Burbank et al., 1996; Douglass et al., 2009).

8.1.3 Second objective - Determine the distinguishing characteristics of direct human impacts on major rivers and whether there are interactions between Earth surface movements and these human impacts

Direct human impacts on the major rivers Karun and Dez in lowland south-west Iran can be distinguished by the human constructions and their remnants associated with the river channels (especially with artificial river development) and by suites of river characteristics. *Major dams* are characterised by a large drop in river water levels across the dam (of the order of about 3 m - 15 m), a reservoir upstream of the dam, and prominent vertical river incision immediately downstream of the dam (about 3 m - 20 m or more below the surrounding plains, with specific stream powers > 16.0 W m^{-2} within downstream channel distances of 6 km). With *ruins of major dams*, only a remnant of the reservoir immediately upstream of the dam ruins may remain (with channel widening to c. 101 m - 850 m within upstream channel distances of 1.5 km). For *major anthropogenic river channel straightening*, river reaches are characterised by very narrow channel-belts (average channel-belt width < 1.1 km), very low channel sinuosities (generally < 1.1) over a greater than 10 km long river course, and relatively broad, shallow channels (mean channel width > 180 m, mean channel width:depth ratio > 20). *Artificial river development* is characterised by prominent vertical river incision (about 2 m - 10 m or more below the surrounding plains) and very limited river channel lateral migration (average channel-belt width < 2.0 km, average channel migration rate < 0.5 m yr^{-1} for the period 1966/1968 - 2001). Since direct human modifications to rivers are distinct entities, it is very likely that the range of river characteristics for each of these categories of human impacts will be notably extended with more cases.

The external factors of Earth surface movements and human activities on the rivers Karun and Dez may have notable interactions where they coincide, mainly over the intermediate timescales of about 100 - 2,000 years and spatial scales of river reaches for which both factors can have significant influences (Schumm, 1991). Interactions between Earth surface movements and major dams and their ruins are slight, since modern major dams only date to about the last 50 years and ruins of major dams only have slight influences on river characteristics. Interactions between Earth surface movements and major anthropogenic river channel straightening are key factors in the persistence of long, near-straight river courses. Three out of four cases of major anthropogenic channel straightening on the River Karun have river courses across the axis of an anticline, and the fourth has a river course immediately upstream of an emerging anticline. Artificial river development with very limited river channel lateral migration may promote incision across an active fold at unusually long distances from the fold "core" and may promote markedly increased sinuosity across a structural lineament. Where direct human impacts on river reaches promote river incision across a fold at a location, over subsequent centuries and millennia these may develop into "fixed" locations of the River Karun and River Dez which shape the subsequent development of their drainage networks and river basins.

8.2 Suggestions for future research

Further research is needed to better understand both the relationships between the major rivers Karun and Dez, active folds, and direct human impacts in lowland south-west Iran, and the relationships between major rivers, active folds, and direct human impacts in general.

8.2.1 Future work on the River Karun and River Dez in lowland south-west Iran

With regards to the River Karun and River Dez, this study has improved our knowledge of vertical Earth surface movements in lowland south-west Iran, both at the regional scale relative to the Zagros Deformation Front (ZDF) and at the local scale of individual folds. These folds include the Shahur Anticline, Naft-e Safid Anticline, the Sardarabad Anticline and the Shushtar Anticline. Nevertheless, for a fuller understanding of the response of major rivers to Earth surface movements, accurate rates of uplift for each of the folds encountered by the major rivers in the study area are important, as are details of the ages and sequential development of their palaeochannels and channels.

Hence, future research work should include a more detailed investigation of the river terraces of lowland south-west Iran, including the detailed mapping of river terrace surfaces and the analysis and dating of many river terrace deposits at a wide range of locations. Such an investigation should include the terraces of the River Karun (building on the work of this study and the work of Vita-Finzi (1969, 1979), Kirkby (1977) and Alizadeh et al. (2004)) and the River Dez (building on the work of Veenenbos (1958) and Kouchoukos and Hole (2003)). Terraces of the rivers Karkheh, Jarrahi and Zohreh could be included if time and resources should permit. Ideally, the investigation would include river terraces associated with the Turkalaki Anticline, Qal'eh Surkheh Anticline and Ahvaz Anticline for the River Karun and associated with the Dezful Uplift and Shahur Anticline for the River Dez, where preserved, in order to determine the rates of uplift for these folds. This could be supplemented by a high-precision GPS survey over about five years to determine short-term rates of deformation for a number of folds, though this would be difficult and expensive and would include errors involved with elevation measurements, geoid models and vertical datums (Higgins, 1999).

This study was limited by the small amount of available data relating to the location, extent and structural geology of oilfields within lowland south-west Iran. If more precise data obtained by seismic survey during oil and gas exploration concerning the sub-surface structures and anticlinal axes associated with these oilfields could be made available, then their influences on major rivers would be better defined. This would be especially useful for the Ramin Oilfield, Ab-e Teymur Oilfield and Dorquain Oilfield with anticlines which interact with the lower reaches of the River Karun. Also, there may be other oilfields and sub-surface structures not known to this study which are interacting with the River Karun and River Dez.

The timing and development of palaeochannels and channels of the rivers Karun and Dez in the study area are often unclear in the study area and are mainly based on limited historical and archaeological evidence. This could be improved upon by targeted archaeological surveys and by sediment coring of palaeochannel deposits, with dating of sediments by radiocarbon dating and Optically Stimulated Luminescence (OSL) dating. In particular, our understanding of developments after the disuse of the ancient Masrukan canal would be improved by sediment coring and archaeological survey in the vicinity of the ruins of the Band-e Mahibazan and the broadened River Gargar floodplain to its south (Figure 6.2), as this should determine the timing and the effects of the collapse of the Band-e Mahibazan more precisely. Also, in the vicinity of Band-e Qir, sediment coring of older channels in the vicinity of the near-straight course of the R. Karun between Band-e Qir and Veys, the short near-straight reach of the R. Dez downstream of Chamlabad, the R. Gargar across the Kupal Anticline, and the palaeochannel between Chamlabad and Ummashiyyeh-ye Yek should enable the development of the unusual configuration of the rivers in this area to be determined more precisely (Figure 4.1 (d); Section 7.2.3). The unusual configuration may be related to the destruction or collapse in antiquity of the "bitumen dike" (Alizadeh et al., 2004), a structure possibly oriented roughly SW-NE in the vicinity of Band-e Qir, and targeted archaeological survey and excavation in the vicinity of Band-e Qir may find traces of its ruins. Also, sediment coring and archaeological survey in the vicinity of the near-straight course of the R. Karun between Dorquain and Masudi (Figure 4.1 (e); Section 7.2.3) should improve understanding of the timing and development of this feature.

8.2.2 Future work on other major rivers

In this study of the major rivers Karun and Dez in the lowland Khuzestan Plains, it has been found that channel width is not a significant discriminative river characteristic, whereas channel-belt width is a key discriminative river characteristic. A narrow average channel-belt width of less than c. 2.7 km is a threshold which probably has a precedence over other geomorphological changes in producing river incision across a fold in response to fold uplift. By contrast, other research in upland catchments has found that channel width is a key discriminative river characteristic, with channel narrowing having probable precedence over other geomorphological changes in producing river incision across a fold in response to relatively high rates of uplift (Lavé and Avouac, 2000, 2001; Amos and Burbank, 2007; Yanites et al., 2010). These differences in river responses are interesting. Further work is needed on a variety of rivers to investigate whether these are consistent differences in the characteristics of river incision across an active fold between upland and lowland catchments, and whether any differences are mainly related to the wider channels and gentler slopes of lowland rivers, to differences in river size, to differences in the degree of fold development, to differences in the rates of fold uplift, or to other factors. This further work should also investigate direct human impacts, to determine better their influences on major river characteristics and responses, and to investigate whether interactions between Earth surface movements and human activities occur for rivers other than the Karun and Dez.

A good starting point would be a detailed investigation of the rivers Karkheh and Jarrahi in lowland south-west Iran in a manner similar to that employed in this study. This would be timely, since some river discharge data and survey data may become available for the River Karkheh and there has been some good recent research on the lower reaches of the River Karkheh and River Jarrahi (e.g. Walstra et al., 2010b; Heyvaert et al., 2012, 2013). A detailed investigation would show the influences of smaller river sizes and show the influences of rates of fold uplift via an investigation of the Karkheh and Jarrahi river terraces. The influence of interactions between direct human impacts and Earth surface movements would include the ancient canal SC2 and the River Shahur branch of the River Karkheh across the Shahur Anticline (Section 4.2.2). Also, the development of the near-straight artificial SE-NW river courses of the Karkheh and Karkheh Kur between Hamidiyyeh and the Huwayzah marshes, may be partly related to Earth surface movements associated with SE-NW trending anticlines, including the Hamidiyyeh, Band-e Karkheh, Susangerd Oilfield and Jufeyr Oilfield Anticlines (Figure 4.1 (a) and (f)).

Further work should also include transverse major rivers in other foreland basins and other tectonic settings, especially where there is a long history of human impacts and there are folds in early stages of their development. Good areas for further studies might be the basin of the River Po and the Apennine rivers in north-east Italy (Alvarez, 1999; Burrato et al., 2003) and the basin of the River Indus in Pakistan (Flam, 1993; Jorgensen et al., 1993). Further research should build on the previous work undertaken in these basins, with a focus on key characteristics like channel-belt width, channel width, channel water surface slope, specific stream power, river discharge, grain size, fold “core” location and fold growth, and the development of wind gaps and water gaps. Field research and remote sensing research of could then provide boundary condition information for numerical models of morphodynamics (such as CAESAR) that could be used to investigate in detail the response of river channels to a range of tectonic forcings over a range of spatial and temporal scales (Coulthard et al., 2007). With such research, it should be possible to determine how and why the key characteristics of the major river responses to active folds vary in different scenarios.

REFERENCES

"I was so long writing my review that I never got around to reading the book."

"Groucho" Marx, American comedian and film star (1890 - 1977 AD)

Abdollahie Fard, I., Braathen, A., Mokhtari, M. and Alavi, S. A. (2006) Interaction of the Zagros Fold-Thrust Belt and the Arabian-type, deep-seated folds in the Abadan Plain and the Dezful Embayment, SW Iran. *Petroleum Geoscience*, **12** (No. 4), 347-362.

Adamiec, G. and Aitken, M. J. (1998) Dose-rate conversion factors update. *Ancient TL*, **16**, 37-50.

Adams, A. E. and MacKenzie, W. S. (1998) *A Colour Atlas of Carbonate Sediments and Rocks Under the Microscope*. London, U.K.: Manson Publishing Ltd., 180 pages.

Adams, A. E., MacKenzie, W. S. and Guilford, C. (1984) *Atlas of sedimentary rocks under the microscope*. Harlow, Essex, U.K.: Longman Scientific & Technical, 104 pages.

Adams, R. M. (1962) Agriculture and Urban Life in Early Southwestern Iran. *Science*, **136** (No. 3,511), 109-122.

Adams, R. M. (1965) *Land behind Baghdad: A history of settlement on the Diyala plains*. Chicago, U.S.A.: The University of Chicago Press, 187 pages.

Adams, R. M. (1981) *Heartland of Cities: Surveys of Ancient Settlement and Land Use on the Central Floodplain of the Euphrates*. Chicago, U.S.A.: The University of Chicago Press, 384 pages.

Afkhami, M. (2003) Environmental effects of salinity in the Karun-Dez Basin, Iran. In: Soliman, M. H. (ed.) *Seventh International Water Technology Conference (IWTC), Cairo, Egypt, 1-3 April 2003: Final Program*. Alexandria, Egypt: El-Fath Printing, Conference Report, pp. 229-233.

Afkhami, M., Shariat, M., Jaafarzadeh, N., Ghadiri, H. and Nabizadeh, R. (2007) Regional water quality management for the Karun-Dez basin, Iran. *Water and Environment Journal*, **21** (3), 192-199.

Agard, P., Omrani, J., Jolivet, L. and Mouthereau, F. (2005) Convergence history across Zagros (Iran): constraints from collisional and earlier deformation. *International Journal of Earth Sciences* (Geologische Rundschau), **94**, 401-409.

Ainsworth, W. F. (1838) *Researches in Assyria, Babylonia and Chaldea, forming part of the Labours of the Euphrates Expedition*. London, U.K.: John W. Parker, 343 pages.

Aitken, M. J. (1990) *Science-based dating in archaeology*. London, U.K.: Longman Archaeology Series, 274 pages.

Aitken, M. J. (1998) *An Introduction to Optical Dating: The Dating of Quaternary Sediments by the Use of Photon-stimulated Luminescence*. Oxford, U.K.: Oxford University Press, 267 pages.

Alai, C. (2010) *Special Maps of Persia 1477-1925*. Leiden, The Netherlands: Brill Academic Publishers, Handbook of Oriental Studies series, 420 pages.

Alavi, M. (1994) Tectonics of the Zagros orogenic belt of Iran: new data and interpretations. *Tectonophysics*, **229**, 211-238.

Alavi, M. (2004) Regional stratigraphy of the Zagros fold-thrust belt of Iran and its proforeland evolution. *American Journal of Science*, **304**, 1-20.

Alexander, J., Bridge, J. S., Leeder, M. R., Collier, R. E. L. and Gawthorpe, R. L. (1994) Holocene meander-belt evolution in an active extensional basin, southwestern Montana. *Journal of Sedimentary Research*, **64** (4b, November 1994), 542-559.

Aleyasin, A. (ed.) (2001) *Applied River Engineering in Dez and Karun Rivers*. Tehran, Iran: Publication No. 33 of Iranian National Committee on Large Dams, 637 pages.

Alijani, B. (2008) Effect of the Zagros Mountains on the Spatial Distribution of Precipitation. *Journal of Mountain Science*, **5**, 218-231.

Alizadeh, A. (1992) *Prehistoric settlement patterns and culture in Susiana, southwestern Iran: the analysis of the F. G. L. Gremliza survey collection*. Ann Arbor, Michigan, U.S.A.: Museum of Anthropology, University of Michigan, Technical Report No. 24, 175 pages.

Alizadeh, A., Kouchoukos, N., Wilkinson, T. J., Bauer, A. M. and Mashkour, M. (2004) Human-Environment Interactions on the Upper Khuzestan Plains, Southwest Iran. Recent Investigations. *Paléorient*, **30** (1), 69-88.

Allen, M. B. and Talebian, M. (2011) Structural variation along the Zagros and the nature of the Dezful Embayment. *Geological Magazine*, **148** (5-6), 911-924.

Allen, M., Jackson, J. and Walker, R. (2004) Late Cenozoic reorganization of the Arabia-Eurasia collision and the comparison of short-term and long-term deformation rates. *Tectonics*, **23** (2), TC2008, doi:10.1029/2003TC001530, 16 pages.

Allen, M. B., Kheirkhah, M., Emami, M. H. and Jones, S. J. (2011) Right-lateral shear across Iran and kinematic change in the Arabia-Eurasia collision zone. *Geophysical Journal International*, **184**, 555-574.

Allen, P. A., Armitage, J. J., Carter, A., Duller, R. A., Michael, N. A., Sinclair, H. D., Whitchurch, A. L. and Whittaker, A. C. (2013) The Q_s problem: Sediment volumetric balance of proximal foreland basin systems. *Sedimentology*, **60**, 102-130.

Alvarez, W. (1999) Drainage on evolving fold-thrust belts: a study of transverse canyons in the Apennines. *Basin Research*, **11**, 267-284.

Amos, C. A. and Burbank, D. W. (2007) Channel width response to differential uplift. *Journal of Geophysical Research*, **112**, F02010, doi:10.1029/2006JF000672, 11 pages.

Andrews, E. D. (1980) Effective and bankfull discharges of streams in the Yampa river basin, Colorado and Wyoming. *Journal of Hydrology*, **46**, 311-330.

Aqrawi, A. A. M., Domas, J. and Jassim, S. Z. (2006) Quaternary Deposits. In: Jassim, S. Z. and Goff, J. C. (eds.) *Geology of Iraq*. Prague and Brno, Czech Republic: Dolin and Moravian Museum, pp. 185-198.

Ashworth, P. J. and Lewin, J. (2012) How do big rivers come to be different? *Earth-Science Reviews*, **114**, 84-107.

Aubry, M.-P., Van Couvering, J. A., Christie-Blick, N., Landing, E., Pratt, B. R., Owen, D. E. and Ferrusquía-Villafranca, I. (2009) Terminology of geological time: Establishment of a community standard. *Stratigraphy*, **6** (No. 2), 100-105.

Azizi, H. and Jahangiri, A. (2008) Cretaceous subduction-related volcanism in the northern Sanandaj-Sirjan Zone, Iran. *Journal of Geodynamics*, **45**, 178-190.

Babault, J., Van den Driessche, J. and Teixell, A. (2012) Longitudinal to transverse drainage network evolution in the High Atlas (Morocco): The role of tectonics. *Tectonics*, **31**, TC4020, doi:10.1029/2011TC003015, 15 pages.

Badripour, H., Suttie, J. M. and Reynolds, S. G. (2006) *Country Pasture/Forage Resource Profiles: Islamic Republic of Iran*. Web page (in nine sections) of the Food and Agriculture Organization of the United Nations: www.fao.org/ag/AGP/agpc/doc/Counprof/Iran/Iran.htm (accessed on 8 March 2011).

Bahroudi, A. and Talbot, C. J. (2003) The configuration of the basement beneath the Zagros basin. *Journal of Petroleum Geology*, **26**, 257-282.

Bak, P., Tang, C. and Wiesenfeld, K. (1988) Self-organized criticality. *Physical Review A*, **38** (1), 364-374.

Bakker, A. J. (1956) Historical Notes. In: Day, T. et al. (eds.) *Iran - The development of land and water resources in Khuzistan - Report to the government*. Rome, Italy: Food and Agriculture Organization of the United Nations, Report No. LA-EPTA 553.

Baltzer, F. and Purser, B. H. (1990) Modern alluvial fan and deltaic sedimentation in a foreland basin tectonic setting: the lower Mesopotamian Plain and the Arabian Gulf. *Sedimentary Geology*, **67**, 175-197.

Bannister, A., Raymond, S. and Baker, R. (1998) *Surveying. Seventh Edition*. Harlow, Essex, U.K.: Pearson Prentice Hall, 502 pages.

Barnard, T. W., Crockett, M. I., Ivaldi, J. C. and Lundberg, P. L. (1993) Design and Evaluation of an Echelle Grating Optical System for ICP-OES. *Analytical Chemistry*, **65** (No. 9), 1,225-1,230.

Barry, R. G. and Chorley, R. J. (1992) *Atmosphere, Weather and Climate. Sixth Edition*. London, U.K. and New York, U.S.A.: Routledge, 392 pages.

Bateman, M. D. and Catt, J. A. (1996) An absolute chronology for the raised beach and associated deposits at Sewerby, East Yorkshire, England. *Journal of Quaternary Science*, **11** (5), 389-395.

Bateman, M. D. and Fattahi, M. (2008) *Quartz Optical Dating Report. Qareh Sultan and Dar Khazineh Terraces, Iran*. Sheffield, U.K.: Unpublished Report of the Sheffield Centre for International Drylands Research, 8 pages.

Bateman, M. D. and Fattahi, M. (2010) *Quartz Optical Dating Report. Batvand, Dar Khazineh, Abgah and Kushkak Terraces, Iran*. Sheffield, U.K.: Unpublished Report of the Sheffield Centre for International Drylands Research, 15 pages.

Bateman, M. D., Frederick, C. D., Jaiswal, M. K. and Singhvi, A. K. (2003) Investigations into the potential effects of pedoturbation on luminescence dating. *Quaternary Science Reviews*, **22**, 1,169-1,176.

Bateman, M. D., Boulter, C. H., Carr, A. S., Frederick, C. D., Peter, D. and Wilder, M. (2007) Detecting post-depositional sediment disturbance in sandy deposits using optical luminescence. *Quaternary Geochronology*, **2**, 57-64.

Bateman, M. D., Murton, J. B. and Boulter, C. (2010) The source of De variability in periglacial sand wedges: Depositional processes versus measurement issues. *Quaternary Geochronology*, **5**, 250-256.

Bates, M. R. and Briant, R. M. (2009) Quaternary sediments of the Sussex/Hampshire Coastal Corridor: a brief overview. In: Briant, R. M., Bates, M. R., Horsfield, R. T. and Wenban-Smith, F. F. (eds.) *The Quaternary of the Solent Basin and West Sussex raised beaches: Field Guide*. London, U.K.: Quaternary Research Association, pp. 21-41.

Ben Avraham, Z. and Emery, K. O. (1973) Structural framework of the Sunda Shelf. *Bulletin of the American Association of Petroleum Geologists*, **57**, 2,323-2,366.

Berberian, M. (1995) Master “blind” thrust faults hidden under the Zagros folds: active basement tectonics and surface morphotectonics. *Tectonophysics*, **241**, 193-224.

Berberian, M. and King, G. C. P. (1981) Towards the paleogeography and tectonic evolution of Iran. *Canadian Journal of Earth Sciences*, **18**, 210-265.

Beroza, G. C. and Jordan, T. H. (1990) Searching for Slow and Silent Earthquakes Using Free Oscillations. *Journal of Geophysical Research*, **95** (No. B3), 2,485-2,510.

Bettess, F. (1992) *Surveying for Archaeologists. Second edition*. Durham, U.K.: Department of Archaeology, University of Durham, 136 pages.

Beydoun, Z. R. (1991) *Arabian Plate Hydrocarbon Geology and Potential - A Plate Tectonic Approach.* Tulsa, Oklahoma, U.S.A.: American Association of Petroleum Geologists, Studies in Geology No. 33, map enclosure and 77 pages.

Beydoun, Z. R., Hughes Clarke, M. W. and Stoneley, R. (1992) Petroleum in the Zagros basin: A Late Tertiary foreland basin overprinted onto the outer edge of a vast hydrocarbon-rich Palaeozoic-Mesozoic passive margin shelf. In: MacQueen, R. W. and Leckie, D. A. (eds.) *Foreland Basins and Fold Belts*. Tulsa, Oklahoma, U.S.A.: American Association of Petroleum Geologists, Memoir No. 55, pp. 309-339.

Bird, E. (2000) *Coastal Geomorphology: An Introduction*. Chichester, U.K.: John Wiley and Sons Ltd., 322 pages.

Birkeland, P. W. (1999) *Soils and Geomorphology. Third Edition*. New York, U.S.A.: Oxford University Press, Inc., 430 pages.

Blanc, E. J.-P., Allen, M. B., Inger, S. and Hassani, H. (2003) Structural styles in the Zagros Simple Folded Zone, Iran. *Journal of the Geological Society of London*, **160**, 401-412.

Blum, M. D. and Törnqvist, T. E. (2000) Fluvial responses to climate and sea-level change: a review and look forward. *Sedimentology,* **47** (Suppl. 1), 2-48.

Blum, M., Martin, J., Milliken, K. and Garvin, M. (2013) Paleovalley systems: Insights from Quaternary analogs and experiments. *Earth-Science Reviews*, **116**, 128-169.

Bobek, H. (1959) Vegetationsverwüstung und Bodenerschöpfung in Persien und ihr Zusammenhang mit dem Niedergang älterer Zivilisationen. In: *Proceedings of the ICUN Seventh Technical Meeting, Athens, 11-19 September 1958, Volume 1*. Brussels, Belgium: International Union for Conservation of Nature and Natural Resources, pp 72-80.

Boggs, S. (2006) *Principles of Sedimentology and Stratigraphy. Fourth Edition*. Upper Saddle River, New Jersey, U.S.A.: Pearson Prentice Hall, 662 pages.

Boss, C. D. and Fredeen, K. J. (2004) *Concepts, Instrumentation and Techniques in Inductively Coupled Plasma Optical Emission Spectrometry*. Shelton, Connecticut, U.S.A.: PerkinElmer Inc., 124 pages.

Bosworth, C. E. (1987) 'Askar Mokram, a town of the medieval Islamic province of Ahvaz (Kuzestan) and also the name of the district of which it was the administrative center. *Encyclopaedia Iranica, Online Edition, 1987* (1 page): http://www.iranicaonline.org/articles/askar-mokram-lit (accessed on 6 December 2012).

Bosworth, C. E., De Planhol, X. and Lerner, J. (1984) Ahvaz, a town of southwestern Iran. *Encyclopaedia Iranica, Online Edition, 1984* (7 pages): http://www.iranicaonline.org/articles/ahvaz-a-town-of-southwestern-iran (accessed on 21 November 2012).

Bottema, S. (1986) A late Quaternary pollen diagram from Lake Urmia (northwestern Iran). *Review of Palaeobotany and Palynology*, **47**, 241-261.

Bowman, S. (1990) *Radiocarbon dating*. Berkeley and Los Angeles, U.S.A.: University of California Press/British Museum, 64 pages.

Bretis, B., Bartl, N. and Grasemann, B. (2011) Lateral fold growth and linkage in the Zagros fold and thrust belt (Kurdistan, NE Iraq). *Basin Research*, **23**, 615-630.

Brett, D. (2013) *Ahwaz: confirmed the most polluted city on Earth*. Web page of the Ahwaz News Agency: http://www.ahwaziarabs.info/2013/03/ahwaz-confirmed-most-polluted-city-on.html (accessed on 25 September 2013).

Bridge, J. S. (2003) *Rivers and Floodplains: Form, Processes, and Sedimentary Record*. Malden, Massachusetts, U.S.A.: Blackwell Science, 491 pages.

Bridgland, D. R. (1986) (ed.) *Clast lithological analysis*. Cambridge, U. K.: Quaternary Research Association, Technical Guide No. 3 of the QRA, 207 pages.

Bridgland, D. R. (1994) *Quaternary of the Thames*. London, U.K.: Chapman and Hall, Title No. 7 in the Geological Conservation Review Series of the Joint Nature Conservation Committee, 441 pages.

Bridgland, D. R. (2000) River terrace systems in north-west Europe: an archive of environmental change, uplift and early human occupation. *Quaternary Science Reviews*, **19**, 1,293-1,303.

Brierley, G. J. and Fryirs, K. A. (2005) *Geomorphology and River Management: Applications of the River Styles Framework*. Malden, Massachusetts, U.S.A.: Blackwell Publishing, 398 pages.

Brocklehurst, S. H. (2010) Tectonics and geomorphology. *Progress in Physical Geography*, **34** (3), 357-383.

Bronk Ramsey, C. (2013) *OxCal 4.2 Manual*. Online program of the University of Oxford Radiocarbon Accelerator Unit: https://c14.arch.ox.ac.uk/oxcal/OxCal.html (accessed on 20 May 2013).

Brookes, A. (1988) *Channelized rivers: perspectives for environmental management*. Chichester, U.K.: John Wiley and Sons, 326 pages.

Brookes, A. (1994) River Channel Change. In: Calow, P. and Petts, G. E. (eds.) *The Rivers Handbook. Volume 2*. Oxford, U.K.: Blackwell Science Ltd., pp.55-75.

Brookes, I. A. (1982) Geomorphological evidence for climatic changes in Iran during the last 20,000 years. In: Bintliff, J. L. and Van Zeist, W. (eds.) *Palaeoclimates, Palaeoenvironments and Human Communities in the Eastern Mediterranean Region in Later Prehistory*. Oxford, U.K.: British Archaeological Reports International Series, No. 133 (i and ii), pp. 191-229.

Brookes, I. A. (1989) *The Physical Geography, Geomorphology and Late Quaternary History of the Mahidasht Project Area, Qara Su Basin, Central West Iran*. Toronto, Canada: Royal Ontario Museum, ROM Mahidasht Project Volume 1, 48 pages.

Brozovic, N., Burbank, D. W., Fielding, E. and Meigs, A. J. (1995) The spatial and temporal topographic evolution of Wheeler Ridge, California: New insights from elevation data. *Geological Society of America Abstracts with Programs*, **27**, 396.

Brunsden, D. and Thornes, J. B. (1979) Landscape sensitivity and change. *Transactions of the Institute of British Geographers, New Series*, **4**, 463-484.

Bull, W. B. (1991) *Geomorphic responses to climatic change*. London, U.K.: Oxford University Press, 326 pages.

Bullard, T. F. and Lettis, W. R. (1993) Quaternary fold deformation associated with blind thrust faulting, Los Angeles Basin, California. *Journal of Geophysical Research*, **98**, No. B5, 8,349-8,369.

Burbank, D. W. (1992) Causes of recent Himalayan uplift deduced from deposited patterns in the Ganges basin. *Nature*, **357**, 680-682.

Burbank, D. W. and Anderson, R. S. (2001) *Tectonic geomorphology*. Malden, Massachusetts, U.S.A.: Blackwell Science, 274 pages.

Burbank, D. W. and Anderson, R. S. (2012) *Tectonic geomorphology. Second edition.* Chichester, U.K.: Wiley-Blackwell, 454 pages.

Burbank, D. W. and Tahirkheli, R. A. K. (1985) Magnetostratigraphy, fission-track dating, and stratigraphic evolution of the Peshawar intermontane basin, northern Pakistan. *Bulletin of the Geological Society of America*, **96**, 530-552.

Burbank, D. W. and Vergés, J. (1994) Reconstruction of topography and related depositional systems during active thrusting. *Journal of Geophysical Research*, **99** (No. B10), 20,281-20,297.

Burbank, D., Meigs, A. and Brozović, N. (1996) Interactions of growing folds and coeval depositional systems. *Basin Research*, **8**, 199-223.

Burbank, D. W., McLean, J. K., Bullen, M., Abdrakhmatov, K. Y. and Miller, M. M. (1999) Partitioning of intermontane basins by thrust-related folding, Tien Shan, Kyrgyzstan. *Basin Research*, **11**, 75-92.

Burberry, C. M., Cosgrove, J. W. and Liu, J. G. (2007) Stream network characteristics used to infer the distribution of fold types in the Zagros Simply Folded Belt, Iran. *Journal of Maps, Student Edition*, **2007**, 32-45.

Burberry, C. M., Cosgrove, J. W. and Liu, J. G. (2008) Spatial Arrangement of Fold Types in the Zagros Simply Folded Belt, Iran, Indicated by Landform Morphology and Drainage Pattern Characteristics. *Journal of Maps*, **2008**, 417-430.

Burberry, C. M., Cosgrove, J. W. and Liu, J.-G. (2010) A study of fold characteristics and deformation style using the evolution of the land surface: Zagros Simply Folded Belt, Iran. In: Leturmy, P. and Robin, C. (eds.) *Tectonic and Stratigraphic Evolution of Zagros and Makran during the Mesozoic-Cenozoic*. Bath, U.K.: The Geological Society of London, Geological Society Special Publication No. 330, pp. 139-154.

Burch, G. J., Bath, R. K., Moore, I. D. and O'Loughlin, E. M. (1987) Comparative hydrological behaviour of forests and cleared catchments in South Eastern Australia. *Journal of Hydrology*, **90**, 19-42.

Burnett, A. W. (1982) *Alluvial stream response to neotectonics in the lower Mississippi Valley*. Unpublished M.Sc. thesis, Colorado State University, Fort Collins, Colorado, U.S.A., 182 pages.

Burrato, P., Ciucci, F. and Valensise, G. (2003) An inventory of river anomalies in the Po Plain, Northern Italy: evidence for active blind thrust faulting. *Annals of Geophysics*, **46** (No. 5), 865-882.

Butzer, K. W. (1976) *Early Hydraulic Civilization in Egypt: A Study in Cultural Ecology*. Chicago, U.S.A.: University of Chicago Press, 134 pages.

Carter, E. and Stolper, M. W. (1984) *Elam: Surveys of political history and archaeology*. Berkeley, California, U.S.A.: University of California Press, 328 pages.

Center for Sustainability and the Global Environment (CSGE) (2010) *River Discharge Database - Station: Ahvaz, River: Karun*. Web page (one large page) of the Global River Discharge Database of the Center for Sustainability and the Global Environment, Gaylord Nelson Institute for Environmental Studies, University of Wisconsin-Madison: http://www.sage.wisc.edu/riverdata/scripts/station_table.php?qual=32&filenum=1079 (accessed on 14 March 2011).

Champel, B., Van der Beek, P., Mugnier, J.-L. and Leturmy, P. (2002) Growth and lateral propagation of fault-related folds in the Siwaliks of western Nepal: Rates, mechanisms, and geomorphic signature. *Journal of Geophysical Research: Solid Earth*, **107** (Issue B6), doi: 10.1029/2001JB000578, 18 pages.

Chang, H. H. (2001) *Fluvial Processes in River Engineering*. Malabar, Florida, U.S.A.: Krieger Publishing Co., 456 pages.

Chappell, A. (1998) Dispersing sandy soil for the measurement of particle size distributions using optical laser diffraction. *Catena*, **31** (4), 271-281.

Chesney, R. F. (1850) *The expedition for the survey of the rivers Euphrates and Tigris: carried on by order of the British Government in the years 1835, 1836, and 1837; preceded by geographical and historical notices of the regions situated between the rivers Nile and Indus. Volume 1 and Volume 2*. London, U.K.: Longman, Brown, Green and Longmans, 1,577 pages & maps.

Chew, L. C. and Ashmore, P. E. (2001) Channel adjustment and a test of rational regime theory in a proglacial braided stream. *Geomorphology*, **37**, 43-63.

Coad, B. W. (2009) *Freshwater Fishes of Iran: Introduction - Drainage Basins - Tigris River*. Web page (one large page) of Brian W. Coad about freshwater fishes of Iran: http://www.briancoad.com/introduction/tigrisriverbasin.htm (accessed on 8 March 2011).

Coe, A. L. (ed.) (2003) *The Sedimentary Record of Sea-Level Change*. Cambridge, U.K.: Cambridge University Press, 287 pages.

Cohen, K. M., Stouthamer, E. and Berendsen, H. J. A. (2002) Fluvial deposits as a record for Late Quaternary neotectonic activity in the Rhine-Meuse delta, The Netherlands. *Netherlands Journal of Geosciences*, **81** (3-4), 389-405.

Collins, B. A. (2001) *The Best Divisions for Knowledge of the Regions: A translation of Ahsan al-taqasim fi marifat al-aqalim by al-Muqaddasi*. Reading, U.K.: Garnet Publishing, 424 pages & maps.

Colls, A. E., Stokes, S., Blum, M. D. and Straffin, E. (2001) Age limits on the Late Quaternary evolution of the upper Loire River. *Quaternary Science Reviews*, **20**, 743-750.

Colman-Sadd, S. P. (1978) Fold Development in Zagros Simply Folded Belt, Southwest Iran. *Bulletin of the American Association of Petroleum Geologists*, **62** (No. 6), 984-1003.

Cooke, G. A. (1987) Reconstruction of the Holocene Coastline of Mesopotamia. *Geoarchaeology*, **2** (No. 1), 15-28.

Coulthard, T. J. and Van de Wiel, M. J. (2007) Quantifying fluvial non linearity and finding self organised criticality? Insights from simulations of river basin evolution. *Geomorphology*, **91**, 216-235.

Coulthard, T. J., Lewin, J. and Macklin, M. G. (2005) Modelling differential catchment response to environmental change. *Geomorphology*, **69**, 222-241.

Coulthard, T. J., Hicks, D. M. and Van de Wiel, M. J. (2007) Cellular modelling of river catchments and reaches: Advantages, limitations and prospects. *Geomorphology*, **90**, 192-207.

Cowie, P. A., Whittaker, A. C., Attal, M., Roberts, G., Tucker, G. E. and Ganas, A. (2008) New constraints on sediment-flux-dependent river incision: implications for extracting tectonic signals from river profiles. *Geology*, **36**, 535-538.

Cox, K. G., Price, N. B. and Harte, B. (1988) *An Introduction to The Practical Study of Crystals, Minerals and Rocks. International Edition*. London, U.K.: McGraw-Hill Book Co. (UK) Ltd., 245 pages.

Cox, R. T. (1994) Analysis of drainage-basin symmetry as a rapid technique to identify areas of possible Quaternary tilt-block tectonics: An example from the Mississippi Embayment. *Bulletin of the Geological Society of America*, **106**, 571-581.

Crampton, S. L. and Allen, P. A. (1995) Recognition of forebulge unconformities associated with early stage foreland basin development: Example from the North Alpine foreland basin. *Bulletin of the American Association of Petroleum Geologists*, **79**, 1,495-1,514.

Cressey, G. B. (1958) The Shatt al-Arab Basin. *Middle East Journal*, **12** (No. 4), 448-460.

Curzon, G. (1890) The Karun River and the Commercial Geography of South-west Persia. *Proceedings of the Royal Geographical Society and Monthly Record of Geography*, **12** (No. 9), 509-532 & Map.

Curzon, G. N. (1892) *Persia and the Persian Question. Volume II*. London, U.K.: Longmans, Green and Co., 653 pages.

Dalongeville, R. and Sanlaville, P. (1987) Confrontations des datations isotopiques aux données géomorphologique et archéologiques à propos des variations relatives du niveau marin sur la rive arabe du Golfe Persique. In: Aurenche, O., Evin, J. and Hours, F. (eds.) *Chronologies in the Near East: Relative Chronologies and Absolute Chronology 16,000-4,000 BP., C.N.R.S. International Symposium, Lyon (France), 24 - 28 November 1986*. Oxford, U.K.: British Archaeological Reports International Series, No. 379 (ii), pp. 567-584.

Daniels, R. B. (1960) Entrenchment of the Willow Creek Drainage Ditch, Harrison County, Iowa. *American Journal of Science*, **258**, 161-176.

DeCelles, P. G. and Giles, K. A. (1996) Foreland basin systems. *Basin Research*, **8**, 105-123.

De Miroschedji, P. (2003) Susa and the Highlands: Major Trends in the History of Elamite Civilization. In: Miller, N. F. and Abdi, K. (eds.) *Yeki bud, yeki nabud: Essays on the archaeology of Iran in honor of William M. Sumner*. Los Angeles, U.S.A.: The Cotsen Institute of Archaeology at UCLA, Monograph No. 48, pp. 16-38.

Deer, W. A., Howie, R. A. and Zussman, J. (1978) *An Introduction to the Rock-Forming Minerals*. (ELBS edition). Harlow, Essex, U.K.: Longman Group Ltd., 528 pages.

Demir, T., Westaway, R., Bridgland, D. R. and Seyrek, A. (2007) Terrace staircases of the River Euphrates in southeast Turkey, northern Syria and western Iraq: evidence for regional surface uplift. *Quaternary Science Reviews*, **26**, 2,844-2,863.

Dewan, M. L. and Famouri, J. (1964) *The soils of Iran*. Rome, Italy: Food and Agriculture Organization of the United Nations, 319 pages.

Dietrich, R. V. (2011) *Marble, limestone and dolostone*. Web page (one large page) of the Central Michigan University: http://stoneplus.cst.cmich.edu/marble.htm (accessed on 20 June 2011).

Dieulafoy, M. (1885) *L'Art antique de la Perse: Achéménides, Parthes, Sassanides. 5e partie: Monuments Parthes et Sassanides*. Paris, France: Librairie
, 239 pages.

Djamali, M., De Beaulieu, J.-L., Shah-hosseini, M., Andrieu-Ponel, V., Ponel, P., Amini, A., Akhani, H., Leroy, S. A. G., Stevens, L., Lahjani, H. and Brewer, S. (2008)

A late Pleistocene long pollen record from Lake Urmia, NW Iran. *Quaternary Research*, **69**, 413-420.

Djamali, M., De Beaulieu, J.-L., Miller, N. M., Andrieu-Ponel, V., Ponel, P., Lak, R., Sadeddin, N., Akhani, H. and Fazeli, H. (2009) Vegetation history of the SE section of the Zagros Mountains during the last five millennia; a pollen record from the Maharlou Lake, Fars Province, Iran. *Vegetation History and Archaeobotany*, **18** (No. 2), 123-136.

Djamali, M., Akhani, H., Andrieu-Ponel, V., Braconnot, P., Brewer, S., De Beaulieu, J.-L., Fleitmann, D., Fleury, J., Gasse, F., Guibal, F., Jackson, S. T., Lézine, A.-M., Médail, F., Ponel, P., Roberts, N. and Stevens, L. (2010) Indian Summer Monsoon variations could have affected the early-Holocene woodland expansion in the Near East. *The Holocene*, **20** (5), 813-820.

Dollar, E. S. J. (2004) Fluvial geomorphology. *Progress in Physical Geography*, **28** (3), 405-450.

Douglass, J. and Schmeeckle, M. (2007) Analogue modeling of transverse drainage mechanisms. *Geomorphology*, **84**, 22-43.

Douglass, J., Meek, N., Dorn, R. I. and Schmeeckle, M. W. (2009) A criteria-based methodology for determining the mechanism of transverse drainage development, with application to the southwestern United States. *Bulletin of the Geological Society of America*, **121** (No. 3/4), 586-598.

Downs, P. W. and Gregory, K. J. (2004) *River Channel Management: Towards Sustainable Catchment Hydrosystems*. London, U.K.: Arnold, 395 pages.

Drury, S. A. (2001) *Image Interpretation in Geology. Third Edition*. Cheltenham, U.K.: Nelson Thornes Ltd., 290 pages.

Dumont, J. F. (1994) Neotectonics and rivers of the Amazon headwaters. In: Schumm, S. A. and Winkley, B. R. (eds.) *The Variability of Large Alluvial Rivers*. New York, U.S.A.: American Society of Civil Engineers Press, pp. 103-114.

Dupin, L. (2011) Mapping the landform assemblages and archaeological record of the Lower Khuzestan plain (SW Iran) using remote-sensing and GIS techniques. In: Brown, A. G., Basell, L. S. and Butzer, K. W. (eds.) *Geoarchaeology, Climate Change and Sustainability*. Boulder, Colorado, U.S.A.: Geological Society of America, Special Paper 476, pp. 53-68.

Dutton, A. and Lambeck, K. (2012) Ice Volume and Sea Level During the Last Interglacial. *Science*, **337**, 216-219.

Edgell, H. S. (1996) Salt tectonism in the Persian Gulf Basin. In: Alsop, G. I., Blundell, D. J. and Davison, I. (eds.) *Salt tectonics.* Bath, U.K.: The Geological Society of London, Geological Society Special Publication No. 100, pp. 129-151.

Ehlers, E. (2001) Glaciers and ice fields in Persia. *Encyclopaedia Iranica*, *Online Edition, 2001*: http://www.iranicaonline.org/articles/glaciers (accessed on 8 March 2011).

El-Moslimany, A. P. (1986) Ecology and late-Quaternary history of the Kurdo-Zagrosian oak forest near Lake Zeribar, western Iran. *Vegetatio*, **68**, 55-63.

El-Moslimany, A. P. (1987) The late Pleistocene climates of the Lake Zeribar region (Kurdistan, western Iran) deduced from the ecology and pollen production of non-arboreal vegetation. *Vegetatio,* **72**, 131-139.

Emami, K., Arab, D. R., Madashti, A., Saarang, A., Shirazi, H., Izadpanaah, T., Izadjoo, F. and Basirzadeh, H. (2003) The value engineering study of Marun regulating dam in Iran. In: Berga, L., Buil, J. M., Jofré, C. and Chonggang, S. (eds.) *Roller Compacted Concrete Dams*. Lisse, The Netherlands: Swets & Zeitlinger, pp. 139-146.

Fairbanks, R. G. (2005) *Radiocarbon Calibration*. Web page (one large page) of the Lamont-Doherty Earth Observatory / Columbia University in the city of New York: http://radiocarbon.ldeo.columbia.edu/research/radiocarbon.htm (accessed on 1 June 2011).

Fairchild, I., Hendry, G., Quest, M. and Tucker, M. (1988) Chemical analysis of sedimentary rocks. In: Tucker, M. (ed.) *Techniques in Sedimentology*. Oxford, U.K.: Blackwell Scientific Publications, pp. 274-354.

Fakhari, M. D., Axen, G. J., Horton, B. K., Hassanzadeh, J. and Amini, A. (2008) Revised age of proximal deposits in the Zagros foreland basin and implications for Cenozoic evolution of the High Zagros. *Tectonophysics*, **451**, 170-185.

Falcon, N. L. (1961) Major Earth-flexuring in the Zagros Mountains of south-west Iran. *Quarterly Journal of the Geological Society of London,* **117**, 367-376.

Falcon, N. L. (1974) Southern Iran: Zagros Mountains. In: Spencer, A. M. (ed.) *Mesozoic - Cenozoic Orogenic Belts: Data for Orogenic Studies.* Edinburgh, U.K.: Scottish Academic Press, Geological Society Special Publication No. 4, pp. 199-211.

Farrand, W. R. (1979) Blank on the Pleistocene map. *Geographical Magazine,* **51** (No. 8), 548-554.

Ferrigno, J. G. (1991) Glaciers of the Middle East and Africa - Glaciers of Iran. In: Williams, R. S. and Ferrigno, J. G. (eds.) Satellite image atlas of glaciers of the World. Denver, Colorado, U.S.A.: *United States Geological Survey Professional Paper* **1386-G-2**, pp. G31-G47.

Flam, L. (1993) Fluvial geomorphology of the lower Indus Basin (Sindh, Pakistan) and the Indus civilization. In: Shroder, J. F. (ed.) *Himalaya to the Sea: Geology, geomorphology and the Quaternary*. London, U.K.: Routledge, pp. 265-287.

Fleitmann, D., Burns, S. J., Mangini, A., Mudlesee, M., Kramers J. and Villa, I. (2007) Holocene ITCZ and Indian monsoon dynamics recorded in stalagmites from Oman and Yemen (Socotra). *Quaternary Science Reviews*, **26**, 170-188.

Fleming, K., Johnston, P., Zwartz, D., Yokoyama, Y., Lambeck, K. and Chappell, J. (1998) Refining the eustatic sea-level curve since the Last Glacial Maximum using far- and intermediate-field sites. *Earth and Planetary Science Letters*, **163**, 327-342.

Flemings, P. B. and Jordan, T. E. (1989) A Synthetic Stratigraphic Model of Foreland Basin Development. *Journal of Geophysical Research*, **94**, No. B4, 3,851-3,866.

Fonstad, M. and Marcus, W. A. (2003) Self-organized criticality in riverbank systems. *Annals of the Association of American Geographers*, **93** (2), 281-296.

Food and Agriculture Organization of the United Nations (FAO) (1992) *Technical Cooperation Programme, The Islamic Republic of Iran: Aquaculture section fact-finding mission*. Rome, Italy: FAO, Field Document FI:TCP/IRA/2251(F), 65 pages.

Frenette, M. and Harvey, B. (1973) River Channel Processes. In: *Fluvial Processes and Sedimentation: Proceedings of Hydrology Symposium held at University of Alberta, Edmonton, May 8 and 9, 1973*. (Prepared and published for the National Research Council of Canada, Subcommittee on Hydrology by the Canada Inland Waters Directorate). Ottawa, Canada: Information Canada, pp. 294-341.

Frey, W. and Probst, W. (1986) A synopsis of the vegetation in Iran. In: Kürschner, H. (ed.) *Contributions to the vegetation of Southwest Asia*. Wiesbaden, Germany: Dr. Ludwig Reichert Verlag, Beihefte zum Tübinger Atlas des Vorderen Orients, Reihe A (Naturwissenschaften) Nr. 24, pp. 9-43.

Frigge, M., Hoaglin, D. C. and Iglewicz, B. (1989) Some Implementations of the Boxplot. *The American Statistician*, **43** (1), 50-54.

Frostick, L. E. and Jones, S. J. (2002) Impact of periodicity on sediment flux in alluvial systems: grain to basin scale. In: Jones, S. J. and Frostick, L. E. (eds.) *Sediment Flux to Basins: Causes, Controls and Consequences*. Bath, U.K.: The Geological Society of London, Geological Society Special Publication No. 191, pp. 81-95.

Gabet, E. J., Burbank, D. W., Pratt-Situala, B., Putkonen, J. and Bookhagen, B. (2008) Modern erosion rates in the High Himalayas of Nepal. *Earth and Planetary Science Letters*, **267**, 482-494.

Galbraith, R. F. and Green, P. F. (1990) Estimating the component ages in a finite mixture. *Radiation Measurements*, **17**, 197-206.

Galbraith, R. F., Roberts, R. G., Laslett, G. M., Yoshida, H. and Olley, J. M. (1999). Optical dating of single and multiple grains of quartz from Jinnium rock shelter, northern Australia: Part I, Experimental design and statistical models. *Archaeometry*, **41** (2), 339-364.

Gale, S. J. and Hoare, P. G. (1991) *Quaternary Sediments: Petrographic Methods for the Study of Unlithified Rocks*. London, U. K.: Belhaven Press, 323 pages.

Gardiner, V. and Dackombe, R. V. (1983) *Geomorphological field manual*. London: George Allen and Unwin Ltd., 254 pages.

Garmin (2011) *Garmin GPS 12 Specifications*. Web page (one large page) of Garmin Ltd.: http://www8.garmin.com/products/gps12/spec.html (accessed on 20 June 2011).

Garrison, E. G. (2003) *Techniques in Archaeological Geology*. Berlin, Germany: Springer-Verlag, 320 pages.

Gasche, H., Paymani, A. R., Baeteman, C., Dupin, L. and Heyvaert, V. (2004) The Persian Gulf Shorelines and the Karkheh, Karun and Jarrahi Rivers: A Geo-Archaeological Approach. A Joint Belgo-Iranian Project. First Progress Report. *Akkadica*, **125** (Fasc. 2), 141-215.

Gasche, H., Baeteman, C., Dupin, L., Heyvaert, V., Paymani, A. R. and Cole, S. W. (2005) The Persian Gulf Shorelines and the Karkheh, Karun and Jarrahi Rivers: A Geo-Archaeological Approach. A Joint Belgo-Iranian Project. First Progress Report - Part 2. *Akkadica*, **126** (Fasc. 1), 1-43.

Gasche, H., Cole, S. W. and Hritz, C. (2007) The Persian Gulf Shorelines and the Karkheh, Karun and Jarrahi Rivers: A Geo-Archaeological Approach. A Joint Belgo-Iranian Project. First Progress Report - Part 3. *Akkadica*, **128** (Fasc. 1-2), 1-72.

Gasse, F. and Van Campo, E. (1994) Abrupt post-glacial climate events in West Asia and North Africa monsoon domains. *Earth and Planetary Science Letters*, **126**, 435-456.

Gay, S. P. (2012) *Joints, Linears, and Lineaments – The Basement Connection*. Search and Discovery Article #41083 (2012) (adapted from oral presentation given at AAPG Rocky Mountain Section Meeting, Grand Junction, Colorado, U.S.A., 9-12 September 2012): http://www.searchanddiscovery.com/documents/2012/41083gay/ndx_gay.pdf (posted on 30 November 2012).

Ghassemi, M. R. (2005) Drainage evolution in response to fold growth in the hanging-wall of the Khazar fault, north-eastern Alborz, Iran. *Basin Research*, **17**, 425-436.

Giardino, J. R. and Lee, A. A. (2011) *Rates of Channel Migration on the Brazos River*. College Station, Texas, U.S.A.: Texas A&M University, Final Report - Contact No. 0904830898 - submitted to the Texas Water Development Board, 45 pages & appendices.

Giesse, P., Makris, J., Akashe, B., Rower, P., Letz, H. and Mostaanpour, M. (1983). Seismic crustal studies in southern Iran between Central Iran and the Zagros Belt. *Geological Survey of Iran, Internal Report*, **51**, 71-84.

Gillespie, R. (1984) *Radiocarbon user's handbook*. Oxford, U.K.: Oxbow Books, Monograph No. 3 of Oxford University Committee for Archaeology, 36 pages.

Gleeson, T. and Novakowski, K. (2009) Identifying watershed-scale barriers to groundwater flow: Lineaments in the Canadian Shield. *Bulletin of the Geological Society of America*, **121** (No. 3/4), 333-347.

Golchin, J. (1977) *Navigation on Karun River*. Ames, Iowa, U.S.A.: Iowa State University of Science and Technology, 182 pages.

Goudie, A., Anderson, M., Burt, T., Lewin, J., Richards, K., Whalley, B. and Worsley, P. (1990) *Geomorphological Techniques. Second Edition*. London, U.K. and New York, U.S.A.: Unwin Hyman Ltd. and Routledge, 570 pages.

Graadt van Roggen, D.-L. (1905) *Notice sur les anciens travaux hydrauliques en Susiane. (Extrait des Mémoires de la Délégation en Perse, VII)*. Chalon-sur-Saône, France: E. Bertrand, 41 pages & Figs.

Great Britain Naval Intelligence Division (GBNID) (1945) *Persia*. London, U.K.: H. M. Stationery Office, B.R. 525, Geographical Handbook Series, 638 pages.

Gregory, K. J. (1987) Environmental effects of river channel changes. *Regulated Rivers: Research and Management*, **1**, 358-363.

Griffin, P. (2004) *Radiometric Measures: Radiocarbon Dating*. Web page (one large page) of Paul Griffin about archaeoastronomy: http://www.bluhorizonlines.org/curv/radio1.html (accessed on 19 July 2011).

Griffiths, H. I., Schwalb, A. and Stevens, L. R. (2001) Environmental change in southwestern Iran: the Holocene ostracod fauna of Lake Mirabad. *The Holocene,* **11** (6), 757-764.

Gutman, G., Byrnes, R., Masek, J., Covington, S., Justice, C., Franks, S. and Headley, R. (2008) Towards monitoring land-cover and land-use changes at a global scale: the global land survey 2005. *Photogrammetric Engineering and Remote Sensing*, **74** (1), 6-10.

Hamilton, W. R., Woolley, A. R. and Bishop, A. C. (1992) *Hamlyn Guide to Minerals, Rocks and Fossils.* London, U.K.: Reed Consumer Books Limited, 320 pages.

Hamzepour, B., Paul, D. J. and Wiesner, E. K. (1999) Views on the structural development of the Zagros simply folded Belt in Khuzestan Province, Iran. *Zeitschrift der Deutschen Geologischen Gesellschaft,* **150** (1), 167-188.

Hansman, J. F. (1978) The Mesopotamian Delta in the First Millennium, BC. *Geographical Journal*, **144** (No. 1), 49-61.

Harbor, D. J., Schumm, S. A. and Harvey, M. D. (1994) Tectonic Control of the Indus River in Sindh, Pakistan. In: Schumm, S. A. and Winkley, B. R. (eds.) *The Variability of Large Alluvial Rivers*. New York, U.S.A.: American Society of Civil Engineers Press, pp. 161-175.

Hardy, S. and Poblet, J. (2005) A method for relating fault geometry, slip rate and uplift data above fault-propagation folds. *Basin Research*, **17**, 417-424.

Hareide, D. (2004) *Iranian Tide Gauge Network. IOC/GLOSS Technical Expert Visit to National Cartographic Center (NCC), Tehran, Iran*. Stavanger, Norway: Norwegian Hydrographic Service, 20 pages.

Haroni, H. A., Erren, H. and Westerhof, P. (2000) Integrated analysis of remote sensing, aeromagnetic, geological and mineral occurrence data for the assessment of a subduction setting along the Zagros Orogenic Belt of Iran. *International Archives of Photogrammetry and Remote Sensing*, **33** (Part B7), 1,700-1707.

Hartley, A. J., Weissmann, G. S., Nichols, G. J. and Warwick, G. L. (2010) Large Distributive Fluvial Systems: Characteristics, distribution and controls on development. *Journal of Sedimentary Research*, **80**, 167-183.

Hartung, F. and Kuros, G. R. (1987) Historische Talsparren im Iran. In: Garbrecht, G. (ed.) *Historische Talsperren, **1***. Stuttgart, Germany: Verlag Konrad Wittwer, pp. 221-274.

Harwood, G. (1988) Microscopical techniques: II. Principles of sedimentary petrography. In: Tucker, M. (ed.) *Techniques in Sedimentology*. Oxford, U.K.: Blackwell Scientific Publications, pp. 108-173.

Hatzfeld, D and Molnar, P. (2010) Comparisons of the kinematics and deep structures of the Zagros and Himalaya and of the Iranian and Tibetan Plateaus and geodynamic implications. *Review of Geophysics*, **48**, RG2005, doi:10.1029/2009RG000304, 48 pages.

Hatzfeld, D., Authemayou, C., Van der Beek, P., Bellier, O., Lavé, J., Oveisi, B., Tatar, M., Tavakoli, F., Walpersdorf, A. and Yamini-Fard, F. (2010) The kinematics of the Zagros Mountains (Iran). In: Leturmy, P. and Robin, C. (eds.) *Tectonic and*

Stratigraphic Evolution of Zagros and Makran during the Mesozoic-Cenozoic. Bath, U.K.: The Geological Society of London, Geological Society Special Publication No. 330, pp. 19-42.

Haynes, S. J. and McQuillan, H. (1974) Evolution of the Zagros Suture Zone, Southern Iran. *Bulletin of the Geological Society of America*, **85**, 739-744.

Heidari, A. (2009) Structural master plan of flood mitigation measures. *Natural Hazards and Earth System Sciences*, **9**, 61-75.

Heinrich, E. M. (1965) *Microscopic identification of minerals*. New York, U.S.A.: McGraw-Hill Book Co., 414 pages.

Hessami, K., Koyi, H. A., Talbot, C. J., Tabasi, H. and Shabanian, E. (2001a) Progressive unconformities within an evolving fold-thrust belt, Zagros Mountains. *Journal of the Geological Society of London*, **158**, 969-981.

Hessami, K., Koyi, H. A. and Talbot, C. J. (2001b) The significance of strike-slip faulting in the basement of the Zagros fold and thrust belt. *Journal of Petroleum Geology*, **24** (1), 5-28.

Heyvaert, V. M. A. and Baeteman, C. (2007) Holocene sedimentary evolution and palaeocoastlines of the Lower Khuzestan plain (southwest Iran). *Marine Geology*, **242**, 83-108.

Heyvaert, V. M. A., Walstra, J., Verkinderen, P., Weerts, H. J. T. and Ooghe, B. (2012) The role of human interference on the channel shifting of the Karkheh River in the Lower Khuzestan plain (Mesopotamia, SW Iran). *Quaternary International*, **251**, 52-63.

Heyvaert, V. M. A., Verkinderen, P. and Walstra, J. (2013) Geoarchaeological Research in Lower Khuzestan: State of the Art. In: De Graef, K. and Tavernier, J. (eds.) *Susa and Elam. Archaeological, Philological, Historical and Geographical Perspectives. Proceedings of the International Congress Held at Ghent University, December 14-17, 2009*. (Volume 58 of Mémoires de la Délégation en Perse Series). Leiden, The Netherlands: Brill Academic Publishers, pp. 493-534.

Higgins, M. B. (1999) Heighting with GPS: Possibilities and Limitations. In: Lilje, M. (ed.) *Geodesy and Surveying in the Future: The Importance of Heights. Proceedings of the Jubilee Seminar, 25 years of Motorised Levelling, Sponsored by Commission 5 of FIG, Gävle, Sweden, 15-17 March, 1999*. Gävle, Sweden: National Land Survey of Sweden, 10 pages.

High-Purity Standards, Inc. (HPS) (2011) *Products - Sediment and Soil Solutions*. Web page (one page) of HPS: http://www.highpuritystandards.com/store/home.php?cat=94 (accessed on 14 June 2011).

Hillman, G. C. (1996) Late Pleistocene changes in wild plant-foods available to hunter-gatherers of the northern Fertile Crescent: Possible preludes to cereal cultivation. In: Harris, D. R. (ed.) *The Origins and Spread of Agriculture and Pastoralism in Eurasia*. London, U.K.: UCL Press, pp. 159-203.

Hodge, A. T. (1992) *Roman Aqueducts and Water Supply*. London, U.K.: Duckworth, 504 pages.

Hogan, D. L. and Luzi, D. S. (2010) Channel Geomorphology: Fluvial Forms, Processes and Forest Management Effects. In: Pike, R. G., Redding, T. E., Moore, R. D., Winkler, R. D. and Bladon, K. D. (eds.) *Compendium of Forest Hydrology and Geomorphology in British Columbia. Volume 1 of 2*. Victoria, Canada: Forest Science Program and FORREX, British Columbia Land Management Handbook No. 66, pp. 331-372.

Holbrook, J. and Schumm, S. A. (1999) Geomorphic and sedimentary response of rivers to tectonic deformation: a brief review and critique of a tool for recognizing subtle epeirogenic deformation in modern and ancient settings. *Tectonophysics*, **305**, 287-306.

Holt, W. E. and Stern, T. A. (1994) Subduction, platform subsidence, and foreland thrust loading: the late Tertiary development of Taranaki basin, New Zealand. *Tectonics*, **13**, 1,068-1,092.

Horton, B. K. and DeCelles, P. G. (1997) The modern foreland basin system adjacent to the Central Andes. *Geology*, **25**, 895-898.

Howard, A. D. (1967) Drainage analysis in geologic interpretation: A summation. *Bulletin of the American Association of Petroleum Geologists*, **51** (No. 11), 2,246-2,259.

Howard, A. D. (1980) Thresholds in river regimes. In: Coates, D. R. and Vitek, J. D. (eds.) *Thresholds in geomorphology*. London, U.K.: George Allen and Unwin, pp. 227-258.

Howard, A. D., Keetch, M. E. and Vincent, C. L. (1970) Topological and Geometrical Properties of Braided Streams. *Water Resources Research*, **6** (No. 6), 1,674-1,688.

Hudson, P. F. and Kesel, R. H. (2000) Channel migration and meander-bend curvature in the lower Mississippi River prior to major human modification. *Geology*, **28** (No. 6), 531-534.

Humphrey, N. F. and Konrad, S. K. (2000) River incision or diversion in response to bedrock uplift. *Geology*, **28** (No. 1), 43-46.

Hurtrez, J.-E., Lucazeau, F., Lavé, J. and Avouac, J.-P. (1999) Investigation of the relationships between basin morphology, tectonic uplift, and denudation from the study of an active fold belt in the Siwalik Hills, central Nepal. *Journal of Geophysical Research*, **104** (No. B6), 12,779-12,796.

Hyndman, R. D. and Wang, K. (1995) The rupture zone of Cascadia great earthquakes from current deformation and the thermal regime. *Journal of Geophysical Research*, **100** (No. B11), 22,133-22,154.

International Atomic Energy Agency (IAEA) (2005) *Fluvial sediment transport: Analytical techniques for measuring sediment load*. Vienna, Austria: International Atomic Energy Agency, IAEA-TECDOC-1461, 61 pages.

Ionides, M. G. (1937) *The regime of the rivers Euphrates and Tigris*. London, U.K.: E. and F. N. Spon Ltd., 278 pages.

Iranian Oil Operating Companies (IOOC) (1969a) *Geological Compilation Map, 1:100,000 Scale, Sheet No. 20829 E, Ahwaz*. Tehran, Iran: IOOC, Geological and Exploration Division.

Iranian Oil Operating Companies (IOOC) (1969b) *Geological Compilation Map, 1:100,000 Scale, Sheet No. 20829 W, Ab Teymur*. Tehran, Iran: IOOC, Geological and Exploration Division.

Iranian Oil Operating Companies (IOOC) (1969c) *Geological Compilation Map, 1:100,000 Scale, Sheet No. 20824 W, Susangerd*. Tehran, Iran: IOOC, Geological and Exploration Division.

Jackson, J. and McKenzie, D. (1988) The relationship between plate motion and seismic moment tensors and the rates of active deformation in the Mediterranean and Middle East. *Geophysical Journal of the Royal Astronomical Society*, **93**, 45-73.

Jackson, J., Haines, J. and Holt, W. (1995) The accommodation of Arabia-Eurasia plate convergence in Iran. *Journal of Geophysical Research*, **100** (No. B8), 15,205-15,219.

Jackson, J., Norris, R. and Youngson, J. (1996) The structural evolution of active fault and fold systems in central Otago, New Zealand: evidence revealed by drainage patterns. *Journal of Structural Geology*, **18** (Nos. 2/3), 217-234.

Jahani, A. (1992) Calculating the suspended sediment load of the Dez River. In: Bogen, J., Walling, D. E. and Day, T. J. (eds.) *Erosion and Sediment Transport Monitoring Programmes in River Basins*. Proceedings of the International Symposium held at Oslo, Norway, 24-28 August 1992. Wallingford, Oxfordshire, U.K.: IAHS Press, International Association of Hydrological Sciences Publication No. 210, pp. 219-224.

James, G. A. and Wynd, J. G. (1965) Stratigraphic nomenclature of Iranian Oil Consortium Agreement Area. *Bulletin of the American Association of Petroleum Geologists*, **49** (No. 12), 2,182-2,245.

Jerolmack, D. J. and Swenson, J. B. (2007) Scaling relationships and evolution of distributary networks on wave-influenced deltas. *Geophysical Research Letters*, **34** (23), L23402, doi:10.1029/2007GL031823, 5 pages.

Jones, S. J. (2002) Transverse rivers draining the Spanish Pyrenees: large scale patterns of sediment erosion and deposition. In: Jones, S. J. and Frostick, L. E. (eds.) *Sediment Flux to Basins: Causes, Controls and Consequences*. Bath, U.K.: The Geological Society of London, Geological Society Special Publication No. 191, pp. 171-185.

Jones, S. J. (2004) Tectonic controls on drainage evolution and development of terminal alluvial fans, southern Pyrenees, Spain. *Terra Nova*, **16** (No. 3), 121-127.

Jones, A. P., Tucker, M. E. and Hart, J. K. (eds.) (1999a) *The Description and Analysis of Quaternary Stratigraphic Field Sections*. London, U.K.: Quaternary Research Association, Technical Guide No. 7 of the QRA, 293 pages.

Jones, S. J., Frostick, L. E. and Astin, T. R. (1999b) Climatic and tectonic controls on fluvial incision and aggradation in the Spanish Pyrenees. *Journal of the Geological Society of London*, **156**, 761-769.

Jordan, T. E. (1995) Retroarc foreland and related basins. In: Busby, C. J. and Ingersoll, R. V. (eds.) *Tectonics of Sedimentary Basins*. Oxford, U.K.: Blackwell Scientific Publications, pp. 331-362.

Jorgensen, D. W. (1990) *Adjustment of alluvial river morphology and process to localized active tectonics*. Unpublished Ph.D. thesis, Colorado State University, Fort Collins, Colorado, U.S.A., 240 pages.

Jorgensen, D. W., Harvey, M. D., Schumm, S. A. and Flam, L. (1993) Morphology and dynamics of the Indus River: Implications for the Mohen Jo Daro site. In: Shroder, J. F. (ed.) *Himalaya to the Sea: Geology, geomorphology and the Quaternary*. London, U.K.: Routledge, pp. 181-204.

Kavanagh, B. F. (2009) *Surveying: Principles and Applications. Eighth Edition*. Upper Saddle River, New Jersey, U.S.A.: Pearson Prentice Hall, 791 pages & colour Figs.

Kehl, M. (2009) Quaternary climate change in Iran – The state of knowledge. *Erdkunde*, **63** (No. 1), 1-17.

Keller, E. A. and Pinter, N. (1996) *Active tectonics: Earthquakes, Uplift and Landscape*. Upper Saddle River, New Jersey, U.S.A.: Prentice-Hall, 338 pages.

Keller, E. A., Zepeda, R. L., Rockwell, T. K., Ku, T. L. and Dinklage, W. S. (1998) Active tectonics at Wheeler Ridge, southern San Joaquin Valley, California. *Bulletin of the Geological Society of America*, **110**, 298-310.

Keller, E. A., Gurrola, L. and Tierney, T. E. (1999) Geomorphic criteria to determine direction of lateral propagation of reverse faulting and folding. *Geology*, **27** (No. 6), 515-518.

Kelletat, D. (2006) Beachrock as Sea-Level Indicator? Remarks from a Geomorphological Point of View. *Journal of Coastal Research*, **22** (6), 1,558-1,564.

Kelts, K. and Shahrabi, M. (1986) Holocene sedimentology of hypersaline Lake Urmia, northwestern Iran. *Palaeogeography, Palaeoclimatology, Palaeoecology*, **54**, 105-130.

Kemp, A. C., Horton, B. P., Donnelly, J. P., Mann, M. E., Vermeer, M. and Rahmstorf, S. (2011) Climate related sea-level variations over the past two millennia. *Proceedings of the National Academy of Sciences of the United States of America*, **108** (No. 27), 11,017-11,022 and doi:10.1073/pnas.1015619108, 6 + 14 pages.

Kennett, D. J. and Kennett, J. P. (2006) Early State Formation in Southern Mesopotamia: Sea Levels, Shorelines, and Climate Change. *Journal of Island and Coastal Archaeology*, **1**, 67-99.

Khalaji, A. A., Esmaeily, D., Valizadeh, M. V. and Rahimpour-Bonab, H. (2007) Petrology and geochemistry of the granitoid complex of Boroujerd, Sanandaj-Sirjan Zone, Western Iran. *Journal of Asian Earth Sciences*, **29**, 859-877.

Khuzestan Water and Power Authority (KWPA) (2003) *Khuzestan Watersheds*. Web page of the KWPA: http://www.kwpa.ir/Latin/WaterDepartment/Khuzestan%20Watersheds.html (accessed on 8 March 2011).

Khuzestan Water and Power Authority (KWPA) (2004) *Map of Dams of Khuzestan Province*. Ahvaz, Iran: KWPA.

Khuzestan Water and Power Authority (KWPA) (2010) *The Khuzistan Water and Power Authority*. Ahvaz, Iran: Unpublished resumé of the KWPA and dams in Khuzestan, 11 pages.

Kirkby, M. J. (1977) Appendix 1. Land and Water Resources of the Deh Luran and Khuzistan Plains. In: Hole, F. *Studies in the Archaeological History of the Deh Luran Plain. The Excavation of Chagha Sefid.* Ann Arbor, Michigan, U.S.A.: Memoirs of the Museum of Anthropology, University of Michigan, Number 9, pp. 251-288.

Knighton, D. (1998) *Fluvial forms and processes: A New Perspective.* London, U.K.: Arnold, 383 pages.

Köhler, U., List, J. and Witt, W. (2007) *Comparison of Laser Diffraction and Image Analysis under Identical Dispersing Conditions*. Paper at PARTEC 2007, International Congress on Particle Technology, Nürnberg, Germany, 27 - 29 March 2007. Four web pages of Sympatec GmbH: http://sympatec.com/docs/ImageAnalysis/publications/IA_2007_ComparisonOfLDandIA_E_1.0.pdf (accessed on 4 July 2011).

Kolstrup, E. (1980) Climate and stratigraphy in northwestern Europe between 30,000 B.P. and 13,000 B.P., with special reference to the Netherlands. *Mededelingen Rijks Geologische Dienst*, **32**, 181-253.

Komura, S. and Simons, D. B. (1967) River-bed degradation below dams. *Proceedings of the American Society of Civil Engineers, Journal of the Hydraulics Division*, **93**, Paper 5335, HY4, 1-14.

Kondolf, G. M. (1997) Hungry water: effects of dams and gravel mining on river channels. *Environmental Management*, **21**, 533-551.

Kondolf, G. M. and Swanson, M. L. (1993) Channel adjustments to reservoir construction and gravel extraction along Stony Creek, California. *Environmental Geology*, **21**, 256-269.

Koop, W. J. and Stoneley, R. (1982) Subsidence history of the Middle East Zagros Basin, Permian to Recent. *Philosophical Transactions of the Royal Society of London, Series A*, **305**, 149-168.

Kopp, R. E., Simons, F. J., Mitrovica, J. X., Maloof, A. C. and Oppenheimer, M. (2009) Probabilistic assessment of sea level during the last interglacial stage. *Nature*, **462**, 863-867.

Kopytin, A. S. (1996) Engineering-geologic analysis of the causes of failure of the chute at the Karun-1 hydroelectric station. *Hydrotechnical Construction*, **30** (No. 12), 716-718.

Kosmas, C., Danalatos, N., Cammeraat, L. H., Chabart, M., Diamantopoulos, J., Farand, R., Gutierrez, L., Jacob, A., Marques, H., Martinez-Fernandez, J., Mizara, A., Moustakas, N., Nicolau, J. M., Oliveros, C., Pinna, G., Puddu, R., Puigdefabregas, J., Roxo, M., Simao, A., Stamou, G., Tomasi, N., Usai, D., and Vacca, A. (1997). The effect of land use on runoff and soil erosion rates under Mediterranean conditions. *Catena*, **29**, 45-59.

Kouchoukos, N. (1999) *Landscape and Social Change in Late Prehistoric Mesopotamia*. Unpublished Ph.D. thesis, Yale University, New Haven, Connecticut, U.S.A., 482 pages.

Kouchoukos, N. and Hole, F. (2003) Changing estimates of Susiana's Prehistoric Settlement. In: Miller, N. F. and Abdi, K. (eds.) *Yeki bud, yeki nabud: Essays on the archaeology of Iran in honor of William M. Sumner*. Los Angeles, U.S.A.: The Cotsen Institute of Archaeology at UCLA, Monograph No. 48, pp. 52-59.

Lahiri, S. K. and Sinha, R. (2012) Tectonic controls on the morphodynamics of the Brahmaputra River system in the upper Assam valley, India. *Geomorphology*, **169-170**, 74-85.

Lambeck, K. (1996) Shoreline reconstructions for the Persian Gulf since the last glacial maximum. *Earth and Planetary Science Letters*, **142**, 43-57.

Lang, A., Bork, H.-R., Mäckel, R., Preston, N., Wunderlich, J. and Dikau, R. (2003) Changes in sediment flux and storage within a fluvial system: some examples from the Rhine catchment. *Hydrological Processes*, **17**, 3,321-3,334.

Larsen, C. E. and Evans, G. (1978) The Holocene Geological History of the Tigris-Euphrates-Karun Delta. In: Brice, W. B. (ed.) *The Environmental History of the Near and Middle East since the Last Ice Age*. London, U.K.: Academic Press Inc., pp. 227-244.

Lavé, J. and Avouac, J. P. (2000) Active folding of fluvial terraces across the Siwaliks Hills, Himalayas of central Nepal. *Journal of Geophysical Research*, **105** (No. B3), 5,735-5,770.

Lavé, J. and Avouac, J. P. (2001) Fluvial incision and tectonic uplift across the Himalayas of central Nepal. *Journal of Geophysical Research*, **106** (No. B11), 26,561-26,591.

Layard, A. H. (1846) A Description of the Province of Khuzistan. *Journal of the Royal Geographical Society of London*, **16**, 1-105.

Le Strange, G. (1905) *The lands of the Eastern Caliphate: Mesopotamia, Persia, and Central Asia from the Moslem conquest to the time of Timur*. Cambridge, U.K.: Cambridge University Press, 536 pages.

Leeder, M. (2011) *Sedimentology and Sedimentary Basins: From Turbulence to Tectonics. Second Edition*. Chichester, U.K.: Wiley-Blackwell, 768 pages.

Lees, G. M. (1955) Recent Earth Movements in the Middle East. *Geologische Rundschau*, **43**, 221-226.

Lees, G. M. and Falcon, N. L. (1952) The Geographical History of the Mesopotamian Plains. *Geographical Journal*, **118**, 24-39 & Figs.

Leopold, L. B. (1994) *A view of the river*. Cambridge, Massachusetts, U.S.A.: Harvard University Press, 298 pages.

Leopold, L. B. and Bull, W. B. (1979) Base level, aggradation and grade. *Proceedings of the American Philosophical Society*, **123** (3), 168-196.

Leopold, L. B. and Wolman, M. G. (1957) River Channel Patterns: Braided, Meandering and Straight. *United States Geological Survey Professional Paper* **282-B**, pp. 39-85.

Leopold, L. B., Wolman, M. G. and Miller, J. P. (1964) *Fluvial Processes in Geomorphology*. San Francisco, U.S.A.: W. H. Freeman and Company, 522 pages.

Leturmy, P. and Robin, C. (2010) Tectonic and stratigraphic evolution of Zagros and Makran during the Mesozoic-Cenozoic: introduction. In: Leturmy, P. and Robin, C. (eds.) *Tectonic and Stratigraphic Evolution of Zagros and Makran during the Mesozoic-Cenozoic*. Bath, U.K.: The Geological Society of London, Geological Society Special Publication No. 330, pp. 139-154.

Leturmy, P., Molinaro, M., and Frizon de Lamotte, D. (2010) Structure, timing and morphological signature of hidden reverse basement faults in the Fars Arc of the Zagros (Iran). In: Leturmy, P. and Robin, C. (eds.) *Tectonic and Stratigraphic Evolution of Zagros and Makran during the Mesozoic-Cenozoic*. Bath, U.K.: The Geological Society of London, Geological Society Special Publication No. 330, pp. 121-138.

Li, C., Wang, P., Fan, D. and Yang, S. (2006) Characteristics and formation of Late Quaternary incised-valley-fill sequences in sediment-rich deltas and estuaries: case studies from China. In: Dalrymple, R. W., Leckie, D. A. and Tillman, R. W. (eds.) *Incised Valleys in Time and Space*. Tulsa, Oklahoma, U.S.A.: Society for Sedimentary Geology, SEPM Special Publication No. 85, pp. 141-160.

Lowe, J. J. and Walker, M. J. C. (1997) *Reconstructing Quaternary Environments. Second Edition.* Harlow, Essex, U.K.: Pearson Prentice Hall, 446 pages.

Ludwig, W. and Probst, J.-L. (1998) River sediment discharge to the oceans: present-day controls and global budgets. *American Journal of Science*, **298**, 265-295.

MacKenzie, W. S. and Adams, A. E. (1994) *A Colour Atlas of Rocks and Minerals in Thin Section*. London, U.K.: Manson Publishing Ltd., 192 pages.

MacKenzie, W. S. and Guilford, C. (1980) *Atlas of rock-forming minerals in thin section*. Harlow, Essex, U.K.: Longman Scientific and Technical, 98 pages.

Mackey, S. D. and Bridge, J. S. (1995) Three-dimensional model of alluvial stratigraphy: theory and applications. *Journal of Sedimentary Research,* **65** (1b, February 1995), 7-31.

Magny, M. and Haas, J. N. (2004) A major widespread climatic change around 5300 cal. yr BP at the time of the Alpine Iceman. *Journal of Quaternary Science*, **19** (No. 5), 423-430.

Maleki, M., Javaherian, A. and Abdollahi Fard, I. (2006) High porosity anomaly with good reservoir properties in the lower Fahliyan formation (Neocomian) of Darquain Field (SW Iran) by 3D seismic. *Journal of the Earth and Space Physics*, **32** (No. 3), 33-39.

Marsh, R. E., Prestwich, W. V., Rink, W. J. and Brennan, B. J. (2002) Monte Carlo determinations of the beta dose rate to tooth enamel. *Radiation Measurements*, **35**, 609-616.

Masih, I. (2011) *Understanding hydrological variability for improved water management in the semi-arid Karkheh Basin, Iran*. Leiden, The Netherlands: CRC Press/Balkema, 182 pages.

Mason, R. (ed.) (1992) *Basement Tectonics 7. Proceedings of the Seventh International Conference on Basement Tectonics held in Kingston, Ontario, Canada, August 17-21, 1987*. Dordrecht, The Netherlands: Kluwer Academic Publishers, 489 pages.

Masson, F., Chéry, J., Hatzfeld, D., Martinod, J., Vernant, P., Tavakoli, F. and Ghafory-Ashtiani, M. (2005) Seismic versus aseismic deformation in Iran inferred from earthquakes and geodetic data. *Geophysical Journal International*, **160**, 217-226.

McGill, R., Tukey, J. W. and Larsen, W. A. (1978) Variations of Box Plots. *The American Statistician,* **32** (1), 12-16.

McManus, J. (1988) Grain size determination and interpretation. In: Tucker, M. (ed.) *Techniques in Sedimentology*. Oxford, U.K.: Blackwell Scientific Publications, pp. 63-85.

McQuarrie, N. (2004) Crustal scale geometry of the Zagros fold-thrust belt, Iran. *Journal of Structural Geology*, **26**, 519-535.

Medwedeff, D. A. (1992) Geometry and kinematics of an active, laterally propagating wedge thrust, Wheeler Ridge, California. In: Mitra, S. and Fisher, G. W. (eds.) *Structural Geology of Fold and Thrust Belts*. Baltimore, Maryland, U.S.A.: John Hopkins University Press, pp. 3-28.

Meghraoui, M., Jaegy, R., Lammali, K. and Albarede, F. (1988) Late Holocene earthquake sequences on the El Asnam (Algeria) thrust fault. *Earth and Planetary Science Letters*, **90**, 187-203.

Meybeck, M., Friedrich, G., Thomas, R. and Chapman, D. (1996) Chapter 6 - Rivers. In: Chapman, D. (ed.) *Water Quality Assessments - A Guide to Use of Biota, Sediments and Water in Environmental Monitoring - Second Edition*. London, U.K.: E. and F. N. Spon on behalf of WHO, 79 pages.

Miall, A. D. (1996) *The Geology of Fluvial Deposits: Sedimentary Facies, Basin Analysis and Petroleum Geology*. Berlin, Germany: Springer-Verlag, 582 pages.

Miller, J. (1988) Microscopical techniques: I. Slices, slides, stains and peels. In: Tucker, M. (ed.) *Techniques in Sedimentology*. Oxford, U.K.: Blackwell Scientific Publications, pp. 86-107.

Milliman, J. D. and Syvitski, P. M. (1992) Geomorphic/Tectonic Control of Sediment Discharge to the Ocean: The Importance of Small Mountainous Rivers. *Journal of Geology*, **100**, 525-544.

Milne, G. A. and Mitrovica, J. X. (2008) Searching for eustasy in deglacial sea-level histories. *Quaternary Science Reviews*, **27** (25-26), 2,922-2,302.

Modi, J. J. (1905) The River Karun. In: Modi, J. J. (collected papers) *Asiatic Papers. Papers read before the Bombay Branch of the Royal Asiatic Society*. Bombay, India: Bombay Education Society's Press, pp. 1-22.

Moghaddam, A. (in press) A Note on the Gargar Irrigation System. In: Abdi, K. (ed) *Mazdesn Shapur ke chihr az yazdan: Essays in Memory of A. Shapur Shahbazi*. Tehran and Persepolis, Iran: Iran University Press and Parsa-Pasargadae Research Foundation, 16 pages.

Moghaddam, A. and Miri, N. (2003) Archaeological research in the Mianab Plain of lowland Susiana, south-western Iran. *Iran*, **41**, 99-137.

Moghaddam, A. and Miri, N. (2007) Archaeological surveys in the "Eastern Corridor", south-western Iran. *Iran*, **45**, 23-55.

Moghaddam, A., Khosrowzadeh, A., Rezaii, A., Zeydi, M., Soleymani, S., Aali, A., Attaei, M. T., Faryadiyan, B., Karimi, K., Lazardusti, A. and Miri, N. (2005) *Archaeological Surveys in Mianab Plain, Shushtar*. Tehran, Iran: Iranian Center for Archaeological Research, Archaeological Report Monograph Series No. 8.

Mohajjel, M., Fergusson, C. L. and Sahandi, M. R. (2003) Cretaceous-Tertiary convergence and continental collision, Sanandaj-Sirjan Zone, western Iran. *Journal of Asian Earth Sciences*, **21**, 397-412.

Molinaro, M., Leturmy, P., Guezou, J.-C., Frizon de Lamotte, D. and Eshragi, S. A. (2005) The structure and kinematics of the southeastern Zagros fold-thrust belt, Iran: From thin-skinned to thick-skinned tectonics. *Tectonics*, **24** (3), TC3007, doi:10.1029/2004TC001633, 19 pages.

Molnar, P., Brown, E. T., Burchfiel, B. C., Deng, Q., Feng, X., Li, J., Raisbeck, G. M., Shi, J., Wu, Z., Yiou, F. and You, H. (1994) Quaternary Climate Change and the Formation of River Terraces across Growing Anticlines on the North Flank of the Tien Shan, China. *Journal of Geology*, **102**, 583-602.

Montgomery, D. R. and Stolar, D. B. (2006) Reconsidering Himalayan river anticlines. *Geomorphology*, **82**, 4-15.

Mook, W. G. and Streurman, H. J. (1983) Physical and chemical aspects of radiocarbon dating. In: Mook, W. G. and Waterbolk, H. T. (eds.) *Proceedings of the First International Symposium ^{14}C and Archaeology, Groningen, August 1981*. Strasbourg, France: Council of Europe (PACT 8, Journal of the European Study Group on Physical, Chemical, Biological and Mathematical Techniques applied to Archaeology), pp. 31-55.

Morozova, G. S. (2005) A Review of Holocene Avulsions of the Tigris and Euphrates Rivers and Possible Effects on the Evolution of Civilizations in Lower Mesopotamia. *Geoarchaeology*, **20** (No. 4), 401-423.

Moseley, M. E. (1983) The Good Old Days Were Better: Agrarian Collapse and Tectonics. *American Anthropologist, New Series*, **85** (No. 4), 773-799.

Mueller, K. and Talling, P. (1997) Geomorphic evidence for tear faults accommodating lateral propagation of an active fault-bend fold, Wheeler Ridge, California. *Journal of Structural Geology*, **19**, 397-411.

Murray, A. S. and Wintle, A. G. (2000) Luminescence dating of quartz using an improved single-aliquot regenerative-dose protocol. *Radiation Measurements*, **32**, 57-73.

Murray, A. S. and Wintle, A. G. (2003) The single aliquot regenerative dose protocol: potential for improvements in reliability. *Radiation Measurements*, **37**, 377-381.

Naddafi, K., Honari, H. and Ahmadi, M. (2007) Water quality trend analysis for the Karoon River in Iran. *Environmental Monitoring and Assessment,* **134**, 305-312.

National Aeronautics and Space Administration (NASA) (2012) *About Landsat: The Enhanced Thematic Mapper Plus.* Web page of NASA: http://landsat.gsfc.nasa.gov/about/etm+.html (accessed on 27 December 2012).

National Iranian Oil Company (NIOC) (1973) *Geological map of Iran Sheet No. 4 South-west Iran, 1: 1,000,000 Scale*. (With map of south-west Iran and northern Persian Gulf Oil Fields). Tehran, Iran: NIOC.

National Iranian Oil Company (NIOC) (1977) *Tectonic map of South-west Iran, 1: 2,500,000 Scale*. Tehran, Iran: NIOC.

Navabpour, P., Angelier, J. and Barrier, E. (2010) Mesozoic extensional brittle tectonics of the Arabian passive margin, inverted in the Zagros collision (Iran, interior Fars). In: Leturmy, P. and Robin, C. (eds.) *Tectonic and Stratigraphic Evolution of Zagros and Makran during the Mesozoic-Cenozoic*. Bath, U.K.: The Geological Society of London, Geological Society Special Publication No. 330, pp. 65-96.

Nissen, E., Tatar, M., Jackson, J. J. and Allen, M. B. (2011) New views on earthquake faulting in the Zagros fold-and-thrust belt of Iran. *Geophysical Journal International,* **186**, 928-944.

Nittrouer, J. A., Shaw, J., Lamb, M. P. and Mohrig, D. (2012) Spatial and temporal trends for water-flow velocity and bed-material transport in the lower Mississippi River. *Bulletin of the Geoogical Society of America*, **124**, 400-414.

Oberlander, T. (1965) *The Zagros Streams: A New Interpretation of Transverse Drainage in an Orogenic Zone*. Syracuse, New York, U.S.A.: Syracuse University Press, 168 pages.

Oberlander, T. M. (1985) Origin of drainage transverse to structures in orogens. In: Morisawa, M. and Hack, J. T. (eds.) *Tectonic geomorphology: Proceedings, 15th Annual Binghamton Geomorphology Symposium, September 1984*. Boston, U.S.A.: Allen and Unwin, pp. 155-182.

O'Connor, C. (1993) *Roman Bridges*. Cambridge, U.K.: Cambridge University Press, 251 pages.

Orfeo, O. and Stevaux, J. (2002) Hydraulic and morphological characteristics of middle and upper reaches of the Paraná River (Argentina and Brazil). *Geomorphology*, **44**, 309-322.

Ori, G. G., Roveri, M. and Vannoni, F. (1986) Plio-Pleistocene sedimentation in the Apenninic-Adriatic foredeep (Central Adriatic Sea, Italy). In: Allen, P. A. and Homewood, P. (eds.) *Foreland Basins*. Oxford, U.K.: Blackwell Scientific Publications, Special Publication No. 8 of the International Association of Sedimentologists, pp. 183-198.

Ouchi, S. (1985) Response of alluvial rivers to slow active tectonic movement. *Bulletin of the Geological Society of America*, **96** (No. 4), 504-515.

Oveisi, B., Lavé, J., Van der Beek, P., Carcaillet, J., Benedetti, L. and Aubourg, C. (2008) Thick- and thin-skinned deformation rates in the central Zagros simple folded zone (Iran) indicated by displacement of geomorphic surfaces. *Geophysical Journal International*, **176** (2), 627-654.

Page, K. J. and Nanson, G. C. (1996) Stratigraphic architecture resulting from Late Quaternary evolution of the Riverine Plain, south-eastern Australia. *Sedimentology*, **43**, 927-945.

Paola, C. and Mohrig, D. (1996) Palaeohydraulics revisited: palaeoslope estimation in coarse-grained braided rivers. *Basin Research*, **8**, 243-254.

PARISH Geomorphic Ltd. (PGL) (2004) *Belt Width Delineation Procedures*. Toronto, Canada: PARISH Geomorphic Ltd., Report No: 98-023 - Final Report, submitted to Toronto and Region Conservation Authority, 68 pages & appendices.

Park, R. G. (1997) *Foundations of Structural Geology. Third revised edition*. Abingdon, Oxfordshire, U.K.: Routledge, 216 pages.

Paul, A., Hatzfeld, D., Kaviani, A., Tatar, M. and Péquegnat, C. (2010) Seismic imaging of the lithospheric structure of the Zagros mountain belt (Iran). In: Leturmy, P. and Robin, C. (eds.) *Tectonic and Stratigraphic Evolution of Zagros and Makran during the Mesozoic-Cenozoic*. Bath, U.K.: The Geological Society of London, Geological Society Special Publication No. 330, pp. 5-18.

Peakall, J. (1995) *The Influences of Lateral Ground-Tilting on Channel Morphology and Alluvial Architecture*. Unpublished Ph.D. thesis, University of Leeds, U.K., 333 pages & pullouts.

Peakall, J., Leeder, M., Best, J. and Ashworth, P. (2000) River response to lateral ground tilting: a synthesis and some implications for the modelling of alluvial architecture in extensional basins. *Basin Research*, **12**, 413-424.

Peng, J., Chen, S. and Dong, P. (2010) Temporal variation of sediment load in the Yellow River basin, China, and its impacts on the lower reaches and the river delta. *Catena*, **83** (Issues 2-3), 135-147.

PerkinElmer (2004) *Optima 5000 Series: Hardware Guide*. Shelton, Connecticut, U.S.A.: PerkinElmer Inc., 352 pages.

PerkinElmer SCIEX (2001) *ELAN DRC II: Hardware Guide*. Shelton, Connecticut, U.S.A.: PerkinElmer SCIEX Instruments, 152 pages.

Permanent Mission of the Islamic Republic of Iran to the United Nations New York (PMIRIUN) (2009) *About Iran: Drainage & Soil*. Web page (one large page) of PMIRIUN: http://www.iran-un.org/index.php?option=com_content&view=article&id=429&Itemid=67 (accessed on 8 March 2011).

Petts, G. E. (1989) Perspectives for ecological management of regulated rivers. In: Gore, J. A. and Petts, G.E. (eds.) *Alternatives in Regulated River Management*. Boca Raton, Florida, U.S.A.: CRC Press Inc., pp. 3-24.

Phillips, J. D. (2003) Sources of nonlinearity and complexity in geomorphic systems. *Progress in Physical Geography*, **27** (1), 1-23.

Pichler, H. and Schmitt-Riegraf, C. (1997) *Rock-forming Minerals in Thin Section*. English language edition. London, U. K.: Chapman & Hall, 220 pages.

Pickering, J. (2010) *Alluvial river response to active tectonics in the Dehradun region, Northwest India: A case study of the Ganga and Yamuna rivers*. Unpublished M.Sc. thesis, University of Durham, U.K., 80 pages.

Pilcher, J. R. (1991) Radiocarbon dating. In: Smart, P. L. and Frances, P. D. (eds.) *Quaternary Dating Methods - a User's Guide*. Cambridge, U.K.: Quaternary Research Association, Technical Guide No. 4, pp. 16-36.

Pirazzoli, P. A. (1996) *Sea-Level Changes: The Last 20,000 Years*. Chichester, U.K.: John Wiley and Sons Ltd., 211 pages.

Pitlick, J. and Wilcock, P. (2001) Relations Between Streamflow, Sediment Transport, and Aquatic Habitat in Regulated Rivers. In: Dorava, J. M., Montgomery, D. R., Palcsak, B. B. and Fitzpatrick, F. A. (eds.) *Geomorphic Processes and Riverine Habitat*. Washington, DC, U.S.A.: American Geophysical Union, pp. 185-198.

Potts, D. T. (1999) *The Archaeology of Elam: Formation and Transformation of an Ancient Iranian State*. Cambridge, U.K.: Cambridge University Press, 490 pages.

Potts, D. T. (2004) Shatt al-Arab, combined effluent of the Euphrates and Tigris rivers. *Encyclopaedia Iranica, Online Edition, 2004*: http://www.iranica.com/articles/shatt-al-arab (accessed on 8 March 2011).

Potts, D. T. (2010) Elamite Ulā, Akkadian Ulaya, and Greek Choapses: A Solution to the Eulaios Problem. In: Potts, D. T. (collected studies) *Mesopotamia, Iran and Arabia from the Seleucids to the Sasanians*. Farnham, Surrey, U.K.: Ashgate Publishing Limited, Variorum Collected Studies Series CS962, Part V, pp 27-44.

Pournelle, J. R. (2003) *Marshland of cities: deltaic landscapes and the evolution of early Mesopotamian civilization.* Unpublished Ph.D. thesis, University of California, San Diego, California, U.S.A., 314 pages.

Prescott, J. R. and Hutton, J. T. (1994) Cosmic ray contributions to dose rates for luminescence and ESR dating: large depths and long-term time variations. *Radiation measurements*, **2/3**, 497-500.

Purser, B. H. (ed.) (1973) *The Persian Gulf: Holocene Carbonate Sedimentation and Diagenesis in a Shallow Epicontinental Sea*. Berlin, Germany and New York, U.S.A.: Springer-Verlag and Heidelberg, 471 pages.

Rakha, K., Al-Salem, K. and Neelamani, S. (2007) Hydrodynamic Atlas for the Arabian Gulf. *Journal of Coastal Research*, **SI 50** (Proceedings of the 9th International Coastal Symposium), 550-554.

Ramsey, L. A., Walker, R. T. and Jackson, J. (2008) Fold evolution and drainage development in the Zagros mountains of Fars province, SE Iran. *Basin Research*, **20**, 23-48.

Reid, H. F. (1910) *The mechanism of the earthquake, in The California Earthquake of April 18, 1906*. Washington, D.C., U.S.A.: Carnegie Institute of Washington, Report of the State Earthquake Investigation Commissiom, Volume 2, pp. 16-28.

Reimer, P. J., Baillie, M. G. L., Bard, E., Bayliss, A., Beck, J. W., Blackwell, P. G., Bronk Ramsey, C., Buck, C. E., Burr, G. S., Edwards, R. L., Friedrich, M., Grootes, P. M., Guilderson, T. P., Hajdas, I., Heaton, T. J., Hogg, A. G., Hughen, K. A., Kaiser, K. F., Kromer, B., McCormac, F. G., Manning, S. W., Reimer, R. W., Richards, D. A., Southon, J. R., Talamo, S., Turney, C. S. M., Van der Plicht, J. and Weyhenmeyer, C. E. (2009) IntCal09 and Marine09 radiocarbon age calibration curves, 0 - 50,000 years cal BP. *Radiocarbon*, **51** (No. 4), 1,111-1,1150.

Rendell, H. M. (1995) Luminescence dating of Quaternary sediments. In: Dunay, R. E. and Hailwood, E. A. (eds.) *Non-biostratigraphical Methods of Dating and Correlation*. Bath, U.K.: The Geological Society of London, Geological Society Special Publication No. 89, pp. 223-235.

Reyss, J. L., Pirazolli, P. A., Haghipour, A. Hatté, C. and Fontugne, M. (1998) Quaternary marine terraces and tectonic uplift rates on the south coast of Iran. In: Stewart, I. S. and Vita-Finzi, C. (eds.) *Coastal Tectonics.* Bath, U.K.: The Geological Society of London, Geological Society Special Publication No. 146, pp. 225-237.

Riba, O. (1976) Syntectonic unconformities of the Alto Cardener, Spanish Pyrenees: a genetic interpretation. *Sedimentary Geology*, **15**, 213-233.

Richards, B. W. M., Owen, L. A. and Rhodes, E. J. (2001) Asynchronous glaciations at Nanga Parbat, northwestern Himalaya Mountains, Pakistan: Comment. *Geology*, **29**, 287.

Rieben, E. H. (1955) The geology of the Tehran Plain. *American Journal of Science*, **253**, 617-639.

Risø National Laboratory (2009) *The Nordic Centre for Luminescence Research. Home page*. Web page of Risø National Laboratory: http://nclr.risoe.dk/images/Risoe-TL-OSL-DA20.jpg (accessed on 5 July 2011).

Rittenour, T. M. (2008) Luminescence dating of fluvial deposits: applications to geomorphic, palaeoseismic and archaeological research. *Boreas*, **37**, 613-635.

Roberts, C. R. (1989) Flood frequency and urban-induced channel change; some British examples. In: Beven, K. and Carling, P. (eds.) *Floods: Hydrological, Sedimentological and Geomorphological Implications*. Chichester, U.K.: John Wiley and Sons, pp. 57-82.

Roberts, N. (2002) Did prehistoric landscape management retard the post-glacial spread of woodland in Southwest Asia? *Antiquity*, **76**, 1,002-1,010.

Rodwell, M. J. and Hoskins, B. J. (2001) Subtropical anticyclones and summer monsoons. *Journal of Climate*, **14,** 3,192-3,211.

Rogerson, P. A. (2006) *Statistical Methods for Geography: A Student's Guide*. London, U.K.: SAGE Publications Ltd., 304 pages.

Rohling, E. J., Grant, K., Hemleben, C., Siddall, M., Hoogakker, B. A. A., Bolshaw, M. and Kucera, M. (2008) High rates of sea-level rise during the last interglacial period. *Nature Geoscience*, **1** (January 2008), 38-42 & Suppl.

Romaniello, L., Quarta, G., Mastronuzzi, G., D'Elia, M. and Calcagnile, L. (2008) ^{14}C age anomalies in modern land snails shell carbonate from land snails shell carbonate from Southern Italy. *Quaternary Geochronology*, **3**, 68-75.

Rosgen, D. L. (1994) A classification of natural rivers. *Catena*, **22**, 169-199.

Sadrolashrafi, S. S., Mohamed, T. A., Mahmud, A. R. B., Kholghi, M. K. and Samadi, A. (2008) Integrated Modeling for Flood Hazard Mapping Using Watershed Modeling System. *American Journal of Engineering and Applied Sciences*, **1** (2), 149-156.

Said, R. (1993) *The River Nile: Geology, Hydrology and Utilization*. Oxford, U.K.: Pergamon Press Ltd., 320 pages.

Salarijazi, M., Akhond-Ali, A.-M., Adib, A. and Daneshkhah, A. (2012) Trend and change-point detection for the annual stream-flow series of the Karun River at the Ahvaz hydrometric station. *African Journal of Agricultural Research*, **7** (32), 4,540-4,552.

Salkind, N. J. (2010) *Statistics for People Who (Think They) Hate Statistics. Second Edition. Excel 2007 Edition*. London, U.K.: SAGE Publications Ltd., 398 pages.

Salvador, A. (1994) *International Stratigraphic Guide: A Guide to Stratigraphic Classification, Terminology and Procedure. Second Edition*. Trondheim, Norway and Boulder, Colorado, U.S.A.: The International Union of Geological Sciences and The Geological Society of America, 214 pages.

Sanlaville, P. (1989) Considérations sur l'évolution de la Basse Mésopotamie au cours des derniers millénaires. *Paléorient*, **15** (2), 5-27.

Sanlaville, P and Dalongeville, R. (2005) L'évolution des espaces littoraux du Golfe Persique et du Golfe d'Oman depuis la Phase finale de la transgression post-glaciaire. *Paléorient*, **31**, 9-26.

Sarnthein, M. (1972) Sediments and history of the Postglacial transgression in the Persian Gulf and northwest Gulf of Oman. *Marine Geology*, **12**, 245-266.

Schröder, J. W. (1944) Essai sur la structure de l'Iran. *Eclogae geologicae Helvetiae*, **37**, 37-81.

Schumm, S. A. (1960) The shape of alluvial channels in relation to sediment type. *United States Geological Survey Professional Paper*, **352B**, 17-30.

Schumm, S. A. (1981) Evolution and response of the fluvial system, sedimentologic implications. In: Ethridge, F. G. and Flores, R. M. (eds.) *Recent and Ancient Nonmarine Depositional Environments: Models for Exploration*. Tulsa, Oklahoma, U.S.A.: Society of Economic Paleontologists and Mineralogists, Special Publication No. 31, pp. 19-29.

Schumm, S. A. (1985) Patterns of alluvial rivers. *Annual Review of Earth and Planetary Sciences*, **13**, 5-27.

Schumm, S. A. (1991) *To Interpret the Earth: Ten ways to be wrong*. Cambridge, U.K.: Cambridge University Press, 133 pages.

Schumm, S. A. (2005) *River Variability and Complexity*. Cambridge, U.K.: Cambridge University Press, 220 pages.

Schumm, S. A., Dumont, J. F. and Holbrook, J. M. (2000) *Active Tectonics and Alluvial Rivers*. Cambridge, U.K.: Cambridge University Press, 276 pages.

Selby, W. B. (1844) Account of the Ascent of the Karun and Dizful Rivers and the Ab-i-Gargar Canal, to Shuster. *Journal of the Royal Geographical Society of London*, **14**, 219-246.

Sella, G. F., Dixon, T. H. and Mao, A. (2002) REVEL: A model for Recent plate velocities from space geodesy. *Journal of Geophysical Research*, **107** (No. B4), ETG 11-1 to 11-30, doi:10.1029/2000JB000033, 30 pages.

Sepahi, A.A. and Malvandi, F. (2008) Petrology of the Bouein Zahra-Naein plutonic complexes, Urumieh-Dokhtar belt, Iran: with special reference to granitoids of the Saveh plutonic complex. *Neues Jahrbuch für Mineralogie - Abhandlungen*, **185** (No. 1), 99-115.

Sepehr, M. and Cosgrove, J. W. (2004) Structural framework of the Zagros Fold-Thrust Belt, Iran. *Marine and Petroleum Geology*, **21**, 829-843.

Sepehr, M. and Cosgrove, J. W. (2007) The role of major fault zones in controlling the geometry and spatial organisation of structures in the Zagros Fold-Thrust Belt. In: Ries, A. C., Butler, R. W. H. and Graham, R. H. (eds.) *Deformation of the Continental Crust: The Legacy of Mike Coward*. Bath, U.K.: The Geological Society of London, Geological Society Special Publication No. 272, pp. 419-436.

Sepehr, M., Cosgrove, J. and Moieni, M. (2006) The impact of cover rock rheology on the style of folding in the Zagros fold-thrust belt. *Tectonophysics*, **427**, 265-281.

Shakun, J. D. and Carlson, A. E. (2010) A global perspective on Last Glacial Maximum to Holocene climate change. *Quaternary Science Reviews*, **29**, 1,801-1,816.

Shanley, K. W. and McCabe, P. J. (1993) Alluvial architecture in a sequence stratigraphic framework: a case study from the Upper Cretaceous of southern Utah, U.S.A. In: Flint, S. S. and Bryant, I. D. (eds.) *The Geological Modelling of Hydrocarbon Reservoirs and Outcrop Analogues*. Oxford: Blackwell Scientific Publications, Special Publication of the International Association of Sedimentologists No. 15, pp. 21-55.

Sherkati, S. and Letouzey, J. (2004) Variation of structural style and basin evolution in the central Zagros (Izeh zone and Dezful Embayment), Iran. *Marine and Petroleum Geology*, **21**, 535-554.

Sherkati, S., Molinaro, M., Frizon De Lamotte, D. and Letouzey, J. (2005) Detachment folding in the Central and Eastern Zagros fold-belt (Iran): salt mobility, multiple detachments and late basement control. *Journal of Structural Geology*, **27**, 1,680-1,696.

Shields, F. D., Simon, A. and Steffen, L. J. (2000) Reservoir effects on downstream river channel migration. *Environmental Conservation*, **27** (1), 54-66.

Shimaki, K. and Nakata, T. (1980) Time-predictable recurrence model for large earthquakes. *Geophysical Research Letters*, **7**, 279-282.

Shoaei, Z. and Ghayoumian, J. (2000) Seimareh Landslide, Western Iran, One of the World’s Largest Complex Landslides. *Landslide News (The Japan Landslide Society)*, **13** (June 2000), 23-27.

Simon, A. (1992) Energy, time and channel evolution in catastrophically disturbed fluvial systems. *Geomorphology*, **5**, 345-372.

Simpson, G. (2004) Role of river incision in enhancing deformation. *Geology*, **32** (No. 4), 341-344.

Sinclair, H. D. and Allen, P. A. (1992) Vertical vs. horizontal motions in the Alpine orogenic wedge: stratigraphic response in the foreland basin. *Basin Research*, **4**, 215-232.

Sinha, R. and Friend, P. F. (1994) River systems and their sediment flux, Indo-Gangetic plains, northern Bihar, India. *Sedimentology*, **41**, 825-845.

Sklar, L. S. and Dietrich, W. E. (2004) A mechanistic model for river incision into bedrock by saltating bedload. *Water Resources Research*, **40**, W06301, doi:10.1029/2003WR002496, 21 pages.

Smith, D. E., Harrison, S., Firth, C. R. and Jordan, J. T. (2011) The early Holocene sea level rise. *Quaternary Science Reviews*, **30**, 1,846-1,860.

Smith, N. (1971) *A History of Dams*. London, U.K.: Peter Davies, 279 pages.

Snyder, J. A., Wasylik, K., Fritz, S. C. and Wright, H. E. (2001) Diatom-based conductivity reconstruction and palaeoclimatic interpretation of a 40-ka record from Lake Zeribar, Iran. *The Holocene*, **11** (No. 6), 737-745.

Soleimani, B., Nazari, K., Bakhtiar, H. A., Haghparast, G. and Zandkarimi, G. (2008) Three-Dimensional Geostatistical Modeling of Oil Reservoirs: A Case Study From the Ramin Oil Field in Iran. *Journal of Applied Sciences*, **8** (24), 4,523-4,532.

Soleimany, B. and Sàbat, F. (2010) Style and age of deformation in the NW Persian Gulf. *Petroleum Geoscience*, **16**, 31-39.

Soleimany, B., Poblet, J., Bulnes, M. and Sàbat, F. (2011) Fold amplification history unravelled from growth strata: the Dorood anticline, NW Persian Gulf. *Journal of the Geological Society of London*, **168** (No. 1), 219-234.

Southon, J., Kashgarian, M., Fontugne, M., Metivier, B., and Yim, W. W.-S. (2002) Marine reservoir corrections for the Indian Ocean and Southeast Asia. *Radiocarbon*, **44**, 167-180.

Sperazza, M., Moore, J. N. and Hendrix, M. S. (2004) High-resolution particle size analysis of naturally occurring very fine-grained sediment through laser diffractometry. *Journal of Sedimentary Research*, **74** (No. 5), 736-743.

Stanford, J. D., Hemingway, R., Rohling, E. J., Challenor, P. G., Medina-Elizalde, M. and Lester, A. J. (2011) Sea-level probability for the last deglaciation: A statistical analysis of far-field records. *Global and Planetary Change*, **79**, 193-203.

Stevens, L. R., Wright, H. E. and Ito, E. (2001) Proposed changes in seasonality of climate during the Lateglacial and Holocene at Lake Zeribar, Iran. *The Holocene,* **11** (6), 747-755.

Stevens L. R., Ito, E., Schwalb, A. and Wright H. E. (2006) Timing of atmospheric precipitation in the Zagros Mountains inferred from a multi-proxy record from Lake Mirabad, Iran. *Quaternary Research*, **66** (3), 494-500.

Stöcklin, J. (1968) Structural history and tectonics of Iran: a review. *Bulletin of the American Association of Petroleum Geologists*, **52**, 1,229-1,258.

Stöcklin, J. and Setudehnia, A. (1991) *Stratigraphic Lexicon of Iran. Third edition.* Tehran, Iran: Geological Survey of Iran, GSI Report No. 18, 376 pages.

Stoffers, P. and Ross, D. A. (1979) Late Pleistocene and Holocene sedimentation in the Persian Gulf - Gulf of Oman. *Sedimentary Geology*, **23**, 181-208.

Stow, D. A. V. (2005) *Sedimentary Rocks in the Field: A Colour Guide*. London, U.K.: Manson Publishing Ltd., 320 pages.

Suppe, J. (1985) *Principles of Structural Geology*. Englewood Cliffs, New Jersey, U.S.A.: Prentice-Hall, Inc., 537 pages.

Sympatec GmbH (1994) *HELOS Central Unit Operating Instructions*. Clausthal-Zellerfeld, Germany: Sympatec GmbH, 70 pages.

Sympatec GmbH (1995) *GRADIS operating instructions*. Clausthal-Zellerfeld, Germany: Sympatec GmbH, 26 pages.

Sympatec GmbH (1998) *VIBRI operating instructions*. Clausthal-Zellerfeld, Germany: Sympatec GmbH, 24 pages.

Sympatec GmbH (2011) *QUIXEL* and *Image Analysis* and *GRADIS/L*. Web pages (three in total) of Sympatec GmbH:
http://sympatec.com/EN/LaserDiffraction/QUIXEL.html
http://www.sympatec.com/EN/ImageAnalysis/ImageAnalysis.html
http://www.sympatec.com/EN/ImageAnalysis/GRADIS-L.html
(accessed on 4 July 2011).

Tandon, S. T. and Sinha, R. (2007) Geology of Large River Systems. In: Gupta, A. (ed.) *Large Rivers: Geomorphology and Management*. Chichester, U.K.: John Wiley and Sons Ltd., pp. 7-28.

Tatar, M., Hatzfeld, D., Martinod, J., Walpersdorf, A., Ghafori-Ashtiany, M. and Chéry, J. (2002) The present-day deformation of the central Zagros from GPS measurements. *Geophysical Research Letters*, **29**, doi:10.1029/2002GL015427, 4 pages.

Tavakoli, F., Walpersdorf, A., Authemayou, C., Nankali, H. R., Hatzfeld, D., Tatar, M., Djamour, Y., Nilforoushan, F. and Cotte, N. (2008) Distribution of the right-lateral strike-slip motion from the Main Recent Fault to the Kazerun Fault System (Zagros, Iran): Evidence from present-day GPS velocities. *Earth and Planetary Science Letters*, **275**, 342-347.

Thatcher, W. (1993) The earthquake cycle and its role in the long-term deformation of the continental lithosphere. *Annali di Geofisica*, **36** (No. 2), 13-24.

Todd, S. P. (1996) Process deduction from fluvial sedimentary structures. In: Carling, P. A. and Dawson, M. R. (eds.) *Advances in Fluvial Dynamics and Stratigraphy*. Chichester, U.K.: John Wiley and Sons Ltd., pp. 299-351.

Torfi, K., Mahjoobi, A., Kiamanesh, H. and Sheikgarga, M. H. (2007) Introduction of historical hydraulic structures of Karoon River in Shushtar districts. In: *Proceedings of the International History Seminar on Irrigation and Drainage, 2 - 5 May 2007, Tehran, Iran*. Organised by: Iranian National Committee on Irrigation and Drainage (IRNCID) and International Commission on Irrigation and Drainage (ICID), pp. 357-372.

Trentesaux, A., Recourt, P., Bout-Roumazeilles, V. and Tribovillard, N. (2001) Carbonate grain-size distribution in hemipelagic sediments from a laser particle sizer. *Journal of Sedimentary Research,* **71** (No. 5), 858-862.

Tucker, M. E. (1993) *The Field Description of Sedimentary Rocks. Geological Society of London Handbook.* Chichester, U.K.: John Wiley and Sons Ltd., 112 pages.

Turcotte, D. L. and Schubert, G. (2002) *Geodynamics. Second Edition*. Cambridge, U.K.: Cambridge University Press, 472 pages.

Turowski, J. M., Lague, D., Crave, A. and Hovius, N. (2006) Experimental channel response to tectonic uplift. *Journal of Geophysical Research*, **111**, F03008, doi:10.1029/2005JF000306, 12 pages.

Uchupi, E., Swift, S. A. and Ross, D. A. (1999) Late Quaternary stratigraphy, paleoclimate and neotectonism of the Persian (Arabian) Gulf region. *Marine Geology,* **160**, 1-23.

Udden, J. A. (1914) Mechanical composition of clastic sediments. *Bulletin of the Geological Society of America*, **25**, 655-744.

University of New Hampshire/Global Runoff Data Centre (UNH/GRDC) (2009) *UNH/GRDC Composite Runoff Fields V 1.0, Karun Basin, Station: Ahvaz.* Web pages (two in total) of the Water Systems Analysis Group at the University of New Hampshire: http://www.grdc.sr.unh.edu/html/Polygons/P2423500.html (accessed on 8 March 2011).

University of Texas at Arlington (UTA) (2011) *Sedimentology and Stratigraphy. Laboratory Exercise 1b. Sediment Textures by Touch*. Web pages (4 pages) of UTA: http://www.uta.edu/ees/courses/GEOL3442/SedstratLabs/Lab%201/Sed%20Strat%20lab%201b%20Textures%20by%20Touch.pdf (accessed on 15 June 2011).

Upton, G. and Cook, I. (1996) *Understanding Statistics*. Oxford, U.K.: Oxford University Press, 657 pages.

Vali-Khodjeini, A. (1994) Regional generalization of flood characteristics in Karun River basin. In: Seuna, P., Gustard, A., Arnell, N. W. and Cole, G. A. (eds.) *FRIEND: Flow Regimes from International Experimental and Network Data.* Proceedings of an international conference held at the Technical University of Braunschweig, Germany from 11 to 15 October 1993. Wallingford, Oxfordshire, U.K.: IAHS Press, International Association of Hydrological Sciences Publication No. 221, pp. 293-297.

Van de Wiel, M. J. and Coulthard, T. J. (2010) Self-organized criticality in river basins: Challenging sedimentary records of environmental change. *Geology*, **38**, 87-90.

Van de Wiel, M. J., Coulthard, T. J., Macklin, M. G. and Lewin, J. (2011) Modelling the response of river systems to environmental change: Progress, problems and prospects for palaeo-environmental reconstructions. *Earth-Science Reviews*, **104**, 167-185.

Van der Beek, P., Champel, B. and Mugnier, J.-L. (2002) Control of detachment dip on drainage development in regions of active fault-propagation folding. *Geology*, **30**, 471-474.

Van der Plicht, J. and Lanting, J. N. (1994) ^{14}C-AMS: Pros and cons for archaeology. *Palaeohistoria. Acta et Communicationes Instituti Bio-Archaeologici Universitatis Groninganae*, **35/36**, 1-13.

Van der Plicht, J., Wijma, S., Aerts, A. T., Pertuisot, M. H. and Meijer, H. A. J. (2000) Status report: The Groningen AMS facility. *Nuclear Instruments and Methods in Physics Research Section B*, **172**, 58-65.

Van Zeist, W. and Bottema, S. (1977) Palynological investigations in western Iran. *Palaeohistoria*, **19**, 19-85.

Van Zeist, W. and Bottema, S. (1991) *Late Quaternary Vegetation of the Near East.* Wiesbaden, Germany: Dr. Ludwig Reichert Verlag, Beihefte zum Tübinger Atlas des Vorderen Orients, Reihe A (Naturwissenschaften) Nr. 18, 156 pages.

Vandenberghe, J. (2003) Climate forcing of fluvial system development: an evolution of ideas. *Quaternary Science Reviews*, **22**, 2,053-2,060.

Vandenberghe, J., Venhuizen, G. and De Moor, J. (2011) Concepts of dynamic equilibrium of interest for river management in Lower Maas catchment. *Geographia Polonica*, **84**, Special Issue Part 2, 141-153.

Veenenbos, J. S. (1958) *Unified report of the soil and land classification of Dizful Project, Khuzistan, Iran.* Rome, Italy: Food and Agriculture Organization of the United Nations, 149 pages (in 1968 Reprint).

Vergés, J. (2007) Drainage responses to oblique and lateral thrust ramps: a review. In: Nichols, G., Williams, E. and Paola, C. (eds.) *Sedimentary Processes, Environments and Basins: A Tribute to Peter Friend*. Malden, Massachusetts, U.S.A.: Blackwell Publishing, Special Publication No. 38 of the International Association of Sedimentologists, pp. 29-47.

Verkinderen, P. (2009) *Tigris, Euphrates, Karun, Karhe, Jarrahi: Tracking the traces of 5 rivers in Lower Iraq and Huzistan in the Early Islamic Period*. Unpublished Ph.D. thesis, University of Ghent, Ghent, Belgium, 524 pages.

Vernant, P., Nilforoushan, F., Hatzfeld, D., Abbassi, M. R., Vigny, C., Masson, F., Nankali, H., Martinod, J., Ashtiani, A., Bayer, R., Tavakoli, F. and Chéry, J. (2004) Present-day crustal deformation and plate kinematics in the Middle East constrained by GPS measurements in Iran and northern Oman. *Geophysical Journal International*, **157**, 381-398.

Vita-Finzi, C. (1969) Late Quaternary Alluvial Chronology of Iran. *Geologische Rundschau*, **58**, 951-973.

Vita-Finzi, C. (1976) Diachronism in Old World alluvial sequences. *Nature*, **263**, 218-219.

Vita-Finzi, C. (1979) *Contributions to the Quaternary geology of southern Iran*. Tehran, Iran: Geological and Mineral Survey of Iran Report No. 47, 52 pages.

Wainwright, J. (2008) Can modelling enable us to understand the rôle of humans in landscape evolution? *Geoforum*, **39**, 659-674.

Walker, R., Andalibi, M., Gheitanchi, M., Jackson, J., Karegar, S. and Priestley, K. (2005) Seismological and field observations from the 1990 November 6 Furg (Hormozgan) earthquake: a rare case of surface rupture in the Zagros mountains of Iran. *Geophysical Journal International*, **163**, 567-579.

Walpersdorf, A., Hatzfeld, D., Nankali, H., Tavakoli, F., Nilforoushan, F., Tatar, M., Vernant, P., Chéry, J. and Masson, F. (2006) Difference in the GPS pattern of North and Central Zagros (Iran). *Geophysical Journal International*, **167**, 1,077-1,088.

Walstra, J., Verkinderen, P. and Heyvaert, V. M. A. (2010a) Reconstructing landscape evolution in the Lower Khuzestan plain (SW Iran): integrating imagery, historical and sedimentary archives. In: Cowley, D. C., Standring, R. A. and Abicht, M. J. (eds.) *Landscapes through the Lens: Aerial Photographs and Historic Environment*. Oxford, U.K.: Oxbow Books, Occasional Publication of the Aerial Archaeology Research Group No. 2, pp. 111-128.

Walstra, J., Heyvaert, V. M. A. and Verkinderen, P. (2010b) Assessing human impact on alluvial fan development: a multidisciplinary case-study from Lower Khuzestan (SW Iran). *Geodinamica Acta*, **23** (5-6), 267-285.

Wang, S. and Ni, J. (2002) Straight river: its formation and speciality. *Journal of Geographical Sciences*, **12** (1), 72-80.

Wasylikowa, K., Witkowski, A., Walanus, A., Hutorowicz, A., Alexandrowicz, S. W. and Langer, J. J. (2006) Palaeolimnology of Lake Zeribar, Iran, and its climatic implications. *Quaternary Research*, **66** (3), 477-493.

Watson, R. A. and Wright, H. E. (1969) The Saidmarreh Landslide, Iran. In: Schumm, S. A. and Bradley, W. C. (eds.) *United States Contributions to Quaternary Research. Papers Prepared on the Occasion of the VIII Congress of the International Association for Quaternary Research Paris, France, 1969*. Boulder, Colorado, U.S.A.: The Geological Society of America, Geological Society of America Special Paper No. 123, pp. 115-139.

Weaver, K. D. and Bruce, D. A. (2007) *Dam Foundation Grouting. Revised and expanded edition*. Reston, Virginia, U.S.A.: American Society of Civil Engineers Press, 473 pages.

Weiss, H. (2000) Beyond the Younger Dryas - Collapse as Adaptation to Abrupt Climate Change in Ancient West Asia and the Eastern Mediterranean. In: Bawden, G. and Reycraft, R. (eds.) *Confronting Natural Disaster: Engaging the Past to Understand the Future*. Albuquerque, U.S.A.: University of New Mexico Press, pp. 75-98.

Weiss, H., Courty, M. A., Wetterstrom, W., Guichard, F., Senior, L., Meadow, R. and Curnow, A. (1993) The Genesis and Collapse of Third Millennium North Mesopotamian Civilization. *Science*, **261**, 995-1,004.

Wenke, R. J. (1976) Imperial investments and agricultural developments in Parthian and Sasanian Khuzestan: 150 B.C. to A.D. 640. *Mesopotamia*, **10/11** (1975 - 1976), 33-221 & Figs. and Plates.

Wentworth, C. K. (1922) A scale of grade and class terms for clastic sediments. *Journal of Geology*, **30** (No. 5), 377-392.

Whipple, K. X. and Tucker, G. E. (1999) Dynamics of the stream-power river incision model: Implications for height limits of mountain ranges, landscape response timescales, and research needs. *Journal of Geophysical Research*, **104**, 17,661-17,674.

Whittaker, A. C., Cowie, P. A., Attal, M., Tucker, G. E. and Roberts, G. P. (2007) Contrasting transient and steady-state rivers crossing active normal faults: new field observations from the Central Apennines, Italy. *Basin Research*, **19**, 529-556.

Whittaker, A. C., Attal, M. and Allen, P. A. (2010) Characterising the origin, nature and fate of sediment exported from catchments perturbed by active tectonics. *Basin Research*, **22**, 809-828.

Williams, G. P. and Wolman, M. G. (1984) Downstream effects of dams on alluvial rivers. *United States Geological Survey Professional Paper* **1286**, 83 pages.

Witt, W. and Heuer, M. (1998) *Quick and Tubeless Suspension Analysis with Laser-diffraction*. Paper at PARTEC 98, 7th European Symposium on Particle Characterization, Nürnberg, Germany, 10 - 12 March 1998. Eleven web pages of Sympatec GmbH: http://www.sympatec.com/docs/LaserDiffraction/publications/LD_1998_QuickandTubeless.pdf (accessed on 4 July 2011).

Witt, W., Köhler, U. and List, J. (2005) *Experiences with Dry Dispersion and High-Speed Image Analysis for Size and Shape Characterisation*. Paper at PSA 2005, 9th Particulate Systems Analysis conference, Stratford-upon-Avon, U.K., 21 - 23 September 2005. Five web pages of Sympatec GmbH: http://www.sympatec.com/docs/ImageAnalysis/publications/IA_2005_Paper_ExperiencesWithQICPIC_2.0_.pdf (accessed on 4 July 2011).

Wohl, E. E. (2000) River management. Entry within: Hancock, P. L. and Skinner, B. J. (eds.) *The Oxford Companion to the Earth*. Oxford, U.K.: Oxford University Press.

Wolman, M. G. and Schick, A. P. (1967) Effects of construction on fluvial sediment, urban and suburban areas of Maryland. *Water Resources Research*, **3**, 451-464.

Wolman, M. G. (1967) A cycle of sedimentation and erosion in urban river channels. *Geografiska Annaler*, **49 A**, 385-395.

Woodbridge, K. P. (2006) The Late Quaternary of the River Karun and the forcing factors of tectonics and relative sea-level change. *Quaternary Newsletter*, **108**, 52-55.

Woodroffe, C. D. (2003) *Coasts: form, process and evolution*. Cambridge, U.K.: Cambridge University Press, 623 pages.

Wright, H. T. (1969) *Archaeological Survey in the Areas of Ram Hormuz, Shushtar, and Gutwand*. Unpublished Report, Museum of Anthropology, University of Michigan, Ann Arbor, Michigan, U.S.A., 14 pages & Figs.

Yanites, B. J., Tucker, G. E., Mueller, K. J., Chen, Y.-G., Wilcox, T., Huang, S.-Y. and Shi, K.-W. (2010) Incision and channel morphology across active structures along the Peikang River, central Taiwan: Implications for the importance of channel width. *Bulletin of the Geological Society of America*, **122**, 1,192-1,208.

Yasuda, Y., Kitagawa, H., and Nakagawa, T. (2000) The earliest record of major anthropogenic deforestation in the Ghab Valley, northwest Syria: a palynological study. *Quaternary International*, **73/74**, 127-136.

Yeromenko, V. Y. and Ivanov, V. P. (1977) Study of river meandering in the search for tectonic structures (as exemplified by the Middle Dniester Region). *Soviet Hydrology, Selected Papers*, **16**, 9-14.

Zámolyi, A., Székely, B., Draganits, E. and Timár, G. (2010) Neotectonic control on river sinuosity at the western margin of the Little Hungarian Plain. *Geomorphology*, **122**, 231-243.

Zeder, M. A. and Hesse, B. (2000) The Initial Domestication of Goats (*Capra hircus*) in the Zagros Mountains 10,000 Years Ago. *Science*, **287** (No. 5,461), 2,254-2,257.

Zhang, J. F., Zhou, L. P. and Yue, S. Y. (2003) Dating fluvial sediments by optically stimulated luminescence: selection of equivalent doses for age calculation. *Quaternary Science Reviews*, **22**, 1,123-1,129.

Zohary, M. (1963) *On the geobotanical structure of Iran*. Jerusalem: Weizman Science Press of Israel, Volume 11 of Bulletin of the Research Council of Israel, Section D, Botany, 113 pages.

LIST OF APPENDICES

The appendices are presented as files on a CD in a pocket at the end of the thesis. Appendices 1 to 6 give details of the results. Appendix 7 gives details of the methods.

Appendix 1.1	SANDSTONES				MUDROCKS				LIMESTONES AND CARBONATE ROCKS								CHERTS			EVAPORITES	OTHER		
Results of gravel	(% per category and **TOTAL %**)				(% per category and **TOTAL %**)				(% per category and **TOTAL %**)								(% per category and **TOTAL %**)			(%)	(% per category & **TOTAL %**)		
lithological analysis of	CALCAREOUS SANDSTONES			Other	CALCAREOUS MUDROCKS			Other	Light	Medium/	Mottled/	Shelly	Foram-	Other	Dolomite	Marble	Light	Red-	Other	(mainly	Other	Quartz	Other
samples associated with	Coarse	Medium	Fine	(non-	Light	Medium/	Other	(non-	grey or	dark grey	speckled	or	inifera	limest.	or	(metam.	brown	brown	chert	gypsum	rock	and	
Karun River beds	500 µm	250 µm	63 µm	calc.)	grey or	dark grey	calc.	calc.)	brown	or brown	limest.	fossilif.	limest.		dolomitic	limest.)	(often	(often		and	fragments	quartzite	
	– 2 mm	– 500 µm	– 250 µm	sandst.	brown	or brown	mudr.	mudr.	limest.	limest.		limest.			limest.		speckled)	speckled)		anhydrite)			
RIVER BEDS OF THE KARUN RIVER SYSTEM																							
AB-E GULESTAN TRIBUTARY																							
Loc. 32°02'00''N 49°08'25''E																							
BAT1GB River bed gravels	6	38	14	—	—	—	2	2	8	—	2	2	2	2	2	—	—	2	—	18	—	—	—
	58				**4**				**18**								**2**			**18**	**—**		
Bed 6 Upper floodplain	4	30	50	—	2	—	—	—	2	—	2	2	2	—	2	—	—	2	—	2	—	—	—
gravels	**84**				**2**				**10**								**2**			**2**	**—**		
RUD-E TEMBI TRIBUTARY																							
Loc. 32°02'08''N 49°06'14''E																							
BFL1GB River bed gravel bar	—	4	6	—	36	—	4	—	32	—	6	—	4	8	—	—	—	—	—	—	—	—	—
	10				**40**				**50**								**—**			**—**	**—**		
RIVER KARUN - Shushtar																							
Anticline area																							
Upstream of Shushtar Ant.																							
Loc. 32°10'04''N 48°49'34''E																							
JAL2GB River bed gravels	2	4	2	2	4	14	—	4	8	12	4	6	24	6	—	2	—	—	2	—	4	—	—
	10				**22**				**62**								**2**			**—**	**4**		
Loc. 32°08'11''N 48°51'33''E																							
KUHKL2 River bed gravels	—	—	6	2	8	12	—	—	10	16	6	10	20	4	—	2	—	2	2	—	—	—	—
	8				**20**				**68**								**4**			**—**	**—**		
Near axis of Shushtar Ant.																							
Loc. 32°03'44''N 48°51'28''E																							
SHTRA1 River bed gravels	2	2	—	—	4	14	—	—	18	10	6	6	16	10	—	8	—	—	4	—	—	—	—
	4				**18**				**74**								**4**			**—**	**—**		
River Karun (Shuteyt)																							
downstream of Shushtar Ant.																							
Loc. 32°01'05''N 48°47'40''E																							
QALSL1 Shuteyt River bed	—	—	2	—	16	12	2	—	14	16	6	10	12	2	2	—	—	2	—	—	4	—	—
gravels	**2**				**30**				**62**								**2**			**—**	**4**		
River Karun (Gargar)																							
downstream of Shushtar Ant.																							
Loc. 32°01'10''N 48°51'04''E																							
GGRBR2 Gargar River bed	—	2	4	—	14	8	2	—	30	14	4	6	14	—	—	—	—	—	—	—	2	—	—
gravels	**6**				**24**				**68**								**—**			**—**	**2**		
RIVER KARUN (SHUTEYT) -																							
Sardarabad Anticline area																							
Upstream of Sardarabad Ant.																							
Loc. 31°56'28''N 48°47'20''E																							
KBS2GB Shuteyt River gravel	10	12	14	2	8	6	2	6	2	8	2	—	2	2	—	—	2	6	6	—	8	2	—
bar	**38**				**22**				**16**								**14**			**—**	**10**		

Appendix 1.2	SANDSTONES				MUDROCKS				LIMESTONES AND CARBONATE ROCKS								CHERTS			EVAPORITES	OTHER		
Results of gravel	(% per category and **TOTAL %**)				(% per category and **TOTAL %**)				(% per category and **TOTAL %**)								(% per category and **TOTAL %**)			(%)	(% per category & **TOTAL %**)		
lithological analysis of	CALCAREOUS SANDSTONES			Other	CALCAREOUS MUDROCKS			Other	Light	Medium/	Mottled/	Shelly	Foram-	Other	Dolomite	Marble	Light	Red-	Other	(mainly	Other	Quartz	Other
samples associated with	Coarse	Medium	Fine	(non-	Light	Medium/	Other	(non-	grey or	dark grey	speckled	or	inifera	limest.	or	(metam.	brown	brown	chert	gypsum	rock	and	
Karun & Dez River beds	500 µm	250 µm	63 µm	calc.)	grey or	dark grey	calc.	calc.)	brown	or brown	limest.	fossilif.	limest.		dolomitic	limest.)	(often	(often		and	fragments	quartzite	
and Karun River terraces	– 2 mm	– 500 µm	– 250 µm	sandst.	brown	or brown	mudr.	mudr.	limest.	limest.		limest.			limest.		speckled)	speckled)		anhydrite)			
RIVER BEDS OF THE KARUN RIVER SYSTEM (continued)																							
RIVER KARUN (GARGAR) -																							
Dar Khazineh area																							
Loc. 31°54'41''N 48°58'19''E																							
DKBRDG River bed gravels	—	—	—	2	6	4	—	—	20	24	4	8	14	2	—	2	2	4	6	—	2	—	—
	2				**10**				**74**								**12**			**—**	**2**		
RIVER KARUN - Ahvaz Ant.																							
Near axis of Ahvaz Anticline																							
Loc. 31°19'09''N 48°40'38''E																							
AZPLCH River bed gravels	—	—	—	—	12	10	—	—	28	2	10	10	22	2	—	—	—	4	—	—	—	—	—
	—				**22**				**74**								**4**			**—**	**—**		
RIVER BEDS OF THE DEZ RIVER SYSTEM																							
RIVER DEZ - Dezful Uplift area																							
Near crest of Dezful Uplift																							
Loc. 32°22'52''N 48°23'24''E																							
DZFLOB River bed gravels	—	2	6	—	4	10	6	—	16	20	2	16	6	6	—	2	—	2	2	—	—	—	—
	8				**20**				**68**								**4**			**—**	**—**		
RIVER DEZ - Sardarabad																							
Anticline area																							
Upstream of Sardarabad Ant.																							
Loc. 32°03'48''N 48°31'46''E																							
RDZUP3 River bed gravels	—	—	—	2	14	14	6	6	16	8	—	10	8	4	—	4	2	2	4	—	—	—	—
	2				**40**				**50**								**8**			**—**	**—**		
RIVER TERRACES OF THE KARUN RIVER SYSTEM																							
DAR KHAZINEH TERRACE																							
Loc. 31°54'35''N 48°59'09''E																							
HGWS05 Bed 2	12	48	34	—	—	—	—	—	—	—	—	—	—	—	—	—	2	2	2	—	—	—	—
	94				**—**				**—**								**6**			**—**	**—**		
BATVAND TERRACE																							
Loc. 32°00'08''N 49°06'06''E																							
BFLS05 Bed 3	—	4	10	—	14	—	—	—	20	2	12	12	10	—	4	—	2	2	—	8	—	—	—
	14				**14**				**60**								**4**			**8**	**—**		
BFLS05 Bed 3 (Second sample)	—	2	16	—	6	—	2	—	22	—	24	4	—	2	—	—	—	—	—	22	—	—	—
	18				**8**				**52**											**22**	**—**		
BFLS05 Bed 6	—	2	12	—	20	4	4	—	18	4	14	8	8	2	2	—	—	—	—	2	—	—	—
	14				**28**				**56**											**2**	**—**		
BFLS05 Bed 7	—	6	8	—	12	2	—	—	24	2	6	10	18	8	—	—	2	2	—	—	—	—	—
	14				**14**				**68**								**4**			**—**	**—**		

Appendix 1.3	SANDSTONES				MUDROCKS				LIMESTONES AND CARBONATE ROCKS								CHERTS			EVAPORITES	OTHER		
Results of gravel	(% per category and **TOTAL %**)				(% per category and **TOTAL %**)				(% per category and **TOTAL %**)								(% per category and **TOTAL %**)			(%)	(% per category & **TOTAL %**)		
lithological analysis of	CALCAREOUS SANDSTONES			Other	CALCAREOUS MUDROCKS			Other	Light	Medium/	Mottled/	Shelly	Foram-	Other	Dolomite	Marble	Light	Red-	Other	(mainly	Other	Quartz	Other
samples associated with	Coarse	Medium	Fine	(non-	Light	Medium/	Other	(non-	grey or	dark grey	speckled	or	inifera	limest.	or	(metam.	brown	brown	chert	gypsum	rock	and	
Karun River terraces	500 µm	250 µm	63 µm	calc.)	grey or	dark grey	calc.	calc.)	brown	or brown	limest.	fossilif.	limest.		dolomitic	limest.)	(often	(often		and	fragments	quartzite	
	– 2 mm	– 500 µm	– 250 µm	sandst.	brown	or brown	mudr.	mudr.	limest.	limest.		limest.			limest.		speckled)	speckled)		anhydrite)			
RIVER TERRACES OF THE KARUN RIVER SYSTEM (continued)																							
KUSHKAK TERRACE																							
Loc. 32°08'07''N 48°50'34''E																							
KUHKL3 Bed 1	—	—	—	—	16	4	—	6	16	10	6	20	8	—	2	—	4	—	6	—	2	—	—
	—				**26**				**62**								**10**			**—**	**2**		
NAFT-E SAFID TERRACE																							
Loc. 31°57'15''N 48°59'32''E																							
DKITEB Bed 1	14	42	36	—	—	—	—	—	—	—	—	—	—	—	—	—	—	2	4	—	—	—	2
	92				**—**				**—**								**6**			**—**	**2**		
Loc. 31°57'16''N 48°59'34''E																							
DKITEA Bed 3	4	38	44	2	—	—	—	—	—	2	—	—	—	—	—	—	4	—	2	—	2	—	2
	88				**—**				**2**								**6**			**—**	**4**		
ABGAH TERRACE																							
Loc. 31°59'32''N 49°05'43''E																							
BAF2BR Bed 1 (Lower part)	—	4	2	—	16	6	—	—	16	2	8	24	18	—	—	—	—	4	—	—	—	—	—
	6				**22**				**68**								**4**			**—**	**—**		
BAF2BR Bed 5 (Lowest	2	6	2	—	14	2	—	—	30	—	8	16	4	—	—	—	—	—	—	16	—	—	—
gravel unit)	**10**				**16**				**58**								**—**			**16**	**—**		
RIVER BEDS OF THE KARUN RIVER SYSTEM - HIGHER TERRACES																							
HIGHER TERRACES NEAR																							
ABGAH																							
Loc. 31°58'48''N 49°04'54''E																							
BAF3LA Gravels	16	46	6	—	2	2	—	4	2	—	—	—	—	—	—	—	8	4	6	—	2	2	—
	68				**8**				**2**								**18**			**—**	**4**		
Loc. 31°58'38''N 49°04'51''E																							
BAF3LD Gravels	16	30	14	—	2	—	—	2	10	—	—	4	—	2	—	—	8	6	6	—	—	—	—
	60				**4**				**16**								**20**			**—**	**—**		
HIGHER TERRACE NORTH OF																							
BATVAND ON WEST BANK OF																							
AB-E GULESTAN																							
Loc. 32°02'06''N 49°08'17''E																							
BA1LPT Unit 1 Set 1	4	22	48	—	2	—	—	2	10	—	4	2	2	—	—	—	—	—	—	4	—	—	—
	74				**4**				**18**								**—**			**4**	**—**		
BA1LPT Unit 1 Set 2	4	32	38	2	6	—	2	—	—	—	2	6	2	—	—	—	—	2	—	2	—	2	—
	76				**8**				**10**								**2**			**2**	**2**		

Appendix 2.1 (a)	QUARTZ						FELDSPARS			ROCK FRAGMENTS													
Results of thin section	(% per category and **TOTAL %**)						(% per category and **TOTAL %**)			(% per category and **TOTAL %**)													
analysis of sediment and	MONO-		POLYCRYSTALLINE				ALKALI		PLAGIOCLASE	LIMESTONES AND CARBONATES							SANDSTONES & MUDROCKS		OTHER ROCK FRAGMENTS				
rock samples associated	CRYSTALLINE		Straight extinction		Undulose extinction		FELDSPAR		FELDSPAR	Undiff.	Undiff.	Fossiliferous limestone/carbonate			Dolomite/	Other	Calcareous	Other	Undiff.	Low-grade	Other	Gypsum/	Other
with the Karun River	Straight	Undul.	Non-sut.	Sutured	Non-sut.	Sutured	Undiff.	Microcline	Undiff.	limest./	iron-stained	Mainly	Mainly	Other	dolomitic	limest./	sandstone	sandstone	metam.	metam. rk.	quartz-rich	anhydrite	rock
	extinct.	extinct.	bound.	boundaries	bound.	boundaries		& Perthite		carbon.	limest./carb.	molluscs	forams.	fossilif.	limestone	carb.	and siltstone	and mudrock	rk. frag.	with chlorite	metam. rk.	rk. frag.	frag.
RIVER BANKS AND BEDS OF THE KARUN RIVER SYSTEM																							
AB-E GULESTAN TRIBUTARY																							
Loc. 32°02'00''N 49°08'24''E																							
BA1LHE Bed 3 Floodplain	1.0	1.7	—	—	1.0	1.0	0.3	—	0.4	37.4	12.3	0.7	0.3	1.0	0.3	—	26.3	—	—	—	5.3	—	—
sands				**4.7**				**0.7**					**52.0**				**26.3**				**5.3**		
RUD-E TEMBI TRIBUTARY																							
Loc. 32°02'08''N 49°06'14''E																							
BFL1GB **B** River bank - upper	4.4	6.0	0.3	—	3.0	1.0	0.6	0.3	0.7	38.7	6.4	1.0	0.3	3.3	2.0	3.3	3.0	0.7	1.3	1.0	2.7	1.3	2.0
sediments/soil				**14.7**				**1.6**					**55.0**				**3.7**				**8.3**		
RIVER KARUN - Shushtar Ant.																							
Upstream of Shushtar Anticline																							
Loc. 32°10'04''N 48°49'34''E																							
JAL2GB River bank	4.4	2.0	0.7	—	2.0	0.6	—	—	0.3	46.7	9.0	1.7	1.3	3.7	5.3	3.3	1.3	—	0.3	—	1.0	0.4	3.0
				9.7				**0.3**					**71.0**				**1.3**				**4.7**		
Near axis of Shushtar Ant.																							
Loc. 32°03'44''N 48°51'28''E																							
SHTRA1 Agha Jari F. bedrock	1.7	0.6	0.3	—	1.7	0.7	1.0	—	0.3	49.7	4.0	0.3	1.7	4.0	2.0	3.0	0.3	4.0	—	4.3	1.7	1.3	4.0
from river bank				**5.0**				**1.3**					**64.7**				**4.3**				**11.3**		
Downstream of Shushtar Ant.																							
Loc. 32°01'05''N 48°47'40''E																							
QALSL1 Shuteyt river bank	6.0	3.7	—	—	2.6	0.7	0.3	—	0.3	35.7	5.3	0.3	0.7	0.3	1.0	3.0	3.7	3.3	0.3	2.4	3.3	0.3	3.7
				13.0				**0.6**					**46.3**				**7.0**				**10.0**		
RIVER KARUN (GARGAR) - Dar																							
Khazineh area																							
Loc. 31°54'41''N 48°58'19''E																							
DKBRDG Gargar River bank	7.3	4.3	—	—	3.0	1.7	0.7	—	0.6	27.7	31.0	0.3	0.3	1.7	1.3	0.4	0.3	—	—	—	1.7	1.3	2.7
nr. Dar Khazineh				**16.3**				**1.3**					**62.7**				**0.3**				**5.7**		
RIVER KARUN - Ramin Oilf. Ant.																							
River Karun (Shuteyt) upstr.																							
of near-straight reach																							
Loc. 31°38'58''N 48°52'54''E																							
BNDEQ1 River bank	5.3	2.7	0.3	—	1.0	0.7	0.3	—	0.3	43.0	5.7	0.3	1.0	1.0	2.0	5.3	2.0	3.7	0.3	1.0	3.4	1.0	2.7
				10.0				**0.6**					**58.3**				**5.7**				**8.4**		
RIVER KARUN - Ahvaz Ant. area																							
Near axis of Ahvaz Anticline																							
Loc. 31°19'09''N 48°40'38''E																							
AZPLCH River bed sand	4.0	0.7	—	—	1.0	1.3	—	0.3	0.7	38.3	6.3	1.0	0.7	1.7	2.0	3.0	3.0	3.7	0.3	1.7	4.7	3.0	4.3
				7.0				**1.0**					**53.0**				**6.7**				**14.0**		

Appendix 2.1 (b)	CHERTS					EVAPORITES	OPAQUE MINERALS		OTHER MINERALS					ACCESSORY	TEXTURE			NAME OF SEDIMENT OR ROCK
Results of thin section	(% per category and **TOTAL %**)					(%)	(% & **TOTAL %**)		(% per category and **TOTAL %**)					MINERALS	Estimated	Estimated	Estimated	and
analysis of sediment and	Undiff.	Undiff.	Fossilif.	Coarse-	Other	Gypsum/	Haematite	Other	MICAS			Glauconite	Other	(%)	average	average	average	SHORT DESCRIPTION
rock samples associated	chert	iron-	chert	grained	chert	anhydrite	(incl.	opaque	Biotite	Chlorite	Mus-		minerals		grain	degree	grain	
with the Karun River		stained		chert/			"earthy"	miner.			covite				size	of	roundness	
		chert		chalcedony			haematite)								(µm)	sorting		
RIVER BANKS AND BEDS OF THE KARUN RIVER SYSTEM																		
AB-E GULESTAN TRIBUTARY																		
Loc. 32°02'00''N 49°08'24''E																		CALCAREOUS SAND - Unlithified sand comprised of mainly limestone and
BA1LHE Bed 3 Floodplain	6.7	2.3	1.3	—	—	—	0.3	0.4	—	—	—	—	—	—	300	Poorly	Sub-	calcareous sandstone/siltstone rock frags. V. poorly cemented with a weak
sands			**10.3**			**—**	**0.7**		—	—	—	—	—	—		sorted	angular	fine-gr. carbonate cement & a coarser-gr. gypsum cement. V. limited matrix.
RUD-E TEMBI TRIBUTARY																		
Loc. 32°02'08''N 49°06'14''E																		CALCAREOUS SAND - Unlithified sand comprised of mainly limestone rock
BFL1GB **B** River bank - upper	2.6	1.7	—	0.7	—	5.3	1.4	2.3	0.3	1.7	0.3	0.4	—	—	120	Well	Sub-	frags. and quartz grains. V. poorly cemented or uncemented. V. slight
sediments/soil			**5.0**			**5.3**	**3.7**				**2.7**			**—**		sorted	rounded	matrix, limited to micrite and iron-stained micrite around grains.
RIVER KARUN - Shushtar Ant.																		
Upstream of Shushtar Anticline																		
Loc. 32°10'04''N 48°49'34''E																		CALCAREOUS FINE SAND/SILT - Unlithified sand and silt comprised of
JAL2GB River bank	2.4	0.4	1.3	0.3	0.3	1.7	2.3	1.7	—	0.7	0.6	1.0	—	0.3	80	Poorly	Sub-	mainly limestone rock frags. Qu. poorly cemented with iron-stained
			4.7			**1.7**	**4.0**				**2.3**			**0.3**		sorted	angular	carbonate. Fairly abundant matrix of fine-gr. iron-stained carbonate.
Near axis of Shushtar Ant.																		LITHARENITE OF MAINLY LIMESTONE CLASTS - Lithified sandstone comp.
Loc. 32°03'44''N 48°51'28''E																		of mainly limestone/carbonate rock frags. Qu. well cemented with micrite/
SHTRA1 Agha Jari F. bedrock	3.0	3.6	1.7	—	0.7	1.7	1.7	0.3	—	0.4	0.3	—	—	—	160	Well	Sub-	iron-stain. micrite & microspar coating cement and blocky calcite spar
from river bank			**9.0**			**1.7**	**2.0**				**0.7**					sorted	rounded	cement between grains. Matrix limited to micrite coatings around grains.
Downstream of Shushtar Ant.																		CALCAREOUS FINE SAND/SILT - Unlithified sand and silt comprised of
Loc. 32°01'05''N 48°47'40''E																		mainly limestone rock frags. and quartz grains. Qu. poorly cemented with
QALSL1 Shuteyt River bank	2.3	0.7	0.4	0.3	—	8.7	2.7	2.6	0.3	1.7	0.3	1.4	—	1.7	80	Poorly	Sub-	iron-stained micrite coating cement and patches of gypsum cement.
			3.7			**8.7**	**5.3**				**3.7**			**1.7**		sorted	rounded	Fairly abundant matrix of micrite/iron-stained micrite.
RIVER KARUN (GARGAR) - Dar																		
Khazineh area																		
Loc. 31°54'41''N 48°58'19''E																		CALCAREOUS SILT - Unlithified silt comprised of mainly limestone rock
DKBRDG Gargar River bank	4.6	—	—	0.7	—	2.0	2.3	1.4	0.7	0.4	0.3	1.3	—	0.3	50	Moderately	Sub-	frags. and quartz grains. Poorly cemented with iron-stained carbonate.
nr. Dar Khazineh			**5.3**			**2.0**	**3.7**				**2.7**			**0.3**		sorted	rounded	Abundant matrix of iron-stained carbonate - mainly matrix supported.
RIVER KARUN - Ramin Oilf. Ant.																		
River Karun (Shuteyt) upstr.																		
of near-straight reach																		CALCAREOUS FINE SAND/SILT - Unlithified sand and silt comprised of
Loc. 31°38'58''N 48°52'54''E																		mainly limestone rock frags. & quartz grains. Poorly cemented with micrite/
BNDEQ1 River bank	2.7	1.7	—	1.0	—	5.0	2.6	0.7	1.0	1.0	0.3	0.7	—	0.3	80	Moderately	Rounded	iron-stain. micrite cement. Qu. abundant matrix of iron-stained micrite and
			5.4			**5.0**	**3.3**				**3.0**			**0.3**		sorted		some crystalline calcite.
RIVER KARUN - Ahvaz Ant. area																		
Near axis of Ahvaz Ant.																		
Loc. 31°19'09''N 48°40'38''E																		CALCAREOUS SAND - Unlithified sand comprised of mainly limestone
AZPLCH River bed sand	5.0	3.6	0.7	0.7	—	4.3	1.7	1.0	0.3	0.3	—	0.4	—	0.3	120	Well	Rounded	and other rock frags. V. poorly cemented with micrite/iron-stained micrite
			10.0			**4.3**	**2.7**				**1.0**			**0.3**		sorted		coatings around most grains. V. slight matrix limited to grain coatings.

Appendix 2.2 (a)	QUARTZ						FELDSPARS			ROCK FRAGMENTS													
Results of thin section	(% per category and **TOTAL %**)						(% per category and **TOTAL %**)			(% per category and **TOTAL %**)													
analysis of sediment	MONO-		POLYCRYSTALLINE				ALKALI		PLAGIOCLASE	LIMESTONES AND CARBONATES							SANDSTONES & MUDROCKS		OTHER ROCK FRAGMENTS				
samples associated with	CRYSTALLINE		Straight extinction		Undulose extinction		FELDSPAR		FELDSPAR	Undiff.	Undiff.	Fossiliferous limestone/carbonate			Dolomite/	Other	Calcareous	Other	Undiff.	Low-grade	Other	Gypsum/	Other
the Dez River & terraces	Straight	Undul.	Non-sut.	Sutured	Non-sut.	Sutured	Undiff.	Microcline	Undiff.	limest./	iron-stained	Mainly	Mainly	Other	dolomitic	limest./	sandstone	sandstone	metam.	metam. rk.	quartz-rich	anhydrite	rock
of the Karun River	extinct.	extinct.	bound.	boundaries	bound.	boundaries		& Perthite		carbon.	limest./carb.	molluscs	forams.	fossilif.	limestone	carb.	and siltstone	and mudrock	rk. frag.	with chlorite	metam. rk.	rk. frag.	frag.
RIVER BANKS AND BEDS OF THE DEZ RIVER SYSTEM																							
RIVER DEZ - Sardarabad Ant.																							
River Dez upstream of																							
Sardarabad Anticline																							
Loc. 32°03'48''N 48°31'46''E																							
RDZUP3 River bank	4.0	2.3	—	—	0.3	0.7	1.0	—	0.7	41.3	6.4	1.0	0.3	1.0	1.7	2.3	1.0	4.0	0.3	1.0	2.7	2.3	3.7
				7.3				**1.7**					**53.0**				**5.0**				**10.0**		
River Dez near axis of																							
Sardarabad Anticline																							
Loc. 31°58'42''N 48°36'41''E																							
RDZSA1 River bank	10.3	3.7	0.3	—	1.0	—	0.7	—	0.3	38.3	11.4	1.3	0.7	2.7	0.3	1.3	0.3	0.4	—	0.7	0.7	0.3	1.3
				15.3				**1.0**					**56.0**				**0.7**				**3.0**		
RIVER TERRACES OF THE KARUN RIVER SYSTEM																							
DAR KHAZINEH TERRACE																							
Loc. 31°54'35''N 48°59'09''E																							
HGWS05 Bed 7 OSL SAMPLE 4	4.0	2.7	0.3	—	0.7	1.3	0.3	—	0.3	43.0	9.0	0.3	0.7	3.4	2.3	7.0	2.0	1.7	1.0	2.0	1.4	1.3	2.0
				9.0				**0.6**					**65.7**				**3.7**				**7.7**		
Loc. 31°54'46''N 48°59'23''E																							
DKLTFH Bed 10	6.0	5.0	—	—	2.6	0.7	1.0	—	0.3	47.3	4.7	2.3	0.7	1.3	0.3	1.7	2.3	0.4	0.7	0.3	1.7	1.7	3.0
OSL SAMPLE 11				**14.3**				**1.3**					**58.3**				**2.7**				**7.7**		
Loc. 31°54'47''N 48°59'29''E																							
DAKS05 Bed 2 OSL SAMPLE 3	3.0	2.0	0.3	—	0.7	0.3	—	—	—	46.0	6.6	0.3	0.7	1.7	3.0	5.7	2.4	3.0	0.7	1.3	2.7	1.7	3.6
				6.3				**—**					**64.0**				**5.4**				**10.0**		
KABUTARKHAN-E SUFLA																							
TERRACE																							
Loc. 31°56'33''N 48°47'19''E																							
KBS4OS Bed 2 OSL SAMPLE 9	2.6	2.0	—	—	0.7	0.7	1.0	—	0.7	38.7	6.6	1.6	0.7	1.0	0.7	1.7	6.7	0.3	—	0.7	1.0	2.0	6.0
				6.0				**1.7**					**51.0**				**7.0**				**9.7**		
BATVAND TERRACE																							
Loc. 32°00'08''N 49°06'06''E																							
BFLS05 Bed 1 (8 cm below	3.6	2.7	—	—	1.4	0.7	0.3	—	0.7	41.0	6.0	0.3	1.7	1.3	2.3	5.4	1.3	2.7	—	1.7	2.3	4.3	2.0
top of bed)				**8.4**				**1.0**					**58.0**				**4.0**				**10.3**		
BFLS05 Bed 2 OSL SAMPLE 2	2.4	1.0	0.3	—	1.7	—	0.3	—	—	30.7	4.7	0.3	1.3	2.0	1.0	7.3	0.7	2.0	—	0.3	0.7	13.0	1.7
				5.4				**0.3**					**47.3**				**2.7**				**15.7**		
BFLS05 Bed 5 OSL SAMPLE 1	1.0	—	—	—	1.3	—	—	—	0.3	38.0	2.0	—	0.3	3.3	1.0	2.4	2.0	1.4	—	—	1.0	20.3	0.4
				2.3				**0.3**					**47.0**				**3.4**				**21.7**		

Appendix 2.2 (b) Results of thin section analysis of sediment samples associated with the Dez River & terraces of the Karun River	CHERTS (% per category and **TOTAL %**)					EVAPORITES (%)	OPAQUE MINERALS (% & **TOTAL %**)		OTHER MINERALS (% per category and **TOTAL %**)					ACCESSORY MINERALS (%)	TEXTURE			NAME OF SEDIMENT OR ROCK and SHORT DESCRIPTION
	Undiff. chert	Undiff. iron-stained chert	Fossilif. chert	Coarse-grained chert/ chalcedony	Other chert	Gypsum/ anhydrite	Haematite (incl. "earthy" haematite)	Other opaque miner.	MICAS Biotite	Chlorite	Mus-covite	Glauconite	Other minerals		Estimated average grain size (µm)	Estimated average degree of sorting	Estimated average grain roundness	
RIVER BANKS AND BEDS OF THE DEZ RIVER SYSTEM																		
RIVER DEZ - Sardarabad Ant.																		
River Dez upstream of																		
Sardarabad Anticline																		CALCAREOUS FINE SAND/SILT - Unlithified sand and silt comprised of mainly
Loc. 32°03'48''N 48°31'46''E																		limestone/carbonate rock fragments and cherts. Quite poorly cemented
RDZUP3 River bank	8.4	1.3	0.3	2.7	0.3	2.7	4.7	1.0	—	0.3	0.3	1.0	—	—	70	Moderately	Sub-	by micrite/iron-stained micrite cement around grains. Abundant matrix of
			13.0			**2.7**	**5.7**				**1.6**			**—**		sorted	rounded	mainly iron-stained fine-grained carbonate.
River Dez near axis of																		
Sardarabad Anticline																		CALCAREOUS SILT/FINE SAND - Unlithified silt and sand comprised of mainly
Loc. 31°58'42''N 48°36'41''E																		limest./carb. rock frags. & quartz grains. Qu. poorly cemented by micrite/
RDZSA1 River bank	2.3	0.7	0.3	—	0.3	9.7	5.3	1.7	0.7	0.7	0.7	1.6	—	0.3	50	Moderately	Sub-	iron-st. micrite, very fine crystall. calcite, and patches of coarser-gr. gypsum
			3.3			**9.7**	**7.0**				**3.7**			**0.3**		sorted	angular	cement. Qu. abundant matrix of mainly iron-st. fine-grained carbonate.
RIVER TERRACES OF THE KARUN RIVER SYSTEM																		
DAR KHAZINEH TERRACE																		
Loc. 31°54'35''N 48°59'09''E																		CALCAREOUS SAND - Unlithified sand comprised of mainly limestone/
HGWS05 Bed 7 OSL SAMPLE 4	2.4	2.3	2.0	0.3	0.3	4.0	1.0	0.3	0.3	0.4	—	—	—	—	150	Moderately	Sub-	carbonate rock frags. Qu. poorly cemented with micrite/iron stain. micrite
			7.3			**4.0**	**1.3**				**0.7**			**—**		sorted	rounded	coating/meniscus cement. V. slight matrix limited to grain coatings.
Loc. 31°54'46''N 48°59'23''E																		CALCAREOUS FINE SAND/SILT - Unlithified sand & silt of mainly limest. rock
DKLTFH Bed 10	3.0	—	—	0.4	0.3	4.0	2.0	1.3	0.3	0.7	1.3	1.7	—	0.7	70	Moderately	Sub-	frags. & quartz grains. Poorly cemented by fine-gr. carb. coating cement &
OSL SAMPLE 11			**3.7**			**4.0**	**3.3**				**4.0**			**0.7**		sorted	rounded	slight gypsum pore-filling cement. Patchy matrix of micrite/iron st. micrite.
Loc. 31°54'47''N 48°59'29''E																		CALCAREOUS SAND - Unlithified sand comprised of mainly limestone/
DAKS05 Bed 2 OSL SAMPLE 3	3.7	1.3	2.0	1.0	1.0	1.0	1.6	0.7	0.7	0.3	—	0.3	—	0.7	200	Moderately	Sub-	carbonate rock frags. Poorly cemented with micrite/iron-stained micrite
			9.0			**1.0**	**2.3**				**1.3**			**0.7**		sorted	rounded	coatings around most grains. V. slight matrix limited to grain coatings.
KABUTARKHAN-E SUFLA																		
TERRACE																		
Loc. 31°56'33''N 48°47'19''E																		CALCAREOUS SAND - Unlithified sand comprised of mainly limestone rock
KBS4OS Bed 2 OSL SAMPLE 9	6.3	2.0	1.0	2.0	1.0	8.6	0.7	1.0	0.3	0.7	0.3	0.7	—	—	100	Poorly	Sub-	frags. and cherts. Poorly cemented with fine-gr. carbonate cement and
			12.3			**8.6**	**1.7**				**2.0**			**—**		sorted	rounded	coarse-gr. gypsum cement. V. slight matrix.
BATVAND TERRACE																		
Loc. 32°00'08''N 49°06'06''E																		CALCAREOUS FINE SAND/SILT - Unlithified sand and silt comp. of mainly
BFLS05 Bed 1 (8 cm below	2.3	0.7	—	0.7	0.3	8.3	2.3	2.0	0.3	0.4	0.3	0.4	—	0.3	90	Well	Sub-	limest. & other rock frags. Qu. poorly cemented with fine-gr. carb. & areas
top of bed)			**4.0**			**8.3**	**4.3**				**1.4**			**0.3**		sorted	rounded	of coarser-gr. gypsum cement. Mod. matrix of micrite/iron-stain. micrite.
BFLS05 Bed 2 OSL SAMPLE 2	1.0	1.0	0.3	—	0.4	20.3	2.3	1.7	0.3	0.3	—	0.7	—	0.3	130	Poorly	Sub-	CALCAREOUS AND GYPSIFEROUS SAND - Unlithified sand of mainly limest.
			2.7			**20.3**	**4.0**				**1.3**			**0.3**		sorted	rounded	& gypsum rock frags. Qu. poorly cemented with fine-gr. carb. & coarser-gr.
																		gypsum/minor anhydrite cement. Mod. matrix of micrite/iron-st. micrite.
BFLS05 Bed 5 OSL SAMPLE 1	1.3	0.7	0.7	—	0.3	21.0	1.0	—	—	—	—	0.3	—	—	350	Well	Sub-	CALCAREOUS AND GYPSIFEROUS SAND - Unlithified sand of mainly limest.
			3.0			**21.0**	**1.0**				**0.3**			**—**		sorted	rounded	& gypsum rock frags. Qu. poorly cemented with fine-gr. carb. & coarse-gr.
																		gypsum/occ. anhydrite cement. V. slight matrix of micrite/iron-st. micrite.

Appendix 2.3 (a)	QUARTZ						FELDSPARS			ROCK FRAGMENTS													
Results of thin section	(% per category and **TOTAL %**)						(% per category and **TOTAL %**)			(% per category and **TOTAL %**)													
analysis of sediment	MONO-		POLYCRYSTALLINE				ALKALI		PLAGIOCLASE	LIMESTONES AND CARBONATES							SANDSTONES & MUDROCKS		OTHER ROCK FRAGMENTS				
samples associated with	CRYSTALLINE		Straight extinction		Undulose extinction		FELDSPAR		FELDSPAR	Undiff.	Undiff.	Fossiliferous limestone/carbonate			Dolomite/	Other	Calcareous	Other	Undiff.	Low-grade	Other	Gypsum/	Other
terraces of the Karun	Straight	Undul.	Non-sut.	Sutured	Non-sut.	Sutured	Undiff.	Microcline	Undiff.	limest./	iron-stained	Mainly	Mainly	Other	dolomitic	limest./	sandstone	sandstone	metam.	metam. rk.	quartz-rich	anhydrite	rock
River	extinct.	extinct.	bound.	boundaries	bound.	boundaries		& Perthite		carbon.	limest./carb.	molluscs	forams.	fossilif.	limestone	carb.	and siltstone	and mudrock	rk. frag.	with chlorite	metam. rk.	rk. frag.	frag.
RIVER TERRACES OF THE KARUN RIVER SYSTEM (continued)																							
KUSHKAK TERRACE																							
Loc. 32°08'07''N 48°50'34''E																							
KUHKL3 Bed 1 Sandy matrix	3.4	1.3	—	—	1.3	0.7	0.3	—	0.3	43.0	12.0	1.0	2.7	4.0	0.7	3.3	7.3	1.7	0.3	—	—	0.7	1.3
of gravel bed	**6.7**						**0.6**			**66.7**							**9.0**		**2.3**				
KUHKL3 Bed 2 OSL SAMPLE 10	4.7	6.7	0.3		2.0	0.3	1.0	—	0.7	45.7	5.3	0.7	0.3	0.3	0.7	0.7	4.3	1.0	—	0.7	1.6	1.7	0.7
	14.0						**1.7**			**53.7**							**5.3**		**4.7**				
NAFT-E SAFID TERRACE																							
Loc. 31°57'15''N 48°59'32''E																							
DKITEB Bed 1 Grey sand	3.0	1.6	—	—	2.0	0.7	0.3	0.7	0.3	42.3	3.7	0.7	0.7	3.0	2.0	4.0	5.0	3.7	1.7	0.3	3.6	1.0	2.7
	7.3						**1.3**			**56.4**							**8.7**		**9.3**				
DKITEB Bed 2 (Lower part)	1.3	2.3	0.3	0.3	2.4	0.7	1.3	—	0.7	36.7	3.7	1.0	—	1.0	0.6	0.7	10.3	1.0	—	0.3	1.0	3.7	0.7
OSL SAMPLE 8	**7.3**						**2.0**			**43.7**							**11.3**		**5.7**				
ABGAH TERRACE																							
Loc. 31°59'32''N 49°05'43''E																							
BAF2BR Bed 1 (Lower part)	4.7	5.7	0.3	—	3.7	2.0	2.0	0.7	1.0	46.7	5.0	1.0	0.3	1.0	—	0.7	6.3	—	—	—	3.7	—	0.3
Fine-grained lens in gravel bed	**16.4**						**3.7**			**54.7**							**6.3**		**4.0**				
BAF2BR Bed 4 OSL SAMPLE 7	1.0	5.0	0.3	—	1.7	0.3	3.0	0.7	1.6	44.3	3.7	1.7	—	—	0.3	1.0	13.7	1.0	—	0.3	2.0	—	1.0
Orange-brown fine sand	**8.3**						**5.3**			**51.0**							**14.7**		**3.3**				
RIVER TERRACES OF THE KARUN RIVER SYSTEM - HIGHER TERRACES																							
HIGHER TERRACES NEAR																							
ABGAH																							
Loc. 31°58'48''N 49°04'54''E																							
BAF3LA Sandy matrix of	3.4	1.3	0.3	—	1.7	1.0	0.4	0.3	0.3	46.3	4.7	1.0	0.3	1.4	2.3	5.0	3.3	4.0	0.3	—	3.0	0.4	3.0
mainly gravel unit	**7.7**						**1.0**			**61.0**							**7.3**		**6.7**				
Loc. 31°58'38''N 49°04'51''E																							
BAF3LD Sandy matrix of	4.7	3.3	—	—	1.0	0.7	—	—	0.3	34.7	5.4	1.7	1.0	0.3	2.3	5.3	2.3	6.0	0.3	2.0	2.0	—	5.0
mainly gravel unit	**9.7**						**0.3**			**50.7**							**8.3**		**9.3**				

Appendix 2.3 (b)	CHERTS					EVAPORITES	OPAQUE MINERALS		OTHER MINERALS					ACCESSORY	TEXTURE			NAME OF SEDIMENT OR ROCK
Results of thin section	(% per category and **TOTAL %**)					(%)	(% & **TOTAL %**)		(% per category and **TOTAL %**)					MINERALS	Estimated	Estimated	Estimated	and
analysis of sediment	Undiff.	Undiff.	Fossilif.	Coarse-	Other	Gypsum/	Haematite	Other	MICAS			Glauconite	Other	(%)	average	average	average	SHORT DESCRIPTION
samples associated with	chert	iron-	chert	grained	chert	anhydrite	(incl.	opaque	Biotite	Chlorite	Mus-		minerals		grain	degree	grain	
terraces of the Karun		stained		chert/			"earthy"	miner.			covite				size	of	roundness	
River		chert		chalcedony			haematite)								(µm)	sorting		
RIVER TERRACES OF THE KARUN RIVER SYSTEM (continued)																		
KUSHKAK TERRACE																		
Loc. 32°08'07''N 48°50'34''E																		CALCAREOUS FINE SAND - Unlithified sand comp. of mainly limestone/carb.
KUHKL3 Bed 1 Sandy matrix	2.0	1.3	3.0	0.7	1.0	1.4	2.0	0.7	0.6	0.4	0.3	0.7	0.3	0.3	100	Poorly	Sub-	rock frags. V. poorly cemented with micrite/iron-stained micrite coating
of gravel bed			**8.0**			**1.4**	**2.7**				**2.3**			**0.3**		sorted	rounded	cement. V. slight matrix of small crystall. calcite and micrite.
KUHKL3 Bed 2 OSL SAMPLE 10	2.0	0.7	—	0.3	0.3	9.3	2.7	1.0	1.0	1.0	1.3	1.0	—	—	70	Moderately	Sub-	CALCAREOUS FINE SAND/SILT - Unlithified sand and silt of mainly limest. rk.
			3.3			**9.3**	**3.7**				**4.3**			**—**		sorted	rounded	frags. & quartz grains. Poorly cemented by iron-stain. fine-gr. carb. cement
																		(esp. as grain coatings), with slight gypsum cement in some pore spaces.
																		V. abundant matrix of iron-stained carbonate - mainly matrix supported.
NAFT-E SAFID TERRACE																		
Loc. 31°57'15''N 48°59'32''E																		CALCAREOUS SAND - Unlithified sand comprised of mainly limestone rock
DKITEB Bed 1 Grey sand	4.3	2.0	4.6	1.7	0.7	1.3	1.7	0.7	—	—	—	—	—	—	200	Moderately	Sub-	fragments and cherts. Poorly cemented with micrite/iron-stained micrite
			13.3			**1.3**	**2.4**				**—**			**—**		sorted	angular	coating cement. V. slight matrix of iron-stained micrite.
DKITEB Bed 2 (Lower part)	2.3	1.4	0.7	1.0	0.3	19.7	1.0	1.0	—	1.0	0.3	1.0	—	0.3	100	Poorly	Sub-	CALCAREOUS SAND - Unlithified sand comp. of mainly limest./carb. and
OSL SAMPLE 8			**5.7**			**19.7**	**2.0**				**2.3**			**0.3**		sorted	angular	evaporite rock frags. Qu. poorly cemented by fine-gr. carbonate and coarse-
																		gr. gypsum cement. Slight matrix of micrite/iron-stained micrite.
ABGAH TERRACE																		CALCAREOUS SILT - Unlithified silt comprised of mainly limest./carbonate
Loc. 31°59'32''N 49°05'43''E																		grains and quartz grains. Qu. poorly cemented by micrite/iron-st. micrite
BAF2BR Bed 1 (Lower part)	4.3	0.4	—	0.3	0.3	2.3	0.7	1.3	0.7	1.0	1.3	2.0	—	0.3	40	Poorly	Sub-	coating, fine calcite spar, and occ. gypsum cement. Abundant matrix of
Fine-gr. lens in gravel bed			**5.3**			**2.3**	**2.0**				**5.0**			**0.3**		sorted	rounded	micrite/iron-stained micrite - matrix supported.
BAF2BR Bed 4 OSL SAMPLE 7	5.3	0.7	—	0.7	—	4.7	1.4	1.3	0.3	0.7	0.3	1.7	—	0.3	80	Moderately	Sub-	CALCAREOUS FINE SAND - Unlithified sand comp. of mainly limest./carb. &
			6.7			**4.7**	**2.7**				**3.0**			**0.3**		sorted	angular	calc. sandst./siltst. rock frags. Poorly cemented by fine-gr. carb. & coarser-
																		gr. gypsum cement in places. Moderate matrix of micrite/iron-st. micrite.
RIVER TERRACES OF THE KARUN RIVER SYSTEM - HIGHER TERRACES																		
HIGHER TERRACES NEAR																		
ABGAH																		
Loc. 31°58'48''N 49°04'54''E																		CALCAREOUS SAND - Unlithified sand comprised of mainly limestone/carb.
BAF3LA Sandy matrix	4.3	2.3	1.7	0.7	—	1.0	1.6	1.7	0.7	0.7	0.3	1.0	—	0.3	160	Very poorly	Sub-	rock fragments. Poorly cemented with fine-gr. carbonate coating cement.
			9.0			**1.0**	**3.3**				**2.7**			**0.3**		sorted	angular	Slight fine matrix of micrite/iron-stained micrite.
Loc. 31°58'38''N 49°04'51''E																		CALCAREOUS SAND - Unlithified sand comprised of mainly limestone/carb.
BAF3LD Sandy matrix of	4.0	3.0	2.4	1.3	—	1.0	4.0	1.7	0.7	0.7	0.3	2.3	0.3	—	120	Very poorly	Sub-	rock fragments and cherts. Poorly cemented with fine-gr. carbonate coating
mainly gravel unit			**10.7**			**1.0**	**5.7**				**4.3**			**—**		sorted	angular	cement. Fairly slight fine matrix of micrite/iron-stained micrite.

Appendix 2.4 (a)	QUARTZ						FELDSPARS			ROCK FRAGMENTS													
Results of thin section	(% per category and **TOTAL %**)						(% per category and **TOTAL %**)			(% per category and **TOTAL %**)													
analysis of rock samples	MONO-		POLYCRYSTALLINE				ALKALI		PLAGIOCLASE	LIMESTONES AND CARBONATES							SANDSTONES & MUDROCKS		OTHER ROCK FRAGMENTS				
associated with ancient	CRYSTALLINE		Straight extinction		Undulose extinction		FELDSPAR		FELDSPAR	Undiff.	Undiff.	Fossiliferous limestone/carbonate			Dolomite/	Other	Calcareous	Other	Undiff.	Low-grade	Other	Gypsum/	Other
constructions and	Straight	Undul.	Non-sut.	Sutured	Non-sut.	Sutured	Undiff.	Microcline	Undiff.	limest./	iron-stained	Mainly	Mainly	Other	dolomitic	limest./	sandstone	sandstone	metam.	metam. rk.	quartz-rich	anhydrite	rock
bedrock samples	extinct.	extinct.	bound.	boundaries	bound.	boundaries		& Perthite		carbon.	limest./carb.	molluscs	forams.	fossilif.	limestone	carb.	and siltstone	and mudrock	rk. frag.	with chlorite	metam. rk.	rk. frag.	frag.
ROCKS ASSOCIATED WITH ANCIENT CONSTRUCTIONS																							
SHUSHTAR CITY AREA																							
Shushtar water mills																							
Loc. 32°02'43''N 48°51'28''E																							
SHRR01 Cliff rocks at water	0.7	0.7	—	—	1.3	1.0	—	0.7	0.3	54.0	2.7	—	2.3	—	0.7	3.0	0.3	4.7	0.3	1.4	4.3	2.3	2.0
mills - grey sandstone	**3.7**						**1.0**			**62.7**							**5.0**		**10.3**				
SHTR01 Cliff rocks at water	3.0	3.7	0.3	0.4	0.7	1.3	0.3	—	1.0	56.0	6.0	—	1.3	1.0	0.4	3.0	—	2.0	—	0.6	1.7	0.3	1.7
mills - red-brown siltstone	**9.4**						**1.3**			**67.7**							**2.0**		**4.3**				
Band-e Qaisar dam-bridge																							
Loc. 32°03'23''N 48°50'58''E																							
SHTR03 Masonry from base	3.7	1.0	—	—	1.3	1.0	0.3	—	0.7	51.4	3.3	0.3	2.7	2.0	1.0	3.7	—	3.3	—	1.7	2.0	0.7	2.0
of Band-e Qaisar	**7.0**						**1.0**			**64.4**							**3.3**		**6.4**				
Band-e Mizan barrage																							
Loc. 32°02'58''N 48°51'35''E																							
BMIZAN Masonry from	2.3	1.7	—	—	2.0	0.4	—	—	0.3	62.0	3.0	0.3	2.0	2.7	1.7	3.3	—	2.0	—	1.0	0.7	2.0	1.0
Band-e Mizan	**6.4**						**0.3**			**75.0**							**2.0**		**4.7**				
BAND-E MAHIBAZAN AREA																							
Loc. 32°00'01''N 48°51'28''E																							
BMHIB4 Foundation block	6.0	2.4	0.3	0.3	1.7	1.0	—	0.3	—	47.3	5.0	0.3	2.4	1.7	1.3	5.7	—	2.0	0.3	3.0	1.7	—	3.0
sandstone	**11.7**						**0.3**			**63.7**							**2.0**		**8.0**				
BEDROCK																							
BAKHTYARI FORMATION																							
Loc. 32°06'37''N 49°53'04''E																							
KNASCO Conglomerate from	2.7	0.7	—	—	1.3	1.3	0.3	0.7	—	45.6	3.0	0.7	4.7	5.0	—	3.7	0.7	0.6	—	0.3	—	0.3	3.4
Shushtar Ant. S of Kushkak	**6.0**						**1.0**			**62.7**							**1.3**		**4.0**				
AGHA JARI FORMATION																							
Loc. 31°59'31''N 49°05'45''E																							
BAF2AJ Sandst. from Shushtar/	3.7	0.3	0.7	—	2.0	1.0	0.7	—	0.3	43.3	2.7	0.7	1.0	3.7	2.3	2.3	4.7	2.3	0.3	0.3	2.4	0.3	1.0
Naft-e Safid Ant. NE of Abgah	**7.7**						**1.0**			**56.0**							**7.0**		**4.3**				
Loc. 31°57'15''N 48°59'33''E																							
Nr. DKITEB Sandstone from	6.7	2.3	0.7	—	2.0	—	0.3	—	0.4	41.0	7.7	1.0	3.0	1.3	1.7	0.3	—	0.3	—	—	0.3	1.7	1.0
Shushtar/Naft-e Safid Ant.	**11.7**						**0.7**			**56.0**							**0.3**		**3.0**				
Nr. DKITEB "Marl" from	8.0	2.3	—	—	1.0	0.7	0.7	—	—	55.4	4.7	0.7	0.3	1.0	1.3	2.3	0.4	1.3	—	—	0.3	—	1.0
Shushtar/Naft-e Safid Ant.	**12.0**						**0.7**			**65.7**							**1.7**		**1.3**				

Appendix 2.4 (b)	CHERTS					EVAPORITES	OPAQUE MINERALS		OTHER MINERALS					ACCESSORY	TEXTURE			NAME OF SEDIMENT OR ROCK
Results of thin section	(% per category and **TOTAL %**)					(%)	(% & **TOTAL %**)		(% per category and **TOTAL %**)					MINERALS	Estimated	Estimated	Estimated	and
analysis of rock samples	Undiff.	Undiff.	Fossilif.	Coarse-	Other	Gypsum/	Haematite	Other	MICAS			Glauconite	Other	(%)	average	average	average	SHORT DESCRIPTION
associated with ancient	chert	iron-	chert	grained	chert	anhydrite	(incl.	opaque	Biotite	Chlorite	Mus-		minerals		grain	degree	grain	
constructions and		stained		chert/			"earthy"	miner.			covite				size	of	roundness	
bedrock samples		chert		chalcedony			haematite)								(µm)	sorting		
ROCKS ASSOCIATED WITH ANCIENT CONSTRUCTIONS																		
SHUSHTAR CITY AREA																		
Shushtar water mills																		
Loc. 32°02'43''N 48°51'28''E																		LITHARENITE OF MAINLY LIMESTONE CLASTS - Lithified sandstone comp.
Cliff rocks at water mills -	4.0	2.6	2.0	0.7	1.0	3.7	1.3	0.4	0.3	—	0.6	0.7	—	—	130	Well	Sub-	of mainly limest./carb. rock frags. & cherts. Well cemented by fine-gr. carb.
grey sandstone			**10.3**			**3.7**	**1.7**				**1.6**			**—**		sorted	angular	coating cement and v. slight gypsum cement. V. slight micrite matrix.
Cliff rocks at water mills -	—	0.4	—	0.3	0.3	6.3	2.7	1.0	1.3	0.7	0.3	1.7	—	0.3	30	Well	Sub-	CALCAREOUS SILTSTONE - Lithified siltstone comp. of mainly limestone and
red-brown siltstone			**1.0**			**6.3**	**3.7**				**4.0**			**0.3**		sorted	rounded	carbonate grains. Qu. poorly cemented by fine-gr. carbonate & microspar
																		cement & occ. sl. gypsum cement. Slight micrite/iron-stained micrite matrix.
Band-e Qaisar dam-bridge																		
Loc. 32°03'23''N 48°50'58''E																		LITHARENITE OF MAINLY LIMESTONE CLASTS - Lithified sandstone comp.
SHTR03 Masonry from base	5.3	4.7	1.0	1.0	1.3	2.0	2.3	—	—	—	0.3	—	—	—	120	Well	Sub-	of mainly limestone/carb. rock frags. & cherts. Well cemented by mainly
of Band-e Qaisar			**13.3**			**2.0**	**2.3**				**0.3**					sorted	rounded	blocky calcite spar cement. Minimal micrite matrix.
Band-e Mizan barrage																		
Loc. 32°02'58''N 48°51'35''E																		LITHARENITE OF MAINLY LIMESTONE CLASTS - Lithified sandstone comp. of
BMIZAN Masonry from	1.7	2.7	1.3	1.0	—	2.3	1.0	1.0	—	0.3	—	—	—	0.3	130	Well	Sub-	mainly limestone/carb. rock frags. Well cemented by fine-gr. carb. coating
Band-e Mizan			**6.7**			**2.3**	**2.0**				**0.3**			**0.3**		sorted	rounded	and fine-gr. calcite spar cement. V. slight micrite/iron stained micrite matrix.
BAND-E MAHIBAZAN AREA																		LITHARENITE OF MAINLY LIMESTONE CLASTS - Lithified sandstone comp. of
Loc. 32°00'01''N 48°51'28''E																		mainly limest./carb. rock frags. & quartz grains. Well cemented by fine-gr.
BMHIB4 Foundation block	2.3	2.7	1.3	1.3	1.7	2.7	1.0	0.7	—	—	—	0.3	0.3	—	150	Well	Sub-	carbonate coating cement and fine-grained calcite spar & microspar
sandstone			**9.3**			**2.7**	**1.7**				**0.6**			**—**		sorted	rounded	cement in pore spaces. V. slight micrite/iron stained micrite matrix.
BEDROCK																		
BAKHTYARI FORMATION																		
Loc. 32°06'37''N 49°53'04''E																		CALCAREOUS SAND MATRIX OF LIMESTONE-CHERT CONGLOMERATE -
KNASCO Conglomerate from	9.0	2.3	8.7	0.7	2.3	—	1.7	0.3	—	—	—	—	—	—	100	Very poorly	Rounded	Lithified conglomerate with matrix of calcareous sand. Very well cemented
Shushtar Ant. S of Kushkak			**23.0**			**—**	**2.0**				**—**			**—**		sorted		by blocky or drusy calcite spar cement. Slight micrite matrix.
AGHA JARI FORMATION																		LITHARENITE OF MAINLY LIMESTONE CLASTS - Lithified sandstone comp. of
Loc. 31°59'31''N 49°05'45''E																		mainly limestone/carbonate rock frags. and cherts. Qu. poorly cemented by
BAF2AJ Sandst. from Shushtar/	7.0	4.7	4.7	2.3	1.0	0.7	1.3	0.7	0.3	0.7	0.4	0.3	—	—	150	Moderately	Sub-	fine-grained carbonate coating cement and grain contact cement. V. slight
Naft-e Safid Ant. NE of Abgah			**19.7**			**0.7**	**2.0**				**1.7**			**—**		sorted	rounded	micrite/iron-stained micrite matrix.
Loc. 31°57'15''N 48°59'33''E																		LITHIC GREYWACKE OF MAINLY LIMESTONE CLASTS - Lithified sandstone of
Nr. DKITEB Sandstone from	1.0	0.4	1.3	0.3	—	17.0	3.3	1.7	1.4	0.3	0.3	1.3	—	—	70	Very poorly	Sub-	mainly limest./carb. & evaporite rock frags. Abundant matrix of iron-stained
Shushtar/Naft-e Safid Ant.			**3.0**			**17.0**	**5.0**				**3.3**			**—**		sorted	angular	micrite which forms a qu. poor cement, with some gypsum pore cement.
Nr. DKITEB "Marl" from	0.7	0.6	—	—	—	2.0	4.0	5.7	0.3	1.0	0.7	3.3	—	0.3	40	Well	Sub-	CALCAREOUS SILTSTONE - Lithified siltstone comp. of mainly limestone/
Shushtar/Naft-e Safid Ant.			**1.3**			**2.0**	**9.7**				**5.3**			**0.3**		sorted	angular	carbonate grains & quartz grains. Qu. well cemented by calcite spar cement
																		and fine-gr. carbonate cement. Fairly sl. matrix of micrite/iron-st. micrite.

Appendix 3.1 Results of grain size analysis of river bed gravels - Ab-e Gulestan tributary

AB-E GULESTAN TRIBUTARY							AB-E GULESTAN TRIBUTARY						
Loc. 32°02'00''N 49°08'25''E			BAT1GB River bed gravels				Loc. 32°02'00''N 49°08'24''E			BA1LHE Bed 6 Upper floodplain gravels			
Clast	10 largest gravel clasts			50 typical gravel clasts			Clast	10 largest gravel clasts			50 typical gravel clasts		
number	Long	Intermed.	Short	Long	Intermed.	Short	number	Long	Intermed.	Short	Long	Intermed.	Short
	diam.	diam.	diam.	diam.	diam.	diam.		diam.	diam.	diam.	diam.	diam.	diam.
	a (mm)	b (mm)	c (mm)	a (mm)	b (mm)	c (mm)		a (mm)	b (mm)	c (mm)	a (mm)	b (mm)	c (mm)
1	526	447	93	65.4	54.1	17.8	1	409	328	246	67.6	57.9	23.7
2	374	318	173	61.0	50.5	23.7	2	354	317	175	86.3	45.6	21.9
3	357	298	98	69.3	49.4	31.4	3	310	257	96	48.4	45.0	28.7
4	302	276	144	54.0	48.8	20.6	4	319	213	128	82.6	42.9	32.9
5	465	266	110	52.6	46.1	33.4	5	320	202	100	68.5	41.4	22.4
6	393	230	115	59.4	41.7	24.2	6	310	194	133	48.3	40.2	16.8
7	305	192	146	54.9	39.7	28.2	7	226	181	165	54.0	39.6	26.0
8	369	189	179	42.8	37.9	15.6	8	299	175	80	56.4	37.8	24.2
9	341	184	173	38.2	37.8	12.9	9	322	166	133	53.6	35.7	17.7
10	287	176	121	45.7	36.5	23.2	10	230	145	85	35.4	34.0	21.4
11				62.2	35.1	21.4	11				34.8	33.6	22.4
12				48.5	35.0	18.7	12				42.7	33.0	28.4
13				45.7	33.4	13.9	13				47.3	32.8	17.0
14				40.3	32.8	24.2	14				42.5	31.0	15.0
15				45.8	31.6	15.0	15				38.6	30.5	12.3
16				34.3	29.2	18.1	16				38.3	29.9	19.1
17				32.0	28.1	17.5	17				44.6	29.7	21.5
18				34.5	27.2	21.8	18				43.0	28.4	13.6
19				36.3	25.4	15.8	19				50.8	26.4	18.3
20				28.9	25.0	16.4	20				37.2	26.4	8.7
21				34.0	24.5	12.3	21				39.3	26.3	14.6
22				26.2	22.9	18.7	22				27.0	25.3	22.0
23				26.0	21.9	14.6	23				39.2	25.2	19.6
24				47.2	19.5	15.3	24				40.5	25.0	12.2
25				23.8	19.0	13.7	25				27.9	24.9	14.7
26				33.8	18.9	12.0	26				29.3	23.5	10.6
27				18.7	18.3	9.9	27				37.4	23.2	11.9
28				22.3	18.2	10.5	28				28.4	22.9	14.6
29				35.5	17.8	13.7	29				37.1	22.8	13.5
30				25.5	17.7	18.2	30				28.5	22.5	17.8
31				19.1	17.6	10.0	31				28.7	20.6	11.4
32				19.1	17.3	12.3	32				21.5	20.3	14.0
33				26.9	16.5	15.4	33				23.2	19.0	17.5
34				28.9	16.4	16.3	34				26.2	18.5	10.4
35				24.2	16.4	7.5	35				24.6	17.6	11.8
36				22.2	16.4	10.1	36				18.0	16.4	12.6
37				19.3	15.7	6.4	37				16.4	14.0	6.9
38				25.6	15.3	13.9	38				28.9	13.9	13.4
39				28.5	15.2	7.1	39				21.3	13.4	9.0
40				16.9	14.9	7.5	40				21.4	12.6	8.4
41				17.7	14.6	4.5	41				15.9	10.7	5.2
42				17.3	14.2	9.3	42				15.3	9.9	7.5
43				17.8	13.2	5.6	43				14.6	9.6	7.3
44				18.3	13.1	3.8	44				12.6	9.6	8.7
45				17.3	12.3	8.4	45				12.0	9.3	7.3
46				13.6	11.8	9.7	46				14.5	8.7	5.5
47				20.6	11.3	9.9	47				14.4	7.8	5.9
48				11.9	11.0	6.0	48				11.9	7.8	6.1
49				16.2	9.2	7.4	49				12.5	7.5	4.6
50				10.7	7.4	6.4	50				11.1	7.3	4.9
Average gravel clast size							Average gravel clast size						
Median	429.0	248.0	112.5	28.8	19.0	12.9	Median	315.0	198.0	116.5	28.6	24.2	12.7
Mean	371.9	257.6	135.2	32.7	24.5	14.6	Mean	309.9	217.8	134.1	34.4	24.4	14.8

Appendix 3.2 Results of grain size analysis of river bed gravels - Rud-e Tembi tributary and River Karun

RUD-E TEMBI TRIBUTARY							RIVER KARUN upstream of SHUSHTAR ANTICLINE						
Loc. 32°02'08''N 49°06'14''E			BFL1GB River bed gravel bar				Loc. 32°10'04''N 48°49'34''E			JAL2GB River bed gravels			
Clast	10 largest gravel clasts			50 typical gravel clasts			Clast	10 largest gravel clasts			50 typical gravel clasts		
number	Long	Intermed.	Short	Long	Intermed.	Short	number	Long	Intermed.	Short	Long	Intermed.	Short
	diam.	diam.	diam.	diam.	diam.	diam.		diam.	diam.	diam.	diam.	diam.	diam.
	a (mm)	b (mm)	c (mm)	a (mm)	b (mm)	c (mm)		a (mm)	b (mm)	c (mm)	a (mm)	b (mm)	c (mm)
1	211	153	136	76.7	73.8	25.4	1	180	143	96	88.5	54.6	35.8
2	165	145	42	73.2	61.0	28.7	2	173	143	64	67.3	52.8	14.6
3	169	141	95	72.8	59.8	40.7	3	193	131	90	75.9	50.3	21.2
4	158	136	74	56.6	49.4	21.7	4	218	123	85	61.4	48.8	13.7
5	198	134	61	70.0	49.2	18.2	5	142	114	61	69.3	48.2	17.3
6	164	125	72	68.5	46.3	17.6	6	167	107	80	45.1	44.1	13.0
7	168	118	68	56.4	46.0	27.6	7	124	99	40	89.9	43.0	27.7
8	184	113	81	60.3	44.9	21.4	8	114	97	76	53.7	40.0	19.3
9	140	104	65	55.4	43.2	25.9	9	214	95	74	59.2	37.8	23.0
10	151	101	96	71.8	42.6	35.4	10	135	89	40	37.6	36.6	15.3
11				48.4	40.2	27.3	11				39.6	35.0	25.9
12				40.0	39.9	20.5	12				52.5	34.3	34.1
13				49.5	39.3	20.0	13				43.3	33.7	19.2
14				52.8	38.9	18.0	14				39.0	32.1	11.3
15				40.5	34.9	19.1	15				37.3	31.9	12.9
16				66.1	34.3	26.7	16				45.7	31.7	24.2
17				63.8	32.3	21.4	17				40.7	31.4	14.4
18				40.9	30.9	20.9	18				40.5	30.6	18.7
19				36.0	29.2	22.0	19				30.2	28.9	18.9
20				30.5	29.2	20.6	20				41.8	28.5	15.4
21				28.7	28.6	12.3	21				30.8	26.3	9.4
22				48.8	28.3	18.2	22				37.8	25.7	12.0
23				29.5	28.1	11.9	23				31.6	24.4	15.9
24				38.6	27.5	19.2	24				31.0	24.0	19.9
25				39.3	27.3	17.0	25				38.2	23.8	19.9
26				26.5	26.8	14.0	26				28.2	23.3	15.9
27				32.9	26.0	20.7	27				28.8	22.8	9.2
28				31.8	25.1	11.8	28				31.9	22.7	9.1
29				32.8	25.0	13.6	29				37.7	21.4	15.6
30				33.2	24.7	8.4	30				33.0	20.9	10.5
31				24.9	24.4	24.0	31				24.6	20.7	17.3
32				30.0	23.2	11.7	32				33.2	20.6	11.4
33				30.0	23.0	12.4	33				21.0	20.5	12.3
34				23.2	22.6	10.2	34				21.0	20.4	11.5
35				32.4	21.7	12.6	35				14.9	18.7	8.5
36				28.5	21.4	11.6	36				25.7	17.5	14.8
37				28.3	20.5	15.4	37				19.8	17.3	11.3
38				35.4	19.4	13.0	38				26.0	17.1	10.2
39				26.0	19.4	12.8	39				24.2	17.0	4.9
40				25.7	19.0	14.9	40				19.3	15.6	9.8
41				25.7	18.1	11.4	41				19.5	15.5	6.3
42				19.6	17.8	14.6	42				17.8	15.4	6.5
43				18.2	17.7	9.3	43				19.2	13.8	12.2
44				28.7	16.5	10.1	44				25.7	13.7	9.9
45				22.3	16.5	11.0	45				15.9	12.8	6.8
46				21.4	15.9	8.9	46				15.5	12.8	9.4
47				17.5	14.5	13.3	47				13.9	12.7	10.5
48				17.0	13.6	8.5	48				26.6	12.5	7.2
49				15.5	13.6	6.5	49				16.2	11.9	5.4
50				16.4	13.2	10.5	50				10.5	9.2	7.6
Average gravel clast size							Average gravel clast size						
Median	181.0	129.5	66.5	32.9	27.1	15.5	Median	154.5	110.5	70.5	33.2	23.6	17.9
Mean	170.8	127.0	79.0	39.2	30.1	17.4	Mean	166.0	114.1	70.6	36.0	26.5	14.5

Appendix 3.3 Results of grain size analysis of river bed gravels - River Karun

RIVER KARUN upstream of SHUSHTAR ANTICLINE							RIVER KARUN near to axis of SHUSHTAR ANTICLINE						
Loc. 32°08'11''N 48°51'33''E			KUHKL2 River bed gravels				Loc. 32°03'44''N 48°51'28''E			SHTRA1 River bed gravels			
Clast	10 largest gravel clasts			50 typical gravel clasts			Clast	10 largest gravel clasts			50 typical gravel clasts		
number	Long	Intermed.	Short	Long	Intermed.	Short	number	Long	Intermed.	Short	Long	Intermed.	Short
	diam.	diam.	diam.	diam.	diam.	diam.		diam.	diam.	diam.	diam.	diam.	diam.
	a (mm)	b (mm)	c (mm)	a (mm)	b (mm)	c (mm)		a (mm)	b (mm)	c (mm)	a (mm)	b (mm)	c (mm)
1	81	56	20	66.6	36.0	32.4	1	155	103	56	68.8	49.3	26.6
2	80	56	49	42.7	35.4	9.6	2	114	102	67	69.9	49.2	48.0
3	75	53	17	69.7	35.0	20.8	3	158	96	58	48.0	40.4	33.6
4	94	52	38	44.4	34.5	24.5	4	104	84	35	40.3	39.5	23.9
5	56	51	11	40.8	30.0	14.0	5	127	83	72	40.2	31.9	23.4
6	65	46	16	34.6	29.2	14.9	6	88	66	44	31.5	31.4	9.6
7	55	43	10	33.9	28.8	10.6	7	81	64	29	41.5	30.6	14.8
8	51	43	28	47.5	28.2	13.2	8	89	61	39	33.7	30.5	15.9
9	63	41	37	30.0	28.2	9.8	9	81	61	30	32.0	30.5	24.8
10	43	39	17	36.3	27.8	15.7	10	76	57	28	31.5	30.4	15.4
11				42.0	26.8	17.3	11				39.3	30.3	21.0
12				32.8	26.8	10.2	12				34.5	30.0	14.4
13				53.3	26.7	17.8	13				42.2	27.5	15.3
14				50.4	25.4	18.0	14				43.6	27.4	10.8
15				29.5	24.9	19.6	15				35.4	27.3	13.3
16				50.6	24.8	12.3	16				31.9	26.4	14.0
17				32.9	24.6	17.3	17				31.4	26.4	12.8
18				40.5	24.2	23.2	18				39.8	25.7	15.8
19				51.0	23.2	10.6	19				33.3	25.7	11.4
20				28.2	23.1	11.1	20				29.2	25.2	13.0
21				28.2	23.0	11.5	21				39.8	25.0	21.2
22				29.3	22.7	11.5	22				31.8	24.6	10.9
23				26.3	21.2	14.2	23				39.2	23.8	11.9
24				25.1	21.0	8.2	24				27.5	23.6	22.8
25				24.7	20.7	15.2	25				31.7	23.2	10.5
26				27.4	20.4	11.9	26				31.2	22.9	17.3
27				31.4	20.0	13.4	27				28.2	22.8	12.7
28				20.4	19.5	10.6	28				30.0	22.4	13.8
29				36.8	19.3	9.7	29				33.0	22.0	8.5
30				27.3	19.2	11.4	30				33.0	21.9	18.7
31				26.6	19.1	13.5	31				25.5	21.9	10.7
32				24.2	18.9	11.5	32				24.7	21.8	12.8
33				32.3	18.8	12.3	33				26.3	19.8	11.0
34				25.3	18.2	11.7	34				30.8	19.7	10.5
35				23.7	18.1	8.0	35				28.6	19.7	9.0
36				22.3	18.0	9.4	36				32.3	19.6	9.7
37				22.3	17.9	9.2	37				26.4	19.5	5.8
38				20.3	17.8	11.7	38				34.7	18.7	9.6
39				20.5	16.2	13.8	39				25.5	18.0	16.8
40				26.6	15.6	9.6	40				23.2	16.5	10.8
41				18.2	15.6	9.0	41				21.2	16.4	10.7
42				18.7	15.4	14.7	42				19.4	16.0	9.4
43				22.7	15.0	9.1	43				23.7	15.8	5.2
44				36.7	14.9	11.5	44				16.0	14.3	5.4
45				20.9	14.4	9.0	45				18.3	12.2	6.0
46				16.9	14.2	5.3	46				17.6	12.0	7.0
47				21.1	13.2	7.5	47				20.8	10.9	8.4
48				15.0	11.9	7.2	48				14.5	10.0	5.9
49				12.3	11.5	8.8	49				11.4	8.7	8.0
50				13.9	10.8	5.3	50				13.4	8.0	6.0
Average gravel clast size							Average gravel clast size						
Median	60.1	48.5	13.6	26.1	20.6	13.6	Median	107.5	74.5	58.0	31.5	23.1	13.9
Mean	66.1	47.9	24.2	31.5	21.7	12.8	Mean	107.3	77.7	45.8	31.6	23.7	14.1

Appendix 3.4 Results of grain size analysis of river bed gravels - River Karun (Shuteyt and Gargar branches)

RIVER KARUN (SHUTEYT) downstream of SHUSHTAR ANTICLINE							RIVER KARUN (GARGAR) downstream of SHUSHTAR ANTICLINE						
Loc. 32°01'05''N 48°47'40''E			QALSL1 Shuteyt River bed gravels				Loc. 32°01'10''N 48°51'04''E			GGRBR2 Gargar River bed gravels			
Clast	10 largest gravel clasts			50 typical gravel clasts			Clast	10 largest gravel clasts			50 typical gravel clasts		
number	Long	Intermed.	Short	Long	Intermed.	Short	number	Long	Intermed.	Short	Long	Intermed.	Short
	diam.	diam.	diam.	diam.	diam.	diam.		diam.	diam.	diam.	diam.	diam.	diam.
	a (mm)	b (mm)	c (mm)	a (mm)	b (mm)	c (mm)		a (mm)	b (mm)	c (mm)	a (mm)	b (mm)	c (mm)
1	166	124	55	89.7	66.9	39.9	1	174	113	54	78.3	62.0	20.7
2	150	110	73	65.5	53.2	21.4	2	113	100	52	60.5	58.2	21.7
3	118	109	82	62.8	44.9	31.9	3	119	96	56	81.3	54.0	30.5
4	153	86	83	49.5	38.5	19.4	4	110	93	21	55.4	53.6	27.3
5	136	82	41	40.5	37.4	14.4	5	89	87	79	57.6	41.4	17.9
6	101	80	43	44.6	36.6	16.7	6	137	84	51	48.8	40.2	17.0
7	96	78	48	40.0	35.2	12.7	7	88	84	43	57.0	39.8	16.7
8	107	76	44	43.7	33.7	13.4	8	87	82	42	46.9	39.3	10.8
9	110	69	46	39.4	31.3	12.8	9	140	77	61	57.9	38.8	22.8
10	99	68	25	37.0	31.0	11.2	10	97	75	32	52.7	38.2	20.0
11				53.8	30.7	22.8	11				44.8	37.8	29.9
12				38.2	30.7	10.9	12				41.6	37.2	21.7
13				42.7	29.8	13.7	13				439.0	36.8	15.8
14				39.3	29.6	18.2	14				49.0	36.3	19.2
15				34.7	28.3	21.8	15				46.9	34.6	15.0
16				29.8	27.6	11.9	16				40.7	33.5	15.7
17				41.0	27.5	13.5	17				47.5	32.5	20.7
18				31.9	26.5	24.5	18				52.4	32.4	16.0
19				27.9	25.7	8.4	19				48.7	31.8	14.9
20				29.8	25.3	21.5	20				31.6	30.9	8.7
21				29.4	25.2	11.4	21				38.8	30.4	13.2
22				31.2	25.0	14.7	22				45.9	30.0	12.0
23				40.3	24.7	10.0	23				37.5	30.0	6.9
24				26.4	23.4	17.3	24				38.7	28.0	12.3
25				23.8	23.2	14.7	25				46.0	27.7	15.3
26				23.6	23.2	13.8	26				34.5	27.0	11.0
27				26.2	21.8	11.9	27				37.0	26.9	10.9
28				32.3	21.5	15.7	28				30.8	26.7	10.7
29				23.3	20.9	13.0	29				42.2	26.3	15.4
30				22.8	19.9	9.4	30				34.2	23.5	15.5
31				20.4	19.3	13.4	31				30.7	23.2	16.9
32				24.0	18.2	12.9	32				30.2	22.9	20.2
33				41.2	18.0	11.4	33				26.6	22.3	10.5
34				25.5	17.9	11.0	34				30.2	21.6	10.0
35				26.7	17.5	12.3	35				26.5	20.6	8.6
36				22.8	17.3	9.5	36				26.7	20.5	7.3
37				23.5	17.2	17.1	37				27.9	19.7	7.5
38				22.8	16.9	14.6	38				35.4	19.2	9.0
39				21.3	16.4	9.0	39				25.0	18.4	10.3
40				19.4	16.2	6.3	40				20.0	18.0	6.9
41				20.5	15.6	6.0	41				26.9	17.8	9.8
42				19.2	15.3	9.3	42				31.2	16.7	10.9
43				18.3	14.6	9.7	43				28.0	16.5	13.9
44				20.8	14.4	5.6	44				18.7	16.4	6.8
45				17.3	14.3	6.9	45				27.8	14.2	7.8
46				22.0	13.9	8.6	46				15.8	12.2	5.4
47				21.5	12.8	11.7	47				14.0	10.8	4.9
48				20.8	12.7	7.5	48				13.5	10.3	5.5
49				14.8	10.3	7.3	49				15.4	9.9	9.4
50				12.7	8.3	7.3	50				11.0	7.3	3.0
Average gravel clast size							Average gravel clast size						
Median	118.5	81.0	42.0	23.7	23.2	14.3	Median	113.0	85.5	65.0	40.3	27.4	13.2
Mean	123.6	88.2	54.0	31.9	24.5	13.8	Mean	115.4	89.1	49.1	46.1	28.5	13.8

Appendix 3.5 Results of grain size analysis of river bed gravels - River Karun (Shuteyt and Gargar branches)

RIVER KARUN (SHUTEYT) upstream of SARDARABAD ANTICLINE							RIVER KARUN (GARGAR) - Dar Khazineh area						
Loc. 31°56'28''N 48°47'20''E			KBS2GB Shuteyt River gravel bar				Loc. 31°54'41''N 48°58'19''E			DKBRDG Gargar River bed gravels			
Clast	10 largest gravel clasts			50 typical gravel clasts			Clast	10 largest gravel clasts			50 typical gravel clasts		
number	Long	Intermed.	Short	Long	Intermed.	Short	number	Long	Intermed.	Short	Long	Intermed.	Short
	diam.	diam.	diam.	diam.	diam.	diam.		diam.	diam.	diam.	diam.	diam.	diam.
	a (mm)	b (mm)	c (mm)	a (mm)	b (mm)	c (mm)		a (mm)	b (mm)	c (mm)	a (mm)	b (mm)	c (mm)
1	217	143	67	94.0	83.2	50.3	1	58	57	29	25.8	25.4	7.5
2	114	111	55	55.9	47.7	31.2	2	57	43	31	28.9	24.9	7.4
3	102	94	78	55.4	43.7	24.4	3	69	41	30	29.6	23.4	7.3
4	133	78	66	45.9	40.2	14.0	4	47	39	26	29.0	22.3	15.3
5	102	77	21	40.7	40.0	25.4	5	42	36	20	24.2	21.7	5.4
6	166	72	69	59.4	37.8	27.5	6	50	34	24	31.5	21.6	6.4
7	122	69	62	54.1	37.2	20.9	7	47	30	21	26.3	20.6	10.4
8	137	66	30	39.3	36.9	19.6	8	41	29	15	21.8	20.5	7.0
9	98	58	53	44.6	36.3	17.7	9	41	27	15	26.6	20.0	11.2
10	88	57	24	36.0	35.0	25.7	10	35	26	17	23.3	20.0	5.7
11				50.6	34.5	29.6	11				31.6	19.9	11.9
12				50.4	32.3	29.1	12				23.3	19.8	13.7
13				58.3	31.9	22.3	13				23.3	19.7	6.5
14				86.8	30.9	24.2	14				25.7	19.2	7.4
15				41.3	30.8	17.3	15				25.6	18.7	10.8
16				40.8	30.4	7.8	16				23.4	18.7	16.8
17				35.0	27.3	13.7	17				19.0	17.7	6.2
18				33.3	27.3	24.9	18				30.2	17.4	8.9
19				48.0	27.2	14.6	19				35.0	17.3	14.5
20				29.6	26.4	25.3	20				27.3	16.3	8.0
21				25.0	24.8	7.4	21				18.2	15.8	5.9
22				29.6	23.0	15.9	22				23.3	15.7	8.2
23				26.7	22.4	14.5	23				18.3	15.3	4.1
24				33.9	21.9	9.0	24				19.0	15.0	3.8
25				25.8	20.9	17.5	25				21.8	14.7	8.7
26				27.0	20.8	20.7	26				19.0	14.7	10.8
27				26.4	19.5	14.8	27				16.4	14.6	9.9
28				23.2	19.5	13.3	28				24.5	14.3	8.2
29				31.5	19.0	11.2	29				22.0	14.3	7.4
30				28.2	18.2	12.2	30				23.3	14.2	10.8
31				28.9	17.8	12.3	31				17.8	14.2	8.2
32				25.3	17.6	9.7	32				20.0	14.1	11.0
33				44.7	16.1	11.8	33				19.2	14.0	8.8
34				30.4	15.8	8.7	34				16.9	13.4	7.0
35				27.9	15.7	11.7	35				13.4	13.4	9.0
36				23.2	15.7	13.3	36				15.4	13.2	8.8
37				23.7	15.5	7.9	37				19.0	12.3	7.7
38				59.6	15.3	10.2	38				17.5	12.2	5.9
39				17.5	15.0	8.9	39				17.8	12.1	6.3
40				18.2	14.9	9.0	40				17.4	12.1	10.0
41				20.5	14.4	8.5	41				15.9	11.8	5.0
42				14.3	14.2	12.8	42				20.3	11.7	5.7
43				17.0	13.9	6.8	43				14.9	11.7	9.4
44				22.3	13.5	10.4	44				16.3	11.4	10.2
45				22.2	13.2	12.7	45				19.2	10.5	7.4
46				24.4	12.8	11.5	46				10.0	9.3	8.9
47				19.8	12.5	11.9	47				13.2	9.2	5.8
48				18.5	10.9	9.6	48				17.3	8.9	7.2
49				16.4	10.8	9.2	49				17.3	8.5	4.2
50				24.3	9.2	6.9	50				10.0	8.2	5.8
Average gravel clast size							Average gravel clast size						
Median	134.0	74.5	45.0	26.4	20.9	19.1	Median	46.0	35.0	22.0	20.4	14.7	9.8
Mean	127.9	82.5	52.5	35.5	24.6	16.1	Mean	48.7	36.2	22.8	21.3	15.7	8.4

Appendix 3.6 Results of grain size analysis of river bed gravels - River Karun

RIVER KARUN near to axis of AHVAZ ANTICLINE						
Loc. 31°19'09''N 48°40'38''E			AZPLCH River bed gravels			
Clast	10 largest gravel clasts			50 typical gravel clasts		
number	Long	Intermed.	Short	Long	Intermed.	Short
	diam.	diam.	diam.	diam.	diam.	diam.
	a (mm)	b (mm)	c (mm)	a (mm)	b (mm)	c (mm)
1	183	93	84	67.9	41.9	28.8
2	120	91	62	47.8	35.5	13.3
3	127	85	51	49.3	35.4	26.1
4	132	72	54	43.7	31.0	13.0
5	87	68	53	41.7	30.7	15.7
6	88	67	45	49.6	29.3	22.3
7	104	62	31	30.5	27.3	17.9
8	86	61	58	32.5	26.9	15.2
9	70	51	40	29.7	26.7	15.2
10	68	45	20	27.5	25.9	14.9
11				30.8	25.2	19.6
12				34.8	24.6	20.5
13				29.3	24.3	13.9
14				31.0	23.7	9.7
15				32.4	23.5	13.6
16				33.0	23.3	12.8
17				29.8	23.3	16.4
18				35.9	22.8	17.3
19				32.3	22.8	14.6
20				35.9	22.5	19.6
21				32.8	22.5	21.6
22				34.8	22.3	105.0
23				28.3	22.3	13.1
24				31.8	21.9	13.4
25				23.5	21.7	13.9
26				31.0	21.4	14.0
27				25.4	21.4	11.0
28				30.2	20.8	10.0
29				22.5	20.8	13.2
30				24.7	20.6	7.4
31				31.9	20.5	14.7
32				29.0	20.4	13.3
33				27.5	19.3	15.0
34				23.7	17.8	10.3
35				17.7	17.2	10.7
36				16.7	16.7	7.3
37				22.3	16.2	10.4
38				22.7	15.6	12.2
39				20.4	14.6	7.8
40				21.5	14.5	13.9
41				24.5	14.4	11.9
42				21.2	13.9	7.6
43				17.3	13.8	9.0
44				23.7	13.6	7.4
45				19.2	13.4	10.2
46				14.2	12.3	6.9
47				22.4	11.3	8.8
48				12.2	10.5	6.1
49				13.2	9.2	6.8
50				11.6	8.3	6.5
Average gravel clast size						
Median	87.5	67.5	49.0	27.3	21.6	14.0
Mean	106.5	69.5	49.8	28.9	21.1	15.2

Appendix 3.7 Results of grain size analysis of river bed gravels - River Dez

RIVER DEZ near to crest of DEZFUL UPLIFT							RIVER DEZ upstream of SARDARABAD ANTICLINE						
Loc. 32°22'52''N 48°23'24''E			DZFLOB River bed gravels				Loc. 32°03'48''N 48°31'46''E			RDZUP3 River bed gravels			
Clast	10 largest gravel clasts			50 typical gravel clasts			Clast	10 largest gravel clasts			50 typical gravel clasts		
number	Long	Intermed.	Short	Long	Intermed.	Short	number	Long	Intermed.	Short	Long	Intermed.	Short
	diam.	diam.	diam.	diam.	diam.	diam.		diam.	diam.	diam.	diam.	diam.	diam.
	a (mm)	b (mm)	c (mm)	a (mm)	b (mm)	c (mm)		a (mm)	b (mm)	c (mm)	a (mm)	b (mm)	c (mm)
1	151	117	54	83.5	60.2	43.9	1	112	87	39	42.5	37.7	12.8
2	157	106	41	65.5	54.1	36.2	2	116	85	51	38.7	33.8	19
3	166	102	91	83.4	52.1	21.5	3	112	81	52	37.8	31.4	22.3
4	176	100	52	53.0	48.6	35.2	4	88	77	40	46.5	31.3	15.9
5	134	99	86	58.4	48.5	26.7	5	87	72	30	39.4	30.5	25.9
6	138	96	45	57.5	44.6	36.6	6	91	67	36	32.6	30.0	15.4
7	113	85	47	62.1	41.8	31.7	7	69	66	55	40.6	29.6	20.6
8	98	74	46	41.5	38.0	12.9	8	89	58	56	36.4	29.4	19.6
9	107	73	45	42.3	33.5	22.3	9	73	56	29	34.8	29.1	21.8
10	101	64	50	43.7	33.3	21.3	10	70	43	13	28.8	28.2	19.4
11				41.0	32.2	11.9	11				29.5	27.5	20.4
12				38.9	32.2	12.5	12				29.9	27.0	11.4
13				40.9	32.0	19.6	13				33.2	26.3	24.2
14				40.2	31.7	28.8	14				26.4	24.9	16.4
15				40.2	30.9	15.5	15				38.2	24.2	17.8
16				37.4	30.6	15.6	16				25.4	24.2	14.9
17				33.4	30.1	20.6	17				43.8	23.7	18.7
18				44.6	29.0	19.2	18				36.8	23.6	10.9
19				37.9	28.8	20.0	19				37	23.4	14.8
20				31.0	28.5	25.3	20				29.2	23.2	11.4
21				36.6	28.3	19.5	21				25.8	23.2	8.4
22				30.1	28.1	7.3	22				27.7	21.9	14.8
23				32.2	27.2	18.3	23				33.7	21.7	7.1
24				52.4	25.2	20.4	24				36.9	19.7	14.4
25				28.6	24.9	10.5	25				31	19.2	10.1
26				27.5	24.5	12.2	26				25.9	18.9	10.4
27				45.5	24.3	17.5	27				30.5	18.7	12.2
28				27.5	23.7	11.2	28				3.9	18.2	9.9
29				34.1	23.2	13.5	29				25.3	18.0	7
30				29.2	22.3	17.1	30				29	17.8	10
31				29.5	21.2	7.7	31				24	17.7	10
32				29.1	20.8	10.5	32				21.4	16.9	12.8
33				23.2	20.6	16.7	33				20.5	16.8	13.4
34				22.6	20.5	11.4	34				18.2	16.5	8.2
35				27.3	19.6	11.6	35				24	16.4	10.8
36				26.2	19.4	16.1	36				22.1	16.3	4.3
37				29.8	18.9	7.9	37				29.8	15.6	18.4
38				34.2	18.8	9.9	38				18.7	15.5	3.7
39				22.2	18.6	10.9	39				21.4	15.3	8.7
40				27.3	18.2	16.6	40				36.4	15.0	14.8
41				31.8	17.4	11.5	41				17.3	14.6	7.8
42				28.2	17.3	6.1	42				21.4	14.4	8.7
43				23.2	17.3	5.8	43				18	13.7	13.4
44				21.8	17.3	8.8	44				15.7	13.7	7.3
45				25.6	16.9	12.3	45				20.8	12.8	12.6
46				28.0	16.8	11.1	46				19.2	12.5	8.7
47				24.8	16.6	12.6	47				13.8	12.0	8.7
48				19.0	15.2	6.4	48				14.3	11.9	7.9
49				35.4	14.6	9.9	49				18.7	10.9	6.9
50				17.5	12.4	8.4	50				13.3	7.6	5.6
Average gravel clast size							Average gravel clast size						
Median	136.0	97.5	65.5	28.1	24.7	11.4	Median	89.0	69.5	33.0	28.5	19.1	10.3
Mean	134.1	91.6	55.7	36.9	27.4	16.7	Mean	90.7	69.2	40.1	27.7	20.8	13.0

Appendix 3.8 Results of grain size analysis of Karun river terrace gravels - Dar Khazineh terrace

DAR KHAZINEH TERRACE													
Loc. 31°54'35''N 48°59'09''E			HGWS05 Bed 2										
Clast	10 largest gravel clasts			50 typical gravel clasts			Clast	10 largest gravel clasts			50 typical gravel clasts		
number	Long	Intermed.	Short	Long	Intermed.	Short	number	Long	Intermed.	Short	Long	Intermed.	Short
	diam.	diam.	diam.	diam.	diam.	diam.		diam.	diam.	diam.	diam.	diam.	diam.
	a (mm)	b (mm)	c (mm)	a (mm)	b (mm)	c (mm)		a (mm)	b (mm)	c (mm)	a (mm)	b (mm)	c (mm)
1	60	49	40	31.7	22.3	12.3	1						
2	63	46	37	30.5	21.4	12.1	2						
3	76	42	31	33.0	21.3	16.1	3						
4	51	39	18	25.9	20.5	12.3	4						
5	41	32	20	29.9	19.7	16.8	5						
6	44	31	15	30.9	19.3	16.0	6						
7	37	29	11	20.4	19.0	4.6	7						
8	31	25	15	20.9	18.7	7.5	8						
9	30	24	13	20.4	18.4	7.8	9						
10	25	23	18	25.0	18.3	8.4	10						
11				21.9	17.3	11.0	11						
12				18.5	17.2	6.2	12						
13				25.2	17.0	5.8	13						
14				17.8	16.4	7.3	14						
15				16.6	16.4	8.7	15						
16				24.4	16.3	12.7	16						
17				17.9	16.2	7.0	17						
18				25.4	16.0	6.4	18						
19				16.3	16.0	4.9	19						
20				16.1	15.9	3.8	20						
21				21.1	15.7	10.5	21						
22				28.3	15.4	13.3	22						
23				21.9	15.2	8.7	23						
24				15.4	14.6	14.6	24						
25				20.1	14.4	9.2	25						
26				19.5	14.4	9.6	26						
27				17.4	14.0	10.5	27						
28				15.0	13.9	11.4	28						
29				16.4	13.4	4.6	29						
30				17.0	13.3	6.8	30						
31				17.3	12.5	7.6	31						
32				18.3	12.2	7.3	32						
33				17.4	12.2	5.7	33						
34				16.4	12.0	6.4	34						
35				14.7	11.9	4.7	35						
36				15.9	11.4	10.3	36						
37				17.7	11.1	8.4	37						
38				16.0	11.0	6.7	38						
39				12.8	11.0	8.0	39						
40				13.3	10.8	5.7	40						
41				12.0	10.7	4.4	41						
42				11.0	10.6	10.0	42						
43				12.9	10.0	5.3	43						
44				11.7	9.6	6.4	44						
45				11.4	9.5	7.3	45						
46				16.5	9.0	8.8	46						
47				17.6	8.8	4.6	47						
48				15.0	8.7	6.6	48						
49				12.3	8.7	6.9	49						
50				13.0	7.8	7.7	50						
Average gravel clast size													
Median	42.5	31.5	17.5	19.8	14.4	9.4							
Mean	45.8	34.0	21.8	19.1	14.3	8.5							

Appendix 3.9 Results of grain size analysis of Karun river terrace gravels - Batvand terrace

BATVAND TERRACE

Loc. 32°00'08''N 49°06'06''E | BFLS05 Bed 3

Clast	10 largest gravel clasts			50 typical gravel clasts		
number	Long	Intermed.	Short	Long	Intermed.	Short
	diam.	diam.	diam.	diam.	diam.	diam.
	a (mm)	b (mm)	c (mm)	a (mm)	b (mm)	c (mm)
1	169	106	42	85.9	38.8	27.1
2	215	91	84	33.3	32.5	9.7
3	74	56	51	33.2	29.0	21.9
4	68	52	43	30.2	28.5	19.9
5	60	52	18	37.0	26.4	17.9
6	52	45	30	29.7	25.6	7.9
7	74	43	34	27.3	24.2	11.9
8	61	42	32	24.6	21.4	11.6
9	54	42	29	25.5	21.2	18.2
10	45	41	33	24.9	20.5	11.9
11				30.4	19.9	18.5
12				22.3	19.6	9.9
13				24.5	18.4	10.5
14				24.2	17.8	10.2
15				21.2	17.7	16.8
16				21.4	17.3	9.0
17				26.3	17.0	11.7
18				21.5	16.8	10.4
19				23.6	16.7	7.5
20				16.6	15.7	4.7
21				23.4	15.4	5.9
22				16.0	15.4	8.2
23				18.4	15.2	14.8
24				18.0	14.7	11.5
25				20.5	14.6	13.5
26				17.7	14.6	6.0
27				24.6	14.4	7.1
28				22.2	14.4	5.7
29				19.4	14.3	4.7
30				22.0	14.0	9.3
31				24.5	13.4	7.5
32				19.1	12.8	7.8
33				15.5	12.3	7.8
34				13.5	11.5	5.4
35				13.7	11.4	6.7
36				19.5	11.3	7.7
37				16.2	11.0	4.8
38				11.5	10.5	5.2
39				15.0	10.4	8.2
40				17.3	10.0	7.5
41				15.0	9.2	5.4
42				14.4	9.2	5.5
43				14.1	8.8	5.5
44				15.3	8.7	4.5
45				13.6	8.7	4.9
46				10.8	8.7	6.7
47				16.8	8.5	7.8
48				14.8	8.5	3.9
49				11.5	8.3	7.4
50				11.0	6.4	4.6
Average gravel clast size						
Median	56.0	48.5	24.0	19.1	14.6	9.8
Mean	87.2	57.0	39.6	21.8	15.8	9.6

BATVAND TERRACE

Loc. 32°00'08''N 49°06'06''E | BFLS05 Bed 3 (Second sample)

Clast	10 largest gravel clasts			50 typical gravel clasts		
number	Long	Intermed.	Short	Long	Intermed.	Short
	diam.	diam.	diam.	diam.	diam.	diam.
	a (mm)	b (mm)	c (mm)	a (mm)	b (mm)	c (mm)
1	127	107	35	57.3	35.8	15.5
2	101	77	51	62.8	35.3	27.9
3	88	74	33	53.4	34.5	14.6
4	76	67	35	31.6	31.0	12.6
5	87	57	40	33.0	30.5	10.1
6	63	56	23	37.4	26.9	18.3
7	85	47	43	28.0	26.0	7.8
8	56	44	22	33.9	25.6	20.6
9	53	40	24	32.3	25.3	12.5
10	48	39	35	27.3	24.5	13.4
11				23.3	23.3	9.3
12				43.3	22.8	21.8
13				26.4	22.3	17.4
14				39.8	21.7	14.5
15				29.4	20.9	15.5
16				43.7	20.7	20.6
17				20.9	19.4	6.3
18				33.7	19.0	16.4
19				23.6	18.4	8.2
20				30.3	18.0	14.8
21				17.9	17.4	8.7
22				20.9	17.0	10.8
23				23.0	16.0	6.9
24				24.2	15.5	8.0
25				16.9	15.4	9.5
26				26.6	15.1	6.7
27				17.7	15.0	10.8
28				17.7	14.9	9.3
29				20.7	14.8	10.7
30				18.4	14.8	10.6
31				23.2	14.6	13.4
32				15.9	14.3	10.0
33				24.0	14.2	11.3
34				22.0	13.8	12.3
35				23.2	13.7	7.8
36				14.5	13.7	9.7
37				14.3	13.0	7.9
38				19.8	12.9	7.0
39				15.6	12.9	4.9
40				13.0	12.7	4.9
41				16.9	12.4	8.6
42				16.7	12.3	7.7
43				19.5	11.7	5.5
44				19.4	11.0	8.3
45				17.7	10.9	8.8
46				17.3	10.8	10.0
47				14.1	10.5	6.8
48				16.8	10.3	7.3
49				12.5	10.3	7.0
50				16.4	9.6	9.4
Average gravel clast size						
Median	75.0	56.5	31.5	21.8	15.3	8.1
Mean	78.4	60.8	34.1	25.4	18.1	11.2

Appendix 3.10 Results of grain size analysis of Karun river terrace gravels - Batvand terrace

BATVAND TERRACE

Loc. 32°00'08''N 49°06'06''E — BFLS05 Bed 6

Clast number	10 largest gravel clasts Long diam. a (mm)	Intermed. diam. b (mm)	Short diam. c (mm)	50 typical gravel clasts Long diam. a (mm)	Intermed. diam. b (mm)	Short diam. c (mm)
1	111	100	70	67.5	48.7	34.5
2	110	91	36	6.8	45.9	11.6
3	102	87	38	79.3	43.7	21.3
4	95	82	46	49.3	34.5	18.2
5	110	79	52	55.2	33.5	20.4
6	88	73	52	41.3	30.9	14.5
7	96	64	47	62..7	29.2	20.9
8	91	63	50	32.3	27.3	11.8
9	89	51	49	34.1	26.4	20.3
10	56	43	22	31.7	24.7	10.0
11				24.5	23.5	9.9
12				23.9	23.0	22.7
13				25.5	22.9	13.2
14				25.8	22.0	12.3
15				24.5	21.4	15.6
16				35.2	21.3	13.7
17				29.2	20.4	12.0
18				31.7	19.9	10.9
19				32.6	19.8	10.2
20				19.9	19.0	13.1
21				27.5	17.7	15.9
22				23.4	16.9	15.0
23				19.4	16.9	9.9
24				23.3	16.5	10.0
25				22.8	16.1	11.4
26				18.0	15.9	5.0
27				21.6	15.6	7.7
28				17.4	14.2	9.4
29				17.5	13.7	6.7
30				17.8	13.5	7.5
31				30.5	13.3	12.7
32				19.8	12.9	5.9
33				18.0	12.6	6.9
34				20.9	12.5	6.9
35				17.4	12.0	10.0
36				19.7	11.5	6.4
37				12.7	11.1	7.7
38				13.7	11.0	6.5
39				12.3	11.0	5.5
40				17.8	10.9	7.0
41				12.6	10.7	8.1
42				20.0	10.3	5.6
43				16.7	10.0	6.4
44				18.6	9.9	6.6
45				12.8	9.8	4.6
46				12.3	9.8	8.4
47				15.9	9.7	5.4
48				12.8	9.6	5.6
49				11.9	9.6	5.5
50				12.7	8.5	6.2
Average gravel clast size						
Median	99.0	76.0	52.0	20.4	15.8	8.2
Mean	94.8	73.3	46.2	24.7	18.6	11.1

BATVAND TERRACE

Loc. 32°00'08''N 49°06'06''E — BFLS05 Bed 7

Clast number	10 largest gravel clasts Long diam. a (mm)	Intermed. diam. b (mm)	Short diam. c (mm)	50 typical gravel clasts Long diam. a (mm)	Intermed. diam. b (mm)	Short diam. c (mm)
1	215	175	84	74.3	44.0	24.3
2	217	134	92	52.0	36.9	15.7
3	155	112	72	55.3	32.3	18.4
4	105	102	75	41.0	30.8	19.9
5	157	97	70	36.6	30.7	15.7
6	129	97	61	46.3	26.8	9.3
7	112	96	41	34.0	26.2	11.0
8	164	95	76	33.9	21.5	11.5
9	116	95	50	26.5	19.1	8.7
10	159	74	45	20.4	17.7	6.0
11				17.8	17.6	10.4
12				18.6	16.9	10.0
13				26.4	16.5	12.6
14				20.9	16.0	9.6
15				20.4	15.6	7.3
16				19.5	15.4	5.9
17				17.2	15.0	6.4
18				15.9	14.5	7.8
19				18.6	14.3	7.4
20				25.6	14.2	5.9
21				21.4	14.0	10.0
22				14.4	13.8	13.0
23				20.0	13.7	6.6
24				21.8	13.5	10.0
25				17.9	12.9	7.3
26				17.4	12.8	6.4
27				15.0	12.7	7.5
28				14.6	12.7	5.9
29				15.8	12.6	3.2
30				18.2	12.3	8.9
31				16.5	12.0	3.5
32				19.3	11.4	5.0
33				23.5	11.1	7.0
34				11.9	10.9	4.7
35				15.5	10.7	6.4
36				19.6	10.6	6.7
37				13.7	10.5	5.4
38				15.7	10.2	5.5
39				12.3	10.2	5.1
40				15.9	10.0	8.2
41				14.1	10.0	6.3
42				12.8	9.6	6.7
43				17.3	9.5	6.3
44				13.9	9.3	5.0
45				14.3	8.5	4.4
46				11.8	8.5	4.6
47				11.9	8.4	5.0
48				10.4	8.1	4.6
49				16.6	7.7	4.6
50				13.6	6.3	4.7
Average gravel clast size						
Median	143.0	97.0	65.5	17.7	12.9	6.9
Mean	152.9	107.7	66.6	22.0	15.3	8.2

Appendix 3.11 Results of grain size analysis of Karun river terrace gravels - Kushkak terrace & Naft-e Safid terrace

KUSHKAK TERRACE							NAFT-E SAFID TERRACE						
Loc. 32°08'07''N 48°50'34''E			KUHKL3 Bed 1				Loc. 31°57'15''N 48°59'32''E			DKITEB Bed 1			
Clast	10 largest gravel clasts			50 typical gravel clasts			Clast	10 largest gravel clasts			50 typical gravel clasts		
number	Long	Intermed.	Short	Long	Intermed.	Short	number	Long	Intermed.	Short	Long	Intermed.	Short
	diam.	diam.	diam.	diam.	diam.	diam.		diam.	diam.	diam.	diam.	diam.	diam.
	a (mm)	b (mm)	c (mm)	a (mm)	b (mm)	c (mm)		a (mm)	b (mm)	c (mm)	a (mm)	b (mm)	c (mm)
1	129	95	64	51.9	44.8	22.0	1	218	181	103	55.5	52.8	10.6
2	86	65	49	52.3	39.9	30.6	2	119	101	89	71.5	48.7	30.8
3	116	64	41	46.9	34.9	24.6	3	132	90	39	50.7	45.5	12.0
4	79	63	30	36.4	33.9	14.9	4	120	71	25	52.8	41.8	11.7
5	87	56	35	43.2	33.7	28.0	5	102	69	36	70.0	40.3	22.8
6	70	56	35	56.9	33.0	13.4	6	95	67	31	81.8	40.0	26.3
7	63	55	26	51.4	32.8	11.7	7	74	63	33	49.9	38.0	12.9
8	81	54	46	34.3	32.3	9.2	8	73	62	22	39.6	35.8	14.4
9	99	52	35	36.8	31.4	13.4	9	81	60	35	44.5	33.8	11.9
10	60	45	37	34.8	30.0	16.0	10	63	59	14	34.2	28.8	13.0
11				30.0	29.4	14.7	11				29.3	27.2	13.9
12				30.0	29.1	10.0	12				28.9	26.4	16.7
13				39.7	28.0	21.6	13				34.3	25.5	15.9
14				49.0	26.4	16.5	14				33.4	25.4	14.9
15				32.3	26.4	14.5	15				41.9	24.6	20.9
16				27.3	26.3	11.8	16				30.8	22.9	16.8
17				35.9	26.0	13.3	17				36.4	22.8	17.3
18				34.5	25.9	14.7	18				36.4	22.5	15.8
19				27.5	25.7	9.6	19				41.9	21.9	20.4
20				37.0	25.4	13.0	20				36.4	21.6	14.9
21				36.8	25.2	11.9	21				27.2	18.8	12.9
22				50.8	24.8	20.4	22				25.3	18.7	11.0
23				33.2	24.6	11.7	23				20.2	18.2	11.4
24				33.6	24.0	9.6	24				28.0	18.0	17.8
25				59.0	23.4	18.6	25				22.3	17.9	11.9
26				27.6	22.8	11.0	26				29.0	17.5	16.4
27				33.0	22.7	16.4	27				20.0	17.4	16.0
28				31.8	22.5	12.8	28				17.8	17.3	13.7
29				36.3	21.9	13.0	29				17.3	16.0	3.5
30				29.0	21.4	18.5	30				16.9	16.0	8.3
31				25.0	21.4	9.5	31				23.0	15.8	7.6
32				24.8	21.4	13.9	32				20.5	15.8	9.3
33				36.7	21.0	13.9	33				29.9	15.7	15.4
34				32.0	19.4	10.4	34				20.5	15.7	9.4
35				29.7	18.7	7.0	35				24.4	15.5	8.4
36				24.3	18.2	14.4	36				23.9	15.4	7.2
37				26.6	18.0	12.0	37				20.6	13.9	10.7
38				31.4	17.5	16.9	38				13.0	12.8	6.7
39				29.4	17.4	14.2	39				26.5	12.4	8.2
40				20.4	17.2	14.6	40				15.7	12.3	3.7
41				36.0	16.8	10.8	41				14.6	12.3	11.0
42				20.0	12.9	6.7	42				15.3	11.8	7.9
43				15.3	12.8	7.4	43				18.7	11.4	5.7
44				15.9	12.3	7.5	44				14.0	10.8	8.9
45				15.8	12.0	7.0	45				13.0	10.8	6.4
46				12.2	11.3	7.8	46				20.5	10.1	7.5
47				14.6	10.9	8.0	47				12.1	10.0	4.7
48				12.8	9.9	5.8	48				18.9	9.3	7.3
49				16.0	9.5	9.1	49				10.2	8.9	7.4
50				9.8	8.2	7.3	50				21.9	7.5	7.3
Average gravel clast size							Average gravel clast size						
Median	78.5	56.0	35.0	43.3	23.1	14.8	Median	98.5	68.0	33.5	25.7	17.7	14.2
Mean	87.0	60.5	39.8	32.2	23.1	13.4	Mean	107.7	82.3	42.7	30.0	21.4	12.4

Appendix 3.12 Results of grain size analysis of Karun river terrace gravels - Naft-e Safid terrace & Abgah terrace

NAFT-E SAFID TERRACE							ABGAH TERRACE						
Loc. 31°57'16''N 48°59'34''E			DKITEA Bed 3				Loc. 31°59'32''N 49°05'43''E			BAF2BR Bed 1 (Lower part)			
Clast	10 largest gravel clasts			50 typical gravel clasts			Clast	10 largest gravel clasts			50 typical gravel clasts		
number	Long	Intermed.	Short	Long	Intermed.	Short	number	Long	Intermed.	Short	Long	Intermed.	Short
	diam.	diam.	diam.	diam.	diam.	diam.		diam.	diam.	diam.	diam.	diam.	diam.
	a (mm)	b (mm)	c (mm)	a (mm)	b (mm)	c (mm)		a (mm)	b (mm)	c (mm)	a (mm)	b (mm)	c (mm)
1	209	163	45	69.4	55.8	19.8	1	142	83	72	75.6	38.9	27.1
2	169	148	105	84.6	50.3	24.7	2	106	69	40	41.9	37.6	15.6
3	176	137	114	62.2	48.3	30.0	3	101	68	54	43.3	33.2	11.4
4	145	122	86	65.2	44.2	20.9	4	84	63	53	3.4	28.2	22.5
5	210	104	73	44.7	38.3	27.2	5	67	53	25	42.4	26.7	9.8
6	153	102	61	37.0	36.2	9.6	6	71	52	32	30.8	26.5	25.6
7	105	98	44	52.5	36.0	28.8	7	70	51	36	40.2	25.1	10.4
8	109	88	59	50.9	35.4	15.6	8	62	46	37	29.5	24.7	20.3
9	130	85	36	36.3	35.3	11.3	9	94	42	25	48.6	23.9	10.5
10	89	83	45	48.2	34.5	8.1	10	61	41	35	31.9	23.5	16.4
11				40.8	34.0	15.8	11				24.6	21.6	8.4
12				37.0	33.9	14.7	12				25.6	21.4	12.7
13				35.3	32.5	6.8	13				24.7	21.4	6.4
14				74.0	32.0	16.7	14				39.8	20.0	13.5
15				33.5	32.0	21.8	15				24.2	19.7	9.6
16				35.8	29.2	13.2	16				24.5	19.6	10.4
17				34.6	28.9	13.2	17				35.2	19.5	8.5
18				32.7	28.6	26.7	18				23.5	19.3	8.1
19				37.0	28.2	19.1	19				29.5	18.9	13.7
20				30.4	27.8	4.3	20				25.3	18.5	15.8
21				33.2	27.3	9.8	21				23.3	18.3	6.5
22				38.2	26.7	13.4	22				26.4	17.8	10.0
23				33.2	26.4	14.6	23				27.6	17.7	7.3
24				28.3	26.4	13.6	24				29.5	17.3	12.7
25				25.1	24.8	11.2	25				16.9	16.4	9.6
26				27.8	24.1	17.5	26				19.6	15.9	8.2
27				23.8	23.6	12.7	27				17.3	15.9	13.6
28				27.3	23.4	7.3	28				19.9	15.8	8.2
29				28.6	23.0	15.9	29				19.2	15.3	8.7
30				46.4	22.1	15.7	30				17.2	15.3	9.2
31				32.9	20.0	11.9	31				18.4	15.1	9.3
32				22.0	19.6	9.0	32				18.2	15.0	13.2
33				30.5	18.9	10.9	33				32.7	14.9	8.3
34				31.2	18.8	11.9	34				22.2	14.9	12.3
35				42.4	18.2	15.4	35				19.3	14.8	6.6
36				17.7	17.6	7.3	36				17.8	14.3	7.3
37				21.0	17.4	6.3	37				17.5	13.4	11.9
38				22.3	17.3	12.9	38				16.9	12.3	9.6
39				17.3	16.5	9.3	39				16.3	12.3	11.9
40				20.5	15.7	8.6	40				27.5	12.1	11.8
41				17.2	15.5	4.6	41				15.8	11.7	7.5
42				24.3	15.0	6.8	42				19.7	11.5	4.3
43				23.0	14.9	13.7	43				18.0	11.5	5.7
44				17.3	14.1	11.9	44				11.5	11.2	7.9
45				10.9	9.5	6.7	45				19.9	10.5	7.7
46				11.0	8.0	6.8	46				17.8	10.4	9.6
47				11.5	7.9	7.3	47				17.3	10.4	7.1
48				15.9	7.6	7.3	48				13.7	10.2	5.7
49				8.2	6.4	5.5	49				17.3	10.0	8.6
50				10.0	6.3	5.0	50				12.0	9.8	5.4
Average gravel clast size							Average gravel clast size						
Median	181.5	103.0	67.0	26.5	24.5	14.4	Median	69.0	52.5	28.5	18.3	16.2	8.9
Mean	149.5	113.0	66.8	33.2	25.1	13.2	Mean	85.8	56.8	40.9	25.0	18.0	10.8

Appendix 3.13 Results of grain size analysis of Karun river terrace gravels - Abgah terrace

ABGAH TERRACE

Loc. 31°59'32''N 49°05'43''E | BAF2BR Bed 5 (Lowest gravel unit)

Clast	10 largest gravel clasts			50 typical gravel clasts			Clast	10 largest gravel clasts			50 typical gravel clasts		
number	Long	Intermed.	Short	Long	Intermed.	Short	number	Long	Intermed.	Short	Long	Intermed.	Short
	diam.	diam.	diam.	diam.	diam.	diam.		diam.	diam.	diam.	diam.	diam.	diam.
	a (mm)	b (mm)	c (mm)	a (mm)	b (mm)	c (mm)		a (mm)	b (mm)	c (mm)	a (mm)	b (mm)	c (mm)
1	181	108	65	59.9	36.0	12.8	1						
2	90	75	49	41.8	35.3	8.3	2						
3	89	68	55	51.6	32.3	6.7	3						
4	101	56	24	31.0	28.2	10.2	4						
5	74	55	29	30.8	24.4	14.6	5						
6	75	51	39	70.8	23.5	10.7	6						
7	75	50	42	29.4	22.6	9.4	7						
8	75	46	29	29.0	22.5	13.7	8						
9	59	46	43	24.5	21.9	10.8	9						
10	77	41	33	22.5	21.9	10.9	10						
11				25.3	21.5	9.6	11						
12				37.0	20.4	12.5	12						
13				33.7	20.0	9.9	13						
14				20.0	19.7	9.9	14						
15				22.0	18.7	11.2	15						
16				33.5	18.3	11.9	16						
17				25.0	18.2	10.4	17						
18				27.3	17.8	15.0	18						
19				23.2	17.4	11.5	19						
20				22.7	17.3	10.8	20						
21				28.4	16.4	8.3	21						
22				18.5	16.4	6.9	22						
23				27.6	16.3	3.5	23						
24				22.8	15.4	8.2	24						
25				15.5	15.2	5.4	25						
26				22.8	14.9	10.5	26						
27				27.9	14.8	13.5	27						
28				21.3	14.2	6.8	28						
29				19.2	13.7	5.7	29						
30				22.9	12.7	7.3	30						
31				17.9	12.7	3.5	31						
32				19.1	12.5	6.3	32						
33				21.8	12.3	8.6	33						
34				17.6	12.2	4.1	34						
35				14.4	11.8	8.2	35						
36				23.6	11.7	9.6	36						
37				15.0	11.5	7.5	37						
38				17.9	11.1	8.6	38						
39				18.1	10.9	7.8	39						
40				13.0	10.6	4.0	40						
41				15.9	10.5	6.6	41						
42				17.2	9.9	7.5	42						
43				13.2	9.9	6.0	43						
44				20.0	9.6	4.9	44						
45				16.5	9.2	4.1	45						
46				17.8	9.1	7.2	46						
47				14.9	9.0	7.4	47						
48				16.1	8.5	5.6	48						
49				16.4	8.3	6.4	49						
50				8.7	6.7	6.5	50						
Average gravel clast size													
Median	74.5	53.0	34.0	19.2	15.1	8.0							
Mean	89.6	59.6	40.8	24.5	16.3	8.5							

Appendix 3.14 Results of grain size analysis of Karun river terrace gravels - Higher terraces near Abgah

HIGHER TERRACES NEAR ABGAH							HIGHER TERRACES NEAR ABGAH						
Loc. 31°58'48''N 49°04'54''E			BAF3LA Gravels				Loc. 31°58'38''N 49°04'51''E			BAF3LD Gravels			
Clast	10 largest gravel clasts			50 typical gravel clasts			Clast	10 largest gravel clasts			50 typical gravel clasts		
number	Long	Intermed.	Short	Long	Intermed.	Short	number	Long	Intermed.	Short	Long	Intermed.	Short
	diam.	diam.	diam.	diam.	diam.	diam.		diam.	diam.	diam.	diam.	diam.	diam.
	a (mm)	b (mm)	c (mm)	a (mm)	b (mm)	c (mm)		a (mm)	b (mm)	c (mm)	a (mm)	b (mm)	c (mm)
1	167	144	32	67.6	52.5	13.7	1	225	156	72	65.3	49.4	47.3
2	132	117	19	49.6	41.7	9.8	2	161	137	62	62.7	47.9	21.1
3	164	115	57	51.9	39.5	17.3	3	119	101	41	114.0	43.9	34.7
4	111	99	48	44.5	36.3	16.0	4	117	96	31	51.7	42.8	14.3
5	125	96	33	46.0	36.0	14.3	5	110	89	35	58.5	37.3	15.7
6	114	95	31	45.5	34.4	13.9	6	129	63	56	50.5	34.3	22.4
7	131	94	62	53.4	32.7	19.1	7	116	58	28	48.0	32.5	21.4
8	1514	88	39	42.8	31.9	18.4	8	67	56	10	50.9	28.4	25.6
9	112	82	22	55.7	31.8	18.5	9	68	53	12	31.4	27.9	6.3
10	118	77	33	58.3	31.5	27.3	10	55	52	12	68.2	27.7	24.6
11				36.9	30.0	20.0	11				34.6	27.5	16.4
12				39.7	29.6	15.5	12				45.3	27.0	15.1
13				32.5	27.3	12.5	13				41.5	26.8	17.0
14				42.0	26.7	14.6	14				50.9	25.4	12.5
15				37.3	25.9	15.3	15				47.5	25.0	17.0
16				49.1	25.6	12.4	16				32.7	23.5	11.7
17				36.0	25.4	14.4	17				27.8	22.6	8.7
18				36.6	24.0	16.7	18				23.7	22.3	7.3
19				33.8	23.7	7.2	19				25.7	20.2	5.6
20				31.5	23.7	18.2	20				36.9	20.1	10.5
21				25.4	22.1	14.8	21				28.4	20.0	8.8
22				40.0	21.8	12.0	22				23.9	20.0	15.4
23				23.2	21.4	12.6	23				25.0	19.6	6.6
24				28.2	20.7	8.9	24				24.5	19.3	4.0
25				32.0	20.4	11.3	25				30.7	19.0	7.1
26				28.5	20.0	12.6	26				28.7	18.7	13.3
27				24.5	19.5	12.3	27				25.5	18.3	16.0
28				30.8	18.2	10.9	28				30.5	17.8	12.0
29				28.9	18.0	12.3	29				19.5	17.3	7.1
30				33.7	17.9	17.8	30				18.6	16.7	8.2
31				25.7	17.8	7.7	31				23.0	16.6	10.7
32				24.0	17.8	11.4	32				18.2	16.5	5.8
33				22.0	17.7	10.2	33				36.3	16.4	7.5
34				30.4	17.6	12.2	34				18.2	15.7	10.6
35				25.7	17.4	11.5	35				32.3	15.5	5.8
36				18.7	17.4	11.9	36				23.4	15.2	5.3
37				20.5	16.2	9.9	37				18.0	15.2	8.7
38				23.8	15.9	13.1	38				23.6	14.9	4.5
39				19.2	15.8	5.9	39				17.8	14.9	8.5
40				25.4	15.5	12.3	40				22.6	14.8	6.9
41				21.4	15.2	10.7	41				19.4	14.6	5.5
42				19.6	14.1	10.3	42				24.6	14.2	11.0
43				17.9	13.7	11.0	43				18.8	13.6	9.4
44				17.6	13.1	9.0	44				18.8	13.3	12.8
45				23.6	12.9	9.4	45				19.9	11.0	7.3
46				18.7	12.8	8.8	46				18.2	10.4	8.4
47				18.4	11.7	8.4	47				12.7	10.3	6.4
48				19.0	11.5	9.6	48				12.8	9.0	5.7
49				26.2	10.5	7.9	49				10.7	8.4	5.7
50				12.3	9.0	6.5	50				9.1	8.2	4.6
Average gravel clast size							Average gravel clast size						
Median	119.5	95.5	32.0	30.3	20.2	12.0	Median	119.5	76.0	45.5	29.7	18.9	10.2
Mean	268.8	100.7	37.6	32.3	22.5	12.8	Mean	116.7	86.1	35.9	32.4	21.4	12.1

Appendix 3.15 Results of grain size analysis of Karun river terrace gravels - Higher terrace north of Batvand

HIGHER TERRACE N. OF BATVAND ON W. BANK OF AB-E GULESTAN							HIGHER TERRACE N. OF BATVAND ON W. BANK OF AB-E GULESTAN						
Loc. 32°02'06''N 49°08'17''E			BA1LPT Unit 1 Set 1				Loc. 32°02'06''N 49°08'17''E			BA1LPT Unit 1 Set 2			
Clast	10 largest gravel clasts			50 typical gravel clasts			Clast	10 largest gravel clasts			50 typical gravel clasts		
number	Long	Intermed.	Short	Long	Intermed.	Short	number	Long	Intermed.	Short	Long	Intermed.	Short
	diam.	diam.	diam.	diam.	diam.	diam.		diam.	diam.	diam.	diam.	diam.	diam.
	a (mm)	b (mm)	c (mm)	a (mm)	b (mm)	c (mm)		a (mm)	b (mm)	c (mm)	a (mm)	b (mm)	c (mm)
1	384	344	129	115.5	81.5	47.7	1	461	257	135	63.8	44.0	33.0
2	483	304	243	68.7	57.7	26.5	2	331	223	145	46.5	35.6	26.5
3	403	283	135	75.9	54.5	22.8	3	346	218	140	39.9	35.0	12.5
4	376	280	207	80.3	49.2	28.4	4	232	155	138	61.9	33.9	26.5
5	303	255	166	50.5	47.5	25.8	5	177	146	41	41.3	32.3	19.2
6	295	239	105	77.1	46.9	31.9	6	260	136	109	39.6	32.0	20.8
7	233	224	41	53.7	42.7	9.0	7	283	119	84	35.6	31.5	15.8
8	375	207	122	62.3	42.5	25.9	8	183	97	84	31.2	30.4	26.7
9	241	191	46	39.0	37.7	17.3	9	197	95	44	52.7	30.3	10.4
10	255	180	141	46.7	36.1	22.5	10	105	75	41	34.8	25.5	8.0
11				48.6	34.7	15.4	11				30.9	24.1	6.5
12				42.8	34.7	12.7	12				27.8	22.8	11.7
13				47.6	34.2	19.9	13				23.2	22.8	8.7
14				56.8	31.6	16.5	14				24.3	22.7	9.6
15				46.9	31.4	15.0	15				30.3	21.4	13.3
16				32.5	29.9	7.9	16				21.9	20.3	2.9
17				82.5	29.5	21.2	17				20.2	19.0	9.8
18				49.6	27.9	16.0	18				20.7	18.9	6.3
19				32.5	26.4	22.0	19				33.7	18.6	10.9
20				52.3	25.9	11.6	20				22.3	18.4	10.3
21				31.9	25.6	12.0	21				29.2	18.3	9.0
22				33.7	25.5	8.7	22				26.9	18.2	9.9
23				43.7	24.9	15.5	23				32.0	17.8	6.7
24				40.7	24.5	9.9	24				19.0	17.7	2.5
25				44.0	24.4	18.0	25				25.0	17.3	10.0
26				31.0	23.5	12.6	26				19.7	16.0	8.0
27				37.3	23.3	13.5	27				24.6	15.9	7.7
28				24.6	23.3	9.6	28				23.3	15.5	9.9
29				31.2	23.2	15.4	29				20.7	15.4	8.9
30				53.3	21.9	13.0	30				20.4	15.4	8.7
31				31.5	21.7	8.7	31				22.7	15.1	12.2
32				22.5	21.3	12.0	32				27.3	15.0	7.3
33				26.4	19.8	7.9	33				20.0	14.9	8.8
34				24.4	19.8	9.0	34				27.3	13.7	8.5
35				26.0	18.5	6.5	35				21.5	13.5	8.0
36				32.6	18.4	15.5	36				14.4	13.5	6.3
37				23.0	18.2	16.4	37				15.0	12.8	9.7
38				24.3	16.9	11.4	38				15.4	12.3	7.2
39				23.0	16.8	11.7	39				13.8	12.2	10.5
40				38.4	16.4	13.5	40				25.9	12.1	8.2
41				28.2	16.0	9.0	41				15.5	12.1	9.0
42				20.7	15.6	12.2	42				15.6	11.5	7.8
43				26.4	15.5	11.7	43				15.0	11.4	7.7
44				21.7	15.5	8.8	44				14.0	11.2	3.5
45				18.4	14.9	6.4	45				17.8	11.0	7.7
46				17.3	14.3	10.2	46				12.6	10.8	4.4
47				17.8	13.4	11.4	47				14.3	10.3	5.5
48				21.9	11.8	8.3	48				12.9	10.0	5.3
49				13.4	11.3	4.9	49				15.6	9.8	3.2
50				13.5	9.3	8.3	50				18.5	9.0	7.8
Average gravel clast size							Average gravel clast size						
Median	299.0	247.0	135.5	37.5	24.0	15.3	Median	218.5	141.0	75.0	22.4	16.7	9.0
Mean	334.8	250.7	133.5	40.1	27.4	15.0	Mean	257.5	152.1	96.1	26.0	19.0	10.4

Appendix 4.1 (a) Results of grain size analysis of fine-grained sediment and rock samples associated with banks and beds of the Karun and Dez river systems	Dry mass of entire sample used for laser particle size analysis (g)	Proportion of sample > 63 µm by dry mass (%)	Proportion of sample < 63 µm by dry mass (%)	Mean grain size within > 63 µm fraction (µm)	Mean grain size within < 63 µm fraction (µm)	Mean grain size of entire sample by calculation (µm)	Summary components of cumulative distribution for the greater than 63 µm fraction (where available) (e.g. 10 % of the grains in this fraction are smaller than the grain size of X_{10} in µm)					Summary components of cumulative distribution for the less than 63 µm fraction (where available) (e.g. 10 % of the grains in this fraction are smaller than the grain size of X_{10} in µm)				
							X_{10}	X_{16}	X_{50}	X_{84}	X_{90}	X_{10}	X_{16}	X_{50}	X_{84}	X_{90}
RIVER BANKS AND BEDS OF THE KARUN RIVER SYSTEM																
AB-E GULESTAN TRIBUTARY																
Approx. Location 32°02'00''N 49°08'24''E																
PSA 100 / BA1SAB River bed sands	2.8911	76.92	23.08	292.0	7.8	226.4	146.81	173.62	292.00	466.30	542.08	1.30	1.88	7.83	21.13	28.58
PSA 101 / BA1SAB River bank surface/silt	1.1314	5.92	94.08	—	5.3	—	—	—	—	—	—	1.16	1.59	5.33	19.75	24.90
PSA 102 / BA1AJR Agha Jari F. bedrock from river bank	6.6187	21.86	78.14	142.2	5.3	35.2	94.45	101.89	142.18	202.00	993.02	1.20	1.65	5.25	18.21	24.63
PSA 103 / Nr. BA1UHT River bank sediment	2.1844	7.86	92.14	250.4	6.0	25.2	134.88	154.35	250.41	488.84	611.13	1.19	1.65	5.97	18.31	22.92
PSA 104 / BA1UHB Agha Jari F. bedrock from river bank	8.4684	19.63	80.37	196.0	14.6	50.2	94.45	103.76	195.96	649.06	872.26	2.81	4.07	14.61	36.91	42.55
RUD-E TEMBI TRIBUTARY																
Location 32°00'08''N 49°06'14''E																
PSA 105 / BFL1GB River bank/bed clay and silt	0.6989	11.10	88.90	112.7	6.8	18.5	81.78	87.11	112.74	164.51	210.73	1.26	1.80	6.76	28.56	35.23
PSA 106 / BFL1GB **A** River bank - lower soft sediment	1.3579	52.69	47.31	181.9	11.0	101.1	107.79	120.19	181.92	278.21	309.64	1.31	1.89	11.00	38.36	59.13
PSA 107 / BFL1GB **B** River bank - upper sediments/soil	1.5132	50.30	49.70	183.8	9.6	97.2	109.27	120.67	183.75	285.75	322.87	1.22	1.71	9.64	39.99	46.27
AB-E SHUR TRIBUTARY																
Location 31°59'31''N 49°05'45''E																
PSA 108 / BAF2AJ Agha Jari F. bedrock from river bank	6.3938	35.01	64.99	703.4	7.1	250.9	281.96	354.50	703.42	1371.24	1868.56	1.86	2.87	7.09	13.67	17.06
RIVER KARUN - Shushtar Anticline area																
River Karun upstream of Shushtar Anticline																
Location 32°08'09''N 48°51'51''E																
PSA 109 / KUHKL1 River bank	4.3424	12.47	87.53	223.6	12.4	38.7	92.37	101.56	223.64	969.75	1262.90	1.55	2.35	12.40	35.42	41.31
River Karun near to axis of Shushtar Anticline																
Location 32°03'44''N 48°51'28''E																
PSA 112 / SHTRA1 River bank fine-grained sediment	7.5842	20.47	79.53	188.8	9.0	45.8	96.55	107.16	188.81	1347.30	2768.36	1.24	1.77	9.02	34.13	40.32
PSA 113 / SHTRA1 Agha Jari F. bedrock from river bed/bank	8.9969	58.00	42.00	321.9	8.6	190.3	193.90	223.21	321.90	464.74	538.71	1.56	2.47	8.57	23.31	30.92
River Karun (Shuteyt) downstream of Shushtar Anticline																
Location 32°01'05''N 48°47'40''E																
PSA 114 / QALSL1 River bank	1.9225	22.08	77.92	105.7	11.9	32.6	78.97	83.01	105.72	157.97	208.05	1.27	1.85	11.94	39.32	45.35
River Karun (Gargar) downstream of Shushtar Anticline																
Location 32°01'10''N 48°51'04''E																
PSA 115 / GGRBR2 River bank	6.4823	34.60	65.40	114.4	9.2	45.6	82.28	87.92	114.38	170.77	199.13	1.16	1.61	9.18	39.63	45.91
RIVER KARUN (GARGAR) - Band-e Mahibazan area																
Approx. Location 32°00'01''N 48°51'28''E																
PSA 123A / BMHIB6 River cliff sands	5.8701	71.20	28.80	150.7	12.7	110.9	92.41	100.11	150.67	309.46	360.32	1.16	1.65	12.73	41.57	46.95
PSA 124 / BMHIB4 River bank	2.8077	3.00	97.00	—	6.9	—	—	—	—	—	—	1.21	1.70	6.90	22.65	27.27

Appendix 4.1 (b) Results of grain size analysis of fine-grained sediment and rock samples associated with banks and beds of the Karun and Dez river systems	Dry mass of entire sample used for laser particle size analysis (g)	Proportion of sample > 63 µm by dry mass (%)	Proportion of sample < 63 µm by dry mass (%)	Mean grain size within > 63 µm fraction (µm)	Mean grain size within < 63 µm fraction (µm)	Mean grain size of entire sample by calculation (µm)	Summary components of cumulative distribution for the greater than 63 µm fraction (where available) (e.g. 10 % of the grains in this fraction are smaller than the grain size of X_{10} in µm)					Summary components of cumulative distribution for the less than 63 µm fraction (where available) (e.g. 10 % of the grains in this fraction are smaller than the grain size of X_{10} in µm)				
							X_{10}	X_{16}	X_{50}	X_{84}	X_{90}	X_{10}	X_{16}	X_{50}	X_{84}	X_{90}
RIVER BANKS AND BEDS OF THE KARUN RIVER SYSTEM (continued)																
RIVER KARUN (SHUTEYT) - Sardarabad Anticline area																
River Karun (Shuteyt) upstream of Sardarabad Anticline																
Approx. Location 31°56'33''N 48°17'19''E																
PSA 116 / KA0402 River bedload - less than 4 mm fraction	9.7071	82.73	17.27	874.0	4.4	723.8	163.79	210.02	874.01	3633.16	4284.87	0.91	1.23	4.38	28.36	36.85
PSA 117 / KA0402 River bed/bank (associated with Bed 1)	4.4243	1.68	98.32	—	3.2	—	—	—	—	—	—	0.77	1.03	3.23	15.41	21.66
PSA117A / KBS1RB River bank sediment	7.3828	38.42	61.58	132.1	7.2	55.1	87.30	95.74	132.05	232.51	312.28	1.05	1.46	7.15	33.45	40.68
River Karun (Shuteyt) near to proj. of axis of Sardarabad Anticline																
Location 31°52'18''N 48°52'46''E																
PSA 118 / QLHKL1 River bed	5.1319	1.00	99.00	—	6.4	—	—	—	—	—	—	1.27	1.99	6.40	12.35	15.25
PSA 119 / QLHKL1 Lower river bank sediment	4.5122	2.67	97.33	151.3	4.3	8.2	84.17	93.86	151.25	255.35	294.81	0.94	1.38	4.28	16.63	23.65
PSA 120 / QLHKL1 Upper river bank sediment	2.5745	0.96	99.04	274.4	3.1	5.7	140.60	162.98	274.35	436.80	503.58	0.82	1.09	3.14	10.71	15.10
River Karun (Shuteyt) downstream of Sardarabad Anticline																
Location 31°40'25''N 48°52'31''E																
PSA 121 / NASHA3 River bed	4.3619	0.81	99.19	—	3.7	—	—	—	—	—	—	0.86	1.15	3.66	13.24	17.55
PSA 122 / NASHA3 River bank	3.3884	10.23	89.77	270.1	11.4	37.9	112.85	142.51	270.13	618.15	796.96	1.38	2.03	11.41	32.98	38.49
RIVER KARUN (GARGAR) - environs of Dar Khazineh area																
Qulramzi area																
Location 31°56'17''N 48°56'42''E																
PSA 125 / QULGR1 River bed	2.8381	5.19	94.81	103.9	19.3	23.6	73.09	79.42	103.86	194.90	250.03	2.11	3.81	19.25	39.48	44.76
PSA 126 / QULGR1 River bank	4.0912	80.81	19.19	202.3	11.4	165.7	118.60	136.40	202.30	276.25	296.39	1.34	1.94	11.36	39.64	45.09
Buneh-ye Ghaleymeh area																
Location 31°53'23''N 48°59'21''E																
PSA 128 / BUNGH2 River bank	2.6330	3.57	96.43	189.3	8.6	15.1	117.34	130.53	189.26	393.56	590.21	1.33	1.91	8.64	26.71	32.08
RIVER KARUN - Ramin Oilfield Anticline area																
River Karun (Shuteyt) upstream of near-straight reach																
Location 31°38'58''N 48°52'54''E																
PSA 130 / BNDEQ1 River bed	3.5057	11.82	88.18	160.1	11.2	28.8	87.55	97.23	160.14	394.73	501.43	1.38	2.04	11.24	32.35	37.37
PSA 131 / BNDEQ1 River bank	2.7309	34.01	65.99	131.5	15.9	55.2	87.68	95.94	131.46	191.03	210.72	1.55	2.45	15.93	40.69	46.78
River Karun along near-straight reach																
Location 31°37'51''N 48°53'12''E																
PSA 132 / MLS071 River bed	1.3692	11.66	88.34	145.8	4.7	21.1	95.48	102.93	145.75	218.18	244.14	0.99	1.33	4.68	18.08	24.42
PSA 133 / MLS071 River bank	4.3784	18.83	81.17	123.3	12.8	33.6	84.72	91.84	123.28	206.05	272.03	1.69	2.66	12.81	34.11	40.04
Location 31°32'30''N 48°52'38''E																
PSA 133A / MLS073 River bed	2.3416	10.64	89.36	116.5	18.6	29.0	81.71	87.23	116.45	276.57	393.16	1.67	2.68	18.55	42.08	47.37
PSA 133B / MLS073 River bank	2.9683	2.71	97.29	148.1	14.4	18.0	82.99	90.75	148.07	312.53	380.16	1.45	2.21	14.39	35.04	40.29
River Karun downstream of near-straight reach																
Location 31°26'16''N 48°48'53''E																
PSA 134 / SEYRZ1 River bed	4.6591	49.36	50.64	126.1	13.4	69.1	86.10	94.57	126.14	173.48	193.52	1.40	2.07	13.43	40.22	46.08
PSA 135 / SEYRZ1 River bank	5.0761	36.44	63.56	113.2	21.0	54.6	83.13	89.17	113.17	152.54	165.57	1.57	2.59	20.97	44.23	49.23

Appendix 4.1 (c) Results of grain size analysis of fine-grained sediment and rock samples associated with banks and beds of the Karun and Dez river systems	Dry mass of entire sample used for laser particle size analysis (g)	Proportion of sample > 63 µm by dry mass (%)	Proportion of sample < 63 µm by dry mass (%)	Mean grain size within > 63 µm fraction (µm)	Mean grain size within < 63 µm fraction (µm)	Mean grain size of entire sample by calculation (µm)	Summary components of cumulative distribution for the greate than 63 µm fraction (where available) (e.g. 10 % of the grains in this fraction are smaller than the grain size of X_{10} in µm)					Summary components of cumulative distribution for the less than 63 µm fraction (where available) (e.g. 10 % of the grains in this fraction are smaller than the grain size of X_{10} in µm)				
							X_{10}	X_{16}	X_{50}	X_{84}	X_{90}	X_{10}	X_{16}	X_{50}	X_{84}	X_{90}
RIVER BANKS AND BEDS OF THE KARUN RIVER SYSTEM (continued)																
RIVER KARUN - Ahvaz Anticline area																
River Karun upstream of Ahvaz Anticline																
Location 31°22'10''N 48°45'26''E																
PSA 136 / ZARGB1 River bed	3.3879	44.51	55.49	114.0	27.0	65.7	82.10	87.96	114.00	157.84	170.02	1.68	2.88	27.01	47.23	51.01
PSA 137 / ZARGB1 River bank	6.2462	20.24	79.76	107.0	20.1	37.7	74.98	81.13	107.01	149.61	166.07	1.53	2.41	20.05	42.03	47.14
Location 31°21'10''N 48°42'13''E																
PSA 138 / AZPOLN River bed	1.7218	2.90	97.10	204.6	4.9	10.7	105.36	122.52	204.59	318.91	386.88	1.02	1.36	4.86	21.31	27.29
PSA 139 / AZPOLN River bank	1.1167	2.56	97.44	—	4.8	—	—	—	—	—	—	1.11	1.60	4.76	19.22	25.04
River Karun near to axis of Ahvaz Anticline																
Location 31°19'46''N 48°40'54''E																
PSA 140 / AZRPL1 River bank	10.1930	34.31	65.69	119.1	8.4	46.4	79.78	86.29	119.11	171.23	195.22	1.11	1.55	8.37	35.28	41.56
Approx. Location 31°19'09''N 48°40'38''E																
PSA 141 / AZPLCH River bed	2.4187	2.99	97.01	162.5	6.0	10.6	96.52	106.03	162.47	265.74	308.69	1.15	1.67	5.95	18.59	22.58
PSA 142 / AZPLCH River bed	4.6211	87.72	12.28	173.5	4.6	152.7	109.78	121.47	173.45	241.54	266.83	1.01	1.35	4.55	26.22	34.97
PSA 143 / AZPLCH River bank	7.5386	50.22	49.78	194.2	5.6	100.3	107.26	120.81	194.19	335.44	437.64	1.02	1.39	5.58	23.63	29.70
PSA 144 / AZWHBR Agha Jari F. bedrock from river bank	14.0706	71.15	28.85	185.2	28.0	139.8	113.03	125.19	185.20	308.61	381.13	7.07	11.66	27.99	45.12	49.31
River Karun downstream of Ahvaz Anticline																
Location 31°13'50''N 48°35'56''E																
PSA 145 / AMEYL1 River bed	4.5867	88.39	11.61	169.5	6.9	150.7	112.74	123.63	169.54	225.91	242.75	1.42	2.25	6.89	34.97	41.84
PSA 146 / AMEYL1 River bank	4.1097	36.19	63.81	119.2	23.2	57.9	82.58	88.91	119.18	190.03	227.91	2.00	3.48	23.16	45.16	49.68
PSA 147 / AMEYL1 River bank - clay/silt	5.2357	25.32	74.68	110.8	12.4	37.3	80.50	85.59	110.76	166.27	220.52	1.26	1.86	12.36	39.10	45.07
PSA 147A / AMEYL1 River bank - sand	3.6892	36.05	63.95	144.6	15.8	62.2	85.83	94.05	144.64	323.55	361.10	1.35	2.01	15.79	43.34	48.66
RIVER BANKS AND BEDS OF THE DEZ RIVER SYSTEM																
RIVER DEZ - Sardarabad Anticline area																
River Dez upstream of Sardarabad Anticline																
Location 32°03'48''N 48°31'46''E																
PSA 148 / RDZUP3 River bed	4.1252	57.46	42.54	161.5	15.9	99.5	97.46	107.17	161.48	246.64	285.11	1.54	2.34	15.87	39.83	45.13
PSA 148A / RDZUP3 River bank	6.7687	48.20	51.80	142.9	12.9	75.6	89.31	98.64	142.86	216.44	248.24	1.42	2.13	12.94	35.77	41.59
River Dez near to axis of Sardarabad Anticline																
Location 31°58'42''N 48°36'41''E																
PSA 149 / RDZSA1 River bank	5.7585	33.01	66.99	108.9	5.3	39.5	80.32	85.05	108.89	149.26	164.87	1.05	1.42	5.33	32.94	39.95
River Dez downstream of Sardarabad Anticline																
Location 31°49'50''N 48°39'54''E																
PSA 150 / RDZDS1 River bed	7.9654	70.36	29.64	174.2	22.0	129.1	92.99	104.08	174.21	295.21	341.81	1.67	2.55	21.97	43.77	48.55
PSA 151 / RDZDS1 River bank	6.5698	31.64	68.36	123.2	16.5	50.3	86.07	93.73	123.19	181.68	217.39	1.72	2.82	16.51	38.95	44.03

Appendix 4.2 (a) Results of grain size analysis of fine-grained sediment and rock samples associated with river terraces and floodplains of the Karun river system	Dry mass of entire sample used for laser particle size analysis (g)	Proportion of sample > 63 µm by dry mass (%)	Proportion of sample < 63 µm by dry mass (%)	Mean grain size within > 63 µm fraction (µm)	Mean grain size within < 63 µm fraction (µm)	Mean grain size of entire sample by calculation (µm)	Summary components of cumulative distribution for the greater than 63 µm fraction (where available) (e.g. 10 % of the grains in this fraction are smaller than the grain size of X_{10} in µm)					Summary components of cumulative distribution for the less than 63 µm fraction (where available) (e.g. 10 % of the grains in this fraction are smaller than the grain size of X_{10} in µm)				
							X_{10}	X_{16}	X_{50}	X_{84}	X_{90}	X_{10}	X_{16}	X_{50}	X_{84}	X_{90}
RIVER TERRACES OF THE KARUN RIVER SYSTEM																
DAR KHAZINEH TERRACE																
Location 31°54'47''N 48°59'29''E																
PSA 157 / DAKS05 Bed 1 (58 cm above base of bed)	7.8670	14.17	85.83	119.6	6.3	22.4	82.17	88.19	119.57	231.88	305.43	1.19	1.64	6.31	21.20	26.97
PSA 10 / DAKS05 Bed 2 OSL SAMPLE 3	10.0000	38.79	61.21	278.9	7.6	112.8	119.46	148.84	278.89	402.02	439.14	1.68	2.64	7.62	17.15	22.21
PSA 158 / DAKS05 Bed 3 (4 cm above base of bed)	7.7796	59.37	40.63	126.6	4.5	77.0	86.42	94.25	126.58	198.94	232.73	1.01	1.36	4.54	23.98	32.03
PSA 158A / DAKS05 Bed 3 (4 cm above base of bed)	3.8578	55.74	44.26	135.8	6.1	78.4	89.62	97.69	135.76	206.69	240.12	1.07	1.45	6.11	32.50	40.19
PSA 159 / DAKS05 Bed 4 (9 cm above base of bed)	7.6945	71.76	28.24	173.6	5.0	126.0	101.48	112.42	173.61	250.89	283.65	0.99	1.33	5.03	30.99	39.08
PSA 160 / DAKS05 Bed 5 (6 cm above base of bed)	9.8183	43.47	56.53	135.4	6.2	62.3	88.65	96.78	135.40	214.63	253.40	1.07	1.46	6.17	28.93	35.02
PSA 161 / DAKS05 Bed 6 (10 cm above base of bed)	7.2559	33.34	66.66	110.4	3.9	39.4	81.92	87.11	110.42	149.59	165.27	0.93	1.23	3.86	18.79	26.35
PSA 162 / DAKS05 Bed 7 (21 cm above base of bed)	5.2245	46.35	53.65	132.2	10.0	66.6	83.96	91.24	132.16	248.25	295.41	1.24	1.77	9.97	38.57	44.72
Location 31°54'46''N 48°59'23''E																
PSA 7 / DKLTFH Bed 10 OSL SAMPLE 11	10.0000	19.65	80.35	98.9	6.0	24.3	72.49	78.76	98.87	128.28	137.51	0.95	1.30	6.03	31.33	40.91
Location 31°54'35''N 48°59'09''E																
PSA 163 / HGWS05 Bed 1 (13 cm below top of bed)	9.2831	23.05	76.95	118.1	6.8	32.4	82.48	88.50	118.08	192.85	231.92	1.11	1.55	6.76	25.95	31.86
PSA 164 / HGWS05 Bed 2 (10 cm above base of bed)	9.1885	80.12	19.88	428.2	9.5	344.9	172.81	213.38	428.16	997.02	1259.63	1.44	2.09	9.51	33.79	40.31
PSA 11 / HGWS05 Bed 7 OSL SAMPLE 4	10.0000	82.22	17.78	308.0	9.9	255.0	134.74	166.56	308.01	481.98	532.09	1.70	2.55	9.89	23.73	26.79
KABUTARKHAN-E SUFLA TERRACE																
Approx. Location 31°56'33''N 48°47'19''E																
PSA 165 / KA0402 Bed 1 Sample of brown laminated clay/silt	15.2970	0.00	100.00	—	7.4	7.4	—	—	—	—	—	1.19	1.75	7.38	24.86	29.62
PSA 166 / KA0402 Bed 2 Sample of light brown sands and silts	14.6258	66.75	33.25	151.9	10.9	105.0	88.63	97.26	151.93	356.94	495.23	1.25	1.84	10.90	35.85	41.73
PSA 5 / KBS4OS Bed 2 OSL SAMPLE 9	10.0000	58.32	41.68	157.3	3.0	93.0	88.43	98.28	157.31	273.35	312.36	0.80	1.01	3.01	9.22	12.21
PSA 167 / KA0402 Bed 3 (Lower part) Light brown sands	11.6670	50.46	49.54	150.4	5.3	78.5	88.12	96.69	150.36	288.00	336.53	0.99	1.35	5.29	27.24	34.99
PSA 168 / KA0402 Bed 3 (Upper part) Red-brown clay/silt	12.0515	0.26	99.74	242.8	4.3	4.9	143.52	160.98	242.77	365.49	412.49	0.96	1.30	4.29	12.57	16.23
PSA 169 / KA0402 Bed 4 Part of solid sample	10.0616	85.06	14.94	1209.3	9.8	1030.1	359.93	482.75	1209.27	2768.95	3317.27	1.34	2.01	9.76	34.66	40.75
PSA 170 / KA0402 Bed 4 Part of solid sample	9.9715	71.18	28.82	709.2	6.3	506.6	171.29	262.34	709.19	5227.29	6472.33	1.11	1.55	6.27	25.97	31.97
BATVAND TERRACE																
Location 32°00'08''N 49°06'06''E																
PSA 173 / BFLS05 Bed 1 (7 cm above base of bed)	7.7379	43.73	56.27	136.1	8.3	64.2	87.89	96.25	136.05	205.37	236.34	1.16	1.64	8.34	35.19	41.36
PSA 9 / BFLS05 Bed 2 OSL SAMPLE 2	10.0000	22.73	77.27	224.2	5.8	55.5	104.07	118.10	224.22	447.22	557.76	1.26	1.86	5.81	20.33	28.96
PSA 174 / BFLS05 Bed 3 (38 cm above base of bed)	17.7193	80.76	19.24	819.2	8.3	663.2	293.86	382.68	819.23	2913.24	3957.77	1.66	2.61	8.26	29.79	36.60
PSA 175 / BFLS05 Bed 4 (18 cm above base of bed)	15.1314	83.51	16.49	807.2	22.4	677.8	299.74	391.48	807.21	1682.27	2116.96	2.65	4.82	22.44	39.77	43.62
PSA 8 / BFLS05 Bed 5 OSL SAMPLE 1	10.0000	89.87	10.13	554.0	3.2	498.2	274.81	320.38	553.99	1119.59	1362.85	0.91	1.20	3.22	17.58	24.62
PSA 176 / BFLS05 Bed 6 (28 cm above base of bed)	15.6186	40.07	59.93	921.2	7.3	373.5	311.39	419.27	921.15	3533.91	4369.29	2.08	3.03	7.32	14.01	17.34
PSA 177 / BFLS05 Bed 7 (54 cm above base of bed)	11.8295	82.37	17.63	746.7	16.4	617.9	161.73	211.37	746.67	3751.56	5138.04	1.92	3.10	16.39	38.70	44.73
KUSHKAK TERRACE																
Location 32°08'07''N 48°50'34''E																
PSA 6 / KUHKL3 Bed 2 OSL SAMPLE 10	10.0000	23.98	76.02	344.8	6.3	87.4	90.99	103.48	344.80	1306.43	1693.73	1.17	1.68	6.26	18.73	26.40

Appendix 4.2 (b) Results of grain size analysis of fine-grained sediment and rock samples associated with river terraces and floodplains of the Karun river system	Dry mass of entire sample used for laser particle size analysis (g)	Proportion of sample > 63 µm by dry mass (%)	Proportion of sample < 63 µm by dry mass (%)	Mean grain size within > 63 µm fraction (µm)	Mean grain size within < 63 µm fraction (µm)	Mean grain size of entire sample by calculation (µm)	Summary components of cumulative distribution for the greate than 63 µm fraction (where available) (e.g. 10 % of the grains in this fraction are smaller than the grain size of X_{10} in µm)					Summary components of cumulative distribution for the less than 63 µm fraction (where available) (e.g. 10 % of the grains in this fraction are smaller than the grain size of X_{10} in µm)				
							X_{10}	X_{16}	X_{50}	X_{84}	X_{90}	X_{10}	X_{16}	X_{50}	X_{84}	X_{90}
RIVER TERRACES OF THE KARUN RIVER SYSTEM (continued)																
NAFT-E SAFID TERRACE																
Location 31°57'15''N 48°59'32''E																
PSA 178 / DKITEB Bed 1 Grey sands	4.7345	90.63	9.37	432.1	9.0	392.5	222.77	264.59	432.14	703.29	800.58	1.47	2.48	8.98	17.82	24.13
PSA 4 / DKITEB Bed 2 (Lower part) OSL SAMPLE 8	10.0000	44.51	55.49	260.5	5.5	119.0	84.72	96.31	260.53	623.82	891.97	1.03	1.43	5.50	22.82	36.42
PSA 179 / DKITEB Bed 2 (Upper part) Light grey sands	5.0239	68.34	31.66	247.9	15.6	174.3	105.07	123.23	247.85	426.49	506.50	1.43	2.13	15.56	43.69	48.83
PSA 180 / DKITEB Bed 3 Fine gravel in sandy matrix	3.8851	77.95	22.05	2014.1	7.8	1571.7	445.45	640.99	2014.05	4242.57	4579.39	1.24	1.79	7.84	26.99	32.72
PSA 181 / DKITEB Bed 4 Coarse sands	3.6299	79.17	20.83	617.0	11.3	490.9	204.36	264.13	617.04	1567.19	1994.39	1.50	2.30	11.26	34.13	40.17
ABGAH TERRACE																
Location 31°59'32''N 49°05'43''E																
PSA 182 / BAF2BR Bed 1 (Lower part) Sandy matrix of gravel bed	3.6917	90.01	9.99	386.4	5.9	348.4	231.80	263.11	386.41	606.75	725.88	1.16	1.65	5.89	23.37	29.40
PSA 2 / BAF2BR Bed 1 (Lower part) Silt/clay lens in gravel bed	10.0000	13.46	86.54	144.2	4.7	23.5	90.84	99.50	144.19	205.20	231.34	0.88	1.15	4.74	27.73	36.98
PSA 183 / BAF2BR Bed 2 Light grey coarse sand	4.7812	72.27	27.73	336.4	10.8	246.1	138.86	185.26	336.40	515.66	587.51	1.18	1.64	10.84	39.77	45.47
PSA 184 / BAF2BR Bed 2 Fine sand	9.3703	27.97	72.03	104.9	8.0	35.1	76.83	81.63	104.93	140.89	161.14	1.22	1.70	8.01	36.73	43.85
PSA 185 / BAF2BR Bed 4 Orange-brown sands	5.4957	44.61	55.39	182.9	6.1	85.0	94.57	105.01	182.92	307.32	361.23	1.15	1.63	6.09	30.61	36.89
PSA 186 / BAF2BR Bed 4 Sand with laminations	5.3536	18.42	81.58	137.1	9.0	32.6	85.18	92.82	137.05	269.06	326.01	1.10	1.53	9.00	36.75	42.39
PSA 3 / BAF2BR Bed 4 OSL SAMPLE 7	10.0000	53.70	46.30	136.2	3.2	74.6	85.07	93.96	136.15	202.30	228.25	0.84	1.07	3.19	11.28	17.51
PSA 187 / BAF2BR Bed 5 Sandy matrix from gravel unit	7.0874	9.64	90.36	2700.1	7.2	266.8	361.32	699.61	2700.11	4338.96	4502.86	1.74	2.61	7.16	18.53	24.25
PSA 188 / BAF2BR Bed 5 Coarse sand unit	10.0191	77.87	22.13	512.3	5.5	400.2	261.28	314.44	512.34	790.86	908.63	1.34	1.93	5.50	16.64	21.49
HIGHER TERRACES																
HIGHER TERRACES NEAR ABGAH																
Location 31°58'48''N 49°04'54''E																
PSA 189 / BAF3LA Matrix	3.9552	82.97	17.03	557.9	9.5	464.5	185.33	247.19	557.87	1590.73	3576.45	1.92	3.25	9.49	31.93	38.97
Location 31°58'38''N 49°04'51''E																
PSA 190 / BAF3LD Sandy deposits	4.4831	61.24	38.76	359.7	13.7	225.6	141.05	177.65	359.74	684.05	886.17	1.53	2.27	13.72	37.36	42.89
HIGHER TERRACE N. OF BATVAND ON W. BANK OF AB-E GULESTAN																
Approx. Location 32°02'06''N 49°08'17''E																
PSA 191 / BA1 LPT Unit 1 Set 1 Matrix	1.5010	30.42	69.58	3038.7	6.9	929.1	1156.40	1538.39	3038.66	5941.73	6271.08	1.70	2.41	6.86	17.24	22.14
PSA 192 / BA1LPT Unit 1 Set 2 Matrix	1.0715	21.89	78.11	442.7	9.7	104.4	137.56	166.95	442.66	2000.09	2212.01	2.24	3.30	9.66	24.71	30.53
PSA 193 / BA1LPT Unit 2 Matrix	4.6789	42.46	57.54	200.4	8.6	90.0	101.70	113.81	200.42	399.87	497.60	1.29	1.83	8.55	33.91	40.39
RIVER FLOODPLAINS OF THE KARUN RIVER SYSTEM																
PALAEOCHANNEL NEAR HUBEYSHI																
Location 31°31'30''N 48°59'37''E																
PSA 194 / HUBEYS Salt-rich sediment near Hubeyshi	10.8151	19.89	80.11	131.8	6.8	31.6	85.03	92.50	131.80	243.69	317.69	1.60	2.30	6.77	23.22	29.60
DARK GREY SEDIMENTS NEAR SEYYED RAZI																
Location 31°26'21''N 48°48'56''E (c. 220 cm below river cliff surface)																
PSA 195 / SRAZNE Dark grey river cliff sediments - Lower part	2.8486	0.56	99.44	166.3	3.1	4.1	93.09	101.51	166.30	507.11	684.07	0.92	1.19	3.14	11.32	16.36
PSA 195A / SRAZNE Dark grey river cliff sediments - Upper part	6.1426	2.00	98.00	164.4	3.8	7.0	87.17	95.86	164.39	397.48	477.16	0.91	1.22	3.78	12.72	17.40

Appendix 4.3

Results of grain size analysis of fine-grained rock samples associated with ancient constructions

	Dry mass of entire sample used for laser particle size analysis (g)	Proportion of sample > 63 µm by dry mass (%)	Proportion of sample < 63 µm by dry mass (%)	Mean grain size within > 63 µm fraction (µm)	Mean grain size within < 63 µm fraction (µm)	Mean grain size of entire sample by calculation (µm)	Summary components of cumulative distribution for the greater than 63 µm fraction (where available) (e.g. 10 % of the grains in this fraction are smaller than the grain size of X_{10} in µm)					Summary components of cumulative distribution for the less than 63 µm fraction (where available) (e.g. 10 % of the grains in this fraction are smaller than the grain size of X_{10} in µm)				
							X_{10}	X_{16}	X_{50}	X_{84}	X_{90}	X_{10}	X_{16}	X_{50}	X_{84}	X_{90}
ANCIENT CONSTRUCTIONS																
SHUSHTAR CITY AREA																
Shushtar water mills																
Approx. Location 32°02'43''N 48°51'28''E																
PSA 152 / SHTR01 Cliff rocks at water mills - grey sandstone	4.0648	25.12	74.88	265.5	7.3	72.1	173.32	188.72	265.46	443.59	539.36	1.83	2.39	7.29	21.35	27.31
PSA 153 / SHTR01 Cliff rocks at water mills - red-brown siltstone	5.4536	3.18	96.82	130.9	22.1	25.5	84.55	92.72	130.86	194.12	217.00	2.58	4.52	22.05	41.76	46.61
Band-e Qaisar dam-bridge																
Approx. Location 32°03'23''N 48°50'58''E																
PSA 154 / SHTR03 Masonry from base of Band-e Qaisar	7.6829	45.75	54.25	193.7	20.0	99.5	130.00	143.34	193.69	294.74	343.49	3.52	5.99	20.03	39.74	45.21
Band-e Mizan barrage																
Approx. Location 32°02'58''N 48°51'35''E																
PSA 155 / BMIZAN Masonry from Band-e Mizan	5.3035	38.90	61.10	127.3	20.6	62.1	85.91	93.67	127.33	189.56	216.35	2.28	3.79	20.59	42.74	47.79
BAND-E MAHIBAZAN AREA																
Band-e Mahibazan barrage																
Location 32°00'01''N 48°51'28''E																
PSA 156 / BMHIB4 Foundation block sandstone	5.4020	34.77	65.23	325.4	19.4	125.8	185.72	207.63	325.37	818.30	1129.82	6.24	8.47	19.35	39.66	45.39

Appendix 5.1 (a)	STRUCTURAL GEOLOGY					LOCATION	HUMAN ACTIVITIES		
Summary of various data for river reaches of the River Karun associated with the Turkalaki and Shushtar Anticlines	Estimate of degree of development (and erosion) of geological structure	Width of geological structure where crossed by river (km) (where applicable)	Approx. probable location of fold "core" (part of fold which probably emerged first, where applicable)	Approx. distance from fold "core" to where crossed by river (km along fold axis or its proj.)	Approx. distance from fold "nose" to where crossed by river (km along fold axis or its proj.)	Location of river reach including General location Start and end survey locations for reach (Location for channel measurements)	Short description of floodplain land use	Short description of human river channel modifications	Estimate of overall degree of human impact
TURKALAKI ANTICLINE						TURKALAKI ANTICLINE (R. Karun)			
Emerged anticline: Fold axis oriented	Well	2.3	32°15' N 48°52' E	3.9	2.7	**Across axis** of fold			
roughly SE-NW, plunging uncertain,	developed				(uncertain	LG2 to LG16 (LG6)	Gen. extensive agriculture (cultivation and	Major dam - Gotvand Regulating Dam (compl.	HIGH
merges with Zagros foothills to NW	fold				due to		fields) over floodplains; veg. of grasses, herbs,	1977 AD) at loc. of anticlinal axis. Reservoir for c.	
	- more than				merging at		bushes and low trees next to river. Fairly	9 km upstream of dam with modern canal from	
Hinge length, L = more than	120 m above				NW end)		extensive urbanization of latter 4 km of W.	W. bank, channel straightening & deepening for c.	
14 km (approx.)	surrounding						through large town of Gotvand	2.5 km downstream of dam.	
Fold width, W = 4.0 km (approx.)	plains								
Aspect ratio, AR = L / W = 3.5						**Downstream** of fold			
Fold Symmetry Index, FSI =	Very					LG16 to LB8 (LG32)	Gen. extensive agriculture (cultivation and	Limited. No bridges	QU. LOW
Shorter limb width / (0.5 W) = 0.70	extensive						fields) & few villages over floodplains; veg. of		
Possible fold type:	erosion of						low trees, bushes, herbs and grasses next to		
Asymmetric detachment fold	SW limb						river depending on extent of fields and		
(or fault propagation fold)							settlements		
SHUSHTAR ANTICLINE						SHUSHTAR ANTICLINE (R. Karun, Shuteyt and Gargar branches)			
Emerged anticline: Fold axis oriented	Well	7.4	Uncertain -	4.5	8.8	**Upstream** of fold			
roughly SE-NW, singly plunging to	developed		possibly in			LB8 to LB19 (LB15)	Veg. of low trees and bushes on flooplains	Very limited. No bridges	QU. LOW
NW, merges with Naft-e Safid	fold		vicinity of			LB19 to LB26 (LB22)	next to river due to limited human impacts.		
Anticline to SE	- more than		32°02' N 48°54' E			(Confluence with Ab-e	Qu. extensive agriculture (cultivation and		
	230 m above					Shur major tributary	fields) on broader floodplains		
Hinge length, L = more than	surrounding					nr. LB26)			
20 km (approx.)	plains					**Across axis** of fold			
Fold width, W = 10.9 km						LB26 to LB31 (LB29)	Veg. of mainly herbs and grasses on very thin	None of note, except for Band-e Mizan barrage	LOW
Aspect ratio, AR = L / W = 1.8						LB31 to LB34 (LB33)	soils. Very slight human impacts limited to	at Shushtar at downstream end of reach at	
Fold Symmetry Index, FSI =							grazing by nomads, except for urbanization	LB34	
Shorter limb width / (0.5 W) = 0.46							for last 1 km through suburbs of Shushtar		
Possible fold type:						**Downstream** of fold		Intensive river channel engineering for first	
Uncertain, maybe a fault bend fold						LB34 to LB46/1 (LB42)	Urbanization for first 3 km through small city	3 km of R. Shuteyt valley through Shushtar -	HIGH
truncated by an oblique lateral ramp						(along R. Shuteyt)	of Shushtar. Downstr. of this, some fields &	ancient hydr. eng. (incl. Band-e Qaisar and	
							some areas of waste ground & light industry	intakes for Darian canal) two modern bridges,	
Though uncertain, the Shushtar							on N. bank	modern canals, drainage, sewage, etc.	
Anticline may be separated from the						**Downstream** of fold		Intensive river channel engineering for first	
Qal'eh Surkheh Anticline to the W and						LB34 to L3 (L2)	Urbanization for first 3 - 4 km through small	3 km of R. Gargar valley through Shushtar -	VERY HIGH
from the Naft-e Safid Anticline to the						L3 to L15 (L12/1)	city of Shushtar. Downstr. of this, some	ancient hydr. eng. (incl. former course of	
SE, by an oblique lateral ramp						(along R. Gargar)	fields, esp. on W. bank, some areas of waste	Masrukan canal, Pol-e Boleiti dam at L3 & water	
oriented roughly SSW-NNE							ground, very few fish tanks.	mills), modern bridges, modern canals, etc.	

Appendix 5.1 (b)	RIVER GEOMORPHOLOGY																RIVER HYDROLOGY		
Summary of various data for river reaches of the River Karun associated with the Turkalaki and Shushtar Anticlines	Straight-line valley length of reach (km)	General course direction of reach (bearing to nearest 10°)	Channel pattern type (using simple classification of Schumm (1981, 1985)	Channel sinuosity (no units) S	Average meander wave-length (m) λ	Meander type	Overall channel width (m) (Approx. range for reach) W_{max}	Channel width (m) w	Channel depth (m) d	Channel width: depth ratio (no units) w / d	Approx. cross-sectional shape of channel(s)	Estimate of av. height of channel banks above channel water surface (m)	Estimate of av. height of floodplain or valley above channel water surface (m)	Channel water surface slope (m m-1) s	Projected-channel water surface slope (m m-1) S_p	Valley slope (m m-1) S_v	Average daily water discharge (data from gauging sta.) (m3 s-1) Q	Specific stream power (W m-2) ω	Stream power per unit length (W m-1) Ω
TURKALAKI ANTICLINE (R. Karun)																			
Across axis of fold																			
LG2 to LG16 (LG6)	5.855	SSW (200°)	Type 2 (m-l S)	1.074	—	—	130	121.60	7.19	16.9	Triang./	3.13	7.5	0.0006427	0.0006901	0.0007857	316	16.339	1986.8
							(Range 60				Irreg.						(Gotvand		
							to 320 m)										R. Karun)		
Downstream of fold																			
LG16 to LB8 (LG32)	6.386	S (170°)	Type 4 (M-B)	1.368	2,200	Irreg., qu.	820	292.85	2.29	127.9	Trapez./	2.14	2.7	0.0008394	0.0011486	0.0010805	316	8.861	2594.9
						smooth,	(Range 170				Irreg.						(Gotvand		
						v. high	to 1,880 m)										R. Karun)		
						migr. rate													
SHUSHTAR ANTICLINE (R. Karun, Shuteyt and Gargar branches)																			
Upstream of fold																			
LB8 to LB19 (LB15)	6.289	SE (130°)	Anastom.	1.704	2,600	Irreg.,	2,180	320.61	2.52	127.2	Rect./Trap.	3.73	3.2	0.0005306	0.0009040	0.0005247	316	5.116	1640.4
LB19 to LB26 (LB22)	2.876	S (180°)	Type 4 (M-B)	1.345	3,100	smooth,	520	284.53	1.62	175.6	Triang.	2.83	5.3	0.0010434	0.0014032	-0.0017040	316	11.336	3225.6
(Confluence with Ab-e						v. high	(Range 100										(Gotvand		
Shur major tributary						migr. rate	to 2,410 m)										R. Karun)		
nr. LB26)																			
Across axis of fold																			
LB26 to LB31 (LB29)	3.782	SSW (200°)	Type 3b (m-l M)	1.431	3,400	Reg., sl.	190	179.55	4.84	37.1	Triang.	4.34	16.6	0.0005988	0.0008568	0.0030674	351	11.451	2056.1
LB31 to LB34 (LB33)	3.108	SSW (200°)	Type 3b (m-l M)	1.329	3,200	angular,	130	99.18	3.60	27.6	Triang.	3.18	8.2	0.0004018	0.0005340	0.0005791	351	13.912	1379.8
						v. low	(Range 60										(Shushtar		
						migr. rate	to 300 m)										R. Shuteyt)		
Downstream of fold																			
LB34 to LB46/1 (LB42)	3.731	WSW (250°)	Type 4 (M-B)	1.392	2,700	Irreg., qu.	330	215.37	3.73	57.7	Triang.	2.66	6.5	0.0006103	0.0008497	0.0021981	351	9.730	2095.7
(along R. Shuteyt)						smooth,	(Range 80										(Shushtar		
						moderate	to 510 m)										R. Shuteyt)		
						migr. rate													
Downstream of fold																			
LB34 to L3 (L2)	0.776	SSW (200°)	Type 2 (m-l S)	1.066	—	Irreg., qu.	30	30.07	3.92	7.7	Triang.	3.62	7.4	-0.0001993	-0.0002125	-0.0024472	46	-2.983	-89.7
L3 to L15 (L12/1)	4.635	S (190°)	Type 3b (m-l M),	1.164	1,300	smooth,	80	72.24	1.16	62.3	Rect./Irreg.	1.21	3.2	0.0028614	0.0033321	0.0011650	46	17.825	1287.6
(along R. Gargar)			Type 2 (m-l S)			v. low	(Range 10										(Shushtar		
						migr. rate	to 120 m)										R. Gargar)		

Appendix 5.1 (c)	RIVER SEDIMENTOLOGY					SUMMARY
Summary of various	Main sediment or	Estimate	Short general description of channel **bed** surface	Short general description of channel **banks**	Estimate	Short overall description of river reach,
data for river reaches	bedrock type in river	of degree	sediments	(including, in some cases, B (% of channel bank	of degree	including estimate of probable overall degree of aggradation or incision
of the River Karun	valley	of general	(including, in some cases, D_{coarse} (mean grain size	sediments less than 63 µm), D_{fine} (mean grain size for	of erosion	
associated with the		erosion	for gravels, intermed. diam. in mm), D_{max} (mean	fine gravels, sands and muds))	resistance	
Turkalaki and Shushtar		resistance	grain size for 10 largest gravel clasts, intermed.		of channel	
Anticlines			diam. in mm), D_{fine} (mean grain size for fine		banks	
			gravels, sands and muds, in µm))			
TURKALAKI ANTICLINE (R. Karun)						
Across axis of fold						
LG2 to LG16 (LG6)	Unlith. floodplain seds.	HIGH	**Partly gravels** (esp. pebbles), **partly sands and silts**	**Partly gravels and sands, partly sands and silts**.	QU. LOW/	Type 2 (m-l S) single-thread straight/very sl. meandering river. Narrow &
	/Bakhtyari F. bedrock			Quite poorly cemented. Veg of banks mainly herbs	MODERATE	deep channels, esp. over first 2.5 km downstr. of Gotvand Reg. Dam due
				and grasses (esp. near edges of fields), some bushes		to channel straightening & deepening; mod. narrow & deep channels
				and low trees		after this. River channel fixed by dam, and has limited mobility throughout
						reach despite widening of valley. Probable VERY HIGH degree INCISION
						over first 2.5 km, prob. lessening to QU. HIGH degree of INCISION downstr.
Downstream of fold						Type 4 (M-B) river with multiple meandering channels separated by veg.
LG16 to LB8 (LG32)	Unlith. floodplain seds.	LOW	**Partly gravels** (esp. pebbles), **partly sands and silts**	**Partly gravels and sands, partly sands and silts**.	QU. LOW	islands and bars; channel belt broadens sl. downstream. Single-thread
				Quite poorly cemented. Quite extensive veg. of banks -		for last c. 0.5 km, though still a broad channel belt. Broad, shallow
				partly low trees and bushes, partly herbs & grasses at		channels. River channels highly mobile within qu. broad valley.
				edges of fields		Probable MODERATE degree of AGGRADATION at upstr. end, increasing
						rapidly to HIGH degree of AGGRADATION for most of reach
SHUSHTAR ANTICLINE (R. Karun, Shuteyt and Gargar branches)						
Upstream of fold			**Mainly gravels** (esp. pebbles with some cobbles,	**Partly gravels & sands, partly sands & silts** (B = 87.5 %,		Type 4 (M-B) river with multiple meandering channels separated by veg.
LB8 to LB19 (LB15)	Unlith. floodplain seds.	LOW	D_{coarse} = c. 21.7 - 26.5 mm, D_{max} = c. 47.9 - 114.1	D_{fine} = c. 38.7 µm). Qu. poorly cem. Variable - at some	QU. LOW	islands & bars, becomes less braided downstr.; last 1 km eff. single-thread
LB19 to LB26 (LB22)	Unlith. floodplain seds.	LOW	mm), **some sands and silts**. Variable - at some	locs. predom. altern. gravels & sands, at some locs.		river. Broad, shallow channels & sl. levées. River channels highly mobile
(Confluence with Ab-e			locs. predom. gravels with matrix of sands & silts,	predom. fine sands & muds. Qu. extensive veg. of		(freq. qu. small avulsions since Islamic Period (Wright, 1969)) within qu.
Shur major tributary			at few locs. predom. sands & silts with occ. gravels	banks - partly low trees & bushes, partly herbs &		broad valley; sl. constrained to SW. Prob. HIGH degree of AGGRADATION,
nr. LB26)				grasses at edges of fields		probably changing to MODERATE degree of INCISION for last 1 km
Across axis of fold			**Mainly gravels** (esp. pebbles with some cobbles,	**Mainly sands & silts** (B = 79.5 %, D_{fine} = c. 45.8 µm) **and**		Type 3b (m-l M) single-thread meand. river. Narrow, deep channels with
LB26 to LB31 (LB29)	Bakhtyari F. bedrock	HIGH	D_{coarse} = c. 23.7mm, D_{max} = c. 77.7 mm), **some**	**gravels**, partly bedrock channel of Bakhtyari F. conglom.	VERY HIGH	very high, steep river cliffs, esp. over first 3 km. River channel constrained
LB31 to LB34 (LB33)	Agha Jari F. bedrock	MODERATE	**sands and silts**. Variable - at many locs. predom.	or Agha jari F. sandst. Gen. well cem. Variable, with	/HIGH	within very narrow valley. Probable VERY HIGH degree of INCISION,
			gravels with matrix of sands & silts, at some	bedrock channels mainly limited to first 3 km. Sparse		possibly lessening to HIGH degree of INCISION for about last 1 km
			downstr. locs. predom. sands & silts	veg. of banks with herbs & grasses and occ. low scrub		
Downstream of fold			**Mainly gravels** (esp. pebbles with some cobbles),	**Partly gravels & sands, partly fine sands & muds**		Type 4 (M-B) river with several meand. channels separated by sl. veg. or
LB34 to LB46/1 (LB42)	Agha Jari F. bedrock/	MODERATE	**some sands and silts**. Predom. gravels for first c.	Qu. well cem., becoming qu. poorly cem. downstream.	MODERATE	unveg. islands & bars; single-thread river for first 1 km. Broad, shallow
(along R. Shuteyt)	Unlith. floodplain seds.	/LOW	3 km, with some sands & silts further downstream	Predom. gravels & sands for first 3 km, becoming	/QU. LOW	channels with slight levées. River channels moderately mobile within qu.
				finer downstream. Qu. sparse veg. on banks - occ.		narrow valley. Probable HIGH degree of INCISION for about first 3 km,
				scrub & low trees away from fields		probably lessening to NO INCISION downstream
Downstream of fold			**Mainly sands and silts, few gravels** (D_{coarse} =	**Mainly sands and muds** (B = 65.4 %, D_{fine} = 45.6 µm),		Type 2 (m-l S) or Type 3b (m-l M) straight or v. gently meand. single-thread
LB34 to L3 (L2)	Agha Jari F. bedrock/	MODERATE	c. 28.5 mm, D_{max} = 89.1 mm). Partly gravels and	partly sands and gravels. Gen. well cem. Variable - river	HIGH	river. Narrow, deep channels, esp. for first 2 km partly cut as a gorge
L3 to L15 (L12/1)	Unlith. floodplain seds.	/LOW	partly sands and silts for first 2 km, predom.	embanked or cut through bedrock for first 2 km,		through bedrock by humans. River channel fixed for first 2 km, slightly
(along R. Gargar)			sands and silts further downstream	further downstr. banks are predom. sands & muds.		mobile further downstr. Probable HIGH degree of INCISION for first 3 km,
				Qu. sparse veg. with few cultivated trees		probably lessening to MODERATE degree of INCISION downstream

Appendix 5.2 (a)	STRUCTURAL GEOLOGY					LOCATION	HUMAN ACTIVITIES		
Summary of various data for	Estimate of	Width of	Approx. probable	Approx.	Approx.	Location of river reach	Short description of floodplain land use	Short description of human river channel	Estimate of
river reaches of the River Karun	degree of	geological	location of fold	distance from	distance from	including		modifications	overall degree
associated with the Qal'eh	development	structure	"core" (part of	fold "core" to	fold "nose" to	General location			of human
Surkheh Anticline and river	(and erosion)	where crossed	fold which	where crossed	where crossed	Start and end survey			impact
reaches of the River Dez	of geological	by river (km)	probably emerged	by river (km	by river (km	locations for reach			
associated with the Dezful	structure	(where	first, where	along fold axis	along fold axis	(Location for channel			
Uplift		applicable)	applicable)	or its proj.)	or its proj.)	measurements)			
QAL'EH SURKHEH ANTICLINE		**For R. Karun, Shuteyt branch**				QAL'EH SURKHEH ANTICLINE (R. Karun, Shuteyt and Gargar branches)			
Emerged anticline: Fold axis oriented	Moderately	7.5	Uncertain -	1.2	11.8	**Upstream** of fold	Urbanization for first 3 km through small city	Intensive river channel engineering for first	
roughly ESE - WNW, singly plunging to	developed	(very approx.	possibly in		(from WNW	LB34 to LB46/1 (LB42)	of Shushtar. Downstr. of this, some fields &	3 km of R. Shuteyt valley through Shushtar -	VERY HIGH
WNW. Interpretation uncertain due	fold	projection)	vicinity of		fold "nose",	(along R. Shuteyt)	some areas of waste ground & light industry	ancient hydr. eng. (incl. Band-e Qaisar and	
to extensive erosion of E part, but	- more than		32°02' N 48°48' E		location of		on N. bank	intakes for Darian canal) two modern bridges,	
possibly merges with Shushtar/	70 m above		(or maybe further		ESE fold "nose"			modern canals, drainage, sewage, etc.	
Naft-e Safid Anticline to E	surrounding		to the E)		not known)	**Across axis** of fold	Qu. extensive agriculture on broader	Limited. Major modern road bridge near LB47	
	plains					LB46/1 to LB49 (LB47)	floodplains. Veg. of low trees and bushes on		LOW/
Hinge length, L = more than						(along R. Shuteyt)	floodplains next to river downstream of		MODERATE
13 km (approx.)							LB47 due to limited human impacts		
Fold width, W = more than	Very								
8.0 km (approx.)	extensive	**For R. Karun, Gargar branch**				**Across axis** of fold	Urbanization for first 3 - 4 km through small	Intensive river channel engineering for first	
Aspect ratio, AR = L / W = 1.6	erosion	7.5	Uncertain -	4.8	15.7	LB34 to L3 (L2)	city of Shushtar. Downstr. of this, some	3 km of R. Gargar valley through Shushtar -	VERY HIGH/
Fold Symmetry Index, FSI =	of E part of	(very approx.	possibly in		(from WNW	L3 to L15 (L12/1)	fields, esp. on W. bank, some areas of waste	ancient hydr. eng. (incl. former course of	HIGH
Shorter limb width / (0.5 W) = 0.78	fold	projection)	vicinity of		fold "nose",	(along R. Gargar for	ground, very few fish tanks.	Masrukan canal, Pol-e Boleiti dam at L3 & water	
Possible fold type:			32°02' N 48°48' E		location of	projection of fold axis)		mills), modern bridges, modern canals, etc.	
Asymmetric detachment fold			(or maybe further		ESE fold "nose"	**Downstream** of fold	Qu. extensive veg. of bushes and low trees	Very limited. No bridges	
(or fault propagation fold)			to the E)		not known)	LB49 to LB56 (LB56)	over most of river channel belt due to limited		LOW/
						(along R. Shuteyt)	human impacts. Extensive agriculture on		MODERATE
							floodplains just beyond channel belt		
						Downstream of fold	Varied - qu. extensive fields on W. bank,	Over first 1 km, Band-e Mahibazan ancient dam	
						L15 to L37	mainly limited veg. on E. Bank, some areas	remnant is eff. linear ESE - WNW Agha Jari F.	QU. HIGH
						(along R. Gargar for	of bushes and low trees next to river, many	sandst. outcrop around which R. Gargar diverts.	
						projection of fold)	fish tanks, esp. on E. Bank	Gen. course of Gargar developed from Masrukan	
DEZFUL UPLIFT						DEZFUL UPLIFT (R. Dez)			
Emerged uplift: Axis of uplift oriented	Moderately	2.8	Uncertain -	15.1	12.5	**Upstream** of fold			
roughly SE - NW, progressively less	developed fold		possibly in		(approx. -	L1A / L2 to L6 (L2)	Urbanization through northern suburbs of	Major dam - Dez Regulating dam (compl. 1965	VERY HIGH
emergence towards SE, merges with	- more than		vicinity of		location of	(L5)	Dezful	AD) in N. Dezful at start of reach. Reservoir for c.	
Zagros foothills to NW, merges with	70 m above		32°28' N 48°16' E		fold "nose"			4 km upstr. of dam, sl. channel straightening &	
Kuhanak Anticline to SE	surrounding				uncertain)			deepening for c. 2 km downstr. of dam. One modern	
	plains							bridge, drainage, sewage, etc.	
						Across axis of fold		Major dam - Dez Diversion Dam (compl. 1963	
Hinge length, L = 35 km (approx.)						L6 to L40 (L6)	Urbanization through large city of Dezful	AD) in S. Dezful 1 km from downstr. end of	VERY HIGH
Fold width, W = 4.7 km						(L10)		reach. Some channel widening for c. 2 km upstr.	
Aspect ratio, AR = L / W = 7.5						(L40)		of dam, two modern canals, anastomosing river	
Fold Symmetry Index, FSI =								imm. downstr. of dam. Two mod. bridges, etc.	
Shorter limb width / (0.5 W) = 0.77						**Downstream** of fold			
Possible fold type:						L40 to L54-A (L44)	Veg. of low trees and bushes on floodplains	Anastomosing river fans out from Dez Diversion	MODERATE/
Monocline or asymmetric						(L51-B)	next to river & limited veg. of channel bars.	Dam at L14 imm. upstream of this reach	LOW
detachment fold							Extensive agriculture (cultivation and fields)		
							on broader floodplains		

Appendix 5.2 (b)	RIVER GEOMORPHOLOGY																RIVER HYDROLOGY		
Summary of various data for river reaches of the R. Karun assoc. with the Qal'eh Surkheh Ant. and of the R. Dez assoc. with the Dezful Uplift	Straight-line valley length of reach (km)	General course direction of reach (bearing to nearest 10°)	Channel pattern type (using simple classification of Schumm (1981, 1985)	Channel sinuosity (no units)	Average meander wave-length (m)	Meander type	Overall channel width (m) (Approx. range for reach)	Channel width (m)	Channel depth (m)	Channel width: depth ratio (no units)	Approx. cross-sectional shape of channel(s)	Estimate of av. height of channel banks above channel water surface (m)	Estimate of av. height of floodplain or valley above channel water surface (m)	Channel water surface slope (m m-1)	Projected-channel water surface slope (m m-1)	Valley slope (m m-1)	Average daily water discharge (data from gauging sta.) (m3 s-1)	Specific stream power (W m-2)	Stream power per unit length (W m-1)
				S	λ		w_{max}	w	d	w / d				s	S_p	S_v	Q	ω	Ω
QAL'EH SURKHEH ANTICLINE (R. Karun, Shuteyt and Gargar branches)																			
Upstream of fold																			
LB34 to LB46/1 (LB42)	3.731	WSW (250°)	Type 4 (M-B)	1.392	2,700	Irreg., qu.	330	214.37	2.96	72.4	Triang.	2.66	6.5	0.0006103	0.0008497	0.0021981	351	9.776	2095.7
(along R. Shuteyt)						smooth,	(Range 80										(Shushtar		
						moderate	to 510 m)										R. Shuteyt)		
						migr. rate													
Across axis of fold																			
LB46/1 to LB49 (LB47)	2.573	SSW (200°)	Anastomosing	1.168	2,900	Irreg., sl.	360	245.87	3.66	67.2	Rect./Irreg.	1.19	3.6	0.0009313	0.0010880	0.0002215	351	13.006	3197.8
(along R. Shuteyt)						angular,	(Range 200										(Shushtar		
						qu. high	to 1,820 m)										R. Shuteyt)		
						migr. rate													
Across axis of fold																			
LB34 to L3 (L2)	0.776	SSW (200°)	Type 2 (m-l S)	1.066	—	Irreg., qu.	30	30.07	3.92	7.7	Triang.	3.62	7.4	-0.0001993	-0.0002125	-0.0024472	46	-2.983	-89.7
L3 to L15 (L12/1)	4.635	S (190°)	Type 3a (s-l M)/	1.164	1,300	smooth,	80	72.24	1.16	62.3	Rect./Irreg.	1.21	3.2	0.0028614	0.0033321	0.0011650	46	17.825	1287.6
(along R. Gargar for			Type 2 (m-l S)			v. low	(Range 10										(Shushtar		
projection of fold axis)						migr. rate	to 120 m)										R. Gargar)		
Downstream of fold						Irreg., var.													
LB49 to LB56 (LB56)	5.729	SW (220°)	Anastomosing	1.283	3,700	roughness,	1,100	461.96	5.33	86.7	Irreg./	2.94	3.7	0.0005987	0.0007680	0.0008972	351	4.450	2055.8
(along R. Shuteyt)						high	(Range 480				Triang.						(Shushtar		
						migr. rate	to 2,850 m)										R. Shuteyt)		
Downstream of fold						Irreg/tort,													
L15 to L37 (L20)	7.372	SE (130°)	Type 3a (s-l M)	1.964	1,500	smooth,	40	34.78	2.09	16.6	Trapez.	3.54	3.8	0.0001378	0.0002706	0.0020076	46	1.783	62.0
(along R. Gargar for						moderate	(Range 20										(Shushtar		
projection of fold)						migr. rate	to 80 m)										R. Gargar)		
DEZFUL UPLIFT (R. Dez)																			
Upstream of fold																			
L1A / L2 to L6 (L2)	2.469	SW (230°)	Type 2 (m-l S)	1.036	—	—	80	75.52	7.40	10.2	Triang.	3.78	19.9	0.0006645	0.0006884	0.0068034	244	21.003	1586.1
(L5)							100	93.52	4.50	20.8	Trapez.	4.73	17.6	0.0006645	0.0006884	0.0068034	244	16.960	1586.1
							(Range 70										(Dezful		
							to 130 m)										R. Dez)		
Across axis of fold																			
L6 to L40 (L6)	3.864	SW (220°)	Type 2 (m-l S)	1.104	—	—	90	85.21	6.00	14.2	Triang.	4.01	5.7	0.0019238	0.0021243	0.0023546	244	53.891	4592.1
(L10)							90	68.19	3.60	18.9	Trapez.	4.41	5.0	0.0019238	0.0021243	0.0023546	244	67.342	4592.1
(L40)							1,050	165.64	2.29	72.3	Trapez.	2.56	3.7	0.0019238	0.0021243	0.0023546	244	27.723	4592.1
							(Range 60 to 1,050 m)										(Dezful)		
Downstream of fold																			
L40 to L54-A (L44)	10.267	SSW (200°)	Anastomosing	1.140	—	—	1,800	241.98	3.86	62.7	Triang.	1.89	2.1	0.0023614	0.0026920	0.0029511	244	23.294	5636.5
(L51-B)							5,400	137.13	1.40	98.0	Trapez./	1.01	1.3	0.0023614	0.0026920	0.0029511	244	41.103	5636.5
							(Range 1,000				Rect.						(Dezful		
							to 5,600 m)										R. Dez)		

Appendix 5.2 (c)	RIVER SEDIMENTOLOGY					SUMMARY
Summary of various	Main sediment or	Estimate	Short general description of channel **bed** surface	Short general description of channel **banks**	Estimate	Short overall description of river reach,
data for river reaches	bedrock type in river	of degree	sediments	(including, in some cases, B (% of channel bank	of degree	including estimate of probable overall degree of aggradation or incision
of the R. Karun assoc.	valley	of general	(including, in some cases, D_{coarse} (mean grain size	sediments less than 63 µm), D_{fine} (mean grain size for fi	of erosion	
with the Qal'eh		erosion	for gravels, intermed. diam. in mm), D_{max} (mean	gravels, sands and muds))	resistance	
Surkheh Ant. and of the		resistance	grain size for 10 largest gravel clasts, intermed.		of channel	
R. Dez assoc. with the			diam. in mm), D_{fine} (mean grain size for fine		banks	
Dezful Uplift			gravels, sands and muds, in µm))			
QAL'EH SURKHEH ANTICLINE (R. Karun, Shuteyt and Gargar branches)						
Upstream of fold				**Partly gravels & sands, partly fine sands & muds**		Type 4 (M-B) river with several meand. channels separated by sl. veg. or
LB34 to LB46/1 (LB42)	Agha Jari F. bedrock/	MODERATE	**Mainly gravels** (esp. pebbles with some cobbles),	Qu. well cem., becoming qu. poorly cem. downstream.	MODERATE	unveg. islands & bars; single-thread river for first 1 km. Broad, shallow
(along R. Shuteyt)	Unlith. floodplain seds.	/LOW	with some sands & silts. Predom. gravels for first	Predom. gravels & sands for first 3 km, becoming	/QU. LOW	channels with slight levées (c. 0.9 m high). River channels moderately
	(esp. qu. poorly cem.		3 km, with some sands & silts further downstream	finer downstream. Qu. sparse veg. on banks - occ.		mobile in qu. narrow valley. Probable HIGH degree of INCISION for about
	cem. sands & muds)			scrub & low trees away from fields		first 3 km, probably lessening to NO INCISION downstream
Across axis of fold						Anastomosing river with a sl. sinuous main channel and qu. sinuous
LB46/1 to LB49 (LB47)	Unlith. floodplain seds.	LOW	**Mainly gravels** (esp. pebbles with some cobbles,	**Partly gravels & sands, partly fine sands & muds** (B =	QU. LOW	side channels; single-thread up to LB47 then channel belt broadens
(along R. Shuteyt)			D_{coarse} = c. 24.5 mm, D_{max} = c. 88.2 mm), with	77.9 %, D_{fine} = c. 32.6 µm). Qu. poorly cem. Qu. extensive		markedly. Moderately broad and deep channels. River channels highly
			some sands & silts. Some sands & silts for first	veg. of banks - partly bushes & low trees (esp. after		mobile in qu. broad valley. Probably NO AGGRADATION for about first
			1 km, predom. gravels downstream	first 1 km), partly herbs & grasses at edges of fields		1 km, probably increasing to HIGH degree of AGGRADATION
Across axis of fold				**Mainly sands and muds** (B = 65.4 %, D_{fine} = c. 45.6 µm),		Type 2 (m-l S) or Type 3b (m-l M) straight or v. gently meand. single-thread
LB34 to L3 (L2)	Agha Jari F. bedrock/	MODERATE	**Mainly sands and silts, few gravels** (D_{coarse} =	partly sands and gravels. Gen. well cem. Variable - river	VERY HIGH	river. Narrow, deep channels, esp. for first 2 km partly cut as a gorge
L3 to L15 (L12/1)	Unlith. floodplain seds.	/QU. LOW	c. 28.5 mm, D_{max} = c. 89.1 mm). Partly gravels and	embanked or cut through bedrock for first 2 km,	/HIGH	through bedrock by humans. River channels fixed for first 2 km, slightly
(along R. Gargar for			partly sands and silts for first 2 km, predom.	further downstr. banks are predom. sands & muds.		mobile further downstr. Probable HIGH degree of INCISION for first 3 km,
projection of fold axis)			sands and silts further downstream	Qu. sparse veg. with few cultivated trees		probably lessening to MODERATE degree of INCISION downstream
Downstream of fold				**Partly gravels & sands, partly fine sands & muds**		Anastomosing river with qu. sinuous main channel and gen. smoother
LB49 to LB56 (LB56)	Unlith. floodplain seds.	LOW	**Mainly gravels**, with some sands and silts	Qu. extensive veg. of banks - bushes & low trees on	QU. LOW	and sl. more sinuous side channels. River channels highly mobile in broad
(along R. Shuteyt)				banks within channel belt, herbs & grasses associated		valley. Probable HIGH degree of AGGRADATION
				with fields at edge of channel belt		
Downstream of fold				**Sands and muds** (River cliffs, B = 28.8 %, D_{fine} =		Type 3a (s-l M) single-thread river. Narrow, deep channels. For first 1 km
L15 to L37	Unlith. floodplain seds.	LOW	**Mainly sands and silts**	c. 110.9 µm; River bank, B = 97.0 %, D_{fine} = c. 6.9 µm).	MODERATE	fixed tight meand. with Band-e Mahibazan remnant, downstr. restricted
(along R. Gargar for				Qu. well cem. Variable veg. of banks - mainly herbs		dev. from disused anc. Masrukan canal. Probable HIGH degree of INCISION
projection of fold)				& grasses, some areas of bushes & low trees		for first 1 km, prob. lessening to MODERATE degree of INCISION downstr.
DEZFUL UPLIFT (R. Dez)						
Upstream of fold						
L1A / L2 to L6 (L2)	Unlith. floodplain seds.	QU. LOW	**Mainly gravels** (esp. pebbleswith some cobbles)	**Partly gravels and sands, partly fine sands & muds**	MODERATE	Type 2 (m-l S) straight single-thread river. Very narrow, deep channels with
(L5)	/occ. Bakhtyari F.	QU. LOW	few sands and silts	Moderately cemented. Veg. of banks mainly limited		qu. steep river cliffs. River channel has very limited mobility. Probable
	outcrops			to grasses through city of Shushtar		HIGH degree of INCISION throughout
Across axis of fold						Type 2 (m-l S) straight single-thread river, except for abrupt change at Dez
L6 to L40 (L6)	Unlith. floodplain seds.	MODERATE	**Mainly gravels** (esp. pebbleswith some cobbles,	**Partly gravels and sands, partly fine sands & muds**	MODERATE	Diversion Dam to anastomosing river for last 1 km. Very narrow, deep
(L10)	/ Bakhtyari F.	/HIGH	D_{coarse} = c. 27.4 mm, D_{max} = 91.6 mm), few sands	Moderately cemented. Veg. of banks mainly limited		channels with steep river cliffs. River channel has v limited mobility, except
(L40)	conglomerate bedrock		and silts	to grasses through city of Shushtar		downstr. of dam where valley widens. Probable HIGH degree of INCISION,
						changing abruptly to MODERATE degree of AGGRADATION for last 1 km
Downstream of fold						
L40 to L54-A (L44)	Unlith. floodplain seds.	LOW	**Mainly gravels** (esp. pebbleswith some cobbles)	**Mainly sands with some gravels, partly fine sands &**	QU. LOW	Anastomosing river comprised of two braided channels fanning out from
(L51-B)	Unlith. floodplain seds.	LOW	few sands and silts	**muds** Qu poorly cemented. Variable veg. of banks -		the Dez Diversion Dam. Broad, shallow channels with numerous bars.
				partly low trees and bushes, partly herbs & grasses		River channels highly mobile, increasing with distance downstr. Probable
				at edges of fields		HIGH degree of AGGRADATION, esp. in downstr. parts of reach

Appendix 5.3 (a)	STRUCTURAL GEOLOGY					LOCATION	HUMAN ACTIVITIES		
Summary of various data for	Estimate of	Width of	Approx. probable	Approx.	Approx.	Location of river reach	Short description of floodplain land use	Short description of human river channel	Estimate of
river reaches of the River Karun	degree of	geological	location of fold	distance from	distance from	including		modifications	overall degree
and the River Dez associated	development	structure	"core" (part of	fold "core" to	fold "nose" to	General location			of human
with the Sardarabad Anticline	(and erosion)	where crossed	fold which	where crossed	where crossed	Start and end survey			impact
and river reaches of the River	of geological	by river (km)	probably emerged	by river (km	by river (km	locations for reach			
Dez associated with the Shahur	structure	(where	first, where	along fold axis	along fold axis	(Location for channel			
Anticline		applicable)	applicable)	or its proj.)	or its proj.)	measurements)			
SARDARABAD ANTICLINE		**For R. Karun, Shuteyt branch**				SARDARABAD ANTICLINE (R. Karun, Shuteyt branch)			
Emerged anticline: Fold axis oriented	Moderately	4.1	31°58' N 48°35' E	32.2	3.8	**Upstream** of fold			
roughly ESE-WNW, curving to c.	developed	(approx.			(approx.	LB56 to LB68/1 (LB66)	On SW side of river, floodplains veg. mainly	Limited. Various canals feed into river on NE side	QU. LOW/
SE-NW at eastern end, eastern half	fold	projection)			projection)	LB68/1 to LB84 (LB75)	herbs & grasses and few fields. On NE side		MODERATE
subdivided into three segments,	- more than						of river and where floodplains broader, veg.		
doubly plunging, possibly merges	70 m above						of low trees and bushes near river, gen.		
with roughly N-S oriented oblique	surrounding						extensive agriculture on broader floodplains		
lateral ramp at eastern end	plains					**Across axis** of fold			
						LB84 to LB101 (LB85)	Veg. near river partly herbs & grasses, partly	Limited. Various canals feed into river on E side.	QU. LOW/
						(LB93)	low trees and bushes. Extensive agriculture	One modern bridge	MODERATE
Hinge length, L = 58 km							(fields and cultivation) over most of broader		
Fold width, W = 8.6 km (approx.)							floodplains		
Aspect ratio, AR = L / W = 6.7						**Downstream** of fold			
Fold Symmetry Index, FSI =						LB101 to LB116 (LB109)	Veg. near river partly herbs & grasses, partly	Limited. Few canals feed into river on E side	QU. LOW
Shorter limb width / (0.5 W) = 0.68							low trees and bushes. Extensive agriculture		
Possible fold type:							(fields and cultivation) over most of broader		
Asymmetric detachment fold							floodplains		
(or fault propagation fold)		**For R. Dez**				SARDARABAD ANTICLINE (R. Dez)			
		4.3	31°58' N 48°35' E	1.3	27.7	**Upstream** of fold			
						L135 to L145 (L136)	Veg. of low trees and bushes on floodplains	Very limited. One modern bridge	LOW
						L145 to L158 (L153)	due to limited human impacts. Some		
						L158 to L168 (L164)	agriculture on broader floodplains		
						Across axis of fold			
						L168 to L175 (L171)	Veg. of narrow floodplains partly herbs and	Very limited. One ancient canal extracted	LOW
							grasses, partly low trees and bushes. Limited	from E bank	
							agriculture (inc. grazing)		
						Downstream of fold			
						L175 to L190 (L183)	Veg. of low trees and bushes on floodplains	Very limited	QU. LOW
						L190 to L199 (L196)	next to river due to limited human impacts.		
							Qu. extensive agriculture on broader		
							floodplains		
SHAHUR ANTICLINE						SHAHUR ANTICLINE (R. Dez)			
Emerged anticline: Fold axis oriented	Moderately	4.9	31°54' N 48°26' E	22.8	6.3	**Upstream** of fold			
roughly ESE-WNW, small "dome"	developed	(approx.			(approx.	***See L175 to L199 for R. Dez associated with the Sardarabad Anticline***			
segment at each end, doubly plunging	fold	projection)			projection)	**Across axis** of fold			
	- more than					L199 to L206 (L202)	Natural veg. low trees and bushes, with some	Very limited	MODERATE
Hinge lengrth, L = 33 km	40 m above					L206 to L214 (L206)	herbs and grasses, confined to narrow band		
Fold with, W = 6.6 km (approx.)	surrounding					(L210)	next to river. Otherwise, extensive agriculture		
Aspect ratio, AR = L / W = 5.0	plains						over entirety of floodplains		
Fold Symmetry Index, FSI =									
Shorter limb width / (0.5 W) = 0.61						**Downstream** of fold			
Possible fold type:	Extensive					L214 to L225 (L219)	Natural veg. low trees and bushes, with some	Very limited	MODERATE
Asymmetric detchment fold	erosion of					L225 to L233 (L227)	herbs and grasses, confined to narrow band		
(or fault propagation fold)	SW limb						next to river. Otherwise, extensive agriculture		
							over entirety of floodplains		

Appendix 5.3 (b)	RIVER GEOMORPHOLOGY																RIVER HYDROLOGY		
Summary of various data for river reaches of the R. Karun and Dez assoc. with the Sardarabad Ant. and of the R. Dez assoc. with the Shahur Ant.	Straight-line valley length of reach (km)	General course direction of reach (bearing to nearest 10°)	Channel pattern type (using simple classification of Schumm (1981, 1985)	Channel sinuosity (no units) S	Average meander wave-length (m) λ	Meander type	Overall channel width (m) (Approx. range for reach) Wmax	Channel width (m) w	Channel depth (m) d	Channel width: depth ratio (no units) w / d	Approx. cross-sectional shape of channel(s)	Estimate of av. height of channel banks above channel water surface (m)	Estimate of av. height of floodplain or valley above channel water surface (m)	Channel water surface slope (m m-1) s	Projected-channel water surface slope (m m-1) Sp	Valley slope (m m-1) Sv	Average daily water discharge (data from gauging sta.) (m3 s-1) Q	Specific stream power (W m-2) ω	Stream power per unit length (W m-1) Ω
SARDARABAD ANTICLINE (R. Karun, Shuteyt branch)																			
Upstream of fold			Type 4 (M-B)/																
LB56 to LB68/1 (LB66)	5.432	SSE (160°)	Type 3b (m-l M)	1.389	2,500	Irreg/tort,	290	188.25	3.63	51.9	Trapez.	4.59	7.2	0.0007075	0.0009830	0.0007179	400	14.706	2768.5
LB68/1 to LB84 (LB75)	9.055	SE (140°)	Type 3b (m-l M)	1.798	3,000	qu. smooth	190	174.35	2.28	76.5	Trapez.	4.45	7.0	0.0002778	0.0004992	0.0002430	400	6.234	1086.9
						moderate	(Range 60										(Arab Hasan		
						migr. rate	to 2,520 m)										R. Shuteyt)		
Across axis of fold											Irreg./								
LB84 to LB101 (LB85)	10.283	S (190°)	Type 3b (m-l M)	1.647	5,500	Qu. irreg.,	180	169.80	4.38	38.8	Trapez.	5.95	9.4	0.0000035	0.0000058	0.0003987	400	0.082	13.9
(LB93)						sl. angular,	230	202.19	4.70	43.0	Triang.	5.04	7.5	0.0000035	0.0000058	0.0003987	400	0.069	13.9
						qu. low	(Range 110										(Arab Hasan		
						migr. rate	to 360 m)										R. Shuteyt)		
Downstream of fold																			
LB101 to LB116 (LB109)	11.052	S (190°)	Type 3b (m-l M)	1.682	5,600	Regular,	260	292.10	4.61	63.4	Trapez.	2.35	3.1	0.0000433	0.0000728	-0.0000271	400	0.580	169.5
						sl. angular,	(Range 80										400		
						moderate	to 370 m)										(Arab Hasan		
						migr. rate											R. Shuteyt)		
SARDARABAD ANTICLINE (R. Dez)																			
Upstream of fold																			
L135 to L145 (L136)	4.118	SW (220°)	Type 3b (m-l M)	1.199	3,500	Variable,	170	152.26	1.70	89.6	Rect.	3.64	4.0	0.0003018	0.0003618	0.0005099	244	4.731	720.4
L145 to L158 (L153)	5.128	ESE (120°)	Type 3b (m-l M)	2.156	2,100	sl. irreg.,	200	179.04	1.70	105.3	Trapez.	1.94	3.9	0.0003328	0.0007157	0.0005460	244	4.437	794.3
L158 to L168 (L164)	5.727	SE (130°)	Type 3b (m-l M)	1.417	2,200	qu. smooth	140	123.97	2.80	44.3	Trapez.	1.99	3.0	0.0003438	0.0004872	0.0001397	244	6.621	820.8
						v. high	(Range 60										(Bamdej		
						migr. rate	to 310 m)										R. Dez)		
Across axis of fold																			
L168 to L175 (L171)	5.834	SW (230°)	Type 3b (m-l M)	1.120	3,700	Regular,	160	153.65	2.70	56.9	Trapez.	3.60	6.5	0.0002999	0.0003360	0.0005142	244	4.659	715.9
			/Type 2 (m-l S)			qu. rough,											(Bamdej		
						v. low	(Range 80										R. Dez)		
						migr. rate	to 320 m)												
Downstream of fold											Irreg./								
L175 to L190 (L183)	10.331	SE (130°)	Type 3b (m-l M)	1.585	6,100	Irreg/tort,	300	285.03	4.80	59.4	Rect.	2.44	2.8	0.0001240	0.0001965	0.0003291	244	1.039	296.0
L190 to L199 (L196)	5.640	S (170°)	Type 3b (m-l M)	1.629	2,700	sl. angular,	220	194.49	3.10	62.7	Trapez.	3.45	3.9	0.0001664	0.0002710	0.0001282	244	2.042	397.3
						moderate	(Range 70										(Bamdej		
						migr. rate	to 460 m)										R. Dez)		
SHAHUR ANTICLINE (R. Dez)																			
Upstream of fold																			
See L175 to L199 for R. Dez associated with the Sardarabad Anticline																			
Across axis of fold																			
L199 to L206 (L202)	3.980	SSW (200°)	Type 3b (m-l M)	1.792		Irreg.,	170	160.84	2.50	64.3	Trapez.	4.03	5.7	0.0001682	0.0003015	0.0002513	244	2.496	401.5
L206 to L214 (L206)	6.359	S (170°)	Type 3b (m-l M)	1.270		qu. smooth	190	161.26	2.70	59.7	Trapez.	3.81	5.3	0.0000718	0.0000912	0.0002202	244	1.063	171.4
(L210)						mod./high	240	208.50	2.90	71.7	Rect./	4.99	5.2	0.0000718	0.0000912	0.0002202	244	0.824	171.4
						migr. rate	(Range 50				Irreg.						(Bamdej		
							to 250 m)										R. Dez)		
Downstream of fold																			
L214 to L225 (L219)	4.811	SE (130°)	Type 3b (m-l M)	2.231	3,900	Regular,	160	119.68	2.80	42.7	Trapez.	3.01	4.1	0.0001211	0.0002702	0.0002079	244	2.416	289.1
L225 to L233 (L227)	5.407	S (190°)	Type 3b (m-l M)	1.537	3,000	qu. angular	270	206.86	3.40	60.8	Irreg./	1.83	1.9	0.0001528	0.0002349	0.0003699	244	1.763	364.7
						mod./high	(Range 70				Triang.						(Bamdej		
						migr. rate	to 520 m)										R. Dez)		

Appendix 5.3 (c)	RIVER SEDIMENTOLOGY					SUMMARY
Summary of various	Main sediment or	Estimate	Short general description of channel **bed** surface	Short general description of channel **banks**	Estimate	Short overall description of river reach,
data for river reaches	bedrock type in river	of degree	sediments	(including, in some cases, B (% of channel bank	of degree	including estimate of probable overall degree of aggradation or incision
of the R. Karun and Dez	valley	of general	(including, in some cases, D_{coarse} (mean grain size	sediments less than 63 μm), D_{fine} (mean grain size for f	of erosion	
assoc. with the		erosion	for gravels, intermed. diam. in mm), D_{max} (mean	gravels, sands and muds))	resistance	
Sardarabad Ant. and of		resistance	grain size for 10 largest gravel clasts, intermed.		of channel	
the R. Dez assoc. with			diam. in mm), D_{fine} (mean grain size for fine		banks	
the Shahur Ant.			gravels, sands and muds, in μm))			
SARDARABAD ANTICLINE (R. Karun, Shuteyt branch)						
Upstream of fold						Type 3b (m-l M) river, with broader channels with bars (Type 4 (M-B) river)
LB56 to LB68/1 (LB66)	Bakhtyari F. bedrock/	MODERATE	**Partly sands and silts** (D_{fine} = c. 723.8 μm), **partly**	**Mainly sands and silts** (B = c. 61.6 %, D_{fine} = c.	MODERATE	at some locations in upstr. half of reach. Moderately broad & shallow
LB68/1 to LB84 (LB75)	Unlith. floodplain seds.	MODERATE	**gravels** (D_{coarse} = c. 24.6 mm, D_{max} = c. 82.5 mm).	55.1 μm), **few gravels**. Qu. poorly cem. Variable veg.		channels with qu. steep, high banks, esp on SW side. River channel has
			Sands and silts predom. at channel edges,	of banks - partly low trees and bushes (esp. on		qu. high mobility, except on SW side where constrained by Bakhtyri F.
			gravels predom in deeper parts of channel	broader channel betls and on NE bank), partly herbs		of Sardarabad Ant. Probable MODERATE to HIGH degree of AGGRADATION,
				& grasses (esp. on SW bank)		lessening to LOW or NO AGGRADATION at dowstr. end of reach
Across axis of fold						
LB84 to LB101 (LB85)	Unlith. floodplain seds.	QU. LOW	**Mainly sands and silts**. Probably some gravels in	**Sands and muds** (B = c. 97.3 - 99.0 %, D_{fine} = c. 5.7 - 8.2	MODERATE	Type 3b (m-l M) single-thread meand. river. Quite narrow, deep channels
(LB93)	/ occ. Bakhtyari F.		deeper parts of channel	μm). Qu. well cemented. Veg. of banks partly herbs		with qu. steep, high banks. River channel moderately mobile, esp on E
	bedrock outcrops			& grasses (esp. near fields), partly low trees and		side (where oxbows form). Probable LOW degree of INCISION or LOW
				bushes		degree of AGGRADATION
Downstream of fold						
LB101 to LB116 (LB109)	Unlith. floodplain seds.	LOW	**Mainly sands and silts**. Probably some gravels in	**Sands and muds** (B = c. 89.8 %, D_{fine} = c. 37.9 μm). Qu.	QU. LOW	Type 3b (m-l M) single-thread meand. river. Quite broad, quite deep
			deeper parts of channel	well cemented. Veg. of banks mainly herbs & grasses		channels, though qu. variable. River channel moderately mobile, though
				(esp. near fields), with low trees and bushes at some		meanders of qu. low amplitude. Probale LOW degree of AGGRADATION
				locations		
SARDARABAD ANTICLINE (R. Dez)						
Upstream of fold		QU. LOW/				
L135 to L145 (L136)	Unlith. floodplain seds.	MODERATE	**Partly sands and silts** (D_{fine} = c. 99.5 μm), **partly**	**Mainly sands and silts** (B = c. 51.8 %, D_{fine} = c. 75.6	MODERATE	Type 3b (m-l M) single-thread meand. river, varying from low to moderate
L145 to L158 (L153)	/ Bakhtyari F. bedrock	MODERATE	**gravels** (D_{coarse} = 20.8 mm, D_{max} = 69.2 mm).	μm), **few gravels**. Qu. poorly cemented. Gen. well veg.		sinuosity. Moderately broad and shallow channels, becoming narrower
L158 to L168 (L164)	on SW side	MODERATE	Sands predom. at channel edges, gravels predom.	banks of low trees and bushes, herbs & grasses at		and deeper downstr. River channel has high mobility, though constrained
			on bars and in deeper parts of channel	few locations		on SW side by Bakhtyari F. of Sardarabad Ant. Probable HIGH degree of
						AGGRADATION, lessening to MODERATE AGGRADATION at downstr. end
Across axis of fold						
L168 to L175 (L171)	Agha Jari F. bedrock/	MODERATE/	**Partly sands and silts, partly gravels**. Sands predom	**Mainly sands and silts** (B = c. 67.0 %, D_{fine} = c. 39.5	MODERATE	Type 3b (m-l M) single-thread meand. river of very low sinuosity. Slightly
	Bakhtyari F. bedrock	HIGH	at channel edges, gravels predom. in deeper	μm), **few gravels**. Qu. poorly cemented. Veg. of banks		narrow and deep channels with qu. high banks. River channel has v.
			parts of channel	partly low trees and bushes, partly herbs and grasses		limited mobility in narrow valley constrained by bedrock outcrops.
						Probable MODERATE to HIGH degree of INCISION
Downstream of fold						
L175 to L190 (L183)	Unlith. floodplain seds.	LOW	**Mainly sands and silts** (D_{fine} = c. 129.1 μm). Sands	**Sands and muds** (B = c. 68.4 %, D_{fine} = c. 50.3 μm). Qu.	QU. LOW	Type 3b (m-l M) single-thread meand. river. Moderately broad and shallow
L190 to L199 (L196)	Unlith. floodplain seds.	LOW	with current ripples and dunes predom. at edges	well cemented. Veg. of banks mainly low trees and		channels, though sl. variable. River channel mod. mobile in sl. Constrained
			of channel. Probably some gravels in deeper parts	bushes, with herbs and grasses at some locations		valley between Shahur and Sardabad Anticlines. Probable MODERATE
			of channel	near edges of fields		degree of AGGRADATION throughout
SHAHUR ANTICLINE (R. Dez)						
Upstream of fold						
See L175 to L199 for R. Dez associated with the Sardarabad Anticline						
Across axis of fold						
L199 to L206 (L202)	Unlith. floodplain seds.	LOW	**Mainly sands and silts**. Sands with current ripples	**Sands and muds**. Qu. well cemented. Veg. of banks	QU. LOW	Type 3b (m-l M) single-thread meandering river. Moderately broad and
L206 to L214 (L206)	Unlith. floodplain seds.	LOW	and dunes predom. at edges of channel. Probably	mainly low trees and bushes, with herbs and grasses		shallow channels with qu. high channel banks. River channel moderately
(L210)			some gravels in deeper perts of channel	at locations near edges of fields		mobile within fairly wide valley, v. slightly constrained by Shahur Ant. to
						the W. Probable LOW degree of AGGRADATION ot LOW degree of
						INCISION (esp. between L206 and L209)
Downstream of fold						
L214 to L225 (L219)	Unlith. floodplain seds.	LOW	**Mainly sands and silts**	**Sands and muds**. Qu. well cemented. Veg. of banks	QU. LOW	Type 3b (m-l M) single-thread meandering river. Moderately broad and
L225 to L233 (L227)	Unlith. floodplain seds.	LOW		mainly low trees and bushes, with herbs and grasses		shallow channels, though qu. variable. River channel moderately to qu.
				at locations near edges of fields		highly mobile within wide valley. Probable MODERATE degree of
						AGGRADATION (possibly slightly less btween L214 and L225)

Appendix 5.4 (a)	STRUCTURAL GEOLOGY					LOCATION	HUMAN ACTIVITIES		
Summary of various data for	Estimate of	Width of	Approx. probable	Approx.	Approx.	Location of river reach	Short description of floodplain land use	Short description of human river channel	Estimate of
river reaches of the River Karun	degree of	geological	location of fold	distance from	distance from	including		modifications	overall degree
associated with the Kupal	development	structure	"core" (part of	fold "core" to	fold "nose" to	General location			of human
Anticline and river reaches of the	(and erosion)	where crossed	fold which	where crossed	where crossed	Start and end survey			impact
River Karun and Dez associated	of geological	by river (km)	probably emerged	by river (km	by river (km	locations for reach			
with the Ramin Oilfield Anticline	structure	(where	first, where	along fold axis	along fold axis	(Location for channel			
		applicable)	applicable)	or its proj.)	or its proj.)	measurements)			
KUPAL ANTICLINE						KUPAL ANTICLINE (R. Karun, Gargar branch)			
Emerged anticline: Fold axis oriented	Well	6.8	31°25' N 49°14' E	43.0	8.4	**Upstream** of fold	Limited veg. and many fish tanks next to	Uncertain. Gen. course of R. Gargar developed	
roughly SE-NW, doubly plunging	developed	(projection)			(projection)	L71 to L78 (L75)	river, qu. extensive fields on broader	from disuse of ancient Masrukan canal, probably	MODERATE/
	fold					L78 to L88 (L 84)	floodplains	further to the NW in this area. In vicinity of L87,	QU. HIGH
Hinge length, L = 70 km (approx.)	- more than					(along R. Gargar for		part of Masrukan may have intersected orthog.	
Fold width, W = 12.6 km	110 m above					projection of fold)		with R. Gargar (Moghaddam and Miri, 2007)	
Aspect ratioo, AR = L / W = 5.6	surrounding					**Across axis** of fold	Limited veg. of herbs and grasses, limited	Some influences from courses of ancient	
Fold Symmetry Index, FSI =	plains					L88 to L95 (L94)	agriculture, very few fish tanks	Masrukan canal, esp. those associated with	MODERATE/
Shorter limb width / (0.5 W) = 0.83						L95 to LM1 (L 99/1)		ancient Askar Mukram town and ancient Band-e	QU. HIGH
Possible fold type:						(along R. Gargar for		Qir dam located at end of reach	
Uncertain - maybe a short fault bend						projection of fold)			
fold or fault propagation fold						**Downstream** of fold			
						See LM1 to LM8 for R. Karun associated with the Ramin Oilfield Anticline			
RAMIN OILFIELD ANTICLINE		**For R. Dez**				RAMIN OILFIELD ANTICLINE (R. Dez)			
Emerging anticline: Fold axis probably	Emerging	4.0	Very uncertain -	9.4	8.7	**Upstream** of fold			
oriented roughly SSE-NNW, other	fold	(very approx.)	possibly in		(approx. -	L246 to L259 (L254)	Veg. of bushes and low trees on floodplains	Probable extensive human channel modifications	HIGH
details uncertain as fold has very	- less than		vicinity of		location of	L259 to L265 (L261)	next to river due to limited human impacts.	- flow orig. to S. from Chamlabad - Ummashiyyeh	
limited surface expression	5 m above		31°33' N 48°53' E		fold "nose"	L265 to LM1 (L269A)	Extensive agriculture on broader floodplains	-ye Yek; in c. 10th-14th Cent. AD, R. Dez maybe	
	surrounding				very uncertain)			diverted by a "dike" nr. Chamlabad and a canal	
	plains							to the NE of L259, and with disuse this may have	
Hinge length, L = 35 km (approx.)								become the new flow regime for R. Dez	
Fold width, W = 5.0 km (approx.)									
Aspect ratio, AR = L / W = 7.0		**For R. Karun, Shuteyt branch**				RAMIN OILFIELD ANTICLINE (R. Karun, Shuteyt branch)			
Fold Symmetry Index, FSI =		4.0	Very uncertain -	1.7	15.0	**Upstream** of fold			
Shorter limb width / (0.5 W) = 0.89		(very approx.)	possibly in		(approx. -	LB116 to LM1 (LB127)	Veg. of bushes and low trees on floodplains	Course of R. Karun prob. orig. further W. into a	QU. HIGH
(approximate values based on			vicinity of		location of		next to river due to limited human impacts.	confluence with R. Dez nr. Chamlabad. In c. 10th	
measurements from Soleimani et al.,			31°33' N 48°53' E		fold "nose"		Quite extensive agriculture on broader	-14th Cent. AD, with poss. diversion of R. Dez, the	
2008 and oilfield maps)					very uncertain)		floodplains	R. Karun may have avulsed to the E. into a former	
Possible fold type:								course of Masrukan canal between Band-e Qir	
Detachment fold								& Veys (Le Strange, 1905; Alizadeh et al., 2004)	
						Across axis of fold			
						LM1 to LM8 (LM3)	Veg. of low trees, bushes, cultivated trees,	Course of R. Karun/R. Dez prob. orig. along	VERY HIGH
						LM8 to LM16 (LM13)	herbs and grasses next to river. Some	palaeochannel from Chamlabad - Ummashiyyeh	
						LM16 to LM20 (LM19)	industry and some urbanization assoc. with	-ye Yek. In c. 10th-14th Cent. AD, river may have	
							large town of Mulla Sani. Gen. extensive	avulsed into a near-straight former course of	
							agriculture on broader floodplains	Masrukan canal which has been maintained	
								since (Le Strange, 1905; Alizadeh et al., 2004)	
						Downstream of fold			
						LM20 to LM36 (LM27)	Veg. of bushes and low trees on floodplain	Course of R. Karun and location of LM20 greatly	MODERATE
							locations next to river, otherwise extrensive	influenced by former course of Masrukan canal.	
							agriculture (fields and cultivation) over	Otherwise, fairly limited human impacts with	
							floodplains	various small canals	

Appendix 5.4 (b)	RIVER GEOMORPHOLOGY																RIVER HYDROLOGY		
Summary of various data for river reaches of the R. Karun assoc. with the Kupal Ant. and of the R. Karun and Dez assoc. with the Ramin Oilfield Ant.	Straight-line valley length of reach (km)	General course direction of reach (bearing to nearest 10°)	Channel pattern type (using simple classification of Schumm (1981, 1985)	Channel sinuosity (no units)	Average meander wave-length (m)	Meander type	Overall channel width (m) (Approx. range for reach)	Channel width (m)	Channel depth (m)	Channel width: depth ratio (no units)	Approx. cross-sectional shape of channel(s)	Estimate of av. height of channel banks above channel water surface (m)	Estimate of av. height of floodplain or valley above channel water surface (m)	Channel water surface slope (m m-1)	Projected-channel water surface slope (m m-1)	Valley slope (m m-1)	Average daily water discharge (data from gauging sta.) (m3 s-1)	Specific stream power (W m-2)	Stream power per unit length (W m-1)
				S	λ		Wmax	w	d	w / d				s	Sp	Sv	Q	ω	Ω
KUPAL ANTICLINE (R. Karun, Gargar branch)																			
Upstream of fold																			
L71 to L78 (L75)	4.100	SSW (210°)	Type 3a (s-l M)	1.354	1,700	Irreg/tort,	30	38.26	4.40	8.7	Triang.	1.57	2.6	0.0002809	0.0003805	-0.0001707	46	3.304	126.4
L78 to L88 (L 84)	2.836	WSW (250°)	Type 3a (s-l M)	2.629	1,100	smooth,	40	34.62	4.10	8.4	Triang.	2.03	5.4	0.0001087	0.0002856	-0.0015869	46	1.411	48.9
(along R. Gargar for						moderate	(Range 10										(Shushtar		
projection of fold)						migr. rate	to 60 m)										R. Gargar)		
Across axis of fold																			
L88 to L95 (L94)	5.222	SSW (210°)	Type 3a (s-l M)	1.259	1,600	Irreg.,	40	39.76	3.70	10.8	Triang.	2.67	9.9	0.0001278	0.0016090	-0.0010533	46	1.446	57.5
L95 to LM1 (L 99/1)	5.485	SSW (210°)	Type 3a (s-l M)	1.301	1,300	smooth,	20	24.86	3.01	8.3	Triang.	1.68	9.7	0.0002047	0.0002662	0.0023700	46	3.705	92.1
(along R. Gargar for						mod./low	(Range 10										(Shushtar		
projection of fold)						migr. rate	to 60 m)										R. Gargar)		
Downstream of fold																			
See LM1 to LM8 for R. Karun associated with the Ramin Oilfield Anticline																			
RAMIN OILFIELD ANTICLINE (R. Dez)																			
Upstream of fold																			
L246 to L259 (L254)	7.620	SE (130°)	Type 3b (m-l M)	1.623	4,100	Variable -	180	153.32	3.90	39.3	Triang.	3.77	4.3	0.0000954	0.0001549	0.0002756	244	1.485	256.4
L259 to L265 (L261)	3.948	NE (040°)	Type 2 (m-l S)	1.062	—	irreg.,	130	113.91	3.40	33.5	Irreg.	3.18	4.1	0.0001360	0.0001444	0.0000760	244	2.849	324.6
L265 to LM1 (L269A)	4.460	E (080°)	Type 3b (m-l M)	2.091	5,400	smooth	230	167.43	2.80	59.8	Irreg.	3.71	4.5	0.0000750	0.0001569	0.0003139	244	1.069	179.2
						then ang.,	(Range 60										(Bamdej		
						qu. high	to 320 m)										R. Dez)		
						migr. rate													
RAMIN OILFIELD ANTICLINE (R. Karun, Shuteyt branch)																			
Upstream of fold																			
LB116 to LM1 (LB127)	6.990	SE (130°)	Type 3b (m-l M)	1.702	4,300	Irreg.,	240	243.92	6.40	38.1	Trapez.	4.13	5.9	0.0001551	0.0002640	0.0004292	400	2.488	606.8
						angular,	(Range 90										(Arab Hasan		
						moderate	to 290 m)										R. Shuteyt)		
						to high													
						migr. rate													
Across axis of fold																			
LM1 to LM8 (LM3)	6.325	S (180°)	Type 2 (m-l S)	1.061	4,800	—	240	200.65	8.07	24.9	Trapez.	4.88	7.6	0.0000007	0.0000008	-0.0005534	575	0.021	4.2
LM8 to LM16 (LM13)	8.202	S (180°)	Type 2 (m-l S)	1.010	—	—	330	306.45	3.20	95.8	Rect.	6.67	6.9	0.0001104	0.0001116	0.0003292	575	2.027	621.1
LM16 to LM20 (LM19)	4.533	S (190°)	Type 2 (m-l S)	1.043	—	—	270	258.86	4.90	52.8	Rect.	4.54	6.9	0.0001354	0.0001412	0.0003309	575	2.941	761.4
							(Range 130										(Mulla Sani		
							to 340 m)										R. Karun)		
Downstream of fold																			
LM20 to LM36 (LM27)	7.291	WSW (250°)	Type 3b (m-l M)	2.468	4,000	Irreg/tort,	330	303.15	5.40	56.1	Rect.	3.69	4.5	0.0000839	0.0002071	0.0001783	575	1.557	471.9
						angular,											(Mulla Sani		
						moderate	(Range 130										R. Karun)		
						to high	to 360 m)												
						migr. rate													

Appendix 5.4 (c)	RIVER SEDIMENTOLOGY					SUMMARY
Summary of various	Main sediment or	Estimate	Short general description of channel **bed** surface	Short general description of channel **banks**	Estimate	Short overall description of river reach,
data for river reaches	bedrock type in river	of degree	sediments	(including, in some cases, B (% of channel bank	of degree	including estimate of probable overall degree of aggradation or incision
of the R. Karun assoc.	valley	of general	(including, in some cases, D_{coarse} (mean grain size	sediments less than 63 µm), D_{fine} (mean grain size for f	of erosion	
with the Kupal Ant. and		erosion	for gravels, intermed. diam. in mm), D_{max} (mean	gravels, sands and muds))	resistance	
of the R. Karun and Dez		resistance	grain size for 10 largest gravel clasts, intermed.		of channel	
assoc. with the Ramin			diam. in mm), D_{fine} (mean grain size for fine		banks	
Oilfield Ant.			gravels, sands and muds, in µm))			
KUPAL ANTICLINE (R. Karun, Gargar branch)						
Upstream of fold						
L71 to L78 (L75)	Unlith. floodplain seds.	QU. LOW	**Mainly sands and silts**	**Mainly muds, with some sands** Gen. qu. poorly	QU. LOW	Type 3a (s-l M) single-thread meand. river. Narrow, deep channels.
L78 to L88 (L 84)	Unlith. floodplain seds.	QU. LOW		cemented. Limited veg. of banks - mainly herbs and		Reach L78 to L88 very tortuous with some channel migration within a
(along R. Gargar for				grasses		narrow channel belt. Probable NO AGGRADATION for about first 1 km,
projection of fold)						increasing qu. abruptly to HIGH degree of AGGRADATION downstr.
Across axis of fold						
L88 to L95 (L94)	Unlith. floodplain seds.	QU. LOW	**Mainly sands and silts**	**Mainly muds, with some sands** Gen. qu. poorly	QU. LOW	Type 3a (s-l M) single-thread meand. river. Narrow, deep channels. Slight
L95 to LM1 (L 99/1)	Unlith. floodplain seds.	QU. LOW		cemented. Limited veg. of banks - mainly herbs and		channel migration within a narrow channel belt, reach L87 to L89 v. low
(along R. Gargar for				grasses		sinuos. with deep channel. Probable QU. HIGH degree of AGGRADATION
projection of fold)						to L87, probable QU. HIGH degree of INCISION downstream of L87
Downstream of fold						
See LM1 to LM8 for R. Karun associated with the Ramin Oilfield Anticline						
RAMIN OILFIELD ANTICLINE (R. Dez)						
Upstream of fold						Type 3b (m-l M) single-thread meand. river, except Type 2 (m-l S) straight
L246 to L259 (L254)	Unlith. floodplain seds.	LOW	**Mainly sands and silts**. Possibly some gravels	**Sands and muds**. Generally poorly cemented. Veg.	LOW	river between L259 and L265. Mod. narrow, deep channels, though qu.
L259 to L265 (L261)	Unlith. floodplain seds.	LOW	in deeper parts of channel	of partly low trees and bushes, partly herbs and		variable. River channel mod. mobile, sl. constrained by N-S oriented ridge
L265 to LM1 (L269A)	Unlith. floodplain seds.	LOW		grasses near edges of fields		to N. and by higher ground to S. - few centuries ago river flowed S along
						palaeochannel Chamlabad to Ummashiyyeh-ye Yek when flow between
						L259 and L265 was reversed. Probable gen. MODERATE degree of
						AGGRADATION, probably LOW degree of AGGRADATION in some parts
RAMIN OILFIELD ANTICLINE (R. Karun, Shuteyt branch)						
Upstream of fold						
LB116 to LM1 (LB127)	Unlith. floodplain seds.	LOW	**Mainly sands and silts** (D_{fine} = c. 28.8 µm near	**Sands and muds** (B = c. 66.0 %, D_{fine} = 55.2 µm). Gen.	LOW	Type 3b (m-l M) single-thread meandering river with qu. angular meanders.
			channel margin). Possibly some gravels in deeper	poorly cemented. Veg. of banks partly herbs and		Moderately narrow, deep channels. River channel mod. mobile, though sl.
			parts of channel	grasses (esp. near fields), partly low trees and		constrained within sl. narrow valley by Kupal Ant. to E and roughly N-S
				bushes		oriented ridge to W. Probable MODERATE degree of AGGRADATION, prob.
						lessening to LOW degree of AGGRADATION at downstr. end
Across axis of fold						
LM1 to LM8 (LM3)	Unlith. floodplain seds.	LOW	**Mainly sands and silts** (D_{fine} = c. 21.1 µm near	**Sands and muds** (B = c. 81.2 %, D_{fine} = 33.6 µm). Qu.	QU. LOW	Type 2 (m-l S) single-thread staright river with very slight, smooth
LM8 to LM16 (LM13)	Unlith. floodplain seds.	LOW	channel margin)	poorly cemented. Veg. of banks partly low trees,		meandering between LM1 and LM8. Moderately broad, shallow channels,
LM16 to LM20 (LM19)	Unlith. floodplain seds.	LOW		bushes and cultivated trees, partly herbs and		though sl. deeper between LM1 and LM8. River channel has limited
				grasses		mobility with sl. meandering between LM1 and LM8, very limited mobility
						elsewhere. Probable HIGH degree of INCISION, possibly QU. HIGH
						degree of INCISION between LM1 and LM8
Downstream of fold						
LM20 to LM36 (LM27)	Unlith. floodplain seds.	LOW	**Mainly sands and silts** (D_{fine} = c. 69.1 µm near	**Sands and muds** (B = c. 63.6 %, D_{fine} = 54.6 µm). Qu.	QU. LOW	Type 3b single-thread meandering river with gen. angular meanders.
			channel margin)	poorly cemented. Veg. of banks partly low trees and		Variable channels - gen. mod. broad & shallow channels, with narrow &
				bushes, partly grasses and herbs (due to extensive		deep channels at meander apices. River channel mobility imited at LM20,
				fields)		otherwise river channel moderately mobile. Gen. MODERATE degree of
						AGGRADATION

Appendix 5.5 (a)	STRUCTURAL GEOLOGY					LOCATION	HUMAN ACTIVITIES		
Summary of various data for river reaches of the River Karun associated with the Ahvaz and Ab-e Teymur Oilfield Anticlines	Estimate of degree of development (and erosion) of geological structure	Width of geological structure where crossed by river (km) (where applicable)	Approx. probable location of fold "core" (part of fold which probably emerged first, where applicable)	Approx. distance from fold "core" to where crossed by river (km along fold axis or its proj.)	Approx. distance from fold "nose" to where crossed by river (km along fold axis or its proj.)	Location of river reach including General location Start and end survey locations for reach (Location for channel measurements)	Short description of floodplain land use	Short description of human river channel modifications	Estimate of overall degree of human impact
AHVAZ ANTICLINE						AHVAZ ANTICLINE (R. Karun)			
Emerged anticline: Fold axis oriented	Well	2.3	31°17' N 48°45' E	8.5	18.1	**Upstream** of fold			
roughly ESE-WNW, curving to c.	developed					LM36 to LM61 (LM55)	Veg. of bushes and low trees on floodplain	Various river channel modifications over last	MODERATE
SE-NW at eastern end, doubly	fold					LM61 to A11/A12	locations next to river, otherwise extensive	7 km assoc. with suburbs of Ahvaz - two modern	
plunging, merges with small anticline	- more than					(LM69)	agriculture over floodplains. Fairly extensive	bridges, drainage, sewage, etc. Various canals,	
at western end, associated with the	150 m above						urbanization over last 7 km assoc. with	including major modern canal from W. bank in	
roughly ESE-WNW oriented Ahvaz	surrounding						suburbs of Ahvaz	latter part of reach serving Lower Khuz. Plains	
Thrust Fault to the south-west	plains					**Across axis** of fold		Various modern bridges, embankments, & ruins	
						A11/A12 to B11/B12	Extensive urbanization through large city	of prob. Sassanian - Abbasid Period "Bund of	HIGH
						(A21/A22)	of Ahvaz	Ahvaz" (used to raise river level for major irrig.	
Hinge length, L = 53 km	Extensive							canals to Lower Khuz. Plains) on outcrops near	
Fold width, W = 8.2 km (approx.)	erosion of							railway bridge (Walstra et al., 2010), increase	
Aspect ratio, AR = L / W = 6.5	SSW limb							the rapids of the first c. 2km of this reach	
Fold Symmetry Index, FSI =						**Downstream** of fold			
Shorter limb width / (0.5 W) = 0.24						B11/B12 to A49/A50	Extensive urbanization for first 8 km through	Various embankments & constructions through	HIGH
Possible fold type:						(A37/A38)	large city and suburbs of Ahvaz. Downstr. of	city and suburbs of Ahvaz inhibit meander	
Fault propagation fold						A49/A50 to A85/A86	this, extensive agriculture (fields and	development and channel migration. Major	
						(A69/A70)	cultivation) over floodplains	canal assoc. with "Bund of Ahvaz" prob. had	
								SSW course c. 1 km from east bank of R. Karun	
								& then S along Nahr Bahreh (Walstra et al., 2010)	
AB-E TEYMUR OILFIELD ANTICLINE						AB-E TEYMUR OILFIELD ANTICLINE (R. Karun)			
Emerging anticline: Fold axis probably	Emerging	4.4	Very uncertain -	0.6	9.0	**Upstream** of fold			
oriented roughly SE-NW, other	fold of very	(approx.)	possibly in		(approx.	A49/A50 to A85/A86	Veg. of bushes and low trees on floodplain	Some irrigation canals, including intakes near	QU. LOW
details uncertain as fold has very	limited		vicinity of		- location of	(A69/A70)	locations next to river, otherwise extensive	A49/A50 serving Nahr Bahreh; otherwise quite	
limited surface expression	surface		31°11' N 48°31' E		fold "nose"		agriculture (fields and cultivation) over	limited	
	expression				very uncertain)		floodplains		
	- less than								
Hinge length, L = 20 km (approx.)	2 m above					**Across axis** of fold			
Fold width, W = 4.7 km (approx.)	surrounding					A85/A86 to B33/B34	Extensive agriculture (fields and cultivation)	Various irrigation canals from N and S banks	QU. LOW/
Aspect ratio, AR = L / W = 4.3	plains					(B19/B20)	over floodplains. Veg of bushes, herbs and	serving very extensive fields on Lower Khuzestan	MODERATE
Fold Symmetry Index, FSI =							grasses on floodplain locations next to river	Plains	
Shorter limb width / (0.5 W) = 0.90									
(approximate values based on									
measurements from Abdollahie Fard						**Downstream** of fold			
et al., 2006 and oilfield maps)						B33/B34 to B49/B50	Extensive agriculture (fields and cultivation)	Various irrigation canals from both banks,	MODERATE
Possible fold type:						(B45/B46)	over floodplains. Veg of bushes, herbs and	including two very large modern canals serving	
Detachment fold						B49/B50 to B63/B64	grasses on floodplain locations next to river	very extensive fields to the S and SW.	
						(B57/B58)			

Appendix 5.5 (b)	RIVER GEOMORPHOLOGY																RIVER HYDROLOGY		
Summary of various data for river reaches of the River Karun assoc. with the Ahvaz and Ab-e Teymur Oilfield Anticlines	Straight-line valley length of reach (km)	General course direction of reach (bearing to nearest 10°)	Channel pattern type (using simple classification of Schumm (1981, 1985)	Channel sinuosity (no units) S	Average meander wave-length (m) λ	Meander type	Overall channel width (m) (Approx. range for reach) W_{max}	Channel width (m) w	Channel depth (m) d	Channel width: depth ratio (no units) w / d	Approx. cross-sectional shape of channel(s)	Estimate of av. height of channel banks above channel water surface (m)	Estimate of av. height of floodplain or valley above channel water surface (m)	Channel water surface slope ($m\ m^{-1}$) s	Projected-channel water surface slope ($m\ m^{-1}$) S_p	Valley slope ($m\ m^{-1}$) S_v	Average daily water discharge (data from gauging sta.) ($m^3\ s^{-1}$) Q	Specific stream power ($W\ m^{-2}$) ω	Stream power per unit length ($W\ m^{-1}$) Ω
AHVAZ ANTICLINE (R. Karun)																			
Upstream of fold																			
LM36 to LM61 (LM55)	10.471	SW (220°)	Type 3b (m-l M)	2.200	6,600	Sl. irreg.,	350	315.04	4.00	78.8	Rect.	3.52	4.1	0.0000516	0.0001137	0.0001433	575	0.921	290.3
LM61 to A11/A12	5.987	SSW (210°)	Type 3b (m-l M)	2.167	6,900	sl. angular,	310	294.48	4.38	67.2	Rect.	3.64	4.4	0.0000347	0.0000752	-0.0000501	575	0.663	195.1
(LM69)						moderate	(Range 110										(Ahvaz		
						migr. rate	to 620 m)										R. Karun)		
Across axis of fold																			
A11/A12 to B11/B12	4.002	SW (220°)	Type 2 (m-l S)	1.047	—	—	360	320.27	9.80	32.7	Triang./	4.06	5.3	0.0006136	0.0006422	0.0003748	575	10.777	3451.4
(A21/A22)							(Range 310				Irreg.						(Ahvaz		
							to 690 m)										R. Karun)		
Downstream of fold																			
B11/B12 to A49/A50	8.778	SSW (200°)	Type 2 (m-l S)	1.078	—	—	280	263.84	8.60	30.7	Irreg.	4.72	5.2	0.0000296	0.0000319	0.0001823	575	0.631	166.4
(A37/A38)						Irreg/tort,													
A49/A50 to A85/A86	6.628	W (270°)	Type 3b (m-l M)	3.283	4,800	angular,	370	343.65	6.30	54.5	Irreg.	1.97	3.7	0.0000597	0.0001962	0.0000151	575	0.978	336.0
(A69/A70)						moderate	(Range 100										(Ahvaz		
						to high	to 580 m)										R. Karun)		
						migr. rate													
AB-E TEYMUR OILFIELD ANTICLINE (R. Karun)																			
Upstream of fold																			
A49/A50 to A85/A86	6.628	W (270°)	Type 3b (m-l M)	3.283	4,800	Irreg/tort,	370	343.65	6.30	54.5	Irreg.	1.97	3.7	0.0000597	0.0001962	0.0000151	575	0.978	336.0
(A69/A70)						angular,	(Range 100										(Ahvaz		
						moderate	to 580 m)										R. Karun)		
						to high													
						migr. rate													
Across axis of fold																			
A85/A86 to B33/B34	11.172	SW (230°)	Type 3b (m-l M)	1.858	4,500	Qu. Regular	310	291.26	9.30	31.3	Trapez./	2.08	2.3	0.0000212	0.0000394	0.0002954	575	0.409	119.3
(B19/B20)						qu. Angular	(Range 100				Irreg.						(Ahvaz		
						qu. low	to 490 m)										R. Karun)		
						migr. rate													
Downstream of fold																			
B33/B34 to B49/B50	9.513	SW (230°)	Type 3b (m-l M)	1.176	4,900	Irreg.,	300	281.12	6.10	46.1	Trapez.	3.36	3.1	0.0000614	0.0000809	0.0002208	575	1.228	345.3
(B45/B46)						qu. smooth,													
B49/B50 to B63/B64	7.638	S (180°)	Type 3b (m-l M)	1.192	10,000	moderate	230	212.80	7.50	28.4	Triang.	3.74	3.9	0.0000758	0.0000903	-0.0000524	575	2.003	426.2
(B57/B58)						to low	(Range 150										(Ahvaz		
						migr. rate	to 390 m)										R. Karun)		

Appendix 5.5 (c)	RIVER SEDIMENTOLOGY					SUMMARY
Summary of various	Main sediment or	Estimate	Short general description of channel **bed** surface	Short general description of channel **banks**	Estimate	Short overall description of river reach,
data for river reaches	bedrock type in river	of degree	sediments	(including, in some cases, B (% of channel bank	of degree	including estimate of probable overall degree of aggradation or incision
of the River Karun	valley	of general	(including, in some cases, D_{coarse} (mean grain size	sediments less than 63 µm), D_{fine} (mean grain size for	of erosion	
assoc. with the Ahvaz		erosion	for gravels, intermed. diam. in mm), D_{max} (mean	fine gravels, sands and muds))	resistance	
and Ab-e Teymur		resistance	grain size for 10 largest gravel clasts, intermed.		of channel	
Oilfield Anticlines			diam. in mm), D_{fine} (mean grain size for fine		banks	
			gravels, sands and muds, in µm))			
AHVAZ ANTICLINE (R. Karun)						
Upstream of fold						
LM36 to LM61 (LM55)	Unlith. floodplain seds.	QU. LOW	**Mainly sands and muds** (D_{fine} = c. 10.7 - 65.7 µm	**Muds and sands** (B = c. 79.8 - 97.4 %, D_{fine} = c. 4.8 -	QU. LOW/	Type 3b (m-l M) single-thread meandering river. Moderately broad and
LM61 to A11/A12	/few outcrops of Agha	QU. LOW/	near channel margin)	37.7 µm). Qu. poorly cemented, qu. cohesive. Variable	MODERATE	shallow channels, though qu. variable. River channel moderately mobile
(LM69)	Jari F. bedrock at	MODERATE		veg. of banks - some low trees and bushes, mainly		within broad valley, though very limited at downstr. end due to water gap
	downstr. end of reach			herbs and grasses - esp. near fields, settlements and		in Ahvaz Anticline. Probable MODERATE degree of AGGRADTION, lessening
				suburbs		over last few km to NO AGGRADATION at downstream end
Across axis of fold						Type 2 (m-l S) single-thread straight river with sinuous thalweg and prom.
A11/A12 to B11/B12	Agha Jari F. bedrock	MODERATE	**Mainly sands and muds** (D_{fine} = c. 10.6 - 152.7 µm	**Sands and muds** (B = c. 49.8 - 65.7 %, D_{fine} = c. 46.4 -	MODERATE	altern. bars. Along first c. 2 km of reach, channel broadens over extensive
(A21/A22)			near channel margin), **some gravels** (D_{coarse} =	100.3 µm). Qu. poorly cemented, fairly cohesive.		rapids & around islands assoc. with Agha Jari F. sandst. bedrock outcrops
			c. 21.1 mm, D_{max} = c. 69.5 mm). Gravels more	Variable veg. of banks - mainly herbs, grasses and		- used as foundations for modern bridges and ancient "Bund of Ahvaz".
			abundant in vicinity of rapids and bedrock outcrops	waste ground, some constructions in city of Ahvaz,		Variable channels - narrow & deep to broad & shallow, very limited
				some bushes and low trees		mobility. Probable HIGH or VERY HIGH degree of INCISION throughout
Downstream of fold						
B11/B12 to A49/A50	Unlith. floodplain seds.	QU. LOW	**Mainly sands and muds** (D_{fine} = c. 150.7 µm near	**Muds and sands** (B = c. 63.8 - 74.7 %, D_{fine} = c. 37.3 -	QU. LOW	Type 2 (m-l S) single-thread straight river, changing abruptly at A49/A50 to
(A37/A38)			channel margin)	62.2 µm). Qu. poorly cemented, fairly cohesive.		Type 3b (m-l M) single-thread meand. River. Variable channels - narrow &
A49/A50 to A85/A86	Unlith. floodplain seds.	QU. LOW		Variable veg. of banks - some trees and bushes,		deep to broad & shallow. Gen. moderately broad and shallow channels
(A69/A70)				mainly herbs and grasses - esp. near fields		up to A49/A50 with very limited mobility, after that more variable with
						moderate mobility. Probable LOW degree of INCISION, changing at
						A49/A50 to MODERATE to HIGH degree of AGGRADATION
AB-E TEYMUR OILFIELD ANTICLINE (R. Karun)						
Upstream of fold						
A49/A50 to A85/A86	Unlith. floodplain seds.	QU. LOW	**Mainly sands and muds** (D_{fine} = c. 150.7 µm near	**Muds and sands** (B = c. 63.8 - 74.7 %, D_{fine} = c. 37.3 -	QU. LOW	Type 3b (m-l M) single-thread meandering river. Variable channel cross-
(A69/A70)			channel margin)	62.2 µm). Qu. poorly cemented, fairly cohesive.		sections - narrow & deep to broad & shallow. River channel of very limited
				Variable veg. of banks - some trees and bushes,		mobility at A49/A50, then fans out with mod. mobility withas very sinuous,
				mainly herbs and grasses - esp. near fields		qu. tortuous meanders within the c. 6 km valley length of this reach.
						Probable MODERATE to HIGH degree of AGGRADATION throughout
Across axis of fold						
A85/A86 to B33/B34	Unlith. floodplain seds.	QU. LOW	**Sands and muds**	**Muds and sands**. Variable veg. of banks - occ. trees	QU. LOW	Type 3b (m-l M) single-thread meandering river. Variable channel cross-
(B19/B20)				and bushes, mainly herbs and grasses - esp. near		sections - wide range from narrow & deep to broad & shallow/qu. deep.
				fields		River channel of quite low mobility with qu. angular meanders of qu. low
						amplitude and slightly decreasing amplitude with distance downstream.
						Probable LOW degree of AGGRADATION or LOW degree of INCISION
Downstream of fold						
B33/B34 to B49/B50	Unlith. floodplain seds.	QU. LOW	**Sands and muds**	**Muds and sands** - esp. clayey silt and clay. Variable	QU. LOW	Type 3b (m-l M) single-thread meandering river. Variable channel cross-
(B45/B46)				veg. of banks - occ. trees and bushes, mainly herbs and		sections - narrow & deep to broad & shallow. River channel of moderate
B49/B50 to B63/B64	Unlith. floodplain seds.	QU. LOW		grasses - esp. near fields		mobility, with meanders of decreasing amplitude over first c. 9 km valley
(B57/B58)						length, then curves to the S as one very long meander. Probable LOW to
						MODERATE degree of AGGRADATION

Appendix 5.6 (a)	STRUCTURAL GEOLOGY					LOCATION	HUMAN ACTIVITIES		
Summary of various data for	Estimate of	Width of	Approx. probable	Approx.	Approx.	Location of river reach	Short description of floodplain land use	Short description of human river channel	Estimate of
river reaches of the River Karun	degree of	geological	location of fold	distance from	distance from	including		modifications	overall degree
associated with the Dorquain	development	structure	"core" (part of	fold "core" to	fold "nose" to	General location			of human
Oilfield Anticline	(and erosion)	where crossed	fold which	where crossed	where crossed	Start and end survey			impact
	of geological	by river (km)	probably emerged	by river (km	by river (km	locations for reach			
	structure	(where	first, where	along fold axis	along fold axis	(Location for channel			
		applicable)	applicable)	or its proj.)	or its proj.)	measurements)			
DORQUAIN OILFIELD ANTICLINE						DORQUAIN OILFIELD ANTICLINE (R. Karun)			
Emerging anticline: Fold axis probably	Emerging	9.2	Very uncertain -	26.5	14.3	**Upstream** of fold (including near-straight reach and flow parallel to E limb)			
oriented roughly S-N, probably	fold of very	(approx.	possibly in		(approx.	C37/C38 to C63/C64	Extensive agriculture (fields and cultivation)	Near-straight NE-SW reach from Dorquain to	HIGH
associated with the N-S trending	limited	projection)	vicinity of		- location of	(C53/C54)	over floodplains, becoming slightly less	Masudi (C79/80 to E3/F3) with gen. deep	
Burgan-Azadegan High of the Abadan	surface		30°43' N 48°16' E		fold "nose"	C63/C64 to C71/C72	downstream. Veg. of bushes, herbs and	channels, probably related to the course of an	
Plain, SE Iraq and Kuwait, other	expresssion				very uncertain)	(C63/C64)	grasses on floodplains next to river	ancient canal (GBNID, 1945). River appears to	
details uncertain as fold has very	- less than					C71/C72 to C79/C80		alter course to flow along this reach, with	
limited surface expression	2 m above					(C73/C74)		meandering courses both upstr. and downstr.	
	surrounding							being roughly N-S. Various irrigation canals	
	plains							extract from both banks	
Hinge length, L = 26 km (approx.)						C79/C80 to C85/C86			
Fold width, W = 13.7 km (approx.)						(C81/C82)			
Aspect ratio, AR = L / W = 1.9						C85/C86 to E3/F3			
Fold Symmetry Index, FSI =						(E3/F3)			
Shorter limb width / (0.5 W) = 0.92									
(approximate values based on									
measurements from Maleki et al.,						E3/F3 to E12/F12			
2006 and oilfield maps)						(E9/F9)			
Possible fold type:									
Detachment fold									
						Across axis of fold (and slightly downstream of fold)			
						E12/F12 to E15/F15	Quite extensive agriculture over floodplains,	Near-straight NE-SW reach associated with the	VERY HIGH
						(E13/F13)	slightly less in the middle reach. Veg. of	Haffar cut (a canal probably orig. dug in 10th	
						E15/F15 to E19/F19	bushes, herbs and grasses next to river	Cent. AD, with significant widening and dam	
						(E16/F16)		construction in mid-18th Cent. AD)	
						E19/F19 to E27/F27			
						(E23/F23)			

Appendix 5.6 (b)	RIVER GEOMORPHOLOGY																RIVER HYDROLOGY		
Summary of various data for river reaches of the River Karun associated with the Dorquain Oilfield Anticline	Straight-line valley length of reach (km)	General course direction of reach (bearing to nearest 10°)	Channel pattern type (using simple classification of Schumm (1981, 1985)	Channel sinuosity (no units)	Average meander wave-length (m)	Meander type	Overall channel width (m) (Approx. range for reach)	Channel width (m)	Channel depth (m)	Channel width: depth ratio (no units)	Approx. cross-sectional shape of channel(s)	Estimate of av. height of channel banks above channel water surface (m)	Estimate of av. height of floodplain or valley above channel water surface (m)	Channel water surface slope (m m-1)	Projected-channel water surface slope (m m-1)	Valley slope (m m-1)	Average daily water discharge (data from gauging sta.) (m3 s-1)	Specific stream power (W m-2)	Stream power per unit length (W m-1)
				S	λ		W_{max}	w	d	w / d				s	S_p	S_v	Q	ω	Ω
DORQUAIN OILFIELD ANTICLINE (R. Karun)																			
Upstream of fold (including near-straight reach and flow parallel to E limb)																			
C37/C38 to C63/C64	6.458	S (180°)	Type 3b (m-l M)	2.751	4,800	Irreg/tort,	250	232.70	8.60	27.1	Triang.	2.18	2.8	0.0000422	0.0001161	0.0001703	644	1.143	266.0
(C53/C54)						qu. angular													
C63/C64 to C71/C72	3.020	S (190°)	Type 3b (m-l M)	1.873	3,500	moderate	330	299.56	6.80	44.1	Triang.	2.54	2.8	0.0000495	0.0000927	0.0002318	644	1.041	312.0
(C63/C64)						to high													
C71/C72 to C79/C80	5.320	SSW (200°)	Type 3b (m-l M)	1.082	5,400	migr. rate	230	196.96	7.20	27.4	Trapez.	3.03	3.0	0.0000087	0.0000094	0.0000188	644	0.278	54.7
(C73/C74)			/Type 2 (m-l S)				(Range 140												
							to 410 m)												
C79/C80 to C85/C86	4.536	SW (230°)	Type 2 (m-l S)	1.002	—	—	340	294.90	12.60	23.4	Trapez./	2.18	1.8	0.0000770	0.0000772	0	644	1.646	485.4
(C81/C82)											Irreg.								
C85/C86 to E3/F3	6.783	SW (230°)	Type 2 (m-l S)	1.002	—	—	200	195.29	8.40	23.2	Rect.	2.88	2.6	0.0000132	0.0000133	-0.0000442	644	0.427	83.4
(E3/F3)							(Range 190												
							to 510 m)												
E3/F3 to E12/F12	11.055	S (180°)	Type 3b (m-l M)	1.675	4,500	Irreg.,	300	268.49	6.00	44.7	Rect.	1.48	1.6	0.0000140	0.0000235	0..0001719	644	0.330	88.5
(E9/F9)						qu. angular	(Range 140										(Khorramshahr		
						mod./low	to 420 m)										R. Karun)		
						migr. rate													
Across axis of fold (and slightly downstream of fold)																			
E12/F12 to E15/F15	5.687	SSW (200°)	Type 2 (m-l S)	1.049	—	—	250	230.69	6.70	34.4	Rect.	1.63	1.9	0.0000637	0.0000668	-0.0001407	644	1.740	401.4
(E13/F13)						Reg, qu.													
E15/F15 to E19/F19	6.719	SW (220°)	Type 2 (m-l S)/	1.088	3,900	smooth,	200	171.64	14.40	11.9	Trapez.	1.51	1.6	0.0000356	0.0000387	0.0001042	644	1.306	224.1
(E16/F16)			Type 3b (m-l M)			low migr. rate													
E19/F19 to E27/F27	7.523	SW (230°)	Type 2 (m-l S)	1.014	—	—	200	181.56	9.50	19.1	Trapez.	1.88	1.5	0	0	0.0000266	644	0	0
(E23/F23)							(Range 130												
							to 320 m)												
E27/F27 to E35/F35	4.234	WSW (250°)	Type 3b (m-l M)	1.270	3,300	Reg, qu.		150.87	13.20	11.4	Trapez./			0.0000911			644	3.805	574.1
(E30/F30)						smooth,					Irreg.						(Khorramshahr		
						low migr. rate											R. Karun)		

Appendix 5.6 (c)	RIVER SEDIMENTOLOGY					SUMMARY
Summary of various data for river reaches of the River Karun associated with the Dorquain Oilfield Anticline	Main sediment or bedrock type in river valley	Estimate of degree of general erosion resistance	Short general description of channel **bed** surface sediments (including, in some cases, D_{coarse} (mean grain size for gravels, intermed. diam. in mm), D_{max} (mean grain size for 10 largest gravel clasts, intermed. diam. in mm), D_{fine} (mean grain size for fine gravels, sands and muds, in µm))	Short general description of channel **banks** (including, in some cases, B (% of channel bank sediments less than 63 µm), D_{fine} (mean grain size for fine gravels, sands and muds))	Estimate of degree of erosion resistance of channel banks	Short overall description of river reach, including estimate of probable overall degree of aggradation or incision
DORQUAIN OILFIELD ANTICLINE (R. Karun)						
Upstream of fold (including near-straight reach and flow parallel to E limb)						
C37/C38 to C63/C64	Unlith. floodplain seds.	QU. LOW	**Sands and muds**	**Mainly muds**. Variable veg. of banks - occ. trees and	QU. LOW/	The river reaches upstream of the fold show considerable variability. From
(C53/C54)				bushes, mainly herbs and grasses - esp. near fields	MODERATE	C37/C38 to C79/C80, there is a Type 3b (m-l M) single-thread meandering
C63/C64 to C71/C72	Unlith. floodplain seds.	QU. LOW				river flowing roughly S - qu. narrow & deep to broad & shallow channels of
(C63/C64)						mod. to high mobility with decreasing meander amplitude and sinuosity
C71/C72 to C79/C80	Unlith. floodplain seds.	QU. LOW				with distance downstream. From C79/C80 to E3/F3 (c. Dorquain - Masudi),
(C73/C74)						the river flows roughly SW as a Type 2 single-thread straight river - gen.
						deep channels of very limited mobility, probably related to the course of
						an ancient canal (GBNID, 1945). From E3/F3 to E12/F12, the river turns to
C79/C80 to C85/C86	Unlith. floodplain seds.	QU. LOW	**Sands and muds**	**Mainly muds** - esp. silt/clay and clay (Gasche et al.,	QU. LOW	flow roughly S once more as a Type 3b (m-l M) single-thread meandering
(C81/C82)				2004). Limited veg. of banks - mainly herbs and grasses		river - mod. narrow & deep channels of moderate to low mobility. Probable
C85/C86 to E3/F3	Unlith. floodplain seds.	QU. LOW				MODERATE degree of AGGRADATION for the meandering reaches,
(E3/F3)						probably changing to LOW degree of INCISION for Dorquain - Masudi near-
						straight reach
E3/F3 to E12/F12	Unlith. floodplain seds.	QU. LOW	**Sands and muds**	**Mainly muds**. Limited veg. of banks - mainly herbs and	QU. LOW	
(E9/F9)				grasses		
Across axis of fold (and slightly downstream of fold)						
E12/F12 to E15/F15	Unlith. floodplain seds.	QU. LOW	**Sands and muds**	**Mainly muds**. Limited veg. of banks - mainly herbs and	QU. LOW	Type 2 (m-l S) single-thread straight river, with very slight meandering in
(E13/F13)				grasses		the middle reach. Generally narrow and deep channels of very limited
E15/F15 to E19/F19	Unlith. floodplain seds.	QU. LOW				mobility. Near-straight reach associated with the Haffar cut, a canal
(E16/F16)						probably originally dug in the 10th Cent. AD, with significant widening and
E19/F19 to E27/F27	Unlith. floodplain seds.	QU. LOW				dam construction in the mid-18th Cent. AD. Probable MODERATE degree
(E23/F23)						of INCISION, with LOW or NO INCISION at downstream end

Appendix 6.1 River reaches of the River Karun (River **Shuteyt** branch) from Gotvand to the Persian Gulf	Valley distance from Gotvand Regulating Dam (m)	Valley distance from Gotvand Regulating Dam (km)	Straight-line valley length of reach (km)	TOTAL ALONG-CHANNEL LENGTH (for "coherent sections" of river) (m)	Channel length of reach (km)	Average river floodplain elevation (m NCC datum)	Average channel bank elevation (m NCC datum)	Average river water surface elevation (m NCC datum)	Deepest channel bed elevation (m NCC datum)	General course direction of reach (bearing to nearest 10°)	Channel pattern type (classif. of Schumm 1981, 1985)	Channel sinuosity (no units)	Braiding index (no units)	Channel width (m)
					Lc							S		w
Gotvand Dam/LG2/LG5 (& upstream of dam)	0.0000	0	-4.371	0	-4.918	69.8	68.17	65.26	55.02	W (280°)	3b / 2	1.125	1	
LG2 to LG16 Turkalaki Ant.	5854.5521	5.855	5.855	6285.6496	6.286	65.2	63.90	61.22	59.39	SSW (200°)	2 (m-l S)	1.074	1	121.60
LG16 to LB8	12240.7119	12.241	6.386	15024.2318	8.739	58.3	57.13	53.88	50.78	S (170°)	4 (M-B)	1.368	2.4	292.85
LB8 to LB19	18529.6021	18.530	6.289	25737.652	10.713	55.0	48.83	48.20	43.55	SE (130°)	Anastom.	1.704	2.0	320.61
LB19 to LB26	21405.1334	21.405	2.876	29604.7458	3.867	59.9	49.45	44.16	39.86	S (180°)	4 (M-B)	1.345	1.7	284.53
LB26 to LB31 Shushtar Ant.	25186.8090	25.187	3.782	35015.7262	5.411	48.3	47.43	40.92	36.72	SSW (200°)	3b (m-l M)	1.431	1	179.55
LB31 to LB34 Shushtar Ant.	28295.1918	28.295	3.108	39146.9001	4.131	46.5	42.68	39.26	28.86	SSW (200°)	3b (m-l M)	1.329	1	99.18
LB34 to LB 46/1	32025.7618	32.026	3.731	44341.0359	5.194	38.3	38.12	36.09	34.09	WSW (250°)	4 (M-B)	1.392	2.0	214.37
LB46/1 to LB49 Qal'eh Surkheh Ant.	34598.7618	34.599	2.573	47347.6478	3.007	37.4	37.09	33.29	30.68	SSW (200°)	Anastom.	1.168	2.0	245.87
LB49 to LB56	40327.7618	40.328	5.729	54697.1446	7.349	32.6	30.55	28.89	23.56	SW (220°)	Anastom.	1.283	3.1	461.96
LB56 to LB 68/1	45760.1090	45.760	5.432	62244.894	7.548	28.7	28.73	23.55	19.95	SSE (160°)	4 / 3b	1.389	2.1	188.25
LB68/1 to LB84	54814.8453	54.815	9.055	78522.54118	16.278	26.5	25.09	19.03	15.61	SE (140°)	3b (m-l M)	1.798	1.1	174.35
LB84 to LB101 Sardarabad Ant.	65097.6889	65.098	10.283	95458.72788	16.936	22.4	22.50	18.97	15.25	S (190°)	3b (m-l M)	1.647	1	169.80
LB101 to LB116	76149.5248	76.150	11.052	114047.8362	18.589	22.7	22.19	18.17	4.68	S (190°)	3b (m-l M)	1.682	1	292.10
LB116 to LM1	83139.0754	83.139	6.990	125946.3861	11.899	19.7	19.52	16.32	10.20	SE (130°)	3b (m-l M)	1.702	1	243.92
LM1 to LM8 Ramin Oilfield Ant.	89464.0040	89.464	6.325	132654.9956	6.709	23.2	18.14	16.32	8.77	S (180°)	2 (m-l S)	1.061	1	200.65
LM8 to LM16 Ramin Oilfield Ant.	97666.3645	97.666	8.202	140941.4029	8.286	20.5	19.84	15.40	9.10	S (180°)	2 (m-l S)	1.010	1	306.45
LM16 to LM20	102199.2478	102.199	4.533	145669.3689	4.728	19.0	18.99	14.76	3.56	S (190°)	2 (m-l S)	1.043	1	258.86
LM20 to LM36	109490.4205	109.490	7.291	163666.7808	17.997	17.7	17.33	13.25	8.25	WSW (250°)	3b (m-l M)	2.468	1	303.15
LM36 to LM61	119961.0900	119.961	10.471	186706.3832	23.040	16.2	15.46	12.06	7.66	SW (220°)	3b (m-l M)	2.200	1.1	315.04
LM61 to A11/A12	125948.1000	125.948	5.987	199678.0984	12.972	16.5	15.80	11.61	5.51	SSW (210°)	3b (m-l M)	2.167	1.2	294.48
A11/A12 to B11/B12 Ahvaz Ant.	129949.8400	129.950	4.002	203866.6132	4.189	15.0	13.27	9.04	4.44	SW (220°)	2 (m-l S)	1.047	1.2	320.27
B11/B12 to A49/A50	138727.7400	138.728	8.778	213330.4728	9.464	13.4	10.68	8.76	-2.94	SSW (200°)	2 (m-l S)	1.078	1	263.84
A49/A50 to A85/A86	145355.2600	145.355	6.628	235090.9715	21.760	13.3	12.73	7.46	2.56	W (270°)	3b (m-l M)	3.283	1	343.65
A85/A86 to B33/B34 Ab-e Teymur O. Ant.	156526.9400	156.527	11.172	255849.3747	20.758	10.0	10.21	7.02	0.92	SW (230°)	3b (m-l M)	1.858	1	291.26
B33/B34 to B49/B50	166039.5100	166.040	9.513	267040.9308	11.192	7.9	9.43	6.25	0.45	SW (230°)	3b (m-l M)	1.177	1	281.12
B49/B50 to B63/B64	173677.3600	173.677	7.638	276147.6636	9.107	8.3	8.66	5.56	1.36	S (180°)	3b (m-l M)	1.192	1	212.80
B63/B64 to B79/B80	178859.2500	178.859	5.182	285813.9946	9.666	7.3	7.73	4.80	-3.10	SSW (210°)	3b (m-l M)	1.865	1	186.82
B79/B80 to B97/B98	187747.5200	187.748	8.888	296533.3872	10.719	6.3	7.66	4.18	-4.52	SSW (200°)	3b (m-l M)	1.206	1	230.23
B97/B98 to C37/C38	198121.8300	198.122	10.374	318252.1795	21.719	5.9	8.09	3.49	-8.11	SE (130°)	3b (m-l M)	2.094	1	286.14
C37/C38 to C63/C64	204579.3700	204.579	6.458	336016.0635	17.764	4.8	5.28	2.74	-4.06	S (180°)	3b (m-l M)	2.751	1	232.70
C63/C64 to C71/C72	207598.9300	207.599	3.020	341670.2085	5.654	4.1	5.07	2.46	-10.74	S (190°)	3b (m-l M)	1.873	1	299.56
C71/C72 to C79/C80	212918.6900	212.919	5.320	347423.7135	5.754	4.0	5.09	2.41	-6.09	SSW (200°)	3b / 2	1.082	1	196.96
C79/C80 to C85/C86	217454.8100	217.455	4.536	351966.7586	4.543	4.0	4.25	2.06	-4.74	SW (230°)	2 (m-l S)	1.002	1.2	294.90
C85/C86 to E3/F3	224238.2700	224.238	6.783	358764.9299	6.798	4.3	5.87	1.97	-6.43	SW (230°)	2 (m-l S)	1.002	1.1	195.29
E3/F3 to E12/F12	235293.1900	235.293	11.055	377276.6443	18.512	2.4	3.19	1.71	-10.49	S (180°)	3b (m-l M)	1.675	1	268.49
E12/F12 to E15/F15 Dorquain O. Ant.	240980.6700	240.981	5.687	383240.5718	5.964	3.2	3.55	1.33	-4.67	SSW (200°)	2 (m-l S)	1.049	1	230.69
E15/F15 to E19/F19 Dorquain O. Ant.	247699.7600	247.700	6.719	390548.2887	7.308	2.5	3.14	1.07	-14.73	SW (220°)	2 / 3b	1.088	1	171.64
E19/F19 to E27/F27	255222.3200	255.222	7.523	398176.6274	7.628	2.3	2.27	1.07	-17.93	SW (230°)	2 (m-l S)	1.014	1	181.56
E27/F27 to E39/F39	260462.4300	260.462	5.240	403943.2984	5.767	2.4	3.42	0.54	-2.76	SE (140°)	3b / 2	1.100	1	159.23
E39/F39 to LK91	310962.4300	310.962	50.500	461943.2984	58.000	1.7	1.88	-0.21	-6.80	SE (140°)	3b (m-l M)	1.149	1	241.77

Appendix 6.1 River reaches of the River Karun (River **Shuteyt** branch) from Gotvand to the Persian Gulf	Channel width: depth ratio (no units)	Channel water surface slope (m m⁻¹)	Projected-channel water surface slope (m m⁻¹)	Valley slope (m m⁻¹)	Total along channel distance	Specific stream power (W m⁻²)	Channel-belt area (km²)	Average channel-belt width (km)	Greatest channel bank migration distance 1966/68 - 2001 (m)	Greatest channel bank migration distance 1966/68 - 2001 (m)	Greatest channel bank migration distance 1966/68 - 2001 (m)	Area of channel migration 1966/68 - 2001 (migration OUT) (m²)	Area of channel migration 1966/68 - 2001 (migration IN) (m²)	Total area of migration polygons 1966/68 - 2001 (m²)	Average channel migration rate 1966/68 - 2001 (m yr⁻¹)
	w / d	s	sp	sv		ω			L BANK	R BANK				A	Rm
Gotvand Dam/LG2/LG5 (& upstream of dam)					0				-275	-196	-275	341531	33198	374729	-2.228
LG2 to LG16 Turkalaki Ant.	17.6	0.0006427	0.0006901	0.0007857	6285.6496	16.339	7.1097	1.214	200	223	223	94426	141146	235572	1.096
LG16 to LB8	127.9	0.0008394	0.0011486	0.0010805	15024.2318	8.861	16.6892	2.613	494	480	494	166410	766792	933202	3.123
LB8 to LB19	127.2	0.0005306	0.0009040	0.0005247	25737.652	5.116	23.1395	3.679	1626	1620	1626	2820077	564903	3384980	9.239
LB19 to LB26	175.6	0.0010434	0.0014032	-0.0017040	29604.7458	11.336	7.1007	2.469	956	907	956	1046249	108133	1154382	8.728
LB26 to LB31 Shushtar Ant.	37.1	0.0005988	0.0008568	0.0030674	35015.7262	11.451	1.8340	0.485	411	371	411	30493	297816	328309	1.774
LB31 to LB34 Shushtar Ant.	27.6	0.0004018	0.0005340	0.0005791	39146.9001	13.912	1.8018	0.580	259	205	259	42620	164780	207400	1.468
LB34 to LB 46/1	72.4	0.0006103	0.0008497	0.0021981	44341.0359	9.776	3.3331	0.893	432	356	432	429186	199697	628883	3.540
LB46/1 to LB49 Qal'eh Surkheh Ant.	67.2	0.0009313	0.0010882	0.0003498	47347.6478	13.006	5.797	2.253	337	802	802	330367	125109	455476	4.430
LB49 to LB56	86.7	0.0005987	0.0007680	0.0008972	54697.1446	4.450	16.587	2.895	1644	1550	1644	3502928	1039534	4542462	18.072
LB56 to LB 68/1	51.9	0.0007075	0.0009830	0.0007179	62244.894	14.706	12.7919	2.355	1119	1104	1119	708694	1560935	2269629	8.792
LB68/1 to LB84	76.5	0.0002778	0.0004992	0.0002430	78522.54118	6.234	16.3417	1.805	1039	1104	1104	2312490	1396799	3709289	6.663
LB84 to LB101 Sardarabad Ant.	38.8	0.0000035	0.0000058	0.0003987	95458.72788	0.082	34.5396	3.359	589	554	589	1793413	757107	2550520	4.403
LB101 to LB116	63.4	0.0000433	0.0000728	-0.0000271	114047.8362	0.580	27.5611	2.494	1598	1564	1598	779995	2696007	3476002	5.468
LB116 to LM1	38.1	0.0001551	0.0002640	0.0004292	125946.3861	2.488	17.4346	2.494	739	689	739	1321986	674675	1996661	4.907
LM1 to LM8 Ramin Oilfield Ant.	24.9	0.0000007	0.0000008	-0.0005534	132654.9956	0.021	4.5876	0.725	76	117	117	7904	159472	167376	0.730
LM8 to LM16 Ramin Oilfield Ant.	95.8	0.0001104	0.0001116	0.0003292	140941.4029	2.027	2.8225	0.344	162	160	162	67313	134326	201639	0.712
LM16 to LM20	52.8	0.0001354	0.0001412	0.0003309	145669.3689	2.941	4.9171	1.085	75	116	116	48379	88657	137036	0.847
LM20 to LM36	56.1	0.0000839	0.0002071	0.0001783	163666.7808	1.557	35.8735	4.920	323	311	323	759798	909151	1668949	2.711
LM36 to LM61	78.8	0.0000517	0.0001137	0.0001433	186706.3832	0.921	46.3959	4.431	651	478	651	1771014	1428511	3199525	4.061
LM61 to A11/A12	67.2	0.0000347	0.0000752	-0.0000501	199678.0984	0.663	12.3349	2.060	95	315	315	67519	279029	346548	0.781
A11/A12 to B11/B12 Ahvaz Ant.	32.7	0.0006136	0.0006422	0.0003748	203866.6132	10.777	2.6270	0.656	173	197	197	102684	41654	144338	1.008
B11/B12 to A49/A50	30.7	0.0000296	0.0000319	0.0001823	213330.4728	0.631	8.0589	0.918	320	274	320	547153	496458	1043611	3.224
A49/A50 to A85/A86	54.5	0.0000597	0.0001962	0.0000151	235090.9715	0.978	33.1509	5.002	323	271	323	1059384	576464	1635848	2.198
A85/A86 to B33/B34 Ab-e Teymur O. Ant.	31.3	0.0000212	0.0000394	0.0002954	255849.3747	0.409	29.0912	2.604	356	374	374	614971	1396543	2011514	2.833
B33/B34 to B49/B50	46.1	0.0000614	0.0000809	0.0002208	267040.9308	1.228	7.9027	0.831	134	177	177	38011	337747	375758	0.982
B49/B50 to B63/B64	28.4	0.0000758	0.0000903	-0.0000524	276147.6636	2.003	8.0620	1.056	256	214	256	91570	718561	810131	2.601
B63/B64 to B79/B80	23.6	0.0000786	0.0001467	0.0001930	285813.9946	2.651	8.4606	1.633	339	295	339	442988	318062	761050	2.302
B79/B80 to B97/B98	26.5	0.0000578	0.0000698	0.0001125	296533.3872	1.582	9.7753	1.100	141	191	191	191447	244835	436282	1.190
B97/B98 to C37/C38	24.7	0.0000318	0.0000665	0.0000386	318252.1795	0.700	35.5582	3.428	748	799	799	1999979	400209	2400188	3.231
C37/C38 to C63/C64	27.1	0.0000422	0.0001161	0.0001703	336016.0635	1.143	33.7872	5.232	634	598	634	838892	1175382	2014274	3.316
C63/C64 to C71/C72	44.1	0.0000495	0.0000927	0.0002318	341670.2085	1.041	7.8022	2.584	239	159	239	66510	353474	419984	2.172
C71/C72 to C79/C80	27.4	0.0000087	0.0000094	0.0000188	347423.7135	0.278	3.1817	0.598	79	93	93	63381	68864	132245	0.672
C79/C80 to C85/C86	23.4	0.0000770	0.0000772	0.0000000	351966.7586	1.646	2.4760	0.546	110	82	110	15261	115466	130727	0.841
C85/C86 to E3/F3	23.2	0.0000132	0.0000133	-0.0000442	358764.9299	0.427	3.2067	0.473	247	43	247	23009	784003	807012	3.471
E3/F3 to E12/F12	44.7	0.0000140	0.0000235	0.0001719	377276.6443	0.330	13.3594	1.208	296	105	296	177563	974053	1151616	1.819
E12/F12 to E15/F15 Dorquain O. Ant.	34.4	0.0000637	0.0000668	-0.0001407	383240.5718	1.740	2.8938	0.509	195	47	195	78669	95804	174473	0.855
E15/F15 to E19/F19 Dorquain O. Ant.	11.9	0.0000356	-0.0002694	0.0001042	390548.2887	1.306	2.5839	0.385	179	56	179	43523	174539	218062	0.873
E19/F19 to E27/F27	19.1	0	0.000115652	0.0000266	398176.6274	0	1.7174	0.228	65	37	65	6955	105110	112065	0.430
E27/F27 to E39/F39	48.3	0.0000919	-0.0002195	-0.0000191	403943.2984	3.636	2.6916	0.514	67	111	111	171741	11011	182752	0.927
E39/F39 to LK91	36.7	0.0000128	0.0000305	0.0000139	461943.2984	0.334	39.9321	0.791	328	323	328	1291522	7367211	8658733	4.365

Appendix 6.2 River reaches of the River Karun (River **Gargar** branch) from Gotvand to near Zargan-e Buzurg	Valley distance from Gotvand Regulating Dam (m)	Valley distance from Gotvand Regulating Dam (km)	Straight-line valley length of reach (km)	TOTAL ALONG-CHANNEL LENGTH (for "coherent sections" of river) (m)	Channel length of reach (km)	Average river floodplain elevation (m NCC datum)	Average channel bank elevation (m NCC datum)	Average river water surface elevation (m NCC datum)	Deepest channel bed elevation (m NCC datum)	General course direction of reach (bearing to nearest 10°)	Channel pattern type (classif. of Schumm 1981, 1985)	Channel sinuosity (no units)	Braiding index (no units)	Channel width (m)	Channel width: depth ratio (no units)	Channel water surface slope (m m^{-1})	Projected-channel water surface slope (m m^{-1})	Valley slope (m m^{-1})	Total along channel distance	Specific stream power (W m^{-2})	Channel-belt area (km^2)	Average channel-belt width (km)	Greatest channel bank migration distance 1966/68 - 2001 (m)	Greatest channel bank migration distance 1966/68 - 2001 (m)	Greatest channel bank migration distance 1966/68 - 2001 (m)	Area of channel migration 1966/68 - 2001 (migration OUT) (m^2)	Area of channel migration 1966/68 - 2001 (migration IN) (m^2)	Total area of migration polygons 1966/68 - 2001 (m^2)	Average channel migration rate 1966/68 - 2001 (m yr^{-1})
					Lc							S		w	w / d	s	sp	sv		ω			L BANK	R BANK				A	Rm
Gotvand Dam/LG2/LG5 (& upstream of dam)	0	0	-4.371	0	-4.918	69.8	68.17	65.26	55.02	W (280°)	3b / 2	1.125	1						0				-275	-196	-275	341531	33198	374729	-2.228
LG2 to LG16 Turkalaki Ant.	5854.5521	5.855	5.855	6285.6496	6.286	65.2	63.90	61.22	59.39	SSW (200°)	2 (m-l S)	1.074	1	121.60	17.6	0.0006427	0.0006901	0.0007857	6285.6496	16.339	7.1097	1.214	200	223	223	94426	141146	235572	1.096
LG16 to LB8	12240.7119	12.241	6.386	15024.2318	8.739	58.3	57.13	53.88	50.78	S (170°)	4 (M-B)	1.368	2.4	292.85	127.9	0.0008394	0.0011486	0.0010805	15024.2318	8.861	16.6892	2.613	494	480	494	166410	766792	933202	3.123
LB8 to LB19	18529.6021	18.530	6.289	25737.652	10.713	55.0	48.83	48.20	43.55	SE (130°)	Anastom.	1.704	2.0	320.61	127.2	0.0005306	0.0009040	0.0005247	25737.652	5.116	23.1395	3.679	1626	1620	1626	2820077	564903	3384980	9.239
LB19 to LB26	21405.1334	21.405	2.876	29604.7458	3.867	59.9	49.45	44.16	39.86	S (180°)	4 (M-B)	1.345	1.7	284.53	175.6	0.0010434	0.0014032	-0.0017040	29604.7458	11.336	7.1007	2.469	956	907	956	1046249	108133	1154382	8.728
LB26 to LB31 Shushtar Ant.	25186.809	25.187	3.782	35015.7262	5.411	48.3	47.43	40.92	36.72	SSW (200°)	3b (m-l M)	1.431	1	179.55	37.1	0.0005988	0.0008568	0.0030674	35015.7262	11.451	1.8340	0.485	411	371	411	30493	297816	328309	1.774
LB31 to LB34 Shushtar Ant.	28307.3337	28.307	3.121	39116.1817	4.100	46.5	42.68	39.26	28.86	SSW (200°)	3b (m-l M)	1.314	1	99.18	27.6	0.0004048	0.0005320	0.0005768	39116.1817	13.912	1.8018	0.577	259	205	259	42620	164780	207400	1.479
LB34 to L3 Qal'eh Surkheh Ant.	29083.7381	29.084	0.776	39944.1581	0.828	48.4	43.21	39.43	33.73	SSW (200°)	2 (m-l S)	1.066	1	30.07	7.7	-0.0001993	-0.0002125	-0.0024472	39944.1581	-2.983	0.0525	0.068	23	20	23	0	3240	3240	0.114
L3 to L15 Qal'eh Surkheh Ant .	33718.9953	33.719	4.635	45341.8478	5.398	43.0	27.09	23.98	22.05	S (190°)	3a / 2	1.164	1	72.24	62.3	0.0028614	0.0033321	0.0011650	45341.8478	17.825	0.8941	0.193	44	42	44	0	14925	14925	0.081
L15 to L20	36755.459	36.755	3.036	49116.0612	3.774	25.8	25.42	21.88	19.78	SE (140°)	3a (s-l M)	1.243	1	34.78	16.6	0.0005577	0.0006932	0.0056645	49116.0612	7.216	1.6648	0.548	0	0	0	0	0	0	0
L20 to L37	44127.5601	44.128	7.372	59821.8198	10.706	28.2	24.27	21.99	17.02	SE (140°)	3a (s-l M)	1.452	1	38.34	11.4	-0.0000103	-0.0000149	-0.0003256	59821.8198	-0.121	5.1025	0.692	20	17	20	0	6763	6763	0.018
L37 to L44	48815.1368	48.815	4.688	65824.6862	6.003	24.3	23.69	21.80	17.00	SE (130°)	3a (s-l M)	1.281	1	38.79	11.1	0.0000308	0.0000395	0.0008320	65824.6862	0.357	1.6873	0.360	24	0	24	0	2507	2507	0.012
L44 to L56	57642.1707	57.642	8.827	76184.6253	10.360	24.2	23.02	21.68	17.18	S (170°)	3a (s-l M)	1.174	1	40.61	14.4	0.0000116	0.0000136	0.0000113	76184.6253	0.129	2.6807	0.304	23	0	23	0	8882	8882	0.025
L56 to L62	62292.611	62.293	4.650	84770.0376	8.585	23.9	22.50	21.55	17.55	S (170°)	3a (s-l M)	1.846	1	48.42	8.6	0.0000151	0.0000280	0.0000645	84770.0376	0.140	2.5497	0.548	23	37	37	6508	6607	13115	0.045
L62 to L71	65396.4862	65.396	3.104	94688.2709	9.918	22.0	21.59	20.99	14.19	SSW (200°)	3a (s-l M)	3.195	1	39.83	8.0	0.0000565	0.0001804	0.0006121	94688.2709	0.638	4.5003	1.450	15	27	27	1346	3666	5012	0.015
L71 to L78	69496.3705	69.496	4.100	100241.2348	5.553	22.7	21.61	19.43	16.34	SSW (210°)	3a (s-l M)	1.354	1	38.26	8.7	0.0002809	0.0003805	-0.0001707	100241.2348	3.304	1.2394	0.302	102	109	109	24427	6117	30544	0.161
L78 to L88	72332.0419	72.332	2.836	107694.9137	7.454	27.2	21.22	18.62	16.42	WSW (250°)	3a (s-l M)	2.629	1	34.62	8.4	0.0001087	0.0002856	-0.0015869	107694.9137	1.411	1.5998	0.564	265	271	271	10294	99220	109513	0.430
L88 to L95 Kupal Ant.	77553.7162	77.554	5.222	114268.1905	6.573	32.7	20.88	17.78	12.98	SSW (210°)	3a (s-l M)	1.259	1	39.76	10.8	0.0001278	0.0001609	-0.0010533	114268.1905	1.446	1.2234	0.234	13	27	27	0	2251	2251	0.010
L95 to LM1 Kupal Ant.	83039.0424	83.039	5.485	121402.115	7.134	19.7	19.52	16.32	10.20	SSW (210°)	3a (s-l M)	1.301	1	24.86	8.3	0.0002047	0.0002662	0.0023700	121402.115	3.705	0.9589	0.175	27	17	27	0	5703	5703	0.023
LM1 to LM8 Ramin Oilfield Ant.	89363.971	89.364	6.325	128110.7245	6.709	23.2	18.14	16.32	8.77	S (180°)	2 (m-l S)	1.061	1	200.65	24.9	0.0000007	0.0000008	-0.0005534	128110.7245	0.021	4.5876	0.725	76	117	117	7904	159472	167376	0.730
LM8 to LM16 Ramin Oilfield Ant.	97566.3315	97.566	8.202	136397.1318	8.286	20.5	19.84	15.40	9.10	S (180°)	2 (m-l S)	1.010	1	306.45	95.8	0.0001104	0.0001116	0.0003292	136397.1318	2.027	2.8225	0.344	162	160	162	67313	134326	201639	0.712
LM16 to LM20	102099.2148	102.099	4.533	141125.0978	4.728	19.0	18.99	14.76	3.56	S (190°)	2 (m-l S)	1.043	1	258.86	52.8	0.0001354	0.0001412	0.0003309	141125.0978	2.941	4.9171	1.085	75	116	116	48379	88657	137036	0.847
LM20 to LM36	109390.3875	109.390	7.291	159122.5097	17.997	17.7	17.33	13.25	8.25	WSW (250°)	3b (m-l M)	2.468	1	303.15	56.1	0.0000839	0.0002071	0.0001783	159122.5097	1.557	35.8735	4.920	323	311	323	759798	909151	1668949	2.711
LM36 to LM61	119861.0537	119.861	10.471	182162.1121	23.040	16.2	15.46	12.06	7.66	SW (220°)	3b (m-l M)	2.200	1.1	315.04	78.8	0.0000517	0.0001137	0.0001433	182162.1121	0.921	46.3959	4.431	651	478	651	1771014	1428511	3199525	4.061

Appendix 6.3	Valley distance fror	Valley	Straight-	TOTAL ALONG-CHANNEL	Channel	Average	Average	Average	Deepest	General	Channel	Channel	Braiding	Channel	Channel	Channel	Projected-	Valley	Total	Specific	Channel-	Average	Greatest	Greatest	Greatest	Area of	Area of	Total area	Average
River reaches of the River Dez	(m)	distance from	line	LENGTH (for "coherent	length	river	channel	river water	channel	course	pattern	sinuosity	index	width	width:	water	channel	slope	along	stream	belt	channel-	channel bank	channel bank	channel bank	channel	channel	of migration	channel
from northern Dezful to near		Dezful	valley	sections" of river)	of reach	floodplain	bank	surface	bed	direction	type	(no units)	(no units)	(m)	depth	surface	water	(m m^{-1})	channel	power	area	belt	migration	migration	migration	migration	migration	polygons	migration
Zargan-e Buzurg		Regulating	length	(m)	(km)	elevation	elevation	elevation	elevation	of reach	(classif.				ratio	slope	surface		distance	(W m^{-2})	(km^2)	width	distance	distance	distance	1966/68 - 2001	1966/68 - 2001	1966/68 - 2001	rate
		Dam	of reach			(m NCC	(m NCC	(m NCC	(m NCC	(bearing	of Schumm				(no units)	(m m^{-1})	slope					(km)	1966/68 - 2001	1966/68 - 2001	1966/68 - 2001	(migration OUT)	(migration IN)		1966/68 - 2001
		(km)	(km)			datum)	datum)	datum)	datum)	to nearest	1981, 1985)						(m m^{-1})						(m)	(m)	(m)	(m^2)	(m^2)	(m^2)	(m yr^{-1})
					Lc					10°)		S		w	w / d	s	sp	sv		ω			L BANK	R BANK				A	Rm
Dezful reg dam / L1-A / L2 (& upstr. of dam)	0	0	-6.899	0	-8.354	141.9	125.80	122.02	114.62	SW (230°)	3b (m-l M)	1.211	1						0			0.300	405	293	405			695410	2.434
L1-A / L2 to L6	2469.343	2.469	2.469	2558.1856	2.558	125.1	120.89	120.32	114.32	SW (230°)	2 (m-l S)	1.036	1	93.52	20.8	0.0006645	0.0006884	0.0068034	2558.1856	15.987	0.5706	0.231	86	45	86	38065	11437	49502	0.566
L6 to L40 Dezful Uplift	6334.1771	6.334	3.865	6825.7402	4.268	116.0	114.34	112.11	109.82	SW (220°)	2 / Anastom.	1.104	1.9	68.19	18.9	0.0019238	0.0021243	0.0023546	6825.7402	63.478	9.9666	2.579	110	270	270	59529	18342	77871	0.534
L40 to L54-A	16601.606	16.602	10.267	18530.8182	11.705	85.7	85.90	84.47	82.27	SSW (200°)	Anastom.	1.140	6.5	137.13	98.0	0.0023614	0.0026920	0.0029511	18530.8182	38.745	78.7966	7.674	754	627	754	954638	1387973	2342611	5.852
L54-A to L76	20726.6201	20.727	4.125	24154.2929	5.623	79.3	74.66	74.13	71.73	S (180°)	Anastom.	1.363	4.1	88.03	40.0	0.0018387	0.0025067	0.0015515	24154.2929	49.857	18.9224	4.587	417	457	457	339474	611662	951136	4.946
L76 to L93	28324.1727	28.324	7.598	32351.7911	8.197	68.3	64.95	63.34	61.24	SSE (150°)	5 (B)	1.079	2.0	154.27	59.3	0.0013163	0.0014202	0.0014478	32351.7911	20.367	22.5941	2.974	774	728	774	415996	138491	554487	1.978
L93 to L100	34611.2961	34.611	6.287	39861.2072	7.509	56.5	55.87	54.07	51.45	SE (140°)	5 (B)	1.194	2.1	97.80	168.6	0.0012345	0.0014744	0.0018769	39861.2072	30.130	21.5916	3.434	682	696	696	1355025	125137	1480162	5.763
L100 to L109	40296.3341	40.296	5.685	46665.2273	6.804	49.7	49.61	47.16	43.96	SE (140°)	5 (B)	1.197	2.1	223.29	139.6	0.0010156	0.0012155	0.0011961	46665.2273	10.391	17.0295	2.995	1572	1322	1572	225995	3465242	3691237	15.863
L109 to L118	45369.3961	45.369	5.073	54178.0469	7.513	46.8	44.46	42.03	39.53	E (090°)	4 / 3b	1.481	1.3	83.50	39.8	0.0006828	0.0010112	0.0005716	54178.0469	19.519	17.1885	3.388	648	716	716	377153	530623	907776	3.533
L118 to L135	51060.712	51.061	5.691	61977.0005	7.799	43.0	42.63	38.30	36.67	SE (140°)	3b / 4	1.370	1.2	93.61	78.7	0.0004783	0.0006554	0.0006677	61977.0005	12.196	27.2485	4.788	1266	1295	1295	1404621	515800	1920421	7.200
L135 to L145	55179.0215	55.179	4.118	66913.7158	4.937	40.9	39.79	36.81	32.61	SW (220°)	3b (m-l M)	1.199	1	152.26	89.6	0.0003018	0.0003618	0.0005099	66913.7158	4.731	14.9140	3.621	1096	997	1096	688529	144867	833396	4.936
L145 to L158	60307.4429	60.307	5.128	77972.9153	11.059	38.1	34.71	33.13	28.93	ESE (120°)	3b (m-l M)	2.156	1	179.04	105.3	0.0003328	0.0007176	0.0005460	77972.9153	4.437	16.2245	3.164	521	462	521	575168	752720	1327888	3.511
L158 to L168	66034.0189	66.034	5.727	86087.0083	8.114	37.3	35.76	30.34	27.04	SE (130°)	3b (m-l M)	1.417	1	123.97	44.3	0.0003438	0.0004872	0.0001397	86087.0083	6.621	16.2153	2.832	1754	1775	1775	443473	2644752	3088225	11.129
L168 to L175 Sardarabad Ant.	71867.8753	71.868	5.834	92622.1561	6.535	34.3	33.98	28.38	23.08	SW (230°)	3b / 2	1.120	1	153.65	56.9	0.0002999	0.0003360	0.0005142	92622.1561	4.659	8.1819	1.402	210	257	257	163595	189017	352612	1.578
L175 to L190	82198.7444	82.199	10.331	108993.222	16.371	30.9	27.06	26.35	20.25	SE (130°)	3b (m-l M)	1.585	1.1	285.30	59.4	0.0001240	0.0001965	0.0003291	108993.222	1.039	50.3625	4.875	929	946	946	455790	2064890	2520680	4.502
L190 to L199	87659.1201	87.659	5.460	117885.7928	8.893	30.2	29.66	24.87	21.87	S (170°)	3b (m-l M)	1.629	1	194.49	62.7	0.0001664	0.0002710	0.0001282	117885.7928	2.042	33.2583	6.091	911	856	911	416376	1267962	1684338	5.538
L199 to L206 Shahur Ant.	91639.1108	91.639	3.980	125019.2776	7.133	29.2	28.46	23.67	20.97	SSW (200°)	3b (m-l M)	1.792	1	160.84	64.3	0.0001682	0.0003015	0.0002513	125019.2776	2.496	16.5687	4.163	308	281	308	243225	449923	693148	2.841
L206 to L214 Shahur Ant.	97998.1646	97.998	6.359	133096.2965	8.077	27.8	27.35	23.09	13.09	S (170°)	3b (m-l M)	1.270	1	161.26	59.7	0.0000718	0.0000912	0.0002202	133096.2965	1.063	25.8605	4.067	317	344	344	344968	367174	712142	2.578
L214 to L225	102809.0865	102.809	4.811	143830.2485	10.734	26.8	26.19	21.79	17.79	SE (130°)	3b (m-l M)	2.231	1	119.68	42.7	0.0001211	0.0002702	0.0002079	143830.2485	2.416	19.0460	3.959	393	405	405	212910	480731	693641	1.890
L225 to L233	108215.7171	108.216	5.407	152141.8459	8.312	24.8	25.47	20.52	10.82	S (190°)	3b (m-l M)	1.537	1	206.86	60.8	0.0001528	0.0002349	0.0003699	152141.8459	1.763	15.8343	2.929	141	220	220	78512	194496	273008	0.960
L233 to L246	115639.9499	115.640	7.424	165938.7651	13.797	23.5	23.86	18.77	10.97	ESE (120°)	3b (m-l M)	1.858	1	230.49	96.0	0.0001268	0.0002357	0.0001751	165938.7651	1.313	30.7322	4.139	179	160	179	398756	501967	900723	1.909
L246 to L259	123259.7779	123.260	7.620	178305.0662	12.366	21.4	21.06	17.59	13.69	SE (130°)	3b (m-l M)	1.623	1	153.32	39.3	0.0000954	0.0001549	0.0002756	178305.0662	1.485	19.8252	2.602	296	293	296	417951	408623	826574	1.954
L259 to L265	127207.9622	127.208	3.948	182496.2996	4.191	21.1	21.29	17.02	10.42	NE (040°)	2 (m-l S)	1.062	1.2	113.91	33.5	0.0001360	0.0001444	0.0000760	182496.2996	2.849	7.6769	1.944	165	105	165	0	124822	124822	0.871
L265 to LM1	131668.3117	131.668	4.460	191824.053	9.328	19.7	19.52	16.32	10.20	E (080°)	3b (m-l M)	2.091	1	167.43	59.8	0.0000750	0.0001569	0.0003139	191824.053	1.069	13.0608	2.928	317	441	441	307891	363063	670954	2.103
LM1 to LM8 Ramin Oilfield Ant.	137993.2403	137.993	6.325	198532.6625	6.709	23.2	18.14	16.32	8.77	S (180°)	2 (m-l S)	1.061	1	200.65	24.9	0.0000007	0.0000008	-0.0005534	198532.6625	0.021	4.5876	0.725	76	117	117	7904	159472	167376	0.730
LM8 to LM16 Ramin Oilfield Ant.	146195.6008	146.196	8.202	206819.0698	8.286	20.5	19.84	15.40	9.10	S (180°)	2 (m-l S)	1.010	1	306.45	95.8	0.0001104	0.0001116	0.0003292	206819.0698	2.027	2.8225	0.344	162	160	162	67313	134326	201639	0.712
LM16 to LM20	150728.4841	150.728	4.533	211547.0328	4.728	19.0	18.99	14.76	3.56	S (190°)	2 (m-l S)	1.043	1	258.86	52.8	0.0001354	0.0001412	0.0003309	211547.0328	2.941	4.9171	1.085	75	116	116	48379	88657	137036	0.847
LM20 to LM36	158019.6568	158.020	7.291	229544.4447	17.997	17.7	17.33	13.25	8.25	WSW (250°)	3b (m-l M)	2.468	1	303.15	56.1	0.0000839	0.0002071	0.0001783	229544.4447	1.557	35.8735	4.920	323	311	323	759798	909151	1668949	2.711
LM36 to LM61	168490.3233	168.490	10.471	252584.0471	23.040	16.2	15.46	12.06	7.66	SW (220°)	3b (m-l M)	2.200	1.1	315.04	78.8	0.0000517	0.0001137	0.0001433	252584.0471	0.921	46.3959	4.431	651	478	651	1771014	1428511	3199525	4.061

APPENDIX 7 METHODS

Appendix 7.1 Methods for investigating Earth surface movement rates

Appendix 7.1.1 Surveying of marine terraces with a dumpy level and surveyor's staff

Surveying was undertaken using levelling equipment, with a dumpy level that incorporated stadia crosshairs for determining horizontal distances, and a metal extendable surveyor's staff with graduations at 1 cm intervals. These surveys with levelling equipment were elementary topographic surveys, using methods outlined by Bettess (1992) and Bannister et al. (1998).

The surveys were undertaken relative to Mean High Water strand lines and relative to temporary bench marks of metal pegs driven into the ground surface. Relative elevation was the main focus of the surveys, with closure of each survey indicating vertical measurement errors of approximately 5 cm or less. The horizontal locations of temporary bench marks were determined as latitude and longitude using the WGS 84 (World Geodetic System 1984) reference system, by use of a Garmin GPS 12 (Global Positioning System) hand-held unit. When placed at the location of the selected bench mark for several hours, this GPS unit had a horizontal positional accuracy of within 100 m (and probably within 15 m) (Garmin, 2011). This was sufficient for locating each survey on the topographical and geological maps available, when distinctive local features were utilised and differences in mapping reference systems were accounted for. The geological maps used were of 1:100,000 scale with a resolution of approximately 50 m.

Appendix 7.1.2 Radiocarbon dating of marine terrace deposits

Radiometric dating of marine terrace deposits was undertaken so that rates of Earth surface movements could be determined. This was achieved by the radiocarbon dating of a few samples of marine mollusc shells from within the marine terrace sediments, with the genus of each shell sample being noted. Radiocarbon dating is a laboratory technique for the dating of carbon-bearing materials (such as marine mollusc shells) using the rate of radioactive decay of ^{14}C (radiocarbon) to ^{14}N within such materials since the last active exchange of radiocarbon with carbon dioxide in the atmosphere and the environment. This is assumed to be similar to the time of the death of the mollusc and the incorporation of its shell into the terrace deposits. As a technique, it has a practical range of applicability of approximately 0.3 ka - 55 ka (Fairbanks, 2005). Care was taken to only sample shells for radiocarbon dating which appeared to be *in situ* (complete shells with intact valves or complete shells from encrustations around a large boulder) and which appeared to be clean and have minimal contamination (no residues, foreign matter, or signs of dissolution) (Gillespie, 1984). The samples for radiocarbon dating were carefully extracted, bagged in polythene bags and transported, using precautions to avoid contamination, for submission without pre-treatment to a laboratory for radiocarbon dating (Gillespie, 1984; Aitken, 1990).

The laboratory used for radiocarbon dating was the Centre for Isotope Research radiocarbon laboratory in the University of Groningen, the Netherlands. The radiocarbon dating undertaken was conventional (beta-radioactivity) radiocarbon dating for larger shell samples (greater than 15g mass) and Accelerator Mass Spectrometry (AMS) radiocarbon dating for smaller shell samples. This was undertaken following the standard procedures used by the laboratory (Mook and Streurman, 1983; Van der Plicht and Lanting, 1994; Van der Plicht et al., 2000), including the physical and chemical removal of the outer layers of the shell (which had undergone greater carbon exchange with the environment) in order to isolate a more reliable dating fraction (Aitken, 1990; Bowman, 1990).

The results obtained were quoted as conventional radiocarbon years Before Present (BP) (years before 1950 AD, using the standard Libby half-life value for ^{14}C of 5,568 ± 30 years) ± one standard deviation (one σ, confidence interval 68.3 %) for each sample (Bowman, 1990; Griffin, 2004). The results were also quoted as calibrated radiocarbon years Before Christ (cal.BC) ± one standard deviation, using the Julian/Gregorian calendar. Calibration was undertaken with the OxCal Version 4.2 calibration program (Bronk Ramsey, 2013), using the Marine09 modelled ocean average calibration curve of Reimer et al. (2009) and a ΔR offset of $^{+}180$ years for the nearest location (Doha in Qatar) within the CHRONO Marine Reservoir Database (Southon et al., 2002).

Appendix 7.1.3 Surveying of river terraces with a Total Station

Surveying was undertaken using Total Station equipment (similar to the Topcon Electronic Total Station GTS-4), with an electronic theodolite with integrated Electromagnetic Distance Measurement (EDM) and a single prism reflector unit mounted on a ranging pole (Figure APP 7.1). These surveys with a Total Station were elementary topographic surveys, using methods outlined by Bettess (1992), Bannister et al. (1998) and Kavanagh (2009).

The surveys were undertaken relative to the nearest river water surface and relative to temporary bench marks of metal pegs or survey discs driven into the ground surface. Wherever available, a temporary bench mark was located on a National Cartographic Center of Iran (NCC) bench mark (such as that shown in Figure 3.1). This was done in order that elevations could be expressed in metres above the NCC Chart Datum. This datum is a “modified” Indian Spring Low Water - a tidal datum approximating the lowest water level observed at a place (similar to the Lowest Astronomical Tide), originally devised by G. H. Darwin for the tides of India at a level below Mean Sea Level (Hareide, 2004). Relative elevation was the main focus of the surveys, with closure of each survey indicating vertical measurement errors of approximately 2 cm or less. The horizontal locations of temporary bench marks were determined as latitude and longitude using a Garmin GPS 12 hand-held unit, in a manner similar to that used for the marine terraces.

Figure APP 7.1 An electronic theodolite and single prism reflector unit in use in the field

Appendix 7.1.4 Optically Stimulated Luminescence (OSL) dating of river terrace sediments

Radiometric dating of river terrace deposits was undertaken so that rates of Earth surface movements could be determined. This was achieved by Optically Stimulated Luminescence (OSL) dating of the river terrace sediments. Radiocarbon dating was not used, since in the warm, dry oxidising environment of south-west Iran, organic matter was only very rarely preserved in any of the sediments. In the calcareous sediments of the river terrace deposits, only very occasional fragments of terrestrial and freshwater mollusc shells were found, and such samples were known to be associated with significant errors in radiocarbon dating, due to factors such as the incorporation of “old” carbon into the shells from carbonate-rich ground water (Aitken, 1990; Romaniello et al., 2008).

Optically Stimulated Luminescence (OSL) dating is a laboratory technique for dating sediments from the time of their last burial (assumed to be similar to the time of sediment deposition), and has a practical range of applicability of approximately 0.3 ka - 300 ka (Rendell, 1995). In nature, all sediments are subject to a weak flux of ionising radiation produced mainly by trace amounts of certain elements within the sediment and by cosmic rays. This ionising radiation is absorbed by quartz grains (and grains of feldspar, zircon and volcanic glass) within the sediment and the resulting radiation damage to these minerals remains as structurally unstable electron traps within the grains. Artificially stimulating such quartz grains with light (usually green or blue-green light) in a laboratory causes a luminescence signal (mainly green light) to be emitted with the release of the stored unstable electron energy. Exposure to sunlight for a few seconds or more (as may occur during sediment erosion, transport and deposition) is generally sufficient to “bleach” or “set to zero” the latent luminescence within the mineral grains, so that “bleached” quartz grains when artificially stimulated by light in a laboratory will not emit any photons in the green wavelengths. Assuming that such “bleached” quartz grains are subsequently buried by sediments and not exposed to sunlight (or other bright lights) until artificially stimulated in the laboratory, the time since burial can be calculated. This is because the intensity of the luminescence signal from the quartz grains is dependent on the amount of radiation absorbed since “bleaching” and on the rate at which the radiation damage to the quartz grains has accumulated (which in turn is dependent on the amount of the radioactive elements in the sample and other factors) (Aitken, 1998).

In short, the OSL age (in years, a, or thousands of years, ka) can be calculated from the equation: Age = Palaeodose / Annual dose-rate

where

Palaeodose, De is the laboratory dose of radiation needed to induce luminescence equal to that acquired subsequent to the last bleaching event (expressed in Grays, Gy)

Annual dose-rate is the rate at which energy is absorbed from the flux of ionising radiation (Grays per year, Gy a^{-1}) (Aitken, 1998)

Sampling for OSL dating was undertaken with care to ensure sampling from relatively homogeneous deposits containing fine and very fine sand (since quartz grains in the size range 90 - 250 µm were to be used for dating), with the homogeneity and near absence of gravels extending to a sphere of radius of about 0.3 m around each sampling point (Rendell, H. M., Loughborough University, personal communication, 2005). Gamma rays emitted up to a distance of 0.3 m from a sample can contribute to the annual dose-rate and by applying these precautions with sampling, the need for on-site measurement of the gamma dose-rate was circumvented. Also, samples were only taken from sediments with an apparent absence of post-depositional disturbances such as soil formation, groundwater leaching, bioturbation, compaction, variable moisture content, and clay formation and transportation (Aitken, 1998).

The sediment samples for OSL dating were only taken where there was a high likelihood that there had been sufficient exposure to sunlight for complete “bleaching” or “setting to zero” of the OSL signal just prior to the sediment deposition and burial (Aitken, 1998). For fluvial sediments, complete resetting by sunlight exposure is more likely for sediments transported mainly as suspended load (as opposed to bedload), with, for instance, the majority of the samples taken by Colls et al. (2001) from the River Loire in France not exhibiting evidence of partial bleaching. Hence, as far as possible, sampling in Khuzestan targeted fine sands at least several decimetres above probable bedload coarse sands and gravels in the cleaned sediment exposures.

The samples were taken according to established protocols, as described by Aitken (1998). The majority of the sediments in the Khuzestan river terrace exposures were very well indurated and cemented, so after scraping away the surface sediment, samples were carefully extracted by carving out two adjacent approximately 10 cm square blocks with a geological hammer and chisel and a very strong, sharp knife (Figure 3.2). By sampling such a relatively large block, the sediments deeper within the block were not exposed to light. Additional protection was provided by immediately wrapping the block in aluminium foil and opaque black plastic bags and maintaining this protection throughout transportation to the laboratory in the U.K.

Laboratory procedures for OSL dating were undertaken by the Sheffield Centre for International Drylands Research (SCIDR) luminescence laboratory in the University of Sheffield, U.K., according to standard procedures (Aitken, 1998) and as outlined in two Quartz Optical Dating Reports (Bateman and Fattahi, 2008, 2010). For the derivation of the annual dose-rate, concentrations of naturally occurring uranium (U), thorium (Th), potassium (K) and rubidium (Rb) (the main elemental sources of ionising radiation) in each sample were determined by inductively coupled plasma spectrometry (Appendix 7.3.3). Elemental concentrations were converted to annual dose-rates using data from Adamiec and Aitken (1998), Marsh et al. (2002) and Aitken (1998), incorporating attenuation factors relating to the sediment grain sizes used, their density, and palaeomoisture. Attenuation of the dose by moisture used present-day moisture values, as measured in the laboratory with a ± 3 % error to incorporate seasonal and longer-term fluctuations which may have occurred since burial. The contributions of cosmic rays to dose-rates were calculated using the expression published in Prescott and Hutton (1994).

Samples were prepared under subdued red lighting using the procedures to extract and clean quartz outlined in Bateman and Catt (1996), including the thorough use of reagents (including concentrated hydrofluoric acid (HF) treatments) for the removal of mineral coatings around quartz grains and the alpha-irradiated skins of quartz grains (Aitken, 1998). Prepared aliquots of samples were taken from the size ranges of 90 - 180 µm or 90 - 250 µm and mounted as a monolayer of about 1,500 to 2,000 grains on 1 cm diameter aluminium discs. All OSL measurements were carried out using an upgraded Risø DA-20 luminescence reader (Figure APP 7.2) fitted with blue-green laser diodes for stimulation with a Hoya-340 filter placed in front of the photomultiplier tube. Samples were dosed using a calibrated strontium-90 beta-radiation source. All samples were analysed using the single aliquot regenerative (SAR) approach of Murray and Wintle (2000, 2003) and all aliquots where the ratio of the first and last dose point exceeded ± 10 % of unity were excluded from further analysis. A dose recovery preheat plateau test showed no systematic correlation of De with preheat temperature, so preheat temperatures of 180 °C or 220 °C for 10 seconds were applied to each sample prior to OSL measurement to remove unstable signals generated by laboratory radiation (Bateman and Fattahi, 2008, 2010).

Figure APP 7.2 The Risø DA-20 luminescence reader (From Risø National Laboratory, 2009)

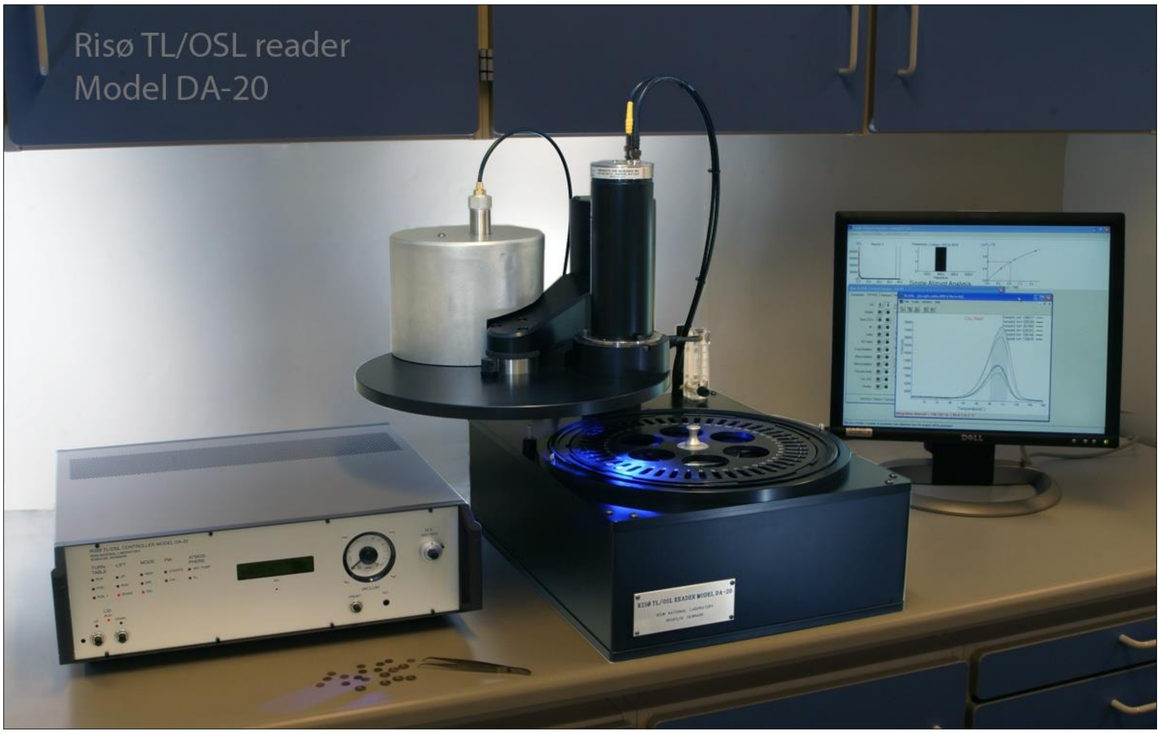

Depending on whether or not samples had good naturally acquired OSL signals with increases in the OSL signal for additional laboratory dose, between 10 and 25 replicate palaeodoses per sample were obtained to give an indication of the reproducibility of De measurements and to assess the bleaching behaviour. Incomplete bleaching during the last period of transport and deposition is frequently a major source of inaccuracies in the calculated palaeodose value, resulting in OSL ages that are older than the true age of sediment burial (Richards et al., 2001). This is difficult to establish with any certainty from OSL data, though, in principle, a well bleached undisturbed sample should have replicate palaeodose data which is normally distributed (Bateman et al., 2003).

By plotting the replicate data for each sample as a probability density function, assessments of where older or younger material had been included in the measurements were made. To varying degrees, all of the samples exhibited some signs of incomplete bleaching (or, possibly, disturbance of grains by bioturbation), with a high amount of replicate scatter and replicates having a wide range of De values. Thus, steps were taken statistically to isolate burial OSL ages for each of the samples. In two cases, this was achieved by removal of aliquots whose palaeodoses were outside of two standard deviations of the dataset mean and by application of the Central Age Model (Galbraith et al., 1999). This statistical model was sufficient where the De replicate datasets produced essentially unimodal De distributions. In the majority of cases, the De replicate datasets were statistically analysed by Finite Mixture Modelling (Galbraith and Green, 1990) to extract the different multiple components contained within the De distributions (Figure 3.3). Where the principal cause of De scatter is partial bleaching the youngest component is generally a better indicator of the true burial age, hence, the lowest component which represented more than 10 % of the data was selected for the calculation of OSL ages (Bateman et al., 2007, 2010).

For calculating the OSL ages, in two cases, a single weighted mean De value was calculated from the selected aliquots. In most cases, the chosen De component extracted by Finite Mixture Modelling was used. The results obtained were quoted as OSL ages in thousands of years before the present day (ka) ± one standard deviation (one σ, confidence interval 68.3 %). This incorporated systematic uncertainties with the dosimetry data, uncertainties with the palaeomoisture content, and errors associated with the De determination (Bateman and Fattahi, 2008, 2010). The results were also quoted as years Before Christ (BC) ± one standard deviation, using the Julian/Gregorian calendar.

Appendix 7.2 Methods for investigating river characteristics influenced by Earth surface movements and human activities

River characteristics were investigated to determine the responses of major transverse rivers to Earth surface movements associated with active folds and to human activities. The River Karun/River Dez system in lowland south-west Iran was chosen for this study for a variety of reasons. It is the largest river system in Khuzestan (and in Iran as a whole), it flows directly into the sea (unlike the River Karkheh and River Jarrahi), it has relatively minor influences from dune fields (unlike the River Karkheh), and it is reasonably accessible by road (except for its lower reaches which are within special security areas relatively near to the border with Iraq). Also, it encounters a significant number of anticlines and emerging anticlines, it has interesting features (such as a bifurcation into two branches at Shushtar, major ancient hydraulic engineering at a number of localities, and a few near-straight reaches), major modern dams have been constructed in the vicinity of Gotvand and Dezful (but no major modern dams further downstream), and some survey and hydrological data had been found to be available.

The river reaches and the survey data, fieldwork data, and map and remote sensing data used in the study were as given in Section 3.3 and Figures 3.4 and 3.5. A standard date of 2000 AD was employed for characteristics, as this was the approximate date of completion of the Dez Ab Engineering Company survey and the approximate date of the analysed Landsat ETM+ satellite images.

Appendix 7.2.1 Data compilation for river longitudinal profiles

The survey and other sources were carefully examined and measured to derive useful elevation data for each river reach. This data included: valley/average river floodplain elevation, average channel banks elevation, river water surface elevation, and deepest channel bed elevation.

The river valley and floodplain surfaces were frequently irregular or sloping, so the average elevation of the main plains nearest to the river banks was used for the valley/average river floodplain elevation measurements (Bridge, 2003; Downs and Gregory, 2004). This meant that, due to features such as levées, the average river floodplain elevation was lower than the average channel banks elevation at some localities, particularly in the lower reaches of the River Karun. For the average channel banks elevation, the river bank surface was taken to be the first major change in the slope of the cross-section above the water surface on each side of the river, with the average of the two bank surfaces being used with a weighting towards the lower bank. For the river water surface elevation, the average of measurements taken on the day of the survey was used. The average river water surface elevation was also used to derive the average height of the channel banks and the average height of the valley/river floodplain above the river water surface. For the deepest channel bed elevation, the lowest surveyed point on the channel cross-section was used. This elevation data was expressed to the nearest cm (or nearest 5 mm), though variations inherent in the data were frequently significantly greater than this. As is natural, the river valley surface and

Figure APP 7.3 Generalised diagrams showing the valley profile, projected-channel profile and channel profile of a river (From Burnett, 1982)

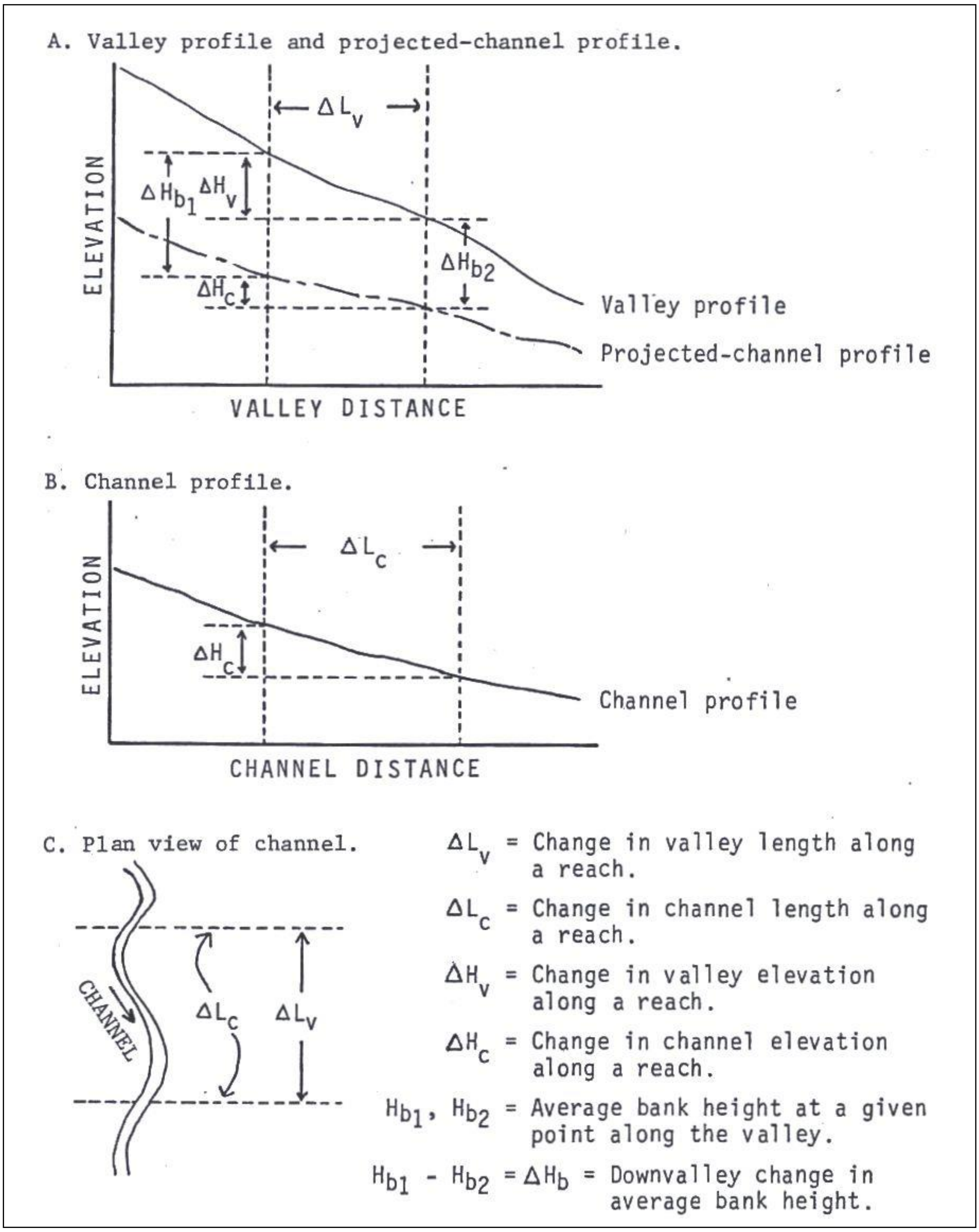

In Diagram A), the slope of the valley profile curve is the valley slope, and the slope of the projected-channel profile curve is the projected-channel water surface slope

Valley slope, $s_v = \Delta H_v / \Delta L_v$

Projected-channel water surface slope, $s_p = \Delta H_c / \Delta L_v$

In Diagram B), the slope of the channel profile curve is the channel water surface slope

Channel water surface slope, $s = \Delta H_c / \Delta L_c$

floodplain surface varied significantly in elevation and average elevations were only expressed to the nearest decimetre. Channel banks were also surfaces of varying elevation, though to a lesser degree, and average elevations were expressed to the nearest cm. River water surface elevations could vary, especially as successive localities may have been surveyed on different days, and the deepest point on the river channel bed varied with the degree of bed scouring and, generally, was deeper near to meander apices (Knighton, 1998; Bridge, 2003).

With consideration of these variations, the data was used to construct longitudinal profiles of the rivers. Since most rivers in the study area had meandering channels, plots of elevation against channel distance (measured along the channel thalweg) would illustrate slopes that were unrepresentatively gentle, particularly for the valley and floodplain slopes. Instead, plots of elevation against valley distance were used. Valley distance was defined as the distance measured along the valley in a succession of straight-line "reaches" from the Gotvand Regulating Dam and the Dez Regulating Dam to the Persian Gulf (Figure 3.5), and elevations were taken orthogonal to the valley axis, in a manner similar to that used by Burnett (1982). On such curves, the plot of average river water surface was the "projected-channel profile" and the slope of the plot was the "projected-channel slope" (Figure APP 7.3). The average channel banks height was shown on such plots as the difference between the projected-channel profile and the average channel banks profile (Burnett, 1982).

Appendix 7.2.2 Data compilation for river characteristics

The topographical maps provided a good overview of the river valley and floodplain, and were used in conjunction with the survey data for determining the elevations relating to the river valley, floodplain and channel banks. The geological maps were mainly used for determining the locations of the geological structures, with the 1:100,000 scale geological maps being used for determining the locations of emerged folds, including their surface extent and other characteristics.

Determining the locations and characteristics of emerging anticlines associated with oil and gas fields was considerably more difficult and subject to larger errors, since only a few were shown in the general sections on the 1:100,000 geological maps and very few deep well logs or seismic profiles were available for the entire study area. The locations of these emerging "oilfield anticlines" were determined from a variety of sources, mainly from published maps of oilfields (including NIOC, 1973; Beydoun, 1991; Sherkati and Letouzey, 2004), but also from a few published articles about the oilfields which included seismic sections (such as Abdollahie Fard et al., 2006; Maleki et al., 2006; Soleimani et al., 2008).

Though the details of folds within the Dezful Embayment are debated (Section 2.4), balanced cross-sections and models (e.g. Blanc et al., 2003; McQuarrie, 2004) have indicated general characteristics. These include: slightly inclined folds associated with thrust faults dipping towards the north-east, décollements at relatively shallow depths, and "typical" Dezful Embayment anticlines that are asymmetric at or near the ground surface, with more steeply dipping forelimbs to the south-west and more gently dipping back-limbs to the north-east (Figure 2.16; Blanc et al., 2003). Due to these features of roughly NW-SE trending oilfield anticlines within the Dezful Embayment, it was considered that the mapped extents of the oilfields for the reservoir rock of the Asmari Formation at depths of about 2 km to 6 km were probably offset to the north-east by a few km relative to the location of the anticlinal crest emerging on the land surface. This assumption was supported by wells of the Ahvaz Oilfield being located about 5 km to the north-east of the axis of the Ahvaz Anticline (IOOC, 1969a). However, due to décollement detachment horizons at a number of different levels effectively separating the stratigraphic column into different structural units (Figure 2.15), it was recognised that the surface configurations of each anticline in the study area often did not reflect the sub-surface structural conditions (Sherkati and Letouzey, 2004). Hence, the anticlinal axis for each of the NW-SE trending oilfield anticlines was plotted 0 km to 5 km to the north-east of the midline of the mapped extent of each oilfield, depending on what was known of the local sub-surface structural geology (especially from published articles like Abdollahie Fard et al., 2006). By contrast, the roughly N-S trending oilfield anticlines within the relatively stable Arabian Platform were more symmetrical and upright (Maleki et al., 2006), so no modifications were applied for these anticlines, with the anticlinal axis being plotted along the midline of the mapped extent of these oilfields.

With the locations of folds and their relationship to the sub-division into river "reaches" recognised, river characteristics were determined for each fold for river reaches upstream of a fold, across the axis of a fold, and downstream of a fold.

Appendix 7.2.2.1 Structural geology

Structural geology data was mainly derived from 1:100,000 geological maps, and other sources given in Section 3.3. The data included aspects of the structural geology of the folds encountered by the major rivers, some of which are described in Table APP 7.1.

Table APP 7.1 Descriptions of some of the structural geology data for folds

Aspect of structural geology	Short description or diagram
Fold measurements and geomorphological indices Hinge length (km), L Fold width (km), W Shorter limb width (km), S Aspect ratio, AR = L / W Fold Symmetry Index, FSI = S / (0.5 W) (Burberry et al., 2007, 2010)	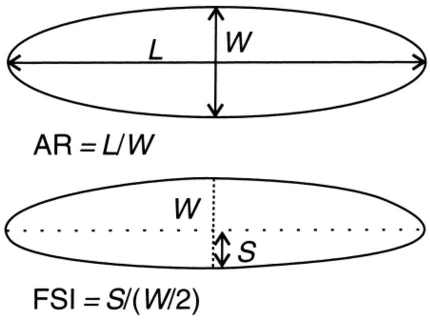 (From Burberry et al., 2010)
Probable fold type, based mainly on fold measurements Folds in the study area were probably mainly on the continuum between detachment folds (usually with short L, low AR, and good symmetry with FSI near to 1.0, though can be 0.6 for asymmetric detachment folds) and fault bend folds (usually with long L, high AR, and some asymmetry with FSI 0.9 typically or less). One other probable fold type in the study area was a monocline (Suppe, 1985; Burberry et al., 2010)	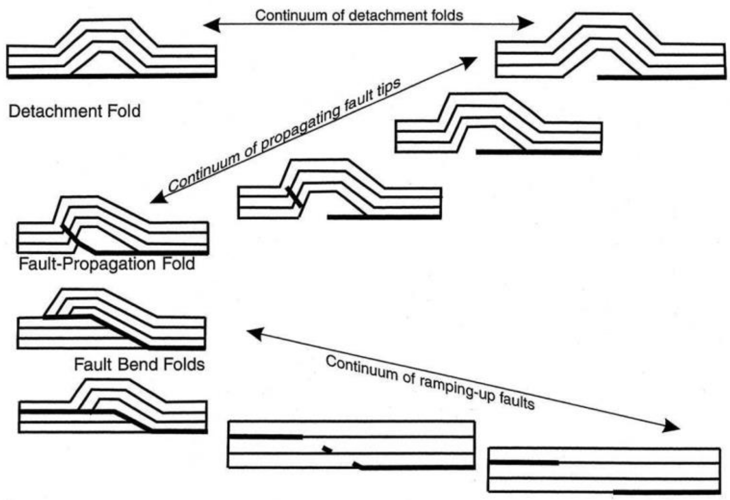 (From Burberry et al., 2010)
Estimate of degree of development of geological structure	Folds were classed according to their maximum topographic expression above the surrounding plains: Well developed fold: More than 100 m Moderately developed fold: 30 m to 100 m Slightly developed fold: 8 m to 30 m Emerging fold: Less than 8 m
Width of geological structure where crossed by river (km) (where applicable)	Horizontal distance over which the fold (or the projection of the fold) had a significant topographic expression, measured orthogonal to the fold axis (or its projection) where it was crossed by the river

Approximate probable location of fold "core"	Approximate location of the centre of the part of the fold which probably emerged first on the ground surface. For younger, emerging folds this was determined with reasonable confidence from the present-day topography. For older, emerged folds this was less certain, especially for more eroded folds and probable fault bend folds. It was generally assigned to be in the vicinity of the structurally highest part of the fold, which depending on the specific fold, could be near its highest topographic expression, midway along the fold axis, or near to where it merged with an older, more developed fold
Approximate distance from fold "core" and fold "nose" to where crossed by river (km)	Horizontal distance measured along the fold axis (or its projection) from the fold "core" (as defined above) and from the nearest fold "nose" (the nearest fold tip as delineated on sources such as 1:100,000 geological maps) to the location of the river crossing
Estimate of degree of general erosion resistance of fold	Descriptive code from least to greatest erosion resistance: 1.0 (Low, unlithified floodplain sediments), 2.0 (Qu. low, unlithified floodplain sediments), 3.0 (Mod/Qu. low), 4.0 (Mod, mainly sandstones and siltstones), 5.0 (Mod/High), 6.0 (High/Mod, mainly conglomerates)

Appendix 7.2.2.2 Human activities

Data for human activities was in the form of short descriptions of floodplain land use, human river channel modifications and an estimate of the overall degree of human impact. This was principally derived from fieldwork (mainly 2002 - 2007 AD) and remote sensing images (mainly Landsat satellite images from 2000 AD and later).

Appendix 7.2.2.3 River geomorphology

Geomorphological data was derived for the river reaches from various sources. The main source was the survey, with considerable contributions from the fine-scale topographical and geological maps, remote sensing images (mainly Landsat satellite images from 2000 AD) and geomorphological fieldwork (mainly from 2002 - 2007 AD). The data was comprised of standard fluvial geomorphological characteristics (as defined in work such as Burnett, 1982; Knighton, 1998; Bridge, 2003), and some of the aspects of river geomorphology are described in Table APP 7.2.

Table APP 7.2 Descriptions of some of the geomorphological data for the river reaches

Aspect of river geomorphology	Short description
General river course direction of reach	Direction towards which the river generally flows, expressed as a compass point and a bearing to the nearest 10°

Channel pattern type	Simple classification based on Schumm (1981, 1985); Knighton (1998): Suspended load straight (Type 1, s-l S); Mixed load straight (Type 2, m-l S); Suspended load meandering (Type 3a, s-l M); Mixed load meandering (Type 3b, m-l M); Meandering-braided transition (Type 4, M-B); Braided (Type 5, B); Anastomosing
Channel sinuosity (no units), S	S = Channel length / Straight-line valley length
Average meander wavelength (m), λ	Distance between successive inflection points or successive meander apices (to the nearest 100 m)
Meander type	Short description included: Regular (Reg.), Irregular (Irreg.), Tortuous (tort), estimate of angularity of meanders, and estimate of meander migration rate
Braiding index	Measure of intensity of braiding, similar to that described by Howard et al. (1970) and Chew and Ashmore (2001). Average number of anabranches across a river section - mean for the river reach determined from sections orthogonal to the valley axis c. 1 km apart
Overall channel width (m), w_{max}	Measured from channel bank to channel bank orthogonal to the thalweg, both at survey locations and as a range for the whole reach (to the nearest 10 m). With multiple channels, the distance between the most widely separated channel banks was measured orthogonal to the valley axis.
Channel width (m), w	Measured across the water surface orthogonal to the thalweg on the day of survey, at survey locations (to the nearest cm). With multiple channels, the sum of the water surface widths was calculated.
Channel depth (m), d	Vertical distance from lowest point on the cross-section to the water surface on the day of survey, measured at survey locations (to the nearest cm)
Channel width:depth ratio (no units), w / d	Calculated as w / d
Channel-belt width (m)	Distance between the extremities of the channel-belt, measured orthogonal to the valley axis
Valley depth over extent of channel-belt (m)	Vertical distance from lowest point of valley (including channel bed) to highest point of valley, within the extremities of the channel-belt
Approximate cross-sectional shape of channel	Irregular (Irreg.), Rectangular (Rect.), Trapezoidal (Trap.), Triangular (Triang.)
Estimate of average height of channel banks and average height of floodplain or valley above channel water surface (m)	Measured relative to the average channel water surface on the day of the survey, in the manner described in Appendix 7.2.1
Channel water surface slope ($m\ m^{-1}$), s	s = Change in water surface elevation / Change in channel distance (measured along the channel thalweg)
Projected-channel water surface slope ($m\ m^{-1}$), s_p	s_p = Change in water surface elevation / Change in valley distance (measured in a straight line along the reach)
Valley slope ($m\ m^{-1}$), s_v	s_v = Change in valley or average river floodplain elevation / Change in valley distance (measured in a straight line along the reach) (Burnett, 1982)

Appendix 7.2.2.4 River hydrology

The river hydrology data for each river reach was mainly derived from data from the nearest river gauging station, as provided by the KWPA and other sources. The main hydrological data available was river water discharge data. The mean annual water discharge (m^3s^{-1} or cumecs), Q from the nearest river gauging station with good data was used, since this was considered to correlate most closely with the river water surface elevation for each reach which had been recorded on "average" days during the survey of about 1997 - 2000 AD. This river water discharge data was combined with morphological data to derive values for stream powers, since various studies (e.g. Jorgensen, 1990; Schumm et al., 2000; Burbank and Anderson, 2001) had shown stream powers to be useful when elucidating river responses to active tectonics. Values calculated included:

Specific stream power ($W\ m^{-2}$), $\omega = \rho_w.\ g.\ Q.\ s\ /\ w$

Stream power per unit length ($W\ m^{-1}$), $\Omega = \rho_w.\ g.\ Q.\ s$

where

$\rho_w.\ g$ is the specific weight of water, which in Khuzestan is c. 9,782.7 $N\ m^{-2}$

Q is mean annual water discharge (m^3s^{-1} or cumecs)

s is channel water surface slope, measured along the channel thalweg ($m\ m^{-1}$)

w is channel width, measured across the water surface orthogonal to the channel thalweg (m) (as described in Appendix 7.2.2.3)

Appendix 7.2.2.5 River sedimentology

Table APP 7.3 Descriptions of some of the sedimentological data for the river reaches

Aspect of river sedimentology	Short description
Estimate of degree of erosion resistance of channel banks	Estimate of low, moderate or high erosion bank resistance based on grain size, cementation, vegetation, etc.
Main sediment or bedrock type in river valley and estimate of general erosion resistance	Unlithified floodplain sediments (low or quite low erosion resistance), Agha Jari Formation bedrock (mainly calcareous sandstones and siltstones of moderate erosion resistance), Bakhtyari Formation bedrock (mainly limestone-chert conglomerates of high erosion resistance)
Short general descriptions of channel bed surface sediments and channel banks	Included in some cases: D_{coarse} (mean grain size for b-axis of 50 typical gravel clasts, in mm), D_{max} (mean grain size for b-axis of 10 largest gravel clasts from a c. 4 m^2 area of river channel bed, in mm), D_{fine} (mean grain size for fine-grained samples - fine gravels, sands and muds, in µm), B (proportion of sediments in silt/clay fraction, i.e. less than 63 µm, %)

Average grain size of channel bed surface sediments and channel bank sediments	Descriptive code from smallest to largest average grain size: 1.0 (mainly muds), 2.0 (mainly muds, with some sands), 3.0 (muds and sands), 3.5 (sands and muds), 4.0 (mainly sands and muds), 4.5 (mainly sands and silts), 5.0 (mainly sands and muds, slight gravels), 5.5 (mainly sands and silts, few gravels) 6.0 (mainly sands and muds, partly sands and gravels), 7.0 (partly sands and silts, partly gravels), 7.5 (partly gravels and sands, partly fine sands and muds), 8.0 (partly gravels and sands, partly sands and silts), 8.5 (partly gravels (esp. pebbles), partly sands and silts), 9.0 (partly gravels (pebbles and cobbles), partly sands and silts), 9.5 (mainly gravels (esp. pebbles with some cobbles), some sands and silts), 10.0 (mainly gravels (esp. pebbles and cobbles), few sands and silts)

Sedimentological data relating to the river reaches was mainly derived from fieldwork in south-west Iran. This data was partly general observations, partly measurements of sediment samples in the field, and partly laboratory analyses of sediment samples in the U.K. The fieldwork in south-west Iran was limited due to security, logistical and time constraints, especially for reaches of the River Karun in the Lower Khuzestan Plains. Hence, this data was supplemented by determinations from river photographs, geological maps, remote sensing images and very occasional previous work (e.g. Gasche et al., 2004, 2005; Heyvaert and Baeteman, 2007). The data included aspects of the river sedimentology described in Table APP 7.3.

Appendix 7.2.5.6 River migration

The CORONA (1966 and 1968) satellite images and the Landsat (2001) satellite images had been processed and geo-referenced using ERDAS IMAGINE and ArcGIS® software by the Geological Survey of Belgium and superimposed into a unified database (Walstra et al., 2010a). This resource, which included 1:50,000 topographical maps and an ArcGIS® shapefile of the main river courses in 1966/1968 from CORONA satellite imagery, was used to determine river migration. Using editing tools available in ArcGIS®, the river reaches were drawn on and the edges of the channel-belt and changes in channel bank location between 1966/1968 and 2001 were drawn on as shape files, using standard methods (e.g. Shields et al., 2000; Giardino and Lee, 2011). From this editing, river migration rates were determined as they may to be proportional to river aggradation rates, since variations in sediment thickness are, generally, of lesser magnitude than variations in sediment lateral extent (Mackey and Bridge, 1995; Miall, 1996). Channel-belt extent was used as an indicator of long-term river migration and long-term rates of river aggradation, perhaps over long time-scales of centuries to several millennia (Alexander et al., 1994; Burbank and Anderson, 2001). River channel changes between 1966/1968 and 2001 were used as indicators of short-term river migration and short-term rates of river aggradation, over a mean time interval of 34.2 years. The data included aspects of river migration described in Table APP 7.4.

Table APP 7.4 Descriptions of some of the river migration data for the river reaches

Aspect of river migration	Short description
Channel-belt area (km^2)	Area of maximum extent of channel-belt, determined using both the CORONA (1966/68) and Landsat (2001) images within the river reach
Average channel-belt width (km)	Calculated as Channel-belt area / Straight-line valley length of reach
Greatest channel bank migration distance 1966/68 - 2001 (m)	Maximum distance between corresponding points on river bank for CORONA (1966/68) and Landsat (2001) images, measured along the probable direction of channel migration within the river reach
Average channel migration rate 1966/68 - 2001 ($m\ yr^{-1}$), R_m	Calculated as $R_m = \frac{(A / L_c)}{yr}$ where A is total area of migration polygons (m^2), drawn as ArcGIS® shape files between corresponding points of a river bank between the CORONA (1966/1968) image and Landsat (2001) image within the river reach L_c is channel length of reach (m) yr is the number of years between the satellite images (mean 34.2 years) (modified from Giardino and Lee, 2011)

Appendix 7.3 Laboratory analyses for investigating Earth surface movement rates and for investigating river characteristics

As part of the fieldwork, both that for investigating rates of Earth surface movements and for investigating river characteristics, a selection of sediment and bedrock samples were carefully taken, bagged in polythene bags and transported to the U.K. These were then subjected to a number of laboratory analyses.

Appendix 7.3.1 Gravel lithological analysis

Gravel lithological analysis was performed on selected sediment samples from river beds and river terrace deposits. This was undertaken mainly to improve the gravel descriptions and interpretations, and to aid in the determination of correlations between samples and likely provenances of samples. Random samples of 50 typical gravel clasts from river beds and river terrace deposits were broken open with a geological hammer in Iran to produce a fragment of each clast that was comprised of both the weathered exterior and unweathered interior. These were subsequently analysed in the U.K. These small sample sizes were less than the usual recommended minimum of 250-300 clasts for lithological analysis of gravel-grade particles (Bridgland, 1986), so only broad differences in lithologies were investigated.

Clasts were identified using a hand lens, a Leica S6 zoom stereo-microscope, a sharp-pointed steel probe, and dropper bottles of hydrochloric acid (10 % HCl and 25 % HCl). This followed standard procedures (Gale and Hoare, 1991) and used guides, such as Bridgland (1986), Cox et al. (1988) and Hamilton et al. (1992) as aids to identification. Broad groupings used in the gravel lithological analysis included: calcareous and non-calcareous sandstones, calcareous and non-calcareous mudrocks, limestones and carbonate rocks, cherts, evaporites, and other rock types. The degree to which a clast underwent effervescence with drops of 10 % and 25 % HCl solution was used as an aid to discriminating between carbonate rock types. Limestone usually exhibited extreme effervescence with drops of 10 % HCl, calcareous rock usually exhibited vigorous effervescence with 10 % HCl, marble usually exhibited some effervescence with 10 % HCl, and dolomite usually exhibited little or no effervescence with 10 % HCl but some effervescence with 25 % HCl (Dietrich, 2011).

Appendix 7.3.2 Thin section analysis

Thin section analysis was performed on selected fine-grained sediment and rock samples from river banks and beds, river terraces, ancient constructions, and bedrock. This was undertaken mainly to improve the fine-grained descriptions and interpretations, to aid in the determination of correlations between samples and likely provenances of samples, to compare the cohesiveness of river banks at different locations, and to aid in the interpretation of sedimentary environments.

Sediment and rock samples with grains mainly in the size range from coarse silts to fine gravels were carefully sub-sampled (Gale and Hoare, 1991) and made into thin sections using established methods (Heinrich, 1965; Adams et al., 1984; Miller, 1988). Rock thin sections were prepared for well consolidated samples and grain mount thin sections were prepared for poorly consolidated samples. Rock samples and well cemented sediment samples were shaped with a diamond-impregnated trim saw and levelled on glass plates using 320 and 600 grade carborundum powder (silicon carbide powder, SiC). Each sample was then bonded onto glass slides using Epotek epoxy resin and cured at approximately 60 - 65°C for about 1 hour. Once cured, each section was trimmed and ground down using a Buehler PetroThin thin sectioning system comprised of a diamond-impregnated cutting blade, a diamond-impregnated grinding wheel and a vacuum slide-holding chuck. Each section was levelled to a thickness of c. 30 μm using 320, 600 and 1,000 grade carborundum grit on glass plates. This standard thickness of 30 μm produced first order white or grey interference colours in quartz when the thin section was viewed under crossed polars. A glass coverslip was attached to each section using Canada Balsam (a standard mounting medium of refractive index, n = 1.535 - 1.540) on a hot plate at approximately 100°C. Excess Canada Balsam was removed from covered slides by immersion in Industrial Methylated Spirits, and slides were warm-cured for about 24 hours before use.

Sediment samples which were too poorly consolidated and too friable to be made into thin sections were placed in plastic moulds. Epotek epoxy resin was poured into these moulds and samples were cold-cured at room temperature (c. 20°C) for about 24 - 48 hours. The cured samples were then removed from the moulds and levelled using 320 and 600 grade carborundum grit on glass plates. These samples were bonded onto glass slides and then prepared in the same manner as for the rock samples (Miller, 1988).

The thin sections were analysed using an Olympus BH-2 petrographic microscope (Figure APP 7.4). For each thin section, a general description was made which included: grain size, sorting, grain roundness, grain types, rock fragment types, matrix, cement, and other characteristics. The general descriptions and identifications of minerals were made with reference to a number of guides, such as Heinrich (1965), Deer et al. (1978), MacKenzie and Guilford (1980), Harwood (1988), MacKenzie and Adams (1994), Pichler and Schmitt-Riegraf (1997) and Adams and MacKenzie (1998). The modal composition of a sediment or rock sample was determined by point counting for a series of traverses across each microscope slide, mainly by use of × 200 magnification and by advancing the microscope stage about 250 μm between each point. A total of 300 points were counted per thin section, as recommended for obtaining sufficiently accurate percentages of the components present by Point Count Analysis (Harwood, 1988; Garrison, 2003). Broad petrological groupings used in the thin section point counting included: quartz (monocrystalline and polycrystalline quartz), feldspars (alkali and plagioclase feldspars), rock fragments (limestones and carbonates, sandstones and mudrocks, and other rock fragments), cherts, evaporites, opaque minerals, other minerals (especially micas) and accessory minerals. A number of distinctive rock fragment types were recognised and their abundance in each thin section was estimated.

Figure APP 7.4 The Olympus BH-2 petrographic microscope

Appendix 7.3.3 Inductively coupled plasma spectrometry

Inductively coupled plasma spectrometry was performed on the river terrace sediment samples of sand on which the OSL dating was carried out. As mentioned in Appendix 7.1.4, for the derivation of the annual dose-rate the concentrations of naturally occurring uranium (U), thorium (Th), potassium (K) and, to a lesser extent, rubidium (Rb) within each sample needed to be determined accurately. These measurements were made by Inductively Coupled Plasma Mass Spectrometry (ICP-MS) and Inductively Coupled Plasma Optical Emission Spectrometry (ICP-OES). Since the metals were only present in very low concentrations in the sediment samples (typically only a few parts per million for U and Th), ICP-MS was the laboratory procedure of choice due to its relatively high precision and low detection limits (a few parts per billion for many elements) (Fairchild et al., 1988; Bateman and Fattahi, 2008, 2010). The ICP-MS results for the analysis of potassium (K, atomic mass 39.098) involved errors due to its atomic mass being close to that of the argon gas (Ar, atomic mass 39.948) used to produce the plasma, so for potassium (K) the results for ICP-OES analysis were mainly used.

A plasma is a luminous volume of gas (such as argon) at very high temperatures (c. 6,000 K - 10,000 K) with atoms and molecules in an ionised state. Inductively coupled plasma spectrometry is a laboratory technique for determining the elemental concentrations of a sediment or rock sample by converting it via a nebuliser into an aerosol which is passed through plasma to produce an atomised and ionised sample. This atomised and ionised sample is then analysed. Inductive coupling refers to the process whereby a radiofrequency generator connected to copper load coils surrounding a torch of argon gas is used to strip electrons off the argon atoms to produce the plasma (Figure APP 7.5; Fairchild et al., 1988; Boss and Fredeen, 2004).

Figure APP 7.5 Schematic diagram of the inductively coupled plasma apparatus (From Fairchild et al., 1988)

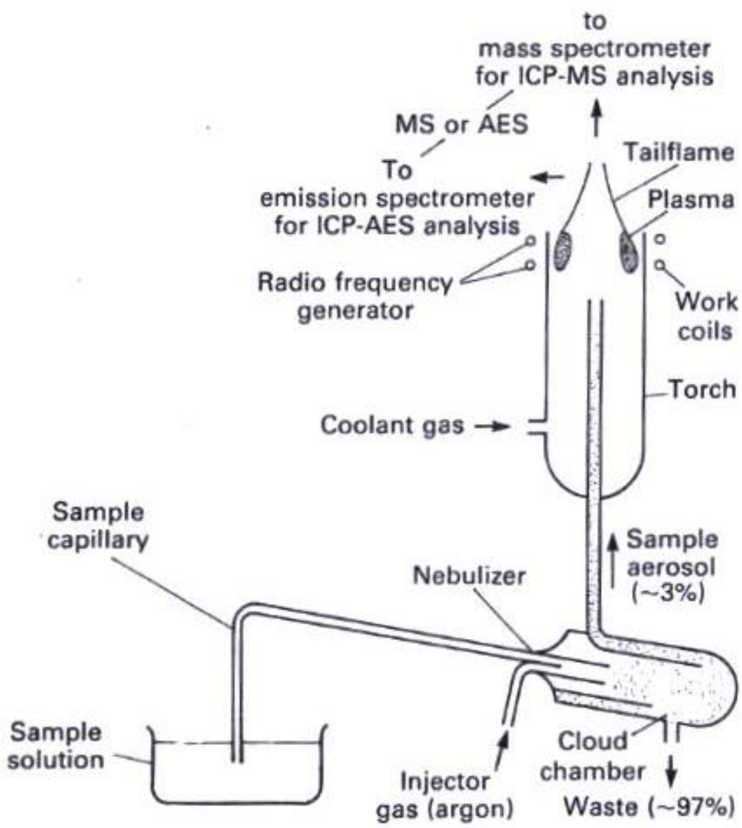

Sample preparation was very similar for both the ICP-MS and ICP-OES analyses. Fine-grained sandy sediment and rock samples were carefully sub-sampled, disaggregated and crushed with a pestle and mortar, and dried in a drying oven set at 105°C for 24 - 48 hours, to obtain accurately weighed powdered sub-samples of about 0.5 g dry mass (Gale and Hoare, 1991). Each of the dry sub-samples was then subjected to decomposition using mineral acid reagents (Fairchild et al., 1988). A solution of 5 ml HF (hydrofluoric acid), 5 ml HNO_3 (nitric acid) and 2 ml HCl (hydrochloric acid) was applied and heated to 200°C in a CEM MARS Xpress microwave system for 20 minutes and cooled gradually. A solution of 30 ml H_3BO_3 (boric acid) was applied and re-heated to 170°C for 10 minutes to neutralise the first pre-treatments and, after cooling, the solution was diluted to 50 g with de-ionised water.

Inductively Coupled Plasma Mass Spectrometry (ICP-MS) used the sample of ions produced by the inductively-coupled argon plasma and passed these ions as a beam through a quadrupole mass spectrometer to determine their mass spectra (Figure APP 7.6) (Fairchild et al., 1988).

Figure APP 7.6 Schematic diagram of the ICP-MS system (From Fairchild et al., 1988)

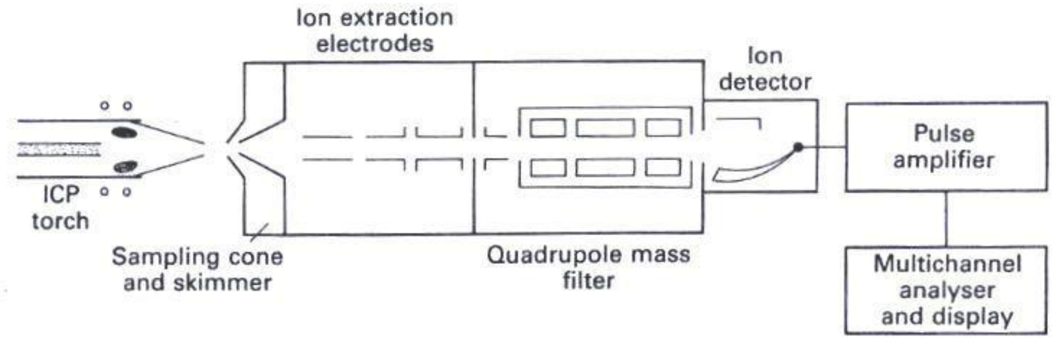

Analysis was carried out using established procedures with a PerkinElmer SCIEX ELAN DRC II Inductively Coupled Plasma Mass Spectrometer (ICP-MS). This system was comprised of: an inductively coupled plasma source (operating at atmospheric pressure at 6,000 K), ion optics, a dynamic reaction cell, an interface with sampler and skimmer cones to reduce pressures with minimal electrical discharges, a quadrupole mass spectrometer (operating at pressures of about 2.7×10^{-3} N m^{-2} or less, with a mass range of 5 to 270 atomic mass units), a detector within the vacuum chamber, and a computer for control and data management (PerkinElmer SCIEX, 2001). After the efficient atomising and ionising of each sample in aerosol form in the plasma torch, the emergent ion beam was passed through the quadrupole mass filter and the mass peaks of the ions were measured in the electron channel multiplier detector on the basis of their mass to charge ratio. The amplified signal was processed by the detection electronics and then sent to the computer for data processing (Fairchild et al., 1988; PerkinElmer SCIEX, 2001).

Inductively Coupled Plasma Optical Emission Spectrometry (ICP-OES) used high resolution spectrometry of the electromagnetic radiation (mainly visible light) emitted from the sample of atoms and ions produced by the inductively coupled argon plasma to determine the elemental composition. Each sample in aerosol form in the plasma torch had the electrons within its atoms and ions excited to higher energy levels, which on returning to their ground states emitted electromagnetic radiation, with unique wavelengths for each metal in the sample. From analysis of these unique emission wavelengths and their intensities with a high resolution spectrometer and the use of calibration curves for standard solutions, the concentration of each metal in the sample was determined (Fairchild et al., 1988; Boss and Fredeen, 2004).

Analysis was carried out using established procedures with a PerkinElmer Optima 5300 DV Inductively Coupled Optical Emission Spectrometer (ICP-OES) (PerkinElmer, 2004). With this instrument, the continuous energy emissions from the plasma were dispersed by an intricate optical system comprised of a plasma image transfer section, an entrance slit, an input collimator, an echelle diffraction grating polychromator, and two output sections (one for visible light and one for ultra-violet radiation) which were independently optimised for resolution and throughput (Figure APP 7.7). The emission line wavelengths were measured with two Segmented-array Charge-coupled Device detectors, covering approximately 6,000 wavelengths over a combined wavelength range of 167 - 782 nm (Barnard et al., 1993). The concentration of a metal within each sample was determined from calibration curves, such as that shown in Figure APP 7.8, though represented mathematically within the memory of the computer. This was based on measurements of emission counts from a blank solution, standard solutions for the element at concentrations of 10 ppm, and standard solutions of Estuarian Sediment Solution in 4 % HNO_3 (nitric acid) (Boss and Fredeen, 2004; HPS, 2011). For each metal analysed one emission line wavelength was selected, providing the greatest sensitivity and the least interference from the matrix and from other emission lines.

Figure APP 7.7 Schematic diagram of the PerkinElmer Optima 5300 DV ICP-OES optical system, with photograph of the plasma torch box (Partly from Barnard et al., 1993)

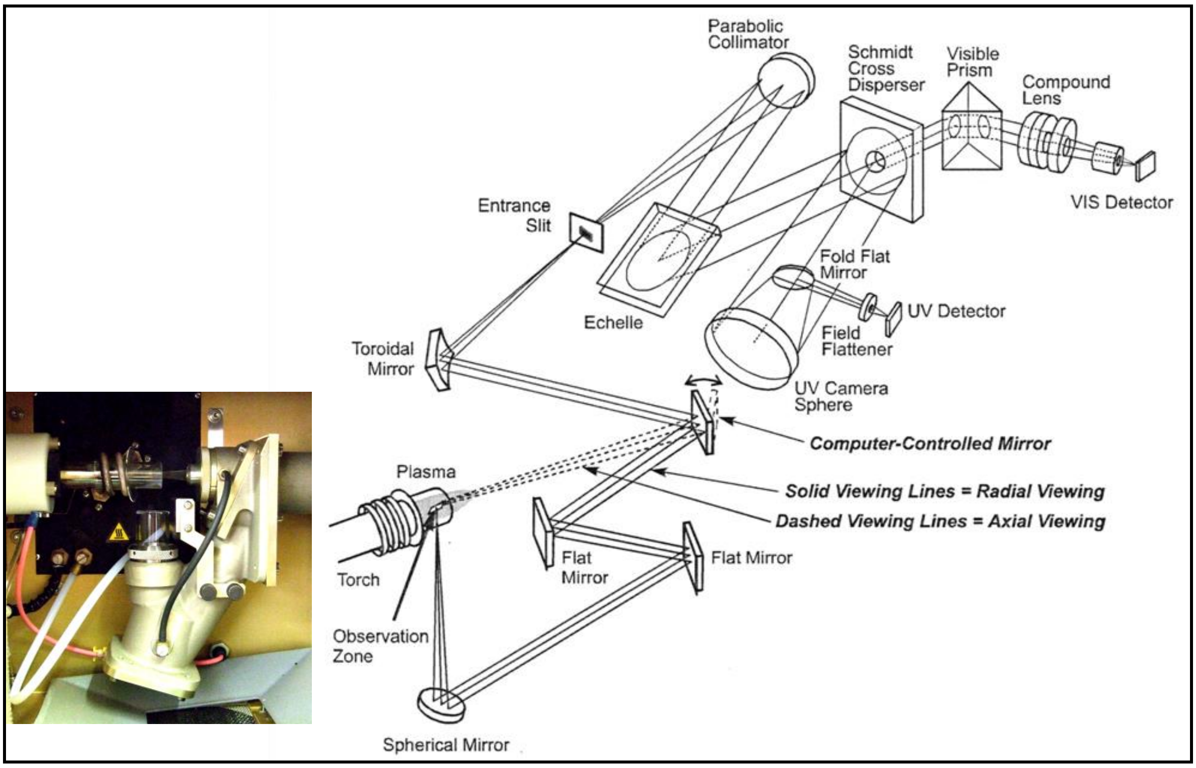

Figure APP 7.8 Example of a calibration curve used for ICP-OES (From Boss and Fredeen, 2004)

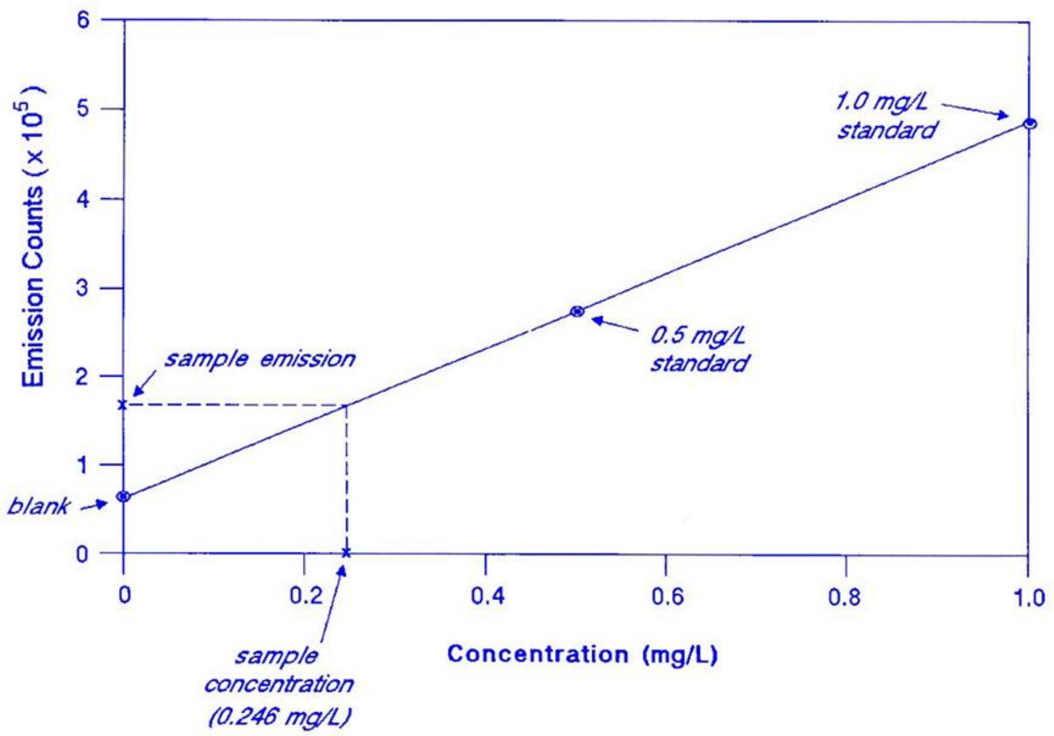

The results obtained by ICP-MS and ICP-OES analysis were expressed as ppm (parts per million, or micrograms per gram) of the metal in the original dry solid for uranium (U), thorium (Th) and rubidium (Rb), and in % (parts per hundred) of the metal in the original dry solid for the more abundant potassium (K).

Appendix 7.3.4 Grain size analysis

Grain sizes in sediments have a wide range from gravels (> 2 mm, up to large boulders more than 1 m in size) through sands (63 µm - 2 mm) and silts (4 µm - 63 µm) to clays (< 4 µm, down to fine clays less than 1 µm in size) (Udden, 1914; Wentworth, 1922). Whilst there are considerable overlaps, these four main groups are distinctive, with gravels being formed mainly from rock fragments, sands being formed mainly from small rock fragments and mono-minerallic crystals, silts from the splitting of sand-sized crystals, and clays from the chemical weathering of rocks. This wide range of sizes and characteristics means that one measurement technique cannot adequately cover the entire range; hence, different techniques are used for the analysis of different grain size ranges (McManus, 1988; Gale and Hoare, 1991; Garrison, 2003).

In the field, grain size assessment and description was based on observations (including drawings, photographs and use of a hand lens), direct measurements (especially for gravels), use of grain size scales (especially for sands), and touch (especially for sands, silts and clays) (UTA, 2011). For some samples of ten or fifty gravel clasts, direct measurements of the a-axis, b-axis, and c-axis were made using vernier calipers to the nearest 0.1 mm, or bow calipers to the nearest mm for larger clasts (Gale and Hoare, 1991). This was undertaken to aid in the interpretation of the sedimentary environments (mainly the energy of the depositional environments) for the river beds and river terraces investigated.

In the laboratory, selected fine-grained sediment and rock samples (fine gravels and smaller) had their grain size distributions analysed in more detail. These samples were from river banks and river beds, river terraces and river floodplains, and ancient constructions. This was undertaken mainly to compare the cohesiveness of river banks at different locations (sediments with a greater silt-clay content may produce more cohesive river banks) (Schumm, 1960; Knighton, 1998), to aid in the interpretation of sedimentary environments (though opinions vary on the reliability of using grain size analysis for this (Boggs, 2006)), and to compare masonry in ancient constructions with possible rock sources In addition, detailed grain size analysis (especially for the size ranges of 90 - 180 μm and 90 - 250 μm) was undertaken on sub-samples from the block sediment samples from river terrace exposures as part of the procedures for optically stimulated luminescence (OSL) dating.

Appendix 7.3.4.1 Sample preparation for all laboratory grain size analysis

Most of the fine-grained sediment and rock samples were cemented with carbonate cements and many contained a high proportion of limestone rock fragments and carbonate grains. For preparation of samples for detailed grain size analysis, this meant that a difficult balance had to be struck between rigorous pre-treatments (to produce and maintain disaggregation of the grains by breaking down and dissolving the carbonate cements) and minimal pre-treatments (to avoid damage to grain surfaces and to avoid breaking down and dissolving limestone rock fragments, carbonate grains and other soft grains) (Trentesaux et al., 2001). Also, there were issues with the grain size analysis equipment available, with the laser diffraction equipment being better suited to wet grain size analysis of clays and silts (with grains larger than c. 9 mm size being undetectable) and the laser imaging equipment being better suited to dry grain size analysis of sands and fine gravels (with grains smaller than c. 5 μm size being undetectable). Thus, since determining the silt-clay content of each sample was one aim of the analysis (as sediments with a greater silt-clay content may produce more cohesive river banks), it was decided to divide each sub-sample by wet sieving through a 63 μm sieve and analyse the coarser and finer fractions separately.

The fine-grained sediment and rock samples were carefully sub-sampled, disaggregated with a mounted needle and gentle application of a rubber pestle and mortar, and dried in a drying oven set at 105°C for 24 - 48 hours, to obtain accurately weighed dry sub-samples of about 1 g - 18 g dry mass (depending on the amount of sample available) (Gale and Hoare, 1991). A Leica S6 zoom stereo-microscope was used to ensure minimal crushing of the softer (mainly carbonate) grains with these treatments. Quite gentle disaggregation of the grains in each sample was undertaken by soaking in a solution of 100 ml de-ionised water and 0.5 ml of 40 grams litre^{-1} sodium hexametaphosphate solution, followed by agitation for 1 minute in an ultrasonic bath. Rock samples and very well cemented sediment samples that were insufficiently disaggregated by these processes were subjected to further soaking in a solution of cold 10 % HCl (hydrochloric acid) until sufficient disaggregation was achieved. Inevitably, this acid pre-treatment resulted in some breaking down and dissolution of limestone rock fragments and carbonate grains, though examination with the stereo-microscope indicated that these effects were fairly limited. Immediately afterwards, all samples were thoroughly rinsed with de-ionised water and were carefully wet sieved through a 63 µm sieve (Chappell, 1998; Trentesaux et al., 2001; Sperazza et al., 2004).

Appendix 7.3.4.2 Grain size analysis of the less than 63 µm fraction

The less than 63 µm fraction was analysed using a laser diffraction particle size analyser, in which grains were passed across a parallel beam of laser light to produce diffraction of the light at angles that were inversely proportional to the grain size. The equipment used was the Sympatec GmbH HELOS helium-neon laser diffraction sensor and the QUIXEL wet dispersing system (Figure APP 7.9), following recommended methods (Sympatec GmbH, 1994; Witt and Heuer, 1998). In this system, a dispersed wet flow of grains was produced by the QUIXEL by capillary and cavitational forces within the solution agitated by ultrasound, and then passed across a parallel beam of laser light produced from a point source via an adaptable beam expansion unit. This collimated laser beam was then diffracted by the flow of grains and transformed into a diffraction pattern by a Fourier lens, which was then recorded by a multi-element photo-detector and processed by a computer system.

After the sample preparation outlined in Appendix 7.3.4.1., the sediment and solution which passed through the 63 µm sieve was transferred to a large dish, with agitation and disaggregation being constantly maintained by use of magnetic stirrers and a small amount of sodium hexametaphosphate solution. A representative sub-sample of 7 ml - 420 ml of this uniformly suspended sediment solution was extracted using a pipette and added to 100 ml - 700 ml of tap water in the reservoir basin of the QUIXEL wet dispersing system. All of the concentrations were carefully balanced to produce a solution with an optical concentration of about 20 % (acceptable range 15 - 25 %) within the equipment. In most cases, for each sample a total of three sub-samples were run using the R2 lens (nominal measuring range 0.25/0.45 µm - 87.5 µm) and three sub-samples were run using the R5 lens (nominal measuring range 0.5/4.5 µm - 875 µm), with rinsing and reference measurements in between. Fewer measurements were taken for samples with only very small amounts of sediment in the fraction passed through the 63 µm sieve. These two lenses were employed (the only lenses available in the laboratory used) to complement each other, since the R2 lens was poor at detecting the larger grains (with sands larger than 87.5 µm not analysed) and the R5 lens was poor at detecting the finer grains (with clays smaller than 0.5 µm not analysed). Computer software presented the results in a number of formats (Veal, J., Sympatec GmbH, personal communications, 2008, 2009).

Figure APP 7.9 Schematic diagram and photograph of the dispersing system (QUIXEL) and laser diffraction sensor (HELOS) used for wet grain size analysis of the less than 63 µm fraction (Modified from Köhler et al., 2007; Sympatec GmbH, 2011)

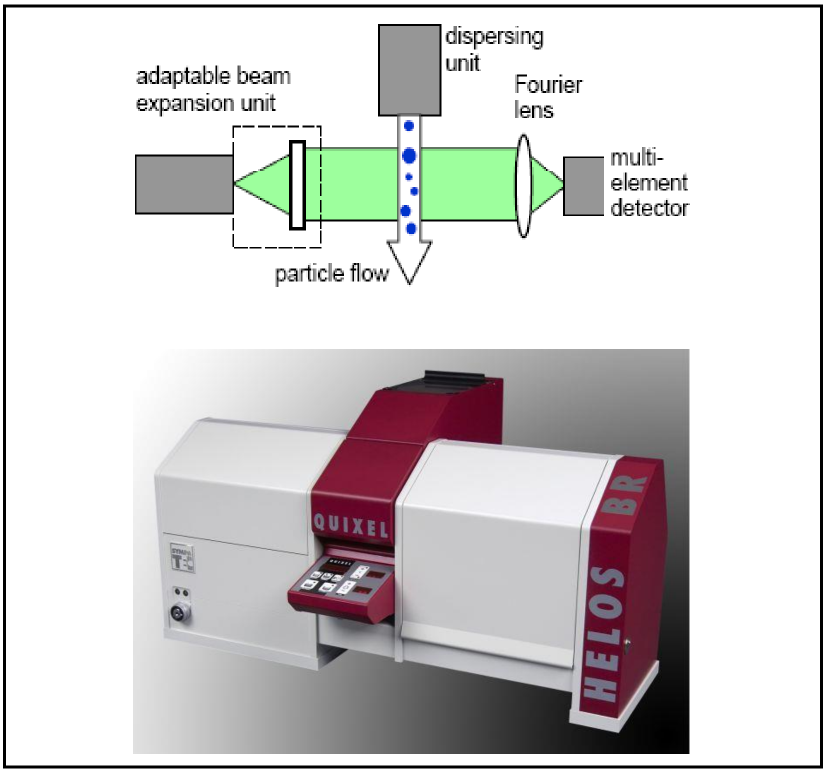

Appendix 7.3.4.3 Grain size analysis of the greater than 63 µm fraction

The greater than 63 µm fraction was analysed using a laser imaging particle size analyser, in which grains were passed across a parallel beam of laser light to produce images that were a record of each grain size and shape. The equipment used was the Sympatec GmbH QICPIC image analysis sensor and the GRADIS dry gravity dispersing system (Figure APP 7.10), following recommended methods (Sympatec GmbH, 1995, 1998; Witt et al., 2005). In this system, a dispersed dry flow of grains produced in the GRADIS by vibratory, collisional and gravitational forces within a vibratory feeder, a fall shaft, and a laminar air flow, was passed across a parallel beam of pulsed laser light produced via an adaptable beam expansion unit in the QICPIC (Figure APP 7.10). Each particle in the flow was imaged as “black” in a high speed CMOS (Complementary Metal-Oxide Semiconductor) camera and computer system, by the use of special imaging lenses which only transmitted light rays nearly parallel to the optical axis and a special pulsed laser light source (with exposure times of less than 1 nanosecond) which eliminated all significant motion blur (Sympatec GmbH, 2011).

Figure APP 7.10 Schematic diagram and photograph of the dispersing unit (GRADIS) and image analysis sensor (QICPIC) used for dry grain size analysis of the greater than 63 µm fraction (Modified from Sympatec GmbH, 2011)

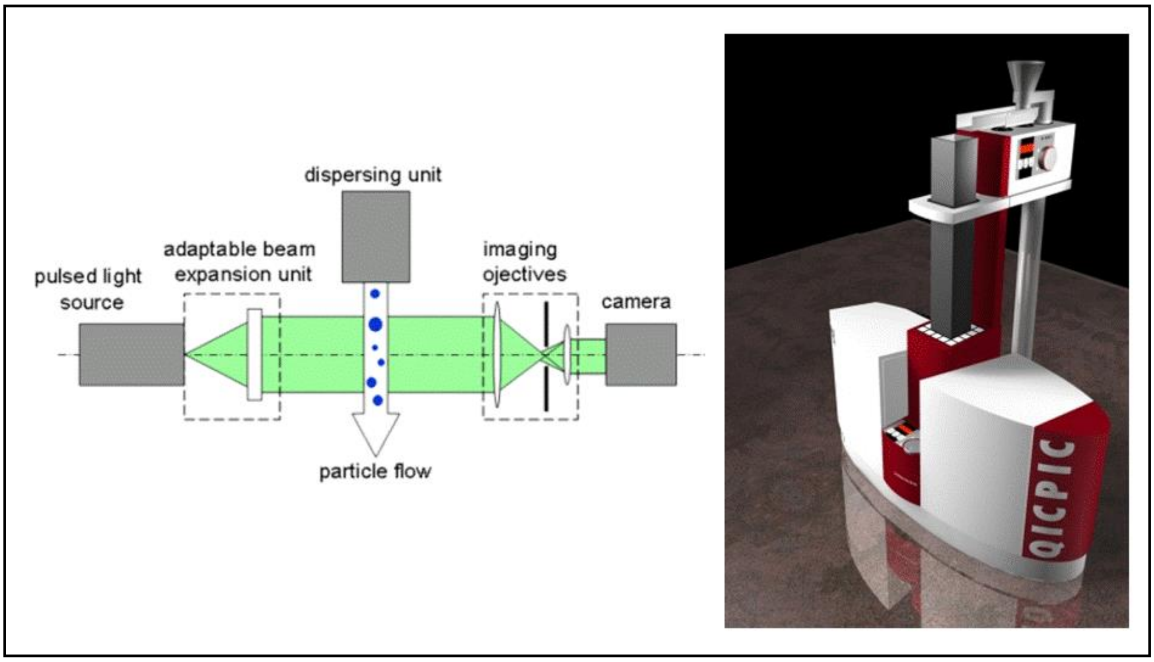

Following the sample preparation outlined in Appendix 7.3.4.1., the sediment and solution retained by the 63 µm sieve was carefully washed off into an evaporating dish using de-ionised water and a fine sieve brush. This was thoroughly dried in a drying oven set at 105°C for 48 hours and the dried sub-sample was accurately weighed to determine the proportion by dry mass of the greater than 63 µm grain size.

Then the entire dried sub-sample was brushed carefully into the vibratory feeder of the GRADIS with a fine brush. In most cases, four consecutive measurements of QICPIC grain size analysis were undertaken, with use of a cone of coffee filter paper fitted at the base of the GRADIS fall shaft to collect and re-use the same sub-sample. This methodology involved some slight loss of grains between measurements, so, generally, the first measurement runs were undertaken with the M8 lens (nominal measuring range 20 µm - 6.82 mm), the second runs were undertaken with the M6 lens (nominal measuring range 5 µm - 1.705 mm), and subsequent runs used the M8 lens again. Fewer measurements were taken for samples with only very small amounts of sediment retained by the 63 μm sieve, and only measurements with more than 5,000 particles recorded for the QICPIC calculations were considered to be sufficiently reliable to be recorded. The M8 lens was employed on all of the sub-samples, since the majority of the grains retained by the 63 μm sieve were detected by the M8 lens (practical measuring range c. 40 μm - 20 mm). The M6 lens was employed on the majority of the sub-samples, due to slightly greater precision for the finer grains with the M6 lens (practical measuring range c. 10 μm - 2 mm). Computer software presented the results in a number of formats (Smith, A. and Veal, J., Sympatec GmbH, personal communications, 2008, 2009).